AD-A261 915

# NONLINEAR DYNAMICS IN OPTICAL SYSTEMS

*Sponsored by*
Air Force Office of Scientific Research
Office of Naval Research

*For*
Optical Society of America

DTIC
ELECTE
MAR 23 1993
S D
E

## 1992 TECHNICAL DIGEST SERIES VOLUME 16

## JUNE 22–26, 1992 ALPBACH, AUSTRIA

DISTRIBUTION STATEMENT
Approved for public release
Distribution Unlimited

93-05071

93 3 9

# Nonlinear Dynamics in Optical Systems

*Summaries of papers presented at the*
*Nonlinear Dynamics in Optical Systems Topical Meeting*

June 22–26, 1992
Alpbach, Austria

1992 Technical Digest Series
Volume 16

CONFERENCE EDITION

DTIC QUALITY INSPECTED 1

*Sponsored by*
Air Force Office of Science Research
Office of Naval Research

*For*
Optical Society of America

Optical Society of America
2010 Massachusetts Avenue, NW
Washington, DC 20036

Accesion For
NTIS CRA&I X
DTIC TAB
Unannounced
Justification $75.00
By
Distribution /
Availability Codes
Dist | Avail and / or Special
A-1 | 21

Articles in this publication may be cited in other publications. In order to facilitate access to the original publication source, the following form for the citation is suggested:

> Name of Author(s), "Title of Paper," in Nonlinear Dynamics in Optical Systems Technical Digest, 1992 (Optical Society of America, Washington, D.C., 1992), Vol. 16, pp. xx–xx.

ISBN Number

| | |
|---|---|
| Conference Edition | 1-55752-258-8 |
| Postconference Edition | 1-55752-259-6 |
| (Note: Postconference Edition includes postdeadline papers.) | |
| 1992 Technical Digest Series | 1-55752-261-8 |

Library of Congress Catalog Card Number

| | |
|---|---|
| Conference Edition | 92-80629 |
| Postconference Edition | 92-80630 |

Copyright © 1992, Optical Society of America

Individual readers of this digest and libraries acting for them are permitted to make fair use of the material in it, such as to copy an article for use in teaching or research, without payment of fee, provided that such copies are not sold. Copying for sale is subject to payment of copying fees. The code 1-55752-261-8/92/$2.00 gives the per-article copying fee for each copy of the article made beyond the free copying permitted under Sections 107 and 108 of the U.S. Copyright Law. The fee should be paid through the Copyright Clearance Center, Inc., 21 Congress Street, Salem, MA 01970.

Permission is granted to quote excerpts from articles in this digest in scientific works with the customary acknowledgment of the source, including the author's name and the name of the digest, page, year, and name of the Society. Reproduction of figures and tables is likewise permitted in other articles and books provided that the same information is printed with them and notification is given to the Optical Society of America. Republication or systematic or multiple reproduction of any material in this digest is permitted only under license from the Optical Society of America; in addition, the Optical Society may require that permission also be obtained from one of the authors. Address inquiries and notices to Director of Publications, Optical Society of America, 2010 Massachusetts Avenue, NW, Washington, DC 20036. In the case of articles whose authors are employees of the United States Government or its contractors or grantees, the Optical Society of America recognizes the right of the United States Government to retain a nonexclusive, royalty-free license to use the author's copyrighted article for United States Government purposes.

The views and conclusions contained in this document are those of the author(s) and should not be interpreted as necessarily representing the official policies or endorsements, either expressed or implied, of the Air Force Office of Scientific Research or the U.S. Government.

This work relates to a Department of the Navy Task issued by the Office of Naval Research. The U.S. Government has a royalty license through the world in all copyrightable material contained herein.

Printed in U.S.A.

# CONTENTS


Agenda of Sessions ..... v

MA Dynamics of Pulse Formation ..... 1

MB Laser Instabilities ..... 17

MC Poster Session 1 ..... 37

TuA Control of Chaos ..... 109

TuB Multiwave Mixing and Phase Conjugation ..... 125

TuC Poster Session 2 ..... 145

WA Spatial Pattern Formation and Dynamics 1 ..... 221

WB Spatial Pattern Formation and Dynamics 2 ..... 239

WC Spatial Pattern Formation and Dynamics 3 ..... 257

ThA Semiconductor Device Dynamics ..... 261

ThB Laser Array Dynamics ..... 285

ThC Invited Paper Session ..... 303

FA Optical Chaos and Noise ..... 309

FB Special Topics in Chaos ..... 329

Key to Authors and Presiders ..... 347

## MONDAY, JUNE 22, 1992

### SCHROEDINGER HALL (KONGRESSHAUS ALPBACH)

**8:20 am–10:40 am**
**MA, DYNAMICS OF PULSE FORMATION**
William J. Firth, *University of Strathclyde, U.K., Presider*

**8:20 am (Invited)**
**MA1 Nonlinear dynamics of ultrashort pulse formation,** speaker to be announced. Abstract not available at press time. **(p. 2)**

**9:00 am**
**MA2 Physical origin of self-mode-locking regime in solid-state lasers,** Michel Piche, *Univ. Laval, Canada;* Francois Salin, *Institut d'Optique, France.* We describe how self-focusing in nonlinear laser resonators leads to self-mode-locking. Changes in beam size produce an effective loss modulation. **(p. 3)**

**9:20 am**
**MA3 Nonlinear effects in a ring resonator,** A. M. Dunlop, D. R. Heatley, W. J. Firth, *Univ. Strathclyde, U.K.* An in-plane ring resonator consisting of a nonlinear lens, a Gaussian aperture, and a gain medium is analyzed. Implications for unidirectional lasing and Kerr-lens mode-locking are explored. **(p. 6)**

**9:40 am**
**MA4 Dynamics of nonlinearly coupled mode-locked laser arrays,** Song Wu, Sandra L. Smith, Richard L. Fork, *Rensselaer Polytechnic Institute.* We discuss the dynamics of arrays of nonlinearly coupled mode-locked laser oscillators as a source of rapidly reconfigurable arrays of ultrashort optical pulses. **(p. 9)**

**10:00 am**
**MA5 Fast and slow self-phase modulation-induced pulse shaping of subpicosecond pulses in semiconductor laser amplifiers,** A. Dienes, M. Y. Hong, J. P. Heritage, *UC-Davis.* Subpicosecond pulse evolution is calculated in semiconductor amplifiers, including dispersion and self-phase modulation by saturation and by fast nonlinear index. Solitonlike compression is predicted. **(p. 11)**

**10:20 am**
**MA6 Optical pulse evolution in fiber laser additive pulse mode-locking,** K. A. Shore, *Bath Univ., U.K.;* T. Geisler, M. P. Sorenson, P. L. Christiansen, *Technical Univ., Denmark;* J. Mork, J. Mark, *TFL, Denmark.* The dynamics of optical pulse compression in an all-fiber APM configuration has been studied taking into account dispersion and phase bias effects. **(p. 14)**

**10:40 am–11:00 am COFFEE BREAK**

## MONDAY, JUNE 22, 1992—*Continued*

### SCHROEDINGER HALL

**11:00 am–1:20 pm**
**MB, LASER INSTABILITIES**
Yakov I. Khanin, *Academy of Sciences, Russia, Presider*

**11:00 am**
**MB1 Time inverted type-I intermittency of a single-mode laser,** D. Y. Tang, C. O. Weiss, *Physikalisch-Technische Bundesanstalt, Germany.* We report experimental observation of an intermittent route to chaos of a single-mode laser. We show that, by analyzing the experimental data time inverted, the observed intermittency can be described well by type-I intermittent dynamics. **(p. 18)**

**11:20 am**
**MB2 Instability and chaos in laser oscillation between highly excited molecular vibrational states,** Feng-Lei Hong, *Riken, Japan;* Maki Tachikawa, Toshiki Sugawara, Takehisa Tohei, Todao Shimizu, *Univ. Tokyo, Japan.* Instability and chaos in hot-band and sequence-band $CO_2$ lasers are used in the study of relaxation processes among highly excited molecular vibrational levels. **(p. 21)**

**11:40 am**
**MB3 Modulation dynamics of a two-mode laser,** Paul Mandel, M. Georgiou, *Brussels Free Univ., Belgium;* Kenju Otsuka, *NTT Basic Research Laboratories, Japan.* We show how the periodic solutions of a two-mode pump modulated class-B laser are organized in the plane of field amplitude vs pump frequency or amplitude. **(p. 24)**

**12:00 m**
**MB4 Diversity of chaos in multimode solid-state lasers,** E. A. Viktorov, A. A. Mak, O. A. Orlov, V. I. Ustyugov, I. B. Vitrischak, *S. I. Vavilov State Optical Institute, Russia.* The conditions for nonstationary processes arising in the multimode spectrum of solid-state lasers caused by different types of mode–mode coupling have been investigated in theory and experiment. We discuss the crowding-attractors situation for free-running generation and homoclinic chaos for intracavity SHG. **(p. 26)**

**12:20 pm**
**MB5 Geometrical phases in self-pulsing lasers,** C. Z. Ning, H. Haken, *Univ. Stuttgart, Germany.* A geometrical formulation of phase accumulation in dissipative systems is given to establish an exact relationship between the geometrical phase and the phase accumulation in lasers. **(p. 29)**

**12:40 pm**
**MB6 Dynamics of monovelocity atomic beam masers,** A. N. Oraevsky, T. V. Sarkissian, *Lebedev Physics Institute, Russia;* D. J. Jones, D. K. Bandy, *Oklahoma State Univ.* The dynamics of monovelocity atomic beam masers is analyzed within the framework of a two-level model. The loss-gain bifurcation curve, irregular pulsations, multistability, and hysteresis are found. **(p. 32)**

**1:00 pm**
**MB7 Interaction of relaxation oscillations and instability in a bidirectional Nd:YAG laser with a nonreciprocal ring cavity,** P. A. Khandokhin, Ya. I. Khanin, *Nizhny Novgorod, Russian Federation.* It is shown that the phase nonreciprocity influences the stability of the traveling wave regime due to changing the interaction between different types of relaxation oscillation. The laser sensitivity to the sign of phase nonreciprocity appears with detuning. **(p. 36)**

**1:20 pm–8:00 pm ATTENDEE FREE TIME**
**(Lunch and dinner on your own)**

## KRENEK HALL

**8:00 pm–10:00 pm**
**MC, POSTER SESSION: 1**

**MC1 Interferometric configurations for laser mode-locking using a nonlinear active medium,** Jean-Francois Cormier, Michel Piche, *Univ. Laval, Canada.* We analyze the operation and the stability of mode-locked lasers with nonlinear interferometric components, where the gain and the nonlinearity originate from the same material. **(p. 38)**

**MC2 Mode-locking dynamics of synchronously pumped color-center lasers,** W. Forysiak, *Heriot-Watt Univ., U.K.;* J. V. Moloney, *Univ. Arizona.* Phase-wave fluctuations in synchronously pumped color-center lasers lead to operating regimes including, quasistationary and fluctuating pulsing, spontaneous unidirectional lasing, and stochastic bidirectional switching. **(p. 41)**

**MC3 Optical bistabilities and autostabilization of the solid-state ring laser generation regimes under colliding USPs dynamic self-diffraction,** A. N. Shelaev, *P. N. Lebedev Physics Inst., Russia.* Abstract not available at press time. **(p. 43)**

**MC4 Nonlinear dynamics of extremely short electromagnetic pulses in passive and active media,** E. M. Belenov, A. V. Nazarkin, *P. N. Lebedev Physics Inst., Russia.* Abstract not available at press time. **(p. 44)**

**MC5 Coexistence of two attractors in lasers with incoherent delayed feedback,** Kenju Otsuka, Jyh-Long Chern, *NTT Basic Research Laboratories, Japan.* Sustained periodic relaxation oscillations and regenerative periodic spiking oscillations leading to chaotic oscillations are found to coexist in single-mode class-B lasers with incoherent delayed feedback. **(p. 45)**

**MC6 Nonlocal adiabatic elimination in the Maxwell-Bloch equation,** P. Ru, P. K. Jakobsen, J. V. Moloney, *Univ. Arizona.* The infinite-dimensional Maxwell-Bloch laser equations can be adiabatically reduced to a nonlocal rate equation set devoid of nonphysical instabilities. **(p. 48)**

**MONDAY, JUNE 22, 1992**—*Continued*

**MC7 Chaos and multistability in a bimodal $CO_2$ laser with a saturable absorber,** K. Tanii, T. Sugawara, M. Tachikawa, F.-L. Hong, T. Tohei, T. Shimizu, *Univ. Tokyo, Japan.* A passively Q-switched $CO_2$ laser exhibits novel types of chaotic mode competition and multistable oscillation caused by transverse spatial coupling of the lasing modes. **(p. 51)**

**MC8 Pulse pattern selection and low-dimensional modulation chaos in fiber lasers,** M. Haelterman, S. Trillo, S. Wabnitz, *Fondazione Ugo Bordoni, Italy.* We introduce a dynamic description of the generation and propagation of dissipative temporal structures in active nonlinear fiber resonators. **(p. 54)**

**MC9 Paper withdrawn. (p. 57)**

**MC10 Quasi vertical Hopf bifurcation for the multimode class-B laser,** Thomas Carr, Thomas Erneux, *Northwestern Univ.* We determine new amplitude equations for the quasivertical Hopf bifurcation of the multimode class-B laser. **(p. 58)**

**MC11 Nonlinear dynamics of photon–phonon lasing in indirect gap semiconductors,** L. A. Rivlin, A. A. Zadernovsky, *Moscow Institute of Radioengineering, Electronics & Automation, Russia.* Conditions are found for phonon lasing and simultaneous lasing of photons and phonons in indirect gap semiconductors. Stability, bistability and hysteresis of generation states are investigated. **(p. 61)**

**MC12 Paper withdrawn. (p. 63)**

**MC13 Instabilities in lasers with an injected delayed-feedback-controlled signal,** N. A. Loiko, A. M. Samson, *Academy of Sciences of the Republic of Belarus.* A theoretical analysis is presented of structurally different attractors and mechanisms of chaos in lasers with a delayed feedback that provides a phase-locked or incoherent injected signal with an amplitude depending on the value of the lasing field. **(p. 64)**

**MC14 Eigenvalues and eigenvectors of the inhomogeneously broadened single-mode laser stability problem,** V. Tu. Toronov, L. A. Melnikov, *Chernyshevsky State Univ., Russia.* New eigenvalues of the stability problem for the inhomogeneously broadened single-mode laser are found. The normal form representation of the inhomogeneously broadened laser equations of motion is considered. **(p. 67)**

**MC15 Successions of bifurcations in a laser with a saturable absorber as the distributed system,** L. A. Kotomtseva, A. M. Samson, *Academy of Sciences of the Belarus Republic.* Results of a theoretical consideration of the dynamics of a laser with a saturable absorber as the distributed system are given, with detuning of the cavity frequency from the frequency of the absorber. **(p. 70)**

**MC16 Pulse train instabilities and pulse structure evolution in a Nd:YAG laser with active mode-locking,** L. A. Melnikov, G. N. Tatarkov, *Chernyshevsky State Univ., Russia.* It is shown that low-frequency laser output instabilities are accompanied by complicated subnanosecond pulse structure evolution under the influence of a small field fluctuation. **(p. 73)**

**MC17 Transitions to chaos in a laser with a saturable absorber,** S. A. Tatarkova, V. V. Tuchin, *Chernyshevsky State Univ., Russia.* We studied the 5-D model for a laser with a saturable absorber which includes polarizations. We identified the transitions to chaos as period-doubling and intermittency. The multistability region is analyzed. **(p. 76)**

**MC18 Generalized finite-dimensional model of an inhomogeneously broadened single-mode laser,** L. A. Melnikov, V. Yu. Toronov, *Chernyshevsky State Univ., Russia.* The finite-dimensional dynamic model of a single-mode laser with arbitrary inhomogeneous broadening is proposed and analyzed. **(p. 79)**

**MC19 Combination tone mode–mode coupling as an instability mechanism in a dye ring laser,** Ya. I. Khanin, I. V. Koryukin, *Nizhny Novgorod, Russian Federation.* It is shown that combination mode–mode coupling is responsible for spectral instabilities in a ring dye laser. The key role of nonequidistant spacing of the modes in the combination tone mode–mode coupling efficiency is proved. **(p. 82)**

**MC20 Chaotic behavior associated with multicodimensional bifuractions in a laser with a saturable absorber,** A. G. Vladimirov, *St. Petersburg State Univ., Russia.* We consider a three-level:two-level model of a laser with a saturable absorber including polarization in the absorbing medium. We find the regions in laser parameter space in which different chaotic attractors exist and investigate the influence of frequency detuning on the bifurcation sequences leading to chaos. **(p. 85)**

**MC21 Dynamics of the solid-state laser with a saturable absorber,** E. A. Viktorov, A. A. Mak, O. A. Orlov, V. I. Ustyugov, *S. I. Vavilov State Optical Institute, Russia.* Experimental results of the dynamics of Nd:YAG laser with an intracavity $Cs^2$ vapor cell are presented. Different types of lasing regime (regular and chaotic) and theoretical models are discussed. **(p. 88)**

**MC22 Thin layer lasers,** A. N. Oraevsky, *Lebedev Physics Institute, Russia.* A theory of a thin layer laser is presented, i.e., a laser whose active medium length along the wave propagation is less than the wavelength. It is shown that such a laser exhibits a number of peculiarities compared with an ordinary laser. **(p. 90)**

**MONDAY, JUNE 22, 1992**—*Continued*

**MC23 Influence of velocity-changing collisions on single-mode inhomogeneously broadened laser dynamics,** B. Meziane, H. Ladjouze, *ENSSAT, France.* The inclusion of spectral cross-relaxation terms owing to strong velocity-changing collisions in the low-D equations is shown to bring noticeable modifications to the low-excitation spontaneous pulsation waveforms that occur in bad cavity-configured high-gain lasers. **(p. 91)**

**MC24 Nonlinear dynamics of the broadband dye ring laser with regulated cavity dispersion,** S. E. Vinogradov, A. A. Kachanov, S. A. Kovalenko, E. A. Sviridenkov, V. V. Ivanov, *Moscow, Russia.* Abstract not available at press time. **(p. 94)**

**MC25 From harmonic to pulsating periodic solutions in intracavity second harmonic generation,** Nicolas Pettiaux, *Brussels Free Univ., Belgium;* Thomas Erneux, *Northwestern Univ.* We show that the solution appearing above the bistability region in intracavity second-harmonic generation is pulsating rather than harmonic and can be described analytically. **(p. 95)**

**MC26 Transient behavior of fiber-optic Brillouin ring lasers,** R. Hereth, D. Garus, F. Schliep, *Ruhr Univ., Germany.* Transient oscillations of fiber-optic Brillouin ring lasers are investigated. Analytical expressions for the damping rate and the frequency of oscillations are presented. **(p. 98)**

**MC27 Density of probability distribution for quantum electro-magnetic field,** I. E. Protsenko, *P. N. Lebedev Physics Insitute, Russia.* Abstract not available at press time. **(p. 101)**

**MC28 Paper withdrawn. (p. 103)**

**MC29 High-dimensional dynamics in semiconductor lasers,** I. Fischer, J. Sacher, W. Elsasser, E. O. Gobel, *Marburg Univ., Germany.* A semiconductor laser coupled to a Michelson-type double-resonator shows slow switching between various regular and chaotic states, which are closely related to the Ikeda delay scenario. **(p. 104)**

**MC30 Transient multimode statistics in nearly single-mode semiconductor lasers,** A. Valle, L. Pesquera, *Univ. Cantabria, Spain;* P. Colet, M. San Miguel, *Univ. Baleariac Islands, Spain.* The transient statistics of nearly single-mode semiconductor lasers is studied for lasers biased below threshold. The side-mode excitation probability is obtained analytically and numerically for different excitation currents and gain differences. **(p. 106)**

## TUESDAY, JUNE 23, 1992

### SCHROEDINGER HALL

**8:20 am–10:20 am**
**TuA, CONTROL OF CHAOS**
Fedor Mitschke, *Univ. Hanover, Germany, Presider*

**8:20 am (Invited)**
**TuA1 Controlling chaos,** Celso Grebogi, *Univ. Maryland.* A method is proposed whereby motion on a chaotic attractor can be converted to a desired attracting time-periodic motion or steady state by making only small time-dependent perturbations of some set of available system parameters. **(p. 110)**

**9:00 am**
**TuA2 Control of chaos in a multimode solid-state laser: numerical results,** P. Colet, Rajarshi Roy, *Georgia Institute of Technology.* We have studied a numerical model for the control of a chaotic multimode solid-state laser using the occasional proportional feedback technique. **(p. 113)**

**9:20 am**
**TuA3 Experimental control of a chaotic laser system,** Rajarshi Roy, T. W. Murphy, Jr., T. D. Maier, Zelda Gills, *Georgia Institute of Technology;* E. R. Hunt, *Ohio Univ.* Dynamic control of a chaotic laser system has been demonstrated experimentally by occasional proportional feedback. A wide variety of stable, complex, periodic waveforms may be generated. **(p. 116)**

**9:40 am**
**TuA4 Control and characterization of unstable stationary states,** S. Bielawski, M. Bouazaoui, D. Derozier, P. Glorieux, *Lille Univ., France.* The characterization of unstable stationary states is reported using an external feedback control which also stabilizes the spontaneous intensity oscillations of an optical fiber laser. **(p. 119)**

**10:00 am**
**TuA5 Controlling laser chaos,** S. Bielawski, M. Bouazaoui, D. Derozier, P. Glorieux, *Lille Univ., France.* We have achieved experimental control of chaos in a doped fiber laser using a method slightly different from that proposed by Ott *et al.* **(p. 122)**

**10:20 am–10:40 am COFFEE BREAK**

## TUESDAY, JUNE 23, 1992—*Continued*

### SCHROEDINGER HALL

**10:40 am–12:40 pm**
**TuB, MULTIWAVE MIXING AND PHASE CONJUGATION**
Rajarshi Roy, *Georgia Institute of Technology, Presider*

**10:40 am**
**TuB1 Deterministic dynamics of the stimulated scattering phenomenon,** R. G. Harrison. Weiping Lu, A. Johnstone, D. S. Lim, J. S. Uppal, *Heriot-Watt Univ., U.K.* Cavity feedback is experimentally shown to dramatically modify the dynamics of stimulated scattering, the results substantiating a recent generalized treatment showing deterministic dynamics to be generic to these interactions. **(p. 126)**

**11:00 am**
**TuB2 Cascaded stimulated Brillouin scattering in high-finesse all-fiber ring resonators,** Dieter Garus, Ralf Hereth, *Ruhr Univ., Germany.* Multiple stimulated Brillouin scattering was observed in all-fiber ring resonators. A simple theoretical model allows the calculation of pump thresholds and laser output power. **(p. 129)**

**11:20 am**
**TuB3 Hamiltonian dynamics of parametric nonlinear wave mixing,** S. Trillo, S. Wabnitz, *Fondazione Ugo Bordoni, Italy.* We investigate the Hamiltonian dynamics of parametric instabilities and chaos in media with both quadratic and cubic nonlinearities. **(p. 132)**

**11:40 am**
**TuB4 Observation of chaos in off-Bragg photorefractive four-wave mixing,** Kenneth D. Shaw, *USAF Phillips Laboratory.* Chaotic oscillations have been observed in the phase-conjugate intensity of an externally pumped photorefractive phase-conjugate mirror when one of the pumping beams deviates slightly from the Bragg angle. **(p. 135)**

**12:00 m**
**TuB5 Self- and mutual phase conjugation via thin layers,** B. Ya. Zeldovich, I. V. Goosev, V. A. Krivoschekov, *Chelyabinsk Technical Univ., Russia.* Mutual phase conjugation is suggested via two thin layers, e.g., quantum well samples, with cross phase nonlinearity of opposite sign. Experiments are reported. **(p. 138)**

**12:20 pm**
**TuB6 Uses of fiber-optic interferometry in nonlinear dynamics,** S. T. Vohra, F. Bucholtz, *U.S. Naval Research Laboratory.* Extremely high strain resolution ($\leq 10^{-12}/\sqrt{\text{Hz}}$) is possible with fiber-optic interferometers, which makes them ideally suited for studying the nonlinear strain dynamics of various materials. **(p. 141)**

**12:40 pm–8:00 pm ATTENDEE FREE TIME**
**(Lunch and dinner on your own)**

## KRENEK HALL

**8:00 pm–10:00 pm**
**TuC, POSTER SESSION: 2**

**TuC1 Transverse modes of microchip solid-state lasers,** G. K. Harkness, W. J. Firth, *Univ. Strathclyde, U.K.* We describe a model for microchip lasers, presenting results on their transverse modes, thresholds, operating frequencies, and dynamic stability at and well beyond threshold. **(p. 146)**

**TuC2 Hexagonal transverse patterns in the interaction of counterpropagated light beams: the many-body approach,** A. A. Afanasev, B. A. Samson, V. M. Volkov, *Academy of Sciences of the Republic of Belarus.* We propose to consider the output hexagonal pattern in the counterpropagating interaction of light beams in a nonlinear medium as the dense packing of filaments in a finite volume, as well as to analyze the spatial pattern formation from the point of view of many-body theory. **(p. 149)**

**TuC3 Spatial symmetry breaking and coexistence of attractors in a nonlinear ring cavity,** M. Sauer, F. Kaiser, *Darmstadt Institute for Applied Physics, Germany.* Resonances between internal and external transverse space frequencies in a passive optical system are investigated. They lead to symmetry breaking bifurcations and to the coexistence of periodic attractors. **(p. 151)**

**TuC4 Dynamics of transverse field structure in a unidirectional ring laser with fast-relaxed active medium,** I. V. Veshneva, L. A. Melnikov, A. A. Sokolov, G. N. Tatarkov, *Chernyshevsky State Univ., Russia.* Steady-state and beat regimes are studied using the transverse flexible modes having the beam parameter as a dynamic variable. The axial symmetrical case and fields with defects are considered. **(p. 154)**

**TuC5 Dynamic 3-D propagation of light pulses,** G. G. Luther, J. V. Moloney, D. E. Hart, E. M. Wright, *Univ. Arizona.* Several characteristic features of the propagation of 3-D light pulses in media with dispersion, spectral absorption, and noninstantaneous cubic nonlinearity are illustrated. **(p. 157)**

**TuC6 Phase singularities in a Fabry-Perot resonator with an intracavity nematic liquid crystal film,** M. Kreuzer, R. Neubecker, T. Tshudi, *Darmstadt Institute of Applied Physics, Germany.* We present what we believe to be the first experimental evidence of optical vortices as a concomitant phenomenon of pattern formation in a nonlinear Fabry-Perot containing a thin liquid crystal film. **(p. 160)**

**TuC7 Laser rate equations with phase-sensitive interactions,** C. Etrich, Paul Mandel, *Brussels Free Univ., Belgium;* Kenju Otsuka, *NTT Basic Research Laboratories, Japan.* We study the influence of space-dependent mode–mode coupling oscillating at wavenumber differences in the framework of multimode rate equations. **(p. 163)**

**TUESDAY, JUNE 23, 1992**—*Continued*

**TuC8 Simple modeling of feedback-induced properties in semiconductor lasers,** B. Meziane, P. Besnard, G. Stephan, *ENSSAT, France.* We transform the infinite-dimensional Lang/Kobayashi rate equations into a much more numerically tractable model, which is shown to describe the well-known distinct regimes of operation of an external-cavity semiconductor laser. **(p. 166)**

**TuC9 Asymmetric behavior and kink shaping by optical feedback,** F. Brivio, *Italtel SIT, Italy;* S. Mazzoleni, M. Milani, *Univ. Milan, Italy.* A nonhomogeneous distribution of carriers inside a semiconductor laser active cavity is induced by optical reinjection, because of its spatial asymmetry. The characteristic *P-I* curve is analytically derived, and the nonlinearity (kink) just above threshold in the presence of optical feedback can be derived. **(p. 169)**

**TuC10 Switch-on time statistics of a single-mode semiconductor laser with an injected signal,** M. C. Torrent, *Catalonia Polytechnic Univ., Spain;* J. M. Sancho, *Barcelona Univ., Spain;* M. San Miguel, S. Balle, *Univ. Balearic Islands, Spain.* Passage time statistics of gain-switched single-mode semiconductor lasers is sensitive to an injected signal. An optimum detuning proportional to the $\alpha$ factor is found. **(p. 172)**

**TuC11 Dynamics of passive FM locking in semiconductor lasers,** K. A. Shore, W. M. Yee, *Bath Univ., U.K.* A multimode formalism has been utilized to study FM locking arising from nonlinear gain in semiconductor lasers. An admixture of FM and AM locked states inhibits pure FM operation. **(p. 175)**

**TuC12 Light dynamics of a bistable element chain,** Yu. A. Logvin, A. M. Samson, *Academy of Sciences of the Republic of Belarus.* The light dynamics of a chain of bistable thin films is theoretically considered. It is assumed that bistable elements are arranged in line and coupled by the light beams. Regular and chaotic dynamic regimes of the system are discussed. **(p. 177)**

**TuC13 Effects of nonlinear gain on the stability of two-element evanescently coupled laser arrays,** D. Nichols, H. Winful, *Univ. Michigan.* We have studied the effect of nonlinear gain saturation on the stability of evanescently coupled laser arrays and found that gain saturation facilitates stable operation. **(p. 179)**

**TuC14 Bifurcation analysis of bistable systems disturbed by external noise: an application of cumulant analysis,** V. S. Anischenko, A. B. Neiman, *Chernyshevsky State Univ., Russia.* Abstract not available at press time. **(p. 182)**

**TuC15 Static and dynamic optical bistability in Fabry-Perot and distributed feedback resonators with QW structures,** F. Castelli, L. A. Lugiato, *Milan Univ., Italy;* G. P. Bava, *Turin Polytechnic, Italy;* P. Debernardi, *CESPA-CNR, Italy.* We study the static and the dynamic behavior of optically bistable systems including a MQW structure. The analysis is based on an accurate description of the optical nonlinearities in the system. **(p. 183)**

**TuC16 Dynamical aspects of polarization-induced switching phenomena in diffusively nonlinear Fabry-Perot resonators,** J. Danckaert, H. Thienpont, I. Veretennicoff, *Brussels Free Univ., Belgium.* The dynamics of polarization-induced switching phenomena occurring in Fabry-Perot resonators with a diffusive nonlinearity are studied, both for low- and high-finesse resonators. **(p. 186)**

**TuC17 Optothermal bistable cavities with localized absorption under modulated excitation,** Jordi Farjas, Francesc Boixader, Gaspar Orriols, *Barcelona Univ. Automona, Spain;* Josep Massaneda, Francesc Pi, *Catalonia Univ. Politecnica, Spain.* We present numerical and experimental results showing complex dynamics in the response of an optothermal bistable cavity with an absorbing mirror and a transparent bilayer spacer of opposite thermo-optic materials, which is irradiated with modulated light. **(p. 189)**

**TuC18 Effect of initial phase factor on the properties of an electro-optical bistable system,** Zhiren Zheng, Jinyue Gao, *Jilin Univ., P.R.C.* The effect of initial phase factor on bistability, instability, resonance, and frequency locking has been studied for a hybrid bistable system with a delay. **(p. 192)**

**TuC19 Dynamic optical bistability in a semiconductor-doped glass etalon,** Chunfei Li, Yinglin Song, Zizhong Zha, Lei Zhang, *Harbin Institute of Technology, P.R.C.* A dynamic theory of transient optical bistability in a Cd-S-Se-doped glass etalon is presented. The quasistable condition for transient optical bistability is $T_p > T_d \geq T_r$. **(p. 195)**

**TuC20 New types of switching waves and diffractive autosolitons in wide-aperture nonlinear interferometers and lasers,** S. V. Fedorov, G. V. Khodova, K. S. Kostritskaya, N. N. Rosanov, *S. I. Vavilov State Optical Institute, Russia.* We propose and analyze the equations of motion of the diffractive autosoliton in a nonlinear interferometer excited by nonuniform radiation, and in a laser with a saturable absorber. New types of patterns are described in bi- and multistable interferometers. **(p. 198)**

**TuC21 Squeezing in a wide-aperture nonlinear interferometer: transverse effects,** A. V. Belinsky, *Moscow State Univ., Russia;* N. N. Rosanov, *S. I. Vavilov State Optical Institute, Russia.* We analyze squeezed states of light in an interferometer filled with Kerr media and excited by external radiation. Effective noise depression in a certain range of temporal and spatial frequencies is predicted. **(p. 199)**

**TuC22 Theory of a photorefractive resonator,** H. Zeghlache, L. Dambly, P. Glorieux, *Lille Univ. Sciences et Technologies, France.* We analyze two-wave mixing in an unidirectional ring cavity containing a photorefractive material and give an analytical expression which approaches the cavity-mode frequency shift. **(p. 200)**

**TuC23 Solvable models of optical resonators,** A. V. Malev, *St. Petersburg State Univ., Russia.* Solvable models of open optical resonators in a 1-D approach are considered. Construction was carried out based on the self-adjoint extension theory of symmetrical operators. **(p. 203)**

**TUESDAY, JUNE 23, 1992**—*Continued*

**TuC24 Phase quasi-integral for stimulated Raman scattering initiated by quantum fluctuations and statistics of solitonlike random pulses in depleted pump,** S. Ya. Kilin, *Academy of Sciences of the Belarus Republic.* The phase quasi-integral for SRS is found; the relative phase of laser, Stokes, and polarization waves is nearly conserved during their propagation in Raman media. Due to this quasi-integral the temporal statistics of solitonlike pulses in depleted pump is defined by phase statistics in the SRS linear stage. **(p. 206)**

**TuC25 Multiparametric criticality in a laser system,** A. P. Kuznetsov, S. P. Kuznetsov, I. R. Sataev, *Saratov Institute of Radioengineering & Electronics, Russia.* The hierarchy of criticality types (Feigenbaum, tricritical, bicritical, multicritical) is found at the onset of chaos in equations of a laser pumped by another Q-switched laser. **(p. 209)**

**TuC26 Bifurcation and chaos in the presence of external noise,** V. S. Anishchenko, A. B. Neiman, *Chernyshevsky State Univ., Russia.* Cumulative analysis is used for studies of nonwhite noise influence on some dynamic system bifurcations. The influence of external noise on dynamic chaos is investigated in the Lorenz model. **(p. 212)**

**TuC27 Rossler chaos in optothermal bistability with localized absorption,** Ramon Herrero, Francesc Boixader, Gaspar Orriols, *Barcelona Autonomous Univ., Spain;* Joan I. Rosell, Francesc Pi, *Catalonia Polytechnic Univ., Spain.* We present numerical and experimental evidences of Rossler chaos in optothermal bistable cavities with an absorbing mirror and a transparent trilayer spacer of alternatively opposite thermo-optic materials. **(p. 215)**

**TuC28 Pulse statistics of modulated gas lasers,** A. Valle, L. Pesquera, M. A. Rodriguez, *Univ. Cantabria, Spain.* The statistics of turn-on delay time, maximum light intensity and pulse width of class-A single-mode lasers is analyzed. An analytic expression for the switch-on time is obtained, in good agreement with numerical simulations. **(p. 218)**

## WEDNESDAY, JUNE 24, 1992

### SCHROEDINGER HALL

**8:20 am–11:20 am**
**WA, SPATIAL PATTERN FORMATION AND DYNAMICS: 1**
Neal B. Abraham, *Bryn Mawr College, Presider*

**8:20 am (Invited)**
**WA1 Patterns and their defects,** Pierre Coullet, *Univ. Nice, France.* Abstract not available at press time. **(p. 222)**

**9:00 am**
**WA2 Statistics of topological defects in linear and nonlinear optics,** P. L. Ramazza, S. Residori, G. Giacomelli, *Italian National Institute of Optics;* E. T. Arecchi, *Univ. Florence, Italy.* We show that the statistical distribution of the number of defects in an optical field does not discriminate between the linear and nonlinear case. **(p. 223)**

**9:20 am**
**WA3 Pattern formation and pattern dynamics in passive systems,** M. Brambilla, F. Castelli, A. Gatti, L. A. Lugiato, F. Prati, *Milan Univ., Italy.* We report on phenomena of pattern formation and pattern dynamics in the transverse profile of the field propagating in an absorbing collection of two-level atoms in a ring resonator with spherical mirrors. **(p. 226)**

**9:40 am**
**WA4 Symmetry breaking and vortices in a sodium-filled Fabry-Perot resonator,** L. M. Hoffer, G.L. Lippi, J. Nalik, C. Vorgerd, W. Lange, *Westfalische Wilhelms-Univ., Germany.* Symmetry broken patterns and vortices are observed in a high Fresnel number nonlinear passive resonator where only a few lowest-order modes are selectively excited. **(p. 229)**

**10:00 am**
**WA5 Spatial and temporal behavior of instabilities generated by counterpropagating laser beams in rubidium vapor,** A. Blouin, M. Pinard, A. Maitre, G. Grynberg, *ENS-Laboratoire de Spectroscopie Hertzienne, France;* J. R. Rios Leite, *Univ. Federal de Pernambuco, Brazil;* R. W. Boyd, *Univ. Rochester.* Spatial and temporal behaviors of instabilities arising from the interaction of counterpropagating laser beams with rubidium atoms are studied for different patterns vs laser frequency and intensity. **(p. 232)**

**10:20 am**
**WA6 Two-dimensional transverse patterns in optical bistability,** W. J. Firth, G. S. McDonald, A. J. Scroggie, *Univ. Strathclyde, U.K.;* L. A. Lugiato, *Milan Univ., Italy;* R. Lefever, *Brussels Free Univ., Belgium.* The mean-field dispersive model of optical bistability is shown to yield hexagonal and other structures. The study is both analytical, using bifurcation theory, and numerical. **(p. 235)**

## WEDNESDAY, JUNE 24, 1992 — *Continued*

**10:40 am**
**WA7 Interaction of spatiotemporal wave structures in nonlinear optical resonators: New routes in optical turbulence,** M. A. Vorontsov, *Moscow State Univ., Russia.* Abstract not available at press time. **(p. 238)**

**11:00 am–11:20 am COFFEE BREAK**

**11:20 am–1:20 pm**
**WB, SPATIAL PATTERN FORMATION AND DYNAMICS: 2**
Paul Mandel, *Brussels Free University, Belgium, Presider*

**11:20 am**
**WB1 Dynamic transverse laser patterns,** M. Brambilla, M. Cattaneo, L. A. Lugiato, R. Pirovano, F. Prati, *Milan Univ., Italy;* A. J. Kent, G.L. Oppo, *Univ. Strathclyde, U.K.;* A. B. Coates, C. O. Weiss, *Physikalisch-Technische Bundesanstalt, Germany;* C. Green, E. J. D'Angelo, J. R. Tredicce, *Drexel Univ.* We consider a cylindrically symmetrical laser with spherical mirrors, and describe the dynamics in terms of the competition among different Gauss-Laguerre modes of the cavity. **(p. 240)**

**11:40 am**
**WB2 Pattern formation in a multimode $CO_2$ laser,** D. Hennequin, C. Lepers, E. Louvergneaux, D. Dangoisse, P. Glorieux, *Lille Univ., France.* The spatiotemporal behavior of a multitransverse-mode Fabry-Perot $CO_2$ laser with and without an intracavity saturable absorber is considered experimentally. Periodic alternation and antiphasing are seen. **(p. 242)**

**12:00 m**
**WB3 Defect dynamics in the evolution of the transverse pattern of a laser,** N. B. Abraham, S. Balle, Z. Chen, *Bryn Mawr College;* E. J. D'Angelo, J. R. Tredicce, *Drexel Univ.* Numerical solutions of the Maxwell-Bloch equations reveal evolving patterns involving many radial and angular modes, which can be simply described in terms of the motion and interaction of defects. **(p. 245)**

**12:20 pm**
**WB4 Optical vortices and dark spatial solitons,** C. O. Weiss, *PTB-Braunschweig, Germany;* K. Staliunas, *Vilnius Univ., Lithuania.* The dynamics of optical vortices in a laser beam cross-section is investigated. The optical vortices are treated as perturbed dark solitons of the 2-D nonlinear Schrodinger equation. **(p. 248)**

**12:40 pm**
**WB5 Turbulent patterns in wide-gain section two-level and Raman lasers,** P. K. Jakobsen, S. G. Wenden, J. V. Moloney, A. C. Newell, *Univ. Arizona.* We establish that a deep analogy exists between turbulent convection patterns in Rayleigh-Benard fluid convection and the output of wide-gain section two-level and Raman lasers. **(p. 251)**

**1:00 pm**
**WB6 Pattern formation due to nonlinear counterpropagation in Kerr and Brillouin-active media,** J. B. Geddes, R. Indik, J. V. Moloney, *Univ. Arizona;* W. J. Firth, G. S. McDonald, *Univ. Strathclyde, U.K.* Analytical and numerical studies are reported for counterpropagating beams in both Kerr and Brillouin-active slabs. The dynamics of hexagonal pattern formation is discussed. **(p. 254)**

**1:20 pm–4:00 pm CONFERENCE RECEPTION AND ATTENDEE FREE TIME**

## SCHROEDINGER HALL

**4:00 pm–5:20 pm**
**WC, SPATIAL PATTERN FORMATION AND DYNAMICS: 3**
Robert G. Harrison, *Heriot-Watt University, U.K., Presider*

**4:00 pm (Invited)**
**WC1 Interference and dislocation patterns in linear waves,** Michael Berry, *Wills Physics Laboratory, U.K.* Phase singularities (dislocations and disclinations) are generic in waves, linear or not, and occur in light, sound, microwaves, quantum waves and the tides. They are complementary to the caustic singularities of geometrical optics. **(p. 258)**

**4:40 pm (Invited)**
**WC2 Pattern formation, pattern recognition, and associative memory,** H. Haken, *Universitat Stuttgart, Germany.* In physical and nonphysical systems, spontaneous pattern formation can be treated by concepts of order parameters and enslaving developed by synergetics. These principles allow one to devise analogue computers for pattern recognition and associative memory. **(p. 259)**

**5:20 pm–8:00 pm ATTENDEE FREE TIME (Dinner on your own)**

## SCHROEDINGER HALL

**8:00 pm–10:00 pm**
**WD, ROUNDTABLE DISCUSSION**
Jerome V. Moloney, *University of Arizona, Presider*



## SCHROEDINGER HALL

**8:20 am–10:40 am**
**ThA, SEMICONDUCTOR DEVICE DYNAMICS**
Daan Lenstra, *Amsterdam Free University, The Netherlands, Presider*

**8:20 am**
**ThA1 Polarization bistability in laser diodes,** Hitoshi Kawaguchi, Tomoyoshi Irie, Naohiro Tan-no, *Yamagata Univ., Japan.* We report a new form of pitchfork bifurcationlike polarization bistability in ' .er diodes which has major speed advantages over conventional polarization bistability. **(p. 262)**

**8:40 am**
**ThA2 Polarization mode sitching and bistability in semiconductor lasers,** A. Klehr, A. Barwolff, G. Berger, R. Muller, M. Voss, *Institut fur Nichtlineare Optik und Kurzzeitspektroskopie, Germany.* The influence of lateral waveguiding on switching behavior between emission states of differently polarized modes in ridge-waveguide lasers was investigated. Measured switching time was 50 ps. **(p. 266)**

**9:00 am**
***ThA3 Transition in the coherence collapse of semiconductor lasers with external optical feedback: two types of low frequency fluctuation,*** J. Sacher, W. Elsasser, E. O. Gobel, *Marburg Univ., Germany.* We demonstrate a transition between ultrahigh-dimensional motion and a high-dimensional attractor in the coherence collapse of semiconductor lasers with external optical feedback. **(p. 269)**

**9:20 am**
**ThA4 Dynamic instability in delay-coupled semiconductor lasers,** David J. Bossert, Richard K. DeFreez, *Oregon Graduate Institute of Science & Technology;* Gregory C. Dente, *G.C.D. Associates;* Herbert G. Winful, *Univ. Michigan.* Self- and mutually coupled semiconductor lasers are examined experimentally and theoretically. Coupling delays and carrier-dependent refractive index result in dynamic instability at moderate coupling levels. **(p. 272)**

**9:40 am**
**ThA5 Modulated semiconductor laser: a Hamiltonian search for its periodic attractors,** P. C. De Jagher, D. Lenstra, *Amsterdam Free Univ., The Netherlands.* Using an analytic approximation, the values of the modulation index which permit periodic output are determined; it is argued that multistability can occur. **(p. 275)**

**10:00 am**
**ThA6 Chaos in semiconductor lasers,** Hua Li, Jun Ye, John G. McInerney, *Univ. New Mexico.* We report investigations of the onset of chaos in a semiconductor laser with weak external optical reflection, and in an AR-coated semiconductor laser in an external cavity. **(p. 278)**

**10:20 am**
**ThA7 Injection locking of a vertical-cavity surface-emitting laser,** D. Boggavarapu, J. W. Grantham, Y. Z. Hu, H. M. Gibbs, G. Khitrova, S. Koch, M. Sargent III, *Univ. Arizona;* Weng W. Chow, *Sandia National Laboratories.* Continuous-wave laser injection into a vertical-cavity surface-emitting laser exhibits pushing and quenching of lasing and new frequency generation shifted up to 50 GHz. **(p. 281)**

**10:40 am–11:00 am COFFEE BREAK**

## SCHROEDINGER HALL

**11:00 am–1:00 pm**
**ThB, LASER ARRAY DYNAMICS**
Peter Davis, *ATR Optical and Radio Communications Research Laboratories, Japan, Presider*

**11:00 am**
**ThB1 Factorial dynamic pattern memory in globally coupled lasers,** Kenju Otsuka, Jyh-Long Chern, *NTT Basic Research Laboratories, Japan.* Chaotic dynamics in globally coupled modulated lasers have been switched into stable orbits, including antiphase periodic states and clustered states, by injection seeding. **(p. 286)**

**11:20 am**
**ThB2 Coherence and phase dynamics of spatially coupled solid-state lasers,** Larry Fabiny, P. Colet, Rajarshi Roy, *Georgia Institute of Technology.* Experimental measurements of the mutual coherence of two lasers with spatially overlapping fields in the active medium are reported and compared with numerical simulations. **(p. 289)**

**11:40 am**
**ThB3 Dynamics of a twin stripe semiconductor laser array: coupled-mode theory vs the PDE model,** Lutfur Rahman, Herbert G. Winful, *Univ. Michigan.* The PDE model for the dynamics of a twin stripe semiconductor laser array is reduced to a coupled-mode ODE model. Dynamic characteristics for the two models are compared. **(p. 292)**

**12:00 m**
**ThB4 Space–time dynamics of semiconductor lasers: many-body theory and phenomenological models,** J. V. Moloney, P. Ru, R. Indik, S. W. Koch, E. Wright, *Univ. Arizona.* We study the dynamical behavior of semiconductor lasers including many-body effects and investigate the validity of the phenomenological laser model. **(p. 295)**

**12:20 pm**
**ThB5 Bifurcation to standing and traveling waves in large laser arrays,** Ruo-ding Li, Thomas Erneux, *Northwestern Univ.* We consider the equations for *N*-coupled semiconductor lasers and investigate the bifurcations to periodic standing and traveling wave solutions in the limit *N* large. **(p. 297)**

THURSDAY, JUNE 25, 1992—*Continued*

**12:40 pm**
**ThB6 Coupled elements, phase transitions, and localized order,** Martin McCall, Ziping Jiang, *Imperial College, U.K.* We examine a distributed nonlinear optical network based on a discretization of the Ginzburg-Landau equation. We demonstrate phase transition and pattern localization effects. **(p. 300)**

**1:00 pm–4:00 pm ATTENDEE FREE TIME**
**(Lunch on your own)**

## SCHROEDINGER HALL

**4:00 pm–5:20 pm**
**ThC, INVITED PAPER SESSION**
Kenju Otsuka, *NTT Basic Research Laboratories, Japan, Presider*

**4:00 pm (Invited)**
**ThC1 Network of chaotic elements,** Kunihiko Kaneko, *Univ. Tokyo, Japan.* Network of chaotic elements exhibits coherent, ordered, partially ordered, and turbulent phases according to the clusterings of oscillations. Novel features include chaotic itinerancy, hierarchical clustering, partition complexity, and hidden coherence. Relevance to information processing is discussed. **(p. 304)**

**4:40 pm (Invited)**
**ThC2 Spatial correlation dimension and critical phenomena in complex Ginzburg-Lardan mode,** M. Rabinovich, *Nighny Novgorod, Russia.* Abstract not available at press time. **(p. 307)**

**5:20 pm–8:00 pm ATTENDEE FREE TIME**
**(Dinner on your own)**

## SCHROEDINGER HALL

**8:00 pm–10:00 pm**
**ThD, POSTDEADLINE PAPER SESSION**
Pierre Glorieux, *Universite des Sciences et Techniques de Lille Flandres-Artois, France, Presider*

## FRIDAY, JUNE 26, 1992

### SCHROEDINGER HALL

**8:20 am–10:20 am**
**FA, OPTICAL CHAOS AND NOISE**
M. San Miguel, *University of Balearic Islands, Spain, Presider*

**8:20 am**
**FA1 Chaos vs noise in experimental data,** F. Mitschke, M. Dammig, C. Boden, *Hanover Univ., Germany.* The distinction of chaos vs noise in experimental data with the recently proposed method of surrogate data is vastly superior to previous approaches **(p. 310).**

**8:40 am**
**FA2 Quantum noise reduction in a spatial dissipative structure,** L. A. Lugiato, F. Castelli, *Milan Univ., Italy.* We demonstrate the presence of quantum mechanical order in the transverse roll pattern predicted by a model of a passive nonlinear optical system. Precisely, the signal beams in the far field are fully quantum correlated twin beams. **(p. 313)**

**9:00 am**
**FA3 Influence of noise and of spatiotemporal nonuniformity on the evolution of optically nonlinear systems,** H. Issler, J. Grohs, M. Kuball, J. Steffen, C. Klingshirn, *Univ. Kaiserslautern, Germany;* S. Apanasevich, A. Lyakhnovich, *Academy of Science of the Republic of Belarus.* We report on spatial structure formation in optically nonlinear elements and the influence of noise on self-oscillations of a hybrid ring resonator containing such elements. **(p. 316)**

**9:20 am**
**FA4 Transient statistics in the switch-on of class B lasers,** S. Balle, M. San Miguel, *Univ. Balearic Islands, Spain;* N. B. Abraham, *Bryn Mawr College.* Transient statistics in the nonlinear regime are a mapping of passage time statistics. Different cases and scaling laws are discussed. **(p. 319)**

**9:40 am**
**FA5 Two-peaked passage time statistics in a Q-switched $CO_2$ laser near threshold,** R. Meucci, M. Ciofini, F. T. Arecchi, Peng-ye Wang, *Italian National Institute of Optics.* The appearance of two-peaked passage time distributions in a Q-switched $CO_2$ laser has been explained as a consequence of the population noise near threshold. **(p. 322)**

**10:00 am**
**FA6 Period-one oscillation in a chaotic system with multimodal mapping,** Yun Liu, Junji Ohtsubo, *Shizuoka Univ., Japan.* Period-one oscillation is observed in a chaotic system consisting of a laser diode active interferometer. The conditions for such oscillations are examined. **(p. 328)**

**10:20 am–10:40 am COFFEE BREAK**

## FRIDAY, JUNE 26, 1992—*Continued*

**10:40 am–12:00 m**
**FB, SPECIAL TOPICS IN CHAOS**
Govind R. Agrawal, *University of Rochester, Presider*

**10:40 am**
**FB1 Radiation trapping: a new mechanism for chaos in optical systems,** M. Moller, W. Lange, *Westfalische Wilhelms-Univ., Germany.* The effect of radiation trapping together with a static magnetic field can give rise to chaotic dynamic behavior in a sodium-filled Fabry-Perot resonator. **(p. 330)**

**11:00 am**
**FB2 Space–time representation of a delayed dynamical system,** F. T. Arecchi, G. Giacomelli, A. Lapucci, R. Meucci, *Italian National Institute of Optics.* A nonlinear system with delayed feedback, whenever the delay time is much longer than the intrinsic correlation time, displays two widely separated time scales. In such a case, a 2-D representation allows use of recognition algorithms developed for spatiotemporal chaos. **(p. 333)**

**11:20 am**
**FB3 Generalized approach to the theory of radiation–atom interaction,** Weihan Tan, *Shanghai Institute of Optics & Fine Mechanics, P.R.C.;* Weiping Lu, Robert G. Harrison, *Heriot-Watt Univ., U.K.* We develop a unified approach to the theory of radiation–atom interaction for arbitrary field strengths in which conventional perturbation and dressed atom theories have been considered. **(p. 336)**

**11:40 am**
**FB4 Neural network applictions to optical chaos,** S. D. Pethel, C. M. Bowden, C. C. Sung, *Redstone Arsenal.* Neural networks trained on chaotic time series are shown to constitute global approximations to the attractors. Data window extension is demonstrated for stationary time series. **(p. 339)**

**12:00 m**
**FB5 Mechanisms of amplification without inversion,** Olga Kocharovskaya, *Russian Academy of Sciences.* We analyze the physical origin of the gain in all schemes of inversionless amplification proposed to date and define two different mechanisms responsible for this process. **(p. 342)**

**12:20 pm**
**FB6 Polarization-sensitive population trapping in an optically pumped laser,** E. Roldan, R. Vilaseca, *Univ. Valencia, Spain;* G. J. de Valcarcel, *Valencia Univ. Politecnica, Spain;* M. Arjona, J. Pujol, *Catalonia Univ. Politecnica, Spain;* R. Corbalan, *Barcelona Univ. Autonoma, Spain.* An optically pumped laser with parallel or orthogonal linear field polarizations is investigated in terms of dressed states. Polarization-dependent inversion without lasing is found. **(p. 343)**

Monday, June 22, 1992

# Dynamics of Pulse Formation

**MA** 8:20am–10:20am
Schroedinger Hall

William J. Firth, *Presider*
*Strathclyde University, United Kingdom*

## Nonlinear Dynamics of Ultrashort Pulse Formation

Speaker to be announced

Summary not available at press time.

# Physical Origin of the Self-Mode-Locking Regime in Solid-State Lasers

Michel Piché
Département de Physique (COPL), Université Laval
Québec, Canada, G1K 7P4
Tel.: (418) 656-2753
FAX: (418) 656-2623

François Salin
Institut d'Optique, CNRS URA14, B.P. 147,
91403 Orsay Cedex, France

During the last two years, it has been found that many solid-state lasers can naturally emit trains of ultrashort laser pulses. This regime of emission, called self-mode-locking, does not require the use of any passive or active modulation element such as loss or phase modulators, saturable absorbers or nonlinear coupled cavities. Indeed, the first report by Spence *et al*[1] indicated that self-mode-locking could be induced by misaligning the resonator. Many similar observations[2-5], combined with simple estimates of the nonlinear phase retardation in the laser material, have indicated that nonlinear transverse effects (self-focussing, self-bending) are playing a key role in the dynamics of pulse formation. In this paper, we describe how the nonlinear lensing effect caused by self-focussing in the laser material produces an effective nonlinear gain when an aperture is properly positioned or gain saturation is taken in account.

The physical mechanism leading to self-mode-locking is the following. When an intense short pulse is amplified in a solid-state gain material, it experiences a phase retardation due to the optical Kerr effect which varies spatially along with the laser beam profile. This nonlinear lensing effect (self-focussing) changes the beam size and divergence at every position in the laser resonator as a function of intensity. Such changes in the beam parameters can be converted into an effective loss modulation using two methods: a) by positioning a hard aperture in the resonator, such that an intense beam suffers lower diffraction losses that a low power (CW) beam; b) by selecting a gain profile such that an intense beam has a better extraction efficiency than a CW beam.

We have made numerical simulations of the evolution of the beam profile in typical Z-type four-mirror laser resonators used for optically pumped solid-state lasers (the resonator included two identical off-axis focussing mirrors and two flat end mirrors in an astigmatism compensated geometry). Our parameters were selected to be appropriate for Ti:Sapphire lasers, which are now used in many laboratories. Our calculations have taken into account diffraction, self-focussing and gain saturation in an active medium pumped by a Gaussian beam; the calculations were made for the tangential and sagittal planes. Two parameters were

identified to evaluate the ability of self-focussing to lead to mode-locking: the change in beam power as a function of nonlinearity (intensity); the residual gain per round-trip experienced by a CW beam once an intense beam has reached steady-state.

Typical results obtained for resonators without any aperture are shown in Fig. 1a and 1b. The output power increases with intensity (or nonlinear parameter $K$) up to a point beyond which it drops rapidly. By adding the contributions along both axes, one can infer a maximum power increase of 8%. Figure 1 also shows that the residual CW gain is negative below a critical power; under such circumstances, the CW beam should be suppressed and self-mode-locking should be stable. This behaviour was reproduced for a broad range of parameters and was maintained as long as the size of the pump beam was below a certain value.

The insertion of a hard aperture at one end of the laser resonator could create conditions favourable to mode-locking (positive differential gain) only if the active (nonlinear) material was displaced towards a focussing mirror, as shown in Fig. 2. This prediction was also observed experimentally. One sees also that the discrimination against the CW oscillations is much larger in presence of an aperture, indicating more stable conditions for mode-locking.

A Gaussian beam model has also been developped and compared with the numerical simulations. Although both models predict the same tendencies, their quantitative predictions may differ, especially when diffraction by hard apertures is taken into account. For instance, the beam size along counterpropagating directions may differ by 30%, as we have experimentally reported in an earlier paper[6]. Other experimental results showing strong beam modifications agree with our calculations.

## References


1. D. E. Spence, P. N. Kean and W. Sibbett, *Opt. Lett.* **16**, 42 (1991).
2. L. Spinelli, B. Couillaud, N. Goldblatt, and D. K. Negus, *CLEO'91 Technical Digest*, post-deadline paper CPDP7.
3. U. Keller, G. W. 'tHooft, W. H. Knox and J. E. Cunningham, *Opt. Lett.* **16**, 1022 (1991).
4. Ch. Spielman, F. Krausz, T. Brabec, E. Wintner and A. J. Schmidt, *Opt. Lett.* **16**, 1180 (1991).
5. G. Gabetta, D. Huang, J. Jacobson, M. Ramaswamy, E. P. Ippen and J. G. Fujimoto, *Opt. Lett.* **16**, 1756 (1991).
6. F. Salin, J. Squier and M. Piché, *Opt. Lett.* **16**, 1674 (1991).

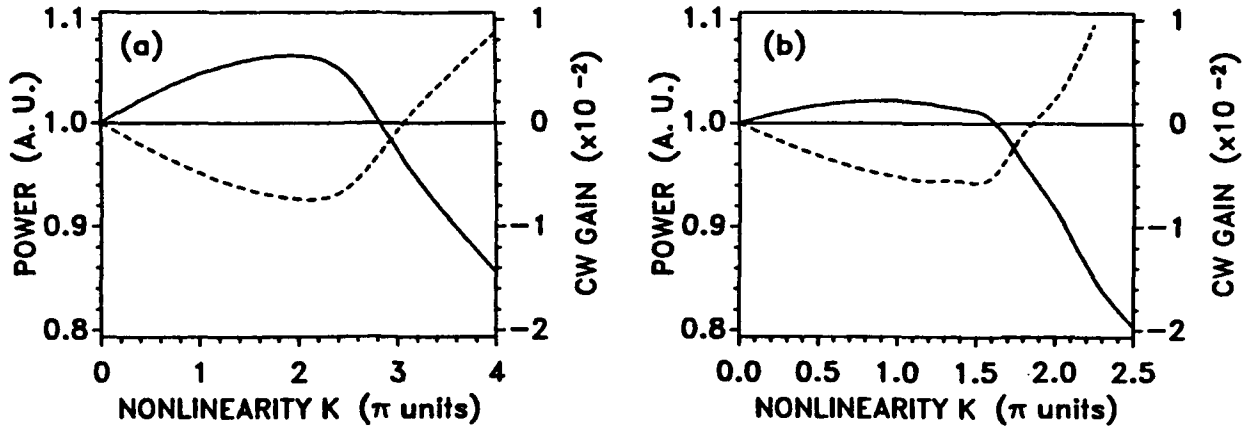


Figure 1. Output power (full curve) and CW residual gain (dashed curve) as a function of nonlinear parameter $K$ : a) sagittal plane; b) tangential plane. One end mirror has a 90% reflectivity; the two focussing mirrors have a focal length of 7.5 cm and are separated by 16.4 cm. The distance from the focussing mirrors to the end mirrors is 75 cm. The gain medium, of index of refraction $n = 1.75$, is 1.5 cm long and pumped by a 30 μm waist Gaussian beam; the single pass power gain is 15% at center at $\lambda = 0.80$ μm.

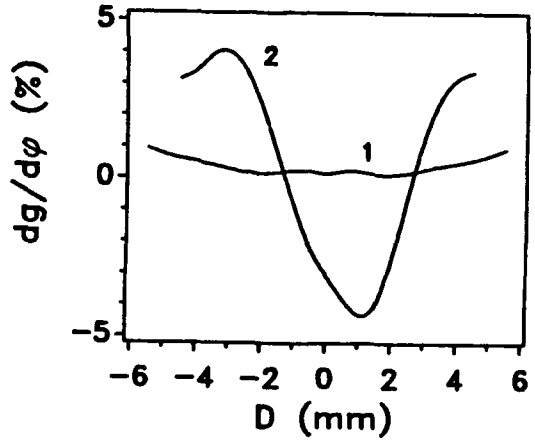


Figure 2. Differential gain per unit of nonlinear phase-shift $dg/d\phi$ when the gain medium is moved from center ($D = 0$) towards a focussing mirror. Curve 1 is obtained without an aperture, and curve 2 with an aperture. The resonator geometry is the same as in Fig. 1. A hard aperture of 2.30 mm full width is placed in the tangential direction. The differential gain is the negative of the CW residual gain.

# Nonlinear Effects in a Ring Resonator

A. M. Dunlop, D. R. Heatley, and W. J. Firth
Department of Physics and Applied Physics
University of Strathclyde
107 Rottenrow, Glasgow G4 ONG
Scotland
Tel. (+) 44 41 552 4400 Ext. 3262
Fax. (+) 44 41 552 2891

There has been much recent interest in using a nonlinear lensing element combined with an aperture to produce a saturable absorber for laser modelocking.[1, 2] This Kerr-lens-modelocking (KLM) technique normally uses the gain medium as the nonlinear element, but lasers with separate gain and nonlinear elements have also been demonstrated,[3] allowing application of this method to lasers in which the gain medium does not provide adequate self-focusing or gain-guiding. The analysis we have carried out seems to indicate that the nonlinear element need not be self-focusing; in fact, it appears that a larger effect can be obtained by a self-defocusing element. Additionally, in the ring resonator geometry we consider, the intensity-dependent lensing leads naturally to unidirectional propagation for continuous-wave lasing.

A suitable cavity (see fig. (1a) consists of an identical pair of thin lenses placed on opposite sides of the ring. Halfway between them on one side is a Gaussian aperture (GA) with transmission $e^{-\gamma r^2}$. We define a normalized lens power to be the separation of the lenses divided by their focal length. The modes of the cavity are found using the ABCD matrix formalism. If lens power is exactly 4, then the beam will focus down through the GA with minimal loss, and focus down again opposite the GA. In this case the counterpropagating modes overlap exactly.

However, choosing a slightly higher lens power causes the beam to focus down at different points for the different propagation directions. The beam waist as it propagates around the cavity is shown in fig. (1b). Ignoring the imperfect mirror reflectivity and linear absorption, the only loss mechanism is the clipping of the Gaussian field profile by the aperture, which in this case has a spot size of 0.36mm.

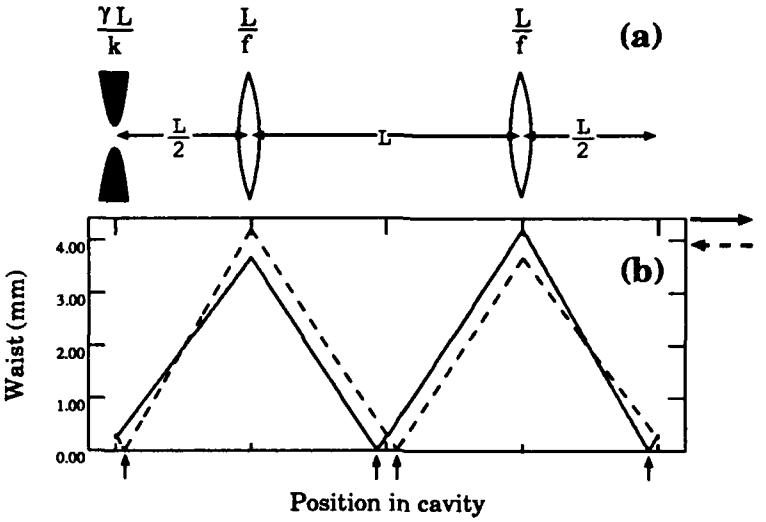


Figure 1: Parameters for linear ring resonator. (a) The Gaussian aperture is characterized by the Fresnel number $\gamma L/k$ (=5.0) and the normalized power of the lenses $L/f$ (=4.02), where $2L$ is the roundtrip distance and $k$ is the wavenumber. (b) The beam waist as a function of position in the cavity. The solid line is for the mode propagating from left to right, the dashed line is for the mode propagating from right to left. Both (a) and (b) share the same horizontal axis.

Adding an intensity-dependent lens (Kerr lens) to the cavity will in general change the loss. Since the nonlinear lensing effect depends on the spot size of the beam as well as its intensity, the power of the nonlinear lens depends on its position within the cavity. Thus the four positions denoted by the arrows in fig. (1b) should yield the largest effects. Clearly the backward and forward propagating beams will have different waists at these points, leading to different changes in the loss due to the nonlinearity.

The relevant quantity from a KLM point of view is the change in loss with respect to the change in the power of the Kerr lens. This quantity is evaluated for a weak lense placed at an arbitrary position within the cavity, for both a slightly "underfocused" cavity (lens power = 3.98) and slightly "overfocused" cavity (lens power = 4.02), as shown in fig. (2). As expected, for the overfocused case, a negative change in the focusing power of the Kerr lens reduces the loss of the cavity. A surprising result is that the magnitude of the curve for the self-defocusing case is roughly four times as large as for the self-focusing case.

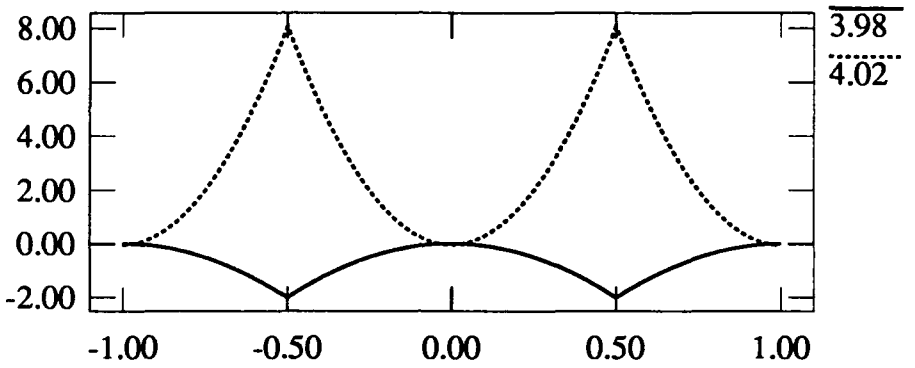


Figure 2: Derivative of the loss with respect to the strength of the Kerr lens, as a function of its position (same horizontal axis as in the previous figure). The top curve is for a underfocused cavity, the bottom is for an overfocused cavity.

# References

[1] François Salin, Jeff Squier, and Michel Piché. Mode locking of Ti:$Al_2O_3$ lasers and self-focusing: a Gaussian approximation. *Opt. Lett.*, 16(21):1674–6, November 1991.

[2] Michel Piché. Beam reshaping and self-mode-locking in nonlinear laser resonators. *Opt. Comm.*, 86(2):156–60, November 1991.

[3] G. P. A. Malcolm and A. I. Ferguson. Self-mode-locking of a diode-pumped Nd:YLF laser. *Opt. Lett.*, 16(24), December 1991.

# Dynamics of Nonlinearly Coupled Modelocked Laser Arrays

Song Wu, Sandra L. Smith, and Richard L. Fork

Rensselaer Polytechnic Institute
Troy, NY 12180
(518) 276-2949

We have used experiments and calculations to explore the dynamics of two nonlinearly coupled modelocked lasers. A special feature of this study is the presence of two distinct adjustable nonlinear mechanisms, where one mechanism causes an attraction of the pulses in the two separate lasers and the other causes a repulsion of the pulses. We find that adjustment of the relative importance of these attractive and repulsive mechanisms, as well as of the relative cavity length, provides a rich variety of dynamical behavior that is not available in alternative laser systems.

The mechanisms that produce this coupling are related to the mechanisms that produce solitons within the modelocked laser. In the operating regime where the shortest pulses are produced the pulses themselves are technically solitons so that we can explore interaction of solitons within the laser structure where the mediating mechanisms are novel and distinct from those that cause interaction of solitons in alternative media, such as optical fibers. The interaction of the pulses themselves in the nonlinear medium is a multiwave mixing effect that permits spatial redirection of the pulses. This furnishes a further capability for influencing the pulse array in the coupled lasers that we intend to, but have not yet, explored.

One motivation for this work is the creation of a capability for producing and rapidly reconfiguring arrays of ultrashort pulses of electromagnetic radiation. The presence of the adjustable attractive and repulsive interactions combined with the capacity to make small alterations in the resonator lengths allows us to obtain pulse synchronization, pulse duration switching, a latching type of amplitude bistability and, in some cases, phase locking of the carrier fields of the pulses.

Stable operation in a given mode of operation can be achieved for extended periods of time. The nonlinear mechanisms can be adjusted to override to some extent the consequence of variations in resonator lengths as a means of reducing the sensitivity of the system to unintentional variations in resonator length. On the other hand the lasers can also be adjusted to be sensitive to small externally introduced optical

perturbations so as to provide a means for the laser system to serve as a sensor of spatially and temporally distributed optical radiation. Similarly, the state of the laser system can be quickly switched to an alternative state by small deliberately introduced perturbations of the laser parameters.

Desirable features of this system are sufficient complexity to explore a variety of nonlinear optical dynamics, adjustable control, well defined high reproducible laser behavior, and generation of arrays of optical pulses that can be shorter than 100 femtoseconds. The capabilities are achieved through the use of a common saturable absorber that produces an attraction of the pulses via the shared bleaching of the absorber and a Kerr lens deflection mechanism that produces, in effect, a repulsion of the pulses in time.

While the initial system has been configured in dye laser media and is limited to two lasers, calculations indicate that this strategy can be extended to solid state lasers and to more complex arrays of modelocked lasers. We are currently exploring these advances and may have additional findings to report at the time of the meeting. The nonlinear interactions in Ti:sapphire, e.g., are highly suitable to producing similar behavior in Ti:sapphire lasers. The advantage of that system is the stability of the solid state material and the large induced refractive index changes.

We are currently exploring means for enhancing the flexibility and speed with which the ultrashort pulse array can be reconfigured by introducing computer controlled phase delays within the laser resonator. Novel electro-optic media, such as DAST, offer large electrically induced phase shifts that can be used to provide adjustable control of the resonator lengths in a computer controlled manner.

The properties of the initial system used to develop this technology are described by Wu, Smith, and Fork in Optics Letters 17 , 276 (1992).

# Fast and slow self-phase modulation induced pulse shaping of subpicosecond pulses in semiconductor laser amplifiers

A. Dienes, M. Y. Hong and J. P. Heritage
Department of Electrical and Computer Engineering
University of California
Davis, CA 95616 (916) 752-0583

Self- and cross-phase modulation (SPM, XPM) of picosecond pulses due to gain saturation in semiconductor laser amplifiers has been investigated, both theoretically and experimentally.[1,2,3] Because of the large value of the so-called linewidth enhancement factor $\alpha$, these effects can result in considerable nonlinear sweep and spectral broadening. The spectrally broadened pulses can be partially compressed[1,2] by providing dispersion externally. It has also been shown[3] that the quadratic shape of the gain spectrum can result in considerable positive second-order phase dispersion. For pulse durations of about 1 ps or shorter (and input energies in the 0.1-1 pJ range) the fast $n_2$ must also be considered. The gain saturation induced "slow" self phase modulation (SSPM) is an integrating, energy dependent effect. On the other hand, the fast $n_2$ responds to the instantaneous intensity of the pulse, resulting in "fast" self phase modulation (FSPM). The interplay of saturation, two kinds of SPM and dispersion will result in complicated pulse shaping. In this paper, we investigate the evolution of subpicosecond pulses in semiconductor amplifiers using a differential equation similar to one used for studying saturated dye laser amplifiers.[4] Under certain conditions, soliton-like compression effects are predicted.

The nonlinear differential equation is

$$\left[\frac{\partial}{\partial z} + i\beta'' \frac{\partial^2}{\partial \tau^2}\right] V = \left[\frac{1}{2}(1-i\alpha)\, g(\tau) - ib_2 |V|^2\right] V . \tag{1}$$

Here, $V$ is the complex amplitude of a pulse of power $P$, $\tau$ is local time, $\beta''$ the group velocity dispersion, and $b_2 = n_2\omega_o/cA$ with $A$ the effective area and $n_2$ the fast nonlinear index in cm$^2$/watt. $g(\tau)$ is the exponential gain governed by the equation

$$\frac{\partial g(\tau)}{\partial \tau} = \frac{g_o - g(\tau)}{\tau_1} - \frac{g(\tau)P(\tau)}{W_s} \tag{2}$$

where $W_s = A\hbar\omega_o/\sigma_e$ is the saturation energy ($\sigma_e$ is the emission cross section taken as constant over the spectrum) and $\tau_1$ is the gain recovery time, the same here as the carrier decay time. For pulses much shorter than $\tau_1$, (2) has the solution $g(\tau) = g_o \exp[-W(\tau)/W_s]$ where $W(\tau) = \int_{-\infty}^{\tau} P(t')\, dt'$.

We note that the above equation results from a considerably simplified model of the very complex effects that occur in semiconductor amplifiers in the subpicosecond domain. In particular, since dispersion in large part results from the gain,[3] it in itself is subject to saturation. Additionally, recent experiments[5,6] have shown the existence of one or more fast lifetimes, on the order of ~500 fs, in the gain dynamics of such media. These fast lifetimes, attributed to relaxation of dynamic heating effects, have been shown to lead to pulse width dependent gain saturation.[7] Their effect on SPM has not yet been studied. The origin and nature of the fast $n_2$ has also not been fully investigated. It is known that above the band-edge it is increasingly large and negative. A value as high as $-4\times10^{-12}$ watts/cm$^2$ has been measured in unpumped AlGaAs[8] and at least in part attributed to the optical Stark effect, which is instantaneous. Recently, a moderately fast negative $n_2$ of even larger magnitude has been identified in InGaAsP lasers.[9] This $n_2$, of response

time of around 0.5-1.0 ps, may be related to the dynamic heating relaxation observed in refs. 5, 6. Thus, it is obvious that, for pulse durations in the ~50 fs to ~1 ps range, the above model is not complete. Nevertheless, we feel that much can be learned from solutions of this equation regarding the interplay of the various nonlinear effects and their relative importance for pulse evolution. Additionally, it is possible that in the ~0.5-2 ps pulse length range it can serve as a reasonably realistic model. Importantly, we note that because $n_2$ is negative and dispersion is relatively large and positive, soliton-like shaping may take place.

The nonlinear equation given above can only be solved numerically. We used the split-step Fourier method to arrive at solutions for the complex amplitude and spectrum. Due to the complicated interplay of the various amplitude and phase shaping effects a large range of parameters must be used. For lack of space, here we only summarize some of the more interesting trends and present two specific results. As shown in Figure 1a, soliton-like pulse shortening is calculated for typical energies of around a fraction of picojoule, input pulse widths of around 1 ps, and linear gain of about 30 dB. Pulse compression by as much as 8 times was found. Figure 1b was calculated by setting $\alpha = 0$. It illustrates the significant role that SSPM plays in producing a large time shift and in reducing uncompressable energy. Another interesting observation is that for a given set of semiconductor amplifier parameters the onset of compression is rather critically dependent on the input pulse parameters. This is illustrated in Figure 2 which shows a 500 fs pulse broadening, but a 1 ps pulse of the same 0.2 pJ energy compressing. This behavior is rather unexpected. More easily understood is the gradual disappearance of the compression as the pulse width is further increased (not shown). This latter trend is attributable to diminishing FSPM. The SSPM, which does not depend on pulse width, cannot alone give compression. We also find that as the input pulse energy is increased, the range of pulse widths over which compression occurs increases. For around 1 pJ input energy, it readily occurs for a large range of pulse durations.

It is not easy to give a simple explanation of the results shown in Figure 2. We are dealing here with dispersion, plus three nonlinear effects sensitive to pulse shape. These four interact in a complex way to alter the pulse shape. In this complex interplay, once compression starts on the major part of the pulse due to a "right" combination of chirp, it can continue to develop and even intensify. However, the opposite effect can also happen.

In conclusion, using a simple model, we theoretically investigated ultrashort pulse evolution in semiconductor laser amplifiers and found some interesting and unexpected trends in soliton-like compression.

## References


1. G. P. Agrawal and N. A. Olsson, *Optics Lett.* **14**, 500 (1989).
2. S. Dijaili et al., *IEEE J. Quantum Electr.* **28**, 141 (1992).
3. G. P. Agrawal, *IEEE J. Quantum Electr.* **27**, 1843 (1991).
4. A. Dienes, L. W. Carr, and M. Y. Hong, *IEEE J. Quantum Electr.* **27**, 1214 (1991).
5. M. S. Stix, M. P. Kesler, and E. P. Ippen, *Appl. Phys. Lett.* **48**, 1722 (1986).
6. K. L. Hall, J. Mark, E. P. Ippen and G. Eisenstein, *Appl. Phys. Lett.* **56**, 1740 (1990).
7. Y. Lai, K. L. Hall, E. P. Ippen and G. Eisenstein, *IEEE Photon. Tech. Lett.* **2**, 711 (1990).
8. M. J. LaGasse et al., *Appl. Phys. Lett.* **56**, 417 (1990).
9. R. S. Grant and W. Sibbett, *Appl. Phys. Lett.* **58**, 1119 (1991).


## Figure Captions

Figure 1. Output pulse shape for amplifier with common parameters $G_o = 30$ dB, $L = 300$ $\mu$m, $W_s = 5$ pJ, $A = 1$ $\mu m^2$, $\beta'' = 18$ $ps^2/cm$, $n_2 = -6 \times 10^{-12}$ $cm^2/w$.

Figure 2. Output pulse shape for amplifier with the same parameters as in Fig. 1, and different input pulses; dashed lines are the input pulses.

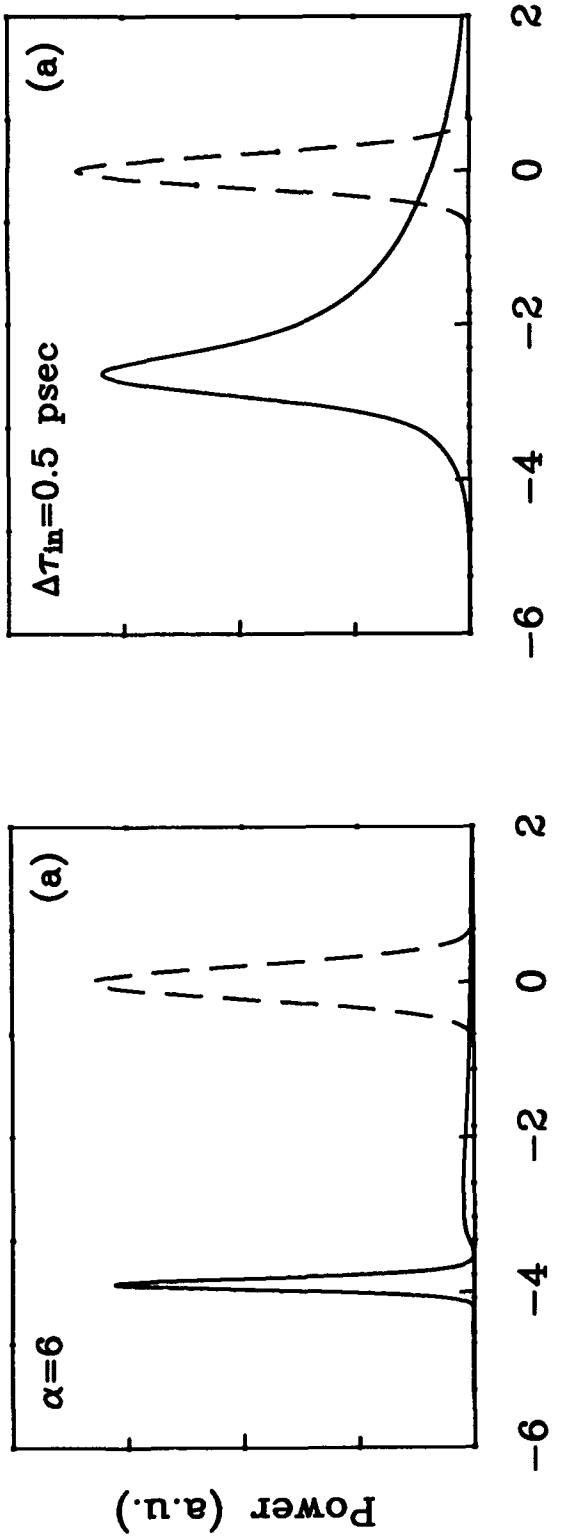


Figure 1




Figure 2

# OPTICAL PULSE EVOLUTION IN FIBRE LASER ADDITIVE PULSE MODELOCKING

K.A.Shore

Bath University,School Electronic and Electrical Engineering
BATH , BA2 7AY , UK

TEL + 44 225 826272

T.Geisler

Technical University of Denmark,Institute of Fundamental
Metrology , DK 2800 Lyngby ,Denmark

M.P.Sorenson and P.L.Christiansen

Technical University of Denmark,Laboratory of Applied
Mathematical Physics,DK 2800 Lyngby ,Denmark

J. Mork and J.Mark

TFL,Lyngso Alle 2,DK-2970,Horsholm,Denmark

## Introduction

The large optical gain bandwidth available in optical fibre amplifiers holds the prospect of optical pulse production of the order of 100 fs . In the present paper it is wished to report on a theoretical study of the utilisation of a fibre amplifier coupled to a nonlinear fibre external cavity configured to permit interferometric additive pulse modelocking (APM).

## Model

The model developed in this work is of rather general application and , for example , includes as a special case a description of pulse effects in fibre laser amplifiers . The model utilises numerical techniques for solving the nonlinear Schroedinger equation appropriate to both the active gain medium of the fibre laser and the passive external cavity nonlinear fibre [1]. Account is taken of bandwidth limited gain in the fibre amplifier and allowance is made for both the anomalous and the normal regimes of dispersion in both fibres . Fine-tuning of the passive cavity length to achieve APM is effected via a phase bias parameter . Coupling losses between the laser and external fibre cavities may also be included in the simulation . Typical parameter values appropriate to erbium-doped fibre amplifiers have been utilised.

## Results

In Figure 1 , optical pulse compression as a function of the number , n , of cavity round trips is shown . The final pulse width is about 230 fs and is thus not limited by the fibre gain bandwidth . The critical role played by the phase bias in achieving APM in this configuration is illustrated in Figure 2 . Similarly,the influence of fibre dispersion in determining the dynamical evolution of the optical pulse is indicated in Figure 3 .

It is shown in this work that a variety of pulse phenomena may arise in the all-fibre coupled cavity configuration depending upon the operating conditions of the fibre laser. The anticipated pulse narrowing is seen but pulse break-up may also occur. The presentation will attempt to categorise these phenomena in accordance with accessible practical control parameters of the device.

References

[1] T.Geisler,P.L.Christiansen,J.Mork and P.S.Ramanujam
J.Comp.Phys.,86,492,1990

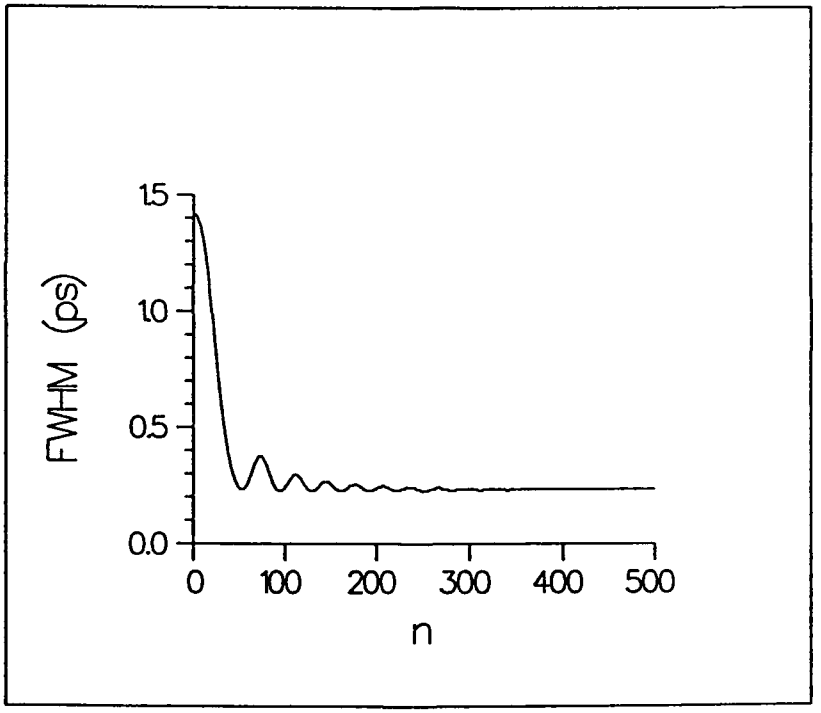


Figure 1

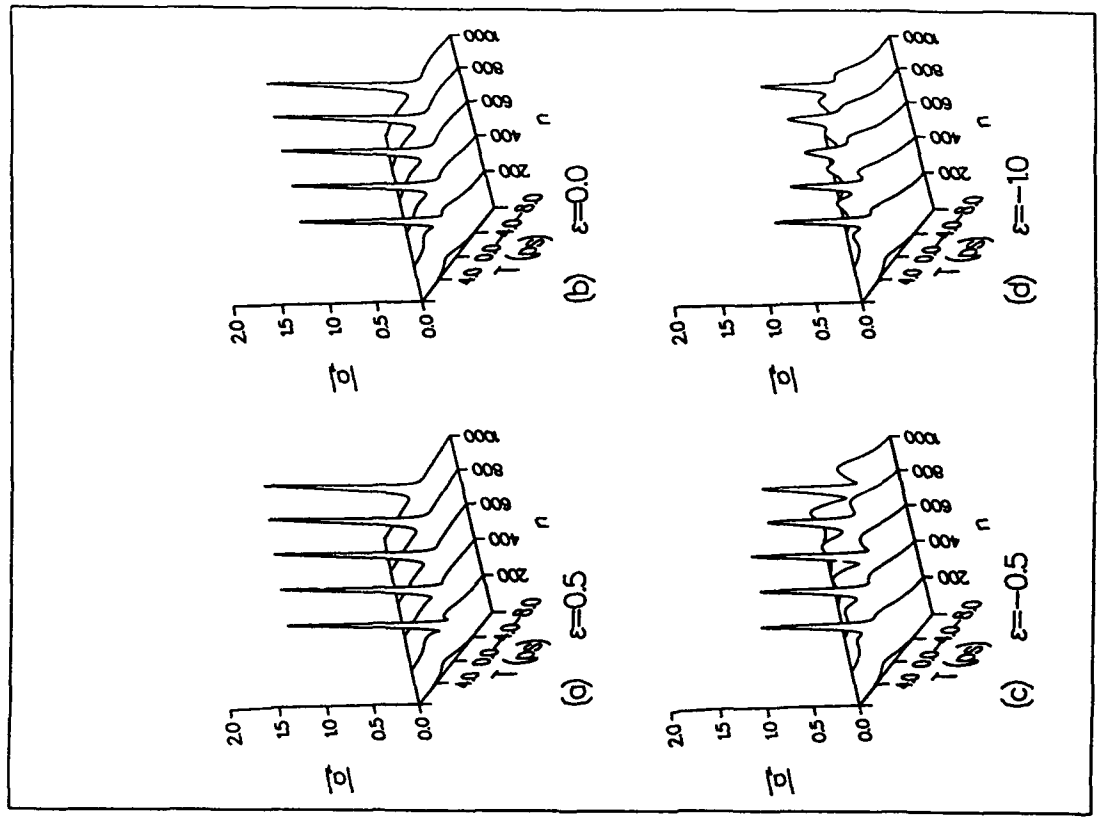


Figure 3

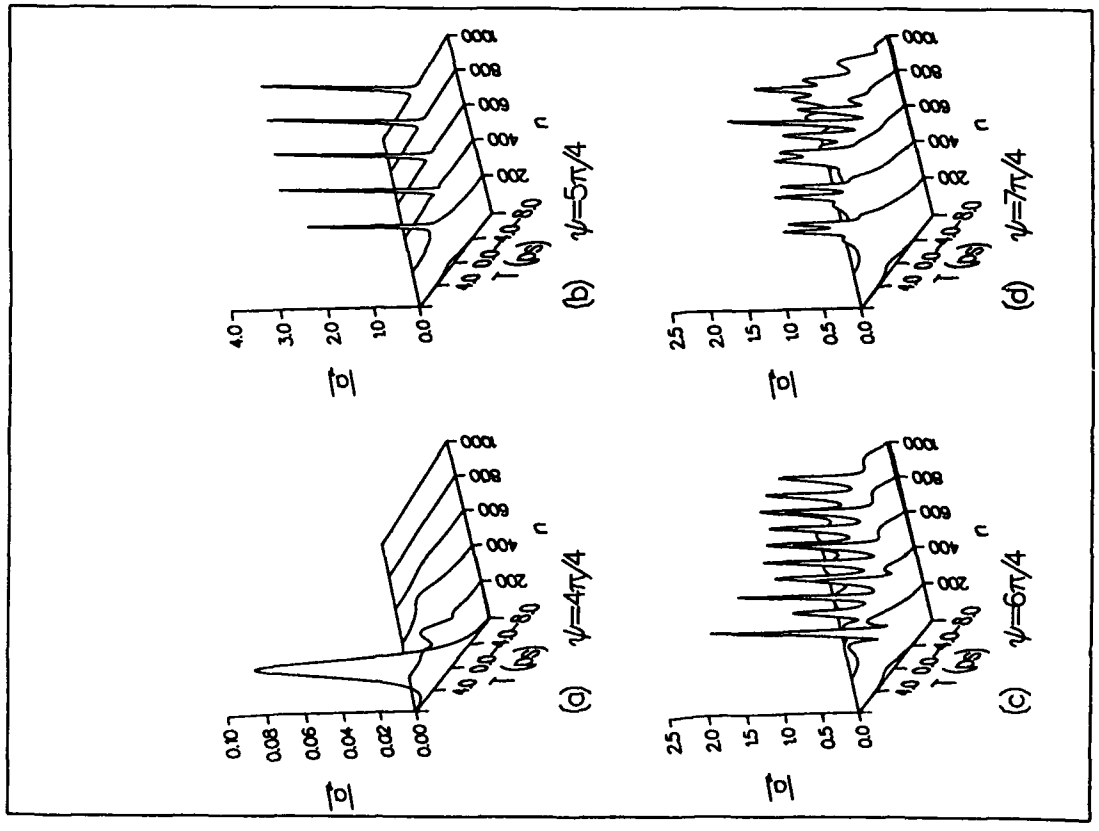


Figure 2

Monday, June 22, 1992

# Laser Instabilities

**MB** 11:00am–1:20pm
Schroedinger Hall

Yakov I. Khanin, *Presider*
*Russian Academy of Sciences, Russian Federation*

# Time inverted type-I intermittency of a single mode laser

D. Y. Tang and C. O. Weiss

Physikalisch-Technische Bundesanstalt,
W-3300 Braunschweig, Germany

Among the three well-known routes to chaos in nonlinear dissipative dynamical systems, onset of chaos via intermittency has been extensively studied. Different types of intermittency have been revealed experimentally /1-3/. Recently intermittent transition to chaos through type-II and type-III intermittency have also been observed in optical systems /4,5/. To our knowledge, however, type-I intermittency has not been observed in optical systems so far.

In this paper we report the experimental observation of type-I intermittency on an optically pumped single mode laser. We show that the observed dynamics is time inverted in comparison with the usual description of type-I intermittency /6/.

The experimental setup used is an optically pumped single mode $NH_3$ FIR ring laser. It operates at the 81 $\mu$m wave length and is pumped by a $N_2O$ laser. Single mode and unidirectional operation of this laser was achieved by tuning the pump laser frequency from the resonance. For the measurement the backward emission of the laser was detected and the resonator detuning was used as control parameter. Details of the experimental setup see /7/.

A typical dynamics observed at the gas pressure of 35 $\mu$bar and pump intensity of 3 W/cm2 is shown in Fig. 1. At larger resonator detuning, the laser pulses periodically, as the resonator detuning decreases to a critical point, this periodic pulsing begins to be interrupted intermittently by irregular pulses as shown in Fig. 1a, decreasing the resonator detuning further, these interruptions become more frequent and consequently the regular pulsing periods (laminar phase) of the laser become short, as to be expected for an intermittent route to chaos.

This kind of intermittency exists only in a small range of resonator detuning and the whole process described occurs at resonator detuning larger than the one for which the period-doubling route to chaos exists.

By analyzing the experimental data time-inverted, we find this kind of dynamics can be good described by the theory of type-I intermittency. First we have compared the first return map of the observed dynamics to that predicted from the type-I intermittency. Fig. 2 shows one of the typical results.

Another characterization of type-I intermittency is by the distribution of the laminar lengths. Different from the laminar length distribution of type-II and type-III intermittency, whose laminar length distribution is exponentially falling towards long lengths, the laminar length distribution of type-I intermittency shows a maximum for long lengths. This difference permits even without knowledge of the reinjection process to distinguish between type-I intermittency and the other two types of intermittency. We have calculated from the experimental data this laminar length distribution. From Fig. 3 the maximum of the distribution at pulse number 8 clearly identifies that it belongs to type-I intermittency.

We have also calculated from the experimental data the scaling law of the observed intermittency. A relation between the average laminar length <N> and the control parameter $\varepsilon$ with

$$<N> \propto \varepsilon^{-0.6}$$

was founded, which is close to the one as expected for type-I intermittency /6/.

References:

1. Y. Pomeau and P. Manneville,
   Physica 1D, 219(1980).
   Y. Pomeau, J. C. Roux, A. Rossi, S. Bachelart,
   and C. Vidal,
   J. Physique Lett. 42, L- 271(1981).
2. J. Y. Huang and J. J. Kim,
   Phys. Rev. A. 26, 2117(1982).
3. M. Dubois, M. A. Rubio, and P. Berge,
   Phys. Rev. Lett. 51, 1446(1983).
4. J. Sacher, W. Elsässer, and E. O. Göbel,
   Phys. Rev. Lett. 63, 2224(1989).
5. D. Y. Tang, J. Pujol, and C. O. Weiss,
   Phys. Rev. A. 44, R35(1991).
6. P. Berge, Y. Pomeau, and C. Vidal,
   Order Within Chaos (Wiley, New York,1984).
7. C. O. Weiss, W. Klische, P. S. Ering, and M. Cooper,
   Opt. Commun. 52, 405(1985).

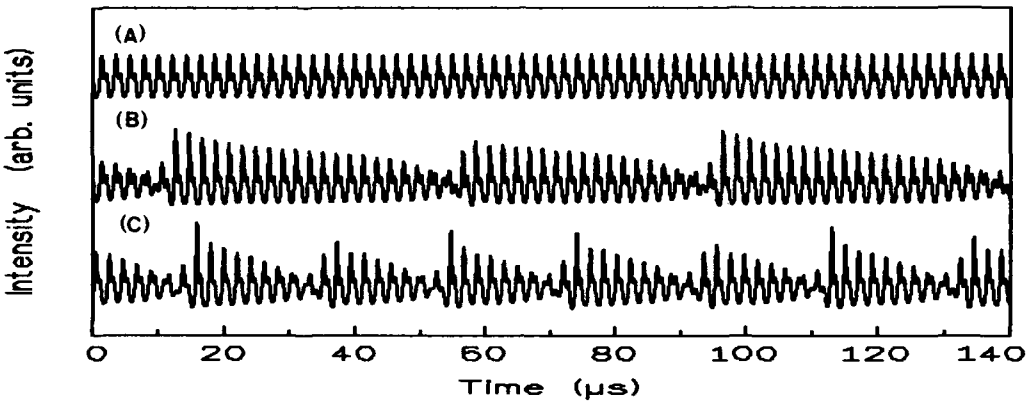


Fig. 1. Time dependence of the laser emission as the resonator detuning is changed. From (a) to (c) the resonator detuning is decreased.

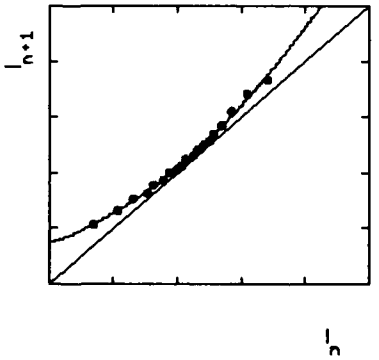


Fig. 2. Return map $I_{n+1}=f(I_n)$ constructed from the experimental data.

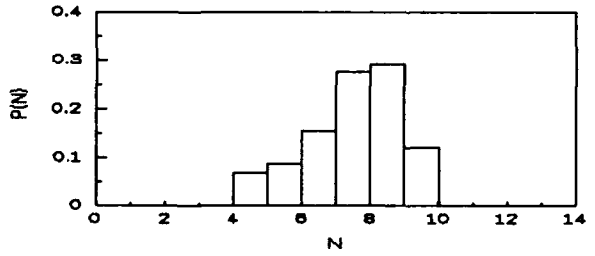


Fig. 3. Histogram of the laminar lengths calculated from the intermittent state shown in Fig. 1c.

# Instability and Chaos in Laser Oscillation between Highly Excited Molecular Vibrational States

Feng-Lei Hong[1)], Maki Tachikawa, Toshiki Sugawara, Takehisa Tohei and Tadao Shimizu

Department of Physics, Faculty of Science, The University of Tokyo
7-3-1 Hongo, Bunkyo-ku, Tokyo-113, Japan
Tel. +81-3-3812-2111, ext. 4169
Fax. +81-3-5684-5291
1) Present address: RIKEN, The Institute of Physical and Chemical Research, Wako, Saitama 351-01, Japan

**SUMMARY:** Dynamic behavior of the laser oscillation has been extensively studied as a paradigm of nonlinear dynamics. Mechanism of laser instability is strongly correlated with detailed relaxation and excitation dynamics in the laser medium. Study of laser instability may open a way to precise measurement of those elementary atomic and molecular processes.

A laser with a saturable absorber (LSA) shows passive Q-switching (PQS) pulsations in the output. PQS instabilities have been extensively investigated in regular-band oscillations in $CO_2$ and $N_2O$ lasers [1-5], and found to be influenced by the relaxation processes of the laser levels [3].

In this paper, we report the first observation of periodic and chaotic PQS instabilities in $CO_2$ hot-band and sequence-band lasers which oscillate among higher vibrational levels than that of the regular-band. We propose a novel rate-equation model to comprehensively describe the PQS instability in the regular, hot, and sequence bands. The three-level:two-level model [3], successfully applied to the regular-band PQS, is extended by introducing the vibration-to-vibration (V-V) resonant energy transfer processes relating to the higher vibrational levels. The rate-equation analysis on the model clarifies the effects of the V-V processes on the temporal structure of the PQS dynamics.

Rate constants of the V-V processes is determined from the analysis of the PQS instability. Figure 1(a) shows a periodic PQS pulse shape observed on the hot-band transition between the $(01^11)$ and $(11^10)$ vibrational states. Note that undamped relaxation oscillation appears in the ending part of the pulse. On the other hand, in the regular-band

oscillation, the relaxation oscillation is superposed on the entire part of the quasi-cw tail, being similar to the pulse shape in Fig. 1(b). Figures 1(b)-1(d) show the calculated PQS pulse shapes on the hot-band transition as a function of the rate constant $K_1$ of the V-V process:

$$CO_2(01^11) + CO_2(00^00) \longleftrightarrow CO_2(00^01) + CO_2(01^10).$$

This population transfer from the lower laser level causes the relaxation oscillation on the pulse tail. When $K_1$ is sufficiently large, the pulse shape approaches those observed in the regular band [Fig. 1(b)]. The pulse in Fig. 1(c) agrees well with the experimentally observed pulse. At considerably small $K_1$, additional relaxation oscillation occurs just after the first peak [see Fig. 1(d)]. The phase portraits in Figs. 2(a) and 2(b) clearly show the difference in the PQS dynamics between the cases of Figs. 1(b) and 1(d). The trajectory visits two saddle focuses associated with the relaxation oscillations when $K_1$ is relatively small. On the other hand, there exists only one saddle focus at larger $K_1$. The rate constant $K_1$ is

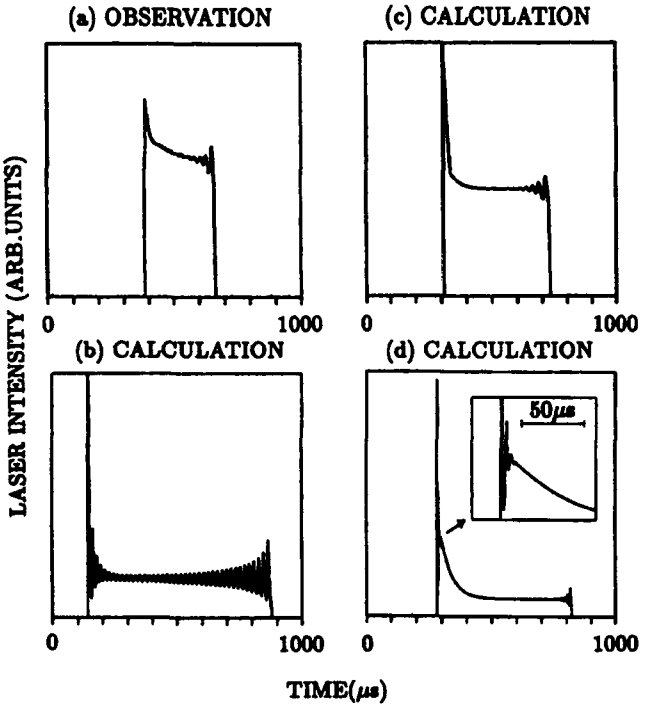


Fig. 1 (a) PQS pulse shape observed in the $CO_2$ hot-band oscillation with a $CCl_2F_2$ absorber. (b)-(d) PQS pulse shapes in the hot-band oscillation calculated as a function of $K_1$; (b) $K_1$ = 3.6 MHz/Torr, (c) $K_1$ = 0.65 MHz/Torr, and (d) $K_1$ = 0.092 MHz/Torr.

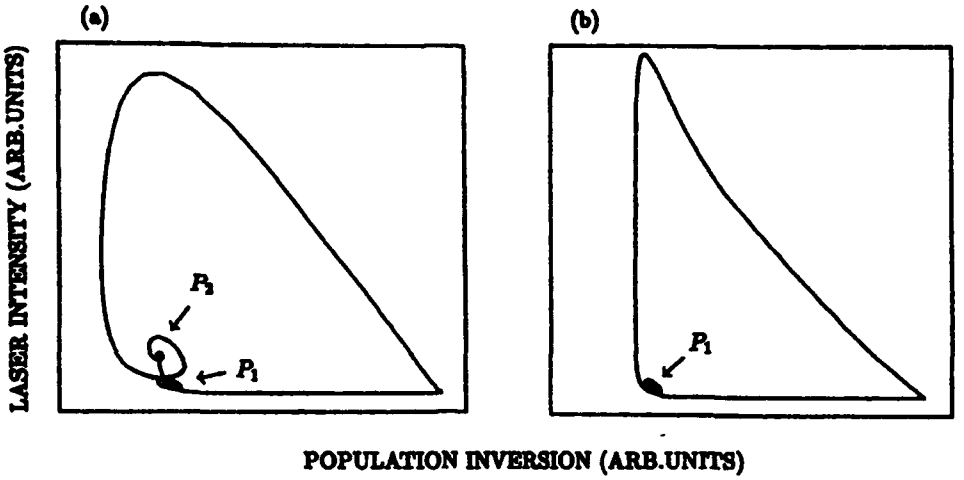


Fig. 2 Portraits of the trajectory calculated in the phase space for the population inversion and the laser intensity. The trajectories in (a) and (b) respectively correspond to the periodic PQS pulsations of Figs. 1(d) and 1(b).

accurately determined from the one-to-one correspondences between experiment and theory. In the sequence-band oscillation between the $(00^02)$ and $(10^01)$ states, the rate constant of V-V process concerning the pumping of the upper laser level is also estimated through the analysis of PQS pulsation.

The Lorenz plot of the hot- and sequence-band chaos are both one-dimensional unimodal curves as well as in the case of the regular-band chaos. This implies that the strange attractor of the chaotic pulsation in any band has a simple geometrical structure. However, detailed analysis reveals that the curvature of the Lorenz plot in the sequence band is appreciably different from those of the regular and the hot bands. This is reproduced quantitatively through the numerical calculation using the proposed model. The V-V energy exchange in the $\nu_3$ mode is found to critically distort the strange attractor. The present analysis suggests even chaos can be used as a method to study molecular processes.

REFERENCES

[1] E. Arimondo et al.: Appl. Phys. B **30**, 57 (1983).

[2] P. Glorieux et al.: IEEE J. Quantum Electron. **QE-21**, 1468 (1985).

[3] M. Tachikawa et al.: J. Opt. Soc. B **4**, 387 (1987).

[4] M. Tachikawa et al.: Phys. Rev. Lett. **60**, 2266 (1988).

[5] F.-L. Hong et al.: J. Opt. Soc. B **5**, 2315 (1988)

# MODULATION DYNAMICS OF A TWO-MODE LASER

Paul Mandel and M. Georgiou

Université Libre de Bruxelles, Campus Plaine, C.P. 231

B-1050 Bruxelles, Belgium; tel +32-2-650 5819.

Kenju Otsuka

NTT Basic Resaerch Laboratory, Musashino-shi, Tokyo 180, Japan

We present new results on the dynamics of solid-state lasers with a few number of modes. Organized collective behavior has been observed in various nonlinear optical systems, suggesting some generic behavior of periodic solutions in multimode lasers [1 - 5]. For instance, antiphase modulation of an N-mode laser is a *self-organized collective behavior* in which each mode is characterized by N relaxation frequencies $\omega_1 < \omega_2 < \omega_3 \ldots < \omega_N$ , while the total frequency oscillates only at $\omega_N$. We have obtained analytic expressions for these frequencies in the N-mode case and we have determined the domain of parameters in which antiphase modulation occurs. In the case of a two-mode laser and near the lasing threshold for the second mode, the two frequencies verify the scaling laws:

$$\omega_L \propto \sqrt{\frac{w - w_2}{T_c T_1}}, \quad \omega_R \propto \sqrt{\frac{w - 1}{T_c T_1}}.$$

where $T_c = 1/\kappa$ is the photon life-time (assumed to be identical for the two modes), $T_1 = 1/\gamma_{\parallel}$ the population inversion life-time, w the dimensionless pump parameter scaled to the laser first threshold and $w_2$ is the scaled threshold of oscillation of the second mode. Since $w_2 > 1$, we also have $\omega_L < \omega_R$. These scalings have been verified experimentally using an optical fibre laser and a solid-state laser. The

physical origin of these antiphase domains can be traced back to the occurrence of cross-saturation. In a Fabry-Perot configuration with standing waves, the cross-saturation coefficients are pump-dependent corresponding to the fact that the spatial hole depth varies with pumping.

Another way to approach the dynamics of the two-mode laser is by considering its response to periodic modulation of the gain parameter $w = w_0[1 + m \cos(\omega_m t)]$. In the case of deep modulation (i.e., when the modulation brings the laser below the first threshold during part of a cycle), a rich bifurcation diagram has been found when the external frequency is in the vicinity of either $\omega_L$ or $\omega_R$. In particular, when the external frequency is in the vicinity of $\omega_R$, there is a coexistence between a Feigenbaum sequence (with its associated chaotic domain) and a stable limit cycle associated with the low frequency resonance $\omega_L$.

References

1 K.Kubodera, K.Otsuka and S.Miyazawa, *Applied Optics* **18** (1979) 884.

2 K.Wiesenfeld, C.Bracikowski, G.James and R.Roy, *Phys.Rev.Lett.* **65** (1990) 1749.

3 K.Otsuka, *Phys.Rev.Lett.* **67** (1991) 1090.

4 C.Bracikowski and R.Roy, *Phys.Rev.* **A43** (1991) 6455.

5 K.Otsuka, P.Mandel, S.Bielawski,D.Derozier and P.Glorieux "New time scale in multimode lasers" (preprint, 1991).

# DIVERSITY Of CHAOS IN MULTIMODE SOLID-STATE LASERS

E. A. Viktorov, A. A. Mak,
O. A. Orlov, V. I. Ustyugov, I. B. Vitrishchak

S. I. Vavilov State Optical Institute
St. Petersburg, 199034, Russia
Phone & FAX: (812) 2185734

Multimode solid-state lasers display deterministic chaos in individual mode intensities (total intensity nearly constant) at free-running generation, and in total output power at intracavity second harmonic generation (ISHG). ("green problem")[1]. The goal of our investigation is comprehensive study for both these cases of lasing.

The equations that govern the dynamics of the multimode lasing were received in semiclassical approach in the frame of third-order theory for homogeneously-broadened-line solid-state lasers (as for class B lasers in general) with spatial hole burning, combination mode coupling (CMC) (four-wave mixing) and nonlinear conversion into second harmonic (SH).

We assume that multimode radiation spectrum is quasiequidistant sequence of frequencies, i.e. nonequidistant mode structure is possible. The possible reasons of the frequency nonequidistancy may be as following: (1) Frequency dispersion of active medium and other intracavity elements. (2) Mode pulling due to frequency selection by intracavity elements. Such selection may be caused for example by: (a) intracavity reflections or scattering (the effect of complex cavity or weak etalon); (b) polarization selector like Lio filter (due to birefringence and polarizer inside a cavity).

Numerical simulation of this model showed that the frequency nonequidistancy of axial-mode spectrum leads to saddle-node (or subcritical Hopf) bifurcation and limit cycle formation with periodical oscillations of individual modes. One can note two features of these periodical oscillations: (1) their spectrum range lays in a region from 10 to 1000 Hz (out of relaxation oscillation frequency region); (2) oscillations have an antiphase characters. The total intensity remains nearly constant. This feature is very important for dynamics analysis in the case of greater number of modes because of the possibility of multistability of solutions called "crowding attractors" situation[3]. Such situation produces special sensitivity of a laser to external

noise sources. So, the chaotic behavior set a dominant due to crowding attractors when the number of lasing modes arises. We have observed the chaos, "metastable" chaotic behavior and a hysteretic phenomena both in the numerical simulation and experiments.

Dynamics of the multimode ISHG have been studied in the frame of similar model. The intracavity SHG is taken into account by the terms that describe additional nonlinear losses. Frequencies that form SH radiation spectrum are the result of summing and doubling of fundamental radiation frequencies. If this spectrum contains N equidistant located frequencies then corresponding SH spectrum will contain 2N-1 frequencies. Quasiequidistant mode sequence of fundamental radiation leads to more complicated set of frequencies in SH range. The total number of spectral components in SH radiation in this case is defined not only by the number of modes but also by the structure of the fundamental laser spectrum. It was shown in the balance treatment of "green problem" that the result of nonlinear conversion mechanism is a breaking of steady-states stability through supercritical Hopf bifurcation and arising of pulsation near relaxation oscillation frequency[2].

As it was mentioned above (for free-running generation) mode-spectrum nonequidistancy leads to saddle-node bifurcation. However, for intracavity SHG the combination of two types of coupling takes place: CMC and mode-mode interaction due to SHG. This provides the situation for which bifurcation point arises not as a result of saddle and sink, but as a result of saddle and focus coalescence. New bifurcation point can be of different types: saddle-focus (at which homoclinic orbit makes tangency - Shil'nikov chaos) or a pure imaginary pair and a simple zero eigenvalue, for example. The dynamics phenomena in cases of points mentioned above has been studied in details. Let us turn to the case of a pure imaginary pair and a simple zero eigenvalue. As it was shown in Ref.4 the possible result of similar situation is a doubly periodic flow on the torus which contains one "fast" frequency (relaxation oscillation frequency in our case) and a slow frequency associated with the secondary Hopf bifurcation. Consequently we can expect to see a rapid oscillation with a slow modulation as well as transverse homoclinic orbits and horseshoes (before homoclinic chaos torus must break-up). Our numerical simulations showed that the treatment model contains rapid processes (due to

intracavity SHG) as well as slow ones. We have demonstrated by consecutive unifying of two types of coupling that solution quasiperiodicity breaks up with strange attractor formation. In the analysis of the process of torus destruction we note intermittency of a second-type (caused by irregularity of trajectory passing near saddle-focus). The interaction between Hopf and homoclinic bifurcations is displayed here as combination of spiral type mapping (this is a feature of second-type intermittence) and homoclinic reinjection to neighborhood of the unstable saddle-focus (spiral center). We have analyzed a power spectrum of mapping and determined that it can be approximate with function $1/f^{0.7}$ near origin. When frequency nonequidistancy increases, the laminar times vanish and dynamics becomes a pure chaotic.

For greater number of modes one can expect that orbits can visit the vicinity of several unstable fixed points so, more rich dynamics may exist . Complexity of dynamics is also possible when the resonance situation takes place for points like a simple zero and a two pure imaginary pairs. Actually, this case can be realized in solid-state lasers due to the existence of low-order resonance near the half of the relaxation oscillation frequency. The origin of such a resonance is a result of multi-mode operation under the condition of spatial hole burning.

REFERENCES

1. E.A.Viktorov, I.B.Vitrishchak, G.E.Novikov, O.A.Orlov, A.A.Mak, V.I.Ustyugov, M.M.Khaleev. "Instabilities and Chaos in Solid-State Lasers as a Result of Mode Coupling" OSA Proceedings on Nonlinear Dynamics in Optical Systems, edited by N.B. Abraham, E.Garmire and P.Mandel (Optical Society of America. Washington. DC. 1991), vol. 7, pp. 410 - 414.

2. X.-G. Wu, P.Mandel. "Second harmonic generation in a multimode laser cavity", JOSA B, vol. 4, pp. 1870 - 1881, 1987.

3. K.Wiesenfeld, P.Hadley. "Attractor crowding in oscillator arrays", Phys. Rev. Lett., vol. 62, No. 12, pp. 1335 - 1338, 1989.

4. J.Guckenheimer, Ph.Holmes. "Nonlinear oscillations, dynamical systems and bifurcations of vector fields", (Shpringer-Verlag, 1983).

## Geometrical phases in self-pulsing lasers

C.Z.Ning and H.Haken
Institut für Theoretische Physik und Synergetik, Universität Stuttgart,
Pfaffenwaldring 57/4, D-7000 Stuttgart 80, F.R.Germany
(Tel: 711-685 4998, Telefax:711-685 4909, Bitnet:NCZ@DS0SYN51)

As observed in detuned lasers [1, 2] the arbitrary constant phase of the laser field in the CW region starts to drift linearly besides pulsations in the self-pulsing region. The fact that this drift might have similarities with the Berry phase [3] was pointed out in [2, 4] and a comparative study was given by us [2]. It has been not easy to establish an exact mathematical relation between the two, however. Thus a compelling analogy is still lacking. The main obstacle is that the original formulation [3] of the Berry phase was given for linear Schrödinger systems, whereas we have here an essentially non-linear and dissipative system. Fortunately we have succeeded in borrowing the geometrical formulation of the Berry phase for linear systems [5] and essentially generalizing it to a certain kind of nonlinear dissipative systems, to which detuned one- and two-photon lasers belong. An exact analogy is therefore established. We show that the whole phase accumulation of the laser field in a period of the intensity pulsation consists of two parts: a dynamical part given directly by the equation of movement and a geometrical part given by the path-integral along the trajectory of limit cycles in a certain phase space. This later part has the same origin as that due to parallel transportations of vectors in a curved space.

Consider a dynamical systems described by the following ordinary differential equations:

$$|\dot{\Psi}\rangle = |\mathcal{F}(|\Psi\rangle)\rangle, \tag{1}$$

where $|\Psi\rangle = (\psi_1, \psi_2, ...\psi_n)$ is a vector describing the states of the system in phase space and $|\mathcal{F}(|\Psi\rangle)\rangle$ is a nonlinear vector-valued function of $|\Psi\rangle$. In general $|\mathcal{F}(|\Psi\rangle)\rangle$ is also a function of the externally controllable parameters, e.g., the pumping in lasers.

We define now a diagonal matrix, $\mathcal{T}(\phi(t))$, whose elements are given by $\exp(i\alpha_1\phi(t))$, $\exp(i\alpha_2\phi(t))$, $...\exp(i\alpha_n\phi(t)$. The $\alpha_i$'s are real numbers and $\phi(t)$ is a real function. Suppose that for certain sets of parameters there exists a kind of asymptotically stable solutions of eq. (1), such that, for certain initial conditions and for $t \longrightarrow \infty$, the following relation holds:

$$|\Psi(t+T)\rangle = \mathcal{T}(-\delta\phi)\,|\Psi(t)\rangle\,, \tag{2}$$

where $\delta\phi$ is a real quantity. We can show [6] that for such systems the whole phase accumulation is given by:

$$\delta\phi = \oint \mathbf{A}_\mu dX_\mu + \int_t^{t+T} \omega_d(\tau)d\tau, \tag{3}$$

where $\mathbf{A}_\mu$ is the so-called vector potential and given by

$$\mathbf{A}_\mu = Im\left\{\frac{\langle\bar{\Phi}|\partial_\mu\bar{\Phi}\rangle}{\langle\bar{\Phi}\,|\Lambda|\,\bar{\Phi}\rangle}\right\}, \tag{4}$$

and $\omega_d$ is the so-called dynamical frequency and defined by

$$\omega_d(t) = -Im\left\{\frac{\langle\Psi\,|\mathcal{F}(|\Psi\rangle)\rangle}{\langle\Psi\,|\Lambda|\,\Psi\rangle}\right\}. \tag{5}$$

The new periodic vector is defined as

$$|\bar{\Phi}(t)\rangle = \mathcal{T}\left(\bar{\phi}(t) + \int^t \omega_d(t')dt'\right)|\Psi\rangle. \tag{6}$$

The $\bar{\phi}(t)$ satisfies

$$\bar{\phi}(t+T) - \bar{\phi}(t) = \delta\phi - \int_t^{t+T} \omega_d d\tau. \tag{7}$$

$\Lambda$ is a diagonal matrix with $\alpha_i$ as its elements.

For one-photon detuned lasers we use the notations in [7], the equations are then given by:

$$\dot{X} = -kX + kY, \tag{8}$$
$$\dot{Y} = -aY + (r - Z)X, \tag{9}$$
$$\dot{Z} = -bZ + \frac{1}{2}(X^*Y + XY^*), \tag{10}$$

where $r = r_1 + ir_2$ , $a = 1 + ir_2$. $r_1$ is related to the pumping. $r_2 = (1-k)\Delta$ and $\Delta$ is the detuning between the cavity and the atomic frequencies. $b$ and $k$ are the relaxation constants of the cavity and of the population inversion scaled by the relaxation constant of the polarization, respectively . The reference frequency is the CW-frequency so that any new frequency will be due to the pulsations of the intensity. Here $|\Psi\rangle$ is a vector with three components $(X, Y, Z)$ and the $\alpha_i$'s are given by $(\alpha_1 = 1, \alpha_2 = 1, \alpha_3 = 0)$. From our earlier analysis [2, 7] we know that this vector is cyclic after the second threshold, when the intensity shows periodic pulsations. Using formula (5) the dynamical frequency is given by

$$\omega_d = -\frac{-r_2|Y|^2 + Im[(r - Z - k)XY^*]}{|X|^2 + |Y|^2}. \tag{11}$$

From this expression we see $\omega_d = 0$, if there is no detuning, because $Y$ is then asymptotically real and $r_2 = 0$. We know that there is no phase accumulation for perfectly tuned lasers in the domain of pulsation except for that induced by the CW-frequency. Therefore there is no geometrical phase for the perfectly tuned lasers. In the presence of detuning the whole phase is given by [7]

$$\phi(t) = -k\int^t d\tau \frac{Im\left[Y\exp(i\phi)\right]}{x_1}, \tag{12}$$

where $x_1 = X\exp(i\phi)$ is a real variable. The dynamical phase is given by the integration of (11). The subtraction of the dynamical part from the total phase gives the geometrical phase.

Our second example is the detuned two-photon laser. Denoting the electric field amplitude by $E$, the polarization of the medium by $P$, and the inversion by $D$ we can write the equations as [8]:

$$\dot{E} = (id - 1)kE - 2iPE^*, \tag{13}$$
$$\dot{P} = -(id + 1)P + iDE^2, \tag{14}$$
$$\dot{D} = b(D_0 - D) + 2i\left[PE^{*2} - P^*E^2\right], \tag{15}$$

where $d$ is the scaled detuning parameter between the cavity and atomic frequencies and $D_0$ denotes the pumping rate. $k$ and $r$ have the same meaning as in the one-photon laser. Again we take the CW-frequency as the reference frequency. It can be easily verified that the $\alpha_i$'s are now given by $(\alpha_1 = 1, \alpha_2 = 2, \alpha_3 = 0)$. The Hopf bifurcation of this set of equations was studied in [8] and there exists a threshold for self-pulsing of the intensity. The cyclicity of $E$ and $P$ as defined in (2) can be easily verified in the parameter region of the periodic intensity pulsations. The dynamical frequency can be calculated from Eq. (5)

$$\omega_d = \frac{d\left[k|E|^2 - |P|^2\right] + Im\left\{iDE^2P^* - 2iPE^{*2}\right\}}{|E|^2 + 2|P|^2}. \tag{16}$$

Again we see $\omega_d = 0$ if $d = 0$, because the polarization is asymptotically imaginary in this case and the second term in the numerator then vanishes. The geometrical phase is therefore zero in this case as well. In the case of detuning we can calculate the geometrical phase in a way similar to that in the one-photon laser. The total phase is now given by [8]:

$$\phi(t) = \int^t d\tau \left[2Re\left\{P\exp(2i\phi)\right\} - kd\right]. \tag{17}$$

The relation between the total, geometrical and dynamical phases can again be determined as above.

In summary we have shown that the geometrical formalism for the parallel transportations of vectors and the geometrical phase expressed as a line integral (3) formulated hitherto for Hamiltonian systems or linear non-Hamiltonian systems can be suitably adapted to dissipative systems showing cyclic attractors. The concept of the geometrical amplitude accumulation can be naturally and generally introduced for nonlinear dissipative systems as well. Finally our work shows that the phase accumulation in self-pulsing lasers is indeed related to the geometrical phase or Berry' phase.

## References


[1] M.F.H.Tarroja, N.B.Abraham, D.K.Bandy and L.M.Narducci, Phys. Rev. **34A**, 3148(1986);H.Zeglache, P.Mandel, N.B.Abraham, and C.O.Weiss, Phys. Rev. **38A**, 3128(1988)

[2] C.Z.Ning and H.Haken, Z.Phys. B, **81**, 457(1990); C.Z.Ning and H.Haken, Phys.Rev.A, **43**, 6410(1991)

[3] M.V.Berry, Proc.Roy.Soc.,A **392**,45(1984)

[4] R.Vilaseca, G.J.de Valcarcel and E.Roldan, Phy.Rev., A **41**, 5269(1990)

[5] B.Simon, Phys.Rev.Lett., **51**,2167(1983); Y.Aharonov and J.Anandan, Phys.Rev.Lett., **58**, 1593(1987); J.Samuel and R.Bhandari, Phys.Rev.Lett., **60**, 2339(1987)

[6] C.Z.Ning, Dissertation, (Universität Stuttgart, 1991)

[7] C.Z.Ning and H.Haken, Phys.Rev.A, **41**, 3826(1990)

[8] C.Z.Ning Z.Phys., B **71**, 247(1988)

# Dynamics of Monovelocity Atomic Beam Maser

A. N. Oraevsky, T. V. Sarkissian,
D. J. Jones, D. K. Bandy
P. N. Lebedev Physics Institute, Russian Federation
Physics Department, Oklahoma State University, Stillwater, OK 74078

The dynamics of a beam maser, the first device in quantum electronics, was the subject of attention more than thirty years ago [1-4]. However, the interest in a beam masers has increased recently due to their applications in the study of fine quantum effects of atom interaction with the cavity field [5,6]. One of the most important feature of the presently used maser is a monovelocity atomic beam. A theory of a monovelocity beam maser was developed by Filipowicz et al. [7] and Guzman et al. [8]. The authors of those theoretical papers analyzed a micromaser, i.e. the maser with a *small* number of atoms in a resonator. The quantum effects are dominating in that case. That is why in [7,8] the statistical but not dynamical approach to the problem has been used.

Our task is to investigate laser dynamics with a *large* number of atoms in the resonator when the quantum effects are negligible but the coherent effects become dominating. In this case, as is known, the polarization of an active medium plays a very important role and the dynamic chaos is possible (see, for example, [4,9] and elsewhere).

Unlike the Maxwell-Bloch model we assume an atomic beam to be a mono-velocity non-selfrelaxing quantum system. The parameter, which determines relaxation properties of the system, is the finite time of atomic interaction with the resonator field. As we shell see, this modifies radically the maser (laser) dynamics, as compared to a laser described within the framework of the Maxwell-Bloch model.

We consider a single-mode microwave maser with a uniform field along the z-axis of the cavity. We assume the eigenfrequency of the cavity $\omega_c$ is resonant with the eigenfrequency $\omega_L$ of atomic transition. The equations of motion in the slowly varying amplitude approximation for the electromagnetic field E, polarization P, and population inversion N are

$$\left[\frac{\partial}{\partial\tau} + \varkappa\right]G = \eta\varkappa \int_0^1 X d\xi \ , \tag{1a}$$

$$\left[\frac{\partial}{\partial\tau} + \frac{\partial}{\partial\xi}\right]X = GY \ , \tag{1b}$$

$$\left[\frac{\partial}{\partial\tau} + \frac{\partial}{\partial\xi}\right]Y = -GX \ . \tag{1c}$$

where

$$\tau = \frac{t}{\tau_o} \ , \ \xi = \frac{z}{L} \ , \ \varkappa = \gamma\tau_o \ , \ G = \mu \frac{E}{\hbar} \tau_o \ , \ X = \frac{iP}{|\mu|N_o} \ , \ Y = \frac{N}{N_o} \ . \tag{2}$$

L is the cavity length and $\varkappa$ represents the cavity losses, v is the velocity of the atoms in the beam, $2\gamma=\omega_c/Q$ where Q is the quality factor of the cavity, $\mu$ is the dipole moment of the atomic transition, $N_o=(I/v)(LS/V)$ where I is the atomic beam intensity in atoms/cm$^2$ s, V is the cavity volume, and S is the beam cross section. The excitation parameter, $\eta = \frac{2\pi\omega|\mu|^2}{\hbar\gamma} N_o\tau_o$.

We consider that all the atoms are in the upper state and there is no polarization at the cavity entrance; i.e.

$$Y(\tau,0) = 1 \ ; \quad X(\tau,0) = 0 \ . \tag{3}$$

The steady-state branches of G as a function of $\eta$ are presented in Fig.1. The branches with negative slope (dashed curve) are unstable. The stability of the positive slope branches depend on the $\eta$ and $\varkappa$ parameters and can be studied by the linear stability analysis. Figure 1 shows the stability for each branch (BI,BII,...) on the steady-state curve for $\varkappa$=0.4 where the stable ranges are indicated by the bolded solid line.

Figure 2 shows the field behaviour in a forward and backward ramp (indicated by arrows) of the parameter $\eta$ for $\varkappa$=0.4 . During the forward scan in the first branch (BI), the system follows the steady-state curve and becomes unstable. For increasing excitation the system continues to oscillate until it jumps to a stable region of the second branch (BII) . The system resides on this branch stably over a small range of the excitation when it again becomes unstable and begins to pulsate. This region of oscillation persists until the system jumps to the fourth branch (BIV), over-shooting the third branch (BIII), and entering an unstable region of the fourth branch.

The reverse ramp as indicated in Fig.2 shows that the oscillations of the fourth branch persist well beyond the transition point of the forward scan until it reaches the branch's stable region, following the steady-state trajectory. It finally drops to the third branch, stably residing on the

third branch, dropping to the second branch and so on. As seen in Fig.2 hysteresis between unstable regions, multistability is possible in the monovelocity atomic beam system.

In general, the parameter space in this system is rich in nonlinear phenomena. There exist: multistability and hysteresis; irregular oscillations for both high and small values of the cavity loss parameter; the dynamical transitions between different steady-state branches.

1. N.G.Basov, A.M.Prokhorov, JETP, 27, 431, (1954).
2. J.P.Gordon,H.J.Zeiger,C.H.Townes, Phys.Rev., 99, 1264, (1955)
3. H.M.Goldenberg,D.Kleppner,N.F.Ramsey, Phys.Rev., 123, 530, (1961)
4. A.N.Oraevsky, Molecular Beam Masers,(Nauka, Moscow, 1964).
5. G.Rempe, H.Walter, P.Dobiasch, in Quantum Optics, Eds., A.Kujawski and M.Levenstein, (Polish Acad. of Sci., Warsaw, 1985),pp.145-164.
6. F.Diedrich, J.Krause, G.Rempe, M.O.Scully, H.Walter, Physica B151, 247(1988).
7. P.Filipowicz, J.Javanainen, and P.Meystre, Phys.Rev. A 34, 3077, (1986).
8. A.M.Guzman, P.Meystre, and E.M.Wright, Phys.Rev. A 40, 2471, (1989).
9. L.Narducci and N.Abraham, "Laser Physics and Laser Instabilities", World Sci. Pub., Singapore, 1988.

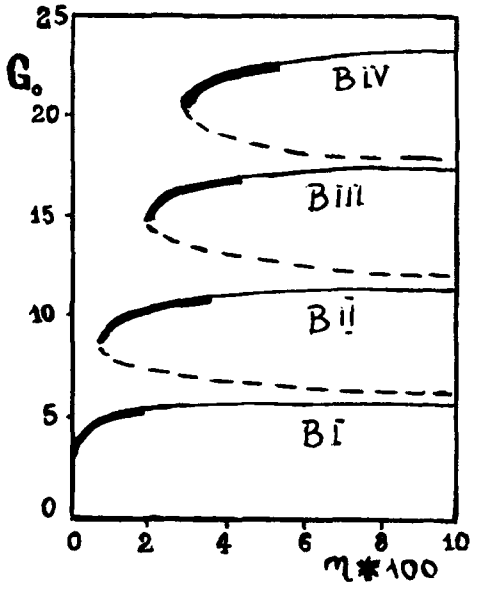


Fig 1

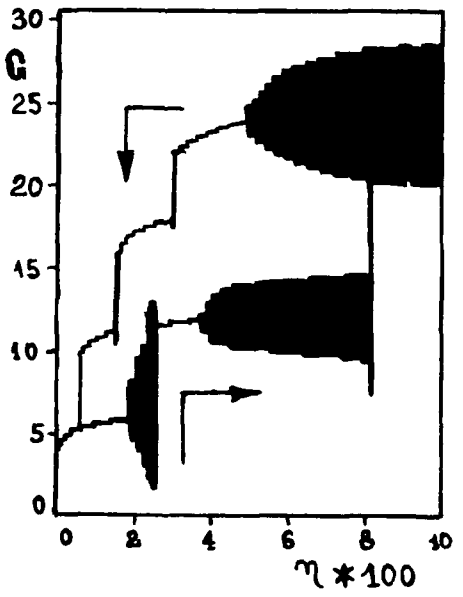


Fig 2

Figure Captions

1. Steady state and linear stability ($\varkappa$=0.4) of the monovelocity atomic beam maser; $G_o$ as a function of $\eta$.

2. Dynamical behavior of the system in a forward and backward excitation ramp for $\varkappa$=0.4.

# Interaction of Relaxation Oscillations and Instability in a Bidirectional Nd:YAG Laser with a Nonreciprocal Ring Cavity

P. A. Khandokhin, Ya. I. Khanin
Nizhny Novgorod
Russian Federation

It is shown that the phase nonreciprocity influences the stability of the traveling wave regime due to changing the interaction between different types of relaxation oscillation. The laser sensitivity to the sign of phase nonreciprocity appears with detuning.

Monday, June 22, 1992

# Poster Session 1

**MC** 8:00pm–10:00pm
**Krenek Hall**

# Interferometric Configurations For Laser Mode-Locking Using a Nonlinear Active Medium

Jean-François Cormier and Michel Piché
Centre d'Optique Photonique et Lasers (COPL)
Département de Physique, Université Laval
Québec (Québec), Canada G1K 7P4
Phone: (418) 656-2753, FAX: (418) 656-2623

## 1. Introduction

The generation of femtosecond optical pulses using the feedback from an external nonlinear cavity is now a well established technique. The principle consists of interfering a reference pulse with a chirped version of itself, where the chirping is due to self-phase modulation (SPM) in a Kerr-like material. By adjusting the relative phase between the pulses, it is possible to achieve pulse shortening at each round-trip and positive differential gain for the short pulse.

Many interferometric configurations have been proposed, where pulse chirping and pulse amplification take place in different materials [1-4]. This paper addresses the problem of establishing the performance and the stability of configurations where both the amplification and the Kerr nonlinearity originate from the same medium, as discussed in Ref. 4. In particular, we look for stable conditions leading to minimum pulse duration and minimum time-bandwidth products.

## 2. Modelling

The four types of configurations shown in Fig. 1 will be examined. A spectral filter $F(\omega)$ is taken either as a complex lorentzian or as a gaussian. The active material is characterized by its gain $G(\omega)$, its nonlinear index of refraction $n_2$ and its dispersion $D_2$. The first scheme involves a two beam-interference effect while the other three involve multiple-beam interference effects which are known to be intrinsically unstable at high intensities. These schemes should be applicable to Ti:Sapphire lasers, fiber lasers and semiconductor lasers. In our modelling, a pulse shape is sent iteratively through the different parts of the laser. The combined effect of amplification, SPM and dispersion of the active medium is treated by the split-step Fourier method which breaks the medium into alternate slices of nonlinear amplifier and dispersive material.

## 3. Results

Typical results obtained for the nonlinear Michelson configuration (Fig. 1a) are described herein. We have chosen this configuration because it is the one likely to be more stable; in fact, the only potential instabilities are due to the laser dynamics, and not to a nonlinear interferometric reflection. In our simulations, we used a gaussian filter with a bandwith of 10 THz and a beam splitter reflectivity of 50%; all other components are assumed nonlossy. To achieve pulse shortening, the phase mismatch between the arms of the interferometer must be appropriately chosen. Convergence of the system parameters to a short

a)

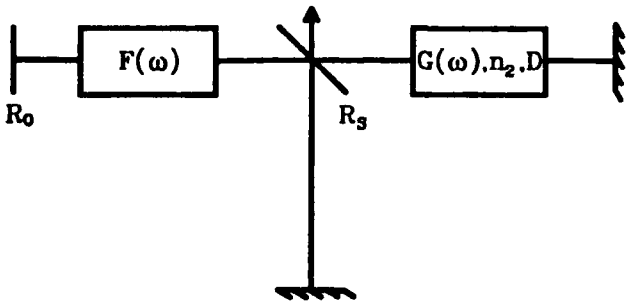


b)

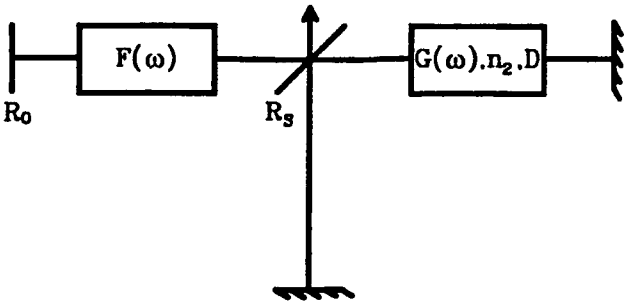


c)

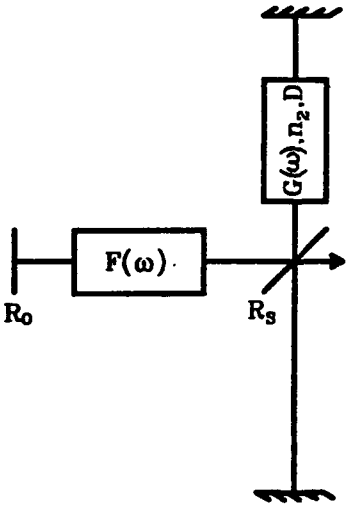


d)

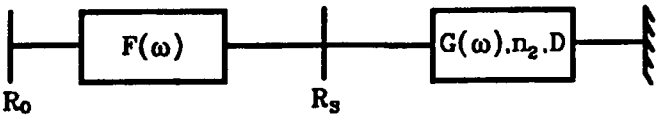


**Figure 1.** Interferential configurations for nonlinear coupled cavity mode-locking; a) Michelson, b) Fox-Smith, c) Modified Fox-Smith, d) Faby-Perot interferometers.

pulse is obtained for a phase mismatch ranging from $-\pi$ to 0, where the interferometric reflectivity increases with intensity. In fact, within this range (as shown in Fig. 2) stability is not garanteed. Periodic oscillations associated to a Q-switching instability tend to narrow the stability zone and break it into two parts at low pumping levels. This instability can be understood as follows: the steep slope of the nonlinear reflectivity as a function of intensity leads to large pulse intensities and energies which must be matched by adequate pumping rates; otherwise, the gain medium is rapidly depleted, resulting in a drop of pulse power and energy. The maximum slope of the interferometer response occurs at a phase mismatch of $-\pi/2$, where a loss of stability is predicted.

With a nondispersive gain medium, the pulse width ranges from 70 fs to 170 fs with a time-bandwidth product almost constant at arount 0.59, giving insight on the large phase content of the pulses. With negative dispersion included into the gain medium, shortening of the pulse is obtained. For a phase mismatch of $-\pi/2$ and a dispersion of -800 $fs^2$, a minimal pulse width of 70 fs is reached with a time-bandwidth product of 0.42. In general, the time-bandwidth product slightly decreases with an increase of negative dispersion.

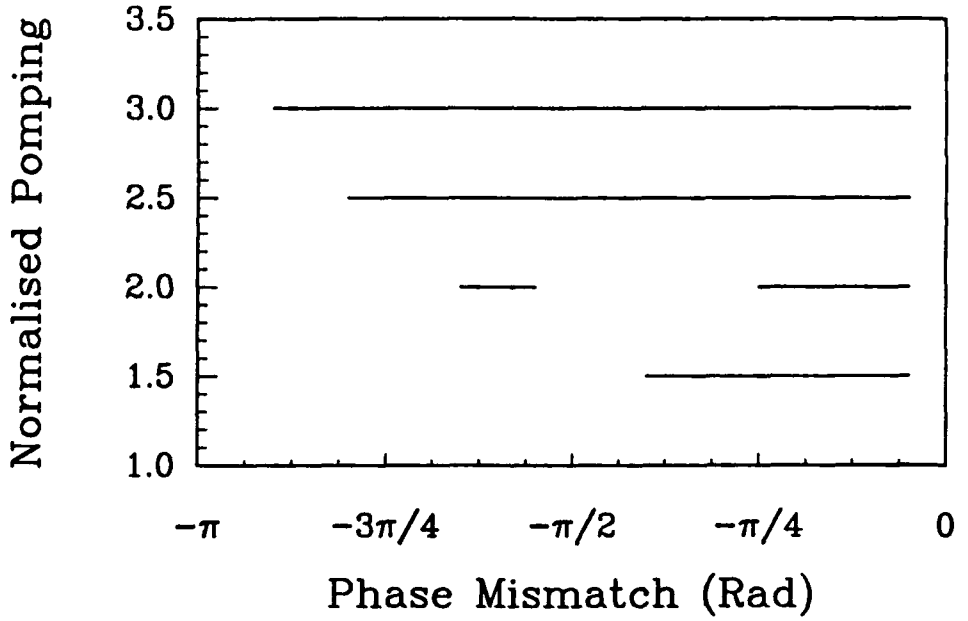


**Figure 2.** Regions of convergence to a short pulse (solid line), for normalized pumping of 1.5, 2, 2.5, 3.

**References**

1. F. Ouellette and M. Piché, Opt. Comm. **60**, 99 (1986).
2. J. Mark, L. Y. Liu, K. L. Hall, H. A. Haus, and E. P. Ippen, Opt. Lett. **14**, 48 (1989).
3. P. N. Kean, X. Zhu, D. W. Crust, R. S. Grant, N. Langford, and W. Sibbett, Opt. Lett. **14**, 39 (1989).
4. H. A. Haus, J. G. Fujimoto, and E. P. Ippen, J. Opt. Soc. Am. B **8**, 2068 (1991).

# Mode-Locking Dynamics of Synchronously Pumped Color-Center Lasers

**W. Forysiak† and J.V. Moloney**

Dept. of Mathematics, University of Arizona, Tucson, Az 85721, U.S.A.
Tel: 602-621-6755, Fax: 602-621-8322
†Dept. of Physics, Heriot-Watt University, Edinburgh EH14 4AS. U.K.

Numerical simulations of the mode-locking dynamics of synchronously pumped $KCl{:}Tl^0(1)$ and $LiF{:}F_2^+$ colour-centre lasers [1,2] in Fabry-Perot and ring geometries are presented. The response of each laser to variation of cavity mismatch is discussed and in particular, their pulse-shaping properties and the conditions required for pulse optimisation and stabilisation. Each of the cavity tuning curves consists of a narrow region of quasi-stationary pulsation, bounded by regions in which the presence of spontaneous emission noise generates episodic phase-wave perturbations, leading to a fundamental pulse jitter [3]. The resulting pulse characteristics are independent of whether the lasers are configured in Fabry-Perot or unidirectional ring geometries, but the detailed pulse shapes and the stability boundaries of the two lasing species differ slightly. Thus, whereas it is possible to minimise the phase-wave fluctuations at the peak of the $Tl^0(1)$ tuning curve to generate optimised, quasi-stationary pulses, in $F_2^+$ a slight detuning from optimum is required, albeit by only approximately 15%. The equivalent bidirectional ring lasers exhibit regions of quasi-stationary, spontaneously unidirectional lasing, bounded by regions of competitive, bidirectional switching. The physical mechanism governing bidirectional switching is the same as that driving pulse jitter in the Fabry-Perot and unidirectional ring configurations, namely, the passage of spontaneous noise induced phase-waves [4]. Consequently, there is a simple correspondence between the two operating regimes of the bidirectional ring lasers and the quasi-stationary and fluctuating regimes of the other laser geometries.

To illustrate the bidirectional switching action, Fig. 1 shows the intensity and phase profiles of the forward and backward-going pulses during a typical switching period. With each cavity round-trip the phase-wave initially ahead of the forward-going pulse (Fig. 1a) sweeps slowly back through it. As it does so, the energy extracted by the forward-going pulse from the inverted medium is diminished, allowing the backward-going pulse to grow from the residual gain. Once passage of the forward-going phase-wave is complete, during which time it is severely attenuated, almost all the available energy has been switched to the backward-going direction. In this particular case, the subsequent passage of the phase-wave just ahead of the backward-going pulse at the end of this sequence (Fig. 1f) switches the lasing direction once again.

Pulse jitter in mode-locking by synchronous pumping has long been recognised as a macroscopic manifestation of quantum noise [3]. A significant problem in the experimental realisation of this phenomenon is the capture of sufficient data describing these ultrashort pulses. The bidirectional switching described above provides a distinct and clear macroscopic signature of quantum fluctuations which could be readily measurable. A more subtle macroscopic switching action of the same origin in the Fabry-Perot geometry will also be described.

[1] L.F. Mollenauer, N.D. Vieira and L. Szeto. *Opt. Lett.* **7**, 414 (1982).

[2] N. Langford, K. Smith and W. Sibbett. *Opt. Lett.* **12**, 817 (1987).

[3] J.M. Catherall and G.H.C. New. *IEEE J. Quantum Electron. QE*-**22**, 1593 (1986).

[4] F.A. Hopf and E.A. Overman II. *Phys. Rev. A***19**, 1180 (1979).

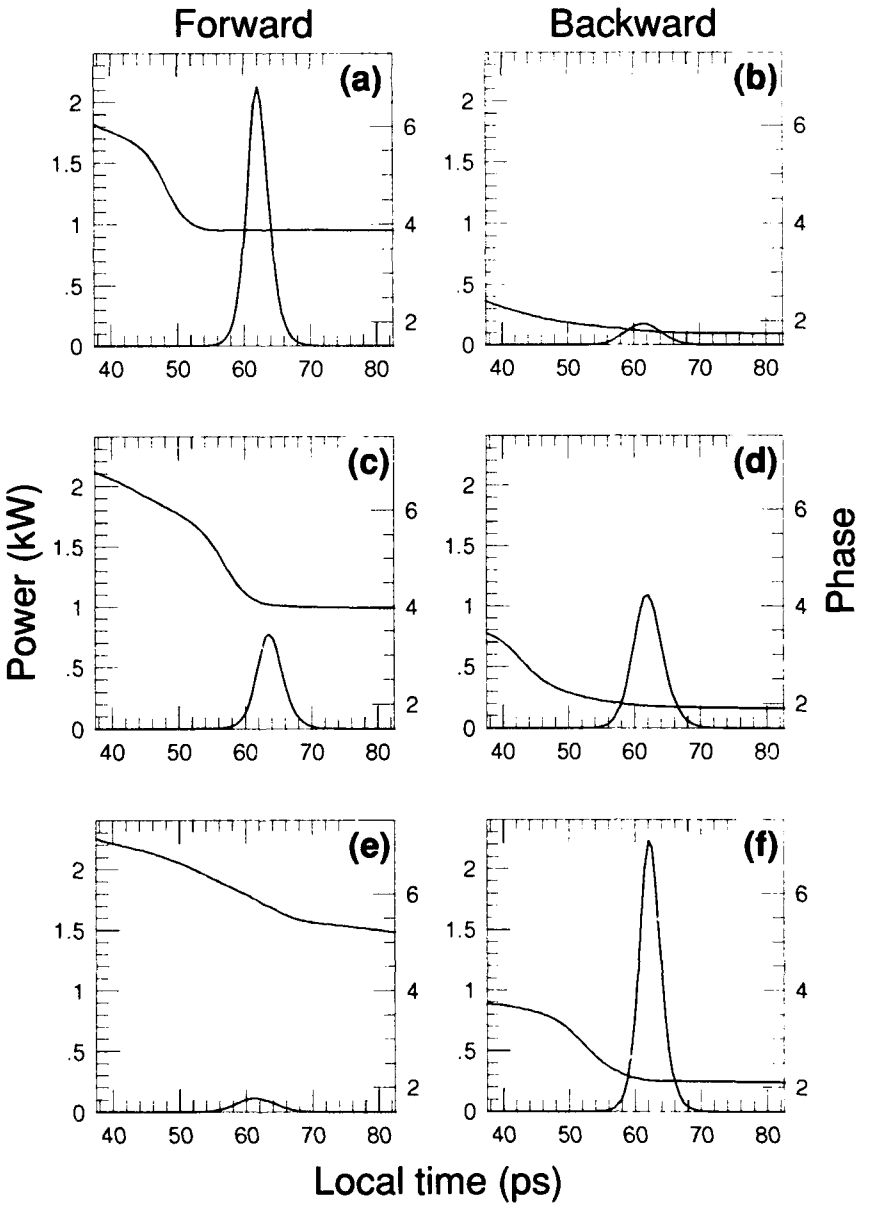


**Figure 1** Forward-going (a,c,e) and backward-going (b,d,f) pulse intensity and phase profiles for the $F_2^+$ bidirectional ring laser during a phase-wave driven switch in pulsing direction. The time interval between each pair of pictures ((a,b), (c,d) and (e,f)) is 80 cavity round-trips.

# Optical Bistabilities and Autostabilization of the Solid-State Ring Laser Generation Regimes under Colliding USPs Dynamic Self-Diffraction

A. N. Shelaev
P. N. Lebedev Physics Institute
Russian Federation

Summary not available at press time.

# Nonlinear Dynamics of Extremely Short Electromagnetic Pulses in Passive and Active Media

E. M. Belenov, A. V. Nazarkin
P. N. Lebedev Physics Institute
Russian Federation

Summary not available at press time.

# Coexistence of Two Attractors in Lasers with Incoherent Delayed Feedback

Kenju Otsuka and Jyh-Long Chern
*NTT Basic Research Laboratories, Musashino-shi, Tokyo, 180 JAPAN*
*Telephone +81 422 59 3367*

Delay-induced complex dynamics in lasers have been investigated in various schemes, such as rich phenomena in semiconductor lasers with external feedback,[1] and quasiperiodicity in $CO_2$ lasers with electro-optic feedback.[2] Recently, we proposed high-speed picosecond pulse generation in semiconductor lasers with incoherent delayed feedback.[3] The basic idea was derived from successive carrier modulation by delayed feedback light whose polarization direction is rotated to be orthogonal to the lasing light. Such a feedback scheme is referred to as *incoherent feedback*.[4] We showed theoretically that periodic spiking oscillations can be excited in a short-delay regime, i. e., delay time $\ll$ carrier lifetime. In this paper, we extend this scheme to general class-B lasers and investigate dynamics in wide parameter regions.

The basic single-mode laser rate equations for population inversion density $n$ and photon density $s$ are expressed as

$$dn(t)/dt = w - n(t)[1 + s(t) + \gamma s(t - T)], \tag{1}$$

$$ds(t)/dt = K[(n(t) - 1)s(t) + \epsilon n(t)]. \tag{2}$$

Here, $w$ is relative pump power scaled by threshold, time $t$ and delay time $T$ are scaled by population lifetime $\tau$, $K = \tau/\tau_p$ ($\tau_p$ is the photon lifetime), $\gamma$ is the effective coupling coefficient, and $\epsilon$ is the spontaneous emission coefficient.

Figure 1 is a stability diagram based on a small signal linear stability analysis of Eqs. (1) and (2). Multiple unstable regions exist. In the unstable regions, the stationary solutions become dynamically unstable and regular and irregular *sustained relaxation oscillations* may appear when intitial values are set near the stationary state, i. e., $\bar{n} = \bar{s}/(\bar{s}+\epsilon)$ and $\bar{s} \simeq (w-1)/(1+\gamma)+\epsilon w/(w-1), (\epsilon \ll 1)$. In addition to this instability born from destabilized statinary states via supercritical

Hopf bifurcation, large signal regenerative *spiking oscillations*,[5] which cannot be predicted by linear stability analysis, are found to be excited by setting initial conditions to be outside the vicinity of the stationary state. In short, these *two* motions coexist at fixed parameter values in the phase space with different basins of attraction. The spiking oscillation corresponds to a repetitive generation of the spike in the onset of relaxation oscillation which builds up from a nonlasing solution, i. e., $n_0 \simeq w$ and $s_0 \simeq \epsilon w/(1-w)$, $(\epsilon \ll 1)$.[5] Such a spiking oscillation has been observed in deeply modulated class-B lasers in which the pump power drops below the threshold during part of the cycle.[5] It is interesting to note that in the present system the spiking oscillation is excited by a delay-induced pulselike modulation of population inversion. Examples of these two motions are shown in Fig. 2. In the case of spiking oscillations (Fig. 2(b)), the delayed feedback photon indicated by | in the figure, which originates from the spike indicated by ⇓, depletes the population inversion in a stepwise manner and controls the buildup process of the next spike. This regenerative spike generation process can be understood in terms of particle motions with a kicked perturbation in an asymmetric Toda-like potential.[6]

From numerical simulations of Eqs. (1) and (2), these two motions are found to be destabilized when the control parameters, $w$, $T$ and $\gamma$, are changed. Each attractor undergoes a complicated bifurcation leading to chaos interrupted by fractional locking. Two qualitatively different oscillation patterns born from different periodic states are shown in Fig. 3. The physical interpretation of such instabilities resulting from a 'history-dependent' perturbation and the interplay between two attractors, such as chaotic itinerancy in large $w$ and $T$ regimes, are now under investigations. (Mutual locking phenomena between these two motions have been demonstrated numerically in a laser array in which emitters are globally coupled through incoherent delayed feedback.[7])

**References**

1. For review, see K. Otsuka, SPIE *Nonlinear Optics and Materials*, **1497**, 432 (1991).
2. F. T. Arecchi, *et al.*, Phys. Rev. A **43**, 4997 (1991).
3. K. Otsuka and J.-L. Chern, Opt. Lett. **16**, 1759 (1991).
4. H. Yasaka and H. Kawaguchi, Appl. Phys. Lett. **53**, 1360 (1988).

5. K. Kubodera and K. Otsuka, IEEE J. Quantum Electron. **QE-17**, 1139 (1981).
6. D. A. Kleinman, Bell Syst. Tech. J. **43**, 1505 (1964); T. Ogawa. Phys. Rev. A **42**, 4210 (1990).
7. K. Otsuka and J.-L. Chern, Phys. Rev. A (April 1992, in press).

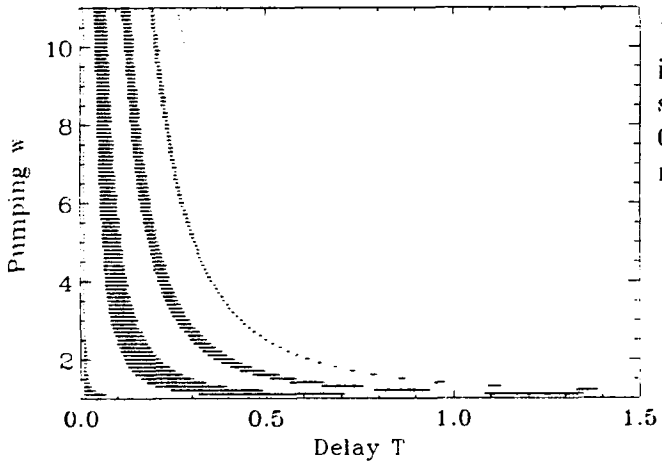


Fig. 1 Stability diagram of class-B lasers with incoherent delayed feedback obtained from small signal linear stability analysis, assuming $\gamma = 0.21$, $K = 10^3$, and $\epsilon = 1.2 \times 10^{-7}$. Stable regimes are indicated by hatching.

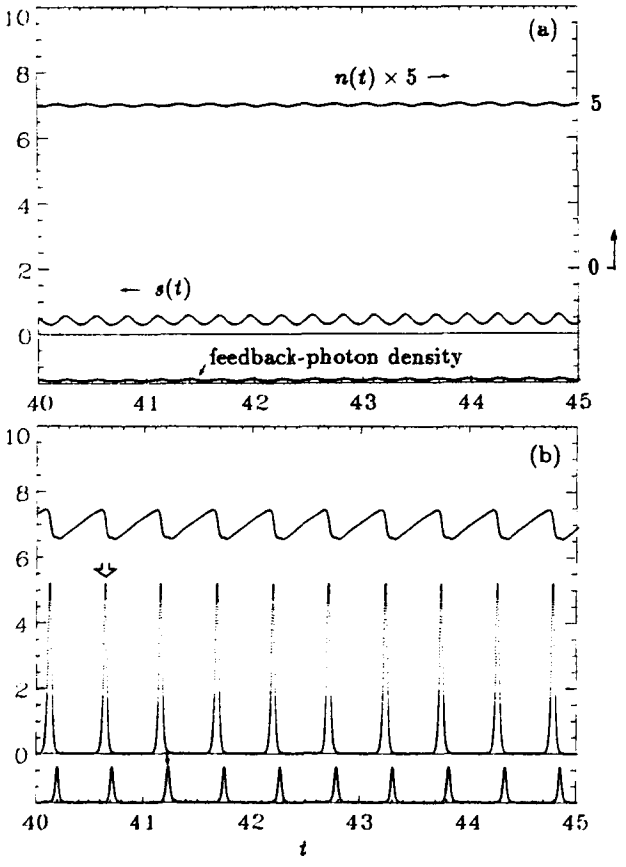


Fig. 2 (a) Sustained periodic relaxation oscillation and (b) periodic spiking oscillation at fixed parameter values of $w = 1.5$, $\gamma = 0.21$, $T = 0.59$, $K = 10^3$, and $\epsilon = 1.2 \times 10^{-7}$.

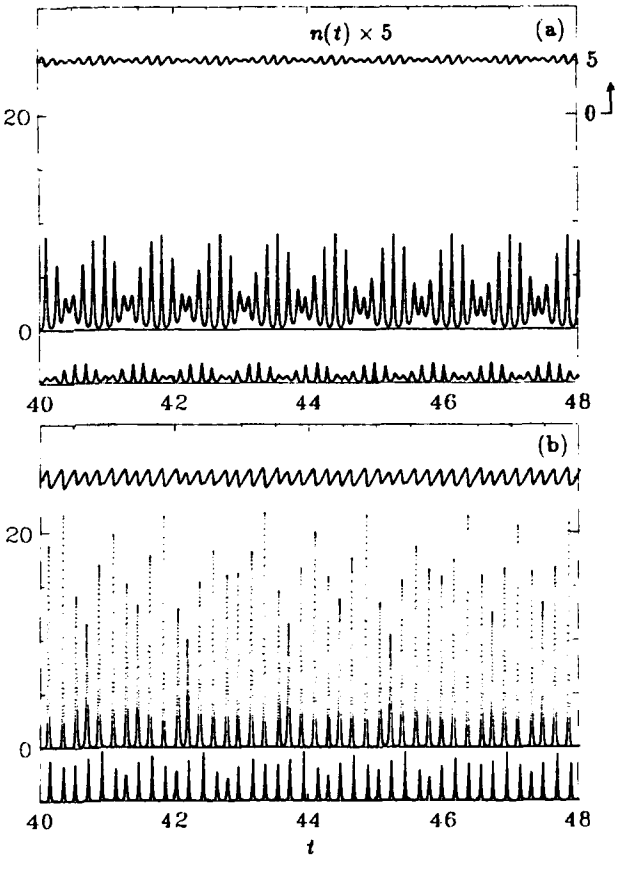


Fig. 3 Coexisting oscillation patterns born from (a) relaxation oscillation and from (b) spiking oscillation at an increased pump value of $w = 3.5$. Other parameter values are the same as Fig. 2.

## Nonlocal Adiabatic Elimination in the Maxwell-Bloch Equation

P. Ru, P.K. Jakobsen and J.V. Moloney
Arizona Center for Mathematical Science
Mathematics Department
University of Arizona
Tucson AZ 85721
Tel: (602)-621-6755, Fax: (602)-621-8322

Adiabatic elimination is a standard procedure applied to the Maxwell-Bloch laser equations when one variable or more is slaved to the remaining variables. An important case in point is a laser with an extremely large gain bandwidth satisfying the condition $\gamma_\perp \gg \gamma_\parallel, k$ where $\gamma_\perp$ is the polarization dephasing rate, $\gamma_\parallel$ the de-energization rate and $k$ the cavity damping constant. For example, color center gain media satisfy this criterion and support hundreds of thousands of longitudinal modes in synchronous pumped mode-locking operation. For simple single mode plane wave models the crude adiabatic elimination step of setting the derivative of the polarization variable to zero can be avoided by using center manifold techniques [1]. In this general class of singular perturbation problem, the idea is to coordinatize the problem using linear stability analysis about some known solution and then to construct an approximation to the center manifold on which the (possibly dynamic) solution remains for all time. This procedure has been successfully applied to the Maxwell-Bloch equations describing a single mode homogenously broadened ring laser [2]. Extension of the procedure to nonlinear partial differential equations is very difficult in general as the resulting center manifold may be an infinite dimensional object. When transverse (or additional longitudinal) degrees of freedom are introduced in the Maxwell-Bloch equations in order to investigate spatial pattern formation (or mode-locking dynamics) we find that a crude adiabatic elimination (henceforth referred to as standard adiabatic elimination SAE) leads to nonphysical high transverse (or longitudinal) spatial wavenumber instabilities [3]. Recent attempts to apply the center manifold technique to the transverse problem have met with mixed success [4]. In fact the high transverse wavenumber instability shows an even stronger divergence than the SAE case for positive sign of the laser-atom detuning. Moreover, the analysis becomes unwieldy even in situations when the center manifold approach appears to work.

We will report on a novel, yet simple approach to adiabatic elimination of the polarization variable from Maxwell-Bloch equations describing transverse spatial pattern formation (and longitudinal mode oscillation) in a homogeneously broadened ring laser.

$$\frac{\partial F}{\partial t} + v\frac{\partial F}{\partial z} = ia\frac{\partial^2 F}{\partial x^2} - \kappa(F + CP)$$

$$\frac{\partial P}{\partial t} = -(1 + i\delta_{AC})P - FD$$

$$\frac{\partial D}{\partial t} = D_f\frac{\partial^2 D}{\partial x^2} - \gamma_\parallel\{-\frac{1}{2}(FP^* + F^*P) + D - 1\}$$

where F, P and D are normalized field, polarization and inversion variables respectively, $\gamma_{\|}\delta_{AC}$ is the atom-cavity normalized detuning, the time $t$ is scaled to the polarization dephasing time $\gamma_{\perp}$, $v$ is the group velocity, $D_f$ a diffusion coefficient and $a$ a diffraction coefficient. The other parameters are $\kappa = \alpha_1|\ln R|/2\pi$ with $\alpha_1 = \frac{2\pi c}{\gamma_{\perp} L}$ the longitudinal intermode frequency spacing. These equations are supplemented by the periodicity boundary conditions

$$F(z=0,x,t) = F(z=1,x,t).$$

Standard adiabatic elimination of the polarization variable from the above set ($P_t = 0$) will decouple the polarization variable from the field equation and introduce arbitrarily high transverse or longitudinal wavenumber instabilites yielding nonphysical behavior. The idea behind our approach is to use the linear dispersion relation

$$\omega_{n,k} = \alpha_n + ak^2$$

for the linear field operator in a rotating wave type of transformation on the Maxwell-Bloch equations in Fourier space, then adiabatically eliminate each Fourier component of the polarization variable before inverting the transform. The end result of this procedure is the following adiabatically reduced set of "rate" equations

$$\frac{\partial F}{\partial t} + v\frac{\partial F}{\partial z} = ia\frac{\partial^2 F}{\partial x^2} - \kappa(F + CP)$$

$$\frac{\partial D}{\partial t} = D_f\frac{\partial^2 D}{\partial x^2} - \gamma\{-\frac{1}{2}(FP^* + F^*P) + D - 1\}$$

where

$$P(z,x,t) = -U(z,x) \otimes \{F(z,x,t)D(z,x,t)\}$$

where $\otimes$ denotes convolution and $U(z,x)$ is the Fourier transformation of the function $1/[1 + i(\delta_{AC} - \omega(n,k))]$. Formally, we have replaced the local operator $P$ in the SAE by a nonlocal operator $P$ which provides a finite gain bandwidth for excitation of transverse and longitudinal modes and a gain discrimination for different modes. In fact, we conjecture that this nonlocal infinite dimensional quantity $P$ defines a globally attracting inertial set, which in the limit $\gamma_{\perp} \to \infty$, reduces exactly to an infinite dimensional global center manifold on which all asymptotic solutions lie.

As an illustration of the robustness of our nonlocal adiabatic elimination technique we have compared instability growth curves for transverse pattern formation and multi-longitudinal mode instabiities for the full model, NAE and SAE models. In order to show a difference between the exact and NAE growth curves we are forced to take $\gamma_{\perp}$ rather small relative to $\gamma_{\|}$ and $\mu$. We remark finally that the condition $\gamma_{\perp} \gg \mu$ is all that is required with no restriction (other than a physical one) placed on the magnitude of $\gamma_{\|}$. In order to test the robustness of the NAE equations (2) we integrated both sets of equation a wide range of initial conditions and found excellent agreement between the two models. By monitoring the nonlocal quantity $P(z,x,t)$, using the exact solution, we verified that the asymptotic solution (after time $t > \gamma_{\perp}^{-1}$) remains within $\gamma_{\perp}^{-1}$ of the inertial set defined by $P$.

# References

[1] J. Carr, "Applications of centre manifold theory (Springer 1981).

[2] G.L. Oppo, A. Politi, in "Instabilities and chaos in quantum optics II". (Plenum Press. New York, London) p. 363 (1988).

[3] P.K. Jakobsen, J.V. Moloney, R.A. Indik and A.C. Newell, Physical Review A (in press).

[4] G.L. Oppo, G. D'Alessandro and W.J. Firth, Physical Review A **44**, 4712 (1991).

# Chaos and Multistability in Bimode $CO_2$ Laser with Saturable Absorber

K.Tanii, T.Sugawara, M.Tachikawa, F.-L.Hong,
T.Tohei, and T.Shimizu

Department of Physics, The University of Tokyo
7-3-1 Hongo, Bunkyo-ku, Tokyo-113, Japan.

Tel. +81-3-3812-2111, ext.4169, Fax. +81-3-5684-5291

**Summary**: Recently, instabilities and chaos in a single-mode $CO_2$ laser with a saturable absorber (LSA) have attracted much attention as a direct access to nonlinear dynamics, such as Shil'nikov chaos and Feigenbaum's period-doubling scenario [1,2]. Introduction of extra lasing modes may bring novel aspects into the laser dynamics and largely extend applicability of the LSA as a model of dynamical systems.

Recently, we have reported that spontaneous periodic mode switching occurs in a bimode oscillation of a $CO_2$ LSA [3]. Our laser oscillates on two lines which are in axial ($TEM_{00}$) and off-axial ($TEM_{01}$) modes of the Fabry-Perot cavity. Only the laser radiation in the axial mode is absorbed by the saturable absorber. The two-mode instability is caused by the combination of the passive Q-switching and the cross saturation between the lasing modes. By considering the transverse spatial overlapping between the modes, we have modified the three-level:two-level model for the single-mode LSA [2] to describe the multimode case. Types of the observed dynamic mode competition have been reproduced with good fidelity by the numerical analysis [3].

In this paper, we report novel aspects of instability and bistability of the bimode $CO_2$ LSA on the basis of the modified version of the three-level:two-level model.

The rate-equation analysis reveals that two types of chaotic bimode pulsation are realized in totally different parameter regions, one of which (type-I) is accompanied by the period-doubling bifurcations as in the case of the single-mode chaos [2,3]. The other (type-II) has no clear standard scenario. Figs.1(a) and (b) show the Lorenz plots constructed from the calculated time series of the axial-mode intensity for the cases of the type-I and type-II chaos, respectively. While the Lorenz plot of the type-I chaos consists of one-dimensional curves, that of the type-II chaos shows two-dimensional distribution.

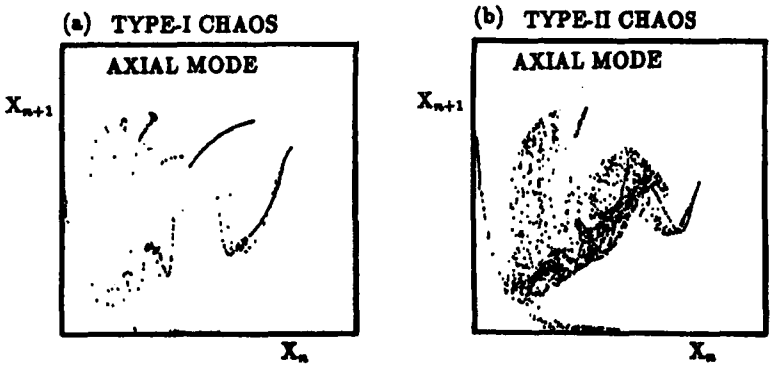


Fig.1 Lorenz plot of the type-I [a] and type-II [b] bimode chaos

In the type-I chaos, the whole laser dynamics is dominated by the temporal behavior of the axial mode and the saturable absorber, and so identical to the single-mode chaos. On the other hand, both modes cooperatively drive the laser system and produce the type-II chaos.

The type-II chaos is observed for the first time in a $CO_2$ laser with a formic acid absorber (see Fig.2). Characteristic features of the Lorenz plot, the fractal dimension, and the Kolmogorov entropy of the observed chaotic pulsation agree quite well with the theoretical predictions.

Besides these instabilities, the present bimode LSA exhibits optical bistability with more complicated hysteresis loops than those generally observed in a single-mode LSA [4] or a multimode laser in the case of strong coupling [5]. Fig.3 shows an example of hysteresis curves calculated as a function of the discharge current. In a real $CO_2$ laser, the excitation efficiency has a peak as a function of the discharge current because of the dissociation of $CO_2$ molecules. This effect is taken into account in the present model. The solid and dashed curves respectively represent stable and unstable stationary solutions of the rate equations.

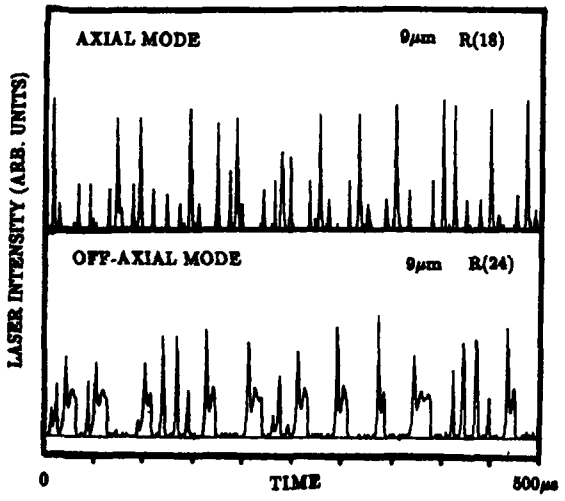


Fig.2 Observed chaotic mode competition.

Below the current of the point D(C'), there are two solutions ($I_C \neq 0, I_S = 0$) and ($I_C = 0, I_S \neq 0$) corresponding to exclusive cw-mode oscillation, where $I_C$ and $I_S$ denote the axial- and off-axial mode intensities, respectively. Below the current of A(A'), both solutions are unstable, and mode-switching instabilities occur. In the current range above D(C'), another solution ($I_C \neq 0, I_S \neq 0$) emerges, corresponding to simultaneous bimode oscillation. When the current is increased from A(A') to E(D'), and then decreased back to A(A'), the axial-mode intensity traces the loop (A→B→C→D→E→F→G→C→B→A), and the off-axial mode goes along (A'→B'→C'→D'→E'→F'→B'→A').

It is interesting to note that the laser system can be switched not only to the state where one mode is on and the other off, but also to the state where both modes are on. So this bistable element can store more information than the ordinary bimode bistable laser [5]. This property may be useful in photonics applications with semiconductor device.

Experiment to search the bistability is now in progress. Preliminary observation supports the present analysis.

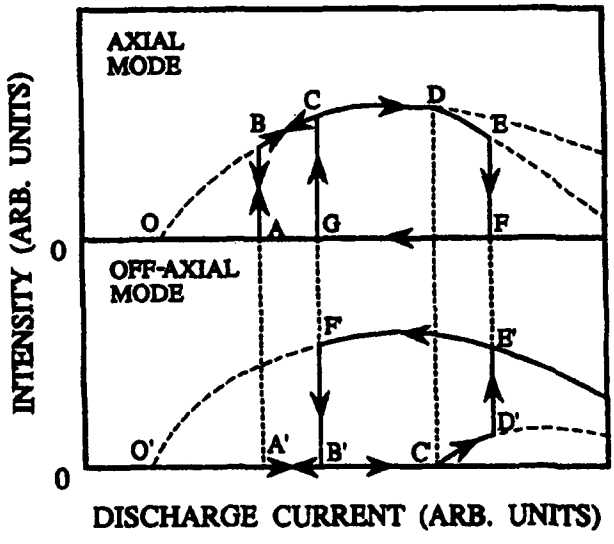


Fig.3 Hysteresis cycle of the laser intensity as a function of the discharge current.

References

[1] D.Dangoisse et al., Europhys.Lett. **6**, 335 (1988)
[2] M.Tachikawa et al., Phys.Rev.Lett. **60**, 2266 (1988)
[3] K.Tanii et al., Phys.Rev.A **43**, 1498 (1991)
[4] E.Arimondo et al., Appl.Phys.B **30**, 57 (1983)
[5] J.R.Rios Leite et al., Tech.Dig. XIV IQEC'86, paper FEE7

# Pulse Pattern Selection and Low Dimensional Modulational Chaos in Fiber Lasers

**M. Haelterman, S. Trillo, and S. Wabnitz**

*Fondazione Ugo Bordoni, Via B. Castiglione 59, 00142 Rome, Italy*

In this work we analyse the process of generation and control of stable or chaotic soliton pulse trains in ultrashort pulse fiber lasers. We reveal the underlying low dimensional homoclinic structure of the nonlinear modulational instability (MI) in a cavity. The onset of spatiotemporal structures in physical systems may often be described in terms of reduced modal expansions which preserve the complexity of the original infinite dimensional model [1]. The advantage of such a reduction procedure is that the transition to chaos may be traced back to the universal bifurcation routes of finite dimensional dynamical systems.

We consider a general model partial differential equation which describes pulse train formation in fiber lasers. This model encompasses several fiber laser structures which have been recently experimentally and theoretically investigated such as the modulational instability ring laser [2], the erbium doped fiber soliton ring laser [3], and coupled cavity lasers [4]. In lossless fibers, the nonlinear dynamics of MI may be well represented by a simple one-dimensional truncated Hamiltonian system [5]. We reveal here that the dissipatively perturbed homoclinic structure of this Hamiltonian system permits a simple description of the nonlinear stage of MI in fiber laser structures.

Pulse propagation in fiber soliton and MI lasers is described by an infinite dimensional map involving the nonlinear Schrödinger (NLS) equation [6,2]. Whenever the characteristic dispersion (or soliton) length which is associated with the propagating pulses is much longer than the length of the fiber in the cavity, pulse formation only occurs over several circulations. As a consequence, averaging procedures may be applied to the periodic pumping and loss and a single partial differential equation results [3,7]. This spatial averaging is similar to the mean field approximation which has previously been introduced for the study of transverse pattern formation in resonators [8]. Note that this result is also valid under large amplitude variations of the field at each passage. In the general case the resulting model for describing the propagation of temporal dissipative field structures in fiber lasers is the following perturbed NLS equation

$$i\frac{\partial v}{\partial Z}+\frac{\eta}{2}\frac{\partial^2 v}{\partial T^2}+|v|^2 v=(\Delta+i\delta)v+(i\nu+\theta)\frac{\partial v}{\partial T}+i\beta\frac{\partial^2 v}{\partial T^2}+i\gamma|v|^2 v+iS, \qquad (1)$$

Here $\eta$ is the sign of group velocity dispersion in the fiber, $\Delta$ is the phase detuning of the cavity, $\delta$ is the residual loss (or gain) in the cavity, $\nu$ is the inverse group velocity in the fiber, $\theta$ is associated with the frequency detuning of the center pulse frequency from the peak value of the gain, $\beta$ is the gain dispersion, $\gamma$ describes the fast saturable absorption (gain) which is introduced by a coupling mirror or a nonlinear switching element, and finally the forcing term $S$ represents an injected signal.

We have examined the role of each term and the interplay between them in eq.(1) in determining the dynamics of the waveform generation process. We have verified that the averaging procedure which leads to eq.(1) is valid over a relatively wide parameter

range by comparing to the numerical integration of eqs.(1) with the solution of the original map. Figure [1a] shows for example the generation of a stable pulse train in the normal dispersion regime of the fiber in a synchronously pumped MI ring laser. Here the only gain mechanism is parametric four wave mixing in the fiber. The repetition rate and the contrast ratio of the pulses may be controlled by varying the frequency and the cavity detuning. Figure [1b] shows pulse train generation in the anomalous dispersion regime in the active fiber soliton ring laser with injected signal. Here there is a finite detuning between the peak frequency of the gain curve and the frequency of the injected signal. Figure [1c] shows the chaotic behavior of the modulated field in a coupled cavity laser.

The low dimensional nature of the dynamics of temporal pattern generation and selection in fiber lasers is revealed by performing a Fourier mode truncation of the field $v$ in eq.(1) to the mean and a few sideband modes [9]. This approach permits to display the stable or chaotic pulse generation from MI by means of phase space trajectories into or around stable attractors (see fig.(2)). This also enlightens the role of the homoclinic structure of the NLS equation [9] in determining the selection between coexisting attractors in the weakly turbulent (chaotic in space, coherent in time) regime. Transition into chaotic regimes is generally characterized by the loss of stability of the pulse train attractors by Hopf bifurcations into limit cycles. The averaged description (eqs[1]) may also be extended to the period-two regime of Ikeda instability in the cavity. In this case the MI is responsible for the regular alternation between two time shifted stable pulse trains over consecutive transits.

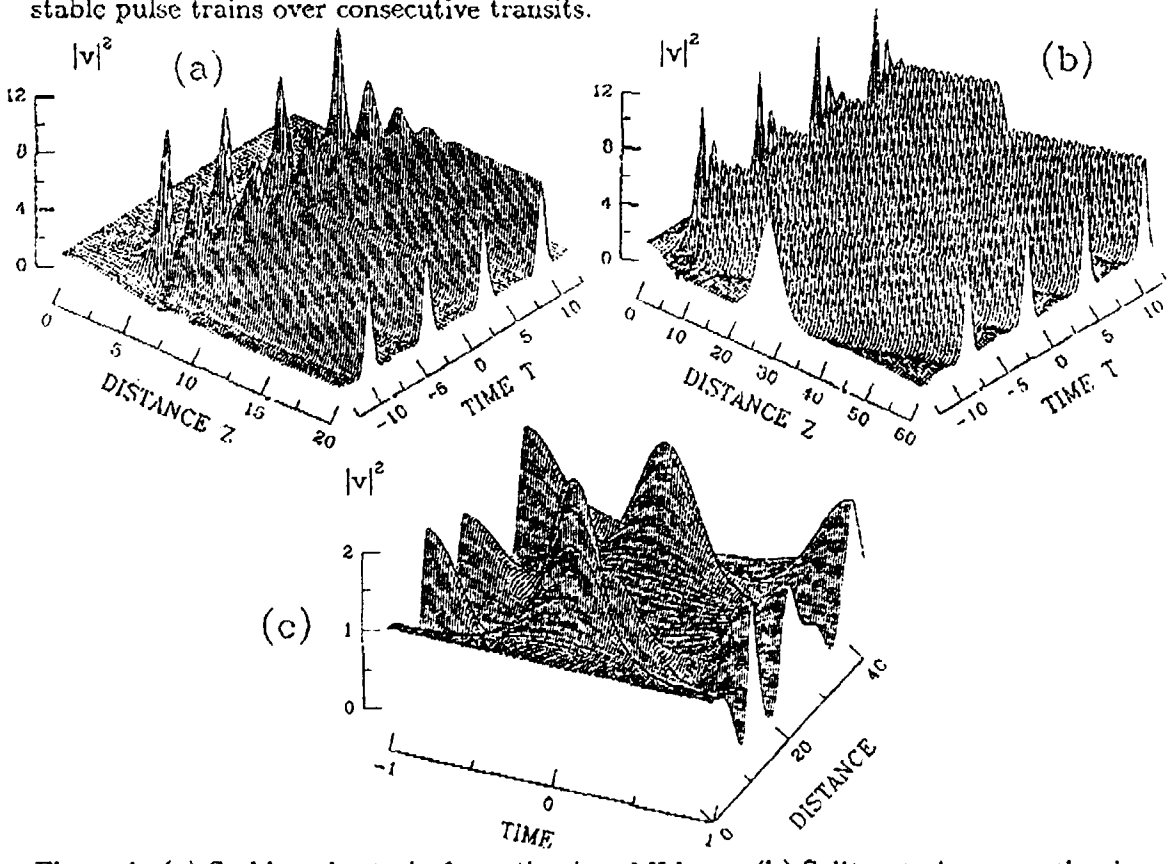


Figure 1: (a) Stable pulse train formation in a MI laser. (b) Soliton train generation in erbium fiber ring laser. (c) Chaotic modulations in a coupled cavity laser.

This work was partially supported by a twinning contract with the Commission of the European Communities, and was carried out under the agreement between Fondazione Ugo Bordoni and the Istituto Superiore Poste e Telecomunicazioni.

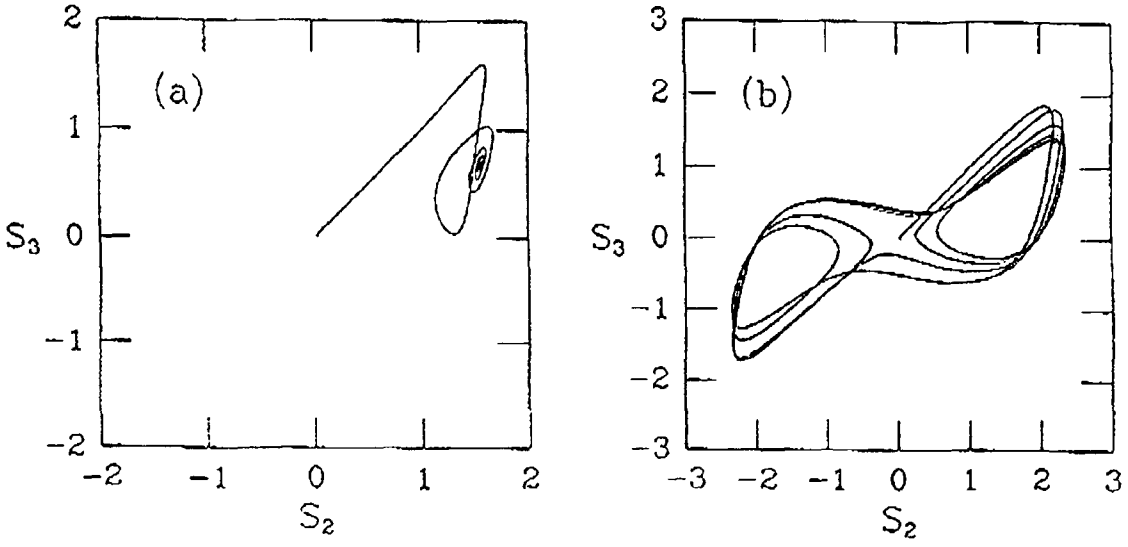


Figure 2: Phase space representation of either (a) stable or (b) chaotic pulse formation process.

## References

[1] P. Manneville, *Dissipative Structures and Weak Tubulence* (Academic, San Diego, 1990).

[2] M. Nakazawa, K. Suzuki, and H.A. Haus, Phys. Rev. A **38**, 5193 (1988).

[3] S.M.J. Kelly, K. Smith, K.J. Blow, and N.J. Doran, Opt. Lett. **16**, 1337 (1991).

[4] P.A. Belanger, J. Opt. Soc. of Am. B **8**, 2077 (1991).

[5] S. Trillo and S. Wabnitz, Opt. Lett. **16**, 1566 (1991).

[6] K.J. Blow and N.J. Doran, Phys. Rev. Lett. **52**, 526 (1984).

[7] A. Hasegawa, and Y. Kodama, Opt. Lett. **15**, 1443 (1990).

[8] L.A. Lugiato and R. Lefever, Phys. Rev. Lett. **37**, 2209 (1988).

[9] A.R. Bishop, M.G. Forest, D.W. McLaughlin, and E.A. Overman, Phys. Lett. A **144**, 17 (1990).

Paper withdrawn

# Quasi Vertical Hopf Bifurcation for the Multimode Class B Laser

Thomas Carr and Thomas Erneux

Northwestern University

Dept. Eng. Sciences and Applied Mathematics

McCormick School of Eng. and Applied Sciences

Evanston, IL 60208

Telephone: (708) 491-5397

Using the rotating wave approximation, Risken and Nummedal [1] have simplified the Maxwell-Bloch laser equations for homogeneously broadened two-level atoms and have analyzed the linear stability of the uniform steady states. They have determined bifurcation points to periodic traveling wave solutions. If I denotes the intensity of the non-zero steady state and a is the spatial wave number of the traveling wave, the first bifurcation occurs at or near $(I,a) = (I_m,a_m)$. See Figure 1. The nonlinear problem has been first investigated by Haken and Ohno [2]. They obtained an amplitude equation of the form

$$\alpha_\tau = A\alpha + B\alpha^2\bar{\alpha} \qquad (1)$$

where $\alpha$ is the amplitude of the traveling wave mode, $\tau$ is a slow time variable and $\alpha_\tau$ means differentiation with respect to $\tau$. The coefficients A and B are complex and were determined numerically for fixed values of the laser parameters. More recently, Fu [3] has reexamined the bifurcation problem for class B lasers. Class B lasers are of particular physical interest and include solid state, semiconductor and $CO_2$ lasers. They are characterized by a small values of $\gamma$, defined as the dimensionless damping constant for the population inversion. As $a - a_m$ is progessively changed from negative to positive values, Fu showed that the direction of bifurcation changes from subcritical (unstable) solutions to supercritical (stable) solutions. This means that Re(B) equals zero at $a = a_m$. The Hopf

bifurcation is called a vertical bifurcation at this order of the perturbation calculations and requires a difficult higher order study. Fu's results are based on a perturbation analysis of Risken and Nummedal's equations valid in the limit $\gamma \to 0$. We have improved his method and derive a new amplitude or bifurcation equation of the form

$$\alpha_\tau = A\alpha + B\alpha^{2-}\bar{\alpha} + C\alpha^{3-2}. \qquad (2)$$

This equation has been obtained assuming first the limit $\gamma \to 0$ and then the limit $I - I_m = O((a - a_m)^2) \to 0$. All coefficients are complex and have been determined analytically. Re(A) and Re(B) are proportional to $I - I_m$ and $a - a_m$, respectively.

This equation leads to a richer discussion of the Hopf bifurcation in the subcritical case (i.e., as $a - a_m < 0$) because it admits two stable steady states. For a large spatial system, the effect of the nearby modes can be taken into account by using the method of multiple scales and by formulating a partial differential equation for the amplitude $\alpha$:

$$\alpha_\tau = A\alpha + B\alpha^{2-}\bar{\alpha} + C\alpha^{3-2} + D\alpha_{\xi\xi}. \qquad (3)$$

In this equation, $\xi$ is a slow space variable and the subscripts $\tau$ and $\xi$ represent partial derivatives. D is new complex coefficient. Because of the $C\alpha^{3-2}$ term, this equation is not the familiar Ginzburg-Landau equation. However, it has been studied recently by van Saarloss and Hohenberg [4]. In the subcritical case, new solutions (localized structures) have been discovered and are of interest for multimode lasers.

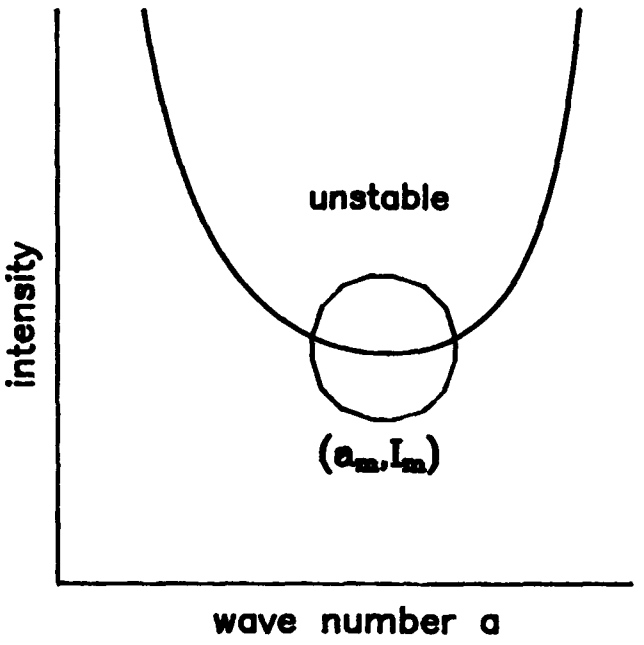


Figure 1. Neutral stability curve of the multimode laser.

References

1. H. Risken and K. Nummendal, Self-Pulsing in lasers, J. Appl. Phys. 39, 4662-4672 (1968).
2. H. Haken and H. Ohno, Opt. Comm. 16, 205 (1976); Opt. Comm. 26, 117 (1978)
3. H. Fu, Analytical self-pulsing solutions and their instabilities in a homogeneously broadened ring laser, Phys. Rev. A40, 1868-1891 (1989)
4. W. van Saarloos and P.C. Hohenberg, Physica D (1992).

# NONLINEAR DYNAMICS OF PHOTON - PHONON LASING IN INDIRECT GAP SEMICONDUCTORS

L.A.Rivlin, A.A.Zadernovsky

Moscow Institute of Radioengineering, Electronics & Automation
78 Vernadsky Prospekt, Moscow 117454, USSR

We investigate nonlinear dynamics of photon-phonon generation in indirect gap semiconductors with aid of rate equations. Due to intrinsic nonlinearity of the two-quantum transitions one can expect a great variety of operation states for the photon-phonon generation.

In indirect gap semiconductors the conduction and valence band extrema are at the different points of the Brillouin zone. Therefore, in such semiconductors interband electron transitions between states close to the band edges can only occur if both photons and phonons are simultaneously involved. If an inverted electronic population is maintained by optical pumping and for sufficiently low temperature of the crystal, these transitions are mainly accompanied by the simultaneous emission of photons and phonons. The emitted phonon can be absorbed in another two-quantum transition including radiation of a photon. Since the phonon energy is much less than that of the photon the probabilities of these processes are similar.

The phonon emission rate, however, can be increased if the photon part of the two-quantum transition including the emission of both photon and phonon is stimulated by light from an appropriate laser source. At a high enough intensity of the stimulating radiation the phonon gain turns out to be equal to the phonon losses in a particular acoustic mode. In this case one can expect the stimulated generation of coherent phonons, i.e. phonon lasing.

The threshold energy flux density P of the stimulating radiation inside the crystal is determined by $P = 2{,}2 \cdot 10^5$ W/cm$^2$ for Ge and $P = 2{,}6 \cdot 10^7$ W/cm$^2$ for Si, whereas the threshold energy flux density of the pumping radiation is $P_o = 5 \cdot 10^2$ W/cm$^2$ for pumping at the wave length $\lambda = 1{,}4$ $\mu$m in Ge and $P_o = 3{,}7 \cdot 10^4$ W/cm$^2$ for $\lambda = 0{,}9$ $\mu$m in Si.

If the phonon lasing is started, the subsequent increase of the pumping rate leads to growth of the photon concentration inside the crystal. This permits us to decrease the intensity externally applied stimulating radiation required to sustain the phonon lasing. At a high enough pumping rate the external source of the stimulating radiation can be switched off and system continues to operate with simultaneous lasing of both photons and phonos.

The threshold value of the energy flux density of the pumping radiation required for the photon-phonon lasing is $P_S = 2{,}2 \cdot 10^5$ W /cm$^2$ for Ge and $P_S = 5{,}3 \cdot 10^7$ W/cm$^2$ for Si.

Routh - Hurwitz criterion is used to investigate stability of the steady state solutions of the rate equations. Conditions are found for the stable operation with phonon lasing and simultaneuos lasing of photons and phonons. The analysis of the rate equations shows that the variations of two controlling parameters - the intensity of stimulating radiation and the pumping rate - leads to a great number of operation states with "smooth" or abrupt change of photon and phonon gain. Stability, bistability and hysteresis of these operation states are investigated.

Paper withdrawn

# INSTABILITIES IN LASERS WITH AN INJECTED DELAYED-FEEDBACK-CONTROLLED SIGNAL

N.A. Loiko, A.M. Samson

Institute of Physics, Academy of Sciences of Belarus,
Skaryna prospekt 70, 220072 Minsk, Republic of Belarus
Fax: 007(0172) 39 31 31

In [1,2] it was shown that control of laser losses or pump by means of delayed feedback (FB) leads to enrichment of the lasing dynamics. Here we present theoretical investigations of a delay effect of the FB forming an injected signal. Both a phase-locked signal and an uncoherent one are considered.

In the first case we investigate a ruby nuclear magnetic resonance (NMR) laser with a phase-locked injection signal which originates from NMR laser itself. Such a device was used in [3] to form the signal with a constant amplitude and a fixed phase difference relative to the laser field. We suggest the modified laser system with a FB that organizes a driving signal with an amplitude depending on a value of the laser output. Moreover, we suppose that the FB includes a delayed line, which keeps the phase locking. The analysis has been made on the basis of Bloch-Kirchhoff equations [3]. In our case a value of the injection signal is proportional to $a \cdot V(t-t_f)$, where $V$ is the transverse nuclear magnetization, $t_f$ is the time of signal passage along the FB loop and $a$ characterizes a FB transition factor.

Investigations of the uncoherent-signal case have been carried out on the basis of a laser model with a delayed loop forming the signal injected into an active medium in the direction perpendicular to the lasing field. The similar system was proposed in [4] for a generation of short pulses in a semiconductor laser and described by rate equations in a case of a small delay time. We have considered an arbitrary length of the FB loop.

Methods for analysis and construction of solutions of the considered systems have been developed. The analysis of the steady-state stability has been carried out. Bifurcation values of the delay $t_f$ at that its effect can change dynamics have been determined. Regular pulsations have been analytically described by means of an asymptotic integration in the instability domains. Their main characteristics and structure have been determined. The stability of the obtained periodic solutions has been investigated.

It is shown that in the case of the NMR-laser with the phase-locked injection signal periodic regimes with a complex relaxational structure exist at considerable values of the delay. Their period $\approx 2t_f$+const and the phase portrait is symmetrical about $V=0$. With decrease in the value $t_f$ the solution structure is simplified tending to harmonic oscillations. A dynamic chaotization arises via a loss of the symmetry and sequential period-dubling bifurcations. At small values of $t_f$ the coexistence of asymetrical solutions is observed.

Steady states of the equations describing a laser with the uncoherent injected signal are unstable if a ratio of

the gain relaxation time to the radiation decay time is comparatively great. There is possible a generation of sequence of short pulses with periods: $T_0=t_f+z$, where z characterizes the time shift between the lasing pulse and nearest of the signal passed along the FB loop and can be considerable, and also $T_n \approx t_f/n$ (n=1,2,3,...). In the last case the pulsing structure depends on the degree of overlapping of this pulses. As the FB depth increases, there appear regimes with periods equal to $(n+1)t_f/n$. They are characterized by the presence on this period of the (n+1)-th pulses with different energies and similar time intervals between them. With increasing $t_f$ these solutions experiences period doubling bifurcations leading to chaos. The regions of realization of individual branches of solutions may overlap, which leads to the coexistence of various attractors in the system.

REFERENCES

1. E.V. Grigoryeva, S.A. Kashchenko, N.A. Loiko, A.M. Samson, Sov. J. Quant. Electr. 20, 938 (1990).
2. E.V. Grigoryeva, N.A. Loiko, A.M. Samson, Technical Digest of EQEC'91, Edinburgh, 89 (1991).
3. R. Holzner, B. Drighetti, M. Ravani, E. Brun, Phys. Rev. A36, 1280 (1987).
4. I.G. Basov, V.N. Morozov, A.N. Oraevsky. DAN SSSR, 168, 550 (1966).

# On the eigenvalues and eigenvectors of an inhomogeneously broadened single-mode laser stability problem

V.Yu.Toronov, L.A.Melnikov

*Chernyshevsky State University,*

*Saratov, 410071, Astrakhanskaya 83, Russia*

Most of works devoted to the stability of inhomogeneously broadened single-mode laser (see Ref.[1] and Refs. in it) concern only the "leading" eigenvalues of corresponding linearized equations which determine the stability of the system steady states. However, in some cases information about all eigenvalues is required, for example to examine the bifurcation of the steady state [2]. The aim of the present work is to find all eigenvalues of the inhomogeneously broadened running-wave single mode laser equations, linearized at the steady state points. Additionally we have considered laser equations in the representation of corresponding eigenvectors (normal form of laser equations [2]).

First we treat as a model system the single mode laser with active medium consisting of $2l + 1$ groups of atoms having different frequencies of spectral lines (one "central" and $l$ pairs of lines, sided symmetrically about "central" line). The equations of motion for this system are:

$$\begin{aligned} dE/dt &= -(\sigma + i\Delta)E + \sigma r \sum_{k=-l}^{k=l} P_k W_k , \\ dP_k/dt &= -(1 + i\omega_k)P_k + ED_k , \\ dD_k/dt &= -b[D_k - 1 + \tfrac{1}{2}(E^* P_k + \text{c.c.})], \end{aligned} \qquad (1)$$

where $E$ is the field amplitude, $P_k$ and $D_k$ are the dipole momentum and population difference of the $k$-th atomic class, $\omega_k$ is the shift of atomic spectral line from the steady-state laser frequency, $W_k$ is the relative amount of atoms of a given class, $\sigma$

and $b$ are the relaxation rates of the field and inversion respectively, $\Delta$ is the difference between the cavity and steady-state frequencies and $r$ is the pump parameter. The Jacoby matrix for this system linearized at the steady state is:

$$\begin{bmatrix} -\sigma, & \Delta, & \sigma r\vec{W}, & \vec{0}, & \vec{0} \\ -\Delta, & -\sigma, & \vec{0}, & \sigma r\vec{W}, & \vec{0} \\ \vec{N}_0^+, & \vec{0}^+, & -\mathbf{I}, & \mathbf{w}, & A_0\mathbf{I} \\ \vec{0}^+, & \vec{N}_0^+, & -\mathbf{w}, & -\mathbf{I}, & B_0\mathbf{I} \\ -b\vec{P}_0^+, & -b\vec{Q}_0^+, & -bA_0\mathbf{I}, & -bB_0\mathbf{I}, & -b\mathbf{I} \end{bmatrix}, \qquad (2)$$

where $\vec{W}$ is the vector with components $(W_{-l},\ldots,W_l)$, $\vec{N}_0$ is the vector of the steady-state values for the population differences of spectral components, $\vec{P}_0$ and $\vec{Q}_0$ are the vectors of the real and imaginary parts of the steady-state dipole momenta , $\vec{0}$ is the zero vector, $A_0$and $B_0$ are the steady-state real and imaginary parts of the field, $\mathbf{I}$ is identical matrix, $\mathbf{w}$ is the diagonal matrix with diagonal elements $\omega_{-l},\ldots,\ \omega_l$ and "+" denotes a column-vector.

We solved the eigenvalue problem for the matrix (2). In Fig.1 the eigenvalues positions are shown. There are few separately placed eigenvalues (denoted as *1,2,3,4,5,6*) and the other ones form three groups (*A*, *B* and *C*) of closely located eigenvalues. The isolated eigenvalues *1,2,3,4* and zero one exist yet for $l$=0 ( pure homogeneous broadening) but the other arise if $l\geq 1$. It was found that the eigenvalues of the groups *A*, *B* and *C* are almost equal to the eigenvalues of the Rabi-flopping problem for the atoms of the partial spectral classes in the steady-state laser field. The eigenvectors corresponding to this eigenvalues have extremely small projections on the field directions in the phase space of the system .

In the limit of continuous atomic spectral distribution the eigenvalues of the groups *A*, *B* and *C* merge in three segments of

lines shown in Fig.1 by dotted lines and the projections of corresponding eigenvectors on the field directions become equal to zero.

We have examined the behavior of the eigenvalues in the wide range of parameters and for different inhomogeneous gain profiles. By decomposing the phase vector of the system along the eigenvectors of the linearized system we have obtained the normal form of laser equations. A study of this equations allows to determine the character of bifurcation from the steady state and to evaluate the role of different degrees of freedom in laser dynamics above second threshold.

References

1. N.B. Abraham, L.A. Lugiato, P. Mandel, L.M. Narducci, D.K. Bandy, J. Opt. Soc. Am. B, 2, 35 (1985)
2. H. Haken, Advanced Synergetics, Springer Series in Synergetics, Vol.20, Springer-Verlag, Berlin, Heidelberg, New York, Tokyo, 1983.

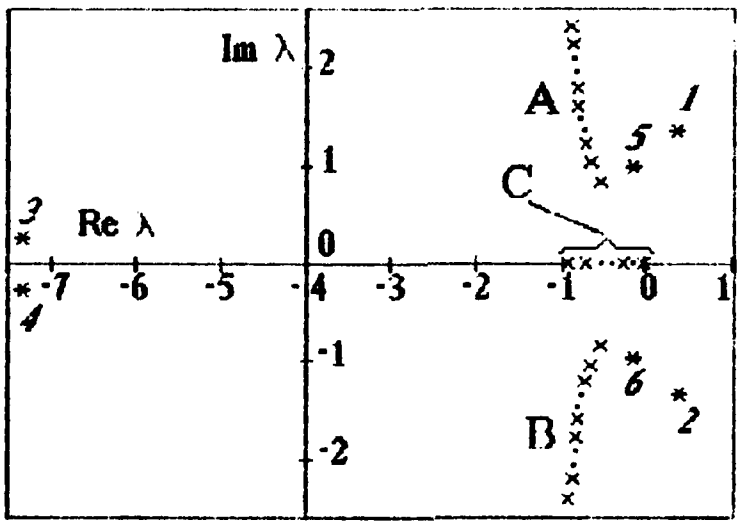


Fig.1 The eigenvalues of the matrix (2) for $l=4$, $\sigma=3$, $r = 15$, $b=0.05$; atomic spectral lines are placed equidistantly with interval $0.5$ and all $W_k$ are equal to $1/(2l+1)$. The detuning of the cavity frequency from the central one is $0.3$.

# SUCCESSIONS OF BIFURCATIONS IN THE LASER WITH A SATURABLE ABSORBER AS DISTRIBUTED SYSTEM

L.A.Kotomtseva, A.M.Samson
B.I.Stepanov Institute of Physics of the
Academy of Sciences of the Republic Belarus
Skaryna prospect 70, Minsk 220072 Belarus
Phone 39-55-21, Fax 7-0172-393131

Results of the investigation of the semiclassical equations for the running wave in the laser with a saturable absorber are proposed on the basis of the system for normalized values and sizeless coordinates

$$\frac{\partial e_i}{\partial z} + \frac{\partial e_i}{\partial t} + f_i e_i = h p_i \sin \Phi_i,$$

$$\frac{\partial \varphi_i}{\partial z} + \frac{\partial \varphi_i}{\partial t} = - h p_i \sin \Phi_i / e_i,$$

$$\frac{\partial p_i}{\partial t} + g_i p_i = a_i k_i e_i \sin \Phi_i , \qquad (1)$$

$$\frac{\partial \psi_i}{\partial t} + g_i (w_c - w_{ai}) = a_i k_i e_i \cos \Phi_i,$$

$$\frac{\partial k_i}{\partial t} = d_i ( 1 - k_i) - b_i e_i p_i \sin \Phi_i,$$

$$\Phi_i(z,t) = \psi_i(z,t) - \varphi_i(z,t).$$

Here $e_i, \varphi_i$ and $p_i, \psi_i$ are the amplitudes and phases of the field and of the polarization of the medium, accordingly, $k_i$ is the relative inversion of populations, $i=1$ for an active medium, $i=2$ for an absorber. Constants $d_i$ and $g_i$ determine the relaxation rates of the inversion of populations and

polarization of the medium, $f_i$ characterizes the distributed losses, $a_i$, $b_i$ and h give the efficiency of the interaction of the polarization and inversion of the medium with the field, $w_c$ and $w_{ai}$ are the frequencies of the cavity and of the medium.

The boundary conditions

$$e_1(0,t)=sRe_2(z_a,t-t_1),\ \varphi_1(0,t)=\varphi_2(z_a,t-t_1)+q_1,$$
$$e_2(z_2,t)=e_1(z_1,t-t_2)/s,\ \varphi_2(z_2,t)=\varphi_1(z_1,t-t_2)+q_2 \qquad (2)$$

connect the amplitude and phase of the field at the input into the active medium $e_1(0,t)$ and $\varphi_1(0,t)$ (into an absorber $e_2(z_2,t)$ and $\varphi_2(z_2,t)$) with their values at the output of an absorber $e_2(z_a,t-t_1)$ and $\varphi_2(z_a,t-t_1)$ (of an active medium $e_1(z_1,t-t_2)$ and $\varphi_1(z_1,t-t_2)$) after reflection on the mirrors R taking into account the time $t_1(t_2)$ of the passage of light from an absorber to the active medium ( from an active medium to an absorber) and additional changes of phases $q_i$.

Steady states of this system taking into account the detuning $w_c-w_{ai}$ are considered and stability of the amplitudes and phases is analyzed.

From one to four pulses during the time of the cavity round trip have been got in computer experiment for the case $w_c=w_{ai}$ with stable phases. Pushing or pulling of the frequencies in such regimes at various parameters is shown. The action of the detuning $w_c-w_{a2}$ on the succession of bifurcations for different beginning conditions is considered. The regular, quasiperiodic and chaotic regimes with constant or alterating

phases are demonstrated for the variation of the leading parameter, such as the rate of the pumping or the length of the cavity. The reasons and mechanisms of the realization of the definite regime in this multistable system are analyzed. The competition of the longitudinal modes , the action of the rates of relaxation and the cavity geomtry explain the amplitude and phase instabilities.

# PULSE TRAIN INSTABILITIES AND PULSE STRUCTURE EVOLUTION IN Nd:YAG LASER WITH ACTIVE MODE-LOCKING

Mel'nikov L.A. Tatarkov G.N.
*Chernyshevsky State University, Saratov, Astrakhanskaya, 83, 410071, Russia*

The low-frequency instability (LFI) of the pulse-train envelope in actively mode locked (AML) laser strongly limits the range of parameters in which the pulse energy and pulse duration may be effectively controlled. It was shown experimentally [1-4] that the detuning of loss modulation frequency about few kHz in Nd:YAG lasers leads to appearance of LFI. Although numerous attempts were made for the theoretical investigation of AML destroying the origins of instabilities remain not clear yet. It was shown also [4,5] that for adequate determination of the width of stable locking region the single-pulse ( for example gaussian pulse [6]) approximation is not valid and it's necessary to include the possibilities of the additive pulse formation within round-trip temporal interval.

The aim of this report is to investigate the subnanosecond pulse autostructure formation and the mechanism determining the LFI and its characteristics.

The pulse transformation in the active medium in the approximation of "thin" amplifier may be written as follows:

$$E'_k(t) = E_k(t) + \alpha P(t) + \eta(t),$$
$$dP/dt = -(\gamma + i\delta)P + NE_k(t),$$
$$dN/dt = -\gamma_{ab}(N-1) - Im(E_k^* P),$$

where $E_k$ is the pulse field envelope at the $k$-th ring cavity round trip ( at the input of active medium ), $E'_k$ is the output field, $\alpha$ is the unsaturated gain, $\gamma$ and $\gamma_{ab}$ are the relaxation rates of medium polarization $P$ and inversion $N$, $\delta$ is the detuning between laser line center and resonator frequencies, $\eta(t)$ is the noise with gaussian statistics which modeled the influence of quantum fluctuation.

The pulse transformation at the loss modulator is:

$$E_{k+1}(t) = E'_k(t) p f(t),$$

where $f(t) = \exp(m(1-\cos(\omega t)))$ is the modulator transmission, $m, \omega$ are loss modulation depth and frequency, $\omega = 2\pi(1/T + \Delta)$, $T$ is the round tripe time, $\Delta$ is the detuning of loss modulation frequency, $p$ is round trip losses. In our calculations $E_k(t)$ is represented as a step-wise function with the step size $0.4\,\gamma^{-1}$.

We investigated the influence of the loss modulation frequency detuning on the dynamics of laser with the next values of parameters: $\alpha = 1.$, $p = 0.9$, $m = 0.2$, $\delta = 0.$, $\gamma = 2\pi \times 100$ GHz, $\gamma_{ab} = 2\pi \times 10$

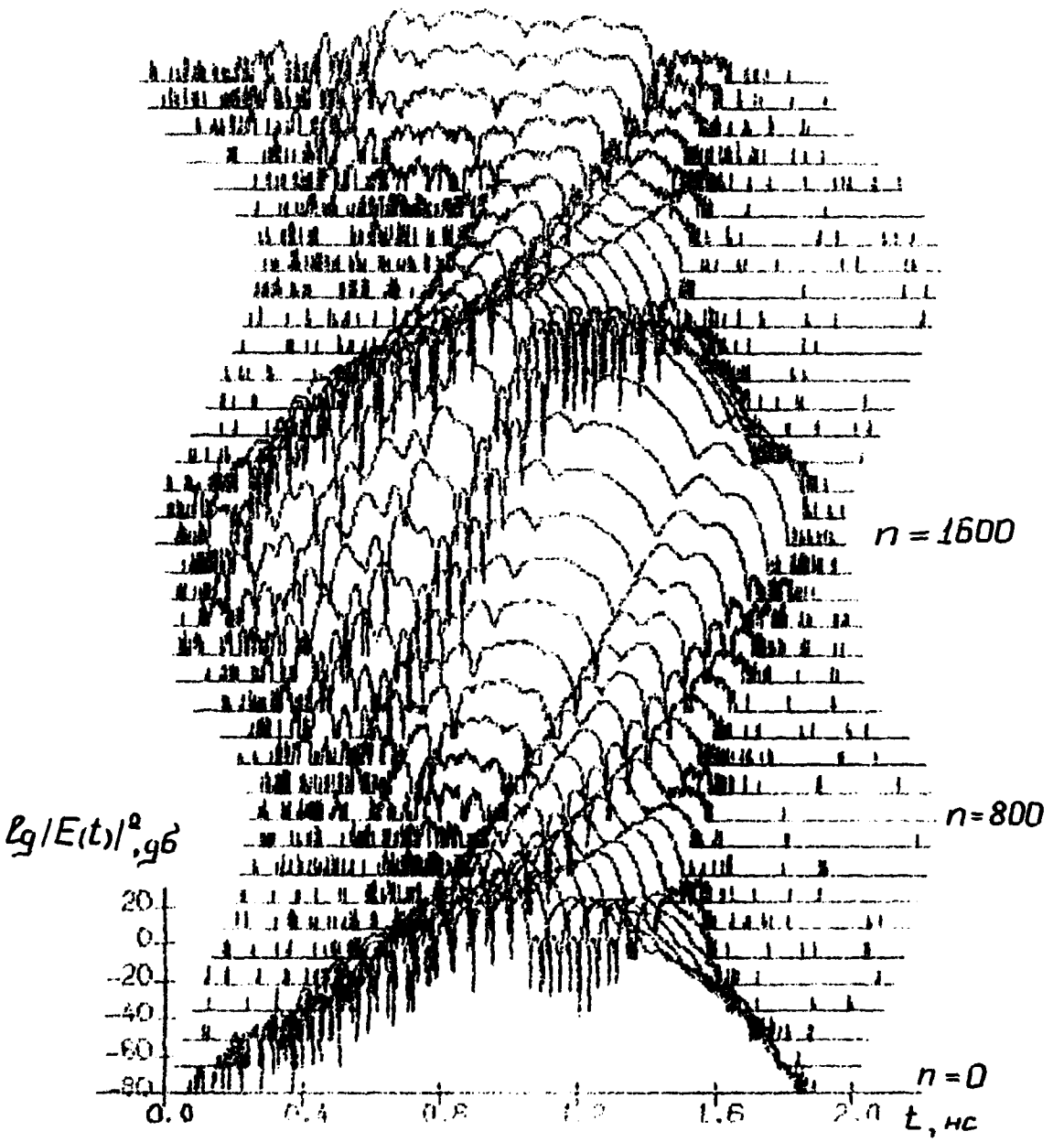


**Fig.1 Pulse shape evolution in the spiking regime. n is round trip number. Δ =10kHz.**

kHz. These values correspond approximately to the Nd:YAG laser.

The noisy distribution $\eta(t)$ was used as an initial field. After some transients the stable AML regime occurred in the region $-8$ kHz$<\Delta<-2$. The pulses with minimum duration about 100 ps are obtained at $\Delta \cong -5$ kHz. This is connected with dispersion delay of pulses in active medium which may be estimated as $\ln(g)/\gamma$, where $g$ is the saturated gain [6].

At the negative and positive detunings $\Delta$ out of stable AML region three types of the unstable regimes were observed: first type is the regime of pulse-train envelope modulation at the frequency $\omega_p$, second type is irregular spiking at frequencies $\omega_p$ or $\omega_p/2$ ( for large $\Delta$ ) and third type is characterized by intermittent temporal behavior between two previous types. In the regime of second type the period of spiking does not vary appreciably meanwhile the instability of the spikes amplitudes increases with the detuning.

The hierarchy of the dynamic regimes observed with the increasing of $\Delta$ is qualitatively similar to the behavior of the Q-switched single-mode laser under the modulation frequency variations and is typical for the systems with nonlinear resonance. The calculations show that the appearance of LFI is connected with the mistuning of pulse period and loss modulation periods which leads to additive effective low-frequency loss modulation. The pulse-structure evolution strongly correlates with the type of the LFI regimes. In the spiking regime as shown in Fig.1 the pulses become multi-humped. During the temporal evolution there is slow sliding of pulses and arising the new ones from noise at the moments of minimum loss. It allows us to suppose that the LFI at these regimes are strongly affected by the level of spontaneous emission as it was pointed out in Ref.4. The arising of subnanosecond pulses from noise fluctuations leads to stochastic structures of pulses, their energy and relative position and consequently to variation of spike amplitude.

*Using the computer simulations the pulse structure evolution and low-frequency pulse-train instabilities in the Nd:YAG laser with active mode-locking are investigated. The different types of laser dynamics are distinguished in the dependence on the loss modulation frequency detuning. The detailed results for pulse profiles and their evolution are presented in the spiking regimes. It was shown that these regimes are characterized by mutual influence of deterministic processes (the nonlinear oscillation of pulse energy) and stochastic sources (spike amplitude modulation due to spontaneous emission). This model may be used for the investigation of other activated-crystal lasers.*


1. Golyaev U.D., Lantratov S.V. -Kvant.elektr. **10**, 925(1983) (Russ.)
2. Eicher H.J., Krauser J.-Opt.Communs. **52**,129(1984)
3. Eicher H.J.-Opt.Communs. **56**, 351(1986)
4. Cormier J., Morin M., Piche M. -Tech.Digest of Nonlinear Dynamics in Optical Systems, 1990 (OSA Washington,1990) p.193
5. Lariontzev E.G. -Kvant.elektr. **12**, 1322(1985) (Russ.)
6. Kuizenga D.J., Siegman A.E. -IEEE J.of Quant.Electr. **QE-6**, 694(1970)

# THE TRANSITIONS TO CHAOS IN THE LASER WITH A SATURABLE ABSORBER

S.A.Tatarkova, V.V.Tuchin

*Chernysheovsky State University*
*Astrakhanskaya 83, Saratov, 410071, Russia*

**Introduction.**

The $CO_2$ laser with a saturable absorber (LSA) generates the continuous pulse sequence which is well known as a passive Q-switching (PQS). Single pulse consists a narrow peak with the long oscillating tail. The pulse length and its shape essentially depends from a choice of the absorbing media and its parameters. The occurrence of chaos in this system has been demonstrated by the experimental and theoretical investigations. Chaos arises according one of the famous scenarios. The theoretical model adequately describing the dynamical characteristics consists of the five differential equations for the field, polarizations and population differences of the amplifying and absorbing cells [1]. In this model LSA has three fixed points corresponding to the trivial laser-off solution and stationary solution. As the recent investigations showed [2,3] depending on the nature of the instability of these points different temporal regimes can arises.

**Model and results.**

For the case of a single mode regime with perfect tuning the equations have the following form [1]:

$$\begin{aligned} dz/dt &= c_1 u + c_2 v - z \\ du/dt &= d_1(xz - u) \\ dv/dt &= d_2(yz - v) \\ dx/dt &= b_1(1 - x - uz) \\ dy/dt &= b_2(1 - y - auz) \end{aligned} \qquad (1)$$

where $1 + z^2$ is dimensionless intensity, $u$ and $v$ are polarizations, $x$ and $y$ are population differences of the amplifying and absorbing cells, $c_1$ is gain coefficient, $c_2$ is absorber coefficient, $d_{1,2} = 2\gamma_{1,2}^{ab}/\Delta\omega_p$, where $\gamma_{1,2}^{ab}$ are the transverse relaxation constants, $b_{1,2} = 2\gamma_{1,2}/\Delta\omega_p$, where $\gamma_{1,2}$ are the longitudinal relaxation constants, $\Delta\omega_p$ is the damping constant of the field in the empty cavity, $a$ is saturation parameter. The system (1) was studied for the parameter values corresponding to $CO_2$ laser with $CH_3I$ as an absorber [4]. These parameters are following: $c_1 = 3.725$, $d_1 = 40$, $b_1 = 0.0024$, $b_2 = 0.001$, $a = 0.5$. As the control parameters the absorber parameters $c_2$ and $d_2$ have been selected.

In Fig.1 the bifurcation diagram of the stationary and pe-

riodic solutions is illustrated. The solution stability and its loss investigated numerically.

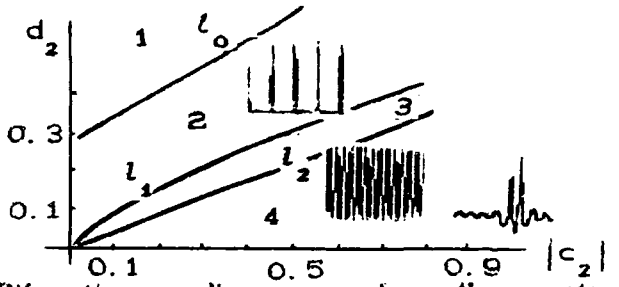


Fig.1. Bifurcation diagram of the steady-state and periodic solutions in the Passive Q Switching Laser.

The trivial laser-off solution is the unstable (saddle) steady-state in the all region of the control parameters - one linear stability coefficient have real positive value. Nonzero steady-state is stable in region 1. This steady-state losses its stability when it is crossing the line $l_0$. The bifurcation is the hard one. As a result the bistability region exists between the continuously oscillating with the constant intensity and pulse generation. The PQS pulse consists of the undamped spikes. The pulse shape essentially depends on the absorber parameter $d_2$. The limit cycle loses its stability on the line $l_1$ when the multiplier crosses the unity circle. For the large absolute value $c_2$ this bifurcation is period-doubling but for the small ones - tangent bifurcation (intermittence). In Fig.2 second case is presented. As illustrated in Fig.2 the temporal evolution of the chaotic attractor is violated by the sudden bursts of the high intensity. This bifurcation arise when the multiplier crosses the unity circle in the point 1.

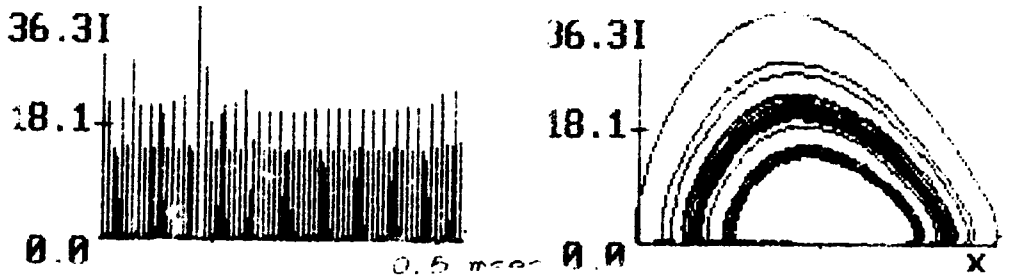


Fig.2. Temporal evolution and phase portrait of the chaotic attractor for the parameters $c_2=-0.6$ , $d_2=0.22$

We study the behavior of the maximum Lyapounov exponent when we move into region 3. The exponent value is equal *0.31* at the appearance moment, and then for $d_2$ *0.2* Lyapounov exponent increases to *0.61*, and for $d_2=0.175$ decreases to *0.40*.

When we cross line $l_2$ limit cycle again becomes stable. The period of this cycle equals *2 μsec* for the point $c_2=-0.6$, $d_2=0.15$

and increases when we move to $c_2=-0.02$.

For the small $d_2<0.001$ the multistability region displays. In this region limit cycles are stable and can be designated $T_{1n}$ in terms [2]. The boundary of the stability regions of these cycles no coincide. When we move to the axis $c_2$ or $d_2$ we discover the transition from the stability region of the cycle with $n$ peaks to the one of the cycle with $n+1$ peaks. Moreover, in this region at least five stable limit cycles can coexist simultaneously which differ in initial conditions. In Fig.3 the shape of PQS-pulses is presented. The period of these pulses equals from 6 to 40 $\mu sec$.

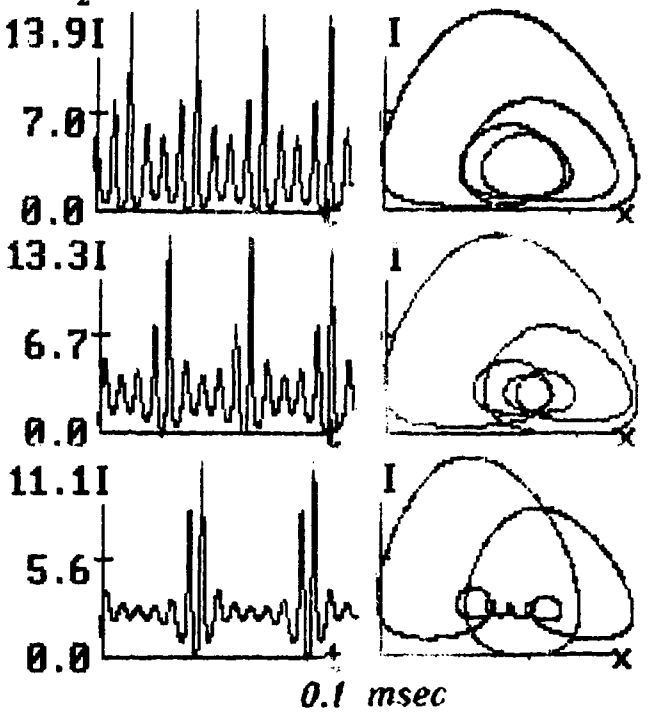


Fig 3. Temporal evolutions and phase portraits of the coexisting limit cycles for $c_2=-0.6$, $d_2=0.0006$.

The unstable fixed points - zero and two nonzero steady states - influence on the form of these cycles. The situation here is similar on the heteroclinic one [5]. The phase trajectory consistently goes round the nonzero steady states and crosses zero point.

**In conclusion** we study numerically system (1) and demonstrate the arising of the chaotic regimes in a Passive Q-Switched Laser. We obtain two scenarios of the transitions to chaos - period-doubling and intermittence. Our results confirm the influence on the laser dynamics the unstable fixed points.

1. L.A.Lugiato, P.Mandel, S.T.Dembinski, A.Kossakovski // Phys. Rev.A **18** (1976) 236.
2. D.Dangoisse, A.Bekkali, F.Papoff, P.Glorieux // Europhys.Lett. **6** (1988) 335.
3. D.Hennequin, F.de Tomasi, B.Zambon, E.Arimondo // Phys.Rev.A **37** (1988) 2243.
4. E.Arimondo, F.Casagrande, L.A.Lugiato, P.Glorieux // Appl. Phys. B **30** (1983) 57.
5. J.C.Antoranz, M.A.Rubio // J.Opt.Am.B 5 (1988) 1070.

# Generalized finite-dimensional model of an inhomogeneously broadened single mode laser

L.A.Melnikov, V.Yu.Toronov

*Chernyshevsky State University,*

*Saratov, 410071, Astrakhanskaya 83, Russia*

Numerical simulation of the dynamics of inhomogeneously broadened lasers requires an enormous computer resources because of their semiclassical models contain infinite degrees of freedom. Therefore the construction of a finite-dimensional models for such lasers is the present-day problem.

In Ref.[1] we have proposed the set of ordinary differential equations which describes the dynamics of the single-mode laser with Lorentz-broadened inhomogeneous spectral line in the case of central tuning of the cavity frequency. The aim of the present work is the generalization of this model for the arbitrary gain profiles and nonzero detuning.

The Maxwell-Bloch equations of motion for the inhomogeneously broadened single mode laser are:

$$dp(\omega,t)/dt=-(1+i\omega)p(\omega,t) + En(\omega,t)$$

$$dn(\omega,t)/dt=-b[n(\omega,t) - 1 + \frac{1}{2}(E^{*}p(\omega,t)+\text{c.c.})] \qquad (1)$$

$$dE/dt= -(\sigma+i\Delta)E + \sigma r\int p(\omega,t)W(\omega)d\omega$$

where $p(\omega,t)$ and $n(\omega,t)$ are the dipole momentum amplitude and population difference of the atoms having transition frequency shift from the line center equal to $\omega$, $E$ is the electric field envelope, $\sigma$ and $b$ are the relaxation rates of the field and population difference, $\Delta$ is the cavity detuning, $r$ is the excitation parameter and $W(\omega)$ is the unsaturated gain profile.

Our model is founded on the decomposition of the atomic dipole momentum and inversion in terms of especially selected set of functions of the frequency shift:

$$p(\omega,t)=\sum_{k=-\infty}^{k=\infty} P_k(t)\phi_k(\omega), \quad n(\omega,t)=\sum_{k=-\infty}^{k=\infty} N_k(t)\phi_k(\omega) \tag{2}$$

where

$$\phi_k(\omega)=exp(ikx), \quad x=2arctg(\omega/\eta). \tag{3}$$

This choice is based on the analysis of $\omega$-dependence of $p(\omega,t)$ and $n(\omega,t)$ in different operation regimes and provide a fast convergence of the series (2). The convergence of these series can be accelerated by choosing of the "width parameter" $\eta$.

Keeping the addenda with $|k|<m$ in expansions (2) one can obtain the set of ordinary differential equations of motion for the coefficients $P_k$ and $N_k$ and the field:

$$\begin{aligned} dP_k/dt &= -P_k + \eta \sum_{l=-m}^{l=m} a_{lk}P_l + EN_k \\ dN_k/dt &= -b[N_k + \delta_{k0} + \frac{1}{2}(E^*P_k + EP^*_{-k})] \\ dE/dt &= -(\sigma + i\Delta)E + \sigma r \sum_{k=-m}^{k=m} W_k P_k \end{aligned} \tag{4}$$

where $a_{lk}=\langle\phi_l|\omega|\phi_k\rangle$, $W_k=\langle\phi_k|W(\omega)|\phi_k\rangle$. In Fig.1 the convergence of solutions of the set (3) to the solutions of original Maxwell-Bloch set (1) is shown. The reliability of our model is examined in the wide range of laser parameters. We consider the possibility to apply our approach to the other laser systems with inhomogeneous broadening.

Reference

1.V.Yu.Toronov, "Simulation of the self-pulsing instability in an inhomogeneously broadened single-mode laser by the finite -dimensional model" in *OSA Proceedings on Nonlinear Dynamics in Optical Systems, N.B.Abraham, E.M.Garmire, P.Mandel,eds. (Optical Society of America, Washington, DC, 1991)*, Vol.7, pp.359-363.

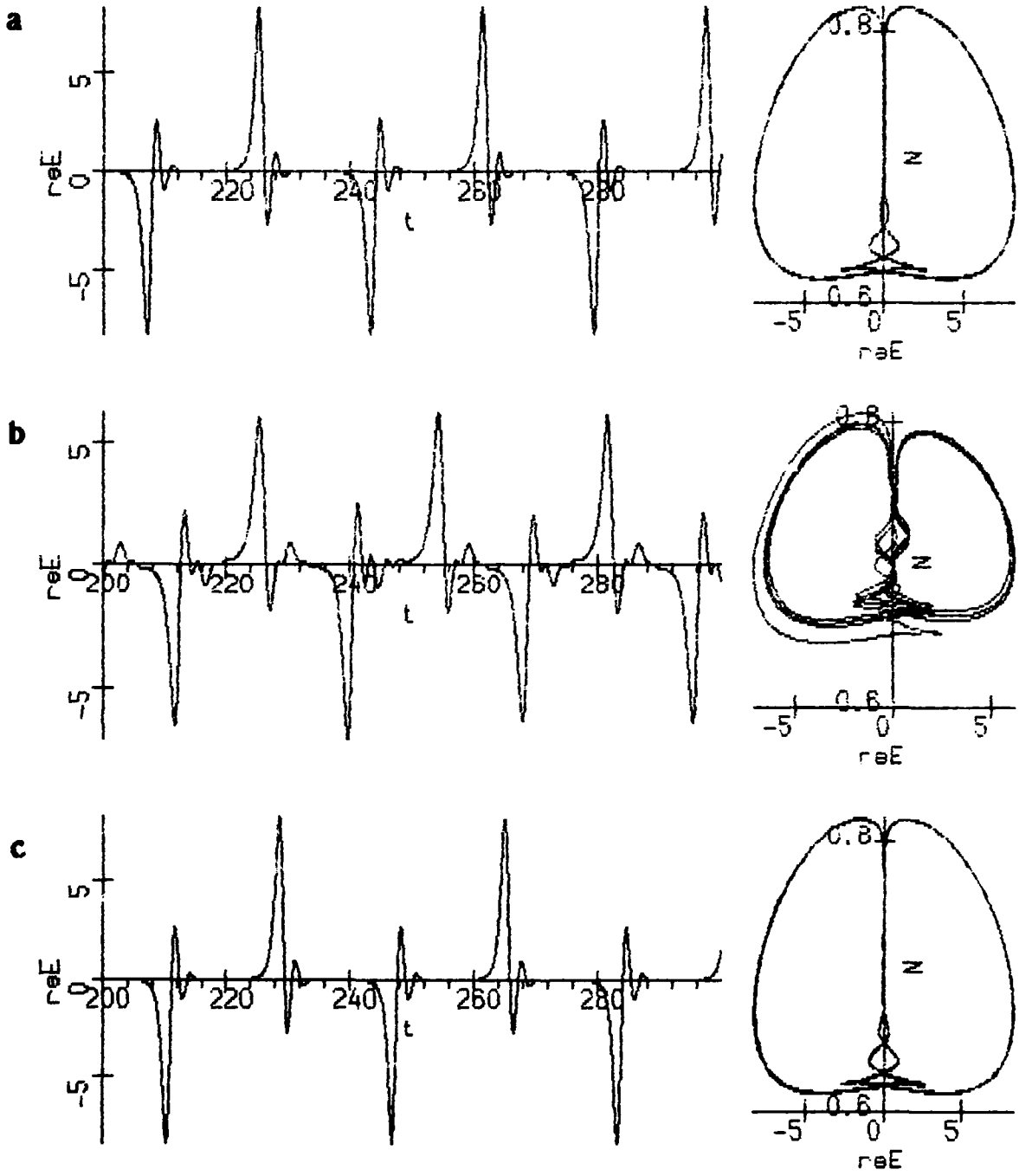


**Fig.1** Time traces of the real part of the field and phase portraits in the field – inversion plane for a) original set of equations (1), and for the set (4): b)$m = 3$, c)$m = 7$. The parameters values are $r = 15$, $\sigma = 5$, $b = 0.05$, $\Delta = 0$. The inhomogeneous gain profile is of the Lorentz-type with halfwidth about five homogeneous ones.

# COMBINATION MODE-MODE COUPLING AS AN INSTABILITY MECHANISM IN A DYE RING LASER

Khanin Ya.I., Koryukin I.V.

Institute of Applied Physics, Russian Academy of Science
46, Uljanov Str., 603600 Nizhny Novgorod, Russia
Tel. (831-2) 384587 Telex 151129 FIZIK SU

The low-frequency time-dependent processes observed in the spectra of class A and class B lasers (according Arecchi [1]) can't be explained using the rate equations. However, by introducing other nonlinear processes of mode coupling in addition to the laser medium saturation one gets a deeper insight into the nature of the multimode laser instability. There was a successful attempt in ref.[2] to take into account the influence of mode coupling on laser action via stimulated Brillouin scattering. However, it should be natural to seek for the reason of the nonlinear mode coupling in the laser medium itself. In the next high-order approximation of the dynamical theory of laser with adiabatically eliminated polarization, the combination mode-mode coupling (CMMC) due to the mode-induced inversion oscillations is taken into account [3-5].

The CMMC as a possible mechanism of time-dependent lasing was considered in a few papers [5-8]. Within the framework of the travelling-wave dye laser model it was shown that the CMMC is responsible for the long-term irregular transient process but it does not lead to an instability [9]. In this paper the mode spectrum was assumed to be equidistant. Under the real conditions, however, the nonequidistancy is highly probable and its key role in the case of the solid-state laser instability has been proven [6,10].

The equations that take CMMC into account can be represented as:

$$dE_k/dt + i(\omega_{ck} - \omega_k)E = kE_k\left\{\mathcal{F}_k\left[n_{\lambda\lambda} - \right.\right.$$

$$\left.\left. - \frac{1}{2}\sum_{\mu,\nu,\rho}\frac{(\mathcal{F}_\mu + \mathcal{F}_\nu^*)n_{k\mu\nu\rho}}{1+i(\omega_\nu-\omega_\mu)/\gamma_\parallel^{-1}}\frac{E_\mu^* E_\nu E_\rho}{E_k}\delta_{k\rho\mu\nu}\right] - 1\right\}.$$

$$\frac{\partial n}{\partial t} = \gamma_\parallel[A - n\ (1+\sum \mathcal{L}_\lambda \psi_\lambda^2\ |E_\lambda|^2)].$$

$$n_{\lambda\lambda} = \int n_0 \psi_\lambda dv, \qquad n_{k\mu\nu\rho} = \int n_0 \psi_\lambda \psi_\mu \psi_\nu \psi_\rho dv,$$

where $E_k$ is the amplitude of the k-th mode of the field, $n$ the normalized saturated inversion, $A$ the nonsaturated inversion (the saturation parameter), $\psi_k$ the eigenfunction of the laser cavity, $\mathcal{L}_k = Re\mathcal{F}_k$, $\mathcal{F}_k = [1+ (\omega_k - \omega_0)^2/\gamma_\perp^2]^{-1}$ the Lorentz function of line shape with the center at the frequency $\omega_0$, $\omega_k$ the laser frequency nearest to the cavity eigenfrequency $\omega_{ck}$, $\gamma_\parallel$ and $\gamma_\perp$ the relaxation rates of the laser medium.

We investigate the influence of control parameters, such as the nonequidistancy, the ratio of the intermode beat frequency to the inversion relaxation rate and the number of modes, on the CMMC efficiency in a ring dye laser. The explicit time dependence of the combination terms, which disappears only in the absence of nonequidistancy, has revealed the analogy between the laser models with CMMC and the balance model with the external modulation of cavity losses. On the basis of this analogy, we obtained the criteria for excitation of deep compensated mode intensity pulsations, witch confine the domain of time-dependent lasing to the low values of nonequidistancy.

These criteria have been confirmed by numerical stimulation. In the absence of nonequidistancy the laser action is steady-state. The same results is obtained in the domain of marginally small nonequidistancies; the modes frequencies calculations show that the laser modes are synchronized in this case. An increase of nonequidistancy leads to time-dependent lasing including chaotic regimes.

witch can again become steady-state with further increase of nonequidistancy. Besides the nonequidistancy, the laser dynamics is strongly dependent on the intermode spacing and the number of lasing modes determining the width and position of the instability region in the parameter space. Inside this region, compensated mode intensity pulsation are developed which can both be regular and chaotic.

1. Arecchi F.T. In: Instabilities and chaos in quantum optics. Eds. F.T.Arecci,R.G.Harrison, N.Y. etc.:Springer Verlag,1987,p.9
2. Aivasijan Yu.M., Baev V.M., Ivanov V.V., Kovalenko S.A. Sviridenkov E.A. Kvantovaya Electronika (Moscow),1987, v.11,p.279
3. Lamb W.E.,Jr. Phys.Rev.,1964,v.A-134,p.1429
4. Khanin Ya.I. JETF,1971,v.60,p.1282
5. Khanin Ya.I. Dynamics of Quantum Oscillators Sov.Radio, Moscow,1975 (in Russian)
6. Viktorov E.A. et al. Optika i spektroskopiya, 1990,v.68, p.920
7. McMackin I.,Radzewicz C.,Beck M.,Raymer M.G. Phys.Rev.A. 1988, v.38,p.820
8. Beck M.,McMackin I.,Raymer M.G. Phys.Rev.A.,1989,v.40, p.2410
9. Kovalenko S.A.,Semin S.P.Toptygin D.D. Kvantovaya Electronika (Moscow),1991,v.18,p.451
10. Viktorov E.A et al. Izvestiya Akad.Nayk.SSSR, Ser.fiz., 1990, v.54, p.2388

# CHAOTIC BEHAVIOR ASSOCIATED WITH A MULTICODIMENSION BIFURCATIONS IN A LASER WITH A SATURABLE ABSORBER

A.G.Vladimirov
Research Institute of Physics,
St.Petersburg State University,1,Ulianovskaya st.,
St.Petersburg-Petrodvoretz, 198904,RUSSIA
Fax: (812) 4286649, E-mail: apver @ onti.phys.lgu.spb.su

It has been shown both theoretically and experimentally that a laser with a saturable absorber (LSA) may exhibit various types of chaotic behavior. Theoretical investigations of such behavior in LSA with $CO_2$ amplifying medium has been carried out on the basis of three level : two level rate equation model [1]. In order to improve the agreement between the model and experimental observations the extension of the model including the polarization of molecular absorber has been proposed in Ref.[2]. It has been shown in [2] that a new types of chaotic regimes arise due to the time lag between the polarization and field. Here we show that these chaotic regimes are associated with a codimension- four bifurcation point. We present the detailed investigation of the bifurcation sequences leading to chaotic operations in the vicinity of this point in the case of detuned LSA .

The equations under consideration are similar to those in Ref.[2] but include the phases of electric field and

polarization in the absorbing medium as well as frequency detuning. We consider the bifurcation point in the parameter space for which complex Jacobian matrix of the zero intensity stationary solution of LSA equations has a triple zero eigenvalue. In the vicinity of this point the application of normal form theory yields three reduced equations governing local dynamics:

$$\begin{aligned} dx/d\tau &= y, \\ dy/d\tau &= x - (\lambda_1 + i\lambda_2)y - xz, \\ dz/d\tau &= -\alpha z + |x|^2, \end{aligned} \qquad (1)$$

where x and y are complex variables, z is real variable. The parameters $\lambda_1$,$\lambda_2$, and $\alpha$ are real. In the case of perfect tuning ($\lambda_2$=0) the dynamics of the reduced equations (1) is equivalent to that of Shimizu- Morioka equations [3]. These equations has been proposed in Ref.[4] and has been shown to posses various types of chaotic solutions [5]. Here we investigate the influence of frequency detuning on the chaotic solutions of reduced equations and find the typical bifurcations leading to chaotic behavior in detuned LSA. We consider the limit $\alpha \to 0$ in Eqs.(1), which more closely represents experimental situation and investigate the bifurcations, which are responsible for the origin of the periodic and chaotic Q- switching in LSA. We study these bifurcations using 1D map.

## REFERENCES

1.M.Tachikawa, K.Tanii, and T.Shimizu, J. Opt. Soc. Am., B5, 1077 (1988)

2.F.de Tomasi, B.Zambon, and E.Arrimondo, OSA Proceedings on Nonlinear Dynamics in Optical Systems, (Optical Society of America, Washington, D.C.,1991),vol.7, pp.377-381

3.A.G.Vladimirov and D.Yu.Volkov in Quantum Electronics Laser Science, 1991 Technical Digest Series,vol.11 (Optical Society of America, Washington, D.C.,1991), p.98

4. T.Shimizu and N.Morioka, Phys. Lett. A76, 201 (1980)

5.A.L.Shil'nikov, submitted to Physica D

# DYNAMICS OF CW SOLID-STATE LASER WITH SATURABLE ABSORBER

E. A. Viktorov, A. A. Mak, O. A. Orlov, V. I. Ustyugov

S. I. Vavilov State Optical Institute

St. Petersburg, 199034, Russia

Phone & FAX: (812) 2185734

The investigations of cw operation of solid-state laser with narrow bandwidth intracavity saturable absorber are interesting from a view point of nonlinear dynamics problems as well as for spectroscopic applications. A number of publications was devoted to the matter, but as for the experimental works, they were carried out only with gas lasers[1,2] (we do not mention here great number of experiments with broad-band saturable absorbers).

The preliminary results of our experiments with YAG:Nd lasers with intracavity molecular cesium cell were reported earlier[3] in connection with frequency stabilization problem and possibility to develop laser frequency standard at the wavelength of 1.06 μm. Frequency servo system with out-of-cavity $Cs_2$-cell provided stability level of the order of $10^{-10}$ - $10^{-11}$ rel. un.[4] Intracavity technique seems to be perspective, one can predict the stability level of the order of $10^{-12}$ rel. un.[3]

In order to realize this potentiality, some problems of dynamics of solid-state laser with intracavity cesium cell should be investigated. In particular this is the dependence of dynamics on fine tuning of laser frequency over Lamb dips of the molecular cesium absorption spectrum. Our report is devoted to these issues.

The sub-Doppler spectrum of saturable absorption of $Cs_2$ on the region of YAG:Nd laser tuning at 1.06 μm represents a rich set of homogeneously broadened lines (Lamb dips) corresponding to various vibration-rotation components of the transition $X_1\Sigma^+_g \rightarrow A_1\Sigma^+_u$. Two relaxation times, both in nanosecond region, appeared to be sufficient for laser dynamics, i.e. decay times of the upper level of molecule $Cs_2$ and lower laser level of $Nd^{3+}$-ion. When the laser is tuned exactly to the center of a Lamb dip, one can expect that experimental results should fit to the theoretical prediction based on

the results of Ref.[5]. Actually, we observed the corresponding sequences of periodical regimes, PQS and PQS with ringing tails, as well as chaotic behavior.

We investigated the dependence of laser dynamics character on saturation power of $Cs_2$. In experiment this saturation power can be varied in the wide range by cesium cell temperature. We founded, that at the exact tuning to $Cs_2$-line center this dependence is in qualitative accordance with the analysis based on Ref.[5]. Our theoretical model was modified in order to analyze the role of detuning. The numerical simulation gave the results which satisfactory fit the experiment. In such experiment we observed various dynamics effects, particular, the dependence of pulse repetition rate on laser frequency tuning over $Cs_2$-line.

**Reference**

1. M.Tochikawa, K.Tanii, T.Shimizu, "Laser instabilities and chaotic pulsation in a $CO_2$ laser with an intracavity saturable absorber". J. Opt. Soc. Amer. B, 1989, vol.5, pp.1077-1088.

2. D.Dangoisse, A.Bekkali, F.Papoff, P.Glorieux, "Shilnikov Dynamics in a Passive Q-switching Laser", Europhys. Lett., 1988, vol.6, pp.335-340.

3. S.N.Labinskii, A.A.Mak, O.A.Orlov, V.I.Ustyugov, "Ultrasensitive intracavity spectroscopy with solid-state lasers and the problem of long-term laser frequency stabilization in the 1-μm region", in Quantum Electronic Laser Science, 1991 Technical Digest, v.11, (OSA, Washington, D.C., 1991), p.234.

4. A.A.Mak, V.I.Ustyugov, "Amplitude and frequency stabilization of solid-state lasers", Proc. SPIE, 1989, vol 1132, pp.58-62.

5.B.Zambon, "Theoretical investigations of models for the laser with a saturable absorber: a case of homoclinic tangency to a periodic orbit", Phys.Rev.A, 1991, vol.44, No.1, pp.688-702.

# Thin Layer Lasers

A. N. Oraevsky
P. N. Lebedev Physics Institute
Russian Federation

A theory of a thin layer laser is presented, i.e., a laser whose active medium length along the wave propagation is less than the wavelength. It is shown that such a laser exhibits a number of peculiarities compared with an ordinary laser.

# Influence of Velocity-Changing Collisions on Single-mode Inhomogeneously Broadened Laser Dynamics

B. Meziane and H. Ladjouze

Ecole Nationale Supérieure des Sciences Appliquées et de Technologie,

6,rue de Kérampont, BP 447, Lannion Cedex, France

The single-mode inhomogeneously broadened [SMIB] laser in the bad cavity configuration has now become a classic example in the demonstration of low-excitation instabilities in nonlinear systems. The general theoretical models in terms of integro-differential "Maxwell-Bloch" equations have for long been shown to be quantitatively accurate for the description of spontaneous pulsations, experimentally obtained in high-gain lasers such as the He-Xe[1,2]. In terms of dynamical aspects these equations are, because of a polarization integral, of infinitely high dimensions, rendering the physics of the behavior rather inscrutable. Recently we have constructed a much more tractable model which consists of only 6 differential equations, yet its deep numerical investigation has shown a one to one qualitative analogy with the infinite-D set of equations in a large range of values of the various control parameters [3]. The simplicity of our model resulted in the clarification of much of the physical insight connected with SMIB laser dynamics.

In this paper we include spectral cross-relaxation terms in the 6-D model and undertake a systematic study of their influence on the general dynamical behavior of the system. The importance of such terms which stem from strong velocity-changing collisions in the lasing medium has already been pointed out [4], but no attempt has been made to characterise their exact role.

Including spectral cross-relaxation terms in the equations derived in ref.3 yields the following set:

$$\frac{d}{dt}E(t) = -k\{E(t) + 2C[2p_r(t) + p_o(t)]\} \tag{1a}$$

$$\frac{d}{dt}p_r(t) = -p_r(t) + wp_i(t) + E(t)D(t) \tag{1b}$$

$$\frac{d}{dt}p_i(t) = -p_i(t) - wp_r(t) \tag{1c}$$

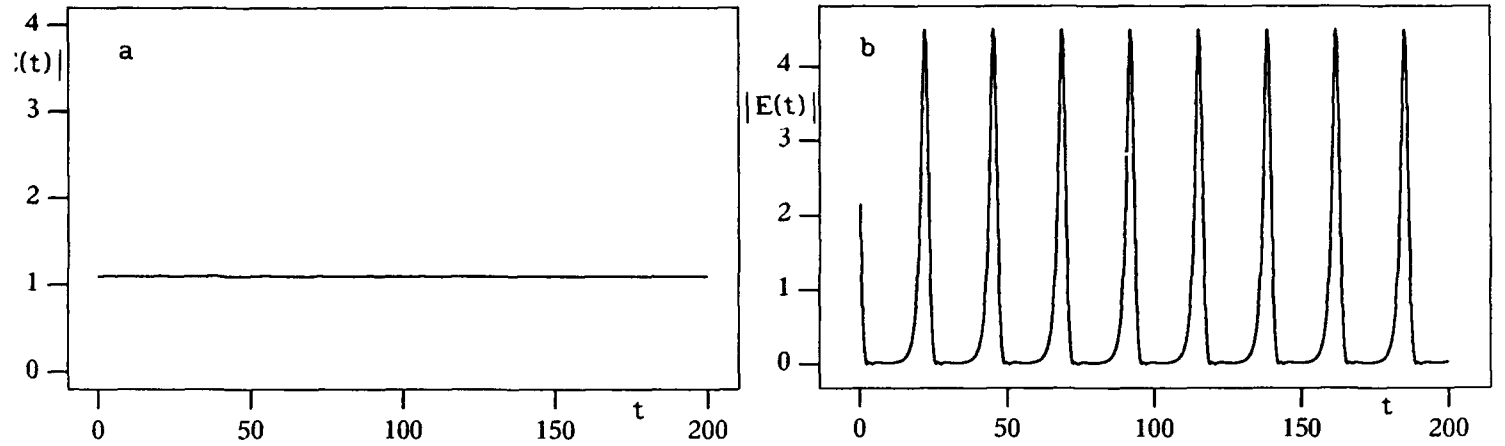


**Fig.1** Time dependence of $|E(t)|$ for k = 5, $\gamma$ = .05, and $X_s$ = 1.1 :a)stable output, and b)regular pulse train, obtained respectively without, and with the inclusion of spectral cross-relaxation terms.

---

$$\frac{d}{dt} D(t) = -\gamma\{D(t) + 1 + E(t)p_r(t) + \varepsilon D(t) - \mu D_o(t)\} \qquad (1d)$$

$$\frac{d}{dt} p_o(t) = -p_o(t) + E(t)D_o(t) \qquad (1e)$$

$$\frac{d}{dt} D_o(t) = -\gamma\{D_o(t) + 1 + E(t)p_o(t) + \varepsilon D_o(t) - 2\mu D(t)\} \qquad (1f)$$

The effect of velocity-changing collisions has been introduced through the parameters $\varepsilon$ and $\mu$.

A set of waveforms as obtained from numerical calculations with parameter values corresponding to the high gain He-Xe laser are shown in Fig.1a and Figs.2a-c, in the case where spectral cross-relaxation terms are neglected , and in Fig.1b and Figs.2b-d when they are included. These first results are suggestive of the following remarks:

i)The inclusion of strong velocity-changing collisions yields a lowering of the instability threshold (compare Fig.1a with Fig.1b, both obtained with the same pumping parameter).

ii)The low excitation period-doubling route to chaos found in the absence of cross-relaxation terms disappears in favor of regular pulse trains as shown in Figs.2a-b, and Figs.2c-d. Other Numerical scans show however that the period-doubling route inherent to the system is still a characteristic of eqs.1 with the inclusion of velocity-changing collisions, but at much higher excitation parameters. This would partly explain the difficulty of experimentally achieving clear hierarchical dynamics such as period-doubling routes with physically accessible pumping levels [5].

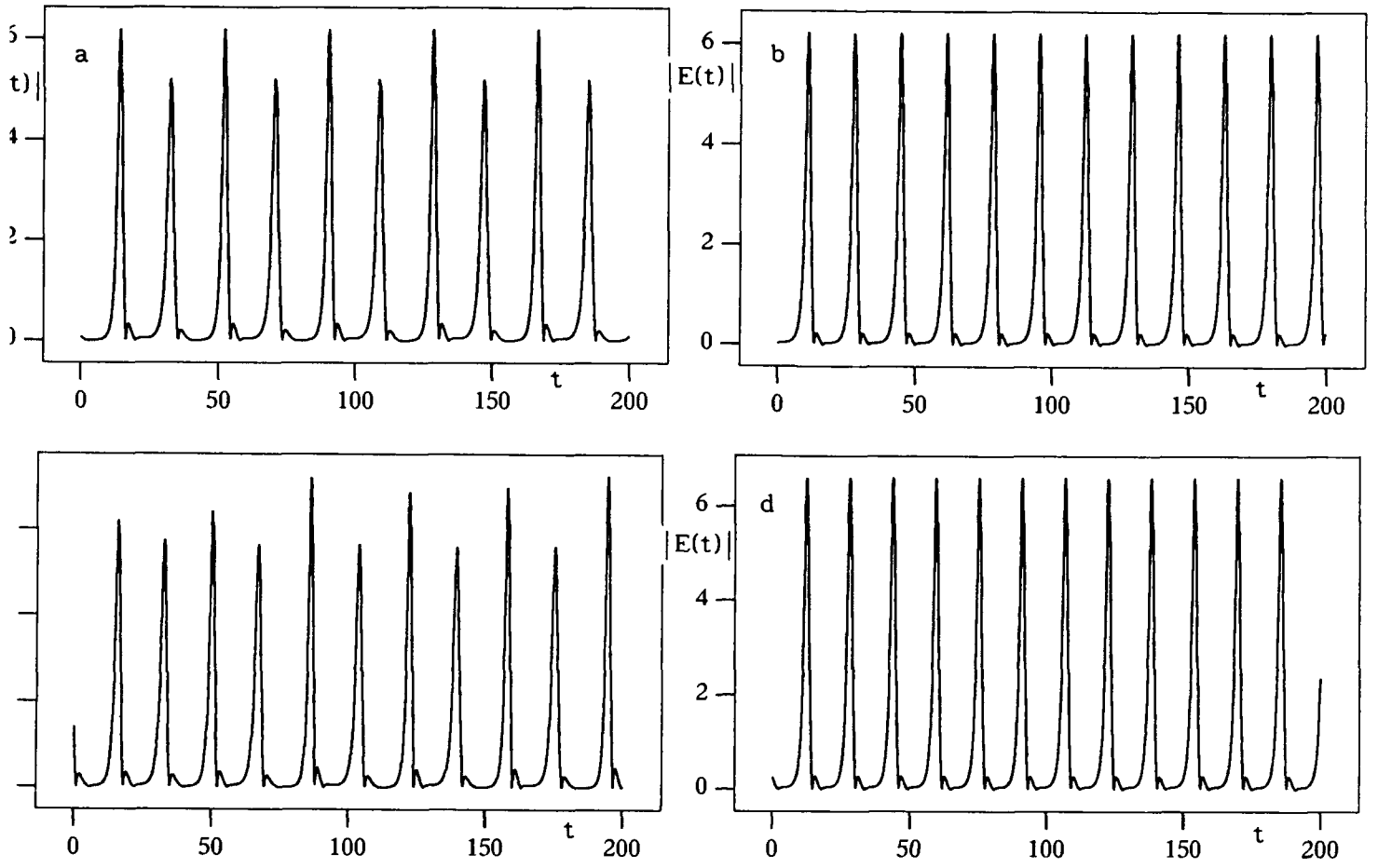


**Fig.2** Comparison of spontaneous pulsation waveforms obtained, respectively without (a,c), and with (b,d) the inclusion of spectral cross-relaxation terms The excitation parameter is $X_s$ = 1.75 (Figs.a,b), and $X_s$ = 1.9 (Figs.c,d).

These first results demonstrate that the description of unstable SMIB laser properties is possible with simple models, which offer straightforward numerical handling, and better insights into the physical mechanisms connected with SMIB laser dynamics than do the usual inscrutable equations. The inclusion of strong velocity-changing collisions in the dynamical equations surprisingly shows a lowering of the instability threshold as well as a reduction of the chaotic behavior.

**References**

**1** - L. W. Casperson and A. Yariv, IEEE J.Quant. Electron., vol.QE-8, 69 (1972)

**2** - L. W. Casperson, J. Opt. Soc. Am. B2, 62, (1985).

**3** - B. Meziane and H. Ladjouze, Phys. Rev. A, to be published.

**4** - L. W. Casperson, J. Opt. Soc. Am. B2, 73 (1985).

**5** - M. F. Tarroja and al., Phys. Rev. A, vol. 34, N°4, 3148 (1986).

# Nonlinear Dynamics of the broadband Dye Ring Laser with Regulated Cavity Dispersion

S. E. Vinogradov, A. A. Kachanov, S. A. Kovalenko,
E. A. Sviridenkov, V. V. Ivanov
Moscow
Russian Federation

Summary not available at press time.

# From harmonic to pulsating periodic solutions in intracavity second harmonic generation

Nicolas Pettiaux
*Université Libre de Bruxelles, Campus de la Plaine, C.P. 231,*
*1050 Bruxelles, Belgium.*
Tel: +32.2.650.58.22,
Fax: +32.2.650.58.24
and
Thomas Erneux
*Department of Engineering Sciences and Applied Mathematics,*
*Northwestern University, Evanston IL 60208, USA*

We consider the problem of Second Harmonic Generation (SHG) inside a resonant cavity, pumped by an external laser. The elementary process that takes place in SHG is the absorption of 2 photons of frequency $\omega$ and the emission of one photon at frequency $2\omega$. Drummond et al[1] have shown that this problem can be modeled by two ordinary differential equations for the (complex) amplitudes of the electrical fields:

$$\frac{dR_1}{ds} = -\gamma R_1 + \bar{R}_1 R_2 + E, \qquad (1)$$

$$\frac{dR_2}{ds} = -R_2 - R_1^2, \qquad (2)$$

where overbar means complex conjugate. We use normalized variables, $R_1$ for the fundamental mode, $R_2$ for the second harmonic mode and $E$ for the input field amplitude that is chosen as real and positive. The real constant $\gamma$ is the ratio of the relaxation constants $\gamma = \gamma_1/\gamma_2$ of modes 1 and 2 in the cavity. The time is scaled to the cavity decay rate $\gamma_2$ of the second harmonic mode.

The steady and time periodic periodic solutions of Eqs.(1) and (2) have been investigated in detail in [2, 3]. They showed that this system displays two important bifurcation features: (i) a Hopf bifurcation to harmonic periodic solutions, (ii) bistability of periodic solutions.

A bifurcation diagram of the periodic solutions for SHG is shown in Figure 1. In this figure, we represent the maximum of $\Im(R_1)$ as a function of $E$. Full (broken) lines correspond to stable (unstable) periodic solutions). The Hopf bifurcation is located at $E = 1$ and bistability occurs for $7 < E < 8$. A dramatic qualita tive change of the periodic solutions appears in this domain of bistability: the "lower" branch, starting at the Hopf bifurcation of the steady state and finishing at the limit point corresponds *harmonic solutions*. The "upper" branch starting at the left limit point and going to the right corresponds to *pulsating solutions*. The first branch is well approximated by the Hopf bifurcation result[3]. The amplitude of the oscillations follows a $(E-1)^{1/2}$ law. On the other hand, the amplitude of the pulsating periodic solutions follows a different law. We show that the amplitude changes as $E^{2/3}$ as $E \to \infty$.

Because the hysteresis domain appears for moderate values of $E$, we cannot analyze the two branches of stable periodic solutions. Since the branch of harmonic solutions is well described by the perturbation analysis valid near the Hopf bifurcation, we propose to describe the branch of pulsating solutions by an asymptotic analysis valid as $E \to \infty$.

For the simplicity, we consider the case $\gamma = 0$. We introduce the new variables $r_1, r_2, t$ and the new parameter $\eta$ defined by

$$R_1 = E^{1/5} r_1, R_2 = E^{1/5} r_2, \quad t = E^{1/2} s \text{ and } \eta = E^{1/2}. \qquad (3)$$

and the decompositions

$$r_1 = x + iu \text{ and } r_2 = y + iv, \qquad (4)$$

The limit $E$ large now corresponds to $\eta$ small.

The long time periodic solution of these equations for $\eta = 0.008$ is shown in Figure 2. The figures suggest that the periodic solution consists of a periodic sequence of pulses first in $u$ and $y$ ($x$ remaining small) and then in $x$ and $y$ ($u$ remaining small). This suggests to apply the method of matched asymptotic expansions[4].

The method consists of determining separate approximations for different parts of the solution. These different approximations are then connected by using appropriate matching conditions.

From Figure 2, we note that the pulsating periodic solution consists of four different parts, namely:

**Stage 1:** $x$ and $v$ are small, $y$ and $u$ are large

**Stage 2:** $u$ and $v$ are small, $x$ and $y$ are large

**Stage 3:** $x$ and $v$ are small, $y$ and $u$ are large

**Stage 4:** $u$ and $v$ are small, $x$ and $y$ are large

We analyze in detail stage 1 and stage 2 as well as their connection. Of particular interest is the matching between the different approximations. We then briefly describe the contributions of the following stages.

We show that the duration of the pulse is

$$\Delta T = -\frac{4a}{C} \ln \eta, \qquad (5)$$

where $C$ is the maximum of $x$ and $a$ is the exponent used in the asymptotic development

$$x(T, \eta^{4a}) = \eta^a \left[ x_0(T) + \eta^{4a} x_1(T) + \ldots \right]. \qquad (6)$$

## References


[1] P.D. Drummond, K.J. McNeil and D.F. Walls, Optica Acta **27**, 321 (1980);

[2] P. Mandel and T. Erneux, Optica Acta **29**, 7-21 (1982).

[3] P. Mandel, N.P. Pettiaux, W. Kaige, P. Galatola and L.A. Lugiato, Phys. Rev. A **43**, 424-432 (1991);

[4] T. Erneux, "Bifurcation analysis in nonlinear optics", ULB Lecture notes in nonlinear optics, 1991.


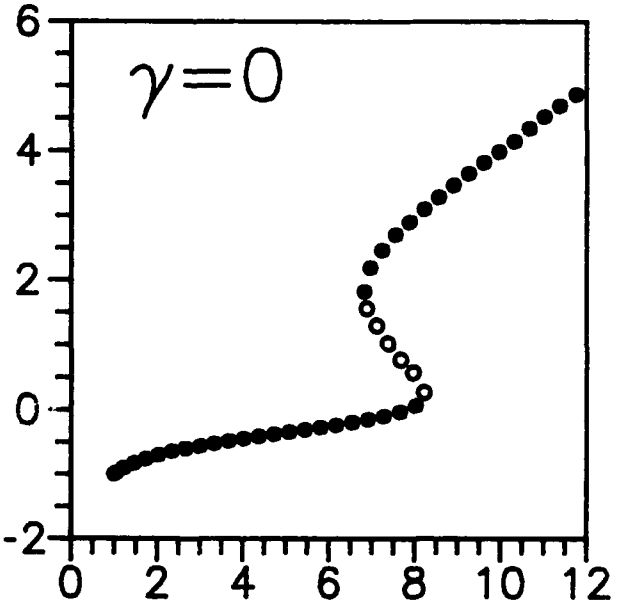


Figure 1: bifurcation diagram for SHG, $\gamma$ =0.

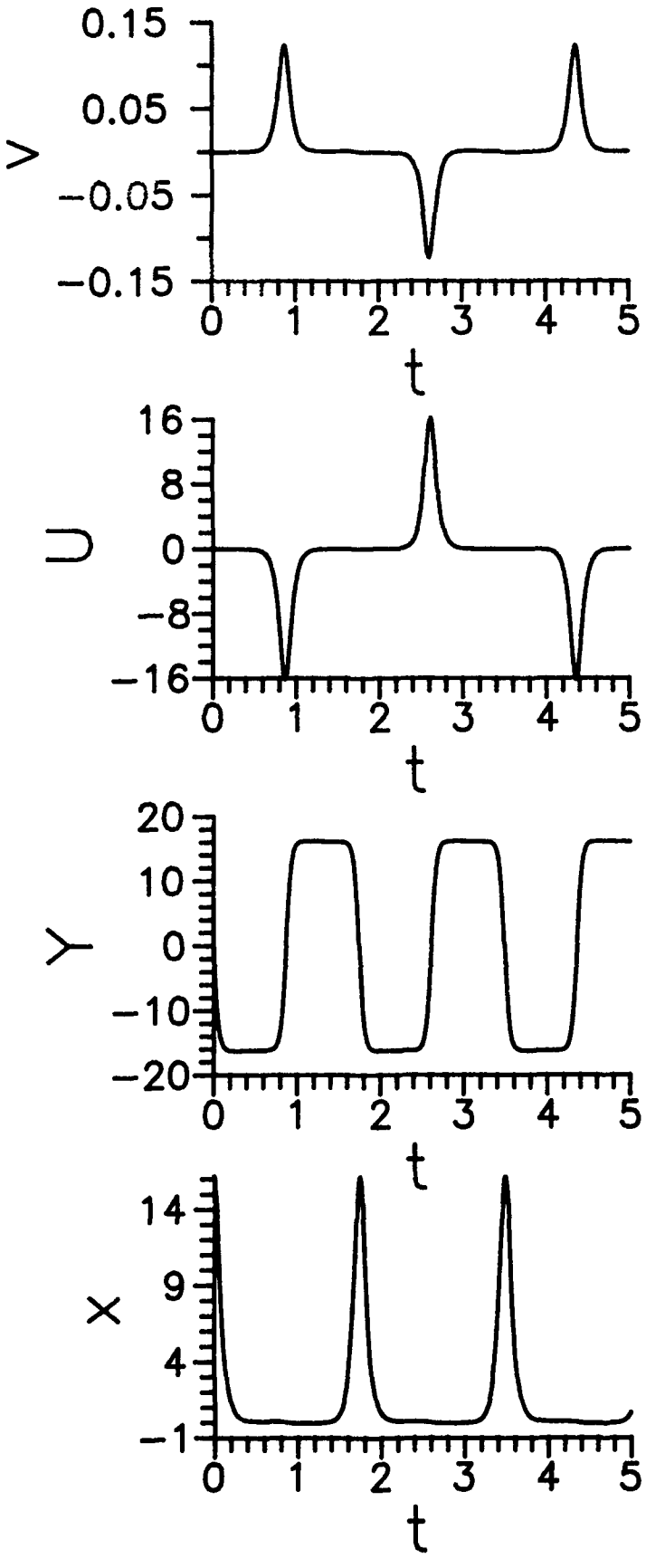


Figure 2: long time periodic solution in the pulsating region.

$\eta$ = 0.08

# Transient behaviour of fibre optic Brillouin ring lasers

R. Hereth, D. Garus, F. Schliep, Ruhr-Universität Bochum, Postf. 10 21 48, D-4630 Bochum, FRG.
Phone: 49/234/700-2098

This work was supported by: Bundesminister für Forschung und Technologie, Förderkennzeichen 13 MV 0059. The authors are responsible for the contents.

## Introduction

Stimulated Brillouin scattering (SBS) is the dominant non-linearity in silica optical fibres. In high-finesse all-fibre ring resonators with fibre lengths of the order of 10 m stimulated Brillouin scattering can be observed at input power levels in the range of 10 to 100 $\mu$W [1]. Above pump threshold fibre optic ring resonators show intensive laser oscillation at the Stokes wavelength and therefore are called Brillouin ring lasers (BRL). An important application of Brillouin ring lasers is the all-fibre optic ring laser gyro [2].

Most types of lasers show transient intensity oscillations with periods that are considerably longer than the cavity decay time. Typical values range between 0.1 $\mu$s and 10 $\mu$s. In this paper analytical and experimental investigations of intensity oscillations of fibre optic Brillouin ring lasers are presented.

## Theory

In the stationary case SBS can be described by a set of two coupled differential equations for the pump intensity $I_1$ and the Stokes intensity $I_2$, respectively:

$$\frac{\partial}{\partial z} I_1 + 2\alpha I_1 = -g_B \cdot I_1 I_2 \qquad (1)$$

$$-\frac{\partial}{\partial z} I_2 + 2\alpha I_2 = g_B \cdot I_1 I_2 \qquad (2)$$

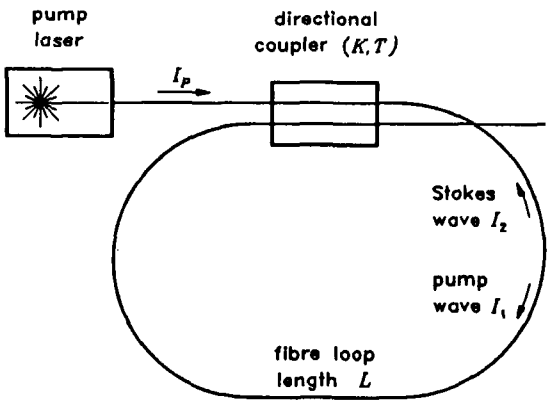


$z$ is the spatial coordinate, $\alpha$ is the damping coefficient of light waves, and $g_B$ is the Brillouin gain coefficient.

The figure on the left shows a schematic diagram of the fibre optic Brillouin ring laser setup. Assuming resonance for both the pump and the Stokes wave, the boundary conditions at the ports of the directional coupler for the pump and the Stokes intensities are given by

$$\sqrt{I_1(0)} = V_k\left(K \cdot \sqrt{I_1(L)} + T \cdot \sqrt{I_P}\right) \quad \text{and} \quad I_2(L) = V_k^2 K^2 \cdot I_2(0)\,. \qquad (3)$$

$K$ and $T$ are the coupling and the transmission factor of the coupler with $K^2 + T^2 = 1$. Coupler loss is considered as lumped loss by the factor $V_K$ with $V_K \le 1$. $I_P$ is the intensity of the pump laser that is coupled into the ring resonator.

In this paper only intensity variations are considered which occure slowly compared to the resonator roundtrip time $T_R$. The time dependence of the pump and Stokes intensities can then be calculated iteratively. For that eqs. (1) and (2) have to be integrated for calculating the intensities after one circulation through the fibre loop from given initial values. New initial values for the next roundtrip can be calculated by the boundary conditions (3). With fibre loop lengths up to about 10 m the gain of the Stokes wave during one circulation is small enough so that the $z$-dependence of $I_2$ in (1) can be neglected [3]. The analogous assumption for (2) is the neglection of pump depletion during one roundtrip through the fibre loop. This leads to approximate solutions of (1) and (2) for one roundtrip:

$$\begin{aligned} I_1(L, t+T_R) &= I_1(0,t)\cdot\exp\left[\left(-g_B I_2(0,t) - 2\alpha\right)L\right] \\ I_2(0, t+T_R) &= I_2(L,t)\cdot\exp\left[\left(g_B I_1(L,t) - 2\alpha\right)L\right] \end{aligned} \tag{4}$$

For analyzing the time dependent behaviour of fibre optic Brillouin ring lasers we derive new differential equations by

$$\frac{I_1(L, t+T_R) - I_1(L,t)}{T_R} \approx \frac{dI_1(L,t)}{dt} \quad \text{and} \quad \frac{I_2(0, t+T_R) - I_2(0,t)}{T_R} \approx \frac{dI_2(0,t)}{dt}, \tag{5}$$

which can be interpreted as an interpolation between the time-discrete values of the iteration. These new differential equations (5) perform a complete description of the temporal behavior of a Brillouin ring laser because they, in contrast to eqs. (1) and (2), take into account the boundary conditions at the ports of the directional coupler. Nevertheless only intensity variations are considered that happen slowly compared to the resonator roundtrip time $T_R$.

The stationary solutions of (5) are

$$I_1^s(L) = \frac{2\pi}{F g_B L} \quad \text{and} \quad I_2^s(0) = \frac{2}{g_B L}\cdot\ln\left(V + (1-V)\sqrt{\frac{I_P}{I_{PT}}}\right) \tag{6}$$

with $V = V_K V_F K$ and $V_F = \exp(-\alpha L)$. $F$ is the finesse of the ring resonator. The relation between $F$ and $V$ is $F = -\pi/\ln(V)$. At pump threshold the loss of the Stokes wave is compensated by the Brillouin gain. The pump intensity at this threshold is given by [4]

$$I_{PT} = I_1^s(L)\cdot\left(\frac{1-V}{V_K V_F T}\right). \tag{7}$$

A solution of (5) shows that time-dependent perturbations of the stationary solutions given by (7) decay in form of damped harmonic oscillations with a damping rate $\alpha_r$ and an oscillation frequency $\omega_r$ given by

$$\alpha_r = \frac{1 - V \cdot \exp\left(-\frac{g_B L I_2^s(0)}{2}\right)}{2T_R} \quad \text{and} \quad \omega_r = \sqrt{\frac{g_B^2 L^2 I_1^s(L) I_2^s(0)}{T_R^2} - \alpha_r^2}\,. \tag{8}$$

## Experiment

A fibre optic ring resonator made of conventional telecom optical fibre was used to observe transient oscillations experimentally. The narrow bandwidth (< 5 kHz) pump laser had a wavelength of 1.32 $\mu$m. The resonator data were: finesse $F$ = 550, coupling factor $K$ = 0.9962, coupler loss factor $V_K$ = 0.9984, fibre damping coefficient $\alpha$ = -0.38 dB/km, and effective mode field area $A_{eff}$ = 78.5 $\mu m^2$. The fibre loop had a length of 9 m which was modulated periodically by a PZT-type phase modulator and a sawtooth generator. Assuming complete polarization scrambling we calculated a pump threshold of $P_{PT} = I_{PT} \cdot A_{eff}$ = 21 $\mu$W (with $g_B = 4.2 \cdot 10^{-11}$ m/W) which compares well to the measured value of 30 $\mu$W. The frequency and the amplitude of the sawtooth generator were chosen in such a way that the free spectral range of the resonator was scanned 13.2 times per second.

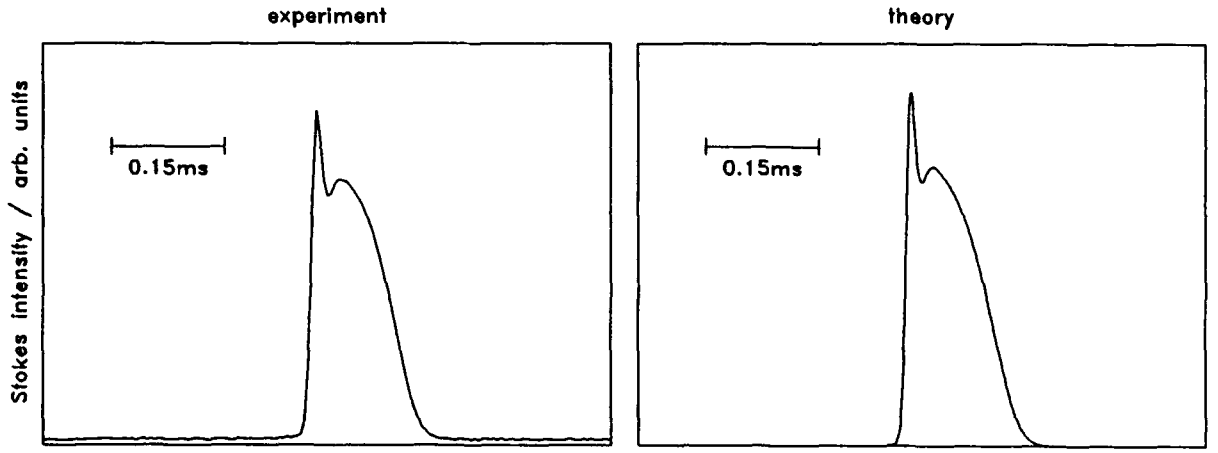


The picture on the left side shows the measured Stokes intensity within the Brillouin ring laser at an input pump power of three times the pump threshold. An overshooting of the Stokes intensity can be seen that decays after some 10 $\mu$s. This overshooting occures due to the above calculated transient oscillations. Before the Stokes intensity could reach its stationary value the ring resonator was detuned by the phase modulator. The picture on the right side shows the Stokes intensity which was calculated iteratively under the same conditions as in the experiment. Both measured and calculated curves match very well.

## References

[1] R. Kadiwar, and I.P. Giles, *Optics Letters* **14** (1989) 332.
[2] F. Zarinetchi, S.P. Smith, and S. Ezekiel, *Optics Letters* **16** (1991) 229.
[3] P. Bayvel, I.P. Giles, and P.M. Radmore, *Optical and Quantum Electronics* **21** (1989) S113.
[4] L.F. Stokes, M. Chodorow, and H.J. Shaw, *Optics Letters* **7** (1982) 509.

# DENSITY OF PROBABILITY DISTRIBUTION FOR QUANTUM ELECTROMAGNETIC FIELD

I.E.Protsenko
P.N. Lebedev Physics Institute, Leninsky prospect 53, 117924,
Moscow, Russia. E-MAIL: protsen@sci.fian.mck.su

Based on the first principles of quantum mechanic the density of probability distribution function W(x,p) is created for quantum electromagnetic field (QEF) - Figs. 1, 2. Unlike a well-known distributions of density of quasi-probability (as Wigner function et.c.) W(x,p) can be measured directly in 8-port homodyne experiment or in the experiment we propose. Using W(x,p) one can calculate the probability to have the field quadratures x and p in a chosen area of a phase space, find the minimum in amplitude or phase fluctuations of QEF. W(x,p) predicts the lemniscate-of-ellipse shape of the dispersion of squeezed QEF (Loudon, 1989; Kimble, 1986). Using a methods of quantum optic in experimental study of W(x,p) one can reconstruct the wave function of QEF and, in principle, the wave function of an emitting substance.

Applied the method to squeezed field being in thermal reservoir one can find a smooth transformation of W(x,p) to classical distribution, while the temperature of reservoir increases.

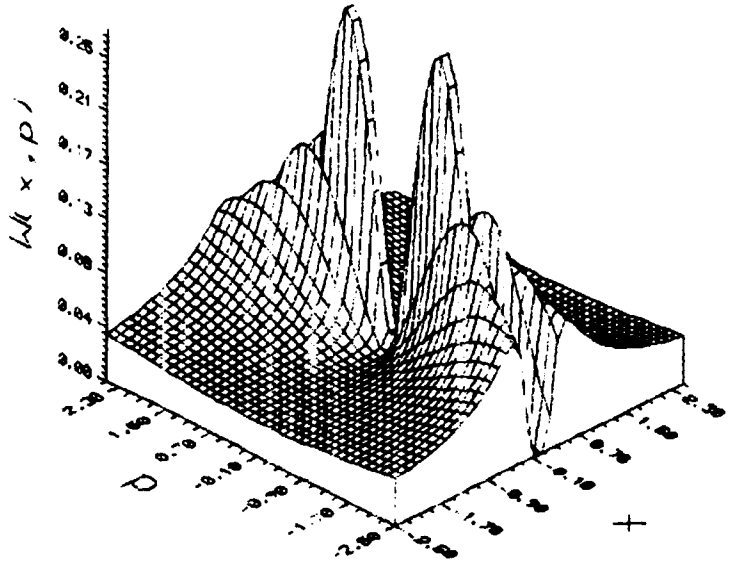

Fig.1 W(x,p) for squeezed vacuum state of QEF

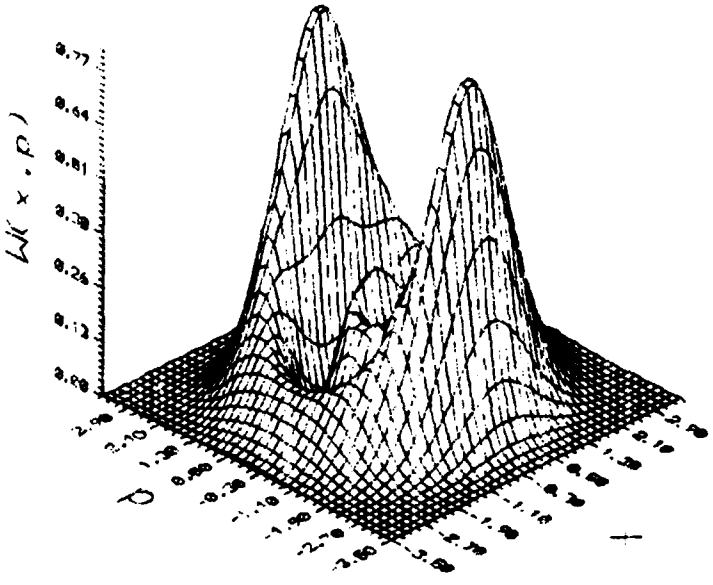

Fig.2 W(x,p) for squeezed number state of QEF, n=3

Paper withdrawn

## High-Dimensional Dynamics in Semiconductor Lasers

I.Fischer, J.Sacher, W.Elsäßer and E.O.Göbel

Fachbereich Physik, Philipps-Universität Marburg, Renthof 5, 3550 Marburg, FRG
Tel.: 01149-6421-282401

We investigate a dynamical system consisting of a one-facet-AR-coated laserdiode coupled to a T-shaped resonator.

The laser shows very complex dynamics depending on the ratio of the two cavity round-trip frequencies. In the vicinity of the ratio 1:2, switching between various states is observed, taking place on a timescale much longer than the fast intensity dynamics. Starting from the mode-locked state, which is related to the modulation of the signal with the compound cavity frequency, the first subharmonic appears. From this state the system switches to different others without changing any control parameter. Some of them belong to a period doubling route to chaos, other states are odd harmonics of the subharmonic, chaotic states belonging to these and finally a state with a broad nearly structureless power spectrum. All these states are closely related to the delay-scenario introduced by Ikeda(1). Estimations of the correlation dimension from a time-series for a state with broad-band power spectrum yields $D_2 \geq 7$ which is also in agreement with the Ikeda-model.

In the vicinity of other simple ratios of the cavity lengths similar switching between different states can be observed, but these states are different from those discussed above with respect to the dominant frequencies.

We explain the coexistence of all these states and the switching between

them in analogy to the model of globally coupled maps representing oscillators as investigated by Kaneko(2). For special parameter regions Kaneko has found chaotic itinerancy between high-dimensional and lower dimensional states related to the coupling of different oscillators. Wiesenfeld et.al.(3) have shown an analogy between laser modes and coupled oscillators. In our system there exist approximately 10-20 competing modes coupled via the inversion. Consequently, the effects studied by Kaneko can be attributed to these modes. Finally, Kaneko has observed clustering to different locked groups of oscillators for, respectively, lower nonlinearity parameters of the single oscillators or stronger coupling. This could be equivalent to the case of one single external resonator, where we have observed many different periodic states.

In conclusion, we have studied an experimental system based on an external cavity semiconductor laser that shows high-dimensional dynamics with switching between various regular and chaotic states that are characteristic for a delay-scenario. The switching might be induced by global coupling of the different laser modes.

## References

(1) K.Ikeda and K.Kondo, Phys.Rev.Lett., **49**,1467 (1982)

(2) K.Kaneko, Physica **54D**,5 (1991)

(3) K.Wiesenfeld, Ch.Bracikowski, G.James and R.Roy, Phys.Rev.Lett., **65**,1749 (1990)

**Transient multimode statistics in nearly single–mode semiconductor lasers**

A. Valle, Dept. de Física Moderna, Univ. de Cantabria. E–39005 Santander, Spain. Telephone: (34)(42)201465. Fax:(34)(42)201402.
P. Colet, Dept. de Física, Univ. de les Illes Balears. E–07071 Palma de Mallorca, Spain.
L. Pesquera, Dept. de Física Moderna, Univ. de Cantabria. E–39005 Santander, Spain.
M. San Miguel, Dept. de Física, Univ. de les Illes Balears. E–07071 Palma de Mallorca, Spain.

Mode partition noise in optical fiber communication systems is still causing an error rate floor even with distributed–feedback (DFB) lasers sources [1,2] having a side–mode suppression ratio larger than 30 dB in stationary conditions. This phenomenon is caused by the laser turning on initially in a side mode having a different wavelength from the principal mode.

We limit our analysis to the case of a two mode laser. This is justified for nearly single–mode DFB lasers, where only one side mode can have an appreciable probability to be excited during the transient. The dynamics of the laser is modelled by using noise driven rate equations for the density of minority carriers $n$ and for the density of photons in the main $I_m$ and side $I_s$ modes [3]. The aim of this work is to analyze the evolution of $I_m$ and $I_s$ when the injected current is suddenly switched from a value $C_b$ below to a value $C$ above the threshold current. The gain margin between the main and side modes $\Delta g$ and the laser operating point, given by $C$, are taken as parameters.

The statistics of the power partition between the two modes during the laser switch on is analyzed in terms of the probability $\Phi(I_m)$ that the main mode intensity is $I_m$ when the total intensity reaches a prescribed reference value $I_T$. We take $I_T = I_{st}/2$, $I_{st}$ being the stationary value of the total photon density in the *on* state.

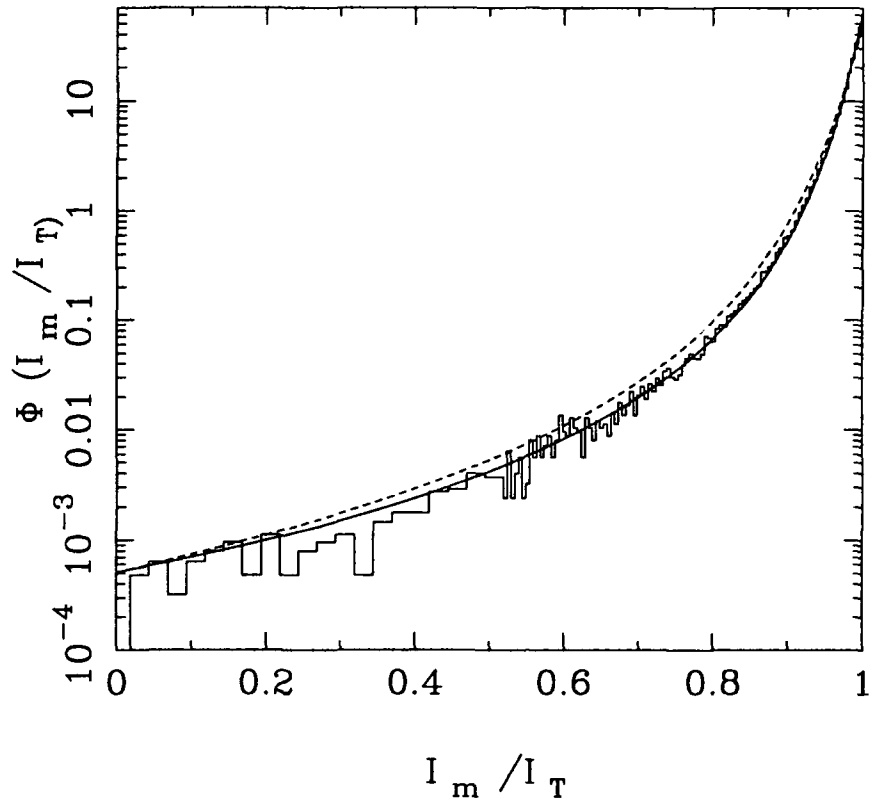


Fig. 1.- $\Phi(I_m/I_T)$ vs $I_m/I_T$ for $\Delta g = 4cm^{-1}$ and $C = 1.2C_{th}$. Linear theory (dotted line); approximation (solid line) and simulation (histogram)

In this way the carrier depletion due to stimulated emission can be neglected. An analytic expression for the probability $\Phi(I_m)$ has been obtained with the use of a linear approximation [3]. We show by performing numerical simulations that this approximation is not accurate when the side mode is highly suppressed, $\Delta g$ increasing and/or $C$ decreasing [3]. A new theory is developed taking into account the gain saturation for the side mode due to the main mode. A better agreement is found between this theory and numerical simulations, including the case of a highly suppressed side mode: $\Delta g$ larger than $4cm^{-1}$ ($7.5cm^{-1}$) and $C = 1.2C_{th}$ ($C = 1.5C_{th}$), $C_{th}$ being the threshold current (see Fig.1). Using this approximation the probability of having a side mode larger than the main mode during the leading edge of the optical pulse is obtained. This corresponds to an integration of $\Phi(I_m)$ from 0 to $I_T/2$ and it is analogous to an error rate

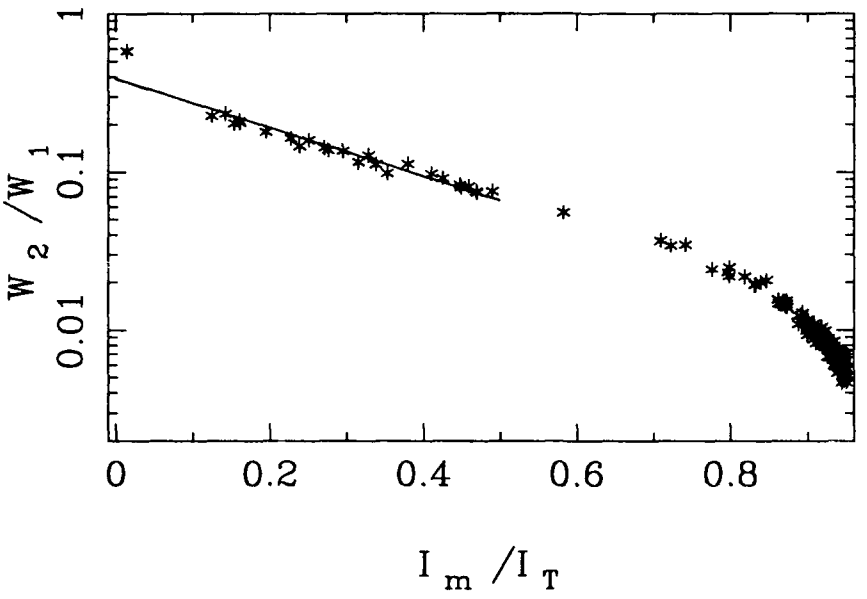


Fig. 2.- $W_2/W_1$ vs. $I_m/I_T$ for $\Delta g = 7.5cm^{-1}$ and $C = 1.5C_{th}$.

in optical communication systems, wherein a threshold near one–half the received pulse power is used to determine whether or not the received pulse is a mark or a space.

The probability density for the main and side mode intensities in the nonlinear regime are also obtained from numerical simulations. The intensity is averaged over different times to analyze the time evolution of both modes.

For highly suppressed side modes the averaged intensity is shown to be independent of the integration time. In this case the evolution is mainly due to the spontaneous emission noise. We have also studied in detail the events such that during the laser switch on $I_m$ is smaller than $I_T/2$. For these events a linear relation is found between this value $I_m$ and the logarithm of the relation between the intensities of the side and main modes both averaged over the first relaxation peak, $W_2/W_1$ (see Fig.2). Finally, the total intensity averaged over the first relaxation peak is found to be constant.

[1] S. Sasaki, M. M. Choy, and N. K. Cheung, Electron. Lett. **24**, 26 (1988).

[2] S. E. Miller, IEEE J. Quantum electron. **26**, 242 (1990).

[3] A. Mecozzi, A. Sapia, P. Spano, and G. P. Agrawal, IEEE J. Quantum Electron. (1991).

Tuesday, June 23, 1992

# Control of Chaos

**TuA** 8:20am–10:20am
Schroedinger Hall

Fedor M. Mitschke, *Presider*
*University of Hannover, Germany*

# Controlling Chaos

Filipe J. Romeiras,[a,b] Celso Grebogi,[a,b], Edward Ott,[b]
and W. P. Dayawansa[c]
(a) Dept. of Mathematics & Inst. for Physical Science and Technology
(b) Laboratory for Plasma Research
(c) Systems Research Center
University of Maryland, College Park, MD 20742

## Summary

It is common for systems to evolve with time in a chaotic way. In practice, however, it is often desired that chaos be avoided and/or that the system be optimized with respect to some performance criterion. Given a system which behaves chaotically, one approach might be to make some large (and possibly costly) alteration in the system which completely changes its dynamics in such a way as to achieve the desired objectives. Here we assume that this avenue is not available. Thus we address the following question: Given a chaotic system, how can we obtain improved performance and achieve a desired attracting time-periodic motion by making only *small* controlling temporal perturbations in an accessible system parameter.

The key observation is that a chaotic attractor typically has embedded densely within it an infinite number of unstable periodic orbits [1]-[5]. In addition, chaotic attractors can also sometimes contain unstable steady states (e.g., the Lorenz attractor has such an embedded steady state). Since we wish to make only small controlling perturbations to the system, we do not envision creating new orbits with very different properties from the already existing orbits. Thus we seek to exploit the already existing unstable periodic orbits and unstable steady states. Our approach is as follows: We first determine some of the unstable low-period periodic orbits and unstable steady states that are embedded in the chaotic attractor. We then examine these orbits and choose one which yields improved system performance. Finally, we apply small controls so as to stabilize this already existing orbit.

Some comments concerning this method are the following:

1. Before settling into the desired controlled orbit the trajectory experiences a chaotic transient whose expected duration diverges as the maximum allowed size of the control approaches zero.

2. Small noise can result in occasional bursts in which the orbit wanders far from the controlled orbit.

3. Controlled chaotic systems offer an advantage in flexibility in that any one of a number of different orbits can be stabilized by the small control, and the choice can be switched from one to another depending on the current desired system performance.

For the sake of simplicity we consider a discrete time dynamical system,

$$\mathbf{Z}_{i+1} = \mathbf{F}(\mathbf{Z}_i, p), \tag{1.1}$$

where $\mathbf{Z}_i \in \Re^n$, $p \in \Re$ and $\mathbf{F}$ is sufficiently smooth in both variables. Here, $p$ is considered a real parameter which is available for external adjustment but is restricted to lie in some small interval, $|p - \bar{p}| < \delta$, around a nominal value $\bar{p}$. We assume that the nominal system (i.e., for $p = \bar{p}$) contains a chaotic attractor. Our objective is to vary the parameter $p$ with time $i$ in such a way that for almost all initial conditions in the basin of the chaotic attractor, the dynamics of the system converge onto a desired time periodic orbit contained in the attractor. The control strategy is the following. We will find a stabilizing local feedback control law which is defined on a neighborhood of the desired periodic orbit. This is done by considering the first order approximation of the system at the chosen unstable periodic orbit. Here we assume that this approximation is stabilizable. Since stabilizability is a generic property of linear systems, this assumption is quite reasonable. The ergodic nature of the chaotic dynamics ensures that the state trajectory eventually enters into the neighborhood. Once inside, we apply the stabilizing feedback control law in order to steer the trajectory towards the desired orbit.

For simplicity we shall describe the method as applied to the stabilization of fixed points (i.e., period one orbits) of the map $\mathbf{F}$. The consideration of periodic orbits of period larger than one is straightforward and is discussed in Sec. II.E. Let $\mathbf{Z}_*(p)$ denote an unstable fixed point on the attractor. For values of $p$ close to $\bar{p}$ and in the neighborhood of the fixed point $\mathbf{Z}_*(\bar{p})$ the map (2.1) can be approximated by the linear map

$$\mathbf{Z}_{i+1} - \mathbf{Z}_*(\bar{p}) = \mathbf{A}(\mathbf{Z}_i - \mathbf{Z}_*(\bar{p})) + \mathbf{B}(p - \bar{p}), \tag{1.2}$$

where

$$\mathbf{A} = \mathbf{D}_{\mathbf{z}}\mathbf{F}(\mathbf{Z}, p),$$
$$\mathbf{B} = \mathbf{D}_p\mathbf{F}(\mathbf{Z}, p),$$
$$(\Delta\mathbf{Z})_i = \mathbf{Z}_i - \mathbf{Z}_*,$$
$$(\Delta p)_i = p_i - \bar{p}.$$

Generically, $(\mathbf{A}, \mathbf{B})$ pair is controllable, and hence we may find a linear feedback control law,

$$(\Delta p)_i = \mathbf{K}(\Delta\mathbf{Z})_i,$$

such that the spectrum of $(\mathbf{A}+\mathbf{BK})$ is in the open unit disc. Furthermore, this control law stabilizes the nonlinear system (1.1) in a neighborhood of the nominal operating point as well.

Although we describe the details only in the case of discrete time systems, this method is applicable in the continuous time case as well by considering the discrete time system obtained from the induced dynamics on a Poincaré section.

In order to illustrate the method we applied it to a periodically forced mechnical system (the kicked double rotor), which results in a four dimensional map. Amongst the examples considered, we studied cases where the unstable orbit of the uncontrolled system has two unstable eigenvalues and two stable eigenvalues, and the stabilization is achieved by variation of one control parameter characterizing the strength of the periodic forcing. The present work generalizes our previous work [6] to the case of higher dimensional systems and also includes new material illustrating the effect of the choice of stabilization on the length of the chaotic transient experienced by the orbit before control is achieved. Other relevant references on the stabilization of periodic or steady orbits embedded in chaotic attractors are the experiments of Ditto et al. [7], Singer et al. [8], Azevedo and Rezende [9], Roy et al. [10], and the paper of Fowler [11].

[1] C. Grebogi, E. Ott, and J. A. Yorke, "Unstable periodic orbits and the dimensions of multifractal chaotic attractors," Phys. Rev. A **37**, 1711–1724, 1988.
[2] D. Auerbach, P. Cvitanovich, J. P. Eckmann, G. Gunaratne, and I. Procaccia, "Exploring chaotic motion through periodic orbits," Phys. Rev. Lett. **58**, 2387–2390, 1987.
[3] T. Morita, H. Hata, H. Mori, T. Horita, and K. Tomita, "On partial dimensions and spectra of singularities of strange attractors," Prog. Theor. Phys. **78**, 511–515, 1987.
[4] A. Katok, "Lyapunov exponents, entropy and periodic orbits for diffeomorphisms," Publ. Math. IHES **51**, 137, 1980.
[5] R. Bowen, "Periodic points and measures for axiom A diffeomorphisms," Trans. Am. Math. Soc. **154**, 377, 1971.
[6] E. Ott, C. Grebogi, and J. A. Yorke, "Controlling Chaos," Phys. Rev. Lett. **64**, 1196–1199, 1990.
[7] W. L. Ditto, S. N. Rauseo, and M. L. Spano, "Experimental control of chaos," Phys. Rev. Lett. **65**, 3211–3214 (1990).
[8] J. Singer, Y.-Z. Wang, and H. H. Bau, "Controlling a chaotic system," Phys. Rev. Lett. **66**, 1123–1125, 1991.
[9] A. Azevedo and S. M. Rezende, "Controlling Chaos in Spin-Wave Instabilities," Phys. Rev. Lett. **66**, 1342, 1991.
[10] R. Roy, T. W. Murphy, T. D. Maier, Z. Gills, and E. R. Hunt, "Dynamical Control of a Chaotic Laser: Experimental Stabilization of a Globally Coupled System," Phys. Rev. Lett. **68**, 1259, 1992.
[11] T. B. Fowler, "Application of stochastic control techniques to chaotic nonlinear systems," IEEE Trans. on Automatic Control **34**, 201–205, 1989.

# Control of Chaos in a Multimode Solid State Laser: Numerical Results

Pere Colet and Rajarshi Roy
School of Physics
Georgia Institute of Technology
Atlanta, Georgia 30332-0430 USA.
Telephone: 404 894 5265

The stabilization of unstable periodic orbits embedded in a chaotic attractor has received great attention recently. In the original algorithm proposed by Ott, Grebogi and Yorke [1] (OGY) control is achieved by means of small perturbations of a system parameter which are proportional to the deviation of the system from the unstable fixed point. A related but different technique to control a chaotic system is the occasional proportional feedback technique (OPF) [2]. Experiments demonstrating the control of chaos in a multimode solid state laser using this technique have been reported recently [3]. Here we study the theoretical model for such laser and compare with the experimental results.

The system considered is a multimode diode pumped solid state Nd:YAG laser with a frequency doubling KTP crystal. In multimode operation, each longitudinal mode can only exist in two orthogonal polarization directions. The rate equations for the intensities $I_k$ and gains $G_k$ of each mode are given by the equations [4]:

$$\tau_c \frac{d I_k}{d t} = \left( G_k - \alpha_k - g\varepsilon I_k - 2\varepsilon \sum_{j \neq k} \mu_{jk} I_j \right) I_k$$

$$\tau_f \frac{d G_k}{d t} = \gamma - \left( 1 + I_k + \beta \sum_{j \neq k} I_j \right) G_k$$

where $\tau_c$ is the cavity round trip (0.2 ns), $\tau_f$ is the fluorescence lifetime of the $Nd^{3+}$ ion (240 μs), $\alpha_k$ is the cavity loss parameter for the kth mode, $\gamma$ is the small signal gain, which is related to the pump rate, $\beta$ is the cross-saturation parameter, and g is a geometrical factor dependent on the birefringence of the YAG and the KTP crystals (its value depends on the phase delays and on the angle between the YAG and KTP fast axes). For modes j having the same polarization as the kth mode, $\mu_{jk} = g$, while $\mu_{jk} = (1-g)$ for modes having orthogonal polarization. The nonlinear coefficient $\varepsilon$ is associated with the conversion efficiency of the fundamental intensity into doubled intensity by the KTP crystal. We assume very similar losses for all the modes with $\alpha_k \approx 0.01$. Chaotic behavior arises as a consequence of the global coupling between the longitudinal modes through the nonlinear process of sum frequency generation.

The OPF procedure to stabilize the system in the chaotic regime is applied as follows. As in the experiments, the total laser output intensity is sampled at a given frequency $\nu_c$. Then, during a short time $t_{on} << t_c = \nu_c^{-1}$, $\gamma$ is modified to $\gamma = \gamma_0 + w(I - I_r)$ where $\gamma_0$ is the ambient value for the pumping, $I_r$ is a given reference value for the total intensity and w is a small proportionality constant. After $t_{on}$, and until the next sampling time, $\gamma = \gamma_0$. The value of $\nu_c$ is related to the oscillation relaxation frequency. We have observed the stabilization of unstable periodic orbits by means of the applied control signal when the parameters $t_c$, $t_{on}$, w and $I_r$ are appropriately chosen. We have studied the range of parameters which yield stabilization. The value of $t_c$ is related to the oscillation relaxation period. In some circumstances control can be achieved for many different values of $t_c$. Preliminary results show that $t_{on}$ has to be chosen much smaller than $t_c$. w is taken around 0.05 (corresponding to modification of the ambient pump rate $\gamma$ by a few percent, and $I_r$ is chosen to be close to the maximum or minimum values of the intensity. A crucial issue in the stabilization procedure is that it only works when system is placed initially close to the unstable orbit to which will be stabilized. We have studied numerically the size of the region around the unstable orbit where the OPF technique works, which is important from a practical point of view.

In conclusion, we have analyzed numerically the control of a multimode solid state laser using the OPF technique. The characterization of the range of parameters which can stabilize the system is of fundamental importance for the practical applicability of this technique.

**References:**

[1] E. Ott, C. Grebogi and J.A. Yorke, Phys. Rev. Lett. **64**, 1196 (1990).
[2] E. R. Hunt, Phys. Rev. Lett. **67**, 1953 (1991); B. Peng, V. Petrov and K. Showalter, J. Phys. Chem. **95**, 4957 (1991).
[3] Rajarshi Roy, T. W. Murphy, Jr. T. D. Maier, Z. Gills and E. R. Hunt, Phys. Rev. Lett. to appear.

# Experimental Control of a Chaotic Laser System

Rajarshi Roy, T.W. Murphy, Jr., T.D. Maier and Zelda Gills
School of Physics
Georgia Institute of Technology
Atlanta GA 30332

and

E.R. Hunt
Department of Physics and Astronomy
Ohio University
Athens OH 45701-2979

## Summary

The exploitation of chaotic and nonlinear dynamical phenomena for practical applications has recently been transformed from concept to reality. Two major approaches to achieving control of chaotic systems have been developed. Hubler and his coworkers have studied control algorithms for driven nonlinear systems where the time dependence of the driving forces necessary to to obtain resonant stimulation are computed from Poincare maps of the system or from detailed mathematical models.[1] A different approach was initiated by Ott Grebogi and Yorke (OGY) ; they suggested that a chaotic attractor typically has many unstable periodic orbits associated with it, that could be stabilized by appropriate modifications to a system parameter.[2] Their approach was experimentally demonstrated by Ditto, Rauseo and Spano in their experiments on a magnetoelastic ribbon.[3]

We report here the results of experiments that demonstrate dynamical control of chaotic intensity fluctuations in a chaotic, intracavity doubled, multimode Nd:YAG laser. It is an autonomously chaotic, higher dimensional system, which we have studied both experimentally and theoretically over the past few years.[4-7] The laser modes (typically from three to ten in number) and their associated gains may be described by a set of coupled, nonlinear ordinary

differential equations. Relaxation oscillations occur in the total intensity output of the laser, resulting from an exchange of energy between the light and active atoms of the laser medium. The potassium titanyl phosphate (KTP) frequency doubling crystal introduces a nonlinear loss for the fundamental frequency (1.06 μ) and also couples the different longitudinal modes through sum frequency generation. In the method of control used in these experiments, it was not necessary for us to utilize a detailed model for the laser system. Comparisons with the theoretical model are made in an accompanying paper.

In a periodically driven system, such as the magnetoelastic ribbon of ref. 3, it is natural to sample a system variable at the driving frequency or its sub-multiples. In the laser system, the relaxation oscillations provide a natural time scale for sampling and feedback to a system parameter. The relaxation oscillations occur in the range of frequencies upto 120 kHz for excitations as large as five times above threshold. A system variable (the total laser intensity in this case) is sampled within a window of selected offset and width. The sampling frequency is chosen to be close to the relaxation oscillation frequency or a rational fraction of it. A signal proportional to the deviation of the sampled intensity from the center of the window is generated and applied to perturb a system parameter from its ambient value. This control signal attempts repeatedly to bring the system closer to a periodic unstable orbit that is embedded in the chaotic attractor. When successful, this dynamical control technique can stabilize the laser output intensity in one of many simple and complex periodic waveforms.

We have been able to control the chaotic intensity fluctuations of the laser system through this method of occasional proportional feedback. These results demonstrate dynamical control of an autonomously chaotic, higher dimensional system for the first time on microsecond time scales. The multimode laser system studied by us is an example of a globally coupled system of nonlinear oscillators. The proportional control signal applied to the pump excitation results in an ordered, periodic state of the originally chaotic ensemble of

oscillators. The results reported here indicate that this technique should be widely applicable to a variety of physical, chemical and biological systems, including arrays and networks of coupled nonlinear elements.

**References:**

1. R. Georgii, W. Eberl, E. Luscher and A. Hubler, Helvetica Physica Acta 62, 290 (1989).
2. E. Ott, C. Grebogi and J. A. Yorke, Phys. Rev. Lett. 64, 1196 (1990).
3. W.L. Ditto, S.N. Rauseo and M. L. Spano, Phys. Rev. Lett. 65, 3211 (1990).
4. G. E. James, E.H. Harrell II, C. Bracikowski, K. Wiesenfeld and R. Roy, Opt. Lett. 15, 1141 (1990).
5. K. Wiesenfeld, C. Bracikowski, G.E. James and R. Roy, Phys. Rev. Lett. 65, 1749 (1990).
6. C. Bracikowski and R. Roy, Chaos 1, 49 (1991).
7. R. Roy, C. Bracikowski and G.E. James, in Proceedings of the International Quantum Optics Conference, edited by R. Inguva and G. S. Agarwal (Plenum Press, to appear, 1992).

# Control and characterization of unstable stationary states

S. BIELAWSKI, M. BOUAZAOUI, D. DEROZIER and P. GLORIEUX
Laboratoire de Spectroscopie Hertzienne, associé au C.N.R.S.
Université des Sciences et Techniques de Lille Flandres-Artois
F-59655 Villeneuve d'Ascq Cedex (France)

The Nd-doped optical fiber laser (OFL) displays spontaneous oscillations when the pump power exceeds some threshold[1]. This will be called hereafter the "second Hopf bifurcation" threshold of the laser since the first Hopf bifurcation corresponds to the onset of laser action.

The present paper reports on the active stabilization of the unstable stationary state that appear following this bifurcation. As shown on figure 1, when the pump power exceeds some threshold (5.8 mW in the conditions of Figure 1), the laser intensity becomes unstable. These spontaneous instabilities start from periodic oscillations and lead to chaos through a period-doubling cascade[1].

Our aim is to suppress these oscillations in order to stabilize the output laser intensity. To reach this goal, we made use of an external feedback method. The laser intensity is detected by a photodetector. The signal output detector is passed through an electronic derivator and sent to the pump laser diode. As a consequence, we force the oscillator to react in the opposite phase with its own oscillations. Figure 2 shows the transition from the spontaneous oscillatory behavior in the absence of the external feedback, to the stabilized steady-state when the control feedback is activated. In this respect, it is worth noticing that in spite of his weakness (limited to 5% of the average pump power) and of the strong oscillations the control becomes effective in a relatively short time after his application. This control strongly affects the qualitative behavior of the system. The dependence of the output laser intensity on the pump power is reported on figure 1. It shows that the laser is stabilized above the second threshold ($P_{th}$ = 5.8 mW), in a state which has the same properties (e.g., dependence on the pump

power) as the previously stable state. We can therefore consider that we have detected and measured the unstable state emerging at the second Hopf bifurcation.

This method of control may also used to characterize this unstable state through the analysis of the relaxation oscillations. Between the two thresholds, the stationary state is stable and a small perturbation of the pump power is followed by damped relaxations. On the other hand, above the second threshold the unstable stationary state is stabilized by the control feedback and when it is desactivated the relaxation oscillations exponentially increases. Figure 3 shows that the square of the oscillation frequencies vanishes at the first bifurcation and increases linearly with the pump power, as predicted by a simple rate equation model of the two level laser[2,3], whereas the damping rate (figure 4) changes of sign at the second Hopf bifurcation (5.8 mW).

In conclusion, we have demonstrated experimentally that a simple external feedback system can be used to suppress the oscillatory behavior and chaos in an optical fiber laser (OFL). The laser is locked to the (unstable) state which destabilized at the bifurcation. The dynamical properties of this state can be studied using the same technique.

---

1 - S. BIELAWSKI, M. BOUAZAOUI, D. DEROZIER and P. GLORIEUX (to be published).

2 - F.T. ARECCHI, R. MEUCCI, G.P. PUCCIONI and J.R. TREDICCE, Phys. Rev. Lett. **49**, 1217 (1982).
- A. E. SIEGMAN, Lasers (University Science Books, California 1986).
- D.DANGOISSE, P. GLORIEUX and D. HENNEQUIN, Phys. Rev. **A36**, 4775 (1987).
- T. MIDAVAINE, D. DANGOISSE, and P. GLORIEUX, Phys. Rev. Lett. **55**, 1989 (1985).

3 - D. DEROZIER, S. BIELAWSKI and P. GLORIEUX , Opt. Comm. **83**, 97 (1991).

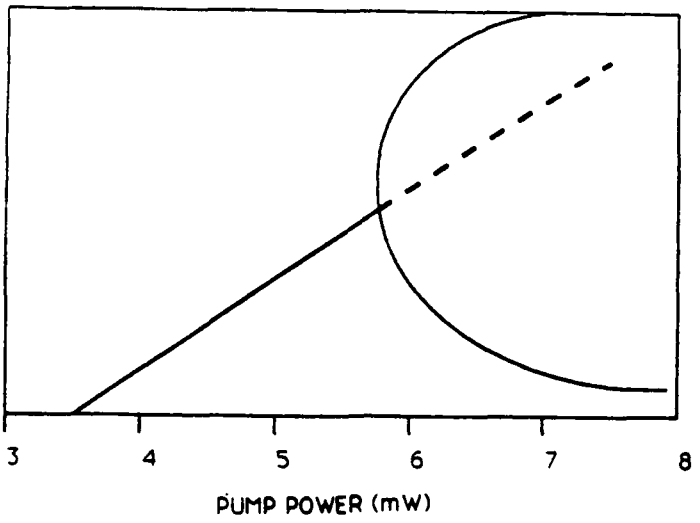


ure.1: Dependence of the laser intensity on the pump power without (solid line, the full line defines the minima and maxima of laser intensity) and with (dashed line) external feedback control.

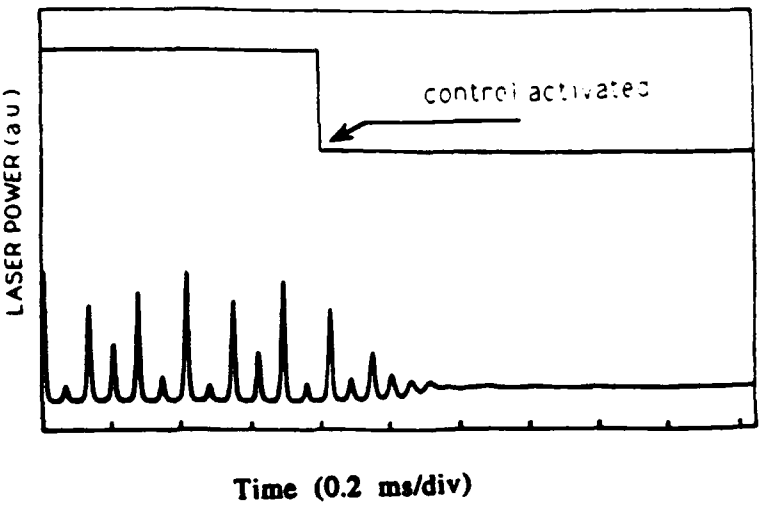


Figure.2: Onset of control.

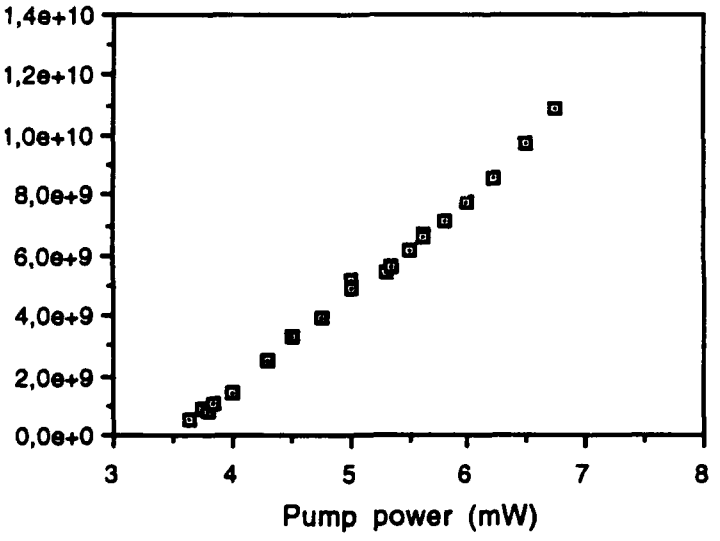


gure.3: Oscillation frequency versus pump power.

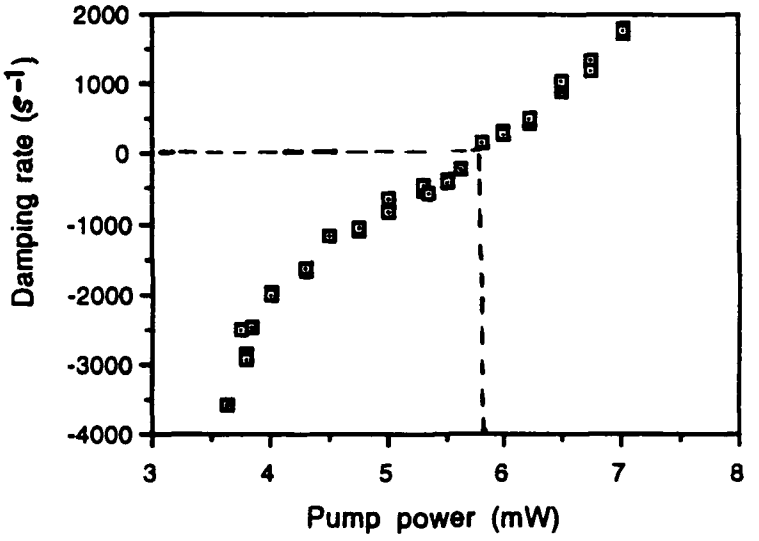


Figure.4: Dependence of the damping rate of the relaxation oscillations on the pump power.

# CONTROLLING LASER CHAOS

S. Bielawski, M. Bouazzaoui, D. Derozier and P. Glorieux
Laboratoire de Spectroscopie Hertzienne, associé au C.N.R.S.
Université des Sciences et Techniques de Lille
F-59655 Villeneuve d'Ascq Cedex (France)

In 1990 Ott, Grebogi and Yorke described an attractive method (OGY) whereby small time-dependent perturbation applied to a chaotic system allowed to stabilize unstable periodic orbits[1]. This method is applicable to experimental situations in which a priori analytical knowledge of the system is not available[2,3]. Their method assumes the dynamics of the system can be represented as arising from a nonlinear map (e.g., a return map). The iterates are then given by $X_{n+1}=F(X_n,p)$, where p is some accessible parameter of the system. To control chaotic dynamics one only needs to learn the local dynamics around the desired unstable periodic orbit (e.g., a fixed point $X_n=X_F$) on the nonlinear map : especially, the derivatives with respect to p of the orbit location. When the motion is near the periodic orbit($X_n \# X_F$), small appropriate temporal perturbations of the control parameter p allow to hold the motion on its unstable periodic orbits.

The control method which is presented here is based on the same approach but it does not need the analysis of the local dynamics and allows to detect, then to stabilize, the periodic orbits embedded in the chaotic motion. Moreover it allows to follow the unstable periodic orbits when the control parameters of the system are slowly changed. The control idea is to monitor the $X_n$' values until $|X_{2n+1}-X_{2n}|$ becomes smaller than a fixed value; in this case, one have detected a candidate for an unstable orbit. Then, one applies a small temporal perturbation $\delta p$, on the control parameter p, proportional to the difference $\alpha(X_{2n+1}-X_{2n})$; $\alpha$ is adapted to minimize the following differences. When one has detected an unstable periodic orbit, the temporal perturbation decreases (its average value tends to zero) and the $X_n$' values tend to a fixed value

$X_F$ corresponding to that determined by the OGY method. Unlike the OGY method, the period of the correction is necessarily double because the fixed value is not beforehand determined (it results of the stability analysis) and so, very unstable orbits are more difficult to stabilize; on the other hand, this method has the advantage, in addition to its simplicity, to stabilize the periodic orbit even when the control parameters slowly change.

Using this methode, we have achieved control of chaos in a $Nd^{3+}$ doped fiber laser pumped by a laser diode[4]. In some experimental conditions and above a threshold value of the pump power, the laser intensity spontaneously oscillates and a period doubling cascade leading to chaos is observed[5]. The evolution of the laser dynamics versus the pump power is summarized in the bifurcation diagram(BD) of figure 1-a.

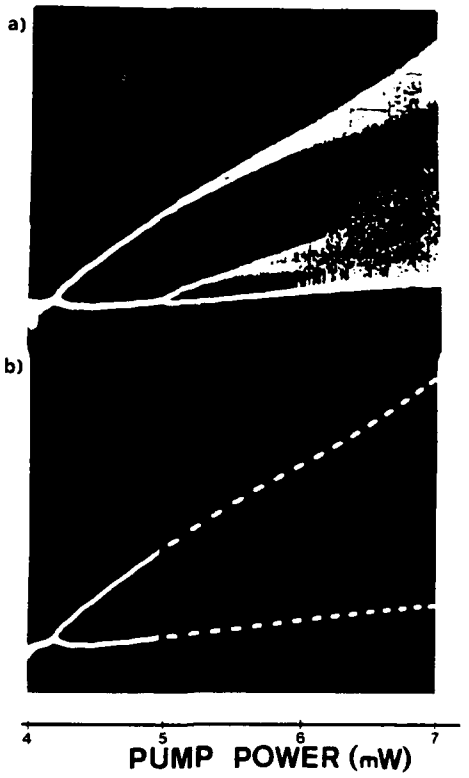


Figure 1 : Bifurcation Diagram of the optical fiber laser. The control parameter is the pump power. (a) without control and (b) with stabilization on the 2-T periodic orbit.
(the dash line represents the unstable orbit).

The BD is obtained using periodic sampling of the laser output intensity synchronously with the spontaneous oscillations. Figure 1-b shows the same BD as the figure 1-a when the system is switched to control the unstable period-2 orbit using small temporal perturbations of the pump power(control parameter) : the full line represents the stable periodic orbit and the dash line shows the unstable 2T-periodic orbit stabilized all over the rangr on which the control parameter is slowly changed. Figure 2 displayss the evolution of the $X_{n'}$ values when the control system is switched on. We clearly observes that the system waits until the attractor reaches the vicinity of the 2-T periodic orbit and then stabilizes it. Similar stabilizations are obtained on higher order unstable orbits.

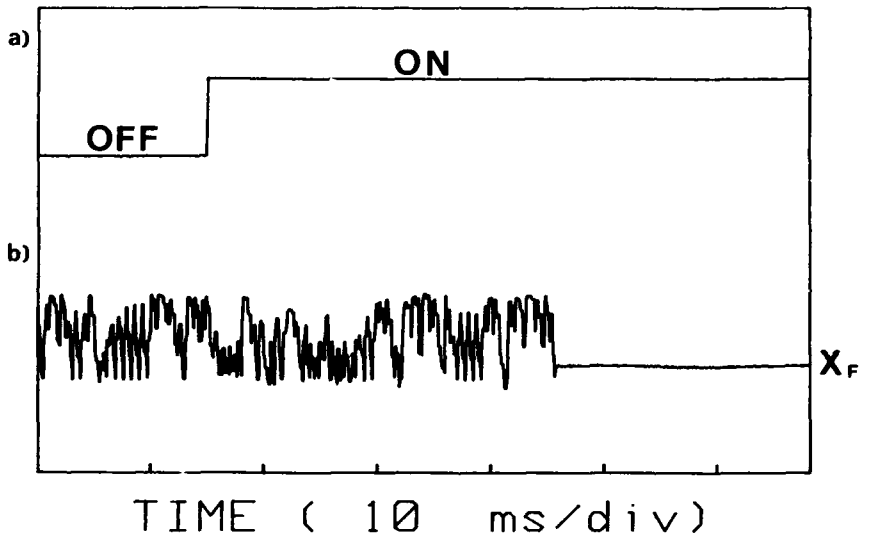


Figure 2 : Times series of Xn' (b) when the control system is switched on (a) to control the period-2 unstable orbit.

In conclusion, we have demonstrated the control of chaos in a physical system using an method analogous to the OGY one. Some advantages of this method are the possibilities to detect the periodic orbits and to follow it when the physical system is modified.

[1] E. Ott, C. Grebogi, and J.A. Yorke, Phys. Rev. Lett. **64**, 1196 (1990)
[2] W.L. Ditto, S.N. Rauseo, and M.L. Spano, Phys. Rev. Lett. **65**, 3211 (1990)
[3] A. Azevedo, and S.M. Rezende, Phys. Rev. Lett. **66**, 1342 (1991)
[4] D. Derozier, S. Bielawski, and P. Glorieux, Opt. Comm. **83**, 97 (1991)
[5] S. Bielawski, M. Bouazzaoui, D. Derozier, and P. Glorieux, to be published

Tuesday, June 23, 1992

# Multiwave Mixing and Phase Conjugation

**TuB** 10:40am–12:40pm
Schroedinger Hall

Rajarshi Roy, *Presider*
*Georgia Institute of Technology*

# On the Deterministic Dynamics of Stimulated Scattering Phenomenon

R.G. Harrison, Weiping Lu and A. Johnstone, D.S. Lim and J.S. Uppal

Department of Physics, Heriot-Watt University, Edinburgh EH14 4AS, U.K.

Tel. 031-451-3033

Fax. 031-451-3136

Lu and Harrison have recently shown [1] in a more complete treatment of stimulated scattering that the interplay of nonlinear refraction with the gain of stimulated scattering lead to rich dynamical instabilities and chaos in the scattered and pump fields; omissions of dispersive effects as in conventional treatments resulting in stable emission only. Such behaviour is shown to be prevalent over broad experimentally accessible operating conditions, in some instances from the onset of stimulated scattering.

In the light of recent well defined cw experiments on SBS, in optical fibre, confirming rich aperiodic behaviour in the emission [2,3] the relative roles of nonlinear dispersion and noise in determining this behaviour is an outstanding issue of some importance. In this report clarification of the role of nonlinear refraction is unambiguously established by considering stimulated scattering in the presence of external feedback. Our experimental findings, so far for SBS, in single mode optical fibre show with the inclusion of *cavity feedback* (pumped at 514 nm) a dramatic modification of the dynamics to sustained and bursting modes of quasi-periodic behaviour. These distinct features provide an excellent basis for quantitative tests of our mathematical description. No evidence is found for sustained stable emission. Our results are shown to be in good quantitative accord with the predictions of our generalised treatment and indicate that spontaneous noise has little or no influence on the deterministic behaviour for this system. Representative data of the SBS emission in a 40 m long fibre (experimental and theory) showing the form and trend of the dynamical features on increasing the pump power from close to threshold to ~ 3 times above are shown in Fig. 1, feedback of ~ 4% being provided by the natural reflectivity of the fibre. Similar features are also obtained for constant pump intensities on varying the feedback (investigated over the range of 1~10%), bursting features prevailing for higher reflectivities. The numerical simulations are based on

physical parameters for silica fibre at 514 nm (gain = $2.6 \times 10^{-11}$ m/W, $\alpha = 4.6 \times 10^{-3}$ m$^{-1}$, $\delta\nu_B$ = 143 MHz, $A_{eff}$ = 14 μm$^2$, $n_2 = 2 \times 10^{-22}$ m$^2$/v$^2$ (electronic). On a contracted time scale (typically ≥ 1 ms) these features show intermittent type behaviour evolving from sustained to bursting emission, the variable separation of which progressively increases with pump power towards eventual quasi cw emission.

Our theoretical and experimental analysis of the dynamical behaviour, through time series, power spectra and phase portraits, establish periodic, quasiperiodic and underlying weak chaotic features. These results, along with current measurements on a longer time scale of the intermittency behaviour, will be presented.

The physical mechanism of nonlinear refraction in promoting the rich dynamics we observe is explained through its induced effect of dynamic phase mismatching between the pump and Stokes waves, details of which will also be discussed.

Towards assessing the role of noise on the dynamics, the inclusion of spontaneous scattering to our model descriptions is currently in progress. Results will be reported for stimulated scattering with and without cavity feedback.

References

[1] Weiping Lu and R.G. Harrison, Europhysics Letts., 16, 655 (1991).

[2] A.L. Gaeta and R.W.Boyd, Phys. Rev., 44, 3205 (1991) and papers cited therein.

[3] R.G. Harrison, J.S. Uppal, A. Johnstone and J.V. Moloney, Phys. Rev. Lett., 65, 167 (1990).

[4] A. Johnstone, Weiping Lu, J.S. Uppal and R.G. Harrison, Opt. Commun., 81, 222 (1991).

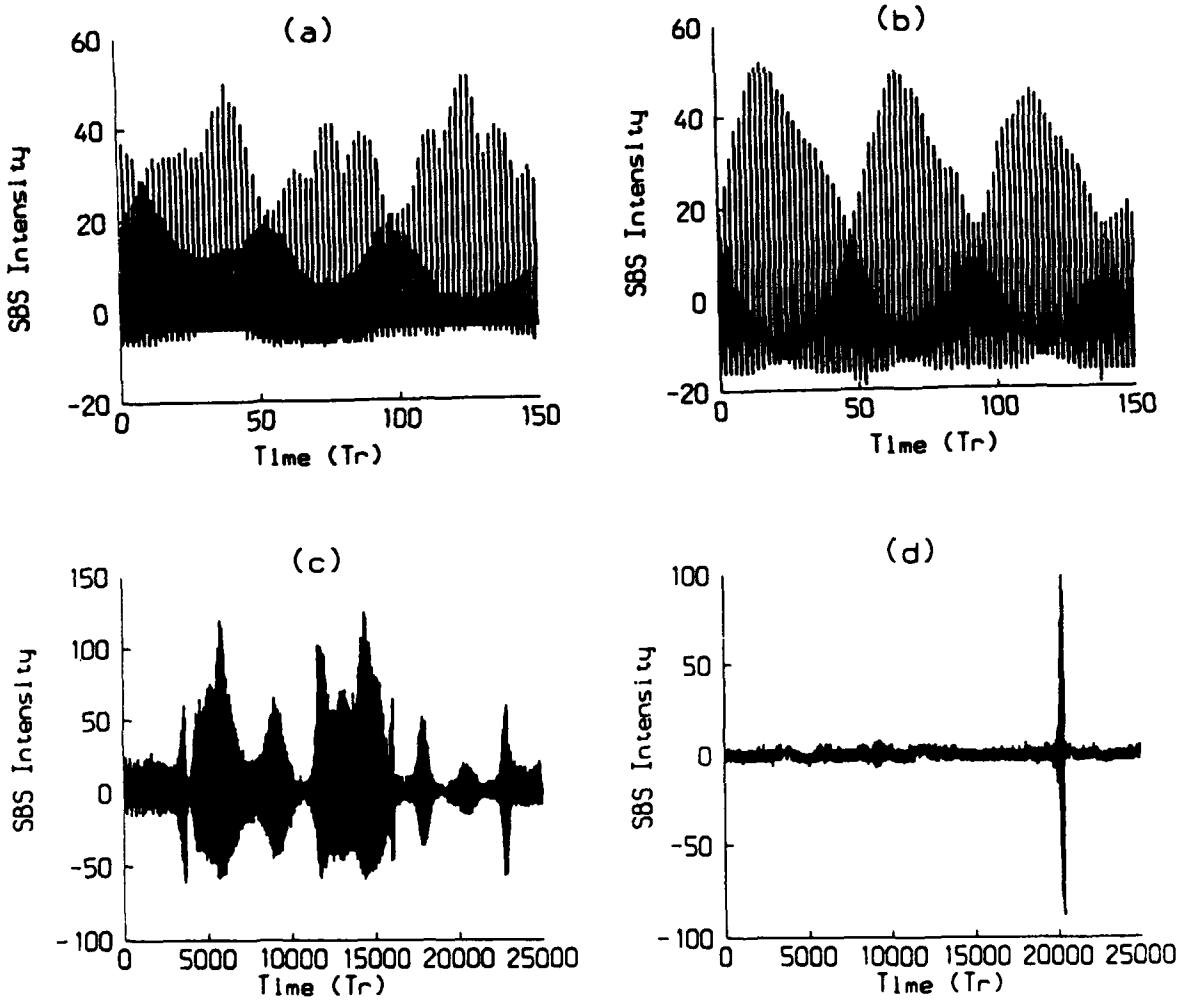


Representative theoretical (left column) and experimental (right column) time series of Stokes intensities on increasing pump power in a 40 m long silica fibre, (a) and (b): Basic periodic oscillation of 2tr (~ 0.4 μs) with a slow regular modulation; (c) and (d): Bursting oscillations, only one bursting profile being presented in the theoretical plot. Note the different time windows between traces (c) and (d).

# Cascaded stimulated Brillouin scattering in high-finesse all-fibre ring resonators

Dieter Garus (member, IEEE), Ralf Hereth
Lehrstuhl für Allgemeine Elektrotechnik und Elektrooptik, Ruhr-Universität Bochum
Universitätsstr. 150, 4630 Bochum, Germany, phone: 49/234/700-2491

One of the most dominant nonlinear effects in single-mode fibers is stimulated Brillouin scattering (SBS). The generation of SBS in a ring resonator can be considered as a lasing action, with the Stokes output downshifted in frequency by an amount equal to the Brillouin frequency. In the stationary case stimulated Brillouin scattering in a length of optical fiber can be described by the following partial differential equations for the slowly varying complex amplitudes of the pump wave $E_p$ and the backscattered first order Stokes wave $E_{B1}$, with the wave amplitudes $E_i$ related to the intensities $I_i$ by $I_i=|E_i|^2$ $(i=p,B1)$ [1]:

$$\frac{\partial E_p}{\partial x} = -\frac{1}{2}(g_B I_{B1}+\alpha)E_p$$
$$\frac{\partial E_{B1}}{\partial x} = -\frac{1}{2}(g_B I_p-\alpha)E_{B1} \qquad (1)$$

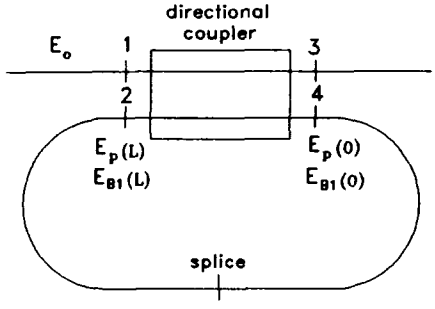


Fig. 1: Ring resonator geometry

In a ring resonator geometry as depicted in Fig. 1 the wave amplitudes at the ports of the directional coupler obey the relations [2]

$$E_p(0) = V_k(-jKE_o+TE_p(L)) ,$$
$$E_{B1}(L) = V_k T E_{B1}(0) , \qquad (2)$$

where $V_k^2$ is the coupler intensity radiation loss, $K$ is the field coupling coefficient, and $T$ is the field transmission coefficient.

The above equations are only valid for limited pump powers, that means the intensity of the backscattered Stokes light at the frequency $\omega_p-\omega_B$ is low enough so that it cannot excite forward Brillouin scattering at $\omega_p-2\omega_B$. If higher order Brillouin scattering has to be considered, the differential equations must be changed adequately. If e. g. second order forward scattering, $E_{F2}$, is taken into account, the differential equations describing the spatial development of pump, backward Stokes and forward Stokes wave amplitudes in the stationary case have the form

$$\frac{\partial E_p}{\partial x} = -\frac{1}{2}(g_B I_{B1}+\alpha)E_p ,$$
$$\frac{\partial E_{B1}}{\partial x} = -\frac{1}{2}(g_B I_p-g_B I_{F2}-\alpha)E_{B1} , \qquad (3)$$
$$\frac{\partial E_{F2}}{\partial x} = -\frac{1}{2}(-g_B I_{B1}+\alpha)E_{F2} ,$$

where the physical meaning of the terms on the right hand side is obvious. If the total Brillouin gain over one loop transit is small, a direct integration of these differential equations yields the following relations for the wave amplitudes at the coupler ports inside the resonator loop:

$$E_p(L) = E_p(0)\exp\left(-\frac{\alpha L}{2}-\frac{g_B L}{2}I_{B1}(0)\right)$$

$$E_{B1}(0) = E_{B1}(L)\exp\left(-\frac{\alpha L}{2}-\frac{g_B L}{2}I_p(0)+\frac{g_B L}{2}I_{F2}(L)\right) \tag{4}$$

$$E_{F2}(L) = E_{F2}(0)\exp\left(-\frac{\alpha L}{2}+\frac{g_B L}{2}I_{B1}(L)\right)$$

An additional equation is obtained from the boundary conditions at the directional coupler, which gives

$$E_{F2}(0) = V_k T E_{F2}(L)\ . \tag{5}$$

Stimulated Brillouin scattering can be described completely by a set of $(4N+2)$ equations, if $N$ scattered waves in forward and backward direction are considered, respectively. $E_{B(\mu+1)}$ denotes the wave amplitude of backscattered Stokes radiation, having a frequency of $\omega_p-(\mu+1)\omega_B$, whereas $E_{F\mu}$ denotes Stokes radiation in forward direction having the frequency $\omega_p-\mu\omega_B$.

The lowest pump threshold, i. e. the threshold for first order backscattering, can be calculated from Equations (2) and (4) as

$$P_{th,B1} = \frac{2A}{g_B L V_k^2 K^2}\frac{\left(1-TV_k\exp(-\frac{\alpha L}{2})\right)^3}{V_k T}. \tag{6}$$

It is possible to derive general expressions for the pump thresholds of backward and forward scattering, respectively. The results are

$$P_{th,B(2N-1)} = \left(\sum_{i=1}^{N}(V_k T)^{-(2i-2)}\right)\left(1+(1-\frac{\alpha L}{2})\sum_{i=1}^{N-1}(V_k T)^{-2i}\right)^2 P_{th,B1} \tag{7}$$

for the pump threshold of the (2N-1)'th order backscattered Stokes wave and

$$P_{th,F(2N)} = \left(\sum_{i=1}^{N}(V_k T)^{-(2i-2)}\right)\left(\sum_{i=0}^{N}(V_k T)^{-2i}\right)^2 P_{th,B1} \tag{8}$$

for the pump threshold of the (2N)'th order forward scattered wave. In the case of negligible fibre and coupler losses, i. e. $V_k \approx 1$ and $\alpha L \ll 1$, and almost critical coupling of the resonator, i. e. $T \approx V_k e^{-\alpha L}$, the pump thresholds can be approximated by

$$P_{th,B(2N-1)} = N^3 P_{th,B1} \tag{9}$$

and

$$P_{th,F(2N)} = N(N+1)^2\ P_{th,B1}\ . \tag{10}$$

If the pump power $P_p$ is in the range $P_{th,B1}<P_p<P_{th,F2}$, the backscattered Stokes power can be calculated from the set of Equations (2) and (4), which yields the result

$$P_{B1} = \frac{2A}{g_B L V_k T}\left(1-TV_k\exp(-\frac{\alpha L}{2})\right)\left[\sqrt{\frac{P_p}{P_{th,B1}}}-1\right]. \qquad (11)$$

If the pump power is in the range $P_{th,B(2N+1)}<P_p<P_{th,F(2N+2)}$, then the backscattered Stokes power at the frequency $\omega_p-(2\mu+1)\omega_B$, $\mu=1...N$, is

$$P_{B(2\mu+1)} = (V_k T)^{2\mu}\, P_{B1}(P_p)-\frac{2A}{g_B L}\left(1-TV_k\exp(-\frac{\alpha L}{2})\right)\sum_{i=2}^{\mu+1}(V_k T)^{2i-5} \quad . \qquad (12)$$

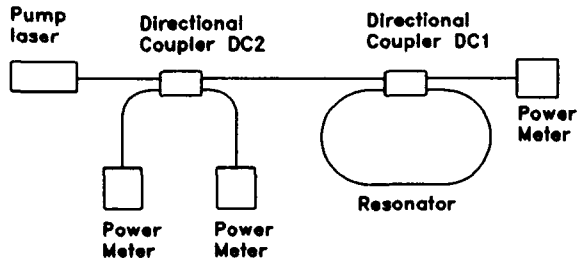


Fig. 2: Experimental setup

The experimental configuration is shown in Fig. 2. The fibre ring resonator, having a finesse $F=145$, is made of 100 m of non-polarization-maintaining single-mode fibre with a damping coefficient $\alpha=0.38\,dB/km$, a core diameter $d=10\,\mu m$ and a core refractive index $n=1.46$. The directional coupler *DC1* has an intensity coupling coefficient $K^2=2.7\,\%$ and a coupler loss $V_k^2=0.035\,dB$. The pump source is a 1319-nm NdYag-laser with a maximum output power of 2 mW. The backscattered Stokes power measured as a function of the pump power coupled into the resonator is depicted in Fig. 3. The pump threshold for the onset of first order Brillouin backscattering was determined as $P_{th,B1}=40\,\mu W$. The good agreement between experiment and theory is shown in Fig. 4 where the output Stokes power was calculated by (12), with the resonator parameters given above.

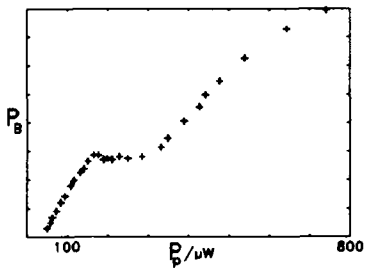


Fig. 3: Measured Stokes power

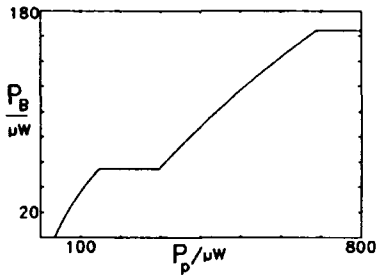


Fig. 4: Calculated Stokes output

This work was supported by: Bundesminister für Forschung und Technologie, Förderkennzeichen 13 MV 0059. The authors are responsible for the contents.

References

[1] Bayvel, P.; Giles, I.; Radmore, P. M.: *Transient and steady-state characteristics of a Brillouin amplifier based on an all-fibre single-mode ring resonator.* Opt. and Quantum Electron., Vol.21, Spec. Issue (1989), pp.113-128

[2] Stokes, L. F.; Chodorow, M.; Shaw, H. J.: *All-single-mode fiber resonator.* Opt. Lett., Vol.7, No.6 (June 1982), pp.288-290

# Hamiltonian Dynamics of Parametric Nonlinear Wave Mixing

**S. Trillo, and S. Wabnitz**

*Fondazione Ugo Bordoni, Via B. Castiglione 59, 00142 Rome, Italy*

Exact solutions in terms of elliptic integrals to the problem of mixing between a wave and its second-harmonic in a medium with quadratic and/or cubic nonlinearity have been reported in the nonlinear optics literature since the early sixties [1-4]. These solutions involve rather cumbersome expressions which do not lead to an immediate insight into the physics of the conversion process.

In this work we introduce a reduced geometrical representation of parametric mixing processes, which is based on the Hamiltonian formalism of nonlinear dynamical systems. The coupling between the complex wave amplitudes is represented by the motion of a point on a given trajectory in the phase plane [2]. The present approach permits to discover the nonlinear eigenmodes of the mixing process and to study their spatial stability. The visualization of the dynamics of the wave coupling process in the phase plane also allows for a powerful immediate physical insight. For example, the phase dependence of the conversion efficiency in the case of seeded second harmonic generation or frequency division is simply explained. Our description also reveals the existence of spatially chaotic regimes for wave propagation in nonuniform media, e.g., in the presence of the periodic variations of the linear or nonlinear properties which are exploited by the quasi-phase matching techniques [5].

Let us briefly outline here the basic steps of our reduction procedure. The equations for the complex fields $a_1 = \sqrt{2}A_\omega$, and $a_2 = A_{2\omega}$, which propagate in a isotropic medium with quadratic and cubic nonlinearity (e.g., an optical fiber), read

$$\begin{aligned} -i\frac{da_1}{d\xi} &= a_2 a_1^* + \chi(\frac{1}{2}\mid a_1\mid^2 + 2\mid a_2\mid^2)a_1 \\ -i\frac{da_2}{d\xi} &= \kappa a_2 + \frac{1}{2}a_2^2 + 2\chi(\mid a_1\mid^2 + \mid a_2\mid^2)a_2, \end{aligned} \tag{1}$$

Here $\chi$ is the ratio between cubic and quadratic nonlinear susceptibilites, $\kappa$ is the linear mismatch, and $\xi = RPz$, where $P = \mid a_1\mid^2 + \mid a_2\mid^2/2$ is the conserved flux and $R$ is coefficient which is proportional to the second order susceptibility. Equations (1) can be written in the Hamiltonian form

$$\frac{\partial a_j}{\partial \xi} = i\frac{\partial H}{\partial a_j^*}, j = 1, 2, \tag{2}$$

where the Hamiltonian reads

$$H = \Delta\kappa \mid a_2\mid^2 + \frac{\chi}{2}\mid a_1\mid^4 + \chi\mid a_1\mid^4 + 2\chi\mid a_1\mid^2\mid a_2\mid^2 + \frac{1}{2}(a_1^2 a_2^* + \text{c.c.}). \tag{3}$$

Equations (1-3) can be reduced to the following one-degree-of-freedom nonlinear oscillator in the conjugate variables

$$\begin{aligned} \eta &\doteq \frac{\mid a_2\mid^2}{P}, \\ \phi &\doteq 2\phi_1 - \phi_2, \end{aligned} \tag{4}$$

where $a_j \doteq \mid a_j \mid exp\{i\phi_j\}, j = 1,2$. The above variables obey

$$\dot{\eta} = \frac{\partial \hat{H}}{\partial \phi}, \dot{\phi} = -\frac{\partial \hat{H}}{\partial \eta}, \tag{5}$$

where the dot denotes derivation with respect to $\xi$, and the reduced Hamiltonian $\hat{H}$ reads

$$\hat{H}(\eta, \phi) = 2\sqrt{\eta}(1-\eta)cos(\phi) + (2\chi - \Delta\kappa)\eta - 2\chi\eta^2, \tag{6}$$

Changing from polar to the cartesian coordinates $u = \sqrt{\eta}\, cos\,\phi$, and $v = \sqrt{\eta}\, sin\,\phi$, this Hamiltonian is

$$\tilde{H} = 2(u^2+v^2)u + 2u + (2\chi - \Delta\kappa)(u^2+v^2) - 2\chi(u^2+v^2)^2 = H_c + H_d \tag{7}$$

where $H_c = 2(u^2+v^2)u$, and $H_d$ is the Hamiltonian of the time-averaged nonlinear Duffing oscillator.

The advantage of the reduced description (eqs.(5-7)) is that one may obtain an immediate physical insight into the conversion process, by a simple visual inspection of the $\tilde{H} = constant$ curves in the phase plane. The geometry of the phase plane is determined by the number and the stability properties of the nonlinear eigenmodes (i.e., the linear superpositions of the two waves which propagate unchanged). Bifurcations and consequent changes of stability of the eigenmodes occur as one parameter (i.e., the mismatch $\kappa$) is varied. Fig.1 shows the bifurcation diagram in the simplest case where the third-order contribution is negligible (i.e., $\chi = 0$). More complex bifurcation diagrams occur in the general case.

Fig.2 contrasts the trajectories which are followed by the point $(\eta, \phi)$ (i.e., the constant $\hat{H}$ curves) in a phase mismatched (a) and matched (b) case, respectively. As can be seen, in the last case the circle of fixed points with $\eta = 1$ is an unstable saddle.

This saddle point instability may lead, in the presence of small longitudinal variations of the linear refractive index or the nonlinear susceptibility, to spatially chaotic behavior in frequency conversion process (see fig.3). We demonstrate analytically the existence of homoclinic chaos in the second harmonic generation by means of the Melnikov analysis [6].

This work was carried out under the agreement between Fondazione Ugo Bordoni and the Istituto Superiore Poste e Telecomunicazioni.

## References

[1] J.A. Armstrong, N. Bloembergen, J. Ducuing, and P.S. Pershan, PHys. Rev. ^a, 1918 (1962).

[2] S.A. Akhmanov, and R.V. Khokhlov, *Problems of Nonlinear Optics*, Gordon and Breach Sciences Publishers, New York, 1972.

[3] T.B. Razumikhina, L.S. Telegin, A.I. Kholodnykh, and A.S. Chirkin, Sov. J. Quantum Electron. **14**, 1358 (1984).

[4] W. Choe, P.P. Banerjee, and F. C. Caimi, J. Opt. Soc. of Am. B **8**, 1013 (1991).

[5] S. Somekh, and A. Yariv, Appl. Phys. Lett. **21**, 140 (1972).

[6] J. Guckenheimer, and P. Holmes, *Nonlinear Oscillations, Dynamical Systems, and Bifurcations of Vector Fields* (Springer, N.Y., 1983).

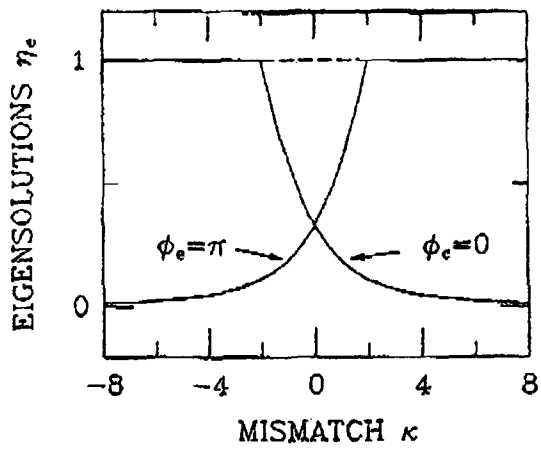


Figure 1: Bifurcation diagram in the absence of third-order contributions: fraction of second-harmonic power of the stable (solid) and unstable (dashed) eigenmodes versus the normalized mismatch $\kappa$.

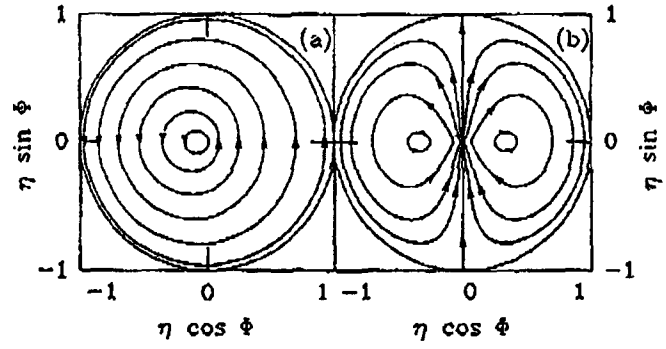


Figure 2: Phase-plane portraits for (a) $\kappa = -5$, (b) $\kappa = 0$.

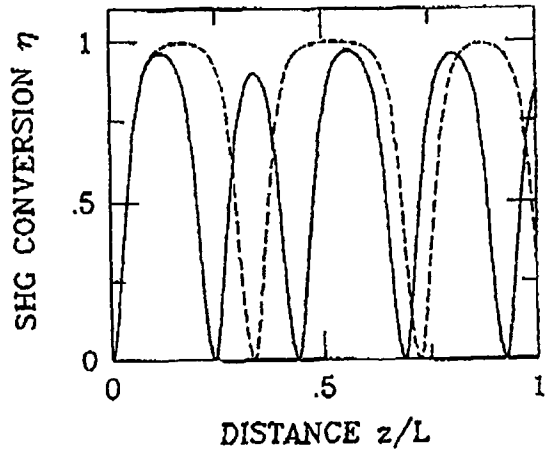


Figure 3: Fraction of second-harmonic power vs. propagation distance z/L, in a quadratic medium with a periodic variation of the linear refractive index, such that $\kappa = \epsilon cos\Omega z$, with $\epsilon = 0.1$, and different values of the spatial frequency $\Omega = 0.5$ (solid), and $\Omega = 1$ (dashed).

# Observation of Chaos in Off-Bragg Photorefractive Four-wave Mixing

Kenneth D. Shaw

Nonlinear Optics Center of Technology

Phillips Laboratory

PL/LITN, Kirtland AFB, NM 87117-6008

Phone: (505)846-4750

Fax: (505)846-4651

In the past few years, several authors have reported observations of chaotic behavior in various photorefractive phase conjugators which involve some form of external feedback, either by way of mirrors or reflections from the crystal faces [1]. We have recently observed such behavior, for the first time to our knowledge, in an externally pumped phase conjugate mirror with no such feedback mechanisms. The origin of chaotic behavior in such a system is fundamentally different from that in either of the former two cases. In the case of the phase conjugate resonator, the chaos apparently arises from a competition between different cavity modes, and in the self-pumped phase conjugator from competition between different photorefractive gratings with different time scales, while in the present case where all the beams are externally supplied, the chaotic behavior is the result of time-dependent phase transfer among the four beams [2]. For the particular set of parameters (coupling constant, geometrical factors, etc.) used in our experiments, theory [3] predicts that such unstable behavior will not occur in ordinary photorefractive four-wave mixing. It will be shown, however, that the observed chaotic oscillations in the phase conjugate intensity

are the result of enhanced gain which can occur when one of the pumping beams deviates slightly from the Bragg angle for the photorefractive phase grating (off-Bragg four-wave mixing, or OBFWM)[4].

Using analytical techniques of nonlinear dynamics, we calculated both the fractal dimension of the phase space trajectory extracted from the experimental time series of the phase conjugate intensity and the number of degrees of freedom (dynamical dimensions) of the system, and found these to have values of 5.7 and 13, respectively. The standard scalar theory of photorefractive four-wave mixing [3] predicts a fractal dimension of 2.4 and the number of dynamical dimensions 5, which are both considerably smaller than those determined in our experiment. Hence it would seem that the scalar coupled wave equations do not provide a correct picture of the dynamics as they occurred in the experiment. These equations comprise four spatial first-order partial differential equations and a fifth first-order PDE which gives the temporal evolution of the refractive index grating. Since they are partial differential equations, they comprise an infinite-dimensional system. Farmer [5] has shown, however, that the dynamics of such an infinite-dimensional system can be represented in a finite-dimensional phase space, the number of dimensions of which are the dynamical dimensions, or the number of degrees of freedom of the system. Comparing this number obtained from the embedding procedure applied to the scalar theory with the number of PDE's in this theory, we see that they are equal. This correspondence implies that since there are 13 degrees of freedom present in the experimental system, the system should therefore be described by 13 first-order partial differential equations. If the coupled wave equations are derived directly from Maxwell's equations for radiation polarized in

the plane of incidence of the beams (see reference [6]), it is found that there are in fact 13 first-order PDE's, 12 of which give the spatial dependence of the electric and magnetic field components of the four beams, and one of which describes the time evolution of the refractive index grating. It is shown in [6] that the vectorial nature of the electromagnetic field plays a vital role in the operation of the double phase conjugate mirror, and so it is not surprising that it would also figure prominently in the dynamics of other photorefractive wave mixing configurations.

[1]. G.C. Valley and G.J. Dunning, Opt. Lett. **9**, 513 (1984); D.J. Gauthier, P. Narum and R.W. Boyd, Phys. Rev. Lett. **58**, 1640 (1987); A.K. Majumdar and J.L. Kobesky, Opt. Comm. **75**, 339 (1990).

[2]. W. Królikowski, M.R. Belić, M. Cronin-Golomb and A. Błędowski, J. Opt. Soc. Am. B **7**, 1204 (1990).

[3]. W. Królikowski, K.D. Shaw, M. Cronin-Golomb and A. Błędowski, J. Opt. Soc. Am. B **6**, 1828 (1989); K.D. Shaw and M. Cronin-Golomb, Opt. Comm. **76**, 151 (1990).

[4]. C. Denz, J. Goltz, and T. Tschudi, Opt. Comm. **72**, 129 (1989).

[5]. J.D. Farmer, Physica D **4**, 366 (1982).

[6]. K.D. Shaw, *The Double Phase Conjugate Mirror is an Oscillator*, submitted to Optics Communications.

# Self and mutual phase conjugation via thin layers.

B. Ya. Zel'dovich, I. V. Goosev, V. A. Krivoschekov.
Technical University, 76 Lenin av., Chelyabinsk,
454080 Russia. Phone (007-3512)-399140

Consider a nonlinear optical layer with small thickness $L$, i.e. with $L \ll \lambda / \theta^2$, where $\theta$ is the angle between interacting waves. If the nonlinearity is of the phase type, the action of the layer on the transmitted beam is the phase modulation only:

$$E_{transm}(x,y) = E_{inc}(x,y)\exp(i\varphi(x,y)) \qquad (1)$$

where $\varphi(x,y)$ is connected with the nonlinear action of the intensity distribution of the field, $\varphi = s|E|^2$. However, the phase modulation produces no extra intensity modulation, and therefore there is no feedback in a thin layer even for a large ($|\varphi| \gg 1$) nonlinearity. This is a strong drawback for such important media as semiconductor quantum wells, for which $L < 1\mu m$, or liquid crystal cells.

The phase modulation $\varphi(x) = g\cos(qx)$ of an incident beam $A\exp(ik_x x)$ results in appearence of diffracted beams:

$$A_{transm}(x) = A\, e^{ik_x x}\left[1 + 0.5ige^{iqx} + 0.5ige^{-iqx} + \ldots\right] \qquad (2)$$

Interference of the +1-st diffraction order with zeroth one virtually gives intensity modulation $\delta I(x) = -|A|^2 g \sin(qx)$, but it is identically compensated by interference $\delta I(x) = +|A|^2 g \sin(qx)$ of zeroth and (-1)-st diffraction orders.

The main idea of this work is to produce by some method the change in the relative amplitudes or phases of these two contributions. Among those methods are: 1) propagation of the wave at some distance $z$, which results in relative phase shift $\gamma_{+1}-\gamma_{-1}=(\sqrt{k^2-(k_x+q)^2}-\sqrt{k^2-(k_x-q)^2})z$, 2) imaging of the output of the layer by a lens with total elimination of (-1)-st diffraction order, like for Foucault knife, 3) the same as in 2), but with introduction extra $180^0$ phase shift into (-1)-st order, like for Zernike phase-contrast microscope.

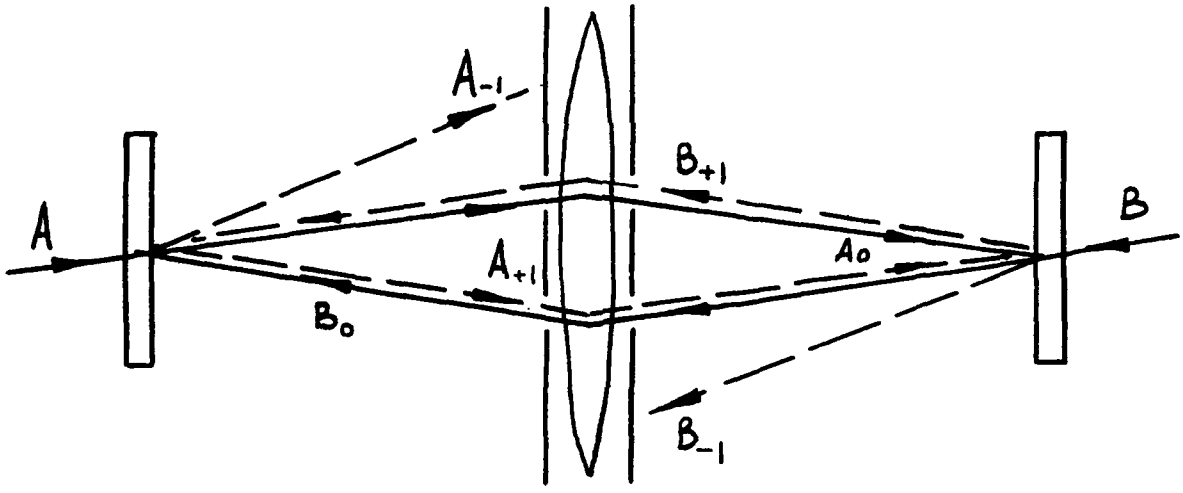


In particular, consider the system of two thin nonlinear layers, illuminated by the beams $A$ and $B$ respectively, and a lens which makes sharp imaging of the illuminated parts of layers to each other, see Figure. Suppose that some grating $g_1$ appeared in the 1-st layer which diffracts the wave $A$ as the +1-st order into the wave which is phase conjugate to $B$.

Interference of $A_{+1}$ and $A_0$ may produce, by cross phase modulation, the grating $g_2$ in the second layer, which will diffract the wave $B$ into $A^*$. The interference of $B_{+1}$ and $B_0$ in the 1-st layer will produce the feedback for original grating $g_1$. Our calculations show that the threshold condition of such mutual conjugation of (generally incoherent to each other) beams $A$ and $B$ is

$$T_1 T_2 \, s_{12} |A|^2 \, s_{21} |B|^2 < -1 \qquad (3)$$

where $\varphi_i = s_{ij} |E_j|^2$ is the cross phase modulation, $T_i$ is intensity transmission coefficient of the $i$-th layer. It is important that the aperture with two holes transmits the beams $A_0$, $A_{+1}$, $B_0$, $B_{+1}$ only and blocks negative diffraction orders.

Experiments were done with nematic liquid crystal cells with thermal nonlinearity which allowed to get $s_{12} > 0$ for ordinary wave and $s_{21} < 0$ for extraordinary wave. We hope to discuss also nonlinear dynamics of the system, a lot of variations of set-up geometry and different types of media.

# Applications of Fiber Optic Interferometry in Nonlinear Dynamics

S.T. Vohra and F. Bucholtz
Naval Research Laboratory, Code 6570
Washington DC 20375-5000
Telephone : (202)-767-9349

The ultimate performance of a fiber optic (FO) interferometer depends on its ability to resolve small differential optical phase shifts. Due to advances in FO technology it has become possible to fabricate interferometers with optical phase resolution of $< 1\ \mu rad/\sqrt{Hz}$ ($f > 100$ Hz) [1]. Such FO interferometers have been successfully utilized in making extremely high resolution acoustic and electromagnetic field sensors [1]. Since the optical phase shift in the fiber is directly proportional to the induced strain in the material bonded to the optical fiber the FO interferometer is also well suited for studying the dynamic strain response of magnetostrictive, piezoelectric and electrostrictive materials [2].

A low noise, high resolution (strain resolution $\leq 10^{-12}/\sqrt{Hz}$ for $f \geq 1$ kHz) fiber optic interferometer is used for the first time to observe several routes to chaos in the nonlinear strain dynamics of piezoelectric (lead zirconate titanate - PZT) and magnetostrictive ($Fe_{78}B_{13}S_9$ - Metglas 2605S-2) materials. The nonlinear time series obtained from the FO interferometer output is used to generate power spectra, display Poincare sections, perform dimension calculations and compute Lyapunov exponents. It is the computation of the Lypunov exponents which especially requires a low noise time series [3]. The experiment has also been utilized to verify various 'universal' models of nonlinear dynamics [4,5]. Due to low noise in the experiment the FO interferometer is particularly well suited in characterizing the effects of noise on dynamical instabilities since noise can be added to the system in a controlled manner.

A Mach-Zehnder fiber optic interferometer [1] used to measure the nonlinear strain dynamics of various materials is depicted in Figure 1. A small portion of the nonlinear material is bonded to the optical fiber comprising one arm of the interferometer. The phase shift of light propagating in the fiber attached to the material is a direct measure of the induced strain in the material. The output from the optical detectors is monitored with a dynamic signal analyzer for real time power spectral analysis and is also digitized with a LeCroy high speed (12 bit) digitizer for generating and storing time series.

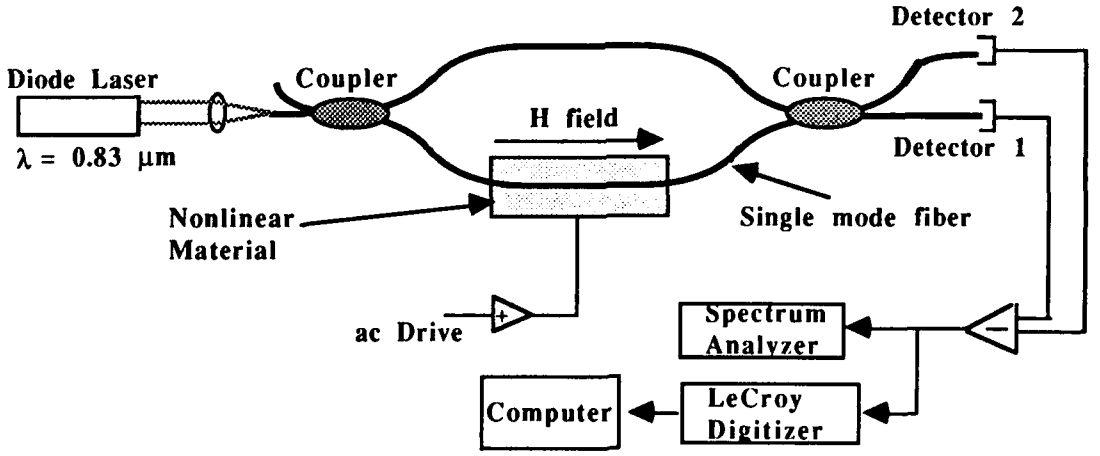


**Figure 1** A schematic of the fiber optic interferometer used to measure the nonlinear strain dynamics of materials.

Nonlinear strain response of magnetostrictive and piezoelectric materials, monitored with a FO interferometer, showed several routes to chaos including period doubling cascades, quasiperiodicity, phase locking and intermittency. A typical nonlinear strain response of a driven magnetostrictive ribbon is shown in Figure 2. A 4" long, vertically held unannealed Metglas ribbon which was clamped at the top end and driven at frequency f = 8.5 kHz with $h_{ac}$ = 0.5 $Gauss_{rms}$ and $H_{dc}$ = 2 Gauss showed a bifurcation at half the drive frequency (period doubling) coexisting with another bifurcation whose frequency was incommensurate with the drive. Figure 2 shows the power spectra of the interferometer output which depicts the drive frequency (f), the period doubled frequency (f/2) and a frequency incommensurate with the drive ($f_q$). Phase space reconstruction of the experimental time series (60 points per period) by the delay coordinate embedding technique showed a two torus as expected (Figure 2b). The corresponding Poincare section depicted in Figure 2c displayed two circles (due to a two torus). Two torus bifurcations have been predicted by Kaneko [6] from studies on coupled logistic maps but have not been experimentally verified. Further changes in drive parameters showed various other bifurcations followed by chaos.

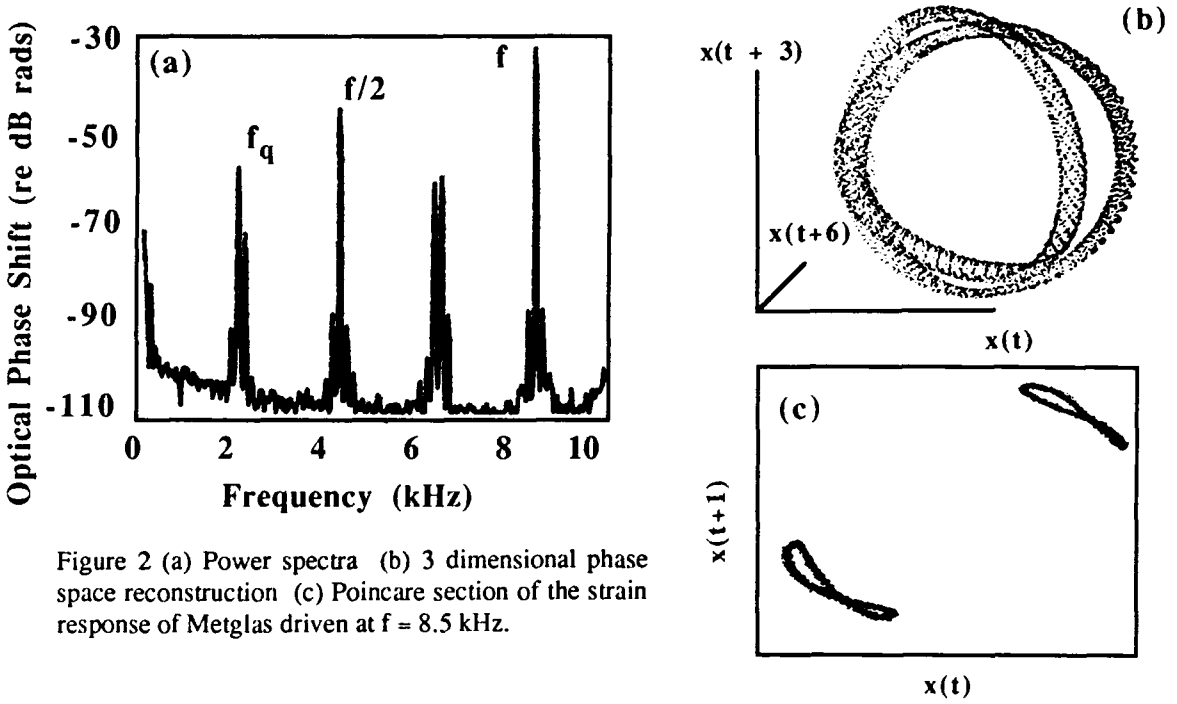


Figure 2 (a) Power spectra (b) 3 dimensional phase space reconstruction (c) Poincare section of the strain response of Metglas driven at f = 8.5 kHz.

The power spectra (Fig. 2) shows the low noise, large dynamic range of the system which makes it well suited in the computation of Lyapunov exponents from experimental time series. Figure 3 depicts a Poincare section generated from a chaotic time series output of a magnetostrictive ribbon. The data was taken for an ac drive amplitude of 0.753 Gauss and a DC bias of 1.5 Gauss at f = 7.68 kHz. The computed Hausdorff dimension of the attractor shown in Figure 3 was approximately 2.1. Table 1 shows the calculated Lyapunov exponents $\lambda_1$, $\lambda_2$, $\lambda_3$ for local dimension 3 and increasing order of mapping from 2 to 4 [7]. The reliable computation of all the Lyapunov exponents (including the negative ones) from experimental system requires such a low noise time series.

Figure 3

| $N_{Tay}$ | $\lambda_1$ | $\lambda_2$ | $\lambda_3$ | Error |
|---|---|---|---|---|
| 2 | -0.01 | -0.12 | -0.68 | 0.32 |
| 3 | 0.11 | -0.07 | -0.65 | 0.20 |
| 4 | 0.14 | -0.07 | -0.63 | 0.14 |

Table 1

The experiment has also been utilized to verify the universality of noise rise in parametric devices. The problem of anomalous noise rise near points of maximum signal gain in a parametric amplifier has recently been theorized to be a universal phenomena [8]. The theory states that the point of maximum signal gain coincides with a bifurcation in the system and as the system approaches the bifurcation it undergoes both signal and noise gain. While this effect had been observed in Josephson junction devices it had not been observed in any other physical system thereby questioning the universality of the theory. By tuning the system near a period doubling bifurcation and adding external noise to the system we not only verified the noise rise phenomena (Figure 4) but also verified the scaling laws predicted by the theory [5].

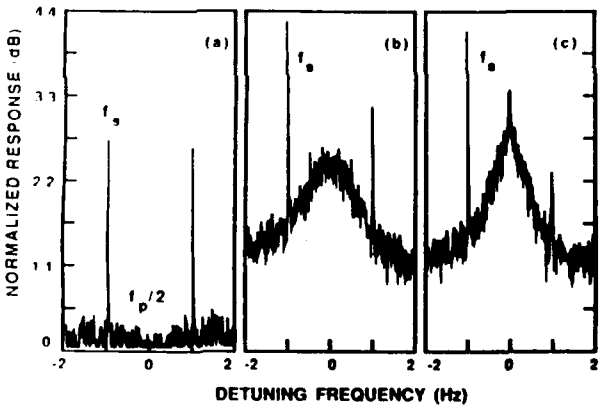


Figure 4 Noise rise near a period doubling bifurcation in a parametrically driven magnetostrictive ribbon. $f_s$ = signal frequency, $f_p$ = pump frequency and $f_p/2$ designates the frequency associated with a period doubling bifurcation. (a) System is tuned far from the point of maximum signal gain (b) system approaches point of maximum signal gain (c) past the point of maximum signal gain.

In conclusion, we have demonstrated that fiber optic interferometry is ideally suited for direct observation of the nonlinear strain dynamics of various materials. The inherently low noise associated with the interferometer allows for direct observation of subharmonic bifurcations with a large dynamic range, allows for reliable computation of Lyapunov exponents and allows for the verification of the universality of theories on noise induced processes near bifurcation.

**References**

1. Fiber Optic Sensors, E.Udd Editor, John Wiley and Sons (1991).
2. S.T. Vohra, F. Bucholtz, D.M. Dagenais and K.P. Koo, *J. Appl. Phys.* **69** (8), 5736 (1991).
3. P. Bryant, R. Brown and H.I. Abarbanel, *Phys. Rev. Lett.* **65** (13), 1523 (1990).
4. S.T. Vohra, F. Bucholtz, K.P. Koo and D.M. Dagenais, *Phys. Rev. Lett.* **66** (2), 212 (1991).
5. S.T. Vohra, F. Bucholtz, K.P. Koo and D.M. Dagenais, *Phys. Rev. Lett.* **66** (22), 2843 (1991).
6. K. Kaneko, *Prog. Theor. Physics* **72** (2), 202 (1984).
7. P.Bryant, Proc. of 1st Experimental Chaos Conference, World Scientific Publishers, (to be published, 1992).
8. P. Bryant, K. Wiesenfeld and B. McNamara, Phys. Rev. B 36, 752 (1987).

# Poster Session 2

**TuC** 8:00pm–10:00pm
Krenek Hall

# Transverse Modes Of Microchip Solid State Lasers

**G.K. Harkness and W.J. Firth**
**Department of Physics and Applied Physics**
**University of Strathclyde**
**107 Rottenrow, Glasgow G4 0NG**
**Scotland**
**Tel. (+) 44 41 552 4400 Ext. 3112**
**Fax. (+) 44 41 552 2891**

In recent years there has been much research into lasers using solid state materials such as Nd:YAG, Nd:YLF and LNP as their active media [1]. Microchip solid state lasers use a thin slab of these materials in a short cavity to ensure single longitudinal mode operation. They may be pumped by a diode laser and they produce single transverse, single longitudinal mode output over a large range of pump powers. It is useful to be able to model the spatial and temporal behaviour of these lasers with a view to design optimisation.

The laser system we have chosen to model is the plane-plane cavity formed by dielectrically coating the ends of the crystal. The single diode laser pump is closely coupled to one end. An empty cavity of this type has no confined transverse modes but the gaussian gain profile induced by the pump produces gain-guided modes. We find that these modes are analagous to the Gauss-Laguerre modes of a non-planar cavity except that certain degeneracies between modes [2] are broken and the gain-guided modes decay exponentially in wings rather than like a conventional gaussian.

Our model is based around the usual Maxwell-Bloch equations for the interaction

of a laser field with the active medium [2]. In steady state the Maxwell-Bloch equations reduce to the following equation for the radial dependence of the laser field $R(r)$

$$\frac{d^2R}{dr^2} + \frac{1}{r}\frac{dR}{dr} - \frac{m^2}{r^2}R + \left[i\alpha + \delta_L - \delta_C + p\chi(r)\frac{\beta\delta_L - i}{\beta^2\delta_L^2 + 1 + I|R(r)|^2}\right] R(r) = 0. \quad (1)$$

Here $m$ is the azimuthal mode index. The other parameters have been scaled into dimensionless units and are: $\delta_L$ the laser output frequency and $\delta_C$ the longitudinal cavity mode frequency - both referenced to the atomic line frequency, $\alpha$ the cavity losses, $\beta$ a linewidth factor, $\chi(r)$ the gain profile shape normalised to unity on axis. The laser intensity $I$, the pump parameter $p$, and $\delta_L$ are considered as unknowns. If we fix one of these three we can solve for the other two by requiring that the mode profile $R(r)$ is bounded for large radii.

For the parameters corresponding to the laser of Zayhowski *et al.* [3] our model shows that, because of its good overlap with the pump profile, the pseudo-gaussian (0,0) mode has the lowest threshold. We also predict that, in the absence of thermal effects, the pump threshold for the intrusion of the (0,1) mode when the (0,0) mode is operating is very high. This is in good agreement with the results of Zayhowski *et al.* However, as figure 1 shows, for other parameter values simultaneous operation of two or more transverse modes may be possible leading to more complicated output patterns. The fact that these lasers show such remarkable stability of their (0,0) mode indicates that a sacrifice is being made in some other aspect of the design. Our model may be useful in answering such questions.

In this paper we will describe the model and its application to this type of laser. We will present results on the thresholds and frequencies of the gain guided transverse modes and discuss their stability. For strong pumping, thermal effects may become relevant [4]. The inclusion of such effects in our model will be described.

## References

[1] IEEE Journal of Quantum Electronics, June 1988 - Special Issue on Solid State Lasers

[2] L.A.Lugiato, G-L.Oppo, J.R.Tredicce, L.M.Narducci and M.A.Pernigo, J. Opt. Soc. of Am. B **7**, 1019 (1990).

[3] J.J. Zayhowski and A. Mooradian, Optics Letters **14**, 24 (1989)

[4] N. MacKinnon, C.J. Norrie, B.D. Sinclair, EQEC 1991, PLWe32

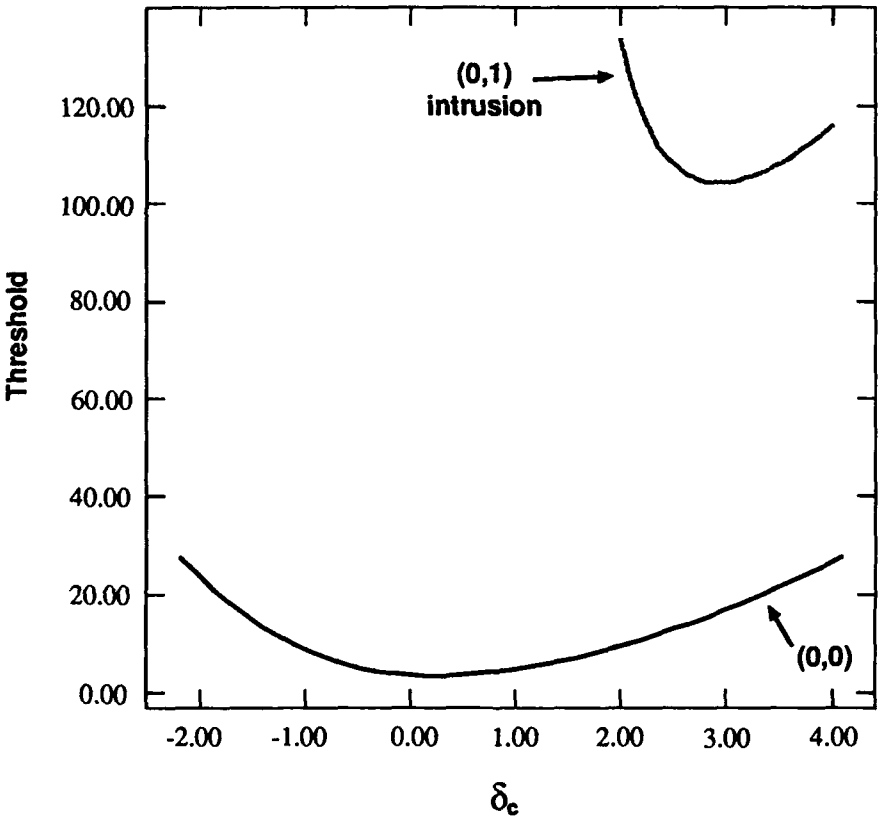


Figure 1 : Pump threshold versus cavity detuning for the pseudo-gaussian (0,0) transverse mode and for the intrusion of the (0,1) mode.

$\alpha' L = 0.05$, $\beta = 1$, $\gamma = 0.05$.

# HEXAGONAL TRANSVERSE PATTERNS IN THE COUNTER-PROPAGATED LIGHT BEAMS INTERACTION: MANY-BODY APPROACH

A.A.Afanas'ev, B.A.Samson
Institute of Physics Belarus Acad.Sci., F.Skarina ave.,70
Minsk 220602, Belarus FAX 7-0172-393131
V.M.Volkov
Institute of Mathematics Belarus Acad.Sci.,Minsk Belarus

The hexagonal patterns in nonlinear optics previously have been discovered experimentally [1,2] and numerically [3]. It was noted that the appearance of the hexagons is one of the displaying of strong counter-propagated light beams instability, in particular, in the media with Kerr-like nonlinearity.

In this work we propose to consider the hexagonal output structure of light beams as a result of dense packing of filaments formed due to a self-focusing. This hypothesis is based on the proof of existence of forces of interaction, in particular, repelling, between filaments. This fact permits to consider the dynamics of transverse light patterns as a many-body problem. Furthermore, it is shown that the finity of thickness of layer of nonlinear medium equivalents to presence of effective repelling border, bounding the region with the "gas" of filaments. In a steady-state limit corresponding to "cooled gas" in a closed volume, the "gas" of filaments crystallizes as a dense hexagonal packing.

The using of many-body theory gives the possibility to assign the vibrational freedom degrees to filaments, and on the basis of that to determine the threshold of transition to a spatial chaos.

Further, we propose to simulate the spatial patterns formation at the interaction of counter-propagating beams in a

Kerr-like medium by the dynamic equations of the following type

$$\partial_t E = i\Delta_\perp E + i|E|^2 E - \sigma E + \sigma W E_o / \int_{r_\perp} E_o E^* dr_\perp + \text{repelling bounds}, \quad (1)$$

where $E_o(r_\perp)=E(t=0)$ is the initial condition, corresponding to the symmetric boundary conditions in the simulation of direct problem [3], $W=\int_{r_\perp}|E|^2 dr_\perp=\int_{r_\perp}|E_o|^2 dr_\perp$ is the unvariable total energy, $\sigma \ll 1$ is the small parameter determined empirically from the comparison between the results of spatial dynamics simulation according to eq.(1) and the direct one [3]. The principal properties of eq.(1) are, first, the permanent adding the initial condition $E_o$ to the evolution of field E, that corresponds to the bounds influence in the counter-propagating interaction. Second, the stability of such solutions as the Townes wave-guide [4], unstable in a Kerr-like media. This stability is achieved at $\sigma > \Omega_k$, where $\Omega_k$ is the instability index of the Townes wave-guide, or the eq.(1) solution at $\sigma=0$. The stability of filaments as the solutions of eq.(1) corresponds to the absence of collapsed solutions in the direct problem statement [3] due to the finity of the interaction length L.

The simulation of the spatial patterns dynamics according to eq.(1) demonstrates the formation of hexagonal structures, oscillating spots, rotating set of vortices and spatial chaos.

REFERENCES

1.G.D'Alessandro, W.J.Firth, Phys.Rev.Lett., 66, 2597 (1991).

2.G.Grinberg, Opt.Comm., 66, 321, (1988).

3.W.J.Firth et al., Digest EQEC'91, Edinburgh, 1991.

4.R.Y.Chiao et al., Phys.Rev.Lett., 14, 1056 (1965).

# Spatial Symmetry Breaking and Coexistence of Attractors in a Nonlinear Ring Cavity

M.Sauer, F.Kaiser

Institute for Applied Physics, Technical University Darmstadt

Hochschulstr.4a, D-6100 Darmstadt

Modulational instabilities in nonlinear optical systems play an important role for pattern formation since they give rise to characteristic internal space frequencies [1]. We address the question how the pattern formation by modulational instabilities influenced by an external spatial modulation of the input. We find a sequence of temporal frequency locking when the wavelength of the modulation is increased. It also leads to a spontaneous symmetry breaking of the solutions which allows for the coexistence of various periodic attractors. This can be explained by the concept of cooperative frequency locking[2, 3].

Our model system consists of a ring cavity of length $\mathcal{L}$ which contains a probe of homogeneously broadened two-level-atoms of length L. Transverse effects are taken into account in one dimension. The wave equation together with the boundary condition read:

$$\left(i\frac{\partial}{\partial z}+\frac{1}{2k}\frac{\partial^2}{\partial x^2}\right)E_n(x,z)-\frac{\alpha}{2}\frac{1+i\Delta}{1+4\mid E_n\mid^2}E_n(x,z)=0 \tag{1}$$

$$E_n(x,0)=\sqrt{T}A(x)+R\exp(ik\mathcal{L})E_{n-1}(x,L) \tag{2}$$

For explanation of the parameters and the parameter values, see [3]. The harmonically modulated input beam A(x) is:

$$A(x)=A_0\left(1+A_m\cos(k_m x)\right)\exp(-\frac{x^2}{\sigma^2}) \tag{3}$$

We investigate the influence of the amplitude and the frequency of the modulation ($A_m$,$k_m$) on a P4-solution in the limit of no modulation. We find alternating bands of periodic and quasiperiodic or chaotic solutions (Fig.1). This structure of the phase diagram is due to the influence of the external frequencies.

The marked points in the region of $k_m = 40$ belong to solutions with broken symmetry to the x=0-axis. This spontaneous symmetry breaking has not been observed without modulation and it leads to qualitatively new bifurcations.

At $A_m = 0.2$ one observes a transition from a non-symmetry-broken P2-solution ($k_m = 36$) to a symmetry-broken P4-solution at $k_m = 40$. At $k_m = 37$ there appears a period-doubling bifurcation which is accompanied by a symmetry-breaking of the output profiles (Fig.2). The resulting P4-attractor is symmetric. The profiles repeat after two resonator passes in the same form, but reflected with respect to the x=0-axis. This

first bifurcation can be explained as a modulational instability with a fractional longitudinal period so that the modulation closes only after two resonator passes. (Fig.4a)

A further increase of the modulation frequency to $k_m = 39$ leads to an additional bifurcation. One finds two coexisting asymmetric P4-solutions which are mirror images of each other (Fig. 3a-b) while their profiles are all different and do not possess any symmetry relations (Fig.3c-f). This second bifurcation is due to a new, independent modulational instability with integer longitudinal period; this modulation closes already after one resonator pass and has therefore the same periodicity as the solution on which the modulation takes place. This is a feature reminiscent of the cooperative frequency locking concept. Since the choice of the phase of the modulation relative to the phase of the unmodulated solution is arbitrary, two completely different coexisting attractors are possible (Fig. 4b). Thus, the coexistence of the periodic attractors results from the locking of different modulations.

The observed bifurcations have been explained as multi-transverse-mode instabilities in the cooperative frequency locking regime. This concept can be applied also in the region of stronger nonlinearity where not only the linear resonator modes are excited. More than that, it explains not only the formation of stationary structures but also bifurcations of periodic attractors.

## References

[1] D.W.McLaughlin, J.V.Moloney, A.C.Newell, Phys.Rev.Lett. 54(1985) 681

[2] L.Lugiato, C.Oldano, Phys.Rev.A 37(1988) 3896

[3] M.Sauer,F.Kaiser,submitted to Applied Physics

## Figure captions

Fig. 1: Phase diagram in the $k_m$-$A_m$-plane.

Fig. 2: symmetric P4-solution: a) complete attractor, b)-e) single profiles.

Fig. 3a)-b): Coexisting symmetry-broken P4-attractors; c)-f) single profiles.

Fig. 4): Sketch of symmetry breaking solutions.

**Fig.1:**

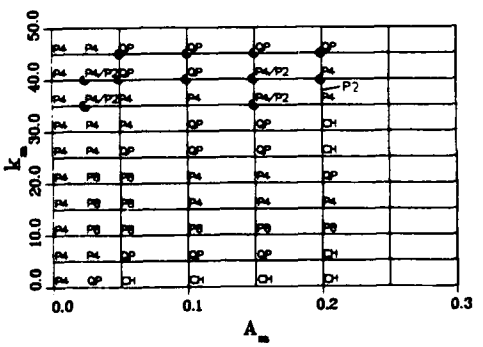

Fig.2:

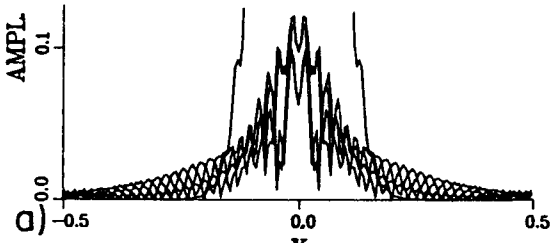


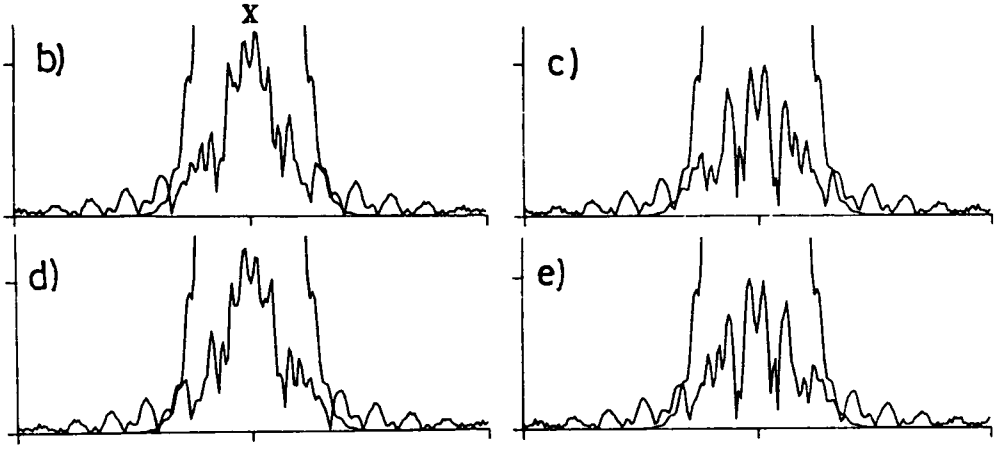


Fig.3:

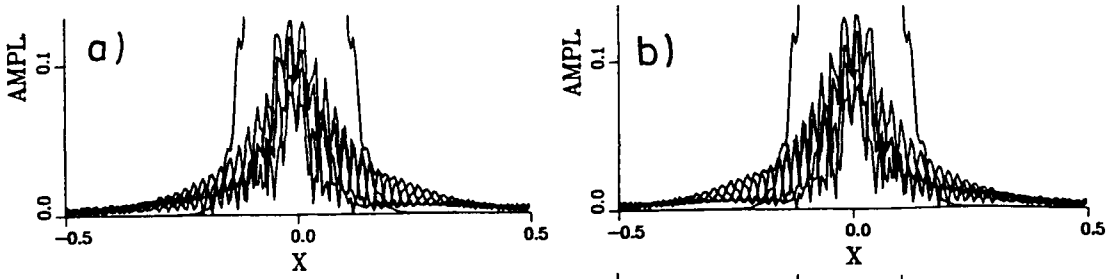


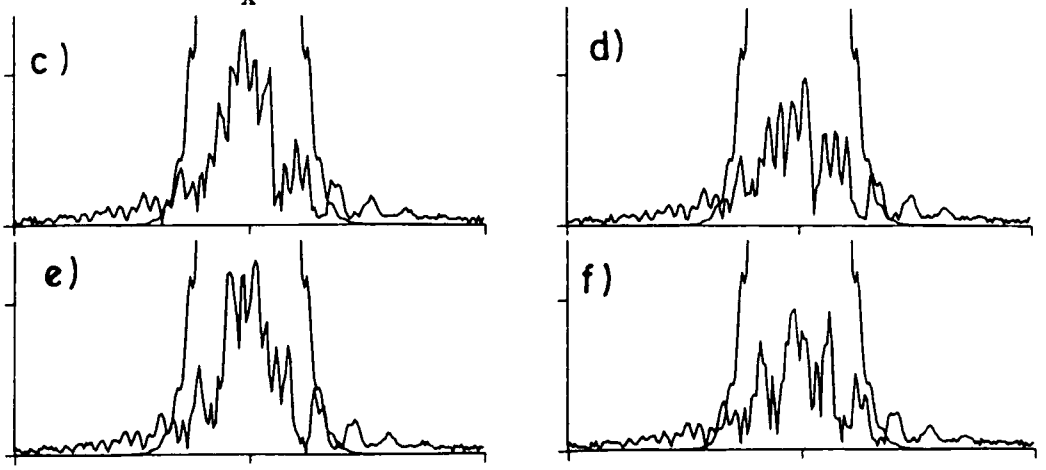


Fig.4:

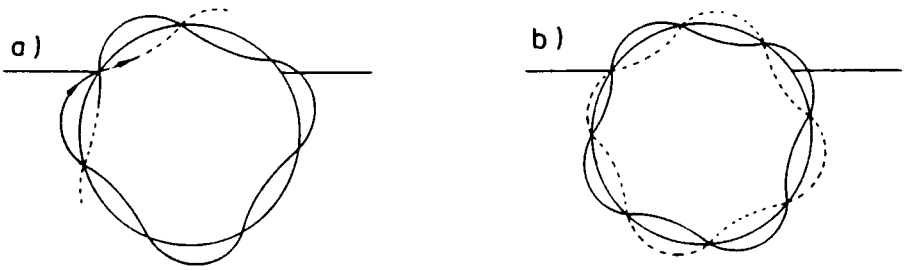

# The Dynamics of Transverse Field Structure in Unidirectional Ring Laser with Fast-Relaxed Active Medium

I.V.Veshneva, L.A.Mel'nikov, A.A.Sokolov, G.N.Tatarkov

*Chernyshevsky State University,*
*Research Institute of Mechanics and Physics,*
*Astrakhanskaya, 83, Saratov, 410071, Russia*

We considered the unidirectional ring cavity formed by mirrors **M1–M4**, lens **L** and Gaussian aperture **D** (Fig.1) and filled with the active medium with homogeneously broadened gain line. We suppose that the relaxation rates of medium polarization $\gamma$ and inversion $\gamma_{\parallel}$ obey the conditions $\gamma L/c$, $\gamma_{\parallel} L/c \gg 1$, where $L$ is cavity length. Thus in running normalized coordinates ( $z \Rightarrow z/L$, $r \Rightarrow r(\lambda L/\pi)^{-1/2}$, $t - z/c$ ) one gets the equation for field envelope:

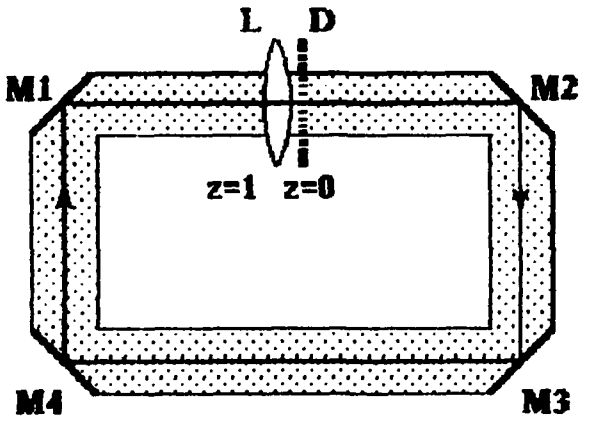


*Fig.1*

$$2i\frac{\partial E}{\partial z} + \nabla_{\perp}^2 E = -\frac{(1+\delta)GE}{1+\delta^2+|E|^2} \qquad (1)$$

where $\delta$ is normalized to $\gamma$ detuning of cavity frequency to the line center, $G$ is round trip gain. Using the model of "flexible" eigenmodes of beam [1,2] we seek the solution (1) as a superposition of Laguerre-Gaussian modes. The parameter of fundamental mode $P$ is dynamics variable like modal amplitudes:

$$E(z,r)=\sum_{m=0,\pm1,\,n=0,1,2} A_n^m(z) L_n^{|m|}(x)\, x^{|m|/2} \exp(im\varphi - P(z)r^2/2), \qquad (2)$$

where $x=\eta(z)r^2$, $P(z)=\eta(z)+i\xi(z)$, $L_n^{|m|}$ is Laguerre polynomials.

The equations for $A_n^m$ may be obtained as follows:

$$2i\frac{dA_n^m}{dz} + \sum_l (L_{nl}^{mk} + \chi_{nl}^{mk})A_l^k = 0, \qquad (3)$$

where $L_{nl}^{mk} = \langle m,n|2i\frac{\partial}{\partial z} + \nabla_\perp^2|k,l\rangle = \delta_{mk}\,[(m+n+1)V\delta_{k,n+l} +$

$+ [-2P+(2iV''-4\eta)(m/2+n) + V(2n+m+1)]\delta_{kn} + nV^*\delta_{k,n-l}]$,

$\chi_{nl}^{mk} = G(i+\delta)\int_0^{2\pi}\frac{d\varphi}{2\pi}\int_0^{\infty} dx\ exp(-x-i(k-m)\varphi)\ L_n^m\ L_k^l\ /[1+\delta^2+|E(x,\varphi)|^2]$.

The equation for $P$ is

$$i\frac{dP}{dz} = P^2 + \eta V \qquad (4)$$

were $V$ is given by the expression from Ref.2. Additionally we use the field transformation on lens and aperture:

$$E(z=0,r) = \sqrt{R}\ E(z=1,r)\ exp(-(\eta_d+iF)r^2/2)$$

were $R$ is the transmission at aperture center, $F$ is lens focal power, $\eta_d$ is the aperture "radius".

The solutions of (3,4) with (5) determines the nonlinear mapping for $(A_n^m,\ P)$.

Previously we report the dynamics of this system in single transverse mode limit [3]. With the same values of parameters $R=0.5$, $\delta=0$ and $\eta_d=0.05$ we have investigate the dynamics of three axially symmetrical "flexible" modes ($m=0$). It was found that bifurcation lines such as threshold line and periodical regimes do not change appreciably. We observe the significant increase of the diameter of beam when $G$ is increased and thus for high gain the confinement of laser

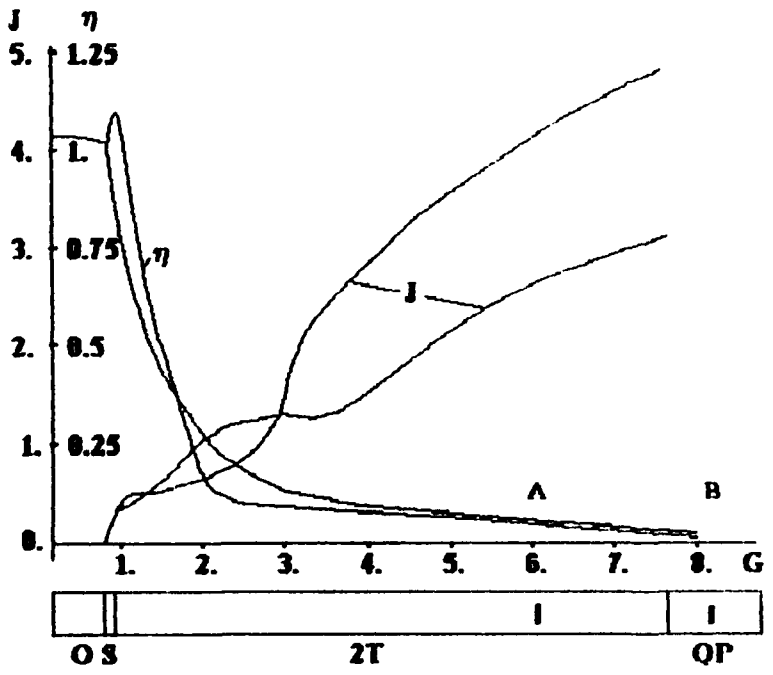


*Fig.2*

beam is due to aperturing. In Fig.2 the dynamic states at $f=2$ (confocal cavity) is shown with the dependence of axial intensity I and $\eta$ from $G$. In Fig.3 the field profiles evolutions is shown at the points $A,B$ of Fig.2. *"O"* denoted zero intensity state, *"S"* denoted steady-state regimes with nonzero intensity, *"2T"* denoted a cycle with period 2, *"QP"* denoted quasi-periodic oscillations. In the regimes $O,S,2T$ the fundamental "flexible" mode prevailed but in $QP$ oscillations $A_1^0$ mode became dominant. This regimes are found to be stable against the appearance of mode with $m=1$. The phase singularities connected with such modes [3] observed at other laser parameters or other initial conditions and is an object of current investigations. We have observed the same behavior of the system with "thin" amplyfier placed at $z=1/2$.

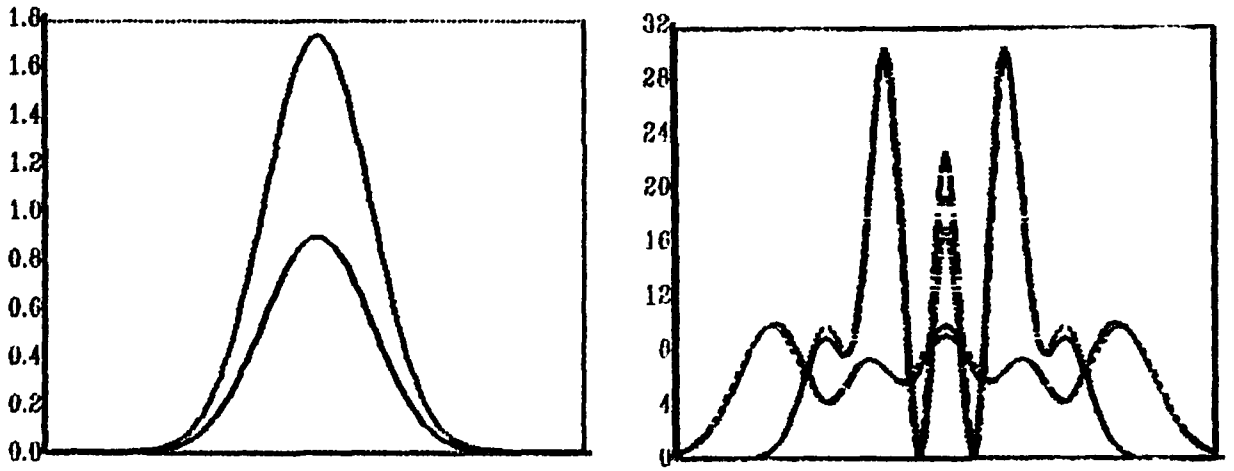


*A* *B*

*Fig.3*

References

**1.** Derbov V.L., Melnikov L.A., Novikov A.D., Potapov S.K. Journ. Opt. Soc. Amer. **7**, 1079 *(1990)*.

**2.** Melnikov L.A., Tatarkova S.A., Tatarkov G.N. Journ. Opt. Soc. Amer., **7**, 1286 *(1990)*.

**3.** Brambilla M., Battipede F., Lugiato L.A., Penna V. et al. Phys.Rev.A, **43**, 5090 *(1991)*.

# Dynamic Three-Dimensional Propagation of Light Pulses

G. G. Luther, J. V. Moloney, and D. E. Hart
Arizona Center for Mathematical Sciences,
Department of Mathematics,
University of Arizona, Tucson, Arizona 85721
Telephone: 602-621-8129, Fax: 602-821-8322

E. M. Wright
Optical Sciences Center
University of Arizona, Tucson, Arizona 85721
Telephone: 602-621-8267

In this paper we illustrate several characteristics of dynamic three-dimensional nonlinear propagation of light pulses. Recent work has shown that the fully spatio-temporal propagation of a light wave envelope in a cubically nonlinear medium displays, in addition to the usual transverse structures, longitudinal dynamics which play an essential role in the evolution of the wave [1, 2, 3]. It has been suggested that the effect of dispersion coupled with self focusing causes short light pulses having beam waists much larger than their pulse length to display spectral characteristics typical of experimental observations of supercontinuum generation [1]. A recent computational effort has illustrated that the presence of dispersion can inhibit collapse due to two dimensional self focusing in normally dispersive media causing structure in the propagation direction as well as the transverse direction [3]. Finally, analysis of three dimensional propagation of light waves in anomalously dispersive media [4, 5] reveals a set of symmetric solutions which would exist in the intermediate state between collapse and dispersal. The practical stabilization of these light pulses is an open problem.

In this paper a numerical investigation of the propagation of light waves in the presence of diffraction, dispersion, spectral absorption, and relaxation of the nonlinear index is presented. The governing equations for the envelope of the light pulse have the form

$$2ik(\partial_z + \frac{1}{c_g}\partial_t)A = -(\partial_x^2 + \partial_y^2)A - 2ik\int_{-\infty}^{\infty} A(t')\hat{R}(t-t')dt' - k^2\,NA\,, \qquad (1)$$

$$\tau_m N_t = |A|^2 n_2 - N\,, \qquad (2)$$

where $\hat{R}(t-t') = \int_{-\infty}^{\infty}(\alpha(\Omega) + i\Delta n(\Omega))e^{i\Omega(t-t')}d\Omega$ is the local linear response function of the medium, and $\alpha(\Omega)$ and $\Delta n(\Omega)$ are respectively, the experimentally measured linear absorption and linear index of refraction. For the purpose of this discussion, consider the simplified model equations with no absorption, $\alpha(\Omega) = 0$, instantaneous nonlinearity, and dispersion given by $\gamma\partial_{tt}^2$ [2, 3, 4, 5]. Results obtained by extending this model to include experimentally determined spectral absorption and dispersion will be presented at the meeting.

Let the initial pulse have Gaussian transverse and longitudinal profiles. As such a pulse propagates, a frequency chirp due to the nonlinearity is formed along the longitudinal direction. This process is enhanced as the pulse begins to self focus. Gradients in the longitudinal profile of the pulse grow as the pulse self focuses causing the effects of dispersion to become significant. In normally dispersive, self-focusing media, the combination of frequency chirp and dispersive spreading cause the up-shifted and down-shifted portions of the pulse to move away from the center of the pulse symmetrically. This redistribution of pulse energy is eventually stopped either due to the weakening of the dispersive effect or as a result of the nonlinearity.

Even though a portion of the initial pulse may have been above the critical power for two-dimensional self focusing, the energy in the resulting symmetrical pair of pulses may have been redistributed in such a way that no portion of the pulse pair is above the critical power. Thus, dispersion may prevent two-dimensional collapse of a pulse which would have self focused in its absence [3]. The spectrum is initially broadened forming a distinct Stokes and anti-Stokes component. Once the splitting occurs the spectrum takes the form of a modulated, single-peaked distribution centered at the carrier frequency. Transverse structure which would appear as a ring in the transverse profile of the pulse may accompany longitudinal pulse splitting. In anomalously-dispersive, self-focusing media the pulse tends to be temporally compressed, enhancing the catastrophic collapse process rather than preventing it.

The importance of the frequency chirp may be illustrated by imposing a phase variation on the initial pulse. In normally dispersive media a frequency chirp which opposes that accumulated during the propagation of the pulse can tend to delay the occurrence of pulse splitting. If the chirp is strong enough the pulse will tend to temporally compress even in the absence of an externally imposed waveguide. A frequency chirp which adds to that accumulated during the propagation of the pulse promotes pulse splitting and may increase

the self-focusing threshold. If the initial chirp is weak compared to the accumulated chirp, it may be ineffective in altering the evolution, so the process may seem insensitive to weak variations in the form of the initial condition.

In media where the nonlinearity does not respond instantaneously, the pulse splitting effect can also occur. Here the pulse evolves asymmetrically in the longitudinal direction. The pulse splits about its peak intensity, but the upstream portion may contains a larger fraction of the pulse energy than the down stream portion. The larger portion may contain enough power to self focus. As a result, in a medium with noninstantaneous response pulse splitting may be less effective in preventing collapse.

These initial results show that self focusing can manifest itself as a dynamic three-dimensional process. Specific characteristics of the propagation of three-dimensional light pulses may be important in understanding the interaction of short light pulses with nonlinear materials.

# References

[1] D. Strickland and P. B. Corkum, *Conference on Quantum Electronics and Laser Science*. 1991 Technical Digest Series (Optical Society of America, Washington DC, 1991), p. 66.

[2] X. O. Cao, C. J. McKinstrie, and D. A. Russell, *Bulletin of the American Physical Society*, **36**, 2273 (1991).

[3] P. Chernev and V. Petrov, *Opt. Lett.* **17**, 172 (1992).

[4] Y. Silberberg, *Opt. Lett.* **15**, 1282 (1990).

[5] N. Desaix, D. Anderson, and M. Lisak, *J. Opt. Soc. Am. B* **8**, 2082 (1991).

[6] P. L. Kelly, *Phys. Rev. Lett.* **15**, 1005 (1965).

[7] M. Karlsson, D. Anderson, M. Desaix, and M Lisak, *Opt. Lett.* **16**, 1373 (1991).

# Phase singularities in a Fabry–Perot resonator with an intra–cavity Nematic Liquid Crystal film

M. Kreuzer, R. Neubecker, T. Tschudi

Institute of Applied Physics, Hochschulstr.6, 6100 Darmstadt, Germany
Telephone: xx49–6151–162379, Telefax: xx49–6151–164123

## Introduction

Formation of transversal patterns and the appearance of phase singularities in nonlinear optical systems have attracted growingly interest in recent years [1, 2]. Up to now, most theoretical and experimental work has been performed for Maxwell–Bloch systems. However, it also turned out that these phenomena can be found in other nonlinear optical feedback configurations as well. Even if the system presented in this paper has in some aspects 'exotic' properties (compared to Maxwell–Bloch models), it nevertheless shows similar pattern formation with broken symmetry [3, 4, 5]. We now present the first experimental evidence of phase singularities in the intracavity wave.

## Setup and basic properties

The Fabry–Perot resonator is made up by two planar mirrors (about 90% reflectivity) with a spacing of some centimeters. The mirror diameter is much larger than the input beam size, so limited mirror aperture must not be taken into consideration. The Fresnel number with respect to the input beam size is typically F=5. As light source we use a c.w. Argon–Ion laser with an output power of up to 700mW. The beam diameter is scaled with a telescope and lies in the range of 0.3..1mm.

Inside the cavity we place a thin film of Nematic Liquid Crystals (NLC). The optical nonlinearity is based on so-called 'reorientation', which in fact is a slight local rotation of the optical axis. In a low–order approximation, the NLC can be modeled as a self-focusing Kerr medium. The medium is spatially and temporally strongly non–local: Reorientation is damped by viscosity with typical time constants in the range of $\tau_{nlc} = 100ms$, which exceeds the time constant of the resonator by some orders of magnitude . As a consequence the dynamics of the electrical field of the intra–cavity wave can be adiabatically eliminated. Furthermore strong spatial coupling with coupling lengths of about $l = 50\mu m$ has to be considered, leading to a diffusion–like behaviour. These material properties significantly determine the systems behaviour.

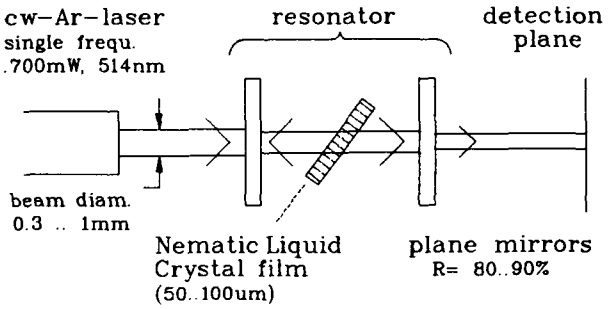


Fig. 1: Experimental setup

It is possible to prove, that diffraction effects inside the sample can be neglected. Hence, the NLC–film can be regarded as a thin phase object. Thus optical nonlinearity and diffraction are spatially separated. The dispersive optical nonlinearity is comparably strong: In one passage through the NLC–film a wave is exposed to an induced phaseshift of up to $\pi$.

## Structure formation

As long as the diameter of the input beam does not exceed the spatial coupling length of the NLC, the system shows classical optical bistability. Using larger beam sizes leads to the formation of transversal patterns with broken symmetry, which can easily be observed in the resonator output field. The input beam dissociates into a number of small spots. Each individual spot has a typical size, given by the spatial resolution of the NLC. Inside the diameter of the input beam, a maximum number of spots develops, holding a certain distance to each other and thus leading to a maximum packing density.

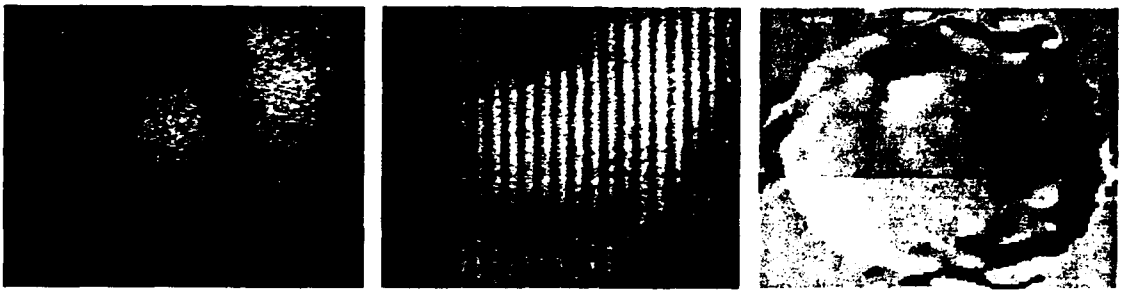

Fig. 2: (a) Intensity pattern, (b) Superposition of reference wave, (c) Phase reconstruction

A typical experimental situation is shown in fig. 2a: One spot is established and a second one is emerging on its right hand side. A theoretical model describing the system has been developed and numerical simulations of pattern formation are in very good agreement with experiment. It is also possible to show, that this spatial instabilities are intrinsic and are caused by diffractional effects [6, 7].

## Phase singularities

In order to observe phase singularities, a plane reference wave is superimposed on the resonator output wave. Like in a hologram, phase information is preserved, even when only the resulting intensity is recorded.

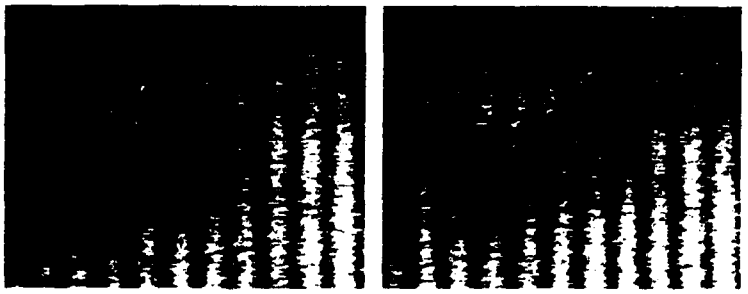

Fig. 3: (a) Magnification of the interference pattern in fig. 2b, (b) same pattern 5 seconds later

For detection, we use a commercial video equipment together with image processing on a personal computer. Due to the slow temporal response of the NLC, it is possible to resolve the dynamics of the system. In the resulting interference pattern an ending equi–phase line indicates a phase singularity. At the point of the singularity itself the amplitude of the field has to be zero. Using a numerical algorithm we are able to reconstruct the phase distribution of the resonator wave. Here a phase singularity is characterized by a $2\pi$–phase edge ending in the singularity. Walking around such a singularity, one crosses such an edge only once (provided the singularity has only single topological charge). Because of this helix–like structure, phase singularities are also called 'optical vortices'.

Fig. 2b shows the same experimental situation as fig. 2a, but now with the reference wave present. A magnification of the central upper area is shown in fig. 3a: The beginning dislo-

cations of the equi-phase lines indicate the creation of a pair of optical vortices with opposite topological charge. About five seconds later, the two vortices have moved away from each other (s. fig. 3b). In real-time, this movement manifests itself in subsequent jumping of equi-phase lines. Vice versa it is possible to observe the annihilation of two vortices with opposite charge.

Fig. 2c finally shows the phase distribution in gray scale (black=$-\pi$, white=$\pi$) reconstructed from fig. 2b : The two vortices are located at each end of the phase edge in the upper part (At the border of the spots the algorithm loses its reliability because of lacking intensity. Thus the structures at the border can be seen as numerical artefacts).

From other observations we can draw the following preliminary conclusions: In our experiment optical vortices always emerge in pairs with opposite charge. They only appear while a transversal structure is forming, and are annihilated, when the structure decays. But we have indications that transversal patterns need not necessarily be accompanied by phase singularities. The vortices are always located in the dark ring, which surrounds each individual spot of a formed transversal pattern. Furthermore, the singularities typically appear in an area where two (or more) spots come into contact. From the studies of pattern formation, we know that typical competition effects take place between individual spots [3, 4]. It seems that the vortices are a result of such a 'pattern competition'. In fig. 4, the phase reconstruction of a rather complex pattern with three dynamically competing spots is shown. At least four pairs of vortices can be identified.

Fig. 4: Phase reconstruction of complex structure formation, at least four pairs of vortices are present

Current work is performed in order to relate the dynamics of pattern formation and the role of stable and metastable patterns to the appearence of phase singularities.

## References


[1] J.Opt.Soc.Am. B, special issues 7 (6) and (7) (1990)

[2] P. Coullet, L. Gil, F. Rocca, Opt.Comm. 73(5), 403-408, Nov 1989

[3] M. Kreuzer, W. Balzer, T. Tschudi, Mol. Cryst. Liq. Cryst., Vol. 198, pp. 231-237, 1991

[4] M. Kreuzer, H. Gottschling, T. Tschudi, Mol. Cryst. Liq. Cryst. Vol.207, pp.219-230, 1991

[5] R. Neubecker, M. Kreuzer, H. Gottschling, T. Tschudi, Proc. of ECOOSA 90-Quantum Optics, Rome 1990, Institute of Physics Conference Series Number 115 IOP-Publishing, Bristol 1991

[6] R. Neubecker, M. Kreuzer, H. Gottschling, T. Tschudi, European Quantum Electronics Conference (EQEC'91), Edinburgh GB, 27.8 - 30.8.91

[7] H. Gottschling, M. Kreuzer, R. Neubecker, T. Tschudi, to be published

# Laser rate equations with phase-sensitive interactions

C. Etrich and Paul Mandel
Université Libre de Bruxelles, Campus Plaine C.P. 231
1050 Bruxelles, Belgium. Tel. +32-2-650-5819

Kenju Otsuka
NTT Basic Research Laboratories, Musashino-shi
Tokyo 180, Japan. Tel. +81-422-59-3367

We derive the following set of equations describing a two-mode semiconductor laser for the case of a Fabry-Perot configuration, taking into account the holes burned into the amplifying medium by the standing field pattern and phase-sensitive interactions:

$$\partial_\tau E_1 = -E_1 + A(1 - i\alpha)(E_1 F + E_2 G)$$

$$\partial_\tau E_2 = -(\kappa - i\delta)E_2 + A(1 - i\alpha)(E_2 F + E_1 G)$$

$$\partial_\tau F = \gamma - \gamma F(1 + |E_1|^2 + |E_2|^2) - \gamma(E_1 E_2^* + E_1^* E_2)G$$

$$\partial_\tau G = -\gamma G(1 + |E_1|^2 + |E_2|^2) - \frac{\gamma}{2}(E_1 E_2^* + E_1^* E_2)F \qquad (1)$$

where $\kappa = \kappa_2/\kappa_1$ is the ratio of the decay rates of the electric fields $E_1$ and $E_2$. It is fixed to be larger than unity. $\gamma$ is proportional to the decay rate of the population inversion, A is proportional to the pump, $\alpha$ the linewidth enhancement factor and $\tau = \kappa_1 t$ the scaled time. $\delta = (\nu_1 - \nu_2)/\kappa_1$ is the scaled difference of the frequencies of the two modes. $E_1$ and $E_2$ are complex and therefore the phase dynamics is fully included in Eqs. (1). The variables F and G are related to the population

inversion D(x,t) via

$$F = \frac{1}{D_0 L}\int_0^L dx\ D(x,t), \quad G = \frac{1}{D_0 L}\int_0^L dx\ D(x,t)\cos[(q_1 - q_2)x] \tag{2}$$

where $q_j = \nu_j/c$, $L$ is the length of the medium filling the cavity and $D_0$ is related to the pumping rate. An important element which is taken into account in Eqs. (1) is the contribution of terms oscillating, in space, at the difference of the wave-numbers. These terms are neglected in the usual multimode approach of Tang, Statz and deMars [1].

The steady state solutions of Eqs. (1) are the trivial solution

$$E_1 = E_2 = 0,\ G = 0 \text{ and } F = 1 \tag{3}$$

and the two single-mode solutions

$$E_1 = \sqrt{A - 1}\ e^{-i\Omega_1\tau}, \quad E_2 = 0, \quad G = 0, \quad F = 1/A, \quad \Omega_1 = \alpha \tag{4}$$

$$E_2 = \sqrt{A/\kappa - 1}\ e^{-i\Omega_2\tau}, \quad E_1 = 0, \quad G = 0, \quad F = \kappa/A, \quad \Omega_2 = \alpha\kappa - \delta \tag{5}$$

which exist for $A > 1$ and $A > \kappa$, respectively. There are also two-mode steady state solutions with both electric fields different from zero and oscillating with the same frequency. The steady state solutions are steady in the sense that the corresponding intensities are constant. Solutions (4) and (5) bifurcate from the trivial solution (3) at their threshold values $A = 1$ and $A = \kappa$. The solution (4) is stable near $A = 1$, whereas solution (5) is unstable near $A = \kappa$.

A typical bifurcation diagram is shown in Fig.1: the single-mode solution (4) becomes unstable via a Hopf bifurcation and restabilizes for sufficiently high pump. Since this restabilization occurs at a relatively high value of A this point is not

considered here. Solution (5) becomes stable via a Hopf bifurcation and destabilizes at a steady bifurcation, where the steady two-mode solutions emerge. These two-mode solutions become unstable via a Hopf leading to stable quasi-periodic solutions. A branch of such solutions connects also the two Hopf bifurcations on either single-mode branch. The transition from one single-mode branch to the other is rather sharp.

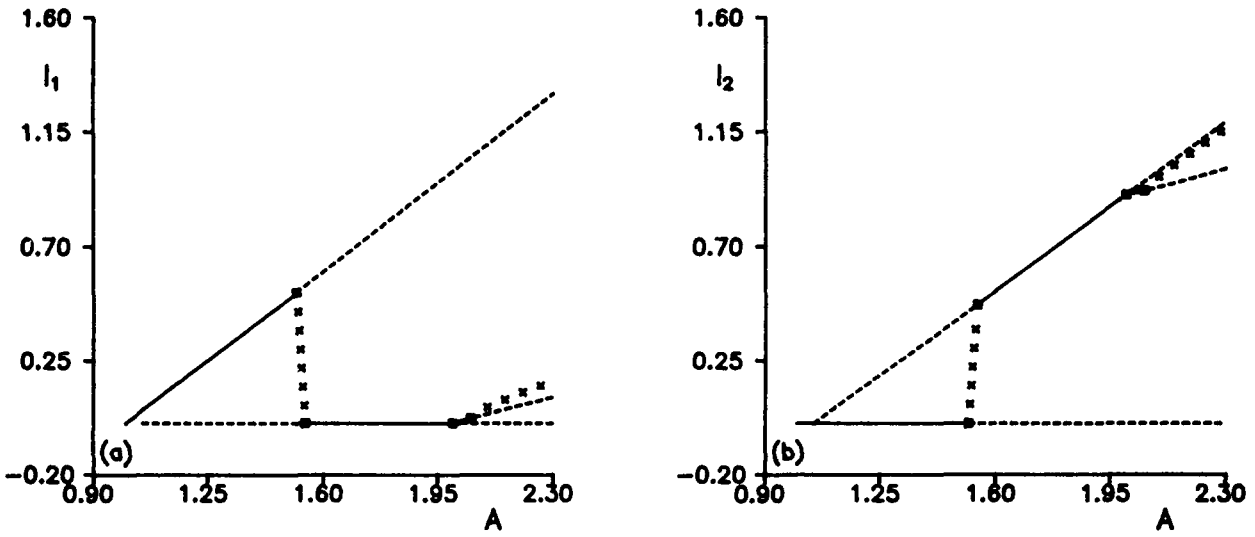


Fig.1. Bifurcation diagrams displaying (a) the intensity $I_1$ and (b) the intensity $I_2$ of all solutions for $\kappa = 1.05$, $\delta = 2$, $\gamma = 0.1$ and $\alpha = 4$. Solid lines indicate stable steady state solutions, dashed lines indicate unstable steady state solutions. Crosses indicate the maxima of stable quasi-periodic solutions. Black squares mark Hopf bifurcation points, the open square marks a steady bifurcation point.

Reference

[1] C.L.Tang, H.Statz and G.deMars, "Spectral output and spiking behavior of solid-state lasers", *J.Appl.Phys.* **34** (1963) 2289-2295.

# Simple Modeling of Feedback-Induced properties in Semiconductor Lasers

B. Meziane, P. Besnard and G. Stephan
Ecole Nationale Supérieure des Sciences Appliquées et de Technologie
6, rue de Kérampont, 22305 Lannion Cedex, France.

The effects of an external optical feedback on semiconductor laser properties have long been a subject of considerable interest[1-7], and continue to attract growing attention among various scientific groups. Such an interest is in great part due to the wealth of reported observations, and the lack of a definite interface between theories, which do not always corroborate, and experiments. For example, based on their experimental data, some authors have suggested that the semiconductor laser with optical feedback could be a good candidate for the observation of optical chaos[2,5,6]. The idea stemmed from the fact that the feedback signal would provide the necessary third degree of freedom which when added to the coupled rate equations would result in a 3D autonomous system (just as in the 'Lorenz' case of turbulence in fluids) which when the conditions of an instability emergence are fulfilled may give rise to some route towards optical chaos. Precise characterisation of such chaotic behavior however still remains obscure.

Although a dramatic linewidth increase has long been known to occur for moderate optical feedback, the exact origin of this linewidth enhancement from a few Mhz to up to 40 Ghz, usually referred to as "coherence collapse" [6,7] has been given distinct interpretations: while many authors attribute the collapse of the output beam to a kind of deterministic and albeit optical chaos[2,6], others interpret this effect as a noise-induced frequency chirp stemming from randomly distributed, noise-induced intensity breakdowns from steady state operation owing to spontaneous emission events[4]. In the theoretical side, the well-known "Lang and Kobayashi" delayed rate-equations[1] have been shown to give fairly good accounts of many of the reported experimental observations, including coherence collapse[6,7]. However, the delayed feedback term in the equations renders the system of infinitely high dimension, the integration of which yields a noise-like output signal just as if it were driven by random forces[6]. On the other hand, a linear stability analysis of these same rate-equations around steady state predicts a stable output signal[4]. This dilemma, in great part explains why no definite model has, so far, cut short so as to the exact physical origin of coherence collapse, or equivalently the tremendous noise which accompanies the output signal of a semiconductor laser subject to moderate optical feedback.

The purpose of this communication is the construction of a low-dimensional model whose numerical analysis will be shown to contain some feedback induced properties inherent to the infinite-D "Lang and Kobayashi" delayed rate-equations. In particular the well-known distinct regimes related to the amount of feedback are correctly described with our model. These regimes are :

i)-low levels, yielding a stable output,

ii)-moderate levels, yielding unstable, and incoherent noisy output with intensity breakdowns, just as in experiments related to coherence collapse,

iii)-high levels, yielding, again, a stable noise-free output.

The dynamical properties of such a system are described in terms of the "Lang and Kobayashi" rate-equations [1,4] :

$$d/dt(\xi(t)) = \{i\omega_o + \Delta G/2(1 + i\alpha)\}\xi(t) + k\xi(t-\tau) \quad (1a)$$

$$d/dt(N(t)) = J - N/\tau_s - G(N)\xi(t)\xi^*(t) \quad (1b)$$

which relate the complex oscillating field $\xi(t)$ with the carrier density of the lasing medium N(t).

In order to transform the infinite-D set of equations 1, two regions of operation are clearly distinguished :

a)-Below solitary laser threshold :

The system behaves as a compound-cavity laser for which coherent interference effects, between the reflected light and the field inside the laser diode, impose the following boundary conditions at the laser facet facing the external mirror :

$$\xi(t-\tau) = \xi(t)$$

b)-Beyond solitary laser threshold :

The bare laser starts to lase by itself, and the interference pattern between the reflected light and the field inside the diode will much depend on the exact amount of reflected intensity :

-For low levels of feedback the reflected waves adjust to the field inside the laser diode yielding coherent interference effects which in turn result in a stable output signal;

-For high feedback levels the field inside the diode adjusts itself to the strong reflected waves yielding also a stable output. This case describes a laser system with an amplifying medium at one end of the cavity;

-In the case of moderate levels, competition effects occur between the external compound-cavity field and the bare laser output. The feedback beam no longer coherently interferes permanently with the diode output field. This results in an extremely noisy output signal. In other words there is no correlation between the laser field and the reflected field. We may regard the system as consisting in two coupled —(1) active bare laser, and (2) passive external— cavities. In order to correctly describe this situation the field is divided into two parts :

$\xi_1(t) = \xi(t)$ in the laser cavity, and

$\xi_2(t) = \xi(t-\tau)$ in the external cavity.

These assumptions are particularly correct for long external cavities with small asymetries in the geometrical configuration of the experimental set-up. This situation allows the external field to be decorrelated to some extent from the bare laser output signal.

With the above transformations we are led to :

$$d/dt(\xi_1(t)) = \{i\omega_o + \Delta G/2(1 + i\alpha)\}\xi_1(t) + k\xi_2(t) \quad (2a)$$

$$d/dt(\xi_2(t)) = \{i\omega_o - 1/2\tau_{p2}\}\xi_2(t) + \varepsilon.\xi_1(t)/2\tau_{p1} \quad (2b)$$

$$d/dt(N(t)) = J - N/\tau_s - G(N)\xi_1(t)\xi_1^*(t) \quad (2c)$$

The second equation only describes the evolution of the field $\xi_2(t)$ which oscillates inside the passive cavity with a lifetime $\tau_{p2}$, and supplied by the laser field $\xi_1(t)$ with an amount $\varepsilon$.

When we write : $\xi_1(t) = E_1(t)\exp i(\omega_o t + \psi(t))$, $\xi_2(t) = E_2(t)\exp i(\omega_o t + \theta(t))$

we obtain a set of 5 equations, which are carefully normalised in order to simplify their numerical handling.

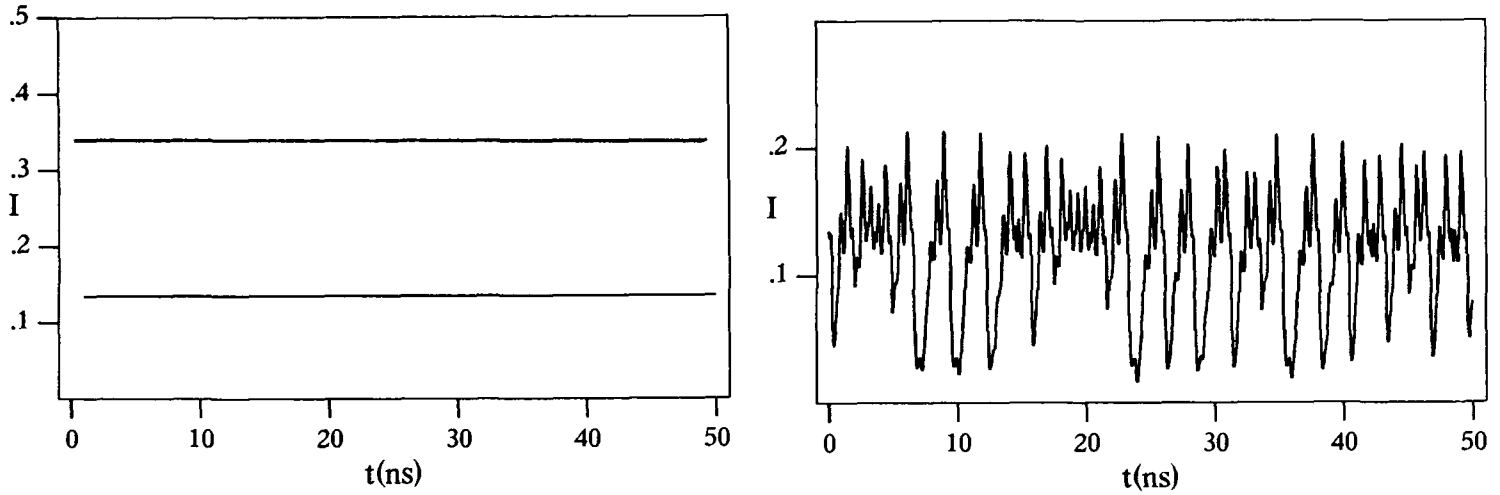


**Fig.1:** Time dependence of the external field showing: a)stable signal for low (lower trace), and high (upper trace) levels of feedback, and b)randomly distributed intensity breakdowns in the moderate feedback regime.

---

Numerical simulations of the normalised equations have been carried out for an excitation level in the vicinity of the diode laser threshold, and for parameter values corresponding to the Hitachi HLP 1400 diode laser. The feedback strength described with the parameter k is scanned from low to high levels.

Preliminary typical results shown in Fig.1 are self explanatory :

-for low feedback strengths the output intensity consists of a stable and constant signal whose value corresponds to the steady state value given by the steady state solutions of eqs.2.

-for moderate feedback levels the output signal consists of irregularly distributed intensity-breakdowns, as experimentally reported by some authors (3,7). This result seems to indicate that the origin of the tremendous noise observed in external-cavity lasers with moderate optical feedback has its roots in the deterministic nature of the non-linearly interacting variables of the system.

This finding constitute the central result of this communication.

-for higher feedback strengths the output signal again consists of a regular and noise-free constant intensity as deduced above from intuitive considerations.

## References

1 - R. Lang and K. Kobayashi, IEEE J. Quant. Electron., vol. QE-16, pp347-355 (1980).

2 - T. Mukai and K. Otsuka, Phys. Rev. Lett., vol. 55, pp 1711-1714 (1985).

3 - H. Temkin, N. A. Olsson, J. H. Abeles, R. A. Logan, and M. B. Panish, IEEE J. Quant. Electron., vol. QE-22, pp 286-293 (1986).

4 - C. H. Henry and R. F. Kazarinov, IEEE J. Quant. Electron., vol. QE-22, pp 294-301 (1986).

5 - Y. Cho and T. Umeda, Opt. Commun., vol. 59, pp 131-136 (1986).

6 - G. C. Dente, P. S. Durkin, K. A. Wilson, and C. E. Moeller, IEEE J. Quant. Electron., vol. QE-24, pp 2441-2447 (1988).

7 - J. Sacher et al., IEEE J. Quant. Electron., vol. QE-27, pp 373-389 (1991).

8 - D. Lenstra et al. IEEE J. Quant. Electron.,vol. QE-21, pp 674-679 (1985).

# Asymmetric Behaviour and Kink Shaping by Optical Feedback

F. Brivio,
*Italtel SIT*
*Cascina Castelletto - 20019 Settimo Milanese (Italy) - phone 39.2.43887987*

S. Mazzoleni, and M. Milani
*University of Milan, Physics Department*
*Via Celoria, 16 - 20133 Milano (Italy) - phone 39.2.2392265*

A systematic investigation of optical feedback induced effects on semiconductor laser diodes shows a variety of phenomena; some of them are linked to (left-right) symmetry properties of the system (symmetric solitary device plus optical feedback source). Attention is devoted to the appearance of feedback induced nonlinearities (kinks) in the **P-I** curves just above threshold [1]. Such nonlinearities are present in the characteristic curves taken from both facets, depend on the feedback ratio, and are reproducible. Kink formation and shaping are not substantially affected by the path between the laser facet and the reflecting surface; in particular they are not dependent on the presence of splices or connectors when a typical transmission line is the subject of investigation. Furthermore the role of optical feedback in destroying the symmetry between light outputs from the (equal reflectivity) front and rear facet of the devices is examined in detail, and a connection is established with the feedback adversely affecting the differential quantum efficiency of the device, in a selected range of values of the feedback ratio.

Experimental results are discussed in the framework of a microscopic model for single-mode semiconductor laser in the presence of optical feedback, with major attention to the **P-I** curves [2]. The discussed approach can be easily related to the standard rate equation treatment for semiconductor laser dynamics. In the presence of optical feedback the couple of equations for the number of carriers and the number of photons are modified as follows:

$$\dot{n}_{ph} = \frac{4\chi^2}{\gamma_\perp} n_{ph} n_c - 2(k-k')n_{ph}$$

$$\dot{n}_c = \frac{4\chi^2}{\gamma_\perp} - \gamma_\parallel(1 + a n_{ph})n_c + \frac{I}{e} \qquad 1)$$

Optical feedback is taken into account by the term ($2k'n_{ph}$) in the photon dynamics and by the term ($-\gamma_\parallel a n_{ph} n_c$) in the carrier dynamics [2]. The first term describes the reinjection of photons into the laser cavity, the second one describes the interaction between the reinjected photons and the carriers, and has its origin in the dependence of the interband carrier lifetime on the electromagnetic field in the laser cavity [3]. Equations (1) apply to the incoherent feedback regime, when the delay time exceeds the laser coherence time. Experimental results confirm the role of the parameter $a = a(f)$ and allow an estimate of the weight of the process that can be ascribed to the feedback effects associated to the term ($-\gamma_\parallel a n_{ph} n_c$) in the carrier dynamics. The proposed model is able to describe the usually neglected situation in which differential quantum efficiency is adversely affected by optical feedback, together with the common features usually reported in the literature [4].

Finally the observed asymmetry between the left and right characteristic curves reflects the symmetry breakdown of the originally symmetric cavity affected by asymmetric single-sided optical feedback. Such an internal asymmetry of the device can be accounted for by sketching the laser cavity as a double cavity: the first section (**right** -or front-) is the one facing the optical feedback source, the second section (**left** -or rear-), i.e. the remaining part of the cavity, is the section poorly affected by optical feedback, in suitable ranges of the feedback ratio (Fig. 1). The two sections of the cavity (denoted with **i=r,l**) will be ruled by two similar couples of rate equations of the type of eqs (1). In the simplest situation $a_l \sim 0$ so that ($-\gamma_{\parallel} a_l n_{c,l} n_{ph} = 0$). The cavity is then described as a whole by coupling the equations ($n_{ph} = n_{ph,l} + n_{ph,r}$ and $n_c = n_{c,l} + n_{c,r}$), introducing the global variables $N_{ph}$ and $N_c$:

$$\dot{N}_{ph} = \frac{4\chi^2}{\gamma_{\perp}} N_{ph} N_c - 2(k - k'_l - k'_r) N_{ph}$$

$$\dot{N}_c = -\frac{4\chi^2}{\gamma_{\perp}} N_{ph} N_c - \gamma_{\parallel} N_c + \gamma_{\parallel} a_r N_{ph} n_{c,r} + \frac{I}{e}$$

In the steady state ($\dot{N}_{ph} = 0$, $\dot{N}_c = 0$) the characteristic **P-I** curve is

$$N_{ph} = \frac{Ib/2ek}{1 - f/2 - \xi f/2 + A/2 - Af/2} - \frac{1 - f/2 - \xi f/2}{b(1 - f/2 - \xi f/2 + A/2 + Af/2)}$$

recalling that $P \propto N_{ph}$, $b = 4\chi^2/\gamma_{\perp}\gamma_{\parallel}$, $f = 2k'/k = 2(k'_l + k'_r)/k$ , $A = A(f) = a_r / b$ , $\xi = 2k'_l/k$. The quantum efficiency ($dN_{ph}/dI$) both increases or decreases as optical feedback increases, depending on **A(f)**. For $n_{c,r} = 0$ the two-section scheme of the active cavity identifies with the **left**-cavity, $N_{ph}$ coincides with the number of photons measured at the rear facet and ($i = I/I_{th} = Ib/2ek$)

$$Nph = \frac{1}{b}\left(\frac{i}{1 - f/2} - 1\right)$$

The quantum efficiency increases or remains unaffected as optical feedback (i.e. $k'_l + k'_r$) increases, as experimentally observed from the rear facet of the device, and the threshold current exhibits the same dependence of the feedback ratio, as the one obtained from the output power on the right side. In the proposed description the dynamics of the system is ruled by the interplay of the dynamics of the two sections. This interplay is substantiated at a microscopic level by a nonhomogeneous distribution of the carriers inside the cavity, because of the asymmetry induced by the optical feedback source. To obtain an explicit link between $\xi$ and **I** the effective dielectric constant and the refractive index dependence on carrier density (via Kramers-Kronig relations) have to be recalled [5]. The absorption coefficient is consequently modified determining the absorption probability

$$\alpha = \alpha_s + (1 - \exp[qV/kT])$$

and, being **V** directly linked to the injection current, $\alpha = \alpha(I)$ giving:

$$\xi(I) = \frac{1 - f/2}{1 + \dfrac{\alpha(I) - (\log R)/L}{\alpha_s - (\log R)/L}}$$

. The analytic form for the **P-I** curve is obtained by inserting the $\xi = \xi(I)$ relationship in the characteristic curve obtained from the rate equations (1) and the expected kink is observed (Fig.2). This procedure will allow the control of the parameter $\xi$ connecting it in a direct way to physical typical parameters of the material.

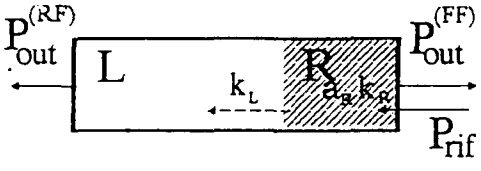


Fig. 1 - The Double Cavity

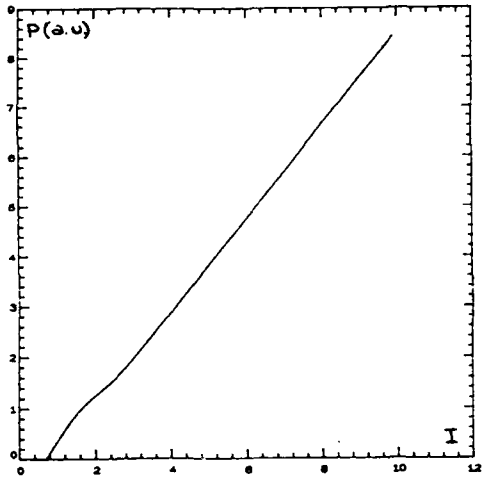


Fig. 2 - The kinked characteristic curve

References

1. K. Petermann, *Laser Diode Modulation and Noise* (Kluwer, Tokyo, 1988);
   G.H.B. Thompson, *Physics of Semiconductor Laser Devices* (Wiley, New York,1980).
2. M. Milani, S. Mazzoleni and F. Brivio, "Semiconductor Laser Diode with Weak Optical Feedback: Self-Coupling Effects on P-I Characteristics", *Proc. Electro-Optics for Signal Processing* 1474, (SPIE, Washington, 1991) 83-88;
   M. Milani, S. Mazzoleni e F. Brivio, "Optical Feedback in Diagnostic Methods and Testing of semiconductor Laser Diodes", *Proc. Laser Testing and Reliability* 1620-03, (SPIE, Washington, in press);
   F. Brivio, C. Reverdito, G. Sacchi, G. Chiaretti e M. Milani "Feedback Effects in Optical Communications Systems: the P-I Characteristic Curve for Single Mode InGaAsP Lasers" *Appl. Optics* (in press).
3. G. Chiaretti, D. Reichenbach, C. Vaccarino and M. Milani, "Analytical Derivation of the Structure of Carrier Lifetime and its Nonlinear Dependence on Optical Field Intensity in Semiconductor Laser Structures", *Appl. Optics* 28, 4556-4559 (1989).
4. H. Temkin, N.A. Olsson, J.H. Abeles, R.A. Logan and M.B. Panish, "Reflection Noise in Index-Guided InGaAsP Lasers", *IEEE J. Quantum Electron.* QE-22, 286-293 (1986);
   M. Ito and T. Kimura "Oscillation Properties of AlGaAs DH Lasers with an External Grating" *IEEE J.Quantum Electron.* QE-16, 69-77 (1980);
   J. Mink and B.H. Verbeek, "Asymmetric Noise and Output Power in Semiconductor Lasers with Optical Feedback Near Threshold", *Appl. Phys. Lett.* 48, 745-747 (1986).
5. K.A. Shore and M.W. McCall, "Nonlinear and Quantum Optics in Semiconductor Lasers", *Progress in Quantum Optics* 14, 63-129 (1990).

# SWITCH-ON TIME STATISTICS OF A SINGLE-MODE SEMICONDUCTOR LASER WITH AN INJECTED SIGNAL.

M.C. Torrent

*Departament de Física i Enginyeria Nuclear, EUETIT, Universitat Politècnica de Catalunya, Colom 1, Terrassa, Spain. Tel. # : (34) - 3 - 739 82 22*

J.M. Sancho

*Departament d'Estructura i Constituents de la Materia, Facultat de Física, Universitat de Barcelona, Diagonal 647, E-08028 Barcelona, Spain. Tel. # : (34) - 3 - 402 11 80*

M. San Miguel and S. Balle

*Departament de Física, Universitat de les Illes Balears, E-07071 Palma de Mallorca, Spain. Tel. # : (34) - 71 - 17 32 34*

Previous studies[1-3] of switch-on times in the presence of an injected signal considered class A-lasers. Here we consider the suitability of semiconductor lasers for detection of weak signals. The main difference with former studies is that now the carrier number cannot be adiabatically eliminated, so that the laser frequency is not constant during the laser switch-on.

Our calculation is based on the usual rate equations for a single mode semiconductor laser[4] with an extra term describing the influence of the external field. In dimensionless units these equations for the complex electric field $z$ and carrier number $n$ read[5]

$$\dot{z} = \frac{\mu z}{2\varepsilon}\left[(n-1)(1+i\alpha) + i\frac{\alpha-\bar{\gamma}}{\mu}\right] + \bar{k}_e f_e + (2\eta m)^{1/2}\xi(t)\ , \tag{1}$$

$$\dot{n} = \epsilon[\lambda + 1 - n(1+|z|^2)]\ . \tag{2}$$

where $f_e$ is the external field with coupling parameter $\bar{k}_e$. In these equations, written in a frame of reference which rotates at the frequency $\bar{\gamma}/2\varepsilon$ of the external field, gain saturation has been neglected. The reason is that the calculation of Passage Times (PT) after the laser is gain-switched involves only the first stages of evolution, when the laser intensity is small. Spontaneous emission noise is modeled by a complex Gaussian white noise $\xi(t')$ with zero mean and correlation

$$< \xi(t')\xi^*(t'') >= 2\delta(t'-t''). \tag{3}$$

In addition, we have normalized the laser intensity and the carrier number to their asymptotic steady state values in the absence of saturation, after scaling the time. It has been shown[5, 6] that the deterministic drift in the carrier number due to the injection current completely dominates the evolution of $n$,so that we can also neglect the nonlinear coupling term in (2). Considering[5] that noticeable laser emission cannot occur until the carrier number has crossed its threshold value $n_{th} = 1$, which happens at a time $\bar{t}$ given by

$$\bar{t} = \frac{1}{\epsilon}\ln\left[\frac{1+\lambda-n(0)}{\lambda}\right]\ , \tag{4}$$

we integrate eqs. (1)-(2) with initial conditions $n(\bar{t}) = 1$, $z(\bar{t}) = z_0$. Since the PT $T$ typically occurs in a time interval much smaller than $\epsilon^{-1}$, and, for usual laser parameters, $(\lambda\mu/2)^{1/2}\,(< T > -\bar{t}\ ) >> 1$, we can approximately solve eq. (1) for times later than $\bar{t}$ as $z(t) = h\ exp[A(t)]$, where

$$A(t) = \frac{\lambda\mu}{4}(1+i\alpha)(t-\bar{t})^2 + i\frac{\bar{\alpha}}{2\epsilon}(t-\bar{t})\ , \tag{5}$$

and

$$h = \int_0^\infty \left[\bar{k}_e f_e + \sqrt{2\eta(1+\epsilon t)}\ \xi(t)\right] e^{-A(t)}\, dt + z_0\ , \tag{6}$$

and where we have defined $\bar{\alpha} = \alpha - \bar{\gamma}$

The function $h$ contains the stochasticity of the process $z(t)$. It plays the role of an effective random initial condition which is exponentially amplified in time. The initial value of the field $z_0$ is a random variable associated with the small fluctuations around zero field in the initial off-state of the laser. Unless the bias current is very close to threshold the effect of $z_0$ in the statistical properties of the Passage Time is negligeable, and in the following we set $z_0 = 0$. Therefore, the PT is determined by the condition

$$i_r = \mid z(T) \mid^2 = \mid h \mid^2 e^{2A_1(T)} ,$$

which can be inverted to obtain $T$ as a function of a random variable $h$ with known Gaussian properties:

$$T - \bar{t} = \sqrt{\frac{2}{\lambda\mu} \ln \frac{i_r}{|h|^2}} .$$

The statistical properties of $T$ are most easily calculated through the generating function $W(\rho)$[3]

$$W(\rho) \simeq e^{-\rho(2\tau/\lambda\mu)^{1/2}} e^{-\beta^2/2} \, \Gamma\left(\frac{\rho}{(2\tau\lambda\mu)^{1/2}} + 1\right) \, M\left(\frac{\rho}{(2\tau\lambda\mu)^{1/2}} + 1, 1, \beta^2/2\right), \tag{7}$$

where $M(a, b, z)$ is the confluent hypergeometric function,[7] and we have defined $\tau = ln(i_r / < |h|^2 >$ and $\beta^2 = 2| < h > |^2 / < |h|^2 >$, the natural scaling parameter which appears in the calculation.[3]

The mean and the variance of the PT are now easily obtained,

$$< T > - \bar{t} = < T >_0 - \bar{t} - \frac{1}{(2\tau\lambda\mu)^{1/2}} \left[E_1(\beta^2/2) - \Psi(1) + \ln \beta^2/2\right], \tag{8}$$

$$< \Delta T^2 > = < \Delta T^2 >_0 - \frac{1}{2\tau\lambda\mu} \left[E_1(\beta^2/2) - \Psi(1) + \ln \beta^2/2\right]^2 + \frac{1}{\tau\lambda\mu} \sum_{n=2}^{\infty} \frac{(-\beta^2/2)^n}{n!n} \sum_{i=1}^{n-1} \frac{1}{i} , \tag{9}$$

where $< T >_0 - \bar{t} = (2\tau/\lambda\mu)^{1/2} [1 - \Psi(1)/2\tau]$ and $< \Delta T^2 >_0 = \Psi'(1)/2\tau\lambda\mu$ are the corresponding values for $\beta = 0$, that is in the absence of external field.[5]

The nontrivial parametric dependence in (8) and (9) appears through the dependence on the scaling parameter $\beta$ which gives the relevant combination of the different parameters in the problem. In particular, $\beta^2$ is proportional to $(\bar{k}_e f_e)^2$. The mean PT is not very sensitive to $\beta^2$: less than a 5% decrease of $< T >$ occurs in 3 decades of variation of $\beta^2$. However, the variance $\sigma(T) = \sqrt{< \Delta T^2 >}$ of the PT distribution shows a very strong dependence on $\beta^2$ with a 20% reduction for $\beta^2/2 = 1.9$, as shown in Fig. (1).

The dependence on $\beta^2$ gives both the dependence on the strength of the injected field $\bar{\kappa}_e^2 f_e^2$ and on the frequency mismatch between the external signal and the laser field. It can be written in the form

$$\beta^2 = \beta_0^2 G(\bar{\alpha})$$

where $\beta_0^2$ is the value of $\beta^2$ when $\bar{\alpha} = 0$. $G(\bar{\alpha})$ is the function which carries the dependence on the frequency mismatch $\bar{\alpha}$,

$$G(\bar{\alpha}) = \left| \omega \left[ \frac{-\bar{\alpha}}{\varepsilon \sqrt{\lambda\mu\sqrt{1+\alpha^2}}} e^{\frac{-i}{2} \arctan \alpha} \right] \right|^2 , \tag{10}$$

where $\omega(z)$ is the scaled error function for complex arguments.[8] From the explicit expression for $\beta^2$ we can conclude that the variance of the PT distribution is much more sensitive to the intensity of the injected signal than the mean PT. A different question is the frequency selectivity or bandwith in which the injected field is detected. Since the whole dependence of $< T >$ and $< \Delta T^2 >$ on the frequency mismatch appears through the function $G(\bar{\alpha})$ in the scaling parameter $\beta^2$, and provided that the mean PT and the variance are monotonously decreasing functions of $\beta^2$, their minima as a function of $\alpha$ occur for those values which

maximize $G(\bar{\alpha})$, and the width of this maximum sets the detection bandwidth. We find that the optimum frequency mismatch $\bar{\gamma}/2\varepsilon$ between the laser field and the external field is close to $\alpha/2\varepsilon$ with a bandwidth of the order of $\approx 100\ GHz$.This optimum value can be understood in terms of a resonance between the external field and the lasing field when amplification becomes first possible (i. e., $t = \bar{t}$): For $\bar{k}_e = 0$, the frequency $\dot{\varphi}$ of the lasing field is

$$\dot{\varphi} = \frac{\alpha\mu}{2\varepsilon}[n(t) - 1 + 1/\mu]$$

and in the domain of validity of our calculation ($\varepsilon << 1$) we find that the optimum detection occurs for $\bar{\gamma}/2\varepsilon = \alpha/2\varepsilon = \dot{\varphi}(t = \bar{t})$.

Since the linewidth enhancement factor $\alpha$ is not generally known with better accuracy that $\pm 1$, the present method could be a promising alternative to better determinations of the $\alpha$-factor.

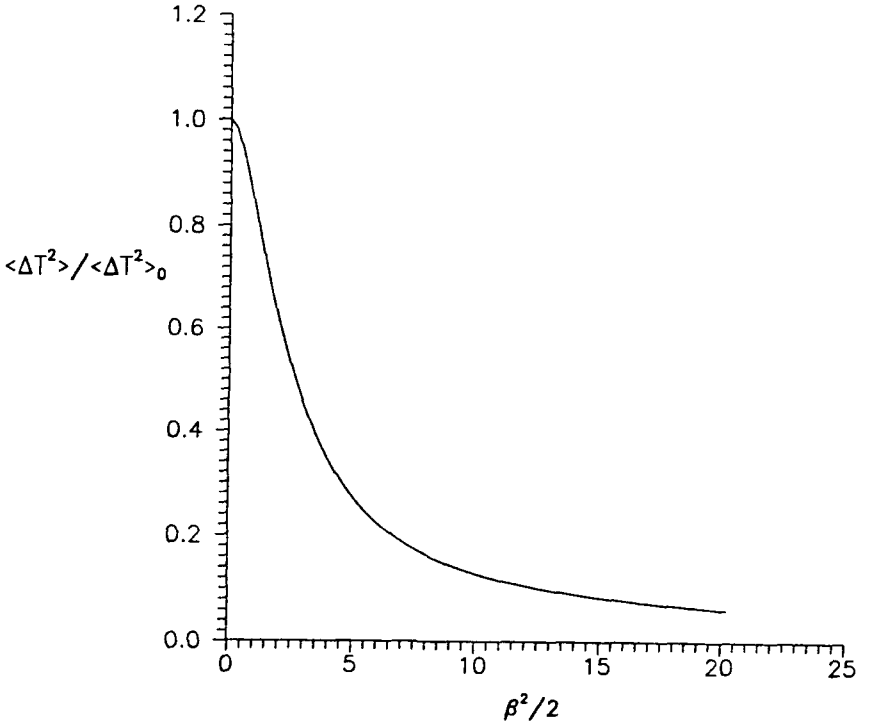


Fig. 1: Variance of the PT distribution normalized to its value when no external signal is applied as a function of $\beta^2/2$.

[1] G. Vemuri and R. Roy, Phys. Rev. A **39**, 2539 (1989).

[2] I. Littler, S. Balle, K. Bergmann, G. Vemuri, and R. Roy, Phys. Rev. **A41**, 4131 (1990).

[3] S. Balle, F.De Pasquale, and M. San Miguel, Phys. Rev. **A41**, 5012 (1990); J.I. Jimenez Aquino and J.M. Sancho, Phys. Rev. **A43**, 589 (1991).

[4] G. P. Agrawal and N. K. Dutta, *"Longwavelength semiconductor lasers"*, Van Nostrand Reinhold Company, New York, 1986; K. Pettermann, *"Laser diode modulation and noise"*, Kluver, Drordrecht, (1988).

[5] S. Balle, P. Colet and M. San Miguel, Phys. Rev. **A43**, 498 (1991).

[6] A. Mecozzi, P. Spano, A. D'Ottavi and S. Piazzalla, Appl. Phys. Lett. **55**, 769 (1989) .

[7] *Handbook of Mathematical Functions*, p. 504, edited by M. Abramowitz and I. Stegun (Dover, New York, 1970).

[8] See [7], p. 297.

# Dynamics of passive FM locking in semiconductor lasers

K.A.Shore and W.M.Yee

Bath University
School of Electronic and Electrical Engineering
BATH BA2 7AY , UK

TEL + 44 225 826272

## Abstract

### Theory

In earlier work [1] the role of gain nonlinearities in effecting self-locked FM supermode oscillation in semiconductor lasers was established and the requisite gain saturation and multiwave mixing nonlinearities were shown to be consistent with the experimental observations of Tiemeijer et al [2]. A three-mode laser model is sufficient to demonstrate the occurrence of intrinsic FM locking in semiconductor lasers but , in order , for example, to calculate the depth of FM modulation in the self-locked state a multimode model is required . In the present work the model of [1] has been extended to take more than three modes into account .

### Results

The model has been applied to the calculation of the intrinsic FM index . As seen from Figure 1, with increasing nonlinearity the index saturates to a value of 1.3 .This value is in agreement with the available experimental evidence.

Consideration of the relative phases in 5 mode , 7 mode and 9 mode locking shows that an admixture of FM and AM locked states is obtained . The inhibition of pure FM operation is evident from time-domain representations of the locked supermodes shown in Figure 2.

Calculations using the nonlinear algebraic equations appropriate to the steady ( locked ) state have indicated the possibility of supermode hopping .Investigations are now underway into the dynamics of supermode hopping in the device.

### Acknowledgement

This work is supported by SERC grant GR/ G 13525.

### References

[1] K.A.Shore and W.M.Yee , " Theory of self-locking FM operation in semiconductor lasers " , IEE Proc. Part J ( Optoelectronics ) 138 , 91-96 , 1991

[2] L.F.Tiemeijer et al , " Passive FM locking in InGaAsP semiconductor lasers " , IEEE J. Quantum Electron.,QE-25 , 1385-1392 , 1989

Figure 1 : Modulation Index Variation

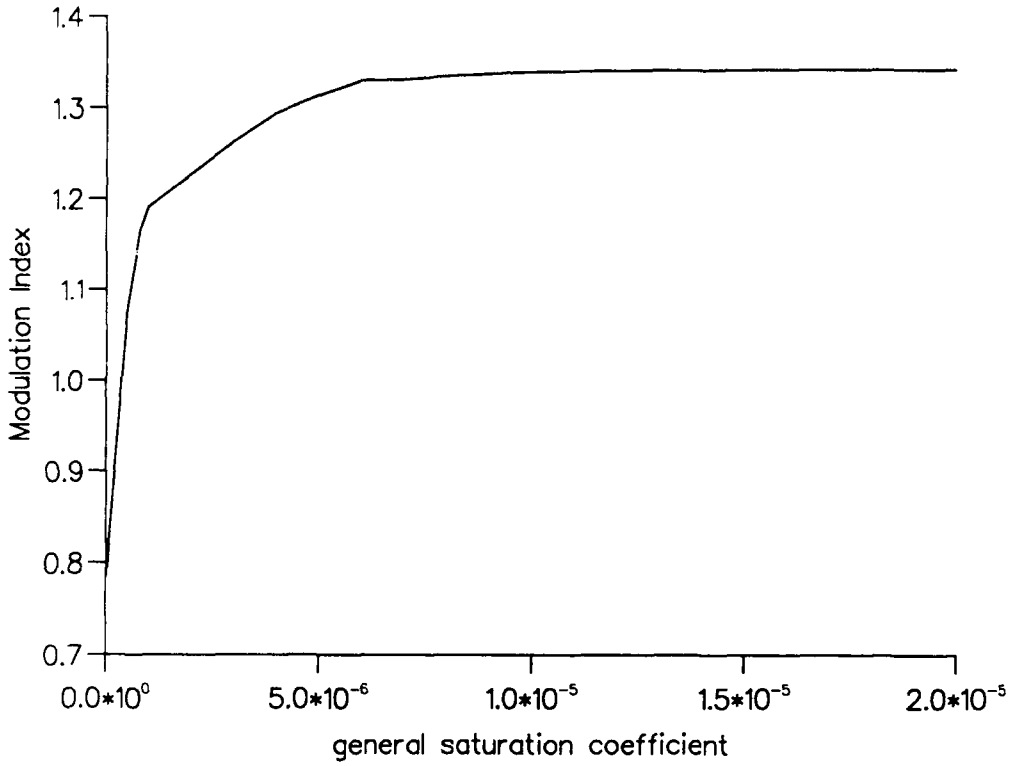


Figure 2 : Output Intensity – Time curve

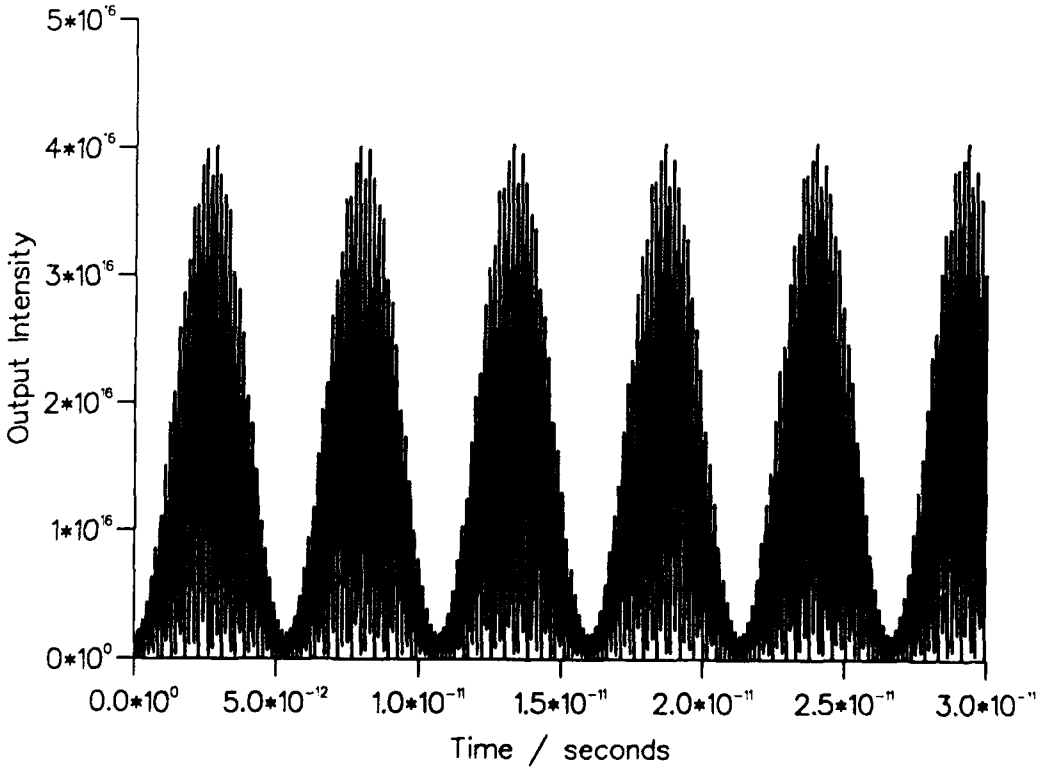

# LIGHT DYNAMICS OF BISTABLE ELEMENT CHAIN

**Yu.A.Logvin, A.M.Samson**

Institute of Physics
Belarus Academy of Sciences
220602 Minsk, Republic of Belarus

The light dynamics of bistable element chain is theoretically considered within the scope of the plane wave approximation. It is supposed that bistable elements are arranged in line and coupled by the light beams (see fig.). As a model is chosen the bistable thin film of two-level atoms [1,2] subjecting to the relation

$$e_i = e_t + \frac{2Ce_t}{1 + e_t^2} \quad , \tag{1}$$

where $e_i$ and $e_t$ - the amplitudes of incident and transmitted field, $C$ - the cooperative parameter of the film [3].

The Maxwell-Bloch equations can be reduced in the limit of short relaxation times (the relaxation times of the matter are smaller than light transit time between the films) to the many-dimension nonlinear map:

$$\vec{x}(m) = \vec{f}\{\vec{x}(m-1)\} \quad , \tag{2}$$

with $\vec{x}(m) = \left[x_1(m), x_2(m), \ldots, x_k(m), \ldots, x_N(m)\right]$, where $x_k(m)$ is proportional to the polarization of the $k$-th film at the

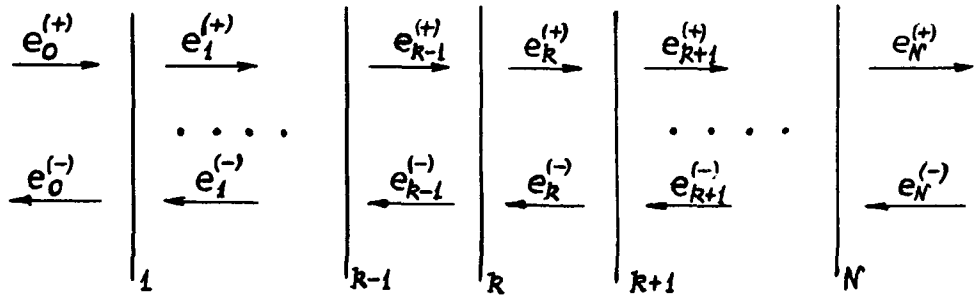

m-th light transit. The form of the function $f_k$ for the $k$-th film in Eq.(2) is given by the expression (1) where incident field depends on $x_{k+1}(m-1)$ , $x_{k-1}(m-1)$ and transmitted field is proportional to $x_k(m)$.

The temporal light dynamics is determined by the map (2) properties which can be summarized as follows:

- the system dynamics is essentially depends on the reflection index of the medium between the films. In case of the transparent medium without absorption and if the distance $l$ is equal to the integer number of wave length, bistable elements tend to the simplest stationary regime. The many-dimensional map (2) has a stable fixed point. The system properties are similar to a single bistable element operation.

- if the distance $l$ holds the odd number of half-waves and the medium has absorption, there occur instability of stationary regime, an appearence of self-pulsations and a spatial-temporal chaosity.

- the basic features of the bistable element chain can be understood with help of $N$=2 model. At the equal amplitudes of the incident field $e_0^{(+)}$ and $e_2^{(-)}$ the problem becomes symmetrical. The system (2) is simplified and reduced to the one-dimension map The problem proves to be equivalent to the study of the dynamics for bistable element which is supplemented with a reflected surface [2,4].

[1] Zakharov S.M., Manykin E.A.// Poverkhnost, No.2 (1988) 137.
[2] Basharov A.M.// Zh. Theor. Eks. Fiz. V.94 (1988) 12.
[3] Lugiato L.A.// In Progress in Optics XXI, Ed. E.Wolf. Oxford-N.Y.-Tokyo: North-Holland Phys. Publ., (1984) 71.
[4] Logvin Yu.A., Samson A.M.// submitted in Kvantovaja Elektronika (Moscow) (1992)

# The Effects of Nonlinear Gain on the Stability of Two-Element Evanescently Coupled Laser Arrays

D. T. Nichols and H. G. Winful
Solid State Electronics Laboratory, University of Michigan, Ann Arbor, MI 48109-2122

Arrays of semiconductor lasers have become widely used as compact sources of intense radiation, generating watts of power in diffraction limited beams. [1] Their high power makes them attractive as potential sources for optical fibers. However, their dynamical behavior is not well understood. Ordinarily, the problem is handled by solving a set of coupled nonlinear differential equations which are descriptive of the coupling of the carrier and photon populations in a single device as well as the the coupling between the individual devices. When writing these equations, one generally assumes that the optical gain is independent of the intensity. However, from a physical perspective, it is reasonable to postulate that the gain will begin to decrease significantly for sufficiently large photon populations. Several models have been utilized in order to describe the phenomenon of gain saturation [2]. One formalism assumes that the gain may be described by $g = g_L(1 - \epsilon X^2)$, where $X$ is a normalized electric field and $X^2$ is proportional to the photon density in the laser cavity. This formalism is, however, only valid for low power levels. A second phenomenological form uses $g = g_L(1 + \epsilon X^2)^{-1}$. This model has its origins in the two-level model and, since a semiconductor laser connot be described completely by the two-level model, a third model, which is taken from a non-perturbative density matrix calculation, has been formulated in which $g = g_L(1 + \epsilon X^2)^{-\frac{1}{2}}$. It is clear that the presence of nonlinear gain will be a stabilizing influence on arrays of lasers, but to what degree is unclear. In the present study, we determine stability criteria for a two-element evanescently coupled laser array using each of the three models mentioned above in an effort to predict the effect of nonlinear gain on these arrays.

It can be shown [3], [4] that the rate equations for a two-element evanescently coupled array may be written

$$\frac{dX_1}{d\tau} = Z_1 X_1 - \eta X_2 \sin\Theta \tag{1}$$

$$\frac{dX_2}{d\tau} = Z_2 X_2 + \eta X_1 \sin\Theta \tag{2}$$

$$\frac{d\Theta}{d\tau} = -\alpha(Z_2 - Z_1) + \eta\left(\frac{X_1}{X_2} - \frac{X_2}{X_1}\right)\cos\Theta \tag{3}$$

$$T\frac{dZ_1}{d\tau} = p - Z_1 - (1 + 2Z_1)X_1^2 \tag{4}$$

$$T\frac{dZ_2}{d\tau} = p - Z_2 - (1 + 2Z_2)X_2^2, \tag{5}$$

where $X_i$ is the field strength, $Z_i$ is the carrier density, $\Theta$ is the phase difference between the two elements, $\eta$ is the coupling strength, $\alpha$ is the linewidth enhancement factor, p is the pumping strength and T is the ratio of the photonic lifetime to the carrier lifetime. These variables are all normalized as in [3]. One can then use first order perturbation theory to arrive at the conditions of pumping strength and coupling strength under which stable operation of the array is possible. These stability criteria are $\eta > \alpha p/(1 + 2p)$ for the in phase mode and $\eta < (1 + 2p)/2\alpha T$ for the out-of-phase mode. The striking thing about this result is that most of the phase space is in the unstable region of operation, indicating that it may be ureasonable to expect that these arrays will ever operate in a stable manner except in the case of very low pumping levels or in the cases of very strong or very weak coupling. As we shall see, the introduction of the nonlinear gain into the model has a strong effect on the behavior of the array, allowing for the stable operation of these arrays over much greater areas of the phase plane.

We may now write the coupled rate equations with the inclusion of the nonlinear gain using the first model presented. These equations are

$$\frac{dX_1}{d\tau} = X_1 Z_1(1 - \epsilon X_1^2) - \frac{\epsilon X_1^3}{2} - \eta X_2 \sin\theta \tag{6}$$

$$\frac{dX_2}{d\tau} = X_2 Z_2(1-\epsilon X_2^2) - \frac{\epsilon X_2^3}{2} + \eta X_1 \sin\theta \tag{7}$$

$$\frac{d\theta}{d\tau} = -\alpha(Z_2 - Z_1 - \epsilon(X_2^2 Z_2 - X_1^2 Z_1)) + \eta\left(\frac{X_1}{X_2} - \frac{X_2}{X_1}\right)\cos\theta \tag{8}$$

$$T\frac{dZ_1}{d\tau} = p - Z_1 - (1+2Z_1)(1-\epsilon X_1^2)X_1^2 \tag{9}$$

$$T\frac{dZ_2}{d\tau} = p - Z_2 - (1+2Z_2)(1-\epsilon X_2^2)X_2^2. \tag{10}$$

Again, first order perturbation theory is invoked and we define the new variables $x = x_2 - x_1$ and $z = z_2 - z_1$, where the subscripted $x$ and $z$ variables, along with $\delta$ represent the small-signal departures from the steady state of the field, carrier density and phase, respectively.

Our differential equations now take the matrix form:

$$\frac{d\mathbf{X}}{d\tau} = \begin{pmatrix} \frac{-\epsilon X_0^2}{1-\epsilon X_0^2} & X_0(1-\epsilon X_0^2) & 2\eta\cos\Theta_0 \\ 2\gamma X_0\left(\frac{\epsilon X_0^2}{1-\epsilon X_0^2} - 1\right) & -\gamma(1+2X_0^2(1-\epsilon X_0^2)) & 0 \\ \frac{\alpha\epsilon^2 X_0^4}{1-\epsilon X_0^2} - 2\eta\cos\Theta_0 & -\alpha X_0(1-\epsilon X_0^2) & 0 \end{pmatrix}\mathbf{X} \tag{11}$$

where

$$\mathbf{X} = \begin{pmatrix} x \\ z \\ X_0\delta \end{pmatrix} \tag{12}$$

We may now solve this perturbation matrix numerically for varying values of $\epsilon$, $\eta$ and p and determine the stable and unstable regions from looking at the real parts of the eigenvalues. The results of this solution were verified via numerical integration of the differential equations and are shown below. Likewise, we invoke a similar procedure for the analysis of the second and third cases. We may write the perturbation matrices for these two cases as

$$\begin{pmatrix} \frac{-\epsilon X_0^2}{1+\epsilon X_0^2} & \frac{X_0}{1+\epsilon X_0^2} & 2\eta\cos\Theta_0 \\ \frac{2\gamma X_0}{1+\epsilon X_0^2} & -\gamma\left(1+\frac{2X_0^2}{1+\epsilon X_0^2}\right) & 0 \\ \frac{2\alpha\epsilon Z_0 X_0^2}{1+\epsilon X_0^2} - 2\eta\cos\Theta_0 & \frac{-\alpha X_0}{1+\epsilon X_0^2} & 0 \end{pmatrix} \tag{13}$$

for the inverse linear dependence, and

$$\begin{pmatrix} \frac{-\epsilon X_0^2(1+2Z_0)}{2(1+\epsilon X_0^2)^{\frac{3}{2}}} & \frac{X_0}{\sqrt{1+\epsilon X_0^2}} & 2\eta\cos\Theta_0 \\ 2\gamma X_0\left[\frac{\epsilon X_0^2(1+2Z_0)}{(1+\epsilon X_0^2)^{\frac{3}{2}}} - 1\right] & -\gamma(1+\frac{2X_0^2}{\sqrt{1+\epsilon X_0^2}}) & 0 \\ \frac{\alpha\epsilon X_0^2}{(1+\epsilon X_0^2)^{\frac{3}{2}}} - 2\eta\cos\Theta_0 & -\frac{\alpha X_0}{\sqrt{1+\epsilon X_0^2}} & 0 \end{pmatrix} \tag{14}$$

for the inverse square root dependence. The stability diagrams of these two systems were also verified via simulation of the differential equations. The stability diagrams of the the first two models are nearly identical. This is simply because, to a first approximation for low output intensities, $1/(1+\epsilon X_0^2) = 1 - \epsilon X_0^2$. The stability diagram for the inverse linear model is shown in Figure 1(a) for $\epsilon = 0.1$, 0.2 and 0.3. From these data, it is clear that the nonlinear gain has the effect of significantly increasing the amount of phase space under which the stable operation of evanescently coupled arrays may occur. One striking feature of these results is the fact that the in-phase mode of operation is substantially unaffected by the presence of the nonlinear gain whereas the out-of-phase mode is clearly very strongly affected. This is indicative of the fact

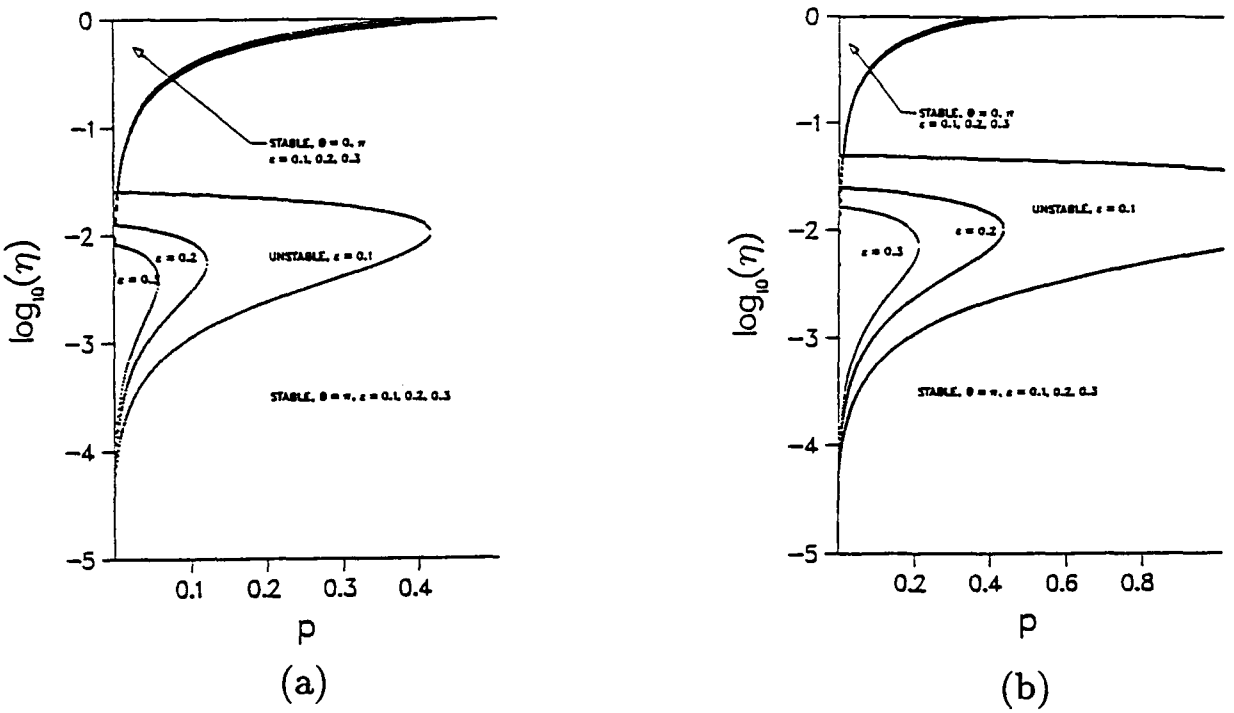


Figure 1: Calculated stability boundaries for (a) an inverse linear dependence of the gain with intensity and (b) an inverse square root dependence of the gain with intensity for $\epsilon = 0.1$, 0.2 and 0.3.

that the stability of the in-phase mode is dependent chiefly upon the extent to which the photons coupled in from the adjacent emitter represent a significant fraction of the photons generated within the device, i.e. the extent to which the array acts as one large laser. The stability of this mode is thus more dependent upon what goes on between the lasers than what goes on within them.

We now examine the third model which exhibits the inverse square root dependence and is derived from consideration of the intraband scattering time. The stability diagram for this model is shown in Figure 1(b) for $\epsilon = 0.1$, 0.2 and 0.3. The diagram is qualitatively very similar to that of the first two cases. Not surprisingly, the major difference is the magnitude of the effect for a given value of $\epsilon$. Quantitatively, one finds that a given value of $\epsilon$ in this model roughly corresponds to $\epsilon/2$ for the first two models. This is because, to a first approximation, we may write $(1+\epsilon X^2)^{-\frac{1}{2}}$ as $(1-\frac{1}{2}\epsilon X^2)$. We thus see a similar though somewhat less pronounced trend for this case to that which was seen for the first two cases, indicating that the presence of gain saturation in evanescently coupled laser arrays enables their stable operation for reasonable amounts of pumping strength and coupling strength.

## References

[1] D. Botez and D. E. Ackley, IEEE Circuits and Devices Mag. **2**, 8 (1986).

[2] G. Agrawal, IEEE Journal of Quantum Electronics, **QE-26**, 1901, (1990).

[3] H. G. Winful and S. S. Wang, Appl. Phys. Lett., **53**, 1894, (1988).

[4] S. S. Wang and H. G. Winful, Appl. Phys. Lett., **52**, 1774, (1988).

[5] G. P. Agrawal and N. K. Dutta, *Long-Wavelength Semiconductor Lasers*, New York: Van Nostrand Reinhold, 1986, p. 227.

# Bifurcation Analysis of Bistable Systems Disturbed by External Noise: an Application of Cumulant Analysis

V. S. Anischenko, A. B. Neiman
Chernyshevsky State University
Russian Federation

Summary not available at press time.

# Static and Dynamic Optical Bistability in Fabry-Pérot and Distributed Feedback Resonators with Quantum Well structures

F.Castelli [1] , L.A. Lugiato [1]
G.P.Bava [2] and P. Debernardi [3]

[1] Dipartimento di Fisica, Università degli Studi di Milano,
Via Celoria 16, 20133 Milano, Italy
[2] Dipartimento di Elettronica, Politecnico di Torino,
[3] CESPA, CNR, c/o Politecnico di Torino,
C.so Duca degli Abruzzi 24, 10129 Torino, Italy
Phone 39 - 11 -5644070, Fax 39 - 11 -5644099

## SUMMARY

Recently relevant results on optical bistability in Multiple Quantum Well (MQW) structures at room temperature have been reported [1].

In this paper a rather complete model for optical bistability in Fabry-Pérot (FP) and Distributed Feedback devices (DFB) including a MQW structure is described. It includes the optical dielectric response of the MQW structure, the static output power vs. input power and finally the dynamical behaviour.

To model the optical response of the material, a sophisticated computer code has been developed which accounts for many–body and Coulomb effects in the electron–hole plasma. The model is based on the work carried out by Haug and coworkers [2], but it is generalized to include finite well thickness and valence band mixing. While the simplified treatment [2] gives rise to only one excitonic resonance, the coupled system of integral equations for the microscopic polarizations resulting from the present model shows, in the dielectric response, a corresponding number of excitonic peaks. The numerical evaluation has included only one electron and two valence (heavy and light hole) subbands; this seems satisfactory in the usual situation for optical bistability, where the working frequency lies below the first exciton absorption peak. However the more complete model applies also to TM polarization, for which the electron–heavy hole transition is ineffective. The numerical results are in satisfactory agreement with experimental measurements reported in the literature.

The material model, previously described, has been used to evaluate the transmission and reflection characteristics of a FP and a DFB device [3]. The role of the most significant parameters on the static response has been analyzed for a GaAs/AlAs MQW. They include the position of the working frequency with respect to the excitonic peak, the shift of this frequency from the cavity frequency or from the Bragg condition, the resonator length and the resonator quality factor due to the grating coupling length. The analysis allows to find the range of the parameter values where optical bistability occurs; it is possible to optimize the structure and the working frequency so to achieve good hysteretic cycles.

We investigated numerically also the dynamical behaviour of the system in order to assess the energy requirements and the time response in the switching processes. Because the cavity buildup time is much shorter than the recombination times of the carriers, we utilized a code in which the field variable follows adiabatically the evolution of the carrier density. The order of magnitude of the response times can be inferred from Fig.1. Fig.2 shows, instead, the " area rule " that the control switching pulse must obey in order to ensure the transition from the low to the high transmission branch.

We started also the investigation of the bistable behaviour in the active counterpart of optical bistability (OB), *i.e.* an amplifier with injected signal (AIS). In this case the MQW structure is subjected to a current which creates population inversion, which however is not enough to let the system lase. We compare the performances of OB and AIS in terms of bistable response and energy requirements.

# References

[1] J.L.Oudar, B.Sfez, R.Kuszelewicz, J.C.Michel, R.Azoulay, Phys. Stat. Sol. B, 159 , 181 (1990)

[2] H.Haug and S.W.Koch, "Quantum Theory of the Optical and Electronic properties of Semiconductors", World Scientific, 1990

[3] G.P.Bava, F.Castelli, P.Debernardi and L.A.Lugiato, Phys. Rev. A **45** (1992), in press.

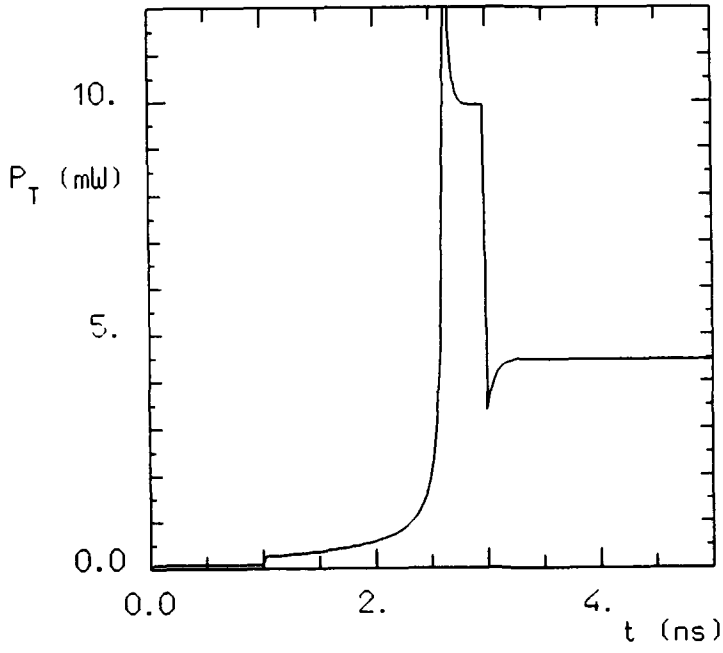


Figure 1: Time evolution of the system towards the high transmission state.

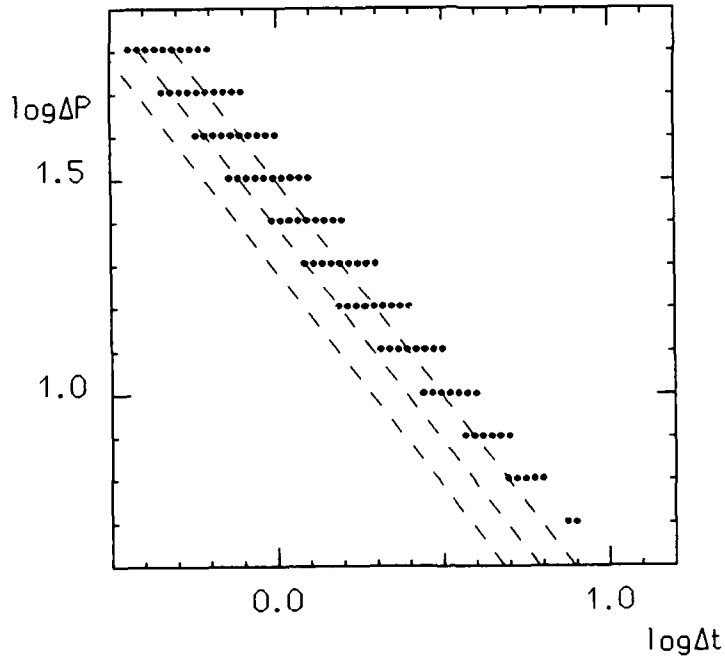


Figure 2: The horizontal (vertical) axis corresponds to the duration (height) of the switching pulse (logarithmic scale). The black balls correspond to the minimum values of the duration for which the switching is obtained. The dashed lines represent pulses with equal energy (pulse area).

# Dynamical aspects of polarization induced switching phenomena in diffusively nonlinear Fabry-Perot resonators.

J. Danckaert, H. Thienpont and I. Veretennicoff

*Applied Physics Dept (TONA/TW), Vrije Universiteit Brussel, Pleinlaan 2, B-1050 Brussel, Belgium.*

The combination of polarization optics and nonlinear optics gives rise to interesting new physical phenomena[1]. In the work presented here we will focus on planar resonators with a nonlinearity of diffusive nature, such as the nonlinear Fabry-Perot resonator (NLFP). There are two ways to display the role of polarization in the bistable response of such a device. First, in a configuration where the light wave is *obliquely incident* on the resonator, as the interface's reflectances depend on the polarization state of the incident light. Second, in a configuration where the beam impinges *normally* on a resonator now filled with an *anisotropic* material, as a phase shift is induced between the linear Airy resonances of the two polarization eigenmodes. In this paper, two *dynamic* theories for planar resonators are presented for both configurations mentioned above, for an arbitrary polarization of the incident *plane* wave.

A first formalism, referred to as the modal approach[2], is valid for nonlinear planar resonators of sufficiently high finesse (F>5). In this model, the evolution in time of the two polarization components of the slowly varying transmitted field amplitude $E_t^{(\sigma)}$ ($\sigma$=s or p, 's' and 'p' being the labels of the two orthogonal polarizations) is governed by the following equation:

$$2i\omega_0 \frac{n_\sigma}{c^2} \frac{dE_t^{(\sigma)}}{dt} + \left[\Delta_\sigma + \eta_\sigma U\right] E_t^{(\sigma)} + i \frac{m\pi T_\sigma}{L^2} E_t^{(\sigma)} = -i\,(-1)^m \frac{m\pi T_\sigma}{L^2} E_i^{(\sigma)}(t) \qquad (1)$$

where $E_i^\sigma$ is the incident field amplitude, $\Delta_\sigma$ is the detuning from the $m^{th}$ resonance, $T_\sigma$ is the transmittance of the interface and L the length of the resonator. The nonlinear term is described by U, where $\eta_\sigma$ is the sign of the nonlinearity. Both the responses for s and p polarized light are governed by similar equations, all parameters differing for s and p polarization in the most general (anisotropic) case. Therefore, in the case of arbitrary polarization, the optical behaviour is governed by two modal equations, which correspond to both polarization states, and which are coupled through the nonlinear term U. In the case of a diffusive nonlinearity, this term U is the same in both modal equations, as it only depends on the total irradiance (s and p components added) inside the cavity. We solved these equations numerically in the dynamical regime, together with the usual Debye equation for the nonlinear term.

In the second approach, an evolution equation in space and time for the forward and backward propagating cavity fields ($E_F^\sigma$ and $E_B^\sigma$) is derived from the nonlinear wave equation by standard procedures (slowly varying envelope approximation, etc...). For simplicity, we present here the case where z, the direction normal to the cavity, corresponds to a principal axis of the system, yielding[3] :

$$\cos\theta\, \partial_z E_F^\sigma + \frac{n_\sigma}{c} \partial_t E_F^\sigma + \frac{\alpha_\sigma}{2} E_F^\sigma = ik\, \eta_\sigma U\, E_F^\sigma \qquad (2)$$

$$-\cos\theta\, \partial_z E_B^\sigma + \frac{n_\sigma}{c} \partial_t E_B^\sigma + \frac{\alpha_\sigma}{2} E_B^\sigma = ik\, \eta_\sigma U\, E_B^\sigma$$

The material parameters $n_\sigma$, and $\alpha_\sigma$ describe the linear index of refraction, and the linear absorption, for s and p polarization, respectively, and $\theta$ is the beam angle inside the cavity. We therefore have to handle a total of four equations, coupled again through the nonlinear term U. We solved these equations numerically with the appropriate boundary conditions. This formalism has the advantage of being valid for resonators of arbitrary finesse. On the other hand, one can see from Eq(1) that in the modal approach the longitudinal spatial coordinate z has been eliminated, reducing the dimension of the problem by one and thus greatly facilitating the numerical integration. The (dis)advantages of both approaches will be further discussed at the meeting.

Essentially two switching phenomena relying on a change of the state of polarization of the incident wave have been observed. We have called *polarization induced switching* the up- *or* down-switching of the device's response at constant input irradiance. In this case, however, no switching *back* to the original state can be established at the same input irradiance. Another interesting phenomenon, is *polarization bistability*, where a full hysteresis cycle is run through as a function of the polarization angle. Polarization bistability has already been demonstrated theoretically in a nonlinear prism coupler[4]. Here it will be shown also to occur in a high finesse, anisotropic NLFP. In general, for polarization bistability to occur it is necessary to have a phase shift between the linear s and p resonances.

At the conference, some dynamical aspects of polarization induced switching will be presented, revealing interesting phenomena such as critical and noncritical slowing down, critical polarization angles, and critical (polarization) modulation times, for high as well as for low finesse resonators, and in both configurations mentioned before. As an example, critical slowing down in a polarization induced up-switching process is shown in the figure on the next page.

This work could not have been performed without the collaboration between the Applied Physics Dept in Brussels and the Laboratoire d'Electromagnétisme, Microondes et Optoélectronique (LEMO) in Grenoble (France), subsidized by the Flemisch Community Government in Belgium and the Centre National de Recherche Scientifique in France (projects 91.3 and 92.9). We are especially indebted to Guy Vitrant from LEMO for providing the numerical codes to solve the modal Eq(1), as well as for the many, most stimulating discussions.

---

1 N.I. Zheludev, Sov.Phys.Usp.**32**, 357 (1989).

2 M. Haelterman and G. Vitrant, in *OSA Proceedings on Nonlinear Dynamics in Optical Systems*, N.B. Abraham, E.M. Garmire & P. Mandel, eds. (Optical Society of America, Washington, DC 1991), Vol.7, p.210; see also G. Vitrant, M. Haelterman and R. Reinisch, J. Opt. Soc. Am. **B7**, 1319 (1990);

3 H. Thienpont, J. Danckaert and I. Veretennicoff, submitted to the Journal of the European Optical Society.

4 J. Danckaert, G. Vitrant and R. Reinisch, in Technical Digest on Nonlinear Guided Wave Phenomena (OSA, Washington DC, 1991), Vol.15, p.313; J. Danckaert and G. Vitrant, accepted for publication in J. Appl. Phys.

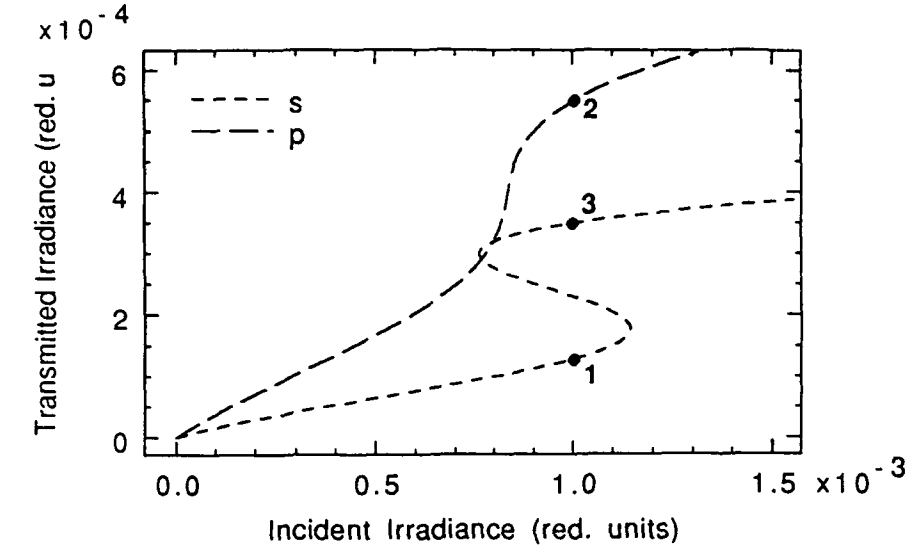


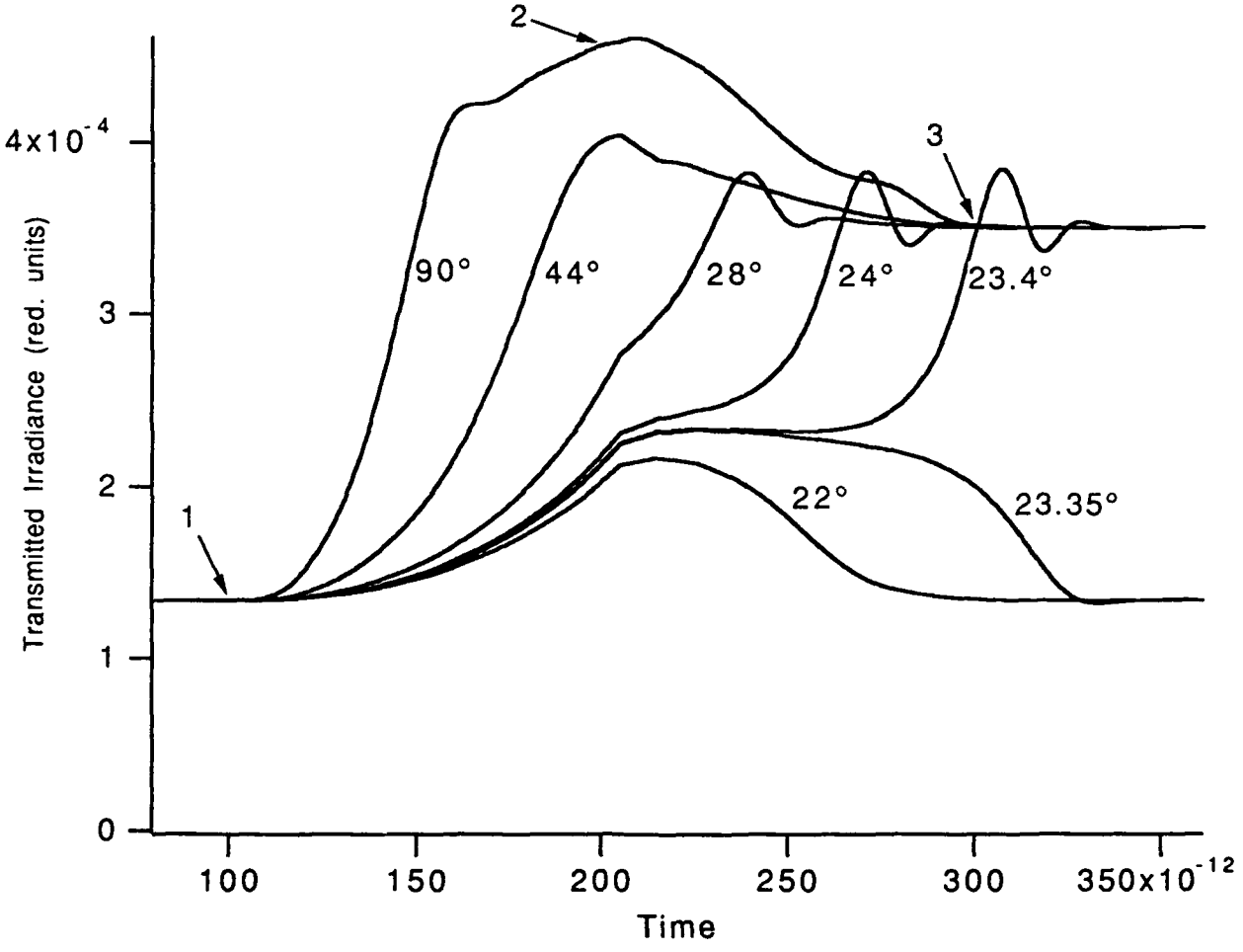


Critical slowing down in the polarization induced up-switching process, for different polarization angle intervals and for a constant value of the incident irradiance ($I_{in}$=1 $10^{-3}$). These curves were calculated using Eqs(2). The different curves in the figure correspond (from the upper to the lower curve) with a maximum value of the polarization angle of resp., 90°, 44°, 28°, 24°, 23.4°, 23.35° and 22°. The polarization angle rises linearly from 0° at a time t=100ps to reach his maximum value at t=200ps, and goes then back to zero in the same time interval. The curves clearly display critical slowing down for values near the critical polarization angle (which is situated between 23.35 and 23.4°). The device under consideration here is a low finesse NLFP illuminated under an angle of incidence of 45°. We suppose the etalon to be uncoated, retaining only the natural reflectances of the interfaces (with an index of refraction n=3.56).

As a reference, also the stationary response curves are shown above. From this and from the dynamical calculation, one sees that the up-switching is established starting from the low (point 1) to the high (point 3) branch for s-polarized light, via an intermediate state (e.g. p-polarized light, point 2).

# Opto-Thermal Bistable Cavities with Localized Absorption under Modulated Excitation

Jordi Farjas, Francesc Boixader and Gaspar Orriols
Departament de Física. Universitat Autònoma de Barcelona.
08193 Bellaterra. Spain. Tel. (34) 3-5812110.

Josep Massaneda and Francesc Pi
Departament d'Òptica i Optometria. Escola d'Òptica.
Universitat Politècnica de Catalunya. 08222 Terrassa. Spain.

Opto-Thermal Bistability with Localized Absorption (BOITAL) deals with etalons in which the light absorption occurs in one of the reflective coatings while the thermo-optic spacer is transparent. The separation of functions within the bistable system permits an independent and, therefore, easier optimisation of both functions and also introduces the possibility of complex structures with more than one absorbing film and/or with various layers of different thermo-optic materials [1]. These kinds of structures possess composite feedback mechanisms and may be used to achieve different logic functions and to study dynamic instabilities in passive optical systems [2].

We are investigating the dynamics of BOITAL cavities with an absorbing mirror and a multilayer spacer of alternatively opposite thermo-optic materials [3,4]. Two remarkable features in the dynamics of such systems are the easy occurrence of homoclinic bifurcations and the fact that their effective dimension is determined by the number of layers in the spacer. In the case of bilayer systems, single-frequency oscillations and a variety of homoclinic bifurcations without complicated orbit structures have been observed both theoretically and experimentally [3]. For systems of higher dimension, the homoclinicity may appear accompanied by a rich dynamics associated with the saddle-focus nature of the invariant set at which the homoclinic orbit makes tangency and Shil'nikov chaos has been numerically observed in trilayer systems [4]. On the other hand, Rössler chaos has been also observed in the response of trilayer systems both numerically and experimentally [5].

This communication deals with BOITAL bilayer cavities irradiated with periodically modulated light. We report numerical and experimental evidences of a variety of instabilities occurring in such a kind of forced two-dimensional system. The modulated cavities exhibit quasi-periodic oscillations, mode locking, period-doubling sequences and other typical phenomena of forced nonlinear oscillators [6]. More interestingly, they provide a natural way to investigate the perturbation of homoclinic bifurcations without complicated orbit structures,

as the ones obtained in the autonomous bilayer system [3], and a variety of chaotic dynamics associated with homoclinicity have been observed.

The figures present experimental results obtained with a bilayer of glass/quinoline and absorbing input mirror [3]. Fig.1 shows and stroboscopic representation of the reflected power as a function of the modulation amplitude when the background power holds the autonomous system in an oscillating state close to a homoclinic transition. The autonomous frequency is 11.0 Hz and the modulation is at 32.6 Hz. Notice the presence of quasiperiodic (QP), periodic (P) and chaotic (C) windows. With holding powers far from the homoclinic transition, chaotic responses have only been obtained in numerical simulations since they appear in extremely narrow windows. Fig.2 shows the time evolution, stroboscopic Poincaré section and phase projection corresponding to the first chaotic window in fig. 1.

Experiments are in good agreement with numerical simulations obtained from integration of a system of homogeneous heat equations subjected to the nonlinear boundary condition describing the input mirror absorption [3].

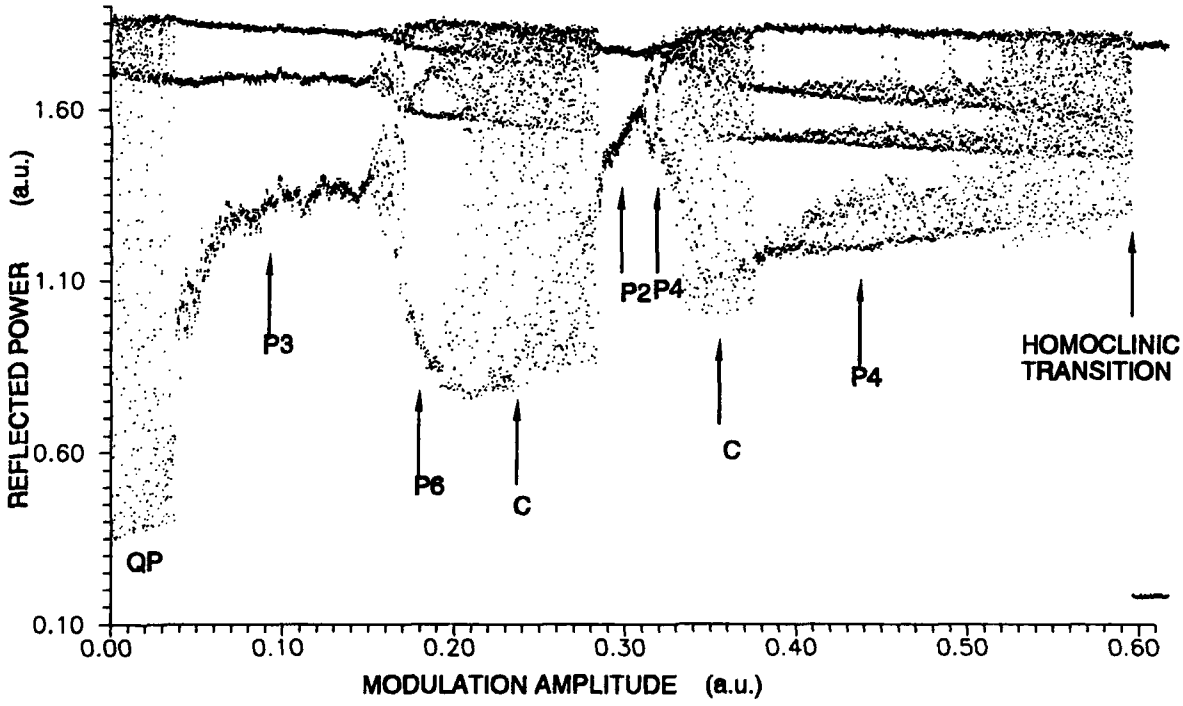


Figure 1

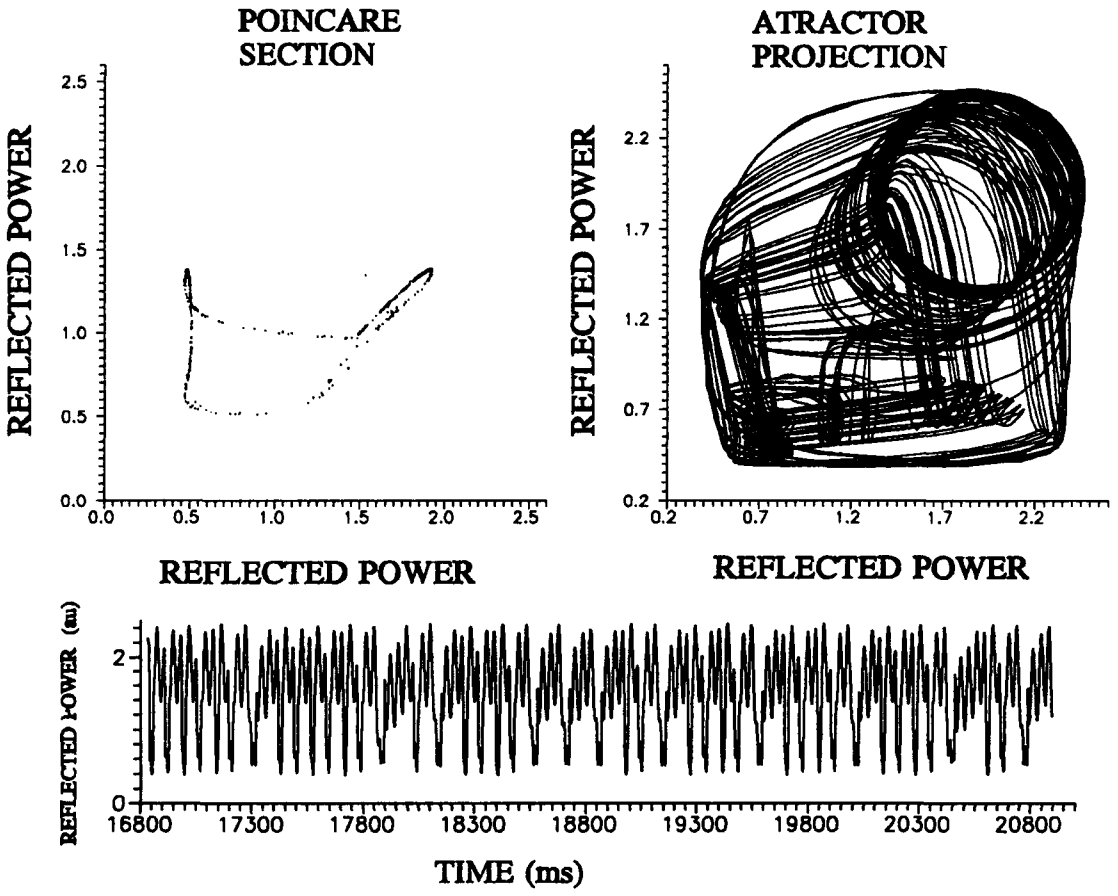


Figure 2

## References

[1] G. Orriols, C. Schmidt-Iglesias, F. Pi, Opt. Commun. 63 (1987) 66.

[2] F. Pi, G. Orriols, in "Interaction of Radiation with Matter. A volume in honor of Adriano Gozzini", eds. G. Alzetta, E. Arimondo, F. Bassani and L. Radicati (Scuola Normale Superiore, Pisa, 1986) 239.

[3] J.I. Rosell, F. Pi, F. Boixader, R. Herrero, J. Farjas, G. Orriols, Opt. Commun. 82 (1991) 162.

[4] J.I. Rosell, F. Pi, F. Boixader, R. Herrero, J. Farjas, G. Orriols, in "ECOOSA'90", eds. M. Bertolotti, E.R. Pike (Adam Hilger, 1991) 289.

[5] F. Boixader, R. Herrero, G.Orriols, J.I. Rosell, F. Pi, "Rössler Chaos in Opto-Thermal Bistability with Localized Absorption", submitted to this Meeting.

[6] T. Kai, K. Tomita, Prog. Theor. Phys. 61 (1979) 54.

# The effect of initial phase factor on the properties of an electro-optical bistable system

Zheng Zhiren and Gao Jinyue
(Physics Department, Jilin University, Changchun, 130023, China)
Tel: China (0431) 822331 Ext. 2976 FAX: China (0431) 823907

The hybrid bistable system with a delay in the feedback loop, which was originally proposed and studied by Ikeda[1], has been widely investigated[2, 3, 4] as this system plays many common instability behaviours of nonlinear dynamical systems. There is an initial phase factor in the equation describing the system dynamics as there are for most other bistable systems, which is equivalent to the bias in the device. We report the important role played by this phase factor in the bistability and instability behaviours, especially when the input intensity of the system is modulated harmonically. The dynamical equation of the system can be written as[4]

$$dV(t)/dt+V(t)=0.5I(1-K\cos(V(t-\tau)+\theta))$$

where V(t) and I are corresponding to the output and input intensities, respectively, K is the extinction coefficient, $\tau$ is the delay time and $\theta$ is the initial phase factor. If a modulation is applied to the steady state, the input intensity could be expressed as

$$I(t)=I_o+A\cos(\omega_o t)$$

where $I_o$ is the steady state value of input intensity where we work on, A and $w_o$ are the modulation depth and modulation frequency, respectively Along with the linear stability analysis[4], it is easy to show that the initial phase factor plays an important role in the bistability and instabilities of the system

(1) The bistability width for the first bistability branch is a function of the phase factor $\theta$, and the necessary condition for the appearance of the first bistability branch is governed by

$$V_o\sin(V_o+\theta)+\cos(V_o+\theta)=1/K$$

with solution of $0<\theta<\pi/2-1/K$.

(2) The resonance peak responding to the modulation at the first eigenfrequency of the system in the stable region without modulation is a function of the phase factor $\theta$ as well as a function of the modulation

depth A . With increasing $\theta$, the resonance peak moves to the higher side of frequency $\omega_o$ , but with increasing A, the resonance peak moves to the lower side of frequency $\omega_o$ . The former could be understood as the eigenfrequency of the linear stability analysis itself is a function of the phase factor, however, the later one is hardly explained simply by the linear stability analysis and its origin need to be further studied.

(3) As it is well known that there are many frequency locking windows in the unstable region without modulation when the input intensity is modulated as shown in Fig. 1 (a) , which is the fundamental frequency $\omega_1$ of the output intensity on the modulation frequency $\omega_o$. It is clearly seen that the fundamental frequency $\omega_1$ eventually approaches its fundamental frequency without modulation, after many locking regions with increasing of the modulation frequency $\omega_o$. This means that the response of the system to the modulation becomes weaker and weaker for larger modulation frequencies. The most interesting is the effect of the phase factor $\theta$ on the frequency locking as shown in Fig. 1. For lower modulation frequency, the locking regions are large. With increasing $\theta$, the function of the fundamental frequency $\omega_1$ versus modulation frequency $\omega_o$ becomes more and more complicated for the lower modulation frequencies and the locking regions become smaller and smaller, Fig. 1 (b), then the first locking region was disappeared , Fig. 1 (c). With increasing $\theta$ further , the all locking regions were disappeared at the same time, Fig. 1 (d). The similar phenomena have been observed in the first frequency locking region . For small $\theta$, the response oscillation is almost sinusoidal. With increasing $\theta$,

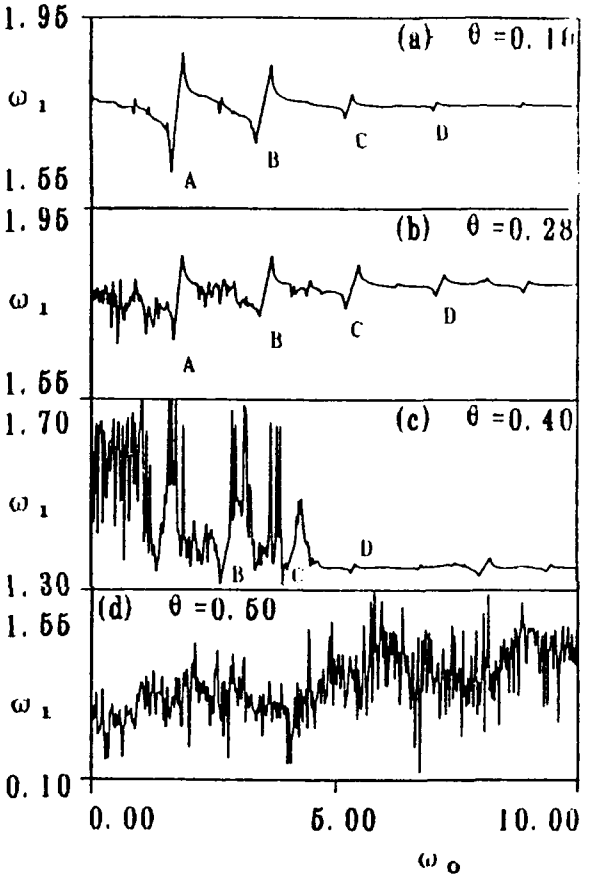


Fig. 1: The curves of the fundamental frequency $\omega_1$ of output intensity Vs. the modulation frequency $\omega_o$ in the unstable region for different initial phase factor $\theta$.
The parameters are K=0.95, V0=4.5 , A=1.0 , $\tau$ =1.2 .
(a) $\theta$ =0.10, $\omega_1$ (A=0) =1.77
(b) $\theta$ =0.28, $\omega_1$ (A=0) =1.79
(c) $\theta$ =0.40, $\omega_1$ (A=0) =1.35
(d) $\theta$ =0.50, $\omega_1$ (A=0) =1.26
A: $\omega_o = \omega_1$ , B: $\omega_o = 2\omega_1$ ,
C: $\omega_o = 3\omega_1$ , D: $\omega_o = 4\omega_1$ .

the response output oscillation undergoes a series of period doubling bifucations and eventually becomes irregular as shown in Fig. 2 and its corresponding power spactrum Fig. 3.

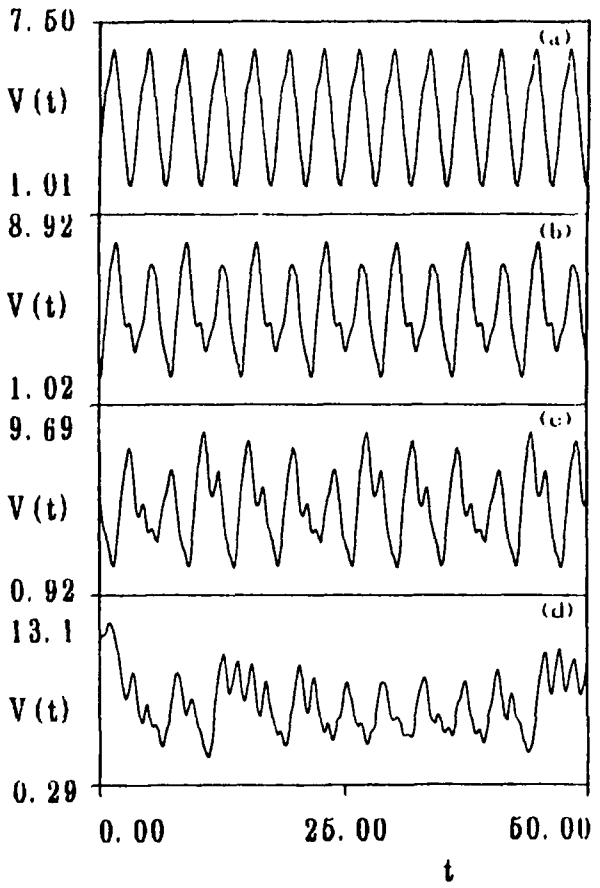


Fig. 2: The curves of the output oscillations V(t) for different initial phase factor θ.

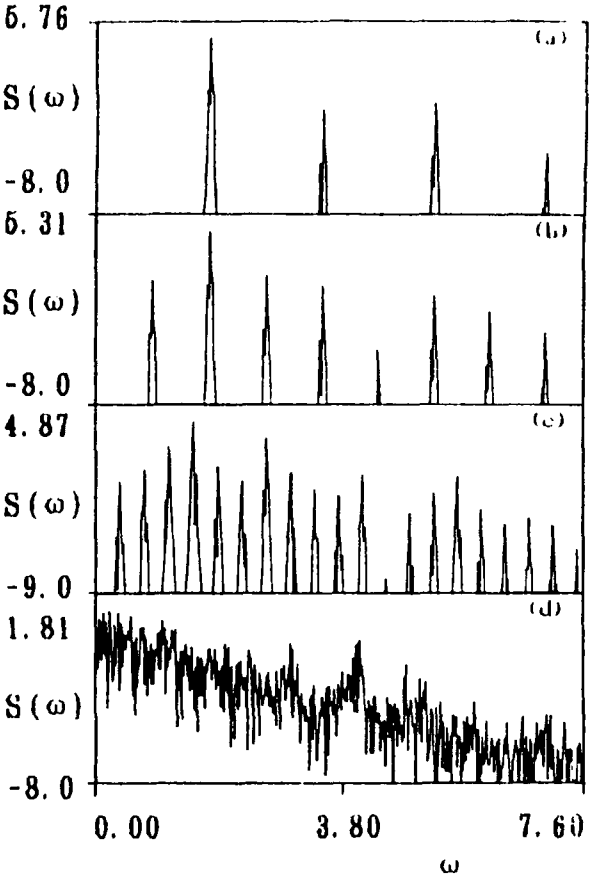


Fig. 3: The power spectra S(ω corresponding to the oscillations in Fig. 2.

The parameters of Fig. 2 and Fig. 3 are K=0.95, $V_0$=4.5, A=1.0, τ=1.2
(a) θ=0.10, $\omega_0=\omega_1$=1.75, (b) θ=0.28, $\omega_0=\omega_1$=1.75,
(c) θ=0.40, $\omega_0=\omega_1$=1.50, (d) θ=0.50, $\omega_0$=1.25.

REFERENCES

(1) K. Ikeda, Optics Comm. 30 (1979) 257
K. Ikeda, H. Daido and O. Akimoto, Phys. Rev. Lett. 45 (1980) 709
(2) M. Okada and K. Takizawa, IEEE J. Quantum Electronics, QE-17 (1981) 2135
(3) H.M. Gibbs, F.A. Hopf, D.L. Kaplan and R.L. Shoemaker, Phys. Rev. Lett. 46 (1982) 474
(4) J.Y. Gao, J.M. Yua and L.M. Narducci, Optics Comm. 44 (1983) 201
J.Y. Gao and L.M. Narducci, Optics Comm. 58 (1986) 360
J.Y. Gao, G.X. Jin, J.W. Sun, X.Z. Guo, Z.R. Zheng, N.B. Abraham, Optics Comm. 76 (1990) 409

# Dynamic Optical Bistability in A Semiconductor Doped Glass Etalon

*Chunfei Li, Yinglin Song, Zizhong Zha and Lei Zhang*
Department of Physics, Harbin Institute of Technology
Harbin, 150006 CHINA Tel:321000-4128

In the past decade, experimental results of transient optical bistabilities in etalons of $CdS_xSe_{1-x}$ doped glasses have been presented by many authors[1-3]. Switching speed of ns to ps orders has been obtained. However, there still do not exist a dynamics theory of this transient optical bistability. This paper emphasizes the dependence of the implementation of transient optical bistabilities on the incident pulse width, the media response time, the FP cavity establishing time, and also, the influence of the incident pulse width on the switching speed.

Applying the band filling theory of the semiconductor and FP cavity model with linear absorption and nonlinear dispersion [4-6], we have obtain the following equations:

$$I_c = T I_i$$

$$T = \frac{A}{1 + F \sin^2 \phi(I_c)}$$

$$\frac{dN}{dt} = \frac{a I_c}{h\nu} - \frac{N}{\tau} - BN^2 - CN^3$$

$$\phi = \phi_0 + \frac{2\pi d \sigma N}{\lambda}$$

where

$$I_c = \frac{I_i T}{C_t}$$

$$\phi_0 = \frac{2\pi d n_0}{\lambda}$$

Assume that the reflectivities $R_1=R_2=R=96\%$, Ic is intensity in a cavity, then A and $C_t$ are constants:
where $\alpha$ is the absorption coefficient, $d$ is the thickness of the

$$A = \frac{e^{-\alpha d}(1-R)^2}{(1-R_\alpha)^2}$$

$$C_t = \frac{\alpha d\, e^{-\alpha d}(1-R)}{(1-e^{-\alpha d})(1+R_\alpha)}$$

material and $R_\alpha$ is called effective reflectivity, $R_\alpha = Re^{-\alpha d}$.

In order to analyze the characteristic of transient optical bistability, the following three temporal parameters should be taken into account, the incident pulse width $T_p$, the response time of the nonlinear media $T_d$ and the cavity round-trip time $T_r$. By choosing different $T_p$, $T_d$ and $T_r$, numerical simulations have given the conditions when optical bistabilities occur. Figure 1 shows the optical bistabilities corresponding to different cavity lengths. When $\Delta\phi_0=0.6$, $T_p=45$ns, $T_d=1$ns, Fig. 1(a) and Fig. 1(b) are the optical bistabilities corresponding to two different $T_r$ ($d_a=20\mu$m and $d_b=300\mu$m), respectively. Figure 2(a), (b) and (c) are optical bistabilities corresponding to $T_d=200$ps, 1ns and 2ns at $\Delta\phi_0=0.6$, $T_p=30$ns, $I_i=220$KW/cm$^2$ and $d=300\mu$m. Figure 3(a), (b) and (c) are optical bistable characteristics when $T_p=20$ns, 30ns and 35ns, respectively, with $\Delta\phi_0=0.6$, $d=300\mu$m, $I_i=220$KW/cm$^2$ and $T_d=1$ns.

The above theoretical simulations indicated that optical bistability could not be obtained when the media response is too slow ($T_p<T_d$) or the life time of the cavity is too long ($T_d<T_r$). Specifying to our cases, we have $T_p/T_d>20$ and $T_d/T_r\geq 1$. Then we have the quasi-stable condition for transient optical bistabilities:

$$T_p > T_d \geq T_r$$

Figure 4 shows the transmissive properties of the optical bistable device with incident pulses of different width. One can observe that the switch-on speed is getting faster when the pulse widths are reduced. Fig.4 (a)-(d) are transmissive waveforms corresponding to the incident pulse widths of 6, 16, 32, and 60ns, respectively, at $I_i=220$KW/cm$^2$, $d=300\mu$m and $T_d=200$ps. The temporal interval of two adjacent points in the curve is 40ps.

In reference [1], only optical limiting characteristics was obtained when $T_p=10$ns and $T_d=2$ns, ie. $T_p/T_d=5$. While in reference [2], optical bistability was observed with $T_p=150$ps, $T_d=3.5$ps and $T_r=3$ps which satisfies the relation $T_p>T_d\geq T_r$.

These experiments have also demonstrated the effectiveness of our theory. For a $CdS_xSe_{1-x}$ doped glass etalon, the quasi-stable condition for optical bistability is $T_p>T_d\geq T_r$. Furthermore, The switch-on speed of the transient optical bistability will be getting faster with the reducing of the incident pulse width. While

the switch-off speed depends on the recombination life time of the carriers. This conclusion can be applied to most of the optical bistable device with the FP etalon structure filled with semiconductors. One effective approach to increasing the switching speed of optical bistability is choosing nonlinear optical materials with fast response time, employing short cavity or cavityless device and using ultra-short laser pulse.

**References:**

[1]. B. Danielzik, et al., Appl. Phys. B., **38**, 31(1985).
[2]. J. Yumoto, et al., Opt. Lett., **12**, 832(1987).
[3]. Wenji Peng, et al., High Speed Photography and Photonics, **20**, 62(1991)(in Chinese).
[4]. D. A. B. Miller, et al., Phys. Rev. Lett., **47**, 197(1981).
[5]. D. A. B. Miller, et al., IEEE. Quantum Electron., QE-**17**, 306(1981).
[6]. J. P. Zheng, et al., Appl. Phys.Lett., **53**, 643(1988).

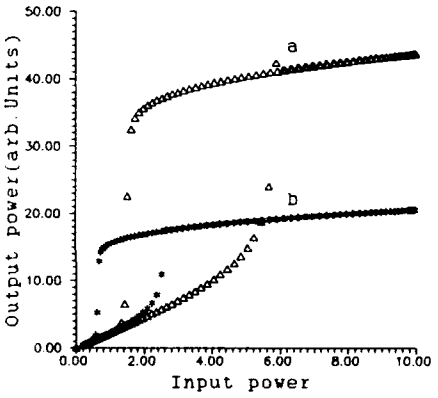


**Figure 1**

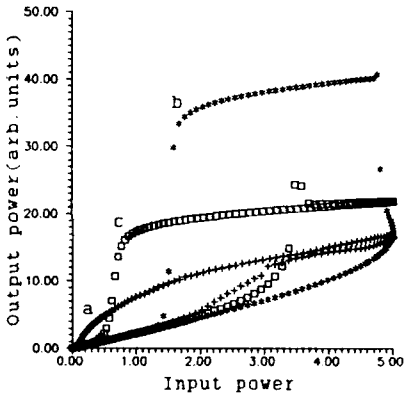


**Figure 2**

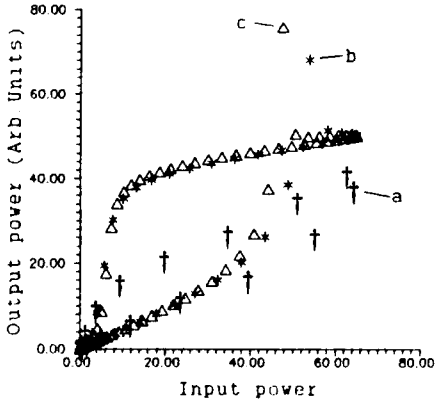


**Figure 3**

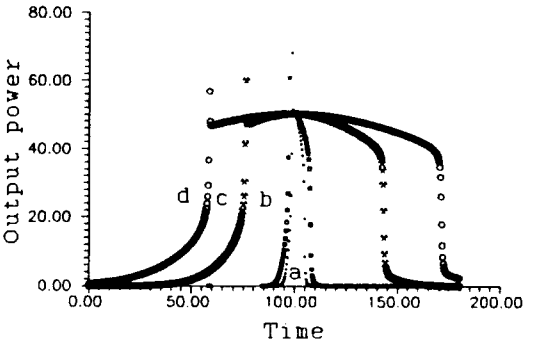


**Figure 4**

# New Types of Switching Waves and Diffractive Autosolitons in Wide-Aperture Nonlinear Interferometers and Lasers

S. V. Fedorov, G. V. Khodova, K. S. Kostritskaya, N. N. Rosanov

S. I. Vavilov State Optical Institute
199034, St. Petersburg, Russia

We investigate the new types of transverse patterns in wide-aperture passive interferometers and lasers. We propose and analyze equations of motion for a diffractive autosoliton in passive nonlinear interferometers excited by external coherent radiation with gradually non-uniform characteristics. If external radiation wave front does not contain dislocations at the interferometer aperture, autosoliton moves along the steepest descent lines of effective potential expressed by linear combination of the intensity and the phase of radiation incident on the interferometer. With the dislocations, the motion with autosoliton rotation becomes possible. The coupled switching wave and autosoliton structures in bistable and multistable interferometers are studied. The dynamics of autosoliton formation in conditions of transverse field structure instability and in nonlinear interferometer with unstable resonator is considered. The peculiarity of autosolitons in lasers with saturated absorption is a diffractive shift of generation frequency. This aspect being taken into account, positive (bright) and negative (dark) laser autosolitons are demonstrated and autosolitons interaction is investigated.

# Squeezing in Wide-Aperture Nonlinear Interferometer: Transverse Effects

A. V. Belinsky[1], N. N. Rosanov[2]

[1] Faculty of Physics, Moscow State University,
Moscow, 117234, Russia
[2] S. I. Vavilov State Optical Institute
St. Petersburg, 199034, Russia

Fluctuations of radiation and of photodetector current present a fundamental limit for capabilities of parallel optical processing. In this connection it seems perspective to use the light squeezed states to depress photon noise of optical images. In this report we consider a possibility of generation of sufficiently wide (multi-mode) beams of sub-Poisson light transmitting coherent radiation through wide-aperture nonlinear interferometer.

The interferometer is filled with Kerr medium, and external radiation consists of regular (classical) and fluctuational components. Fluctuation spectrum at temporal $\Omega$ and spatial $\kappa$ frequencies is determined by nonlinear interferometer response to perturbations with frequencies $(\Omega, \kappa)$ and $(-\Omega, -\kappa)$ (here we omit optical frequency $\omega$, $\kappa$ being the transverse projection of the perturbation wave vector). The spectrum calculations show an appreciable squeezing in a certain range of temporal and spatial frequencies. The optimal squeezing may be obtained in a scheme with output radiation heterodyning.

# Theory of a Photorefractive Resonator.

H. Zeghlache, L. Dambly and P. Glorieux.
Laboratoire de Spectroscopie Hertzienne,
Université des Sciences et Technologies de Lille,
59655 Villeneuve d'Ascq Cedex, France.
Phone : +33.20.43.68.26 Fax : +33.20.43.40.84.

A theory of the two-wave mixing in a photorefractive medium placed in a ring cavity is developped following the model first derived by Yariv and Kwong [1] : a steady refractive index involving the photorefractive effect is used as a non-linear source-term ($\mathbf{P}_{NL}$) in the Maxwell equations, and the cavity field is expanded on the transverse cavity modes. In this model we take into account the intensity change of both the pump and resonator beams inside the crystal due to the mutual power exchange : we have developed a multimode model which gives in the long-time limit the z-dependance of the fields (z is the optical axis) for a passage in the crystal, using the expansion in terms of the complete set of the cavity transverse modes. [2]

In the case of a uniform shining of the PR, a perturbative but detailed analysis of a monomode oscillation is presented and we give an analytical expression for the frequency-shift in terms of a ratio of integrals which presents poles. The presence of a pole implies that the frequency-shift can be as large as required, as soon as the parameters are suitably adjusted. Depending on the length of the crystal (directly related to the convergence of our expansion

and then to the intensity exchange between the oscillating and the pump beams) and $\Phi$ the phase mismatch of the gratings, we analyze the pole number. For different experimental situations, we use two parameters in our description : L the crystal length (for the dominant order calculation) or $m$ the ratio of the cavity intensity to the input intensity (for the exact calculation) and $\Phi$. We show in Fig 1a and 1b the position of the poles on the $\Phi$ axis (presented at the roots of the S function) for L=0.1cm and L=1cm.

Fig 1a : L=0.1cm

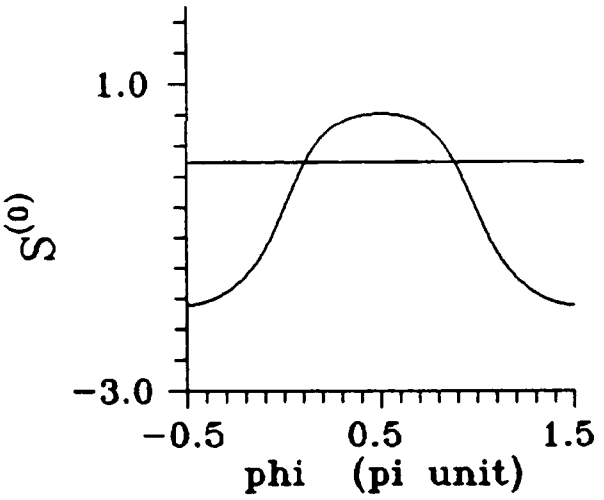


Fig 1b : L=1cm

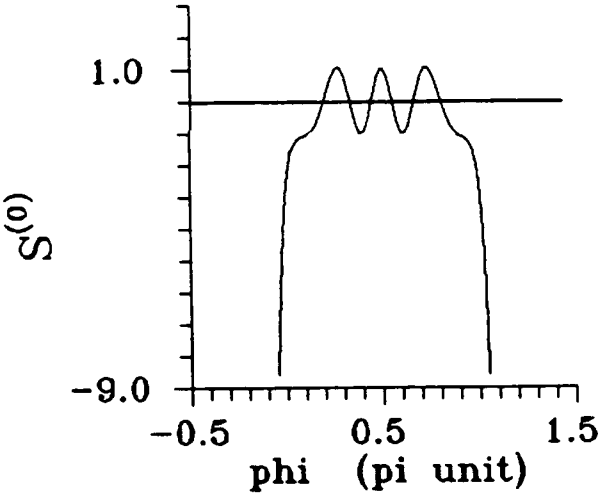


One gets qualitatively the same results by a direct integration of the equations. We present on Figs 2a and 2b the poles frequency shift versus $\Phi$ for $m$=0.5, and consequently for the power transfert of 50%, and $m$=0.2. The pole number increases as $m$ or the length of the cavity increases. One can note the nascent pole for the 20% power transfert.

Fig 2a : $m=0.2$

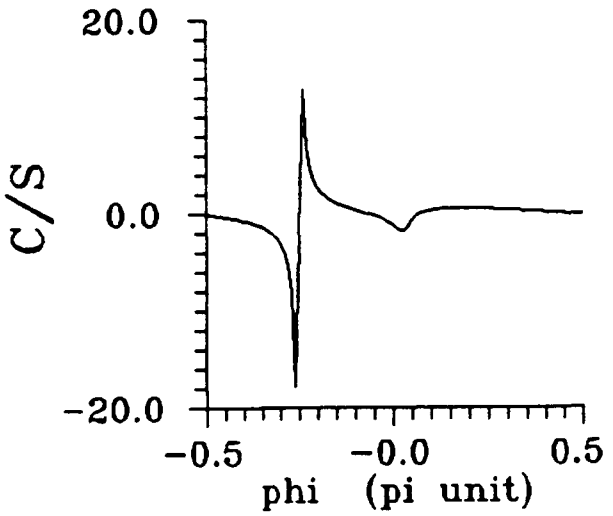


Fig 2b : $m=0.5$

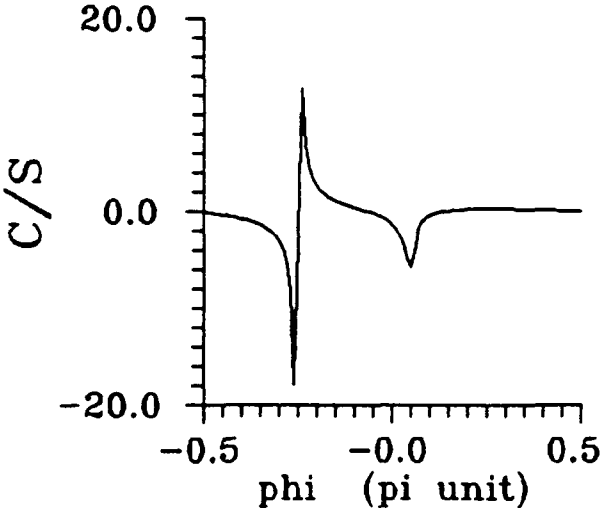


We also analyze the dependance of the poles with respect to $m$. As $m$ increases, the $\Phi$-distance between the poles decreases and at least for $\Phi = 0$ and $\pi$, two new poles appear.

This large frequency-shift, which should be still present in a multimode description, can explain the successive appearance of the cavity modes observed experimentally in [3,4], and could then match the transverse mode spacing which is around $10^8$ Hz. Our calculations are pursued in that direction. We plan also to derive a dynamical bimode model to describe some of the experimental observations made on such a system in the LSH Laboratory in Lille.

[1] A. Yariv and S. K. Kwong, Opt. Lett., **10**, 454 (1985).

[2] D. Z. Anderson and R. Saxena, J. Opt. Soc. Am. B, **4**, 164 (1987).

[3] H. Rajbenbach and J. P. Huignard, Opt. Lett., **10**, 137 (1985).

[4] F. T. Arecchi, G. Giacomelli, P. L. Ramazzi and S. Residori, Phys. Rev. Lett., **65**, 2531 (1990).

# SOLVABLE MODELS OF OPTICAL RESONATORS.

A. V. Malev
St.-Petersburg State University, Research Institute of Physics
Uljanovskaya str. 1, Petrodvorets, St.-Petersburg, Russia
phone: (812)428-72-20, fax: (812)428-66-49

Transverse effects in optical systems have been intensively studied in last years/1,2/. But it is rather difficult to analyze resonator diffraction effects and especially to take into account the influence of space inhomogeneities on laser generation in the framework of standard approach. However one can solve this problems in a mathematically sound way using the self-adjoint extension theory. The extension theory technique provides almost analytically describing of different physical processes (see /3,4/ for details and examples). This technique was used in /5/ for chaotic behavior studies of quantum systems.

In the present work solvable models of open resonators based on the extension theory are considered. Spectral analysis of open resonators is carried out and scattered waves (which are of great importance for laser dynamics studies) are obtained. An open resonator is described as a set of coupled subsystems. Each subsystem is a certain space region where the wave dynamics is assumed to be known. Subsystems interaction is described in terms of boundary conditions on regions boundaries. In the framework of this approach resonator wave dynamics is determined by subsystems wave dynamics and special properties of the binding channels. Thus an open resonator consisting of two mirrors may be considered as two regions: $\Omega^{IN}$ and $\Omega^{EX}=R_3\setminus\Omega^{IN}$. Mirrors surface and caustic form the boundary of $\Omega^{IN}.\Omega^{EX}$ interacts with $\Omega^{IN}$ through this boundary though boundary conditions on the mirror and caustic are different. Analyzing the same resonator but with local inhomogeneity put in it we are to include into consideration supplementary external region. In the limit of single scattering approximation on the inhomogeneity this supplementary external region has simple structure and joins to the resonator through the inhomogeneity surface.

In this paper both cases are discussed using one dimensional

approximation. Unfortunately within one-dimensional analysis no diffraction losses occurring due to the finite mirrors aperture can be described in a mathematically rigorous way. However these losses may be formally taken into account by means of finite dimensional model of the inner space of functions $H^{IN}$. Namely it is considered here the inner space basis to be a set of N eigenfunctions $\varphi_n$, n=1,...,N of the Laplace operator in $L_2([0,1])$ with Dirichlet boundary conditions

$$\varphi_n(0)=\varphi_n(1)=0 \qquad (1)$$

In accordance with above mentioned assumptions two models of open resonators are investigated here. In the first case an open resonator is explored as a scattering system consisting of nontrasmitting point x=1 and partially transmitting point x=0 with reflection **r**. In the second case the system under consideration consists of nontransmitting points x=0, x=1, $x=x_0\in[0,1]$. The point $x=x^0$ models local inhomogeneity.

In the first case $\Omega^{IN}$ is the interval [0,1] and $\Omega^{EX}$ is the region $]-\infty,0]$. $\Omega^{IN}$ and $\Omega^{EX}$ interact through the point x=0. Reflection **r** plays the role of binding parameter. In the second case again $\Omega^{IN}$ is the interval [0,1] and $\Omega^{EX}$ is the axis $]-\infty,\infty[$. $\Omega^{IN}$ and $\Omega^{EX}$ interact through the point $x=x_0$. In both cases the inner operator is the Laplace operator $(-\Delta^{IN})$ defined on the finite set of its eigenfunctions with boundary conditions (1). The external operator is the Laplace operator $(-\Delta^{EX})$ in $L_2(]-\infty,0])=H_1^{EX}$ defined with Dirichlet boundary conditions at the point x=0 in the first case. In the second case the external operator is the Laplace operator in $L_2(]-\infty,\infty[)=H_2^{EX}$.

Starting from the orthogonal sum of inner and external operators its restriction to the domain $D_0=\{f\in D(-\Delta^{IN}\oplus-\Delta^{EX}), f=f^{IN}\oplus f^{EX}, f^{IN}\in H^{IN}, f^{EX}\in H^{EX}, F(f)=0\}$ is obtained. The condition F(f)=o reads

$$F(f)=\int_0^1 f^{IN}(x)\left\{\sum_{n=1}^{N}\varphi_n'(0)\bar{\varphi}_n(x)\right\}dx +$$

$$+\sqrt{\frac{1+r}{1-r}}\;e^{-i\frac{\pi}{2}}\frac{2}{\pi}\int_{-\infty}^{0}dk\int_{-\infty}^{0}dx\;k\sin(kx)\;f^{EX}(x)=0 \qquad (2)$$

in the first case and

$$F(f)=\int_0^1 f^{IN}(x)\left[\sum_{n=1}^{N}\varphi_n(x_0)\bar{\varphi}_n(x)\right]dx +$$

$$+\frac{1}{2\pi}\int_{-\infty}^{\infty}dk\int_{-\infty}^{\infty}dx\, e^{ikx_0}e^{-ikx}f^{EX}(x)=0 \qquad (3)$$

in the second one.

Having in mind conditions (2) and (3) thus obtained symmetrical operators can be extended to self-adjoint ones. Using Krein's method /6/ one can carry out spectral analysis of the extended operators and describe scattered waves. Spectral analysis provides resonator eigenfrequencies, losses and spatial field structure. Scattered waves as it was mentioned are of great importance for laser dynamics studies.

It is worth to mark that one can realize the similar constructions in case of three dimensions and take into account finite aperture of resonator mirrors in the framework of the extension theory. Different resonator configurations including the ring one may be analyzed using this method. Describing inner resonator passive optical elements by means of supplementary coupled inner external subspaces all diffraction effects may be taken into account.

Considering processes in active medium and supposing the latter to be optically thin one can assume no dispersion effects and the characteristic relaxation times of the medium are much greater than the round-trip time between the nonlinear medium and the feedback mirrors. This allows to model processes in active medium by means of finite dimensional maps /7/. The nonlinear effects analysis in this approach is now in progress.

REFERENCES

1. H.Lin, N.B.Abraham, in Technical Digest on Nonlinear Dynamics in Optical Systems 1990 (Optical Society of America, Washington, D.C., 1990), pp.313-315.
2. L.A.Lugiato, C.Oldano and L.M.Narducci, J.Opt.Soc.Am. B, 5, pp.879-888 (1988).
3. B.S.Pavlov, Sov. UMN, V.42, 6, pp.99-131.
4. S.Albeverio, F.Gesztesy, R.Hoeghkrohn, H.Holden: Solvable Models in Quantum Mechanics, Springer,Berlin (1988).
5. P.Seba, Phys.Rev.Lett., 64(1990), 1855.
6. M.G.Krein, Sov.DAN USSR, V.52, 8, pp.657-660 (1946).
7. A.Yu.Okulov, A.N.Oraevsky, J.Opt.Soc.Am.B, vol.3, pp.741-766, (1986).

# PHASE QUASIINTEGRAL FOR STIMULATED RAMAN SCATTERING INITIATED BY QUANTUM FLUCTUATIONS AND STATISTICS OF SOLITON-LIKE RANDOM PULSES IN DEPLETED PUMP

S.Ya.Kilin

Institute of Physics ,
Academy of Sciences of Belarus,
220602, Minsk, F.Skorina avenue 70, BELARUS
Telex 252277 NAUKA SU
Fax 7 0172 393131

Stimulated Raman scattering is a quantum macroscopic process starting from unstable state. Any fluctuations, initial or boundary, classical or quantum in nature, lead to the macroscopic output fluctuations of the Stokes amplitude. Manifestation of these fluctuations in the statistics of the Stokes pulse energy and its spectrum have been studied extensively for the linear stage of the SRS [1]. Another fluctuation phenomena arises in nonlinear stage of the SRS - the random spikes ,usually called soliton-like, are observed in the depleted pump [2]. Here we show that the reason for these soliton-like spikes is the conservation of the relative phase $\Delta\phi=\phi_L - \phi_S + \phi_Q$ of the laser ,Stokes and the polarization waves [3] .

We start from the quantum equation of motion for the SRS presented in the form of the Bloch-like equations:

$$ic(\partial S^+/\partial z)= q^+S_z, \quad (1); \qquad ic(\partial S_z/\partial z)= (q^-S^+-q^+S^-)/2, \quad (2);$$

*where the operators* $S^+$ *and* $S_z$ *are connected with the laser* $E_L^+$ *and the Stokes* $E_S^+$ *amplitude* $S^+= X+iY =E_L^+E_S^-/|E_0(\tau)|^2$, $S_z\equiv Z\equiv[|E_L^+|^2 - (\omega_L/\omega_S)|E_S^+|^2]/|E_0(\tau)|^2$, $|E_0(\tau)|^2$ is the input laser intensity , $\tau = t-z/c$. The role of the "Rabi frequency " for the equations is played by

normalized polarization $q^+$ obeing the stochastic equation

$$(\partial/\partial\tau + \Gamma)q^+ = ig_1g_2|E_0(\tau)|^2S^+ + 2g_2(D\omega_L/\omega_S)^{1/2} F^+(z,\tau)\,, \qquad (3)$$

with the stochastic δ-correlated term ( $\sim F^+(z,\tau)$ ). Using the straightforward numerical calculations we show that in spite of the difference between the random trajectories on the Bloch-like sphere for different z , the stereographical projection of the trajectories are almost similar each other. The calculations clearly demonstrate the existence of the quaziintegral for the equations -the value of $\Delta\phi$ is nearly conserved during propagation in Raman media. We showed that in the z-t plane two types of regions with different phase relations are created : the strips stretched along t-z/h -lines with nearly zero relative phase $\Delta\phi$ ($\Delta\phi \simeq 0$) , and the parallel strips with the $\pi/2$ phase difference ($\Delta\phi \simeq \pi/2$). The first type of the strips are characterized by small gain (small gain strips (SGS)), large value of time derivative of the phases $d\phi_Q/d\tau$ , $d(\phi_L - \phi_S)/d\tau$ and small temporal width of the strips. The second type of the strips have the largest (for possible phase relations) value of gradient for the Stokes and the laser intensities (high gradient strips (HGS)), small time derivatives of the phases $d\phi_Q/d\tau$ , $d(\phi_L - \phi_S)/d\tau$ and rather wide temporal width of the strips.

It should be noted that such a structure of the z-t plane is similar to the z-t plane in the case of phase wave in superfluorescence [4]. The alternation of the SGS and HGS in time is to be detected as the temporal spikes in the depleted laser pulse, the time position of the spikes is coincided with the position of the SGS. Therefore it is possible to calculate the frequency of the soliton-like spikes as the frequency of large phase $\Delta\phi$ changes.

Using known solution for the SRS in linear regime we have obtained the simple formulae for the frequency of the soliton-like spikes in the depleted laser pulse intensity for highly nonlinear regime of scattering [3]. The time dependent frequency of large phase $\Delta\phi$ changes for the Gaussian form of the laser input (3) at different propagation distances qz=25 (1); 45 (2) is presented on figure.

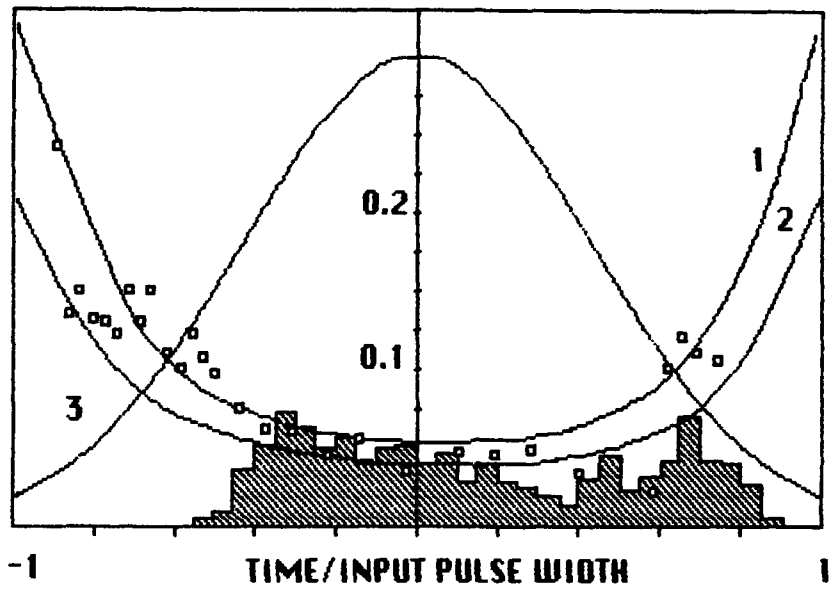


The squares mark the obtained from numerical simulations of Eq.(1)-(3) reverse time differences $(t_i-t_{i-1})^{-1}$ between the nearest values $t_i$ at which $\Delta\Phi=\pi n$.

The obtained relations are agreed with the numerical calculations of the starting equation and experimental results (presented on the figure by the histogram of the soliton appearance frequency) for the SRS in $H_2$ gas [5].

REFERENCES

[1]. M.G.Raymer and I.A.Walmsley, *Progress in Optics* (Elsevier, Amsterdam,1990) Vol.28, p.181.

[2]. J.C. Englund and C.M.Bowden, Phys.Rev.Lett. 57, 2661 (1986); D.C. MacPherson, R.C.Swanson, and J.L.Carlsten, Phys.Rev.A 41, 6745 (1989).

[3]. S.Ya. Kilin , Phys.Rev.A (to be published,1992)

[4]. F.A.Hopf, Phys.Rev. A 20 , 2064 (1979)

[5]. S.Ya.Kilin, V.A.Orlovich, A.S.Grabchicov, D.E.Gakchovich (to be published,1992)

# MULTIPARAMETRIC CRITICALITY IN A LASER SYSTEM

A.P.Kuznetsov, S.P.Kuznetsov, I.R.Sataev

*Institute of Radioengineering & Electronics, Saratov Branch, Saratov, Russia*

Beside chaotic and regular dynamics, the special kind of behaviour occurs in nonlinear systems. This is the critical state arising usually just at the onset of chaos. Its distinctive peculiarity is a presence of the wide band of characteristic temporal scales up to infinitely large ones in the generating signal.

The simplest critical behaviour type was discovered 15 years ago by Feigenbaum [1]. It is associated with road to chaos via period doubling bifurcations under variation of a control parameter. If we undertake a multiparametric consideration of transition to chaos, some other types of criticality may appear in typical situations. Each of these types is characterized by presence of some specific universal hierarchically organized structure in a parameter space having a property of scale invariance.

Here we consider the critical behaviour types taking place in a laser device consisting of two unidirectionally coupled subsystems. The first one is the periodically Q-switched single-mode laser. The second subsystem is also the single-mode laser using four-level scheme pumped by the first laser without some backward influence. The next equations may be obtained for the device dynamics:

$$\dot{\Delta}_1=\gamma_1(r-n_1\Delta_1-\Delta_1),\quad \dot{n}_1=K_1 n_1(\Delta_1-1-m\cos\omega t), \qquad (1)$$

$$\dot{N}=\Gamma(n_2-N),\quad \dot{\Delta}_2=\gamma_2(kN-n_2\Delta_2-\Delta_2),\quad \dot{n}_2=K_2 n_2(\Delta_2-1). \qquad (2)$$

Here $\Delta_1$, $\Delta_2$ are population inversions at working levels of the both lasers, $n_1$, $n_2$ are the field intensities, $N$ is a population of the highest energy level in the second laser intermediate for inversion obtaining. Parameters $K_1$ and $K_2$ characterize the cavity dumping rates, $r$ is the pump rate for the first laser, $k$ is the coupling coefficient, $\gamma_1$, $\gamma_2$ and $\Gamma$ are the relaxation rates for corresponding transitions, $\omega$ and $m$ are the parameters of cavity dumping modulation for the first laser.

The first subsystem describing by Eqs.(1) is independent of the second one. It is known that it demonstrates transition to chaos via period doubling bifurcations [2]. On the other hand, if we choose the parameters for the first subsystem to demonstrate periodic pulsations, then the period doubling scenario may be expected possible to observe in the second subsystem under variation of its own parameters. We know that the simplest representative of Feigenbaum's universality class is a logistic map [1]. So, we expect that the critical phenomena in the composite system (1,2) will be just the same as in two logistic maps with unidirectional coupling:

$$x_{n+1}=1-\lambda x_n^2,\quad y_{n+1}=1-Ay_n^2-Bx_n^2\ . \qquad (3)$$

Here $x$ and $y$ are the dynamical variables, $n$ is the discrete time, $\lambda$ and $A$ are the parameters controlling transition to chaos in both subsystems, $B$ is the coupling parameter.

Fig.1 shows the disposition of critical surfaces, lines and points of different type in the three-dimensional parameter space of the model system (3). There are two Feigenbaum critical surfaces *F1* and *F2* corresponding to onset of chaos in the first and in the second subsystems, respectively. These surfaces intersect along the bicritical line *B*. The surface *F2* is bounded also by the tricritical line *T*. The lines *B* and *T* meet in the multicritical point *BT*. The second end of the bicritical line is the double Feigenbaum point *DF*, where the system breaks down two uncoupled critical logistic maps. The universal constants for phase space and parameter space scaling are presented in the Table for all critical situations. (For *F* and *T* they were found earlier [1,2], for *B* and *BT* we have calculated them numerically by specially developed renormalization group analysis [4].)

| Type of criticality | | Phase space scaling factors | Parameter space scaling factors |
|---|---|---|---|
| Feigenbaum | *F* | -2.502907876 | 4.66920161 |
| Tricritical | *T* | -1.690302971 | 7.28468622<br>2.85712413 |
| Bicritical | *B* | -2.502907876<br>-1.505318159 | 4.66920161<br>2.39272443 |
| Multicritical | *BT* | -2.502907876<br>-1.2416604 | 4.66920161<br>2.654654<br>1.54172055 |
| Double Feigenbaum | *DF* | -2.502907876<br>-2.502907876 | 4.66920161<br>4.66920161<br>2 |

Also we find all the mentioned critical situations directly in the differential equations (1,2). For example, the bicritical point may be easily found if one changes the parameters of both subsystems (1) and (2) to lead each of them just onto the border of chaos. Fig.2 shows the phase portraits for both lasers in the bicritical point. The attractor has fractal, Cantor-like structure, controlling by scaling factors from the Table.

We believe that investigation of multiparametric criticality has a key significance for understanding of fine hierarchically organized parameter space structure for nonlinear systems demonstrating transition to chaos. Particularly, the presence of somewhat kind of criticality gives a possibility to use such simple models as logistic maps for quantitative description of complicated systems in suitable domains of their parameter space.

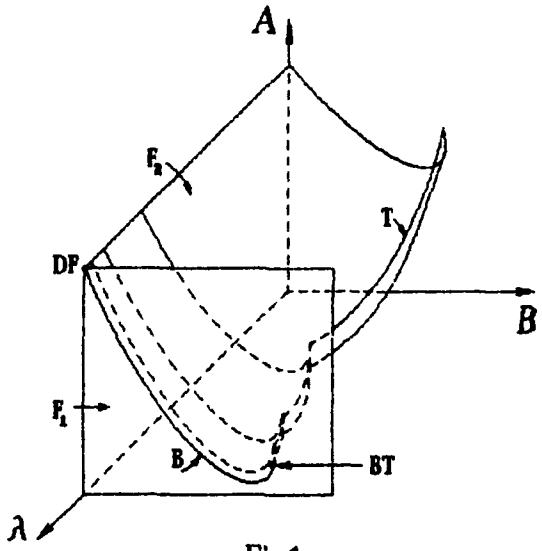


Fig.1

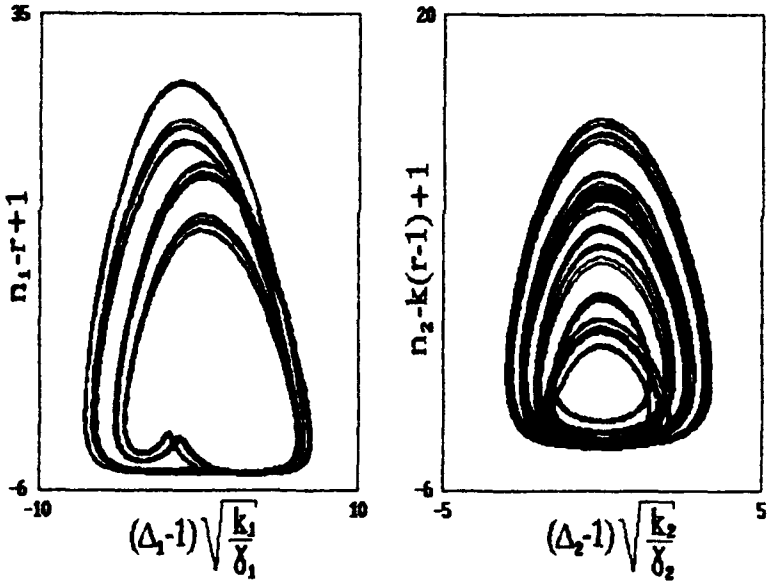


Fig.2

R e f e r e n c e s

[1] Feigenbaum M.J. J.Stat.Phys. 1978. Vol.19. No 1. P.25.

[2] Arecchi F.T., Meucci R., Piccioni G., Tredicce J. Phys.Rev. Lett. 1982. Vol.49. No 17. P.1217.

[3] Chang S.J., Wortis M., Wright J.A. Phys.Rev. 1981. Vol.24A. No 5. P.2669.

[4] Kuznetsov A.P., Kuznetsov S.P., Sataev I.R. Int.J of Bifurcation & Chaos. 1991. Vol.1. No 4.

# BIFURCATION AND CHAOS IN THE PRESENCE OF EXTERNAL NOISE

V.S.ANISHCHENKO and A.B.NEIMAN
*Chernysheusky State University, Department of Physics*
*Saratou, 410071, Russia*

The present work investigates the influence of external non-white noise on some bifurcations of states of equilibrium, period-doubling bifurcation and on the dynamical chaos regimes. Lorenz system [1] and Anishchenko–Astakhov oscillator [2] are used as models. The peculiarities of the present investigation are in combination of numerical simulations with physical experiment and also in the use of cumulant analysis.

For many-parametrical analysis of noise influence the technique based on transition from stochastic differential equations (SDE) (or Fokker-Planck equation (FPE)) to dynamical ones, describing process cumulant evolution, is used [3-5].

The investigation of codimensional two bifurcation is carried out in the instance of model [6]:

$$dx/dt = \alpha + \beta x - x^3 + \xi(t) + x\eta(t), \qquad (1)$$

where $\alpha$ and $\beta$ are parameters, $\xi(t)$ and $\eta(t)$ are statistically independent gaussian noises, describing additive and multiplicative action respectively. It was found that additive action does not lead to qualitative changes of system bifurcational diagram. Multiplicative noise changes bifurcational picture drastically: noise intensity $D$ becomes a natural control parameter of the system (1). Colored noise leads to some bifurcational shift.

One of the most interesting phenomena associated with the influence of colored noise on the bistable systems is the noise induced transition which is accompanied by the formation of a hole in the two-dimensional probability density of process [7-8]. Cumulant analysis applied here allowed to explain this noise effect in terms of qualitative theory of ordinary differential equation: the hole formation corresponds to the bifurcation of "saddle-node - repeller" of the sate of equilibrium of the corresponding system of cumulant equations.

A number of detailed works were devoted to the investigation

of influence of non-correlated noise on period doubling bifurcation [9–11]. The present work investigates the influence of colored noise on the period doubling bifurcation. The one-dimensional mapping is used as the main model

$$X_{n+1} = f(X_n) + \xi_n, \qquad (2)$$

where $f(x)$ – the function with quadratic maximum, $\xi_n$ – the Gaussian source of colored noise, which is simulated by the stochastic mapping

$$\xi_{n+1} = \Gamma\xi_n + \eta_n, \qquad (3)$$

where $\Gamma$ – the parameter, associated with noise correlation time, $\eta$ – white noise with the following characteristics:

$$\langle\eta_n\rangle = 0, \ \langle\eta_n\eta_{n+m}\rangle = (1-\Gamma^2)D\delta(m), \ |\Gamma|<1, \ D\ll 1. \qquad (4)$$

Parameter $D$ determines the intensity of random process $\xi_n$. The linear analysis in the vicinity of bifurcational points has shown that the intensity of spectral subharmonics depends resonancewise on noise correlation time. The values of parameter $\Gamma$, at which for cycle period $2^k$ the intensity of subharmonic reaches its maximum are determined by the following expression

$$\Gamma_m^{(k)} = [1-\sin(\omega_0)]/\cos(\omega_0), \quad \omega_0 = (2n+1)\pi/k \qquad (5)$$

The bifurcational analysis of correspondent cumulant equations system performed numerically has shown that the bifurcational lines of birth of doubled period cycles on the plane of parameters "supercriticity – $\Gamma$" have extrema corresponding to the parameter values $\Gamma=\Gamma_m^{(k)}$, at which the intensities of subharmonics reach maximum values.

The SDE of Lorenz model has the following form:

$$\frac{dx}{dt} = -\sigma x+\sigma y+\xi_1(t), \ \frac{dy}{dt} = -y+rx-xz+\xi_2(t), \ \frac{dz}{dt} = -bz+xy+\xi_3(t), \qquad (6)$$

where $\xi_i(t)$ are gaussian noises. The investigations of the finite intensity noise influence have shown that increase of the noise intensity results in chaosity degree decrease and in smoothing the structure of the two-dimensional probability density. For Anishchenko-Astakhov oscillator, SDE of which is written in the form

$$\frac{dx}{dt} = mx+y-xz+\xi_1(t), \ \frac{dy}{dt} = -x, \ \frac{dz}{dt} = -gz+g1(x)x^2+\xi_2(t) \qquad (7)$$

$$1(x)=0, \ x\le 0 \ \text{ and } \ 1(x)=1, \ x>0,$$

the analogous results have been obtained. In addition to that,

the physical experiments have been carried out. The realizations of radio-physical oscillator excited by external noise generator were entered into computer and the two-dimensional probability density $p(x,y)$ was constructed.

For Lorenz system in the regime of quasi-attractor [12] ($r$=210,$\sigma$=10,$b$=8/3) a noise-induced transition has been found, which is realized in combination of two independent attractors into one chaotic set. It was also found that in the vicinity of the transition point the intermittency of "chaos-chaos" type was realized.

The investigations of colored noise influence on Lorenz system were conducted in two regimes: the first regime of Lorenz attractor ($r$=28) and the second regime of quasi-attractor ($r$=210). Whereupon the noise sources in (6) were simulated by Ornstein-Uhlenbeck processes. The numerical experiments have shown that the characteristics of Lorenz attractor were invariant relative to the change of noise correlation time. The above mentioned effects are explained by the presence in the realization of quasi-attractor of hierarchy of characteristic time scales and by origination of non-linear resonant phenomena due to the change of noise correlation time.

## REFERENCES


[1] E.Lorenz// J.Atmos.Sci., 1963, v.20, p.130.
E.V.Astashkina, A.S.Mikhailov and A.V.Tolstopyatenko// Radiofizika, 1981, v.24. p.1035 (in Russian).

[2] V.S.Anishchenko "Complicated oscillations in simple systems". Moscow: Nauka Publishers, 1990 (in Russian).
V.S.Anishchenko and A.B.Neiman// Nonlinear dynamics of structures/Ed by R.Sagdeev et al. World Scientific,1991,p.21.

[3] A.N.Malakhov "Cumulant analysis". Moscow: "Sov.Radio", 1978 (in Russian).

[4] G.V.Tatarnikova and V.D.Shalfeev//Radiotekhnika, 1986, №3, p.40, №5, p.50 (in Russian).

[5] W.Just and H.Sauermann// Phys.Lett.,1988, v.A131, p.234.

[6] A.D.Basykin, Yu.A.Kuznetzov and A.I.Khibnik "Bifurcational diagram of the dynamical system on plane". Pushcheno, AN USSR, 1985 (in Russian).

[7] F.Marchesoni and F.Moss, Phys.Lett.A **131**, 322 (1988).

[8] G.Debnath, F.Moss, Th.Leiber, H.Risken and F.Marchesoni, Phys.Rev.A **42**, 703 (1990).

[9] E.Vul, Ya.Sinai and K.Khanin// Russ.Math.Surv.,1984,v.39,p.1.

[10] M.Napiorkowski and U.Zaus//J.Sata Phys.,1986,v.43,p.349.

[11] B.Shraiman, C.Wayne and P.Martin//Phys.Rev.Lett,1981,v.41, p.935.

[12] V.V.Bykov and A.L.Shil'nikov//Metods of qualitative theory of differential equations. Gorkii, GGU, 1989, p.151.

# Rössler Chaos in Opto-Thermal Bistability with Localized Absorption

Ramon Herrero, Francesc Boixader and Gaspar Orriols
Departament de Física. Universitat Autònoma de Barcelona.
08193 Bellaterra. Spain. Tel. (34) 3-5812110.

Joan I. Rosell
Departament de Física i Enginyeria Nuclear. ETSIIB.
Universitat Politècnica de Catalunya. 08017 Barcelona. Spain.

Francesc Pi
Departament d'Òptica i Optometria. Escola d'Òptica.
Universitat Politècnica de Catalunya. 08222 Terrassa. Spain.

We present numerical and experimental evidences of Rössler chaos in the response of BOITAL trilayer systems. BOITAL devices are opto-thermal bistable cavities in which the absorption occurs localized in the input mirror and the spacer is made of transparent thermo-optic materials [1]. In the case of multilayer spacers of alternatively opposite thermo-optic materials, the competing phase-shift contributions of the various layers are affected by different time delays according to the relative position with respect to the localized heat source and, in this way, it is possible to have self-sustained oscillations and other sorts of instabilities in the response of the system [2-4]. A remarkable feature in the dynamics of such systems is the fact that their effective dimension is determined by the number of layers in the spacer and, therefore, they permit the analysis of gradual complexity [6]. Another remarkable features are the easy occurrence of homoclinic bifurcations in their response and the really good agreement between experiments and numerical simulation by integration of either the corresponding partial differential equations or a simplified ODE's model of order equal to the number of layers [6].

In the case of bilayer systems, single-frequency oscillations and a variety of homoclinic bifurcations without complicated orbit structures have been observed both theoretically and experimentally [3]. For systems of higher dimension, the homoclinicity may appear accompanied by a rich dynamics associated with the saddle-focus nature of the invariant set at which the homoclinic orbit makes tangency and Shil'nikov chaos has been numerically observed in trilayer systems [4]. In this work we describe the observation of Rössler chaos [7] and related homoclinic phenomena [8] in the response of a trilayer system.

In fact, in the response of BOITAL trilayers we have essentially observed two different families of phase space structures associated with complex behaviour and a variety of hibrids of both structures. The first one of such families is the natural extension to a tridimensional phase space of the bilayer dynamics [3]: On varying the input power, a node point experiences a Hopf bifurcation and the generated limit cycle grows approaching to a neighbouring saddle invariant set up to become an homoclinic orbit to this set. Such a saddle connection is of codimension-one and, according to the actual configuration of the saddle invariant set, it originates more or less complex dynamics [6].

The other family of aperiodic structures appear relatively far from the saddle invariant set and the basic evolution on varying the control parameter is essentially that of the Rössler chaotic band: The limit cycle generated from a node point grows initially in a plane which does not contain the other fixed points, it soon experiences some kind of bending followed by a period-doubling sequence and becomes a folded chaotic band of the spiral-type [7]. The evolution follows from spiral- to screw-type attractors with successively increasing number of screw turns and, finally, the attractor approaches to the saddle invariant set experiencing a homoclinic bifurcation of the kind mentioned above. As pointed out by other authors [8], the evolution from spiral- to screw-type attractors lies on successive codimension-two homoclinic orbits arising from the reinjection of trajectories close to the internal fixed point due to the attractor bending.

As an example, the figure presents two experimental results obtained with a {glass/sunflower oil/glass} trilayer system and which illustrate a simply folded chaoic band and a periodic orbit near the codimension-two homoclinic connection, respectively. The fine structure of attractors have been analyzed by means of first-return time return maps

## References


[1] G. Orriols, C. Schmidt-Iglesias, F. Pi, Opt. Commun. 63 (1987) 66.

[2] F. Pi, G. Orriols, in "Interaction of Radiation with Matter. A volume in honor of Adriano Gozzini", eds. G. Alzetta, E. Arimondo, F. Bassani and L. Radicati (Scuola Normale Superiore, Pisa, 1986) 239.

[3] J.I. Rosell, F. Pi, F. Boixader, R. Herrero, J. Farjas, G. Orriols, Opt. Commun. 82 (1991) 162.

[4] J.I. Rosell, F. Pi, F. Boixader, R. Herrero, J. Farjas, G. Orriols, in "ECOOSA'90", eds. M. Bertolotti, E.R. Pike (Adam Hilger, 1991) 289.

[5] J. Farjas, F. Boixader, G.Orriols, J. Massaneda, F. Pi, "Opto-Thermal Bistable Cavities with Localized Absorption under Modulated Excitation", submitted to this Meeting.

[6] J.I. Rosell, F. Pi, J. Farjas, R. Herrero, G. Orriols, to be published.

[7] O.E. Rössler, Ann. N.Y. Acad. Sci. **316** (1979) 376.

[8] P. Gaspard, R. Kapral, G. Nicolis, J. Stat. Phys. 35 (1984) 697.

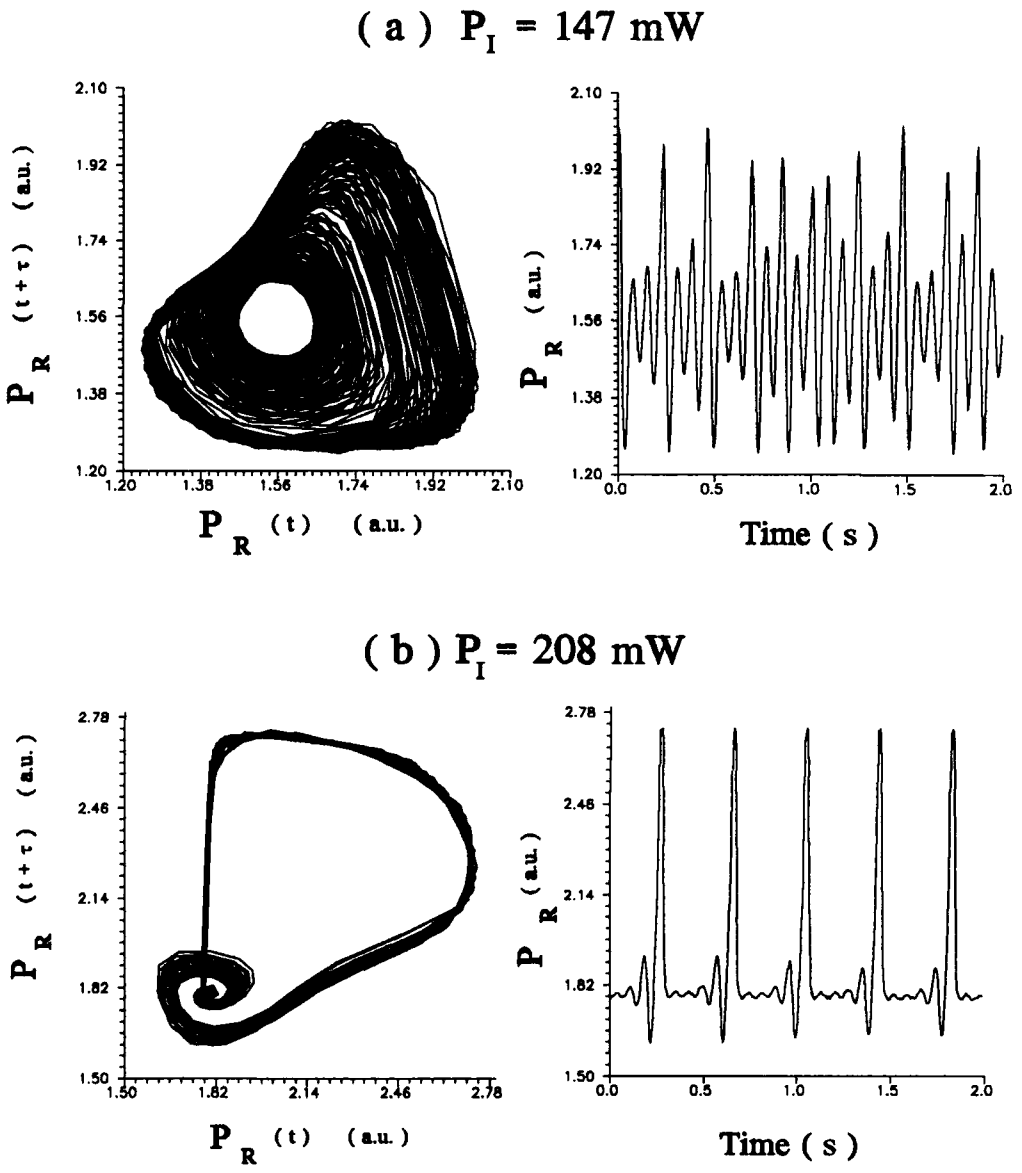


Figure. Time evolution of the reflected power and corresponding phase portrait in the $P_R(t)$, $P_R(t+\tau)$ representation, where $\tau$ = 18 ms, for two input powers upon the trilayer system.

**Pulse statistics of modulated gas lasers**

A. Valle, L. Pesquera, and M. A. Rodríguez

Dept. de Física Moderna, Univ. de Cantabria. E–39005 Santander, Spain.

Telephone: (34)(42)201465. Fax: (34)(42)201402.

Pulse statistics of modulated class A single mode lasers is analyzed both numerically and analytically. The time evolution of the electric field is described by the following equation

$$\dot{E} = a(t)E - \mid E \mid^2 E + \psi(t),$$

where $a$ is the pump parameter and $\psi$ is the spontaneous emission noise of intensity $D$. An analytic approximation is developed for the switch–on time probability density. In this approximation the time evolution is divided in two regimes: a linear one with noise, where saturation is not important, and a nonlinear deterministic domain. Using a kind of self–consistency condition for the switch–on time probability density $P(t)$, an integral equation is derived for $P(t)$. Numerical simulations show that this approximation is very accurate (see Fig.1).

We consider the case when the pump parameter is suddenly switched between a value $a_b$ below to a value $a$ above threshold with a modulation period $T$. The laser is above threshold during a fraction $\alpha$ of the modulation period, $T_{on} = \alpha T$ and above threshold during $T_{off} = (1 - \alpha)T$. Two different situations can be distinguished. First, when $a_b$ and/or $T_{off}$ are large the laser intensity below threshold is mainly due to the spontaneous emission noise. In this case the results obtained in the repetitive Q–switching (no modulation effects) are recovered. This corresponds to the constant limit reached by the mean value and variance of the switch on time in Fig.2.

The second situation happens when $a_b$ is small and/or $T_{off}$ is a small fraction of the

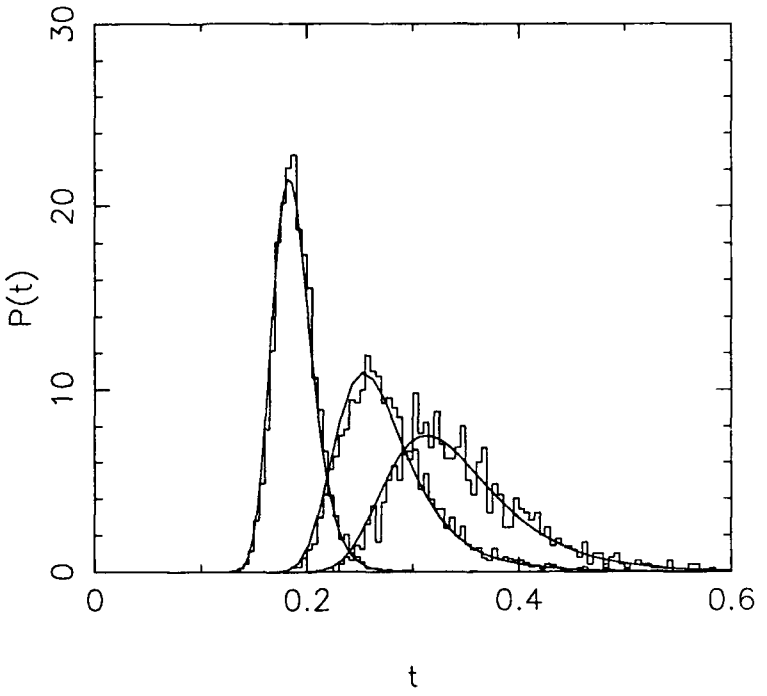


Fig. 1.- P(t) for three different values of $a_b T$:13, 16 and 20(from left to right). Parameters are $a = 10, D = 0.001$ and $A = 1$. Theory (solid line) and simulation (histogram).

period. In this case the steady state is always attained in each pulse and it is found that the mean switch–on time is a linear function of $a_b T$ (see Fig.2). In the limit $a_b T \to 0$ the theory predicts the deterministic value $\frac{a_b T(1-\alpha)}{a}$ for the switch on time, that agrees with the simulation result. It is also found that the variance of the switch–on time is a function of $a_b T$ (see Fig.2).

As concerns the pulse we have analyzed the maximum light intensity $I_m$ and width $\Delta$. The probability densities for $I_m$ and $\Delta$ are obtained from that of the switch on time using the deterministic evolution. The results agree well with the numerical simulations. In the second situation considered previously $I_m$ is a constant given by the steady state value.

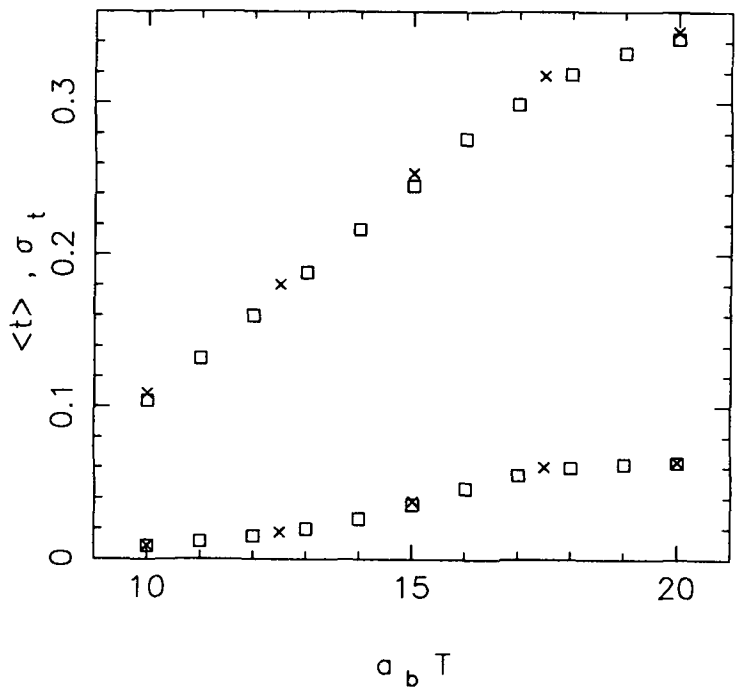


Fig. 2.- Averaged siwtch-on time and variance. The parameters are the same than in Fig. 1. Theory (squares) and simulation (crosses).

Finally, the effect of sweeping with a finite velocity of a modulated pump parameter is also analyzed.

Wednesday, June 24, 1992

# Spatial Pattern Formation and Dynamics 1

**WA** 8:20am–11:00am
Schroedinger Hall

Neal B. Abraham, *Presider*
*Bryn Mawr College*

# Patterns and Their Defects

Pierre Coullet
University of Nice
France

Summary not available at press time.

# STATISTICS OF TOPOLOGICAL DEFECTS IN LINEAR AND NONLINEAR OPTICS

P.L.Ramazza, S.Residori, G.Giacomelli, F.T.Arecchi(+)

Istituto Nazionale di Ottica,
Largo E. Fermi, 6, 50125 Firenze (Italy)
(+) also Dept. of Physics, University of Firenze

Phone:39-55-221179, Fax:39-55-2337755

## SUMMARY

A topological defect of a complex field is a point where the intensity of the field vanishes and the circulation of the phase gradient around it has a value that is an integer (called topological charge) multiple of $2\pi$. In optics, defects have been theoretically predicted [1,2] and experimentally observed both in linear [3] and in nonlinear [4] systems. Linear experiments consist in scattering coherent light from random diffusers, resulting in a speckle field. We compare the experimental statistical distributions of defects for the linear and the nonlinear case at large F. The nonlinear experiment [4] consists of a ring cavity in which a photorefractive BSO crystal, pumped by an $Ar^+$ laser, acts as a light amplifier via a two-wave mixing mechanism. At small F, where only one mode per time is present in a periodic or chaotic alternation [5], the defects are a trivial signature of the symmetry of that specific mode. On the contrary at high F, where many modes coexist, the defect dynamics reflects the mode competition and have a role in mediating turbulence [6]. For a fixed high Fresnel number we study the fluctuations of the total number of defects in the nonlinear field. We repeat the same measurement in the linear case where the fluctuations are trivially due to a translational motion of the random diffuser. The histograms relative to the nonlinear and linear case are plotted in Fig.1a and 1b together with a Poissonian best fit. In Fig.1a we report also the result of a theoretical prediction by Gil et al. [7]. The hypothesis of their work is that defects can only be created and annihilated by pairs, with rates of creation $\Gamma = \alpha$ and annihilation $\Gamma = \beta n^2$ where n is the number of pairs present. This lead to a distribution which is a square Poissonian in the number n of pairs. When reported to the number N=2n of defects, it becomes:

$$P(N) = \gamma \frac{(\bar{N}/2)^{N} e^{-\bar{N}}}{[(N/2)!]^2} \quad . \qquad (1)$$

In Fig.1a the distribution (1) correspond to the dashed line. The difference between this distribution and the Poissonian (solid line) is below the resolution allowed by our experiment as shown by the size of the error bars. Therefore, we conclude that the above statistical indicator is not able to discriminate between the linear and the nonlinear case. It was shown [4] that the mean nearest neighbor separation of defects is close to the correlation length of the field. In order to investigate how defects play a role in breaking also the time correlation of the field we measure, in the nonlinear case, the probability distribution of the time separation between defects within

a space correlation range which contain in general 0 or 1 defect. We build the probabilities $P_n(t)$ of having n successive events within a time t where an event is the entrance of a defect into the correlation area. Experimental results for n=0 to n=3 are shown in Fig.2. The continuous curve is a Poissonian of the same mean value as the experimental data. The Poissonian would be the correct distribution of the data if the probability rate w(t) of occurrence (entrance in the square) of a defect in the unit time was a constant, independent of t. However, the fit of the Poissonian to our data shows systematic deviations. In particular, the experimental values of $P_n(t)$ for $n \geq 2$ are below the Poissonian for very short t and above around the maximum of the curve, thus showing a sort of antibunching effect. This means that each defect has an associated refractory time $\tau$ so that the occurrence of one defect reduces the probability of a next one in the successive instants.
We thus conjecture that, if a defect has entered the square at time $t_0$, then the rate of occurrence of a new defect varies in time as

$$w(t) = w_0\left[1 - e^{-(t-t_0)/\tau}\right]. \qquad (2)$$

This prediction leads to the statistics Q(t) of empty intervals shown in Fig.3a (solid line).The dashed curve in the same figure reprents the Poissonian $P_0(t)$ with the same mean value.Comparing this distribution with the experimental data, for the best fit that minimize the mean square deviations, we get the values $\tau = 0.46$ s and $w_0 = 0.62\ s^{-1}$. Notice that if we evaluate the correlation time of the sequence N(t) (upper inset of Fig.2a) we obtain a value close to $\tau$, which then represents the average permanence time of a defect within the observation area. We conclude that the arrival of a defect in the square implies a refractory time equal to the average permanence time of the defect in the square. Moreover, the arrival of each defect induces a loss of correlation in the time series, since at each arrival time of a defect the probability w(t) looses its memory.
The results of the same measurement in the case of the speckle field are reported in Fig.3b. In this case $\tau$ is trivially related with the uniform speed at which the diffuser is moving.

## REFERENCES


1 M.Berry in "Physics of Defects", edited by R.Balian et al. (North Holland, Amsterdam, 1981), pp 456-543
2 P.Coullet, L.Gil, and F.Rocca, Opt.Comm. **73**, 403 (1989)
3 N.B.Baranova, B.Ya.Zel'dovich, A.V.Mamaev, N.F.Pilipetskii, and V.V.Shkukov, Zh.Eksp.Teor.Fiz. **33**, 206 (1981) [JETP Lett.**33**, 195 (1981)]
4 F.T.Arecchi,G.Giacomelli,P.L.Ramazza, and S.Residori,Phys.Rev.Lett. **67**, 3749 (1991)
5 F.T.Arecchi,G.Giacomelli,P.L.Ramazza, and S.Residori,Phys.Rev.Lett. **65**, 2531 (1990)
6 P.Coullet, L.Gil, and J.Lega, Phys.Rev.Lett. **62**, 1619 (1989)
7 L.Gil, J.Lega, and J.L.Meunier, Phys.Rev.A **41**, 1138 (1990)

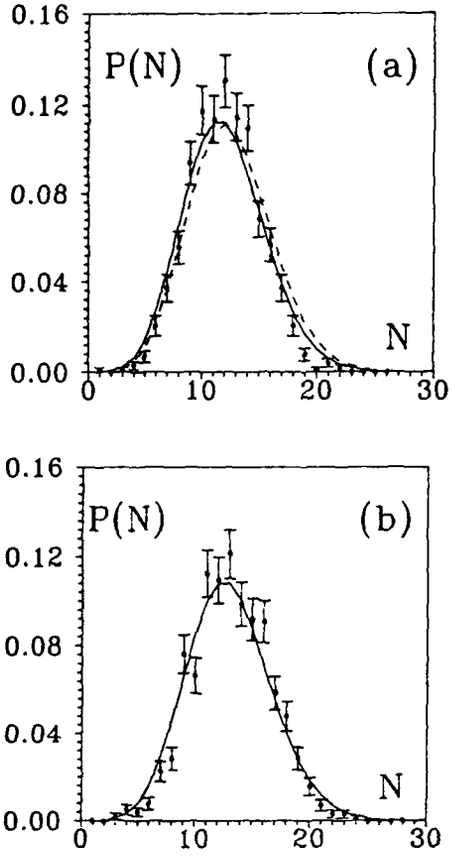


FIG. 1

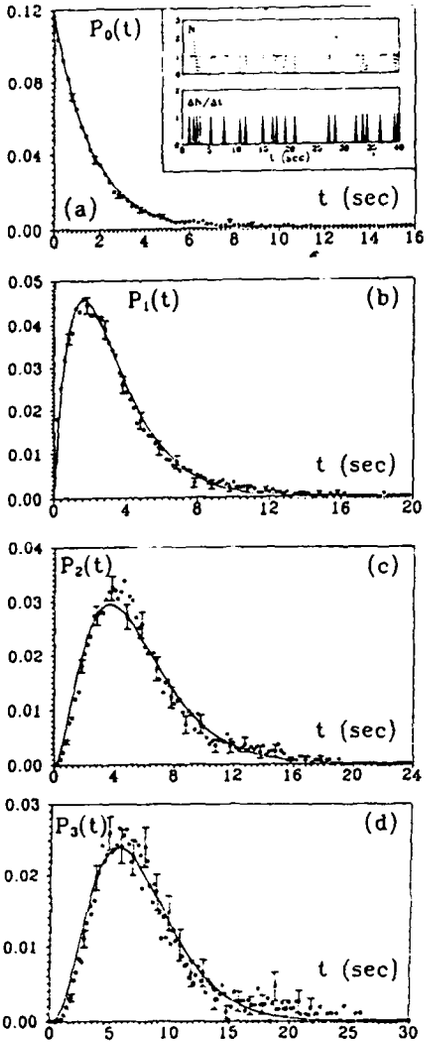


FIG. 2

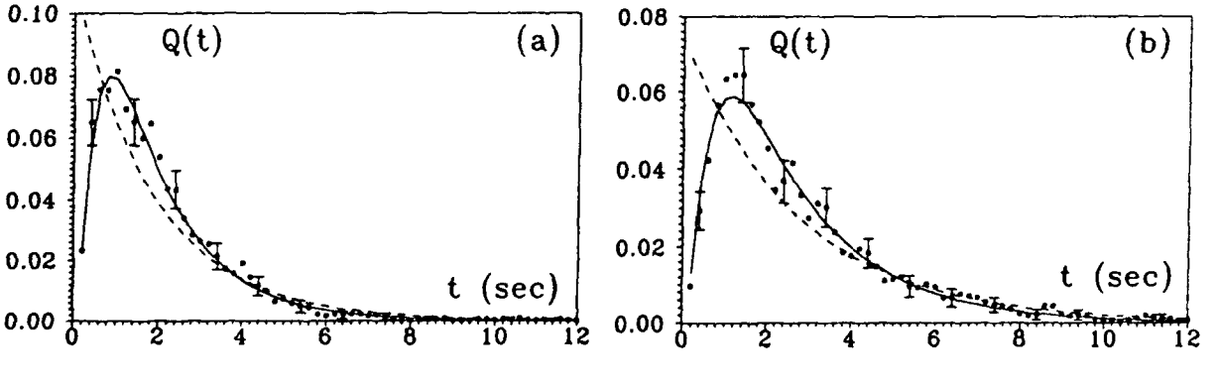


FIG. 3

# Pattern Formation and Pattern Dynamics in Passive Systems

M. Brambilla•, F. Castelli, A. Gatti, L. A. Lugiato and F. Prati•
*Dipartimento di Fisica dell' Università di Milano,*
*via Celoria 16, 20133 Milano, Italy, Tel. +39-2-2392264*
• *also Physik Institut, Universität Zürich, Switzerland*

## Summary

The theoretical modeling and systematic investigation of the transverse effects, due to diffractive phenomena in the propagation of electric fields in nonlinear optical systems, have recently received increasing interest, for both passive and laser systems [1,2].

In optical systems, the onset of spatial and spatiotemporal phenomena can be profitably described in terms of interaction and competition among the modes of the empty cavity. Relevant for the evolution are the mode frequency and the spatial configuration of each mode with respect to that of the available gain and of the loss profile [3]. This mode interaction can lead to the formation of spatial patterns having symmetry properties different from those of the empty cavity and to irregular spatiotemporal regimes [4,5] where diffraction assumes the role played by diffusion in hydrodynamical and open chemical systems.

In this presentation we introduce the model equations describing the evolution of the electric field and atomic variables for a two-level absorbing medium in a ring cavity. Provided that the absorbing region is much smaller than the Rayleigh length, one can describe the transverse spatial profile of the field in terms of fre-

quency degenerate families of Gauss-Laguerre (GL) modes, while the system's evolution is determined by the time behaviour of the modal amplitudes.

In suitable conditions, we derive the generalized stationary solution equation and provide the analytical solution for the fundamental $TEM_{00}$ stationary solution . The presentation includes a linear stability analysis showing how the onset of the modes of a higher-order family destabilizes the singlemode $TEM_{00}$ stationary solution, giving rise to more complex spatiotemporal structures. We study then the dynamical regimes that are observed scanning the parameter space, in both the good cavity and the bad cavity limits. Occurrence of optical vortices [3] is reported and in the bad cavity limit, we present some of the many different dynamical patterns the system displays and identify experimentally-accessible parameter regions where the time behaviour becomes irregular.

Finally, we show that in the limit of good cavity with large atomic detuning and large cooperativity, the three-mode model (which includes the $TEM_{00}$ and the two modes of the next higher order family $q = 1$ ) simplifies drastically and reduces to a parametric set of ODEs (one for each modal amplitude) that can be derived from a parametric Hamiltonian [6] . In this case both the steady state and linear stability equations can be solved analytically, and we present the scenario of stationary single- and multi- mode patterns as well as the onset of dynamical patterns which can be obtained under these conditions. In particular it is shown that when an external field with a transverse $TEM_{00}$ configuration is injected, all possible stable steady states are stationary , while when the injected field has a $TEM_{10}$ structure, a large variety of dynamical patterns is met, ranging from periodic to chaotic. One can also derive a parametric model in the case of a single frequency-degenerate family of modes (in our case the family $q = 2$ , consisting of three modes), and the same steps can be retraced as in the previous case. The system exhibits here the onset of stationary transverse patterns presenting four vortices in a regular array structure.

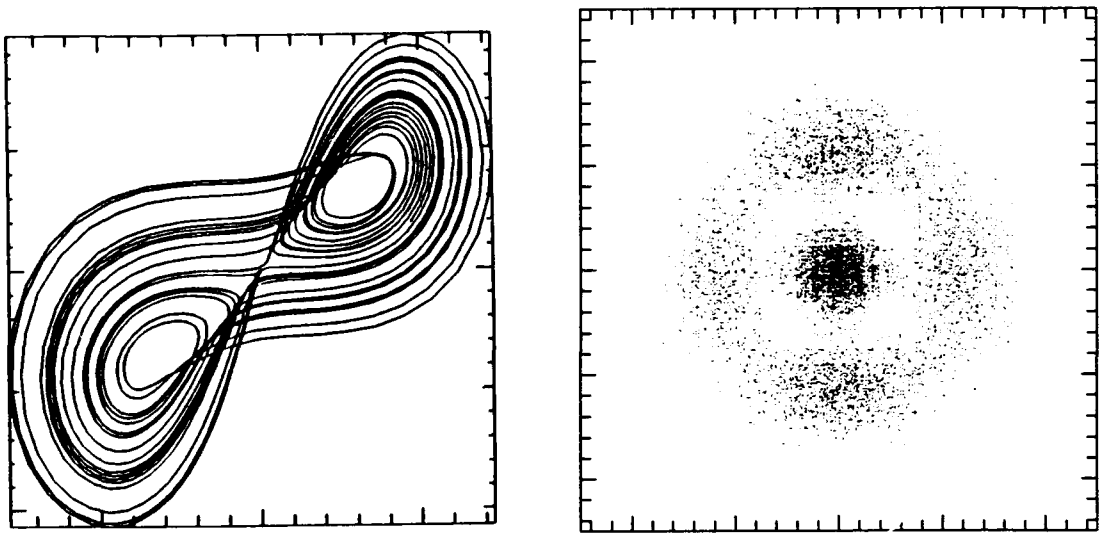

Fig. 1 a) Chaos in passive optical system: plot of the projection of the phase-space trajectory. b) Parametric model: the intensity distribution plot in the transverse plane shows a five-peaked structure with four optical vortices is shown.

## References

1. L.A. Lugiato, in Proceedings of the Solvay Conference on Quantum Optics, ed. by P. Mandel, Physics Reports, in press.

2. N. B. Abraham and W. J. Firth eds., Special issues on *"Transverse Effects in Nonlinear Optical Systems"*, J. Opt. Soc. Am. **B7**, June and July 1990, and references therin quoted

3. M. Brambilla, F. Battipede, L.A. Lugiato, V. Penna, F. Prati, C. Tamm and C.O. Weiss, Phys.Rev.**A43**, 5090 (1991)

4. F.T. Arecchi, G. Giacomelli, P.L. Ramazza and S. Residori, Phys.Rev.Lett. **65**, 2531 (1990)

5. M. Brambilla, G. Broggi and F. Prati, *"Spatiotemporal Pattern Formation and Chaos in Passive Optical Systems "* , to appear in Physica D

6. M. Brambilla, F. Castelli, L. A. Lugiato, F. Prati and G. Strini, Opt. Comm. **83**, 367 (1991)

# Symmetry Breaking and Vortices in a Sodium-filled Fabry-Pérot Resonator

L.M. Hoffer, G.L. Lippi, J. Nalik, Ch. Vorgerd, and W. Lange
Institut für Angewandte Physik, Westfälische Wilhelms-Universität Münster
Corrensstraße 2/4, D-4400 Münster, Federal Republic of Germany
Tel. +49-251-833512; Fax +49-251-833513

In the last few years it has been found, both theoretically and experimentally, that interactions among different transverse modes may produce complicated patterns, vortices and spatiotemporal chaos in active and passive optical systems [1]. In a passive nonlinear resonator with high Fresnel number but where only a few modes are selectively excited, symmetry broken patterns and vortices have been observed. We find that, in our system, the total number of vortices in any one pattern is generally small and the total topological charge is zero. Among the symmetry broken structures observed in our experiments, we find a recurrent sequence that is similar to one particular sequence observed in an experiment performed in a laser.

In our experiment a single longitudinal mode, frequency stabilized cw ring dye laser pumps sodium vapor in a confocal, or nearly-confocal, Fabry-Pérot resonator. The input beam is intensity stabilized, spatially filtered, and mode-matched to the optical resonator. The light is circularly polarized and slightly detuned from the sodium $D_1$ line, to operate in the predominantly dispersive regime. Argon is added as a buffer gas (200 mbar) to mask the effects of the hyperfine structure of sodium, and the transverse components of the Earth's magnetic field are well compensated. The control parameters for this system are: input power, detuning of the laser from the sodium resonance frequency, sodium density, resonator length, working point on the transmission function of the resonator (resonator phase) and the amplitude and phase with which the empty resonator modes are excited by the input beam (mode-mismatch). The saturable medium provides an intensity dependent index of refraction which is radially nonhomogeneous because of transverse diffusion of the oriented atoms (the laser beam diameter is much smaller than that of the cell, at whose walls the atoms lose their orientation).

In a small range of sodium densities, where the nonlinearity is weak, all the structures that appear possess circular symmetry [2]. For higher atomic densities and over a much wider range of parameters, the angular symmetry is lost, in spite of the symmetry of the input beam and of careful alignment of the cavity. The sequences of patterns that we observe in this region strongly depend on the values of the control parameters and may be very complicated. The appearance of similar sequences of symmetry broken patterns in different systems, regardless of the details of the nonlinearity or of whether the system is active or passive, may be indicative of certain general symmetry properties. Examining the sequences that we obtained we find a simple one that strongly resembles the intensity patterns observed in a laser (a↔b↔e↔i in Fig. 2 of ref. [3]), and predicted with the help of group theory (0↔3↔9↔14 in Fig. 1 of ref. [3]). In addition, we observe at least two longer sequences that contain this four-piece one in full. The similarity between full sequences (as opposed to isolated patterns), although verified only in one case, is not necessarily a pure coincidence and may imply a similarity in the basic symmetry properties of the two systems. It is in itself quite remarkable that such different systems have any full sequences in common. Indeed, our sequences of patterns were obtained by varying the resonator phase whereas in ref. [3] they were obtained as a function of the resonator configuration.

An example of the development of symmetry breaking is given by the succession of pictures shown in Fig. 1, taken for successively lower oven temperatures. In Fig. 1a, we see a ring structure, generated by interference of the beam with itself in the presence of a sharp gradient of the index of refraction in the radial direction at high temperature. As soon as the gradient is reduced, the symmetry of the pattern begins to break (Fig. 1b) and within a degree centigrade, the break is complete (Fig. 1c). The range of parameters over which a symmetry broken structure exists is related to the relative phase with which the input beam excites the resonator modes.

With careful alignment, the patterns that do not possess cylindrical symmetry tend to randomly change their direction, for lack of a preferential orientation. However, for appropriate

Fig. 1 a) Cylindrically symmetric pattern transmitted by the nonlinear resonator: T=252°C; b) the rings begin to break up: T=251°C.

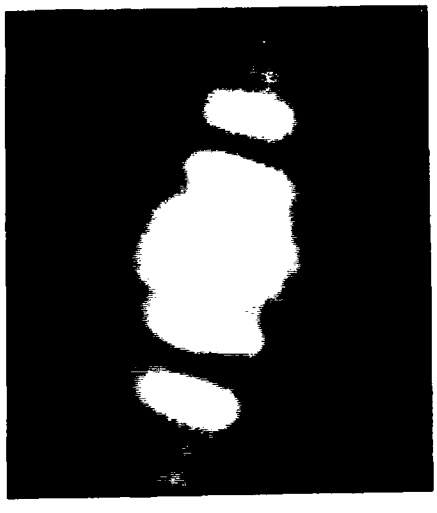

Fig. 1 c) completely broken pattern symmetry: T=250°C.

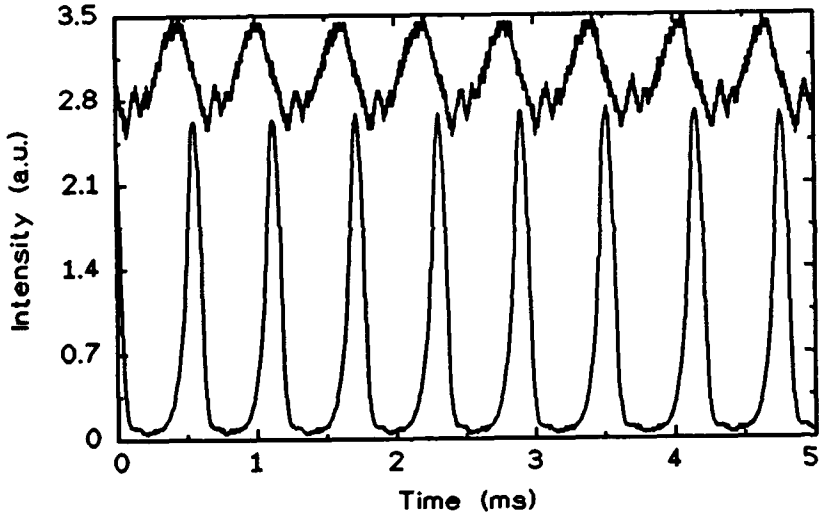


Fig. 2 Time dependent signals detected by two photodiodes for a pattern similar to that of Fig. 1c. Bottom trace: outer detector; upper trace: inner detector. The upper trace also is somewhat modulated probably because the sensitive area of the inner detector is large enough to receive the central peak and the first asymmetric spot.

parameter values these patterns seem to rotate as shown by the two time traces of Fig. 2, detected at the center and at the edge of the intensity distribution for a pattern similar to Fig. 1c. Note that this rotation can not be related directly to that observed in lasers [3], since in our resonator there is only one optical frequency present at any one time: the frequency of the injected laser field. Although different transverse modes may, and in general will, have different resonance frequencies, the rotation of this pattern can not be explained in terms of a beat between different modes. In our system, patterns rotate with frequencies that are of the same order as the time constant for the atomic diffusion, and therefore the rotation mechanism may be related to this effect.

Intertwined with the patterns that have (relatively) simple broken symmetries, we find more complex structures which at least in some cases contain vortices (Fig. 3). The appearance of vortices in nonlinear optical systems is now well established, but in our observations up until now we

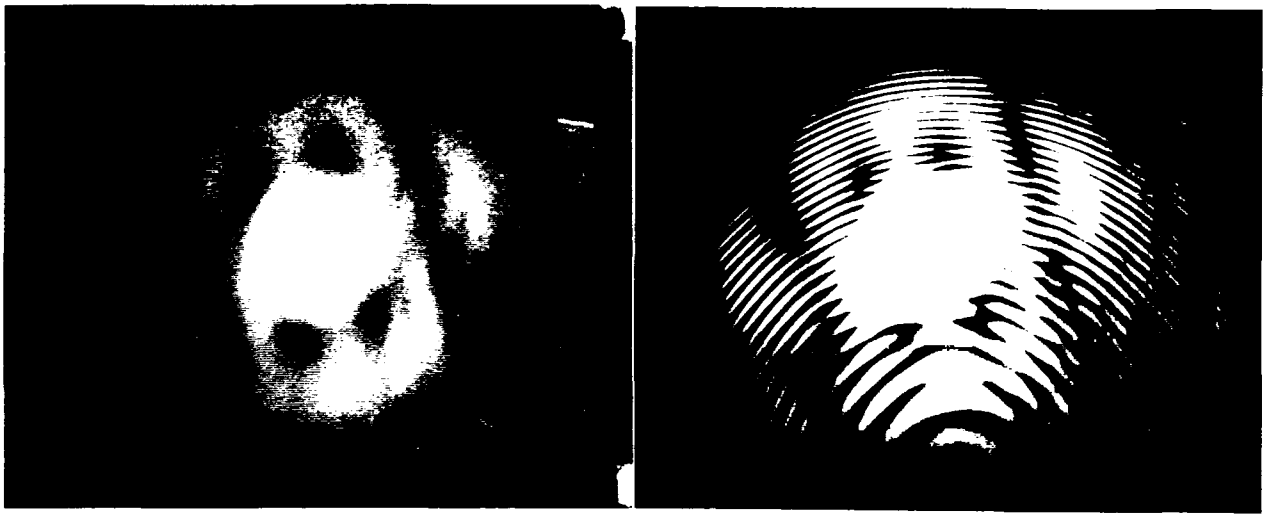

Fig. 3 a) Intensity pattern containing vortices; b) Interference picture of the pattern in (a), where four pairs of vortices with opposite topological charge are identifiable. The interference is a result of mixing the output of the resonator with a reference beam from the dye laser, which is formed by tightly focussing down onto a pinhole, and then collimating the center of the resulting spherical wave.

obtained structures where the total topological charge is zero. This result is at variance with what is predicted (and observed) in lasers [4] and observed in a passive system when the Fresnel number is kept small [5]. At present, we believe that this discrepancy is due to the presence of an open boundary in our system and to the zero topological charge that we input into the resonator [6]. In spite of the large Fresnel number of our cavity, the modes that are excited are extremely limited in number and are restricted to those of lowest order, due to mode-matching between input beam and resonator. Under these conditions, the resonator aperture does not act as a boundary for the creation of vortices. Instead of the extremely large number of vortices that one would expect, based on the empirical scaling law as a function of Fresnel number of ref. [5], we observe a very small number of vortices (only up to eight have been observed so far), because of the small number of low order modes active in our system. This result indicates that the Fresnel number is not necessarily the most appropriate parameter to use when characterizing transverse effects in an optical system. In all cases where the system is diffraction limited, (i.e., most lasers and a few passive systems), the Fresnel number is a meaningful quantity, but in the other cases (e.g., optically pumped lasers or mode-matched passive systems) it carries very little information and its use may be misleading.

References

[1] J. Opt. Soc. Am. B Special Issue, June-July 1990; L.A. Lugiato, Wang Kaige, and N.B. Abraham, submitted to Physical Review A; M. Brambilla, G. Broggi, and F. Prati, Preprint 1991; E.J. D'Angelo, C. Green, J.R. Tredicce, N.B. Abraham, S. Balle, Z. Chen, and G.L. Oppo, submitted to Physica D.

[2] a) Paper NOWe26 presented at the EQEC '91, Edinburgh (Scotland) August 27-30, 1991; b) paper submitted to Physical Review A; c) paper submitted to IQEC '92.

[3] C. Green, G.B. Mindlin, E.J. D'Angelo, H.G. Solari, and J.R. Tredicce, Phys. Rev. Lett. 65, 3124 (1990).

[4] M. Brambilla, F. Battipede, L.A. Lugiato, V. Penna, F. Prati, C. Tamm, and C.O. Weiss, Phys. Rev. A 43, 5090 (1991).

[5] F.T. Arecchi, G. Giacomelli, P.L. Ramazza, and S. Residori, Phys. Rev. Lett. 67, 3749 (1991).

[6] P. Coullet, L. Gil, and F. Rocca, Opt. Commun. 73, 403 (1989).

# SPATIAL AND TEMPORAL BEHAVIORS OF INSTABILITIES GENERATED BY COUNTERPROPAGATING LASER BEAMS IN RUBIDIUM VAPOR

A. Blouin, M.Pinard, A.Maître, J.R. Rios Leite*, R.W. Boyd** and G.Grynberg

Laboratoire de Spectroscopie Hertzienne de l'Ecole Normale Supérieure

Université Pierre et Marie Curie, T12, 75252 Paris Cedex 05, FRANCE

Tel ( 33 1 44 27 44 09 ) FAX ( 33 1 44 27 38 45 )

* Departamento de Fisica, Universidade Federal de Pernambuco, 50739 Recife, PE Brazil.

** The Institute of Optics, University of Rochester, Rochester, New-York 14627, USA.

Summary:

Pattern formation in nonlinear systems is a very active subject in many areas of physics. For example, in hydrodynamics the arrangement of the convective cells of the Rayleigh-Bernard instability [1] constitutes a model problem for pattern formation. In optics, important advances have been recently obtained in the case of lasers [2]. In contrast, transverse pattern formation in mirrorless optical passive systems [3] is no so wellknown because of the intrinsic complexity of a system without cavity and of the fact that the first experiments were done with pulsed lasers [4]. We present here results obtained with c.w. lasers and rubidium atoms. In particular, we show some interesting relationship with the hydrodynamics observations.

Two beams originating from a Ti-saphire laser counterpropagate through a n long cell containing rubidium vapor at a temperature of about 100°C. The laser is scanned over the

$D_1$ resonance line. The instabilites appear as coherent off- and on-axis emission of light cross-polarized with the incident beam. The far-field pattern of the off-axis emission may be an hexagon, a ring, double spots or more complicated shapes (see Fig.1) depending on laser frequency and intensity. The observation of the near field pattern shows the self organisation of light inside the nonlinear medium with apparition of an hexagonal lattice, concentric rings, rolls etc...

We have also studied bifurcation diagrams for the intensity instability $I_i$ versus the pump beam intensity $I_p$. In most situations, a supercritical bifurcation is observed (Fig 2.a). Bifurcation with a sudden jump of intensity and hysteresis (Fig 2-b) is also observed. Several features similar to those encountered in hydrodynamics have been observed, like bifurcations with transition from an hexagon to a double-spot pattern, which corresponds in the near-field to a transition from an hexagonal lattice to rolls.

The preceeding bifurcation diagrams correspond to an average instability intensity. In fact, one may as well observe temporal instabilities [5]. We are presently studiyng the temporal behaviour of both off- and on-axis emission. Near threshold both emission present a static or a periodic behaviour ( the frequency of the instability being on the order of 0.5 MHz). We have also observed a quasi-periodic road to chaos while pattern remains apparently unchanged. For each patterns, correlation between temporal behavior of on and off-axis instabilities will also be discussed. A deeper understanding of the route towards optical turbulence may be deduced from these investigations.

References :

[1] P. Manneville "Dissipative structures and weak turbulence", Academic Press (San Diego 1990), for recent results see E. Bodenschatz et al Phys. Rev. Lett. 67, 3078 (1991)

[2] M. Brambilla et al Phys. Rev. A43, 5090 and 5114 (1991)

[3] G.Grynberg et al Opt. Comm. 66, 321 (1988)

[4] G.Grynberg et al Opt. Comm. 67, 363 (1988)

[5] D.J. Gauthier et al Phys.Rev.Lett. 64, 1721 (1990)

Figure captions :

Fig. 1 : Far-field (a) and near-field (b) for hexagonal transverse pattern of the instability .

Fig. 2 : Bifurcation diagrams for the intensity of the instability versus the pump beam intensity $I_p$. (a) Supercritical bifurcation observed for a wide range of parameters. (b) Bifurcation with a sudden jump of intensity associated to an hysteresis cycle, observed on the low frequency side of the instability diagram.

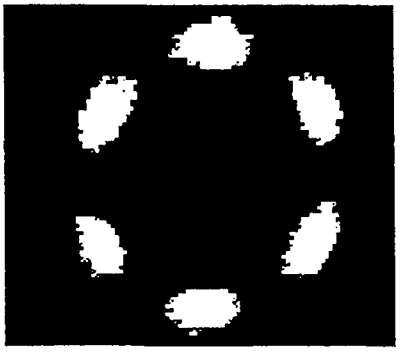

Fig. 1.a

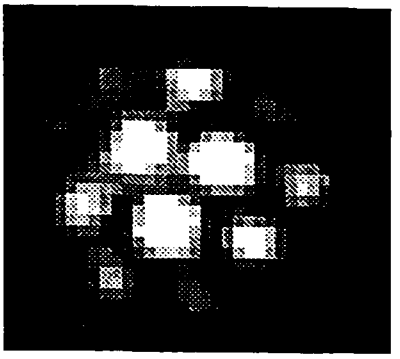

Fig. 1.b

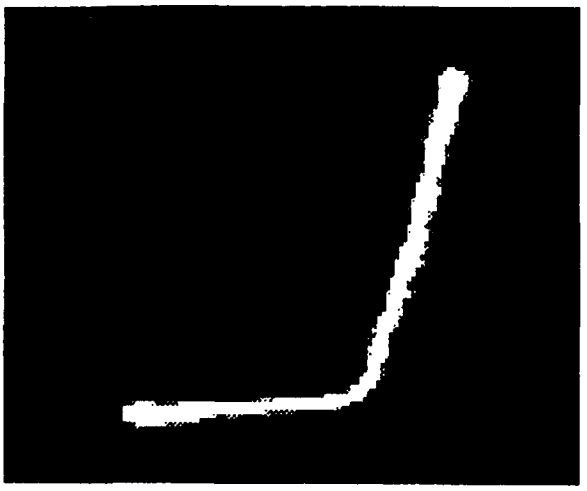

Fig. 2.a

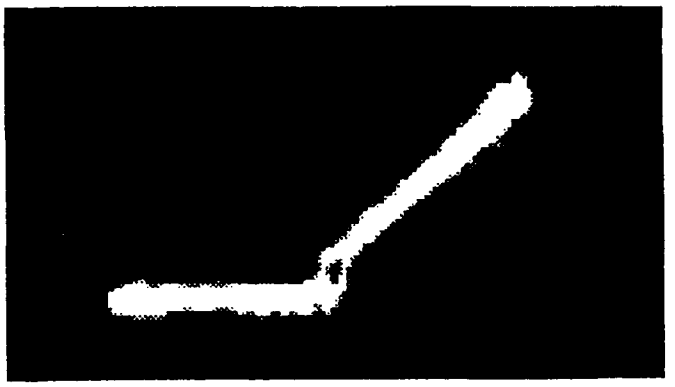

Fig. 2.b

# 2 Dimensional Transverse Patterns in Optical Bistability

W.J. Firth, G.S. McDonald, A.J. Scroggie
Department of Physics & Applied Physics
University of Strathclyde
John Anderson Building, 107 Rottenrow
Glasgow, G4 0NG, UK.

Telephone No. (UK) 41 552 4400
Fax No. (UK) 41 552 2891

L.A. Lugiato
Dipartimento di Fisica, Universita' di Milano
Via Celoria 16, Milano, Italy.

R. Lefever
Service de Chimie Physique, Université Libre Bruxelles
1050 Bruxelles, Belgium.

Pioneered by Moloney and collaborators [1], transverse effects of nonlinear passive systems in a ring cavity have been the object of extensive study. Analytical investigations with diffractive coupling in one transverse dimension have demonstrated [1] that static and dynamic transverse structures occur in this system. Extension of the mean-field dispersive model developed from optical bistability to include diffraction [2] independently demonstrated qualitatively similar features, again in one transverse dimension. Investigations in two transverse dimensions have been largely confined to numerical studies by the Moloney group [1], showing for gaussian beam illumination ring structures which develop through azimuthal instability to a pattern of spots which typically execute a slow chaotic motion with a progressive loss of symmetries.

In cavity-less counterpropagating beam configurations hexagonal structures have recently been experimentally observed [3] and subjected to intensive numerical and analytic study [4,5]. In optical media with third-order nonlinearity, the hexagonal patterns arise typically from forward four-wave mixing [3]. Hexagon structures have been observed experimentally also in the case of unidirectional propagation. All these considerations suggest that the unidirectional ring cavity geometry ought to be suitable for hexagonal pattern formation, and we present a

combination of analytical and numerical evidence that this is indeed the case (Figures 1 and 2). We start from the two dimensional extension of the ring-cavity model of [2]:

$$\frac{\partial E}{\partial t} = -E + E_i + i\eta E(|E|^2 - \theta) + ia\left(\frac{\partial^2 E}{\partial x^2} + \frac{\partial^2 E}{\partial y^2}\right) \qquad (1).$$

By setting $E = E_s(1 + A)$ where A is the deviation (not necessarily small) of the circulating field from its plane wave steady-state value $E_s$, Eq.(1) can be cast in the form

$$\frac{\partial A}{\partial t} = -(1 + i\eta\theta)A + i\eta|E_s|^2(2A+A^*+A^2+2AA^*+|A|^2A) + ia\left(\frac{\partial^2 A}{\partial x^2} + \frac{\partial^2 A}{\partial y^2}\right) \qquad (2).$$

We have undertaken a bifurcation analysis [6] to calculate the pattern (with a roll, or a rhomboedric, or a hexagonal structure) which can arise from the modulational instability of the transversely homogeneous stationary state, and to investigate their stability. We have also performed the first numerical investigations of Eqs.(1),(2); the numerics indicate that hexagons are stable over a range below the instability threshold of the plane-wave solution. Defect structures in the patterns are also observed. These observations are typical of hexagon-forming systems. A key point about these results is that they are obtained in the framework of a model which does not demand supercomputer resources on the one hand, and for which there is considerable experience and expertise in experimental realisation on the other.

References

[1] J.V. Moloney, H. Adachihara, R. Indik, C. Lizaragga, R. Northcutt, D.W. McLaughlin and A.C. Newell, JOSA B7, 1039 (1990) and op.cit.

[2] L.A. Lugiato and R. Lefever, Phys. Rev. Lett. 58, 2209 (1987).

[3] G. Grynberg, E. LeBihan, P. Verkerk, P. Simoneau, J.J.R. Leite, D. Bloch, S. Le Boiteaux and M. Ducloy, Opt. Commun. 66, 321 (1988).

[4] R. Chang, W.J. Firth, R. Indik, J.V. Moloney and E.M. Wright, Opt. Commun. (in press).

[5] G. D'Alessandro and W.J. Firth, Phys. Rev. Lett. 66, 2597 (1991).

[6] P. Manneville, "Dissipative structures and weak turbulence", Academic Press, 1990, ch.8.

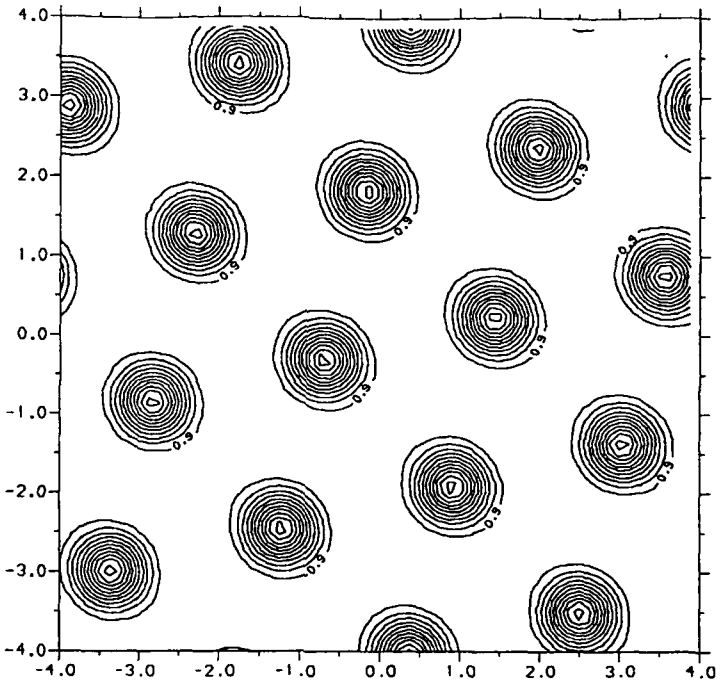


Fig. 1: Contour plot of a stationary hexagon pattern in the transverse plane, obtained at 3% above the linear instability threshold. Mean field, $\theta = 0$, and plane-wave pumping .

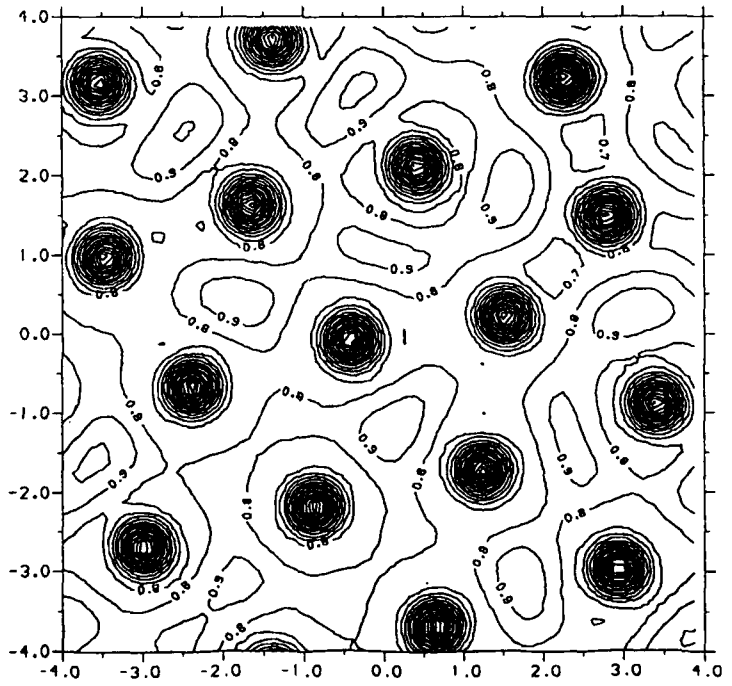


Fig. 2: Defected hexagon pattern at 6% above the linear threshold, $\theta = 1$.

# Interaction of Spatiotemporal Wave Structures in Nonlinear Optical Resonators: New Routes in Optical Turbulence

M. A. Vorontsov
Moscow State University
Russian Federation

Summary not available at press time.

Wednesday, June 24, 1992

# Spatial Pattern Formation and Dynamics 2

**WB** 11:20am–1:20pm
Schroedinger Hall

Paul Mandel, *Presider*
*Brussels Free University, Belgium*

# Dynamical Transverse Laser Patterns

M. Brambilla * , M. Cattaneo, L. A. Lugiato, R. Pirovano and F. Prati *
*Dipartimento di Fisica dell' Università di Milano, via Celoria 16, 20133 Milano, Italy*
* *also Physik Institut, Universität Zürich, Switzerland*

A. J. Kent and G.-L. Oppo
*Department of Physics and Applied Physics, University of Strathclyde*
*107 Rottenrow, Glasgow, G4 0NG, Scotland, U.K.*

A. B. Coates and C. O. Weiss
*Physikalisch-Technische Bundesanstalt, 3300 Braunschweig, Germany*

C. Green, E. J. D'Angelo, and J. R. Tredicce
*Department of Physics, Drexel University, Philadelphia, PA. U.S.A.*

The spatial and spatio-temporal phenomena that emerge in the transverse structure of the electromagnetic field have attracted a lot of attention in recent years [1,2] . We consider a cylindrically symmetrical laser with spherical mirrors, and describe the dynamics in terms of the competition among different Gauss-Laguerre modes of the cavity . In this presentation we focus on the case in which the mode compe-

tition leads the laser to approach a dynamical state which, according to the values of the control parameters, can be periodic or quasiperiodic.

The linear stability analysis of the singlemode stationary solution , in which the laser oscillates with the fundamental Gaussian mode, provides an initial guideline in our search of the various spatio-temporal patterns which arise. We consider cases in which the gain line activates one, or two, or three frequency degenerate families of modes. The motion of optical vortices, from simple rotation to creation and annihilation in pairs, is analyzed, together with the correlated movement of the peaks of the intensity distribution in the transverse plane.

We study also the patterns which appear when the cylindrical symmetry of the system is broken.

We analyze experimentally the simplest dynamical transverse patterns which appear in $Na_2$ and $CO_2$ lasers, selecting values of the control parameters which correspond closely to those considered in the theoretical studies, and we perform a systematic comparison between theoretical predictions and experimental observations.

## References

1. N. B. Abraham and W. J. Firth eds., Special issues on *"Transverse Effects in Nonlinear Optical Systems"*, J. Opt. Soc. Am. B**7**, June and July 1990

2. L.A. Lugiato, in Proceedings of the Solvay Conference on Quantum Optics, ed. by P. Mandel, Physics Reports, in press.

# Pattern formation in a multimode $CO_2$ laser

D. Hennequin, C. Lepers, E. Louvergneaux, D. Dangoisse and P. Glorieux
Laboratoire de Spectroscopie Hertzienne
Université des Sciences et Technologies de Lille
F-59655 Villeneuve d'Ascq cedex - France

The spatio-temporal dynamics of a Perot-Fabry $CO_2$ laser is experimentally studied. The cavity is composed of two mirrors with a lens inserted between them. This system permits to reach very large Fresnel numbers by adjusting the location of the lens, and so to vary the frequency spacing between transverse modes on a wide range [1], typically from almost 0 to 20 MHz in our case, while the free spectral range is 80 MHz. Two other control parameters are available: the pump parameter and the cavity length.

For small Fresnel numbers, we systematically compare our observations of the spatial behavior of the laser with the results obtained by Lugiato et al on a model of a class C ring laser [2]. This numerical work describes the transverse profile of the active modes as a function of the modes of the empty cavity present in the gain profile. Our experimental system differs from the theoretical case studied in [2]

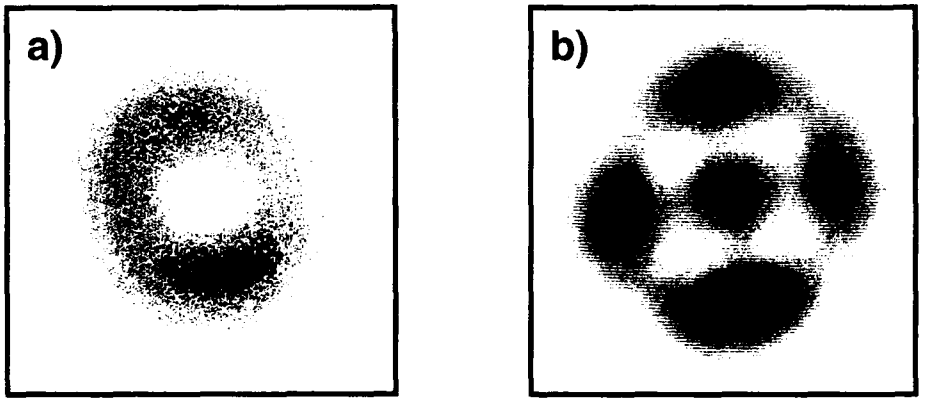


Fig. 1: In a), high contrast video record of the transverse section of the output beam of the laser when the $TEM_{01}$ and $TEM_{10}$ modes are oscillating. The asymmetry of the pattern originates in the symmetry breaking of the system due to the two-mode frequency degeneracy lift. In b), video record of the transverse section of the output beam of the laser when the $TEM_{02}$, $TEM_{20}$ and $TEM_{11}$ modes are oscillating. This pattern is called "4-hole" mode in [2] because of the presence of four phase singularities in it.

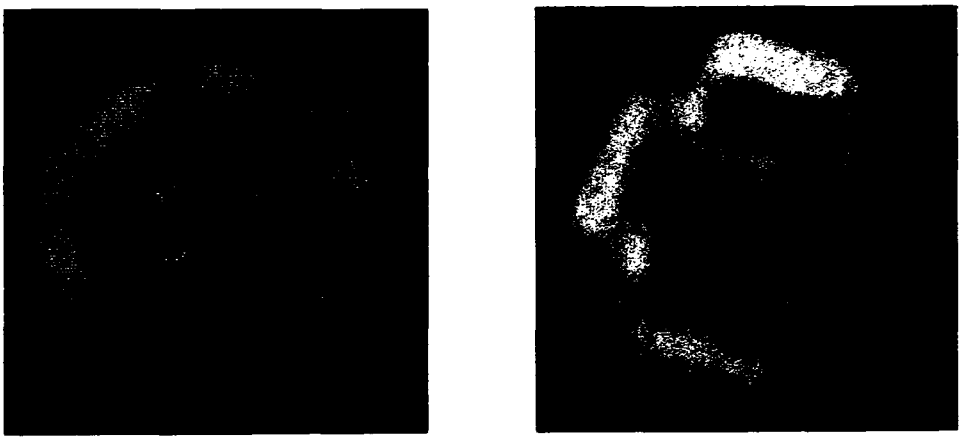

Fig. 2: Two patterns obtained for large Fresnel number.

on two points: (i) we use a class B laser in a Fabry-Pérot cavity and (ii) the cylindrical symmetry of the system is slightly broken by astigmatism effects. However, our observations remain in good agreement with the results of the model, although the symmetry breaking may induce some asymmetry in the patterns (fig. 1). On the opposite, some modes predicted by the model are not observed in this experiment.

The symmetry breaking in our system partially originates from the astigmatism effects in the optical elements, which also induces a degeneracy lift of the frequency of the modes considered in [2]. This results in a temporal dynamics that cannot be considered in the model as the interacting modes have the same frequency. The experimental study of this dynamics shows frequency locking and antiphase behavior, as for example between the $TEM_{01}$ and the $TEM_{10}$ modes.

As the Fresnel number increases, the spatial behavior looses completely the cylindrical symmetry and much more complex structures are observed. The symmetries of all the different patterns that appear then have their main axes oriented following the astigmatism direction (fig. 2). So it appears that as the Fresnel number is increased, the response of the system is more sensitive to the deviation from perfect cylindrical symmetry.

Similar experimental investigations has been carried out on a $CO_2$ laser with an intracavity saturable absorber. This system displays new spatial features in addition to those of the simple $CO_2$ laser. In particular, we observed bistability between patterns corresponding to different mode frequencies.

As a conclusion, we observe that small symmetry losses of the laser geometry have a very weak influence on its behavior as long as the Fresnel number remains low. On the contrary, these defects hold the spatial behavior symmetry at large Fresnel number.

**References**

[1] C. Green, G. B. Mindlin, E. J. D'Angelo, H. G. Solari and J. R. Tredicce, Phys. Rev. Lett. 65 3124 (1990)

[2] M. Brambilla, F. Battipede, L.A. Lugiato, V. Penna, F. Prati, C. Tamm and C. O. Weiss, Phys. Rev. A 43 5090 (1991)

# Defect dynamics in the evolution of the transverse pattern of a laser

N. B. Abraham, S. Balle+, and Z. Chen
Department of Physics, Bryn Mawr College, Bryn Mawr, Pennsylvania 19010-2899, USA

E. J. D'Angelo and J. R. Tredicce*
Department of Physics and Atmospheric Science, Drexel University,
Philadelphia, Pennsylvania 19104, USA

Recently we reported[1] numerical solutions of the full set of Maxwell-Bloch equations for a laser with transverse profile variations, finding examples of multimode pulsations without defects and examples of defect-mediated pulsations that could be periodic or turbulent. The onset of turbulence was illustrated by the loss of spatial correlation -- the decorrelation of intensity fluctuations at separated points -- as the number of defects increased. In that work, we also reported the first results of parallel studies using more physical limitations on the transverse profile of the excitation mechanism and using spatially distributed spontaneous emission noise. The transverse profile limitations effectively suppressed the higher order radial modes, thereby enlarging the spatial extent of the coherent structure surrounding each defect. The enlarging of the size of coherent structures around each defect, reaching a significant fraction of the size of the overall patterns, was sufficient to increase their interaction to a global one, causing entrainment of the motion of the defects after long transients, with the final states being periodic motion. We elaborate on these results in the present work.

The equations of motion for a homogeneously broadened laser are[2]:

$$\begin{aligned}
\frac{\partial E(\rho,\varphi,t)}{\partial t} &= -\kappa\left[ f(\rho) - i\,\Delta - i\,\frac{a}{2}\left(\frac{1}{4}\nabla_{\perp}^{2} - \rho^{2} + 1\right)\right] E(\rho,\varphi,t) - 2\,C\,\kappa\,P(\rho,\varphi,t) \\
\frac{\partial P(\rho,\varphi,t)}{\partial t} &= -\gamma_{\perp}\left[ E(\rho,\varphi,t)\,D(\rho,\varphi,t) + (1 + i\,\Delta)\,P(\rho,\varphi,t)\right] \qquad (1) \\
\frac{\partial D(\rho,\varphi,t)}{\partial t} &= -\gamma_{\parallel}\left\{ -\frac{1}{2}\left[E(\rho,\varphi,t)\,P^{*}(\rho,\varphi,t) + E^{*}(\rho,\varphi,t)\,P(\rho,\varphi,t)\right] + D(\rho,\varphi,t) - \chi(\rho)\right\}
\end{aligned}$$

where $\rho$ and $\phi$ are the radial and angular coordinates in a plane transverse to the direction of propagation of the field; E and P are the slowly varying amplitudes for the electric field and the atomic polarization, respectively; and D is the population inversion; $\kappa f(\rho)$, $\gamma_{\perp}$, and $\gamma_{\parallel}$ are the respective loss rates of the three variables, where $f(\rho)$ describes transverse variations in the cavity loss such as might occur due to apertures or finite extent of the mirrors; $2C\chi(\rho)$ is the pump rate for excitation of the inversion; $\chi(\rho)$ is the radial distribution of the pump normalized to 1 at $\rho=0$; $\Delta$ is the detuning parameter; a is a parameter that depends on the radius of curvature of the mirrors composing the optical cavity; and $\nabla^{2}_{\perp}$ denotes the transverse Laplacian.

The boundary conditions imposed by the spherical mirrors and the length of the cavity in conjunction with the atomic resonance frequency determine the optical frequency of operation of the laser output but do not provide absolute restrictions on the transverse size or boundary values of the electromagnetic field. The diameter of the laser tube and/or the optical elements inside the cavity limit the size of the pattern by increasing the cavity losses at large values of the radial coordinates. Assuming ideal reflectors, and a cylindrical medium we take the losses to be nearly constant in the central region of the laser and then near an effective boundary ($\rho=\rho_{o}$) the losses increase rapidly and

saturate at a higher level when $\rho >> \rho_o$. This approximates the situation in a real laser where the losses become almost infinite at radial distances larger than the radius of the tube. In our case, in order to avoid numerical difficulties, it is important to have a smoothly varying function, hence the value of the gain, C, must be kept small enough so that the ratio between the gain and losses is smaller than the laser threshold for $\rho > \rho_o$. The parameter a in Eq. 1a depends on the radius of curvature of the mirrors and the geometry of the boundaries, and it governs the detuning between the fundamental mode of the cavity and all the higher order modes.

For the numerical integration of Eqs. 1 we have used a Gallerkin method with Gauss-Laguerre polynomials as interpolating functions[3]. This method does not require specific boundary conditions. We adopted the Gauss-Laguerre polynomials as a convenient basis set because they are eigenmodes of the empty cavity. We have used 190 collocation points distributed in 19 different angular directions. To avoid numerical artifacts from sharp boundaries, we have used a smooth function for the cylindrically symmetric form of the pump profile $\chi(\rho)$. For the parameters we used $\kappa = 0.1$, $\gamma_\perp = 1.0$, $\gamma_\parallel = 0.01$, $\Delta = -0.4$, and $\rho_o = 5.0$. The values of a were chosen so that the minimum intermode frequency spacing ($\kappa a/2$) was of the order of 0.1.

The effects of spontaneous emission noise were simulated by adding random white noise to the polarization equation[4], as is appropriate for macroscopic optical systems. We took the strength of this noise to be proportional to the transverse pump profile (a simplification over the more exact, though cumbersome, strategy of taking it proportional to the instantaneous spatial profile of the upper state population). Of course several simplifications are being used at once, since the Maxwell Bloch equations for a two-level medium do not permit identification of the upper and lower state populations since only the inversion is monitored with the variable D.

As the excitation parameter is increased and as the Fresnel number is increased, we find a smooth transition from a nearly Gaussian transverse profile to patterns with more and more defects. If the higher order modes are attenuated by transverse profiles of the loss and the pump, the defects take on larger size and tend to develop correlations in their positions and motions. We tend to find patterns in this case which are fixed except for a uniform rotation rate which is nearly equal to the spacing of the adjacent angular modes. Such a pattern would result if modes of different radial index and the same angular index have the same frequency to avoid radial oscillations in the positions of the defects. Uniform rotation of the pattern results if the modes of different angular indices are equally spaced, with the spacing frequency equal to the rotation frequency. The asymmetry of some of the patterns suggests that modes of odd indices dominate, but the fixed rotation frequency at the minimum mode spacing frequency indicates that all modes contribute and that they are locked to equal spacings.

A wide range of phenomena for different parameter values is summarized in Table 1. Increasing the pump amplitude sharpens the gradient of the pump profile and this seems to tend to force the defects to lock without significantly changing the number of defects. In contrast, increasing the parameter a leads to more defects, which we can understand since the increase leads to a larger Fresnel number while increasing the intermode spacing. In general, the pump profile with its reduced excitation far from the axis of symmetry of the medium suppresses higher order spatial modes found when the profile was assumed to be uniform[1] and this smooths the irregularities in the patterns without eliminating the defects. However, in the absence of these more rapidly varying functions, each defect is of far greater size. This greater size leads to stronger defect-defect interaction and after long transients we find that patterns of two, three, or four defects eventually reach stable, locked configurations which then rotate at a common frequency. In some cases the defects lock to a common radius, in other cases they lock to different radii. In each case the signature of the locking is the absence of temporal oscillations at the center of the pattern.

**Table 1: Defect Phenomenology**

| Mode Spacing Parameter a | Pump Parameter C | Number of Defects | Characteristics |
|---|---|---|---|
| 3.0 | 3.5 | 1 | periodic |
| 3.0 | 6.0 | 2 | periodic, locked, different radii |
| 3.0 | 7.0 | 2 | periodic, locked, different radii |
| 3.0 | 8.0 | 2 | periodic, locked, different radii |
| 3.0 | 10.0 | 2 | periodic, locked, same radii |
| 3.0 | 11.0 | 2 | periodic, locked, same radii |
| 3.0 | 13.0 | 2 | periodic, locked, same radii |
| 3.0 | 14.0 | 2 | periodic, locked, same radii |
| 2.0 | 14.0 | 1 | periodic |
| 2.5 | 14.0 | 2 | periodic, locked, same radii |
| 3.0 | 14.0 | 2 | periodic, locked, same radii |
| 4.0 | 14.0 | 3 | periodic, locked, different radii |
| 5.0 | 14.0 | 4 | periodic, locked, different radii |
| 2.5 | 14.0 | 2 | periodic, locked, same radii |
| 2.5 | 12.0 | 2 | periodic, locked, different radii |
| 2.5 | 10.0 | 2 | periodic, locked, different radii |

In conclusion, our numerical simulations demonstrate a sequence of symmetry breaking bifurcations that signal the arrival of more defects. The increasing Fresnel number is more important than the mode-spacing in increasing the number of the defects. When the higher order radial modes are suppressed, the coherent spatial structures in the vicinity of the defects are relatively large and develop highly correlated motion. The periodic rotation of the pattern of defects indicates that modes of different radial index but the same angular index are locked to the same optical frequency, while modes differing in angular index are equally spaced in frequency. This locking of the mode spacings must be broken before individualized defect motion can occur, and it is the liberating of the individual defects from the overall pattern that is essential to the onset of turbulent phenomena.

The computations were accomplished in part with a grant of supercomputing time from the National Center for Supercomputing Applications. This work was also supported in part by a grant from the NATO Scientific Affairs Programme #CRG.910004.

1. E. J. D'Angelo, C. Green, J. R. Tredicce, N. B. Abraham, S. Balle, Z. Chen, and G. L. Oppo, "Symmetry breaking, dynamical pulsations, and turbulence in the transverse intensity patterns of a laser: the role played by defects", Physica D, to be published.

2. G. L. Oppo, G. D'Alessandro and W. J. Firth, Phys. Rev. A **44**, 4712 (1991); and G. L. Oppo, and L. Gil, private communication.

3. J. Villadsen and M. L. Michelsen, *Solution of Differential Equation Models by Polynomial Approximation* (Prentice Hall Inc., Englewood Cliffs, 1978).

4. H. J. Carmichael, *Quantum statistical methods in quantum optics*, Chapter 7 (Springer, Heidelberg, to be published) and H.J. Carmichael in *Lasers and Quantum Optics*, edited by L. M. Narducci, E. J. Quel and J. R. Tredicce (World Scientific, New Jersey, 1990) pp. 52-85.

+Present Address: Departament de Física, Universitat de les Illes Baleares, E-07071 Palma de Mallorca, SPAIN

*Also with: Institute Nonlineaire de Nice, Université de Nice, Nice, FRANCE

# Optical Vortices and Dark Spatial Solitons

C.O.Weiss, K.Staliunas*

Lab.4.42, PTB Braunschweig, Bundesallee 100
3300 Braunschweig, GERMANY
tel: 49-531-5924400, FAX: 49-531-5924006,
E-mail: STALI426@RZ.Braunschweig.PTB.DBP.DE

Since Zacharov and Shabat integrated one-dimensional Nonlinear Schrödinger Equation (1D NLSE) and found solitons [1,2], much have been done in one-dimensional, but very little in two-dimensional soliton physics. The integrability of 2D NLSE as well as existence of solitons in it is under the question to the time.

We analyse 2D NLSE in a defocussing case:

$$\frac{\partial A}{\partial \tau} = i \cdot \nabla^2 A - i|A|^2 A; \qquad (1)$$

A particullar stationary solution of this equation is so named optical vortex. In the limit $r \to 0$ (r and $\phi$ are the pollar coordinates in a plane) it is of the following asymptotic form:

$$A(\vec{r}) = \frac{r}{r_{core}} \cdot \exp(-i\omega t \pm i\phi) \qquad (2)$$

where $r_{core}$ is the vortex core radius. Characteristic for this vortex is vanishing intensity on its core and that the circullation of phase gradient on a close loop around it is $\pm 2\pi$. In virtue of that, the vortex is an object with nontrivial phase topology.

The direct correspondence for the optical vortex (2) in a 1D NLSE case is a standing dark soliton:

$$A(x) = \exp(-i\omega t) \cdot A_0 \cdot \mathrm{th}\left(\frac{x}{x_{core}}\right) \qquad (3)$$

here the parameters $\omega$, $A_0$ and $x_{core}$ are uniquelly defined by baundary conditions. Our hypothesis is, that the vortex solution (2)

*Alexander von Humboldt fellow, visiting from:

Dep.Quant.Electr. of Vilnius University,

Sauletekio av.9, corp.3, 2054 Vilnius, LITHUANIA

of 2D NLSE is also a soliton in a strict sense of the therm "soliton".

The hyphothesis was checked in numerical experiment, where two opposite charge vortex pairs were collided (if a single vortex is stationary, the pair of opposite charge vortices is moving with a constant velocity). The two examples of such numerical vortex pair collision are presented in Fig., where ⊕ and ⊖ signs represent the location of vortices of positive and negative topological charges correspondingly.

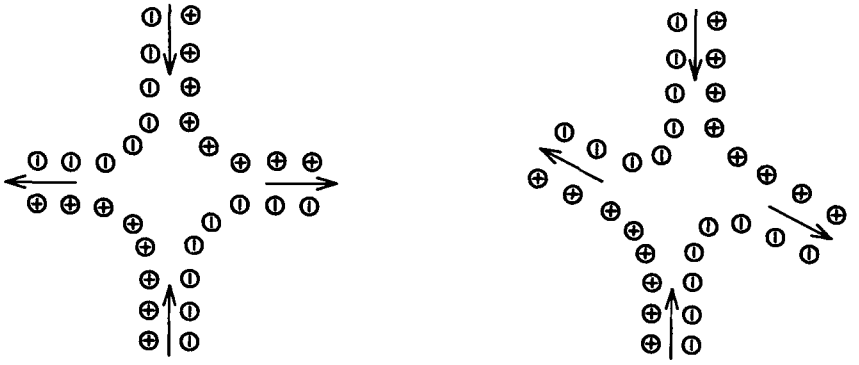

Characteristic for the collision is that not only the total topological charge of the system is integral of motion, but also the number of vortices (the vortices of opposite charge does not anihillate in 2D NLSE!). No energy was observed to be lost in form of radiation during the collision, what is very characterical for "real" the solitons.

The dynamics of vortices in lasers [3,4] and passive systems [5] are governed by Complex Ginzburg-Landau Equation (CGLE):

$$\frac{\partial A}{\partial \tau} = \beta \cdot A + (i + d) \cdot \nabla^2 A - (\beta + i) |A|^2 A; \qquad (4)$$

which can be treated as perturbed NLSE. The diffusion term $d \cdot \nabla^2 A$ and the saturated amplification term $\beta \cdot A \cdot (1 - |A|^2)$ converts NLSE into nonconservative one, and the vortices in it are no more pure solitons.

The two opposite charge vortices can anihillate as well as to be activated in (4). The few vortex ansemble enclosed in potential well can arrange into ordered structures as well as to evolute periodically or chaotically in time, depending on the parameters of a physical system described by (4). In the Fig. the stationary four vortex ensemble is presented obtained by numerical simulations (left) and experimentally in lasers [4] (right).

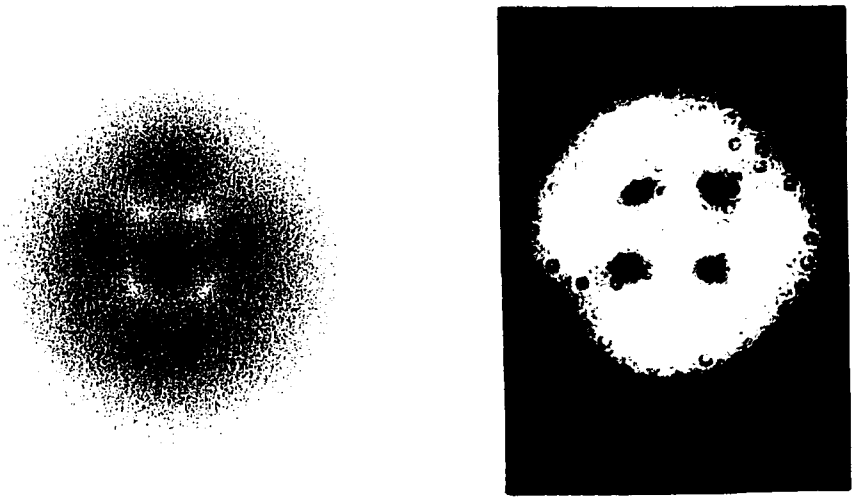

In virtue of said above it is possible to observe the phase transitions between "chaotic vortex gas" state and "vortex crystal" state in optical systems. The properties of this phase transition are further investigated.

*Alexander von Humboldt fellow, visiting from: Dep.Quant.Electr. of Vilnius University, 2054 Vilnius, LITHUANIA

1.V.E.Zacharov and A.B.Shabat Sov.Phys.JETP 34 (1972) 62
2.V.E.Zacharov and A.B.Shabat Sov.Phys.JETP 37 (1973) 823
3.P.Coullet, L.Gil and F.Rocca Optics Comm. 73 (1989) 403
4.M.Brambilla, F.Battipede, L.A.Lugiatto, V.Pena, F.Prati, C.Tamm and C.O.Weiss Phys.Rev. A43 (1991) 5090
5.F.T.Arecchi, G.Giacomelli, P.L.Ramazza and S.Residori: Vortices and defect statistics in two-dimensional optical chaos (to be published in Phys.Rev. Letts.)

# Turbulent Patterns in Wide Gain Section Two-Level and Raman Lasers

P.K. Jakobsen, S.G. Wenden. J.V. Moloney and A.C. Newell

Arizona Center for Mathematical Science

Mathematics Department

University of Arizona

Tucson AZ 85721

Tel: (602)-621-6755, Fax: (602)-621-8322

The close synergism between experiment and theory for Rayleigh-Benard fluid convection has led to the development of sophisticated theoretical models which accurately predict the onset of widely diverse pattern forming turbulent convection. Close to threshold a multiple scales weakly nonlinear analysis yields a universal class of amplitude equations which accurately predict the formation of roll, hexagon, defect patterns and various instabilities of the underlying roll solutions. An elegant study by Busse of the nonlinear regime established that turbulent patterns and stable rolls could coexist beyond the first instability threshold.

We will report on a close analogy between turbulent convection in large aspect ratio fluids and traveling wave turbulent patterns in lasers with wide gain sections. In contrast to the fluid case, exact traveling wave solutions can be easily derived for the Maxwell-Bloch equations including diffraction effects. As in the fluid case, we can identify regions in physical parameter space where stable traveling wave and turbulent patterns can coexist. For a two-level laser, the stable traveling wave region (Busse balloon) extends down to the first laser threshold. However the Busse balloon for a Raman laser may lie well above the instability threshold or may extend down to the first laser threshold, depending on the sign of the intermediate level detuning from the pump. The physical manifestation of these stable traveling wave solutions is a controllable (under, for example, PZT tuning) off-axis far-field emission of the laser. Figure 1(a) shows a single frame of both near- and far- field two transverse dimensional emission patterns for an infinite plane wave-pumped Raman laser initiated from noise. The system lies at a level of pumping $V_0$ coinciding with the Busse balloon region. We observe a turbulent sea of rolls and defects being transported to the right in the near-field and a strong far-field emission at a fixed angle surrounded by a weak fluctuating background. Figure 1(b) shows a single frame of the near- and corresponding

far-field emission for noise initiated patterns at a pump level lying below the Busse balloon. Here the rolls and defects are being transported to the left and right simultaneously, as evidenced by the pair of strong sidebands in the far-field emission.

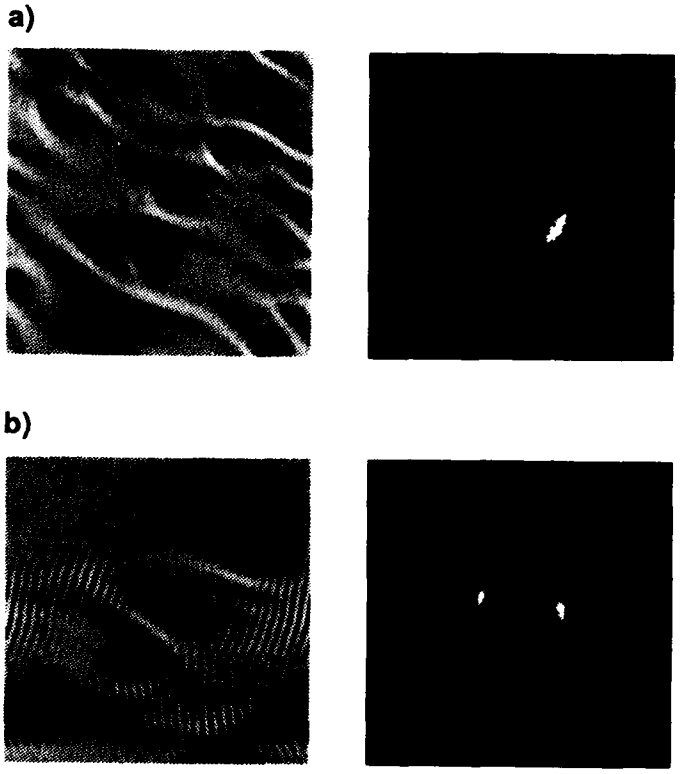


**Figure 1** Single frame from a movie showing near- and far-field two dimensional turbulent output from a plane pumped Raman laser initiated with noise. (a) pump strength coincident with Busse balloon region. (b) pump strength below Busse balloon region.

The onset of turbulent patterns beyond first threshold in the Raman laser is caused by a sideband (Benjamin-Feir) instability occurring at right angles to the underlying traveling wave (roll) solution. This instability which is absent in the two-level laser and the fluid case, causes the spontaneous nucleation of defects from finite amplitude solutions. A weakly nonlinear analysis of the Maxwell-Bloch equations near threshold, leads to an amplitude equation of the complex Newell-Whitehead type. A detailed analysis of this equation is underway and will allow us to compare and contrast pattern forming instabilities for the two-level, Raman lasers and fluid problems. Finite boundary effects are expected to strongly affect pattern formation. Figure 2 shows four frames from the dynamical evolution of patterns

in the more realistic case of a super Gaussian-pumped Raman laser. Observe the appearance of a zig-zag cross roll type instability with rolls and defects being transported to the right.

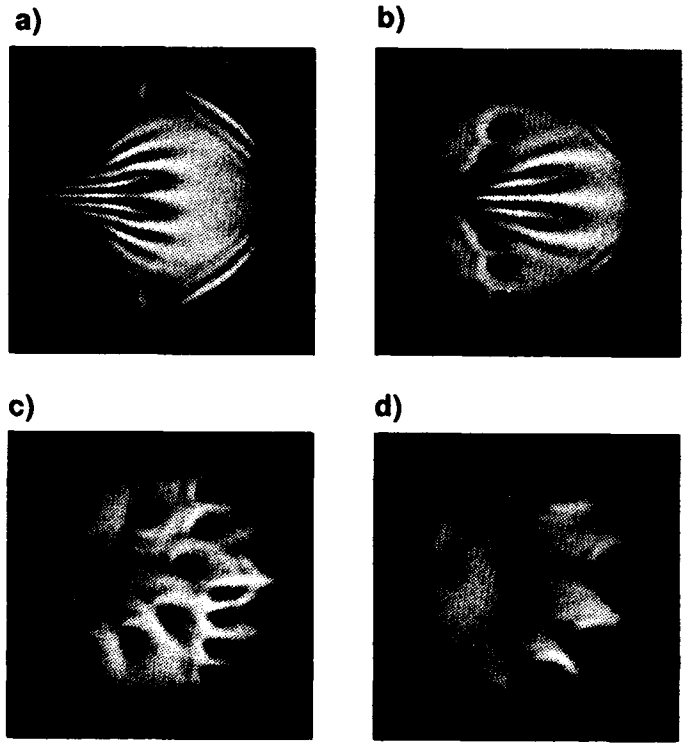


**Figure 2** Four frames from a movie showing turbulent roll and defect patterns under super Gaussian external pumping.

Our more recent results predict a remarkably rich pattern forming phenomenonology which will depend sensitively on the sign of the pump detuning in the Raman laser and on the mode of initiation of lasing. A distinction can be made between noise initiated or probe beam selected transverse spatial patterns. The latter can be viewed as a spatial injection-locking of the wide gain section laser.

# Pattern Formation Due to Nonlinear Counterpropagation in Kerr and Brillouin-active Media

J.B. Geddes, R. Indik and J.V. Moloney
Arizona Center for Mathematical Science
Mathematics Department
University of Arizona
Tucson AZ 85721
Tel: (602)-621-6755, Fax: (602)-621-8322

W.J. Firth and G.S. McDonald
Dept. of Physics and Applied Physics
University of Strathclyde
John Anderson Building, 107 Rottenrow
Glasgow G4 ONG UK

Spontaneous hexagon formation has been observed when two counterpropagating laser beams interact in sodium vapor [1] and carbon disulfide [2]. Here we report on investigations into the nature, stability and range of patterns in such systems. We model an anti-reflected slab of either a Kerr or Brillouin-active medium irradiated on each side by smooth constant input fields. These may be Gaussian beams [3] or plane-waves.

Linear stability analysis of the Kerr slab is well-understood [4], but with two transverse dimensions, all small-amplitude solutions are unstable at the linear threshold. We performed a weakly nonlinear analysis for this system with three space variables plus time. This nonlinear expansion is more difficult than usual because of the longitudinal structure. We have derived amplitude equations, similar to those in fluid convection [5], describing hexagons near the linear threshold for self-focusing media.

Two transverse-dimensional numerical simulations have been undertaken on Cray and Convex machines in the USA and the UK, and the results are in broad agreement with the analysis and the experiments. In particular, we find that for self-focusing media, stable hexagon patterns persist to about 15% below threshold both with and without the wavelength-scale index grating [4]. In self-defocusing media hexagons are not favored, small-amplitude rolls are the only stable pattern found.

A new phenomenon we have noted is the occurrence of a Hopf bifurcation near threshold, through which the hexagonal pattern destabilizes. The resultant oscillation, which has a

period of order a few transit times, exchanges energy between the fundamental hexagon and a "mixed" hexagon - Figures 1 and 2. In K-space this is identifiable as a four-wave mixing interaction involving the pump field and an adjacent pair of the fundamental hexagon vectors, generating dynamics for a new transverse wavevector of magnitude $\sqrt{3}$ times the fundamental. Figures 1 and 2 show different phases of this oscillation obtained by numerical simulation.

To analyze this new instability we have derived a family of equations by projecting onto modes of the linearized equations. The choice of modes is motivated by numerical experiment. Most of these modes can be slaved to a few active ones - in fact if all but three are slaved we return to our original amplitude equations. This model can capture the dynamics of the full system and Fig. 3 shows the output generated by the AUTO package.

In Brillouin-active media, we have seen [6] that pattern formation in one transverse dimension is possible. Whereas patterns in the Kerr slab are observed at the same frequency as the pump beams, there is a frequency-mismatch in the Brillouin-active slab. This frequency mismatch seems to preclude the usual mechanism for the formation of hexagonal patterns in two-transverse dimensions. It is intriguing that hexagonal patterns have been observed for this system in at least one experiment [2]. We will report on the results of our numerical simulations.

# References

[1] G. Grynberg, E. LeBihan, P. Verkerk, P. Simoneau, J.J.R. Leite, D. Bloch, S. Le Boiteaux and M. Ducloy, Opt. Commun. **66**, 321 (1988).

[2] A.L. Gaeta, M.D. Skeldon, R.W. Boyd and P. Narum, JOSA **B6**, 1709 (1988).

[3] R. Chang, W.J. Firth, R. Indik, J.V. Moloney and E.M. Wright, Opt. Commun. (in press).

[4] W.J. Firth, A. Fitzgerald and C. Parè, JOSA **B7**, 1087 (1990).

[5] S. Ciliberto, P. Coullet, J. Lega, E. Pamploni and C. Perez-Garcia, Phys. Rev. Lett. **65**, 2370 (1991).

[6] J.B. Geddes, J.V. Moloney and R. Indik, Opt. Commun. (in press).

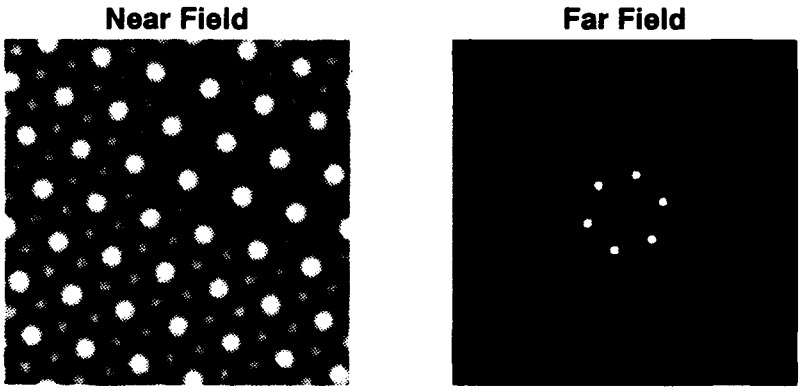


**Figure 1**

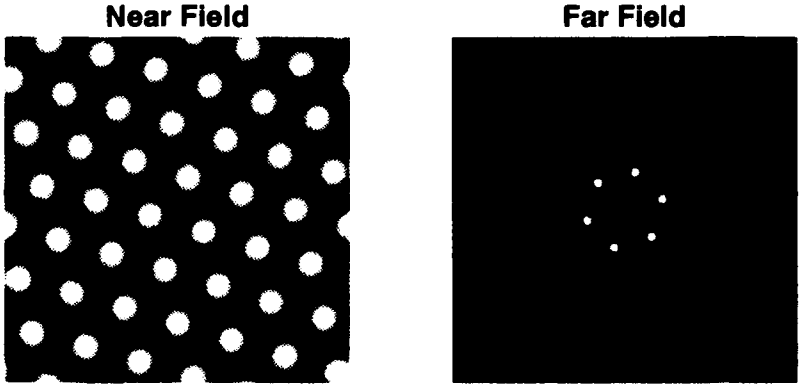


**Figure 2**

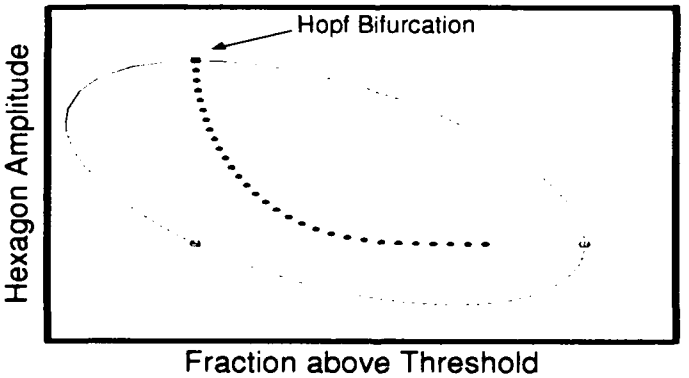


**Figure 3**

Wednesday, June 24, 1992

# Spatial Pattern Formation and Dynamics 3

**WC** 4:00pm–5:20pm
Schroedinger Hall

Robert G. Harrison, *Presider*
*Heriot-Watt University, United Kingdom*

# Interference and Dislocation Patterns in Linear Waves

Michael Berry
Wills Physics Laboratory
United Kingdom

Phase singularities (dislocations and disclinations) are generic in waves, linear or not, and occur in light, sound, microwaves, quantum waves and the tides. They are complementary to the caustic singularities of geometrical optics.

# Pattern Formation, Pattern Recognition, and Associative Memory

H. Haken
Institut für Theoretische Physik und Synergetik
Universität Stuttgart
Pfaffenwaldring 57
7000 Stuttgart 80

Spatial and temporal patterns can be spontaneously formed in a variety of systems treated in physics, chemistry, biology and other disciplines. Such patterns may be coherent oscillations in the laser and their interactions with each other, spatio-temporal patterns in fluids, chemical reactions and a great variety of morphogenetic processes in biology.

The interdisciplinary field of synergetics has shown that in large classes of systems pattern formation obeys the same basic principles irrespective of the nature of the individual components. When an open system that is controlled by one or several control parameters such as the power input into laser, reaches an instability point, its dynamics is governed by few degrees of freedom, the order parameters, that govern the behavior of the individual parts of the system by means of the slaving principle of synergetics. Order parameters may compete or cooperate which leads to different kinds of a spatio-temporal behavior of the system. Examples for competion and cooperation are provided from laser physics and fluid dynamics.

So far, the formation of patterns was studied for a given system. The question arises whether we can devise systems, which form specific wanted patterns by their internal dynamics. Using the concept that pattern recognition is pattern formation we show how such systems may be constructed and implemented as a program on a conventional computer. It will be shown how such an algorithm acts as associative memory and a number of examples for recognition tasks will be given. Possible analogue computer realisations by lasers and solid-state devices will be discussed.

Thursday, June 25, 1992

# Semiconductor Device Dynamics

**ThA** 8:20am–10:40am
Schroedinger Hall

Daan Lenstra, *Presider*
*Amsterdam Free University, The Netherlands*

# Polarization Bistability in Laser Diodes

Hitoshi Kawaguchi, Tomoyoshi Irie, and Naohiro Tan-no
Faculty of Engineering, Yamagata University
4-3-16, Jonan, Yonezawa-shi, Yamagata 992, JAPAN
Tel: +81-238-22-5181, Fax: +81-238-24-2752

## Introduction

Bistable laser diodes (BLDs) are expected to be key components in future optical communication and switching systems, because of the advantage in providing inherent optical gain. Several kinds of BLDs have been developed thus far [1]. One of the most important remaining problems with such devices is their limited switching speed and repetition rates.

In this paper a rate equation simulation is carried out to demonstrate a new from of pitchfork polarization bistability which has significantly different properties from the conventional hysteresis form of bistability. The simulation shows that the occurence of each form of bistability depends on the strength of the polarization self- and cross-saturation. The theory also shows that pitchfork bifurcation bistability allows switching at high rates. This is attributed to two causes: (1) the switching can be obtained by using only ON switching with optical trigger pulses and (2) switching speed can be increased by the high bias current ($I_b >> I_{th}$) as is expected in direct intensity modulation of LDs. Experiments are in progress to investigate such ultrafast switching. We have observed clear polarization bistability by using a novel configuration in which the TE and TM mode gain are balanced.

## Numerical Model and Results

We analyze the behavior of polarization bistability in LDs using the following equations [2].

$$\frac{dn}{dt} = P - \frac{n}{\tau_s} - v_g\, g(n)\,(1 - \varepsilon_{EE} S_E - \varepsilon_{EM} S_M)\, S_E - v_g\, g(n)\,(1 - \varepsilon_{ME} S_E - \varepsilon_{MM} S_M)\, S_M \quad (1)$$

$$\frac{dS_E}{dt} = v_g \Gamma_E\, g(n)\,(1 - \varepsilon_{EE} S_E - \varepsilon_{EM} S_M)\, S_E - \frac{S_E}{\tau_{pE}} + \beta B n^2 \quad (2)$$

$$\frac{dS_M}{dt} = v_g \Gamma_M\, g(n)\,(1 - \varepsilon_{ME} S_E - \varepsilon_{MM} S_M)\, S_M - \frac{S_M}{\tau_{pM}} + \beta B n^2 \quad (3)$$

Here $S_E$ and $S_M$ are the photon densities of TE and TM modes, respectively. $\varepsilon_{EE}$ and $\varepsilon_{MM}$ are the contributions to self-saturation, and $\varepsilon_{EM}$ and $\varepsilon_{ME}$ are those to cross-saturation from the nonlinear gain. When the coherent optical signal $S_{iE/M}$ at a wavelength within the injection locking band is injected into the BLD, the term $\sqrt{S_{E/M}\,\eta\, S_{iE/M}} / \tau_{pE/M}$ is added in Equation (2) or (3) depending on its polarization. Here, $\eta$ is the coupling coefficient.

TE/TM polarization bistability is found under the following conditions: (i) coexistence probability for both the TE and the TM modes and (ii) mutual coupling of both modes via gain saturation. Bistability occurs if $\varepsilon_{ME}\,\varepsilon_{EM} > \varepsilon_{EE}\,\varepsilon_{MM}$. From the calculations, taking into account the intra-band relaxation processes, the following relations can be expected: $\varepsilon_{ME} = \varepsilon_{EM} = 2\,\varepsilon_{EE} = 2\,\varepsilon_{MM}$ [3,4]. The enhancement of the cross-saturation effect can be expected owing to additional effects such as transverse-mode deformation or polarization-dependent saturable loss[5,6].

Figure 1 shows the computed variations in photon density against the excitation rate using following values: in (a), $\varepsilon_{EE} = \varepsilon_{MM} = 7\times10^{-18}$ [cm$^3$], $\varepsilon_{EM} = 6\times10^{-17}$ [cm$^3$], $\varepsilon_{ME} = 1.4\times10^{-17}$ [cm$^3$], $\Gamma_E = 0.15$, $\Gamma_M = 0.158$, $\tau_{pE} = 3\times10^{-12}$ [s], and $\tau_{pM} = 2.838\times10^{-12}$ [s], and in (b) $\varepsilon_{EE} = \varepsilon_{MM} = 1\times10^{-7}$ [cm$^3$], $\varepsilon_{EM} = \varepsilon_{ME} = 2\times10^{-7}$ [cm$^3$], $\Gamma_E = 0.15$, $\Gamma_M = 0.1505$, $\tau_{pE} = 3\times10^{-12}$ [s], and $\tau_{pM} = 2.989\times10^{-12}$ [s]. Other parameters for both cases are the same. In order to attain hysteresis like bistability (Fig. 1(a)) an enhanced cross-saturation effect is included. However only the intraband relaxation processes need to be taken into account to allow the demonstration of bifurucation-like bistability (Fig. 1(b)). In this case, as the pump rate is increased from zero, the solutions of the outputs of TE and TM polarization bifurcate at the critical point, and form Branch A. Branch B is obtained by injection of a coherent optical trigger input with TM polarization at the appropriate bias pump rate.

Ultrafast all-optical flip-flop operation is realized at a rate of 50 Gb/s as shown in Fig.2 With the system parameters the same as those used for Fig.1(b), the BLD is biased in the regime of the bifurcated solution, and trigger pulses, with either TE or TM polarization, are injected. The pump rate P is set at 26 x $P_{th}$ ($P_{th}$ is the threshold pump rate), $\eta = 1$, and $S_{iE} = S_{iM} = S_E(P=26\times P_{th})$.

## Experiment

We have used a T-shaped two-armed cavity configuration as shown in Fig.3. A 1.3 μm InGaAsP buried heterostructure LD is AR coated on one facet. The optical loss of the TE mode cavity is changed by the variable attenuator. We can adjust the oscillation wavelengths for TE and TM modes by the gratings independently.

The current versus light output (I-L) curves for TE and TM modes were straight lines above the threshold when one arm was cut off. When both arms were coupled simultaneously, the I-L curves were drastically changed (Fig.4). Polalization switching from TE to TM occured at the point A which coincided with the anti-phase condition for the LD chip cavity and the external cavity of the TE mode. Although this system does not include any additional enhanced cross-saturation effect, the I-L curve shows clear bistable characteristics. We have observed almost complete bistable ON-OFF switching for both TE and TM modes with increasing the optical loss of the TE arm.

Another interesting bistable characteristic was observed. At the current grater than the point A in Fig.4, the TE output changed to the upper branch, when the TM arm was cut off. And then the output stayed on the upper branch even when the TM arm was recoupled (Fig.5). Polarization switching from TE to TM occurred repeatedly with increasing the current as shown in Fig.5. These results suggest that the system shows pitch-fork like polarization bistability.

## Conclusion

This paper reports ultrfast all-optical flip-flop operation in new pitchfork bifurcation like polarization bistability in LDs. We believe that this theoretical approach taken here is also applicable for bistable switching between longitudinal modes in LDs. We have observed clear polarization bistable switching by using a T-shaped two-armed cavity configuration.

## REFERENCES

[1] for example, H.Kawaguchi, Opt.Quantum Electron., 19(1987)S1.
[2] H. Kawaguchi, I.H.White, M.J.Offside, and J.E.Carroll, Opt. Lett., 17(1992)130.
[3] M.Yamada, IEEE J. Quantum Electron., QE-19 (1983)1365.
[4] B.M.Yu and J.M.Liu, J. Appl. Phys., 69(1991)7444.
[5] B.Rheinlander et al, Opt.Comm.80 (1991)259.
[6] Y.Ozeki and C.L.Tang, Appl. Phys. Lett., 58(1991)2214.

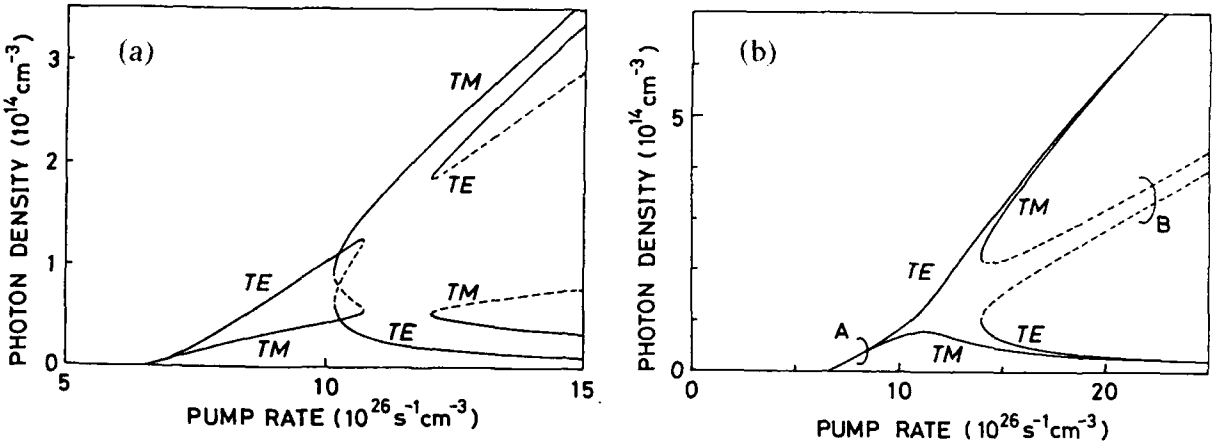


Fig.1 Photon density against excitation rate.

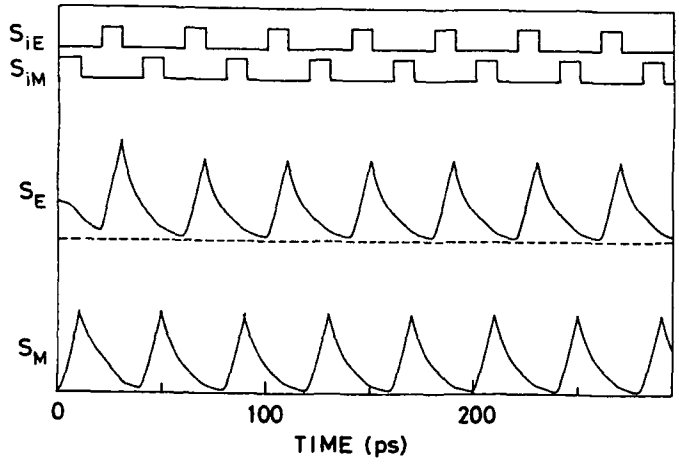


Fig.2 Flip-flop operation in pitchfork bifurcation-like polarization bistability.

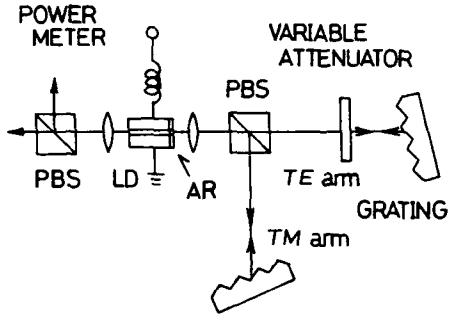


Fig.3 Experimental setup.

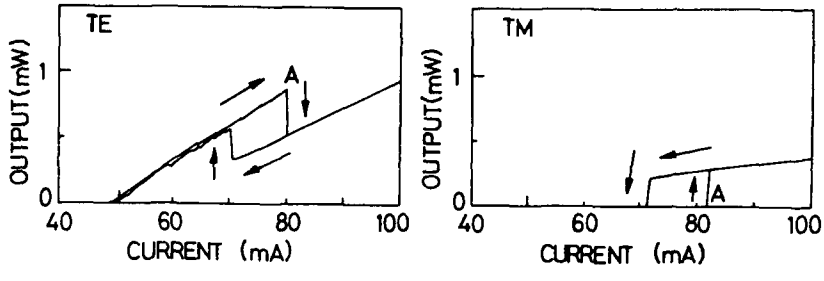


Fig.4 Observed current versus light output curves.

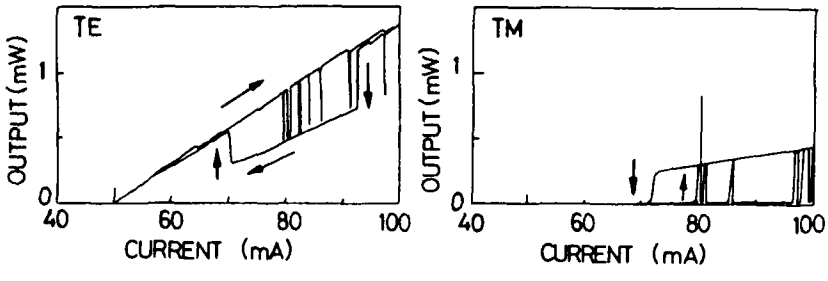


Fig.5 Observed current versus light output curves. TM arm was cut off, and then recoupled.

# Polarization Mode Switching and Bistability in Semiconductor Lasers

A.Klehr, A.Bärwolff, G.Berger, R.Müller and M.Voß

Institut für Nichtlineare Optik und Kurzzeitspektroskopie
O-1199 Berlin, Rudower Chaussee 5, Germany, Phone: 6704 3963

Generally, TE-mode emission (the transverse electric field is polarized parallel to the active-layer plane) is favored in unstrained semiconductor lasers in comparison with TM-mode emission (the magnetic field is polarized parallel to the active-layer plane) due to a larger reflectivity for the TE wave at the cleaved facets forming the laser cavity. The optical gain delivered from the active medium is the same for both modes, i. e., $g_{TE} = g_{TM} = g$ given by $g = A\ (N - N_0)$ where A is the gain coefficient, N is the carrier density, and $N_0$ denotes the carrier density required to achieve transparency, $g = 0$.
However, tensile biaxial strain in the active layer plane as caused by a lattice misfit between the active and the cladding layers may increase the optical gain for the TM mode and, simultaneously, decrease that for the TE mode according to a change in the structure of light-and heavy-hole bands of the active medium, e. g. /1/, expressed by the relations $A_{TM} > A_{TE}$ and $N_{0TM} < N_{0TE}$. Hence the effective (small-signal) gain for TM emission, defined as the difference between optical gain and loss, may approach and, finally, exceed that for TE emission provided that N becomes sufficiently large. Then mode switching from TE to TM may be initiated by several mechanisms such as nonlinear gain suppression, /2/, and lateral waveguiding effects, /3/, see below.

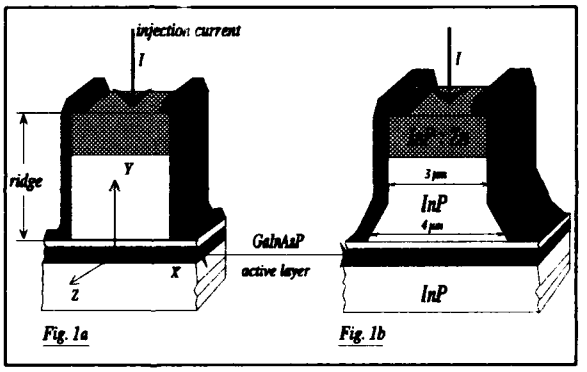


Fig. 1a Fig. 1b

This paper presents experimental and theoretical results of TE-TM mode switching and bistability in InGaAsP/InP ridge-waveguide (RW-) lasers with lasing wavelength at 1.3 $\mu$m. Besides RW-lasers with commonly used ridges of rectangular cross section, Fig. 1a, also lasers with "waist shape" ridges have been employed in our experiments. These ridges consist of a trapezoidal bottom part and a rectangular top part, see Fig. 1b. The z-axis in Figs. 1a,b points to the direction of light wave propagation in the laser. We have found that lasers with waist shape

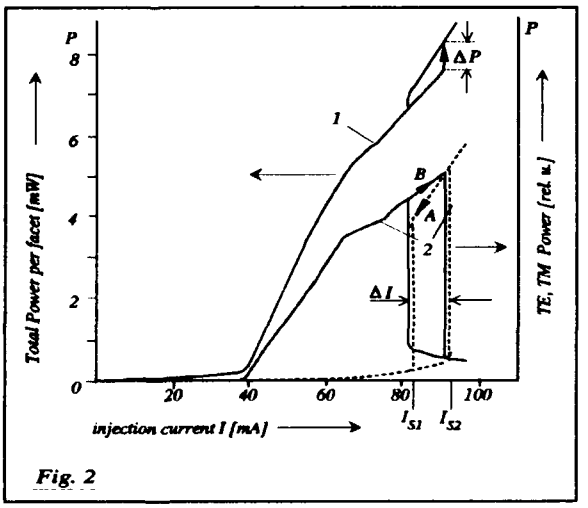


Fig. 2

ridges exhibit TE-TM switching and bistability at room temperature whereas lasers with rectangular ridges do not.

Fig. 2 shows the measured light power-current characteristics for the total output power per facet, curve (1), and for the output power of the TE (full line) and TM (dashed line) modes, curve (2) . Lasing starts at about 39 mA in the TE mode. The polarization of the emitted radiation changes abruptly from TE to TM at switching current $I_{S2}$ connected with an increase of the total output power, $\Delta P$.

Above $I_{S2}$ stable TM emission was found. With decreasing injection current the polarization flipped back from TM to TE at $I_{S1}$. The width of the hysteresis, $\Delta I$, is about 10 mA, see Fig.2.

The switching dynamics have been investigated by means of injection current modulation with modulation frequencies up to 900 MHz. As can be seen from Fig. 3a a switching time of about 50 ps is found being the shortest switching time between polarization modes of a laser measured so far, /4/. Fig. 3b shows alternating TE- and TM-mode emission in the case of 500 MHz current modulation indicating stable TE/TM modulation of laser radiation.

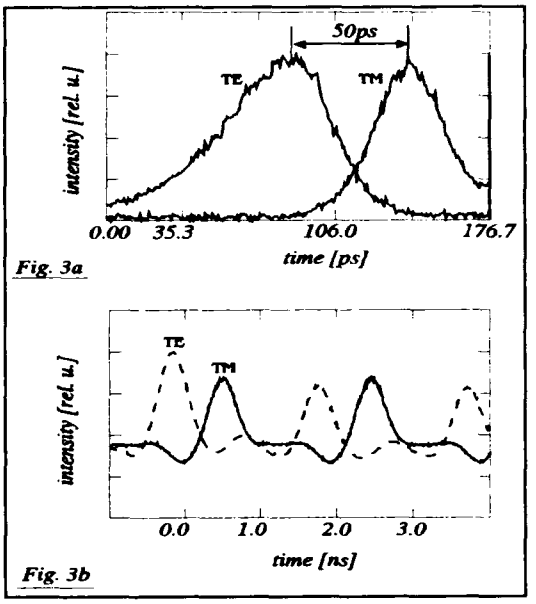

Fig. 3a

Fig. 3b

Also respective theoretical investigations have been carried through. In particular, the lateral behavior (i.e., along the x-axis, see Fig.1) of the refractive index has been studied from which it may be deduced that lateral waveguiding of the TM mode, as compared with the TE mode, is relatively more effective

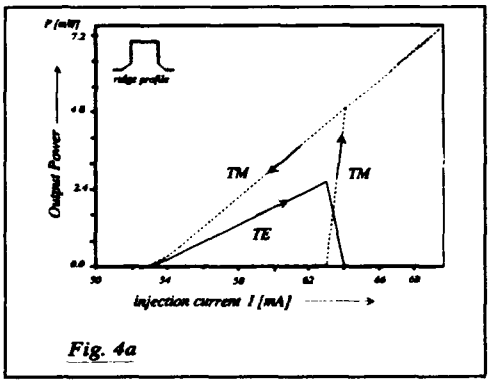

Fig. 4a

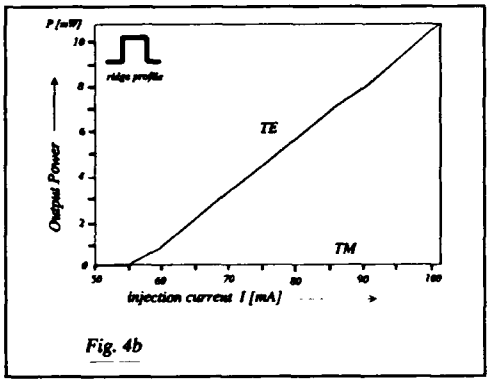

Fig. 4b

in lasers with a waist shape ridge than in lasers having a rectangular ridge. Furthermore, the light power of TE and TM mode has been calculated for both types of lasers at various parameter values. As an example Figs 4a,b represent the steady-state TE and TM output power versus injection current, where the following parameter values have been used:

$A_{TE} = 2.0 \times 10^{-16} cm^2$, $A_{TM} = 2.6 \times 10^{-16} cm^2$, and $N_{0TE} = N_{0TM} = 1.0 \times 10^{18} cm^{-3}$ .

The numerical calculations are based on the beam-propagation method (BPM) considering

the longitudinal (along the z-axis) and lateral distributions of carrier density and complex field amplitudes of the TE, TM modes in the active-layer plane. From Figs. 4a,b it follows that, in agreement with the experiments, TE-TM switching and bistability is obtained for the laser with a waist shape ridge, Fig. 4a, while the laser with an assumed rectangular ridge, Fig. 4b, exhibits only TE-mode emission.
The aforementioned switching between TE- and TM-mode emission can be explained as follows:
Due to a smaller cavity loss the TE mode reaches the laser threshold first. In lasers with a rectangular ridge a strong depletion of carrier density prevents the onset of TM-mode lasing. By contrast, carrier depletion is smaller in diodes with a waist shape ridge because of a worse lateral confinement of the TE mode. In this case the TE mode is not able to prevent TM- mode emission when the injection current reaches a certain value. Detailed numerical calculations show that the onset of TM emission leads to a change of the lateral carrier behavior accompanied by a respective change in the index of refraction which gives rise to a stronger curvature of the lateral phase fronts of the TE mode. This, in turn, causes a further decrease in TE confinement resulting in the suppression of TE-mode emission by the TM mode.

References:

/1/ T.C. Chong and C.G. Fonstad
IEEE J. Quantum Electron., QE 25, 1989, 171

/2/ B.M. Yu and J.M. Liu
J. Appl. Phys. 69, 1991, 7444

/3/ M.C. Amann and B. Stegmüller
J. Appl. Phys. 63, 1988, 1824

/4/ A. Klehr, A. Bärwolff, R. Müller, M. Voß, J. Sacher, W. Elsässer and E.O. Göbel
Electron. Lett., 27, 1991, 1680

# Transition in the coherence collapse of semiconductor lasers with external optical feedback: Two types of low frequency fluctuations

J.Sacher, W.Elsäßer and E.O.Göbel

Fachbereich Physik der Philipps Universität Marburg

Renthof 5, D–3550 Marburg, Germany

Phone: ..49 6421 282401

FAX: ..49 6421 284239

Semiconductor laser diodes with external optical feedback (EOFSL) have found considerable interest within the last 10 years /1–6/. This is due to the practical importance of this system as well as the EOFSL can serve as a model system for the investigation of the dynamics of nonlinear systems with countable infinite dimensions. EOFSL exhibit drastic changes in the output behavior for specific values of the operation parameters, especially a coherence collapse of the laser output can be found /1/. Experiments and numerical simulations have explained these changes by a quasiperiodic route to chaos for the variation of the feedback level /2/ as well as by an intermittency route /3/ for the variation of the injection current.

In the present contribution, we analyze the regime of the intermittency. For the relevant parameter regime the time evolution of the light intensity (Fig.1) shows typical break down events and a subsequent relaxation process. These break down events are called low frequency fluctuations (LFF) because their frequency is small in comparison to the external cavity resonance frequency. We have found a transition and a coexisting regime of two different types of LFF (Fig.2) characterized by the dependance of this characteristic frequency on the injection current. On the base of these data and the data shown in Fig.1, we

propose the coexistence of two different kinds of LFF (type I and type II LFF). The Type I LFF are charcterized by intermittant break downs of the light intensity /3–5/ while the characteristic frequency of the type II LFF is determined by the relaxation oscillations of the external cavity semiconductor laser /4,6/.

In the present contribution we will report on investigations of the transition regime between the two types of LFF (Fig.2) in order to study its dynamical origin. For this purpose we have characterised the attractors belonging to type I and type II LFF by evaluation of their correlation dimensions. We find a correlation dimension of about 11 for type I LFF and between 5 and 6 for type II LFF. Consequently, the system undergoes a transition between ultra–high dimensional motion ($C_2 \sim 11$) and a high dimensional attractor ($5 < C_2 < 6$). The transition itself is interpreted as a subharmonic bifurcation with irregular switching between the two branches of the corresponding hysteresis.

**References**

/1/ R.W.Tkach and A.R.Chraplyvy, J. Lightwave Technol. **LT–4**, 1655 (1986)

/2/ J.Mørk, J.Mark, and B.Tromborg, Phys. Rev. Lett. **65**, 1999 (1990)

/3/ J.Sacher, W.Elsässer, and E.O.Göbel, Phys. Rev. Lett. **63**, 2224 (1989)

/4/ J.Sacher, W.Elsässer, and E.O.Göbel, EQEC 1991, Edinburg

/5/ J.Mørk, B.Tromborg, P.L.Christansen, IEEE J.Quant. Electron. **QE–24**, 123 (1988)

/6/ J.Sacher, W.Elsässer, and E.O.Göbel, IEEE J.Quant. Electron. **QE–27**, 373 (1991)

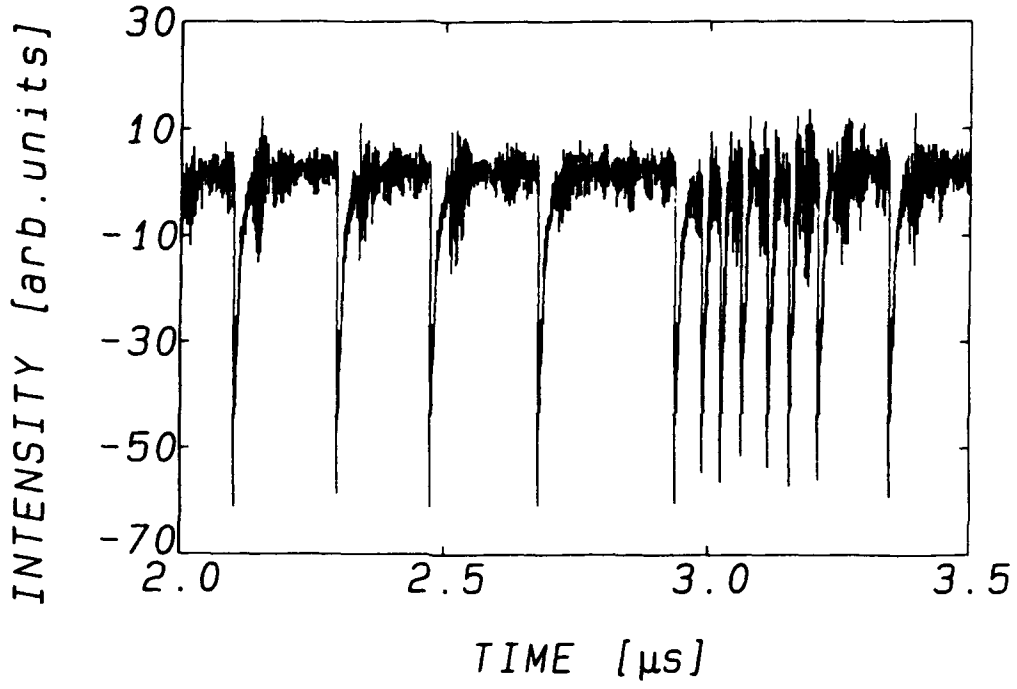


**Fig.1** Oscilloscope trace of the time evolution of the emitted light intensity in the coexistence regime of both types of LFF.

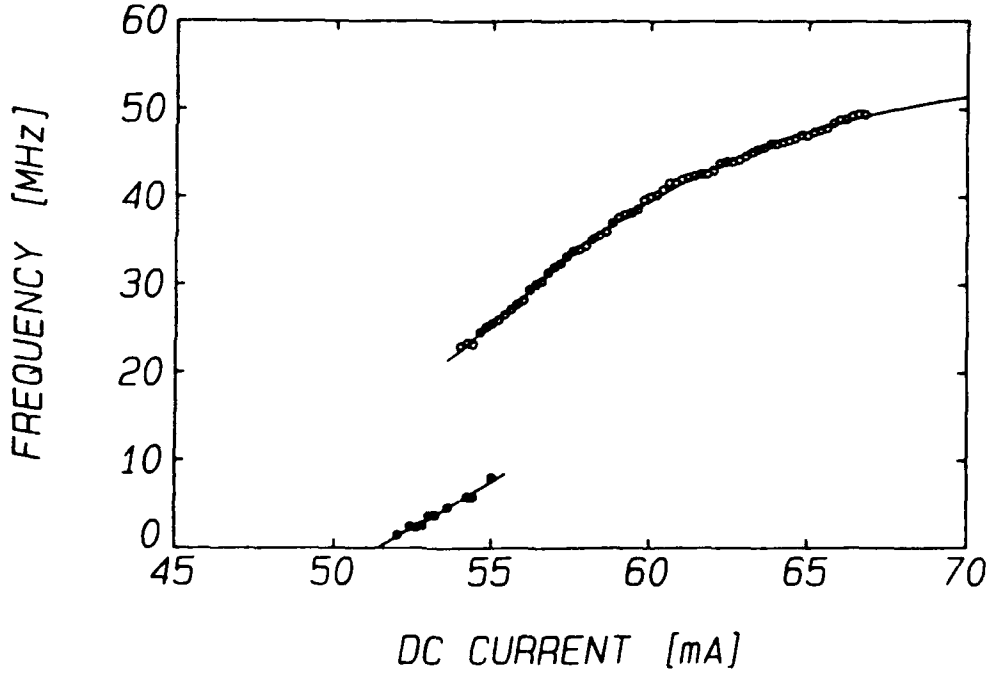


**Fig.2** Characteristic fluctuation frequency as a function of current. Type I LFF are observed for low currents, whereas for higher currents type II LFF occur. The transition regime is around 55 mA.

# Dynamic Instability in Delay-Coupled Semiconductor Lasers

David J. Bossert and Richard K. DeFreez
Department of Applied Physics and Electrical Engineering
Oregon Graduate Institute of Science and Technology
19600 N.W. Von Neumann Drive, Beaverton, OR 97006, (503) 690-1121

Gregory C. Dente, G.C.D. Associates
2100 Alvarado NE, Albuquerque, NM 87110 (505) 268-8337

Herbert G. Winful
Department of Electrical Engineering and Computer Science
University of Michigan, Ann Arbor, MI 48109-2122, (313)747-1804

Although semiconductor lasers are inherently large-linewidth and low-power devices, these limitations can be overcome by coupling their output to another laser or resonator. A coupling delay, however, is known to cause an extreme loss of coherence for a self-coupled diode laser above a critical coupling level.[1] Unstable operation has also been observed recently in a system of two semiconductor lasers mutually coupled at a distance,[2] a phenomenon referred to as *overcoupling*. In this paper, systematic spectral and coherence measurements are described for a single, self-coupled diode laser and two mutually coupled lasers, demonstrating extreme dynamic instability at moderate coupling levels.

Fig. 1 displays the optical spectrum of a CSP diode laser with feedback from an external reflector 40 cm away. The vertically displaced traces represent increasing levels of coupling, in which $\varepsilon^2$ denotes the fraction of power transmitted one way through the coupling region. Stable operation is interrupted above a critical coupling level, manifesting in spectral broadening and a reduced coherence length, a phenomenon known as *coherence collapse*. Sidebands, separated from the carrier by the relaxation resonance frequency are clearly visible, while the spectrum pulls to low frequencies at stronger coupling levels. Numerical simulations, based on coherent rate equations, account for all these features. It is now generally accepted that the coherence collapse represents a state of deterministic chaos.

While coherence collapse is well documented, we found that mutually coupled diode lasers exhibit similar spectral broadening and reduced mutual coherence. Here, in order to quantify the degree of phase-locking, the laser outputs were interfered. The depth of modulation (visibility) of the resulting fringe pattern measured the mutual coherence between the lasers. The phase of the optical interaction was controlled by varying the laser separation in fractions of a wavelength. In Fig. 2, error bars indicate the extremes in recorded visibility at a given coupling level for two mutually coupled TJS diode lasers separated by 45 cm. Relatively high visibilities are obtained at extremely small coupling levels, indicating that a substantial degree of coherence has been established. Below $\varepsilon^2 = -60$ dB, maximum visibilities are limited by spontaneous emission noise, while the large variation is a result of mode hopping. High quality phase-locks, independent of $\omega_o\tau$, are confined to a $\approx 10$ dB "window" near $\varepsilon^2 = -50$ dB. Dynamic instability rapidly degrades this highly coherent state,

for $\varepsilon^2$ larger than -50 dB. The drop in visibility is accompanied by spectral broadening similar to Fig. 1.

The unstable operation is well accounted for by single-longitudinal-mode coupled rate equations describing the time evolution of the slowly-varying complex electric field amplitude $E$ and carrier number $N$ in each laser cavity:

$$\frac{dE_j(t)}{dt} = \frac{1}{2}\left[\left(G(N_j,P_j) - \frac{1}{\tau_p}\right) + i\alpha\frac{\partial G}{\partial N}\Delta N_j\right]E_j(t) + \kappa E_k(t-\tau)\exp(-i\omega_o\tau) + E_{sp}(t) \qquad (1)$$

$$\frac{dN_j(t)}{dt} = J_j - \frac{N_j(t)}{\tau_s} - G(N_j,P_j)P_j(t) \qquad j \neq k = 1,2. \qquad (2)$$

where the absolute squared value of the electric field amplitude gives the total number of photons, $P_j$, in the lasing mode. $J_j$ denotes the pumping rate, $G$ is the stimulated emission rate and $\Delta N_j \equiv N_j - N_{th}$ is the deviation in carrier number from threshold. The lasers are taken to be identical, characterized by photon lifetime $\tau_p$, carrier lifetime $\tau_s$, free-running angular oscillation frequency $\omega_o$ and linewidth enhancement parameter $\alpha$. $\tau$ is the coupling delay and $E_{sp}$ describes spontaneous emission noise. The coupling coefficient $\kappa$ is related to $\varepsilon$ by

$$\kappa = \frac{1}{\tau_D}\frac{(1-R)}{\sqrt{R}}\varepsilon \qquad (3)$$

where $\tau_D$ is the round-trip time in the diode laser, and $R$ is the power reflectance of the output facet. Parameters necessary for the preceding model were measured for the experimental lasers; those of a ML5101a TJS device are compiled in Table I.

Fig. 3 compares numerical simulations of overcoupling to the data in Fig. 2. Visibilities, at selected $\omega_o\tau$, were determined via time series integrated from rate equations (1) and (2). The rapid decline in mutual coherence is well represented. With $\alpha = 0$, however, the visibility was found to remain higher than 0.9 for all coupling levels shown in Fig. 3. Stability analysis of the rate equations has shown that the collapse in mutual coherence is initiated by the system's inability to damp relaxation oscillations due to the optical coupling, although the full nonlinear rate equations are necessary to predict the severity of instability. Note that the lasers are truly incoherent only near $\varepsilon^2 = -30$ dB. (Experiment does not indicate the partial recovery in coherence above -30 dB, due to the emergence of multiple longitudinal diode modes.) Time series have indicated that in regions of partial coherence the system undergoes rapid transitions between its stable states. Below -30 dB, these transitions predominantly occur between modes which minimize fluctuations in the phase difference between the lasers, while above this level the dominant modes possess the minimum threshold gain. The latter modes oscillate at frequencies negatively detuned from $\omega_o$, explaining the frequency pulling in Fig. 1. Collapse in coherence is interpreted as a transition between these distinct stability regions.

The authors gratefully acknowledge the support of the Air Force Office of Scientific Research and the National Science Foundation.

## References


1. D. Lenstra, B. H. Verbeek and A. J. Den Boef, "Coherence collapse in single-mode semiconductor lasers due to optical feedback," *IEEE J. Quantum Electron.*, QE-21, pp. 674-679, June 1985.
2. G. C. Dente, C. E. Moeller and P. S. Durkin, "Coupled oscillators at a distance: applications to coupled semiconductor lasers," *IEEE J. Quantum Electron.*, vol. 26, pp. 1014-1022, June 1990.


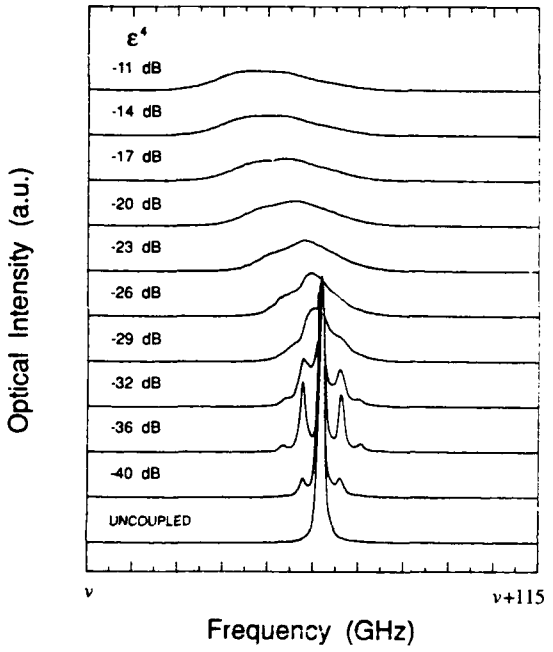


**Figure 1**

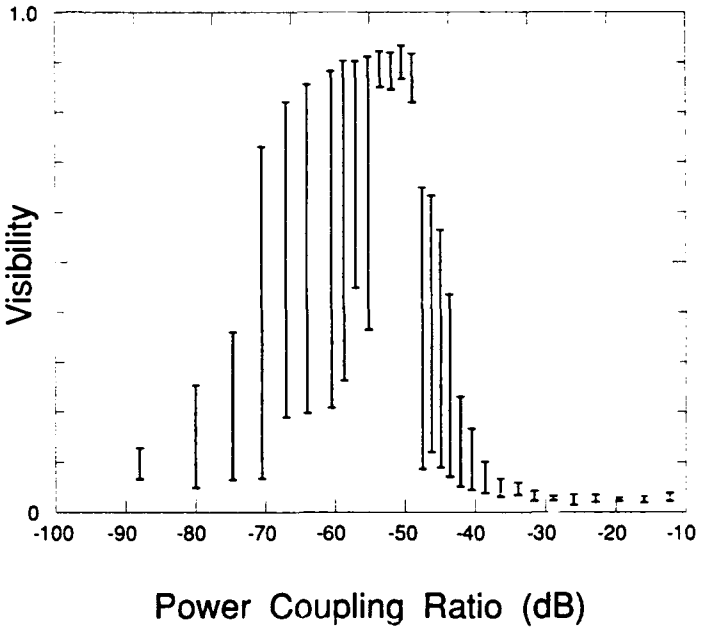


**Figure 2**

| Parameter | Symbol | Value |
|---|---|---|
| Output power (front facet) | - | 7 mW |
| Relaxation resonance frequency | - | 3.8 GHz |
| Round-trip time in laser cavity | $\tau_p$ | 8.7 ps |
| Modal gain derivative | $\partial G/\partial N$ | $6.1\times10^{4}\ s^{-1}$ |
| Photon lifetime | $\tau_p$ | 1.1 ps |
| Carrier lifetime | $\tau_s$ | 1.7 ns |
| Linewidth enhancement parameter | $\alpha$ | 2.7 |
| Spontaneous emission rate | - | $2.5\times10^{12}\ s^{-1}$ |
| Gain compression coefficient $G(N_j,P_j)=G_L(N_j)(1-\beta P_j)$ | $\beta$ | $6.8\times10^{-8}$ |

TABLE I
ML5101a TJS Laser Parameters

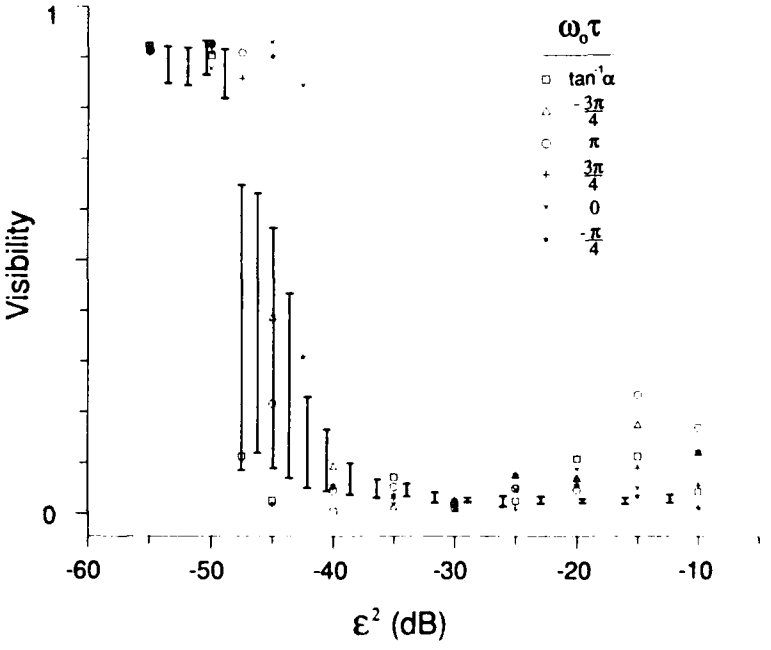


**Figure 3**

# The modulated semiconductor laser: a Hamiltonian search for its periodic attractors

P. C. De Jagher
and
D. Lenstra

Vrije Universiteit, De Boelelaan 1081, 1081 HV Amsterdam, The Netherlands.
Tel: +31 20 5484498; FAX: +31 20 6461459; E-mail: pdj@nat.vu.nl

February 20, 1992

Modulated lasers have been investigated for over a decade now, c.f. *ref.* [3] and references cited therein. Periodic as well as chaotic types of operation have been observed. In this paper we put forward a mathematical technique to calculate lower and upper bounds for the modulation strength which is needed to sustain a periodic large amplitude output.

A simple set of rate equations for a modulated laser is given by

$$\frac{dn}{dt} = -\lambda_n n - (\lambda_c + \xi(n - n_0))S + J_0 + J_1(t)\,, \tag{1}$$

$$\frac{dS}{dt} = \xi(n - n_0)S\,, \tag{2}$$

where $n$ is the inversion density, $\lambda_n$ and $\lambda_c$ are the reciprocal inversion- and photon decay times, $\xi$ is the gain coefficient, $S$ is the photon-density, $J_0$ and $J_1$ are the dc- and the time-dependent component if the injection current, and $n_0$ is the stationary inversion density. The stationary photon density $S_0$, $S_0 = (J_0 - \lambda_n n_0)/\lambda_c$, the stationary inversion density, and the relaxation-oscillation frequency $\omega_R$, $\omega_R = \sqrt{S_0 \lambda_c \xi}$, are used to rescale the rate equations by introducing $\hat{S}$, $\hat{n}$, and $t'$ according to $\hat{S} = S/S_0$, $\hat{n} = \frac{\xi n_0}{\omega_R}\frac{n-n_0}{n_0}$, and $t' = \omega_R t$. Doing so, we obtain:

$$\dot{\hat{n}} = -2\gamma_R \hat{n} - \beta \hat{n}(\hat{S} - 1) - (\hat{S} - 1) + \hat{J}_1(t') \tag{3}$$

$$\dot{\hat{S}} = \hat{n}\hat{S}\,, \tag{4}$$

where the dot denotes the operator $\frac{d}{dt'}$. Further we introduced $\beta$, $\gamma_R$, and $\hat{J}_1$: $\beta = \frac{\omega_R}{\lambda_c}$, $2\gamma_R = \frac{\lambda_n}{\omega_R} + \beta$, and $\hat{J}_1(t') = \frac{\xi J_1(t'/\omega_R)}{{\omega_R}^2} = \frac{J_1}{J_0 - \lambda_n n_0}$.

In order to see the structure of (3) and (4) somewhat better we transform them to the variables $\sigma$ and $\nu$ which are given by $\sigma = \log \hat{S}$, and $\nu = \frac{1}{\beta} \log(\beta \hat{n} + 1)$. This leads to

$$\dot{\sigma} = \frac{1}{\beta}(e^{\beta\nu} - 1)\,, \tag{5}$$

$$\dot{\nu} = -(e^{\sigma} - 1) + \hat{J}_1 - (2\gamma_R + \beta \hat{J}_1)\frac{1 - e^{-\beta\nu}}{\beta}\,. \tag{6}$$

Obviously, eq.(5) and (6) are the equations of motion for a damped, driven, nonlinear oscillator. The nonlinear oscillation itself is given by the Hamiltonian $\mathcal{H}(\nu,\sigma) = \beta^{-2}(e^{\beta\nu} - \beta\nu - 1) + (e^{\sigma} - \sigma - 1) + \sigma \hat{J}_1$. A similar observation was made in *ref* [1]. However our Hamiltonian is more general: one easily sees that in case $\beta\nu \ll 1$ and $\hat{J}_1 = 0$, $\mathcal{H}$ can be approximated by the Hamiltonian for the Toda oscillator which was discussed in *ref*[1]. In case $\gamma_R = 0$ and $\hat{J}_1 = 0$ the solution $\sigma_E$ of (5) and (6) with period time $T_E = 2\pi/\Omega$ and initial condition $\dot{\sigma}_E = 0$ can be written as $\sigma_E = \sum_{k=-\infty}^{\infty} \sigma_k e^{ik\Omega t}$. An algorithm to calculate the $\sigma_k$ for some given value of $\Omega$ is given in *ref*[2].

Now we introduce the 'energy' $E(t')$ according to

$$E(t') = \beta^{-2}(e^{\beta\nu(t')} - \beta\nu(t') - 1) + (e^{\sigma(t')} - \sigma(t') - 1)\,, \tag{7}$$

for which one easily finds $\dot{E} = \frac{\dot{\sigma}}{1+\beta\dot{\sigma}}\{-2\gamma_R\dot{\sigma} + \hat{J}_1(t')\}$. This equation can be read as the rate of energy exchange of the oscillator due to damping and a driving force. Provided this exchange per period is small, one can use the solution $\sigma_E$ of the free running oscillator as a zeroth order trajectory in a perturbation scheme, which will give us an analytic approximation for the Poincaré mapping function.

To see how this works out we consider a periodic modulation $\hat{J}_1(t') = j_1 \cos\omega_j t'$, where $j_1$ is the modulation index. Let $\sigma_j(t')$ be a solution of (5), (6) for this $\hat{J}_1$. Since we need two initial conditions for integrating these equation, the phase space is 2-dimensional. Hence the solution for $\sigma$ and $\nu$ can be represented as a time-parameterized curve in this phase space. The interesting property is the attractor of such a trajectory, *viz.* the trajectory it approaches when $t \to \infty$. For our driven dissipative system this attractor must be either locked periodic or chaotic.

Here we will study the locked periodic attractor. The period time $T_\sigma = 2\pi/\omega_\sigma$ must be some multiple of $2\pi/\omega_j$. At the same time an integer number of output cycles is generated. If it is possible to approximate the output by an orbit of the Hamiltonian system, $T_\sigma$ must also be a multiple of $2\pi/\Omega$. So we have

$$T_\sigma = m\,2\pi/\omega_j = n\,2\pi/\Omega;\ n, m \in I\!N\,. \tag{8}$$

Instead of representing the system in the phase space $(\sigma,\nu)$, we consider successive times $t'_i$ at which $\sigma(t')$ reaches a minimum and we represent the system by the value of $E$ and the phase $\varphi_j$ of $\hat{J}_1$ at this time, *i.e.* by the points $(E = E(\sigma(t'_i)),\ \varphi_j = \omega_j t'_i)$. We are now dealing with the phase space $(E,\ \varphi_j)$ which can conveniently be used when looking for stationary orbits.

The problem we have tackled is the question under what conditions the attractor characterized by (8), with $\omega_j$, $n$, and $m$ fixed, exists. We have been able to find an answer which states that:

**There exist an upper and a lower bound for the modulation index $j_1$. Below the lower bound, the 'energy' supply is not sufficient to compensate for the dissipative losses; above the upper bound the periodic attractor becomes unstable, presumably starting a period doubling route to chaos. We have obtained expressions for these upper and lower bounds as well as for the position of the attractor in phase space.**

**In practice, when all parameters are fixed, it is possible that more than one attractor exist. So we found a new type of multistability, characterized by different values of $n$ and $m$ in (8). A numerical simulation indeed confirmed this multistable character.**

As an example of such a numerical calculation fig.1 shows three attractors in the ($\sigma$,$\nu$) plane; fig.2 displays the corresponding output. These figures were calculated for $2\gamma_R = 0.064$, $\beta = 0.035$, $\omega_j = 0.4$, and $j_1 = 0.7$.

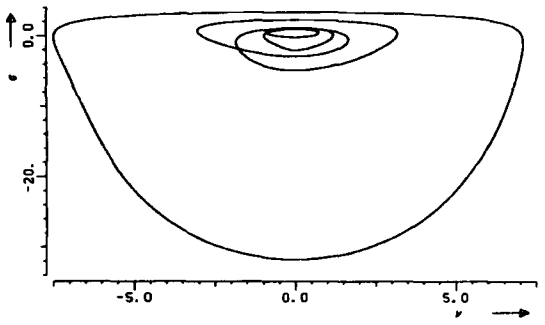


fig. 1

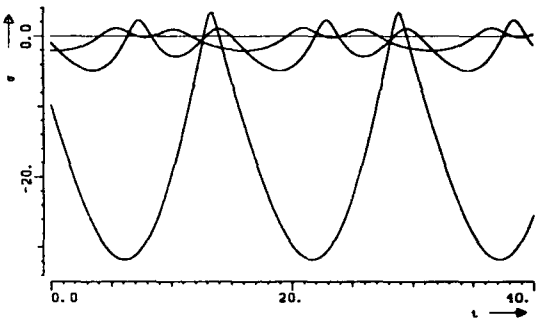


fig. 2

# References

[1] Toda potential for laser equations, G.L. Oppo and A. Politi, Z. Phys B **59** (1985) 111.

[2] The Fourier series for a "double Toda" oscillator, P.C. De Jagher, Internal Report: Quantum Electronica Dossiers, QED 1992 - 1.

[3] Dynamic behaviors of semiconductor lasers under strong sinusoidal current modulation. E. Hemery, L. Chusseau, and J.M. Lourtioz, IEEE J. Quantum Electron. **26** (1990) 633.

# CHAOS IN SEMICONDUCTOR LASERS

Hua Li , Jun Ye and John G. McInerney
Center for High Technology Materials
The University of New Mexico
Albuquerque, NM 87131, USA
Tel. (505) 277-0768

Semiconductor lasers are typical class-B lasers in which the decay rates obey $\gamma_p, \gamma \ll \gamma$ , where $\gamma_p, \gamma$ . and $\gamma$ are the decay rates of the photons, population inversion and polarization, respectively. Therefore an isolated semiconductor laser is well described by rate equations with only two independent variables (photon number and carrier population) so that chaos is not observed. Here we show two different geometries to make chaos feasible in a semiconductor laser system. The results clearly demanstrate the origin of instability in the semiconductor laser: the interaction in the nonlinear laser medium between undamped relaxation oscillation (which expresses the energy exchange between carrier population and photons) and some external modulation (which may include optical feedback).

In the first experiments we used a commercial CSP semiconductor laser (Hitachi HLP1400) with an external reflector which provides weak optical feedback (<0.1% in power) to the laser. This optical feedback modulates the carrier population N and the optical field (both intensity I and phase $\Phi$) in the laser resonator and also causes coupling between them. Using this geometry a rich variety of dynamic behavior has been observed /1,2/, but the physical basis for the instability was hitherto unclear. We show here the measured intensity noise spectrum by changing system parameters, mainly by changing feedback levels (Figs.1 and 2). For increasing feedback level the relaxation oscillation is undamped at first, then the external cavity modes are excited. Fig. 1 shows that chaos can be reached through a pure period-doubling route if the relaxation oscillation frequency $\nu_R$ remains an integer multiple of the external cavity mode spacing $\nu_{ext}$, i.e. $\nu_R=n\nu_{ext}$ (n: integer). The fundamental period corresponds to the roundtrip time of photons in the external cavity ($T=1/\nu_{ext}$). Fig.2 shows the quasiperiodic route to chaos observed when $\nu_R \neq n\nu_{ext}$. The latter situation is found more frequently in the experiment. The optical spectra are also monitored during the measurements, clearly showing symmetry breaking in the system.

Although the pure period-doubling route to chaos happens only in a narrow range of system parameters, initial period-doubling is found in quasiperiodic behavior (Fig.2), indicating that period-doubling is a fundamental process in the system. For most system parameters we see a mixture of period-doubling and quasiperiodicity, culminating in chaos.

The above experiment has been modeled theoretically /3/ using a rate equation approximation including coupling between the intensity and phase, weak feedback and gain saturation effects. The rate equations are integrated numerically to obtain the time series of the three variables $N(t),I(t),\Phi(t)$ which are further utilized to calculate the autocorrelation function, correlation dimension and other fundamental dynamical properties. Period-doubling and quasiperiodic routes to chaos are obtained in the theoretical analysis, in good agreement with the experimental measurements /4/.

The phenomena described above are easy to understand in the general context of nonlinear oscillators: the interaction of two or more modulations applied to a nonlinear oscillator can cause chaotic behavior. If the two modulation frequencies have a rational ratio, frequency locking may result and period-doubling will occur when the system symmetry is broken. Otherwise the two incommensurate modulation frequencies will beat together, and for increasing modulation depth more new frequencies corresponding to combinations of the existing frequencies will appear because of nonlinearity of the oscillator. Both processes cause chaos in the oscillator. In our laser system only one external modulation is added due to the external cavity modes, but the intrinsic relaxation oscillations are also undamped by the optical

feedback, so in effect two oscillations are applied to the laser system, and interaction between them causes the chaos.

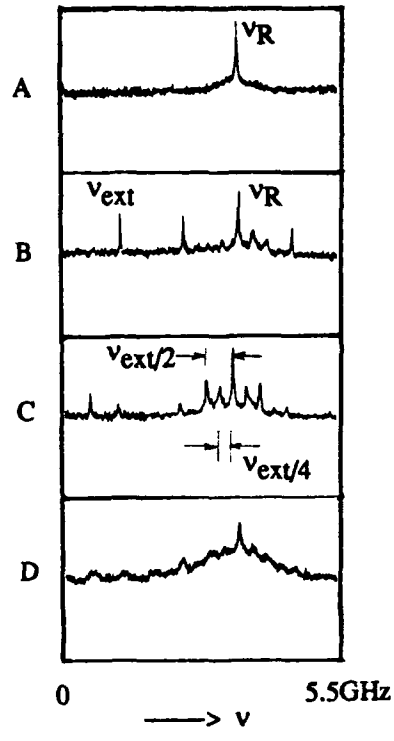


Fig.1 Measured intensity power spectra for the laser diode with an external reflector. $L_{ext} \cong 9$cm, pump current $I/I_{th} \cong 1.38$. Feedback level was increased from A to D.

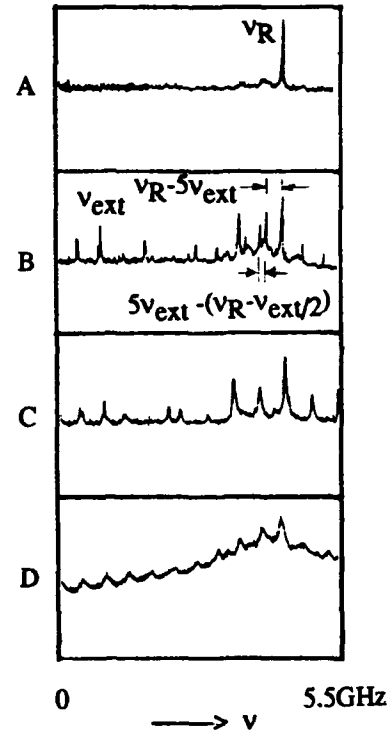


Fig.2 Measured intensity power spectra for the laser diode with an external reflector. $L_{ext} \cong 15.5$cm, pump current $I/I_{th} \cong 1.59$. Feedback level was increased from A to D.

Armed with this understanding, we set up another experiment to investigate the dynamic behavior of an anti-reflection (AR) coated semiconductor laser in an external cavity with a grating reflector. The residual reflectivity of the AR-coating on the internal facet was less than 0.1%. A solid etalon with FSR ≅ 100 GHz and finess ≅ 30 was inserted in the cavity to create strong dispersion and hence longitudinal mode selection. The external cavity mode spacing was chosen as ≅ 520MHz so that the envelope of the etalon resonance curve could include several cavity modes, therefore multi-mode behavior was possible. At first the cavity detuning was chosen so that the cavity resonance was at the center of the etalon resonance curve. In this case a single external cavity mode was obtained (Fig.3A) and maximum output power observed. As the external cavity was detuned from the center of the etalon resonance, a sharp peak at several tens of MHz appeared (marked in Fig.3 as $\nu_R$) which was accompanied by a low frequency component (marked as $\nu_1$ in Fig.3) and its harmonics. With different cavity detuning the value of $\nu_R$ was almost constant but $\nu_1$ changed, so that different ratios of $\nu_R$ to $\nu_1$ were obtained. The corresponding intensity spectra showed quasiperiodicity (Fig.3D) or period-doubling (Fig.3C). The corresponding optical spectra showed multi-mode behavior and different ansymmetries. Chaotic behavior appeared upon further cavity detuning(Fig.3E).

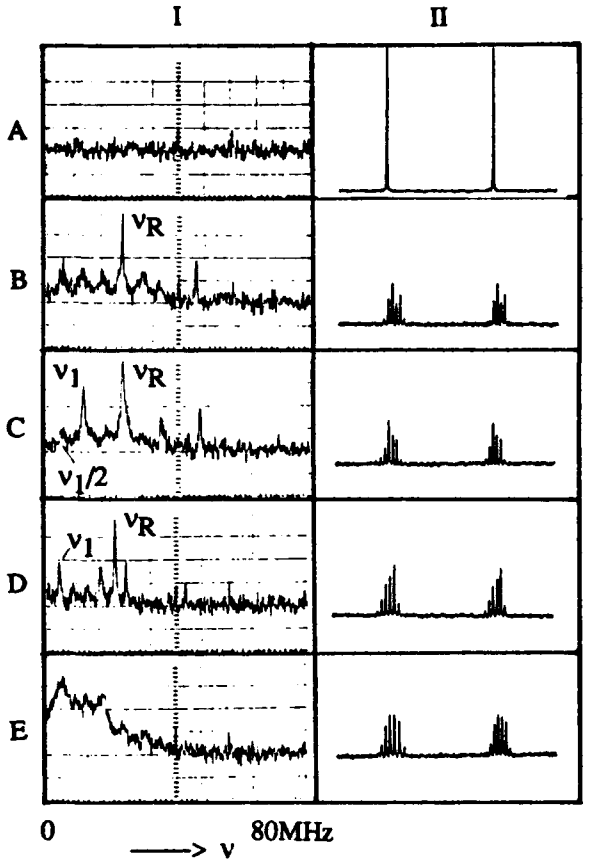


Fig.3 Measured intensity power spectra (I) and optical spectra (II) for an AR-coated laser diode in an external cavity. $L_{ext} \cong 26$cm, pump current $I/I_{th} = 1.07$. External cavity length is detuned from A to D by an amount $< \lambda/2$. Optical spectra were measured by using a plane-plane scanning F-P interferometer with FSR=11GHz and finesse>100.

In the experiments $\nu_R$ could be changed most effectively by adjusting the pump current, while $\nu_1$ could be varied mainly by setting the cavity detuning. This suggests that $\nu_R$ was the relaxation oscillation frequency of the external cavity laser, and $\nu_1$ was the beat frequency between different cavity modes; these modes had unequal mode spacings because they were located at different parts on the etalon dispersion curve. Further experimental measurements are continuing.

Both experiments agree in associated indicating strongly that the origin of instabilities in a semiconductor laser system is the interaction between undamped intrinsic relaxation oscillation and same external modulation.

References:

/1/ G. C. Dente, P. S. Durkin, K. A. Wilson and C. E. Moeller, IEEE J. Quantum Electron., QE-**24**, 2441(1988).
/2/ J. Mork, J. Mark and B. Tromborg, Phys. Rev. Lett., **65**, 1999(1990).
/3/ Jun Ye, Hua Li and John G. McInerney, Submitted to Phys. Rev. Lett..
/4/ Hua Li, Jun Ye and John G. McInerney, unpublished.

# Injection Locking of Vertical-Cavity Surface-Emitting Laser

D. Boggavarapu, J. W. Grantham, Y. Z. Hu, H. M. Gibbs, G. Khitrova, S. Koch, M. Sargent III
Optical Sciences Center
University of Arizona
Tucson, AZ 85721
phone: (602)621-2452 / fax: (602)621-4323

and

Weng W. Chow
Sandia National Laboratory, Division 2535
Albuquerque, NM 87185
phone: (505) 844-9088

Injection locking phenomena in oscillators has been studied in many laser systems (see for example [1]) including semiconductor lasers [2]. The vertical-cavity surface-emitting laser (VCSEL) provides an interesting system to investigate injection locking behavior due to its short cavity length ($\sim 1$ $\mu$m), which also results in a single lasing cavity longitudinal mode. We have studied locking dynamics in a highly noisy laser system in the strong external injection regime and observed relaxation oscillation frequency generation of up to 50 GHz.

The VCSEL is grown by molecular beam epitaxy: (100) GaAs substrate, 1 $\mu$m GaAs buffer, bottom mirror consisting of 22.5 periods of alternating quarterwave layers of AlAs and $Al_{0.127}Ga_{0.873}As$, 3$\lambda$ GaAs gain medium, top mirror consisting of 17 periods of AlAs and AlGaAs. The $\sim 0.99$ reflectances result in a single transmission peak of width $\sim 0.5$ nm within the $\sim 830$ nm to 920 nm mirror stopband. Excitation of the VCSEL was by optical pumping using a cw dye laser. The injected laser beam was produced by another cw ring dye laser frequency stabilized to $\sim 1$ MHz linewidth.

When the injection frequency approximately coincides with the peak of the VCSEL lasing and the injected power exceeds 0.06 mW, new frequencies appear labeled $I_3$ and $I_4$ in Fig. 1. The separation $\Delta\nu = \nu_{inj} - \nu_3$ between the injected frequency $\nu_{inj}$ and the new frequency $\nu_3$ varies strongly with the injected power $P_{inj}$, following $\Delta\nu(\text{GHz}) = 11.15 + 20.3\sqrt{P_{inj}(mW)}$ for $0.06 \leq P_{inj} \leq 2.7$ mW and is of similar magnitude to relaxation oscillations recently reported for a highly excited VCSEL [3]. Previous studies have reported enhanced relaxation oscillations with weak injection [4] but not of the strength or frequency separation reported here. As in other studies [4] we observe asymmetry in the locking range as the injected signal is detuned, with larger locking range on the negatively detuned side.

To understand the mechanism of the injection locking in short cavity semiconductor lasers, we have calculated power spectra and steady state properties by solving the coupled equations [5]

$$\begin{aligned}
\frac{dE}{dt} &= (g-\kappa)E + \frac{c}{2Ln(n)}tF\cos(\phi) \\
\frac{d\phi}{dt} &= \Delta + \alpha\frac{dg}{dN}\Delta N - \frac{c}{2Ln(N)}tF\sin(\phi) \\
\frac{d\Delta N}{dt} &= \Gamma - \gamma N - \frac{2gn(N)}{c}\frac{I}{\hbar\nu},
\end{aligned} \tag{1}$$

where the rate equation approximation is employed. $\alpha$ in Eq. (1) is the linewidth enhancement factor. In addition to Eq. (1), we also assumed linear dependence of the optical refractive index, $n(N)$, and the gain, $g(n)$, on the carrier density, $N$. As a first step, we obtained the steady state solutions. There exist three possible steady states for low injection intensities. However, as noted by Spencer and Lamb [5], the lower two branches of the solutions are not stable. The existence of the asymmetry for different detuning was verified in the steady state calculations.

We also integrated Eq. (1) to obtain the laser field strength $E$, and the phase $\phi$, as functions of time by using the Runge-Kutta method. Given the injection detuning frequency $\Delta$, we found that the laser emission is locked into the injection frequency if the injection intensity $F$, is larger than a certain critical intensity. $E$ and $\phi$ reached their corresponding steady state values within the time of $1/\omega_R$, where $\omega_R$ is the oscillation frequency in the absence of the injection. The Fourier transform power spectra of the injected-laser system show new frequencies other than the injection frequency or the freerunning laser frequency when the VCSEL is not in the locked state.

## REFERENCES


1. A. E. Siegman, *Lasers*, University Science Books, 1986, chapter 29.
2. R. Lang, IEEE J. Quant. Elect. **QE-18**, 976 (1982).
3. J. Lin, J.K. Gamelin, K.Y. Lau, S. Wang, M. Hong, J.P. Mannerts, Appl. Phys. Lett. **60**, 15 (1992).
4. F. Mogensen, H. Olesen, G. Jacobsen, IEEE J. Quant. Elect. **QE-21**, 784 (1985).
5. M.B. Spencer and W.E. Lamb Jr., Phys. Rev. **A5**, 884 (1972).

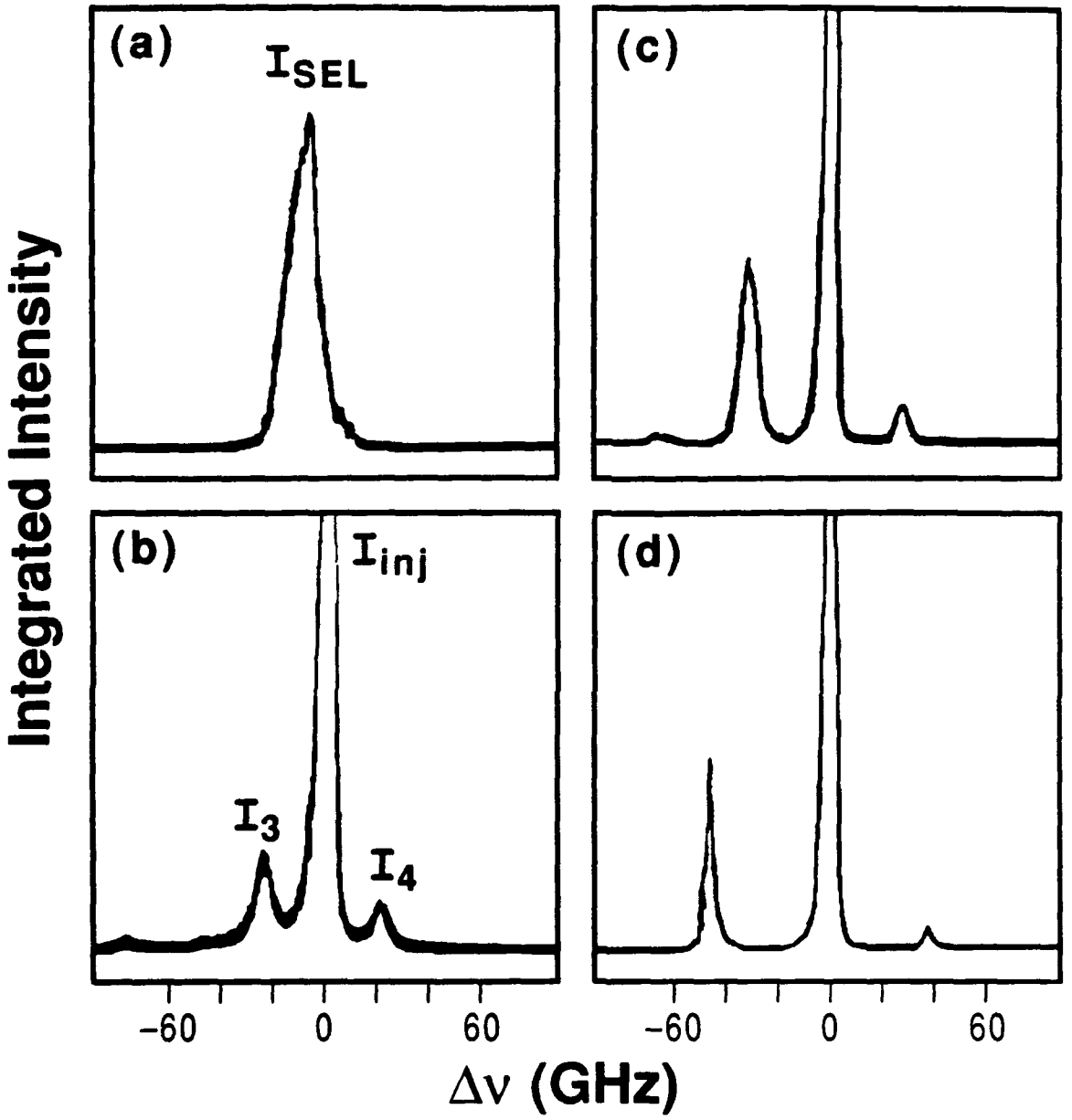


Figure 1. Unmodified and modified frequency spectra of the VCSEL lasing. (a) VCSEL lasing without injection: peak at 874.5 nm with and output power of 0.1 mW (well above threshold). (b)-(d) VCSEL output with injection at a frequency slightly above $\nu_{VCSEL}$ and with power (mW) of (b) 0.23, (c) 1.2, (d) 2.5.

Thursday, June 25, 1992

# Laser Array Dynamics

**ThB** 11:00am–1:00pm
Schroedinger Hall

Peter Davis, *Presider*
*ATR Optical and Radio Communications Research Laboratories, Japan*

# Factorial Dynamic Pattern Memory in Globally Coupled Lasers

Kenju Otsuka and Jyh-Long Chern
*NTT Basic Research Laboratories, Musashino, Tokyo, 180 JAPAN*
*Telephone +81 422 59 3367*

Recently, applicability of complex dynamics to information storage (memory) has been discussed in nonlinear optical systems. *Spatial chaos* memory was proposed in a bistable pixelsl[1] and in a coupled bistable chain.[2] *Dynamic memory* in a delayed feedback bistable system was demonstrated experimentally.[3] On the other hand, Otsuka demonstrated that $m_a = (N-1)!$ ($N$: number of oscillating modes) coexisting *dynamical spatial patterns*, i. e., antiphase periodic motions, can be selectively excited by applying seed signals to the modulated multimode lasers whose modes are globally coupled through spatial hole burning.[4] In this paper, we discuss the detailed bifurcation scenario, featuring clustered states and chaotic itinerancy[5] among destabilized clustered states. Also, factorial dynamical pattern memory associated with antiphase and clustered states as well as the effect of spontaneous emission on memory operation are demonstrated by numerical simulations.

From linear stability analysis, an N-mode free-running laser is found to be always stable in time and the relaxation oscillation at $\omega_r = [(w-1)/\tau\tau_p]^{1/2}$ ($w$: relative pump, $\tau$: population lifetime, $\tau_p$: photon lifetime) is damped out. If the modulation depth $m$ increases to where the pump power drops below the threshold during part of the pump modulation cycle, the total output behaves just like a single mode laser and exhibits spiking mode oscillations at $\omega_s < \omega_r$, while each emitter exhibits N-alternative spiking pulsations at $\omega_s/N$, resulting from winner-takes-all dynamics based on the cross-saturation mechanism. This is manifested as the antiphase states in modulated multimode lasers.[4] For small $N$, the antiphase states are globally attracting and are obtained after short transients for arbitrary initial conditions.

When $N$ increases, the basin of attraction of antiphase states shrinks very rapidly and antiphase attractors tend to coexist with chaotic orbits in the phase space. In addition, clustered states appear, where the system breaks into p-clusters which exhibit different synchronized motions. There coexist at least $m_c = N!/N_1!N_2!....N_p!$ clustered states in the phase space, where $N_i$ is the number of modes belonging to the $i$-th cluster. The bifurcation diagram for a five mode laser is shown in Fig. 1(a) as a function of modulation frequency, where $w_0 = 2.7$, $m = 0.74$, $\tau/\tau_p = 1000$, and spontaneous emission coefficient $\epsilon = 1.2 \times 10^{-7}$ are assumed. In the high modulation frequency side near $\omega_r$, synchronized relaxation oscillations are realized. When the modulation frequency is decreased, clustered states like Fig. 1(b) appear. Figure 1(b) shows a 2-cluster state $[(1,2,3),(4,5)]$. It is interesting to note that the total output exhibits the alternative spike pulses of the spiking mode and the resonant relaxation oscillation which was observed experimentally in a modulated *single mode* LNP laser.[6] This implies that the dynamics of individual modes are self-organized such that the total output behaves just like a single mode laser similarly to antiphase states. It should be noted that these stable synchronized relaxation oscillations or stable clustered motions coexist with both the chaotic attractor and antiphase states with different basins of attraction in the phase space.

If the modulation frequency is decreased further, clustered states are destabilized and then the system exhibits self-induced switching among coexisting destabilized clustered motions (chaotic itinerancy[5]) leading to a global chaos (GC in the figure). This process repeats when the modulation frequency is decreased as shown in the figure. Figure 1(c) shows an example of chaotic itinerancy at $\tau\omega_m = 19.5$, where at point $A$, for example, the switching from a destabilized $[(1,4,5),2,3]$ cluster to a destabilized $[(1,3,4),2,5]$ cluster is occurring.

The basin of attraction of antiphase states for $N = 5$ is extremely small in this parameter range and it is hard for the system to find it. However, one can assign the system to the desired

antiphase dynamics states by injecting small light pulses [≈ (laser pulse height)/60 ] to $(N-1)$ modes in the desired sequences as seeds at the time interval of $2\pi/\omega_s$ only during the $(N-1)$ modulation cycle in the region indicated in Fig. 1(a). Examples are shown in Fig. 2 for $\tau\omega_m = 35$. In Fig. 2(a), the system shows chaotic evolutions initially and is switched to the antiphase state by the seed pulses. In the case of Fig. 2(b) with slightly different initial conditions from Fig. 2(a), the system is attracted by the 2-cluster state $[(1,2,3,4),5]$ after some transients, and is switched to the antiphase states by seed pulses. These results imply that chaotic, cluster and antiphase attractors indeed coexist in the phase space for $\tau\omega_m = 35$, and switching among them can be established by injection seeding. Moreover, even switching from one antiphase state to another is possible.[4]

Next, let us consider the assignment to desired clustered states. From the numerical analysis, it is found that direct assignment to the desired clustered states is possible when "key patterns" of the desired clustered states are applied to some modes as seeds in the first modulation cycle. Examples are shown in Fig. 3 for $\tau\omega_m = 25$. In Fig. 3(a), the system is initially in the chaotic attractor and the chaotic dynamics are switched to a 3-cluster state $[(1,2,3),4,5]$ by applying "key patterns" to $k = 1$, 2, and 3 modes, where seed pulse height $s_{k,i}(k = 1,2,3)$ is 0.2 and pulse width is 0.06. In Fig. 3(b), the system is switched to a 3-cluster state $[(1,4,5),2,3]$ by applying "key patterns" to $k = 2$ and 3 modes, where seed pulse heights are $s_{2,i} = 0.2$ and $s_{3,i} = 0.1$. Here, other modes are self-organized such that the total output behaves just like a single mode and exhibits alternative spike pulses similar to Fig. 1(b). In other words, the desired clustered state can be *associatively* memorized by injection seeding of "key patterns" during one modulation cycle. It is very likely that injection seeds give a driving force to the system such that the trajectory will fall on the basin of attraction of these periodic states surrounded by a chaotic sea through saddles (homoclinic crossing). Such an assignment process can be called *seeding-assisted crisis*.

The basin of attraction of antiphase states depends on the spontaneous emission coefficient $\epsilon$. In general, if $\epsilon$ is decreased, the basin of attraction increases as a result of the reduction of fluctuations due to the spontaneous emission term $\epsilon n_0$ in the rate equation, where $n_0$ is the population density. For $\epsilon \geq 5 \times 10^{-8}$, antiphase attractors are destroyed for $N \geq 6$. In the case of $N = 6$, antiphase attractors are divided into $N = 5$ antiphase motions and the chaotic motion. However, the *sequential playback* of the "forced" $N = 6$ antiphase motions which do not exist previously in the phase space, can be accomplished by applying clock optical pulses to the first firing mode in addition to the injection seeds. The result is shown in Fig. 4, where the antiphase state is destroyed into $N = 5$ antiphase motion and chaotic motion when the clock pulse is cut. When the spontaneous emission coefficient $\epsilon$ is decreased to below $5 \times 10^{-8}$, the $N = 6$ antiphase states ($m_a = 120$) have a finite basin of attraction and one can assign the system to these antiphase states without applying clock pulses. If $\epsilon$ is decreased further to $< 1.2 \times 10^{-9}$, which is an attainable value in solid state lasers[4], sequential playback by clock pulses (like Fig. 4) is possible even for $N = 7$ (, i. e., $m_a = 720$).

Assignment to periodic states in the present system is attractive in terms of application to a memory of fractional "dynamical spatial patterns" resulting from automatic parallel processing among oscillating modes with cross-saturation. The memory capacity in the present system is expressed by $C_a = log(N-1)!/log2$ for antiphase states and $C_c = log(N!/N_1!N_2!...N_p!)/log2$ for p-clusters states. This implies that the memory capacity per mode exceeds ordinary 1-bit binary memory.

**References**

1. W. J. Firth, Phys. Lett. A **125**, 375 (1987).
2. K. Otsuka and K. Ikeda, Phys. Rev. A **39**, 5209 (1989).
3. T. Aida and P. Davis, Jpn. J. Appl. Phys. **29**, L1241 (1990).
4. K. Otsuka, Phys. Rev. Lett. **67**, 1090 (1991).
5. For a review, see K. Otsuka, Int. J. Modern Phys. **B 5**, 1179 (1991).
6. K. Kubodera and K. Otsuka, IEEE J. Quantum Electron. **QE-17**, 1139 (1981).

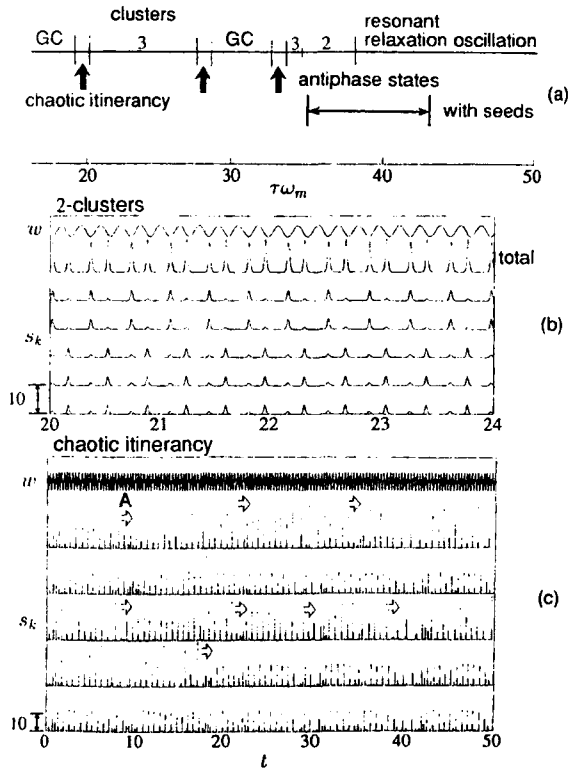


Fig. 1 (a) Bifurcation diagram for a 5 mode laser, (b) 2-clusters state; $\Omega_m \equiv \tau\omega_m = 35$, and (c) chaotic itinerancy; $\Omega_m = 19.5$ Here, $s_k$ indicates the photon number and time $t$ is normalized by $\tau$.

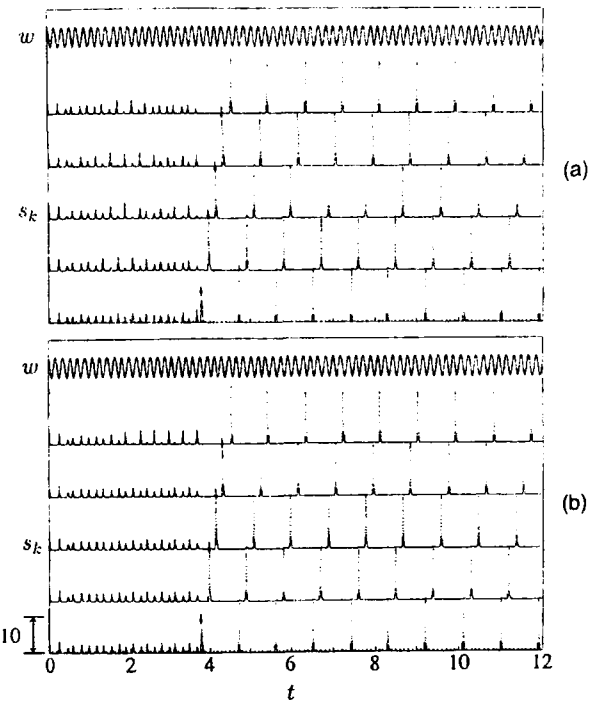


Fig. 2 Assignment to antiphase states. Parameter values are the same as for Fig. 1. $\Omega_m = 35$, seed pulse height = 0.2, and pulse width = 0.06.

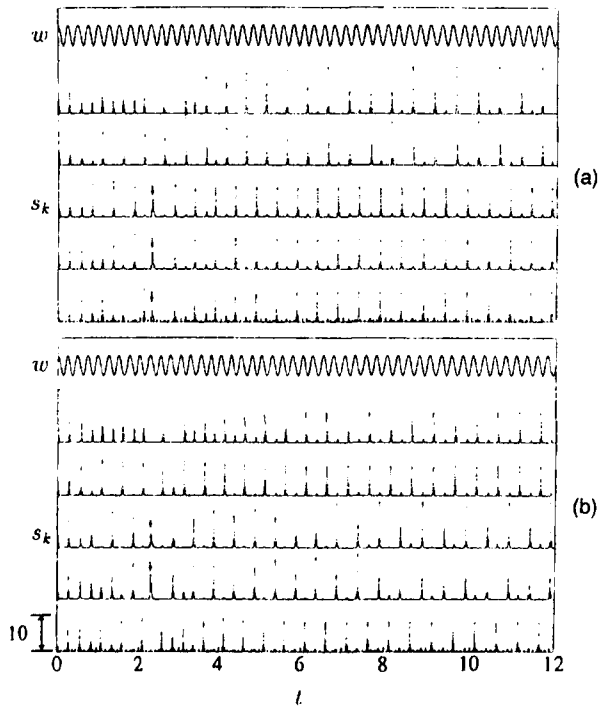


Fig. 3 Assignment to clustered states for the same parameters. $\Omega_m = 25$.

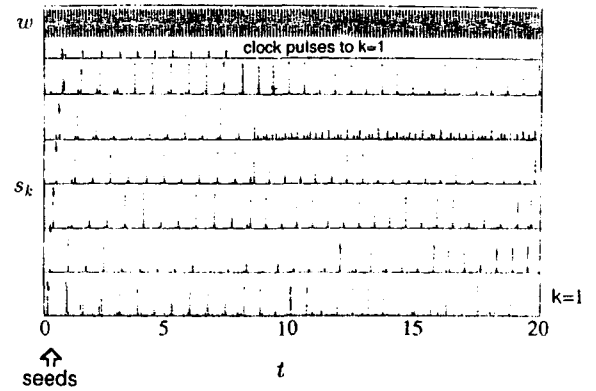


Fig. 4 Sequential playback of forced antiphase states for $N = 6$ with $\epsilon = 1.2 \times 10^{-7}$ by clock pulses. $w_0 = 4.2$, $m = 0.76$ and pulse $\Omega_m = 51$. Seed pulse height = 0.2 and pulse width = 0.02. Clock pulse height = 0.2 and pulse width = 0.05

# Coherence and Phase Dynamics of Spatially Coupled Solid State Lasers

Larry Fabiny, Pere Colet and Rajarshi Roy
School of Physics
Georgia Institute of Technology
Atlanta, Georgia 30332-0430 USA.
Phone 404 894 5265

Although coherence properties of semiconductor laser arrays have been the subject of extensive investigations for many years [1], solid state laser arrays are only recently receiving much interest. The two systems are described by similar dynamical equations, but the solid state laser dynamics occur on much slower time scales. In addition, spatial coupling is varied more easily in a solid state array. The solid state array then presents some advantages as a tool in investigating coupled dynamical systems. In this paper we study the coherence properties of two spatially coupled Nd:YAG lasers.

Our laser system produces two parallel, spatially separated lasers in a single Nd:YAG crystal, with each laser excited by its own Argon pump beam. The symmetric cavities consist of two plane end mirrors and rely upon positive thermal lensing in the Nd:YAG active medium for optical stability. The coupling between the two lasers is varied by changing the amount of overlap between the two lasing fields. This overlap is a function of the lasing spot size and the separation of the two pump beams, L. The coupling strength can be varied continuously simply by changing the spacing between the two pump beams.

Intrinsic noise and detuning between the output beams act to destabilize the coupling. The detuning between the uncoupled beams has been measured to be in the range 25 - 100 MHz. In order to determine the mutual coherence of the two output beams, we superimpose them at a small angle and measure the visibility of the interference fringes. For large L, the beams are completely incoherent. For small L, the two beams are phase-locked and produce a visibility approaching 1. The transition from incoherence to coherence occurs abruptly in a narrow range of separation of the two lasers. The phase-locked beams are observed to lase with a $\pi$ phase difference.

We describe our system in terms of the rate equations for the slowly varying complex amplitude of the electric field and the population inversion for each of the beams. We have included a coupling term between the two electrical fields and a Gaussian white noise term to model random fluctuations in the laser fields. The value of the coupling coefficient is determined by the overlap integral of the two beams.

In the steady state, neglecting the fluctuations of the intensity of each beam, the visibility can be simply expressed in terms of the phase difference between the two beams. When the intensities of the two beams have the same mean value, it is possible to reduce our model to a closed equation for the phase difference of the two output beams. This equation corresponds to the Adler equation [2], which has been widely used in the study of coupled oscillators, plus a stochastic term which describes the fluctuations. In the limit of small noise and for values of the coupling much larger than the detuning, the two lasers are phase-locked and mutually coherent. For small values of the coupling constant the phases of the two beams become uncorrelated.

We have compared the experimentally measured visibility for different separations between the pump beams with numerical simulations of our simple model and obtained very good agreement.

**References:**

[1] R.K. DeFreez et. al., Nonlinear Dynamics in Optical Systems, ed. N. B. Abraham, E.M. Garmire and P. Mandel, p. 106 (Optical Society of America, Washington D.C. 1991).

[2] R. Adler, Proc. IRE **34**, 351 (1946), reprinted in Proc. IEEE, **61**, 1380 (1973).

# Dynamics of a Twin Stripe Semiconductor Laser Array: Coupled Mode Theory vs The PDE Model

Lutfur Rahman and Herbert G. Winful
*Department of Electrical Engineering and Computer Science*
*The University of Michigan, 1301 Beal, Ann Arbor, MI 48109*
*Phone: (313)747-1804*

In this paper we present numerical solutions for a partial differential equation (PDE) model[1] for the dynamics of a twin stripe semiconductor laser array. The model includes carrier diffusion and the effects of propagation. A coupled-mode ordinary differential equation (ODE) model[2] is then derived from this PDE model. The two models are compared in predicting the dynamical behavior of the laser array. We obtain good qualitative and quantitative agreement between the two models. The results obtained can be readily extended to larger arrays.

The ODE model greatly facilitates the determination of the domain of stability of the device, the conditions and nature of bifurcations leading to instability and of subsequent bifurcations.

We start with the evolution equations for the field ampliude $X$, in arbitrary units, and carrier densities $Z$, in normalized units.

$$\frac{\partial X}{\partial \tau} = iC\Delta\eta_{\text{eff}}(x)X + (1 - iR)ZX + iL_p^2\frac{\partial^2 X}{\partial x^2}, \tag{1}$$

$$T\frac{\partial Z}{\partial \tau} = p(x) - Z - (1 + 2Z)|X|^2 + L_e^2\frac{\partial^2 Z}{\partial x^2}, \tag{2}$$

where $C$ is a constant dependent on material and waveguide parameters, $R$ is the antiguiding parameter, $L_p^2\partial^2 X/\partial x^2$ allows for diffraction and $\Delta\eta_{\text{eff}}(x)$ is the lateral built-in effective index profile. $T$ is the ratio of the carrier lifetime, $\tau_s$, to photon lifetime, $\tau_p$, and $L_e$ is the diffusion length of the carriers. The lateral coordinate is $x$ and $\tau$ is the time normalized to $\tau_p$. The injection current $p(x)$ is assumed constant under the stripes and zero elsewhere.

In the coupled-mode formalizm, each element of the laser array is considered separately and inter-element coupling is accounted for through coupling coefficients. With the injection current about 2.5 times the threshold current and with typical parameter values for an AlGaAs laser, we see that gain guiding is significant in addition to the index guiding provided by $\Delta\eta_{\text{eff}}(x)$. With this in mind, we take the single element dielectric profile as $C\Delta\eta_{\text{eff}}(x) - (i + R)Z_0$, and the single element field as $X_0$, where $(X_0, Z_0)$ is the steady state solution of Eqs. (1)-(2). The change in the single element dielectric profile due to temporal instabilities is expected to be small and can be taken as a perturbation. $X_0$ and $Z_0$ are readily obtained by advancing Eqs. (1)-(2) in time, for a single stipe, long enough to reach a steady state starting from an arbitrary field and gain profile.

The usual coupled mode expansion is now made for the total field $E_t$ in terms of the laterally shifted versions of the single element field $X_0$.

$$E_t(x,\tau) = a_1(\tau)X_{01}(x) + a_2(\tau)X_{02}(x). \tag{3}$$

The time dependent total carrier profile, $Z_t$, can be written as

$$Z_t(x,\tau) = Z_{t0}(x) + \tilde{z}(x,\tau), \tag{4}$$

where $Z_{t0}$ can be expressed in terms of $Z_{0m}$, the laterally shifted versions of $Z_0$. As noted earlier $|\tilde{z}(x,\tau)| \ll |Z_{t0}(x)|$. We further assume that

$$z(x,\tau) = z_1(\tau)X_{01}(x) + z_2(\tau)X_{02}(x). \tag{5}$$

With Eqs. (1)-(5), the coupled mode equations can be written down.

$$\sum_{m=1}^{2} c_{nm}\frac{\partial a_m}{\partial \tau} = (1-iR)a_n z_n + i\sum_{m=1}^{2}\tilde{\kappa}_{nm}a_m, \tag{6}$$

$$T\frac{\partial z_n}{\partial \tau} = P - (1-\delta)z_n - (1+\gamma z_n)|a_n|^2. \tag{7}$$

with $n = 1, 2$. $\delta$ and $\gamma$ are constants independent of the separation between the elements of the array and are integrals involving $X_0$ and $Z_0$ and $c_{nm}$ are modal overlap integrals close to the identity matrix elements. The coupling constants $\tilde{\kappa}_{nm}$ and the pump parameter $P$ are given by

$$\tilde{\kappa}_{nm} = \int X^*_{0n}X_{0m}[(\eta(x) - \eta_m(x)) - (i+R)(Z_{t0}(x) - Z_{0m}(x))]dx, \tag{8}$$

$$P = \int \left(p(x) - Z_{t0} + L_e^2\frac{\partial^2 Z_{t0}}{\partial x^2}\right)dx, \tag{9}$$

where $\eta(x)$ is the total built-in refractive index and $\eta_m$ is the built-in refractive index for a m'th guide alone. The pump parameter $P$ depends upon the separation between the lasers because of coupling between the lasers through carrier diffusion.

The dynamical behavior of the laser array according to Eqs. (1)-(2) was obtained by advancing an initial field and carrier profile in time using a time-splitting finite difference scheme. The width of the stripes are $4\mu$m, $R = 3$, and $\Delta\eta_{\text{eff}} = 0.01$. The other parameters are as given in Ref. 1. Two such sets of simulations, for varying center to center separation $S$ between stripes, were performed for $L_e$, equal to 0 and $3\mu$m. When $L_e = 0\mu$m, the array loses the stability of the out of phase steady state, through a (generalized) Hopf bifurcation, in favor of self-sustained oscillations at $S = 9.0\mu$m. As $S$ is decreased further, the dynamical behavior of the array becomes more complicated and eventually it becomes chaotic through the quasiperiodic route. On the other hand when $L_e = 3\mu$m, the stability of the out of phase steady state is lost at $S = 8.4\mu$m. With further decrease in $S$ the system becomes chaotic through a sequence of period doubling bifurcations.

The coupled-mode equations, Eqs. (5)-(6), support both in-phase and out of phase equilibria. The stability of these equilibria is determined by the eigenvalues of the linearized rate equations corresponding to Eqs. (5)-(6). When $S \leq 13.2\mu$m, for both $L_e = 0$ and $3\mu$m, the in-phase state is stable while the out of phase state is unstable. At this value of $S$ a steady state bifurcation leads to the exchange of stability of the two states. As $S$ is decreased, the out of phase steady state loses stability at $S = 8.9$ and $7.8\mu$m for $L_e = 0$ and $3\mu$m, respectively. The qualitative agreement between the PDE and the coupled-mode

models is good as far as the nature of bifurcations and the routes to chaos are concerned. For $L_e = 0\mu$m, there is also good quantitative agreement. The quantitative agreement is, however, less than desirable for $L_e = 3\mu$m. This is primarily because for this case the stripes are coupled not only by their evanescent fields but also through the exchange of carriers. Diffusion of carriers result in the carrier peaks of the two stripes being pulled towards each other resulting, in turn, the modal fields being pushed out because of index anti-guiding. The amount of pulling (pushing) depends upon the separation between the stripes. A more refined coupled-mode expansion, corresponding to Eq. (3), is needed for this case.

In conclusion, we have reduced the PDE model for the dynamics of a semiconductor laser array to a coupled-mode ODE model using a basis for the coupled-mode field expansion which incorporates both index guiding and gain guiding. For diffusionless carriers, there is good qualitative and quantitative agreement between the two models. However, when inter-element coupling of carriers is allowed through diffusion, the agreement is only qualitative.

**References:**

1. S.S.Wang and H.G. Winful, in OSA Proceedings on Nonlinear Dynamics in Optical Systems, N.B. Abraham, E.M. Garmire, P. Mandel, eds., (OSA, 1991) vol. 7, pp 114-118.
2. S.S. Wang and H.G. Winful, Appl. Phys. Lett, **52**, 1774(1988).

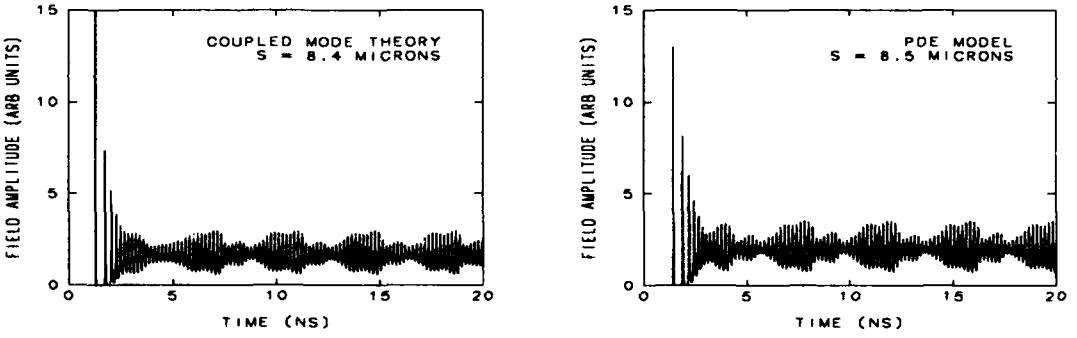


Figure 1. $L_e = 0$. Evolution of the field amplitude according to the coupled mode model and the PDE model past the point of a bifurcation to a torus.

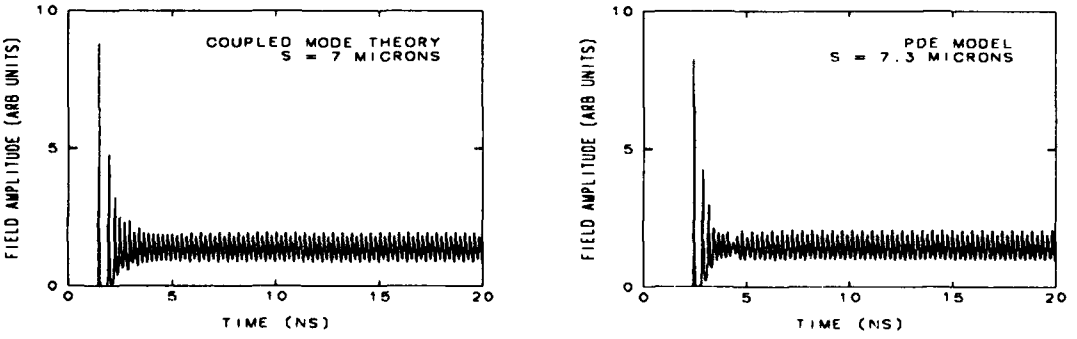


Figure 2. $L_e = 3\mu$m. Evolution of the field amplitude according to the coupled mode model and the PDE model past the point of a period doubling bifurcaton.

# Space-Time Dynamics of Semiconductor Lasers: Many-Body Theory and Phenomenological Models

J.V. Moloney, P. Ru, and R. Indik
Department of Mathematics, University of Arizona
Tucson, Arizona 85721
S.W. Koch, and E. Wright
Optical Science, Univeristy of Arizona
Tucson, Arizona 85721
Tel: (602)-621-6755 , Fax: (602)-621-8322

The space-time dynamical behaviour of multi-stripe index/gain guided semiconductor laser arrays and broad area lasers is studied using the semiconductor Maxwell-Bloch laser model including transverse diffraction of the counterpropagating optical fields and transverse diffusion of the excited carriers. Our results confirm that evanescently coupled multi-stripe lasers are a fascinating manifestation of spatio-temporal complexity in spatially extended nonlinear systems. Stabilization of the laser output can be achieved by injection-locking the array with a weak external injected signal. The broad area laser shows random intensity filamentation in free-running mode and can be stablized to produce high power output by using the unstable resonator configuration for transverse mode discrimination.

In the usual phenomenological semiconductor laser model approach a linewidth enhancement factor is introduced in an ad hoc fashion. The magnitude of this factor plays an important role in promoting instability in evanescently coupled semiconductor laser arrays [1, 2]. The issue can best be resolved by appealing to a fundamental many-body theory [3] of the interaction of light with semiconductor media. An obvious advantage of such a theory is that one can dispense entirely with ad hoc parametrization and compute the material parameters directly from first principles.

In the present paper we will study the space-time dynamics of the semiconductor laser by numerically integrating the *time-dependent*, fully transverse dimensional partial differential equations while using the many-body semiconductor theory to obtain the carrier induced gain, refractive index and nonlinear carrier diffusion coefficient changes. To investigate the validity of the phenomenological approach, we use the many-body theoretical data to

construct the usual phenomenological model and study the dynamics of the laser model. By linear curve fitting the gain and the refractive index changes at the laser threshold we obtain parameters that can be used in the phenomenological model. Our studies show that these parameters depend not only the properties of the material, but are also strongly dependent on the laser device and working conditions. In the strong index guiding case, the phenomenological approach gives qualitative agreement with the many-body theory. For weak index guided or gain guided laser arrays and broad area lasers, the phenomenological model fails to describe the complex dynamical behavior of the laser system.

# References

[1] S.S. Wang and H.G. Winful, *Dynamics of phase-locked semiconductor laser arrays*, Appl. Phys. Lett. **52**(21), pp. 1774-1776, 1988.

[2] H.G. Winful and S.S. Wang, *Stability of phase locking in coupled semiconductor laser arrays*, Appl. Phys. Lett. **52**, pp. 1894-1896, 1988.

[3] H. Haug and S.W. Koch, *Quantum theory of the optical and electronic properties of semiconductors*, (World Scientific) 1990.

# Bifurcation to Standing and Traveling Waves in Large Laser Arrays

Ruo-ding Li and Thomas Erneux

Northwestern University

Dept. Eng. Sciences and Applied Mathematics

McCormick School of Eng. and Applied Sciences

Evanston, IL 60208

Telephone: (708) 491-5397

Arrays of semiconductor diode lasers are promising devices for applications that require high optical power from a laser source (high-speed optical recording, high-speed printing, free-space communications, pumping of solid-state lasers) [1]. Experimental and numerical studies of arrays consisting of a small number of lasers have shown that they are unstable devices and may exhibit a large variety of spatio-temporal responses [2-5]. In order to control these instabilities by various external mechanisms (injection locking, periodic modulations), systematic bifurcation studies are needed. The laser equations are however stiff and accurate solutions for a large population of lasers require long computation times. Asymptotic methods based on the limit of weak coupling [6] also fail to provide simple phase equations because the semiconductor laser is not a limit cycle oscillator. We have recently reformulated the laser equations as a weakly perturbed system of coupled conservative oscillators which eliminate part of the stifness of the problem and allow an analytical study of the first Hopf bifurcation as the coupling strength is progressively increased. If N is even, the Hopf bifurcation is simple and corresponds to a transition from a nonuniform steady state to a time periodic standing wave solution [7]. However, if N is odd, bifurcation to periodic standing and traveling wave solutions are both possible. This multiple bifurcation problem is difficult analytically but can be simplified if we consider the limit N large.

Specifically, we determine small amplitude periodic solutions of the following equations describing the evolution of N coupled semiconductor lasers

$$\frac{dY_j}{d\sigma} = (1 - i\alpha)Z_jY_j + i\eta(Y_{j+1} + Y_{j-1}), \qquad (1)$$

$$T\frac{dZ_j}{d\sigma} = p - Z_j - (1 + 2Z_j)|Y_j|^2. \qquad (2)$$

In these equations, the variables $Y_j$ and $Z_j$ are defined as the normalized electrical field and normalized excess carrier density in the jth laser, respectively. The basic time $\sigma$ is defined as $\sigma = t/\tau_p$ where $\tau_p$ denotes the photon lifetime. The parameter p is the normalized excess pump current ($p \approx 0.05$), $\eta$ is the coupling strength ($\eta \approx 10^{-3}$-$10^{-4}$), $\alpha$ is the linewidth enhancement factor ($\alpha \approx 5$) and T is equal to the ratio $\tau_s/\tau_p$ where $\tau_s$ is the spontaneous carrier lifetime $\tau_s$ ($T = 2\times10^3$). Typical values of these parameters are shown in parentheses and suggest the scaling $\eta = O(T^{-1}) \ll 1$. As Otsuka [5], we consider a ring geometry (looped Coupled Waveguide Lasers) and introduce periodic boundary conditions. The bifurcation analysis is easier for the ring geometry but can be extended to the more interesting case of fixed boundary conditions. We determine the bifurcation diagram of the periodic solutions by investigating the limits

$$\eta = O(T^{-1}) \to 0 \text{ and } \nu = O(N^{-1}) \to 0 \qquad (3)$$

where $\nu$ denotes the amplitude of the time periodic mode. In [8], a system of partial differential equations were obtained for solutions depending on time t and a slow space variable $\xi = j/N$. By using a different method, we determine a solution that depend on time t, the position j of the jth-laser and the slow space variable $\xi = j/N$. We obtain a Ginzburg-Landau-type equation of the form

$$\alpha_\tau = A\alpha + B\alpha^2\bar{\alpha} + C\alpha_\xi + D\alpha_{\xi\xi} \qquad (4)$$

where $\alpha$ denotes the complex amplitude of a spatio-temporal mode, $\tau$ is slow time and all the coefficients are complex. The unusual term $C\alpha_\xi$ results from the fact that the basic steady state solution is a function of the laser position j. Boundary conditions are important for this problem and differ if N is even or odd. As $N \to \infty$, we find

$$\alpha(0) = \alpha(1) \text{ (N even) and } \alpha(0) = -\alpha(1) \text{ (N odd)}. \qquad (5,6)$$

If N is even, we have verified that Eq. (4) predicts the amplitude of the standing wave solution, as previously obtained [7]. If N is odd, the effect

of the coefficient $C\alpha_\xi$ as well as the boundary conditions (6) is to split the multiple bifurcation point to standing and traveling wave solutions. See Figure. The two primary bifurcations correspond to traveling wave solutions and the secondary bifurcation corresponds to a standing wave solution. Full lines (dashed lines) mean stable (unstable) solutions. The separation between primary and secondary bifurcation points is a small $O(T^{-1}N^{-2})$ quantity. Our results are in agreement with a numerical study of Eqs. (1) and (2) with N equal to 6 and 7.

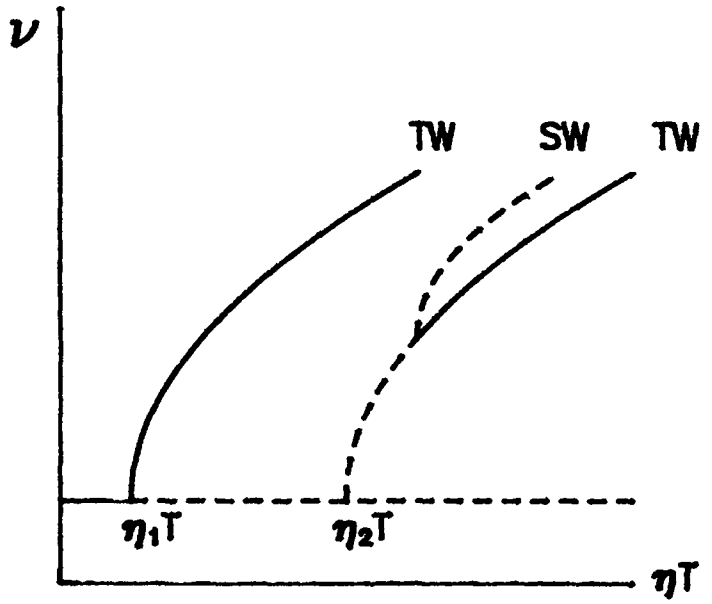


References
1. D. Botez and D.E. Ackley, IEEE Circ. and Dev. Mag., 8 (1986).
2. S.S. Wang and H.G. Winful, Appl. Phys. Lett. 52, 1774 (1988).
3. H.G. Winful and S.S. Wang, Appl. Phys. Lett. 53, 1894 (1988).
4. H.G. Winful and L. Raman, Phys. Rev. Lett. 65, 1575 (1990).
5. K. Otsuka, Phys. Rev. Lett. 65, 329 (1990).
6. P.C. Matthews and S.H. Strogatz, Phys. Rev. Lett. 65, 1701 (1990)
7. Ruo-ding Li and T. Erneux, Phys. Rev. A, submitted (1992).
8. P.K. Jakobsen, R.A. Indick, J.V. Maloney, A.C. Newell, H. G. Winful and L. Raman, JOSA B8, 1674 (1991).

# Coupled elements, phase transitions and localized order

Martin McCall and Ziping Jiang
Optics Section, Blackett Laboratory, Imperial College, London SW7 2BZ
Tel: 071 589 5111 ext 6821
Fax: 071 589 9463

Two-dimensional optoelectronic device arrays have considerable potential for applications ranging from the production of high power coherent beams (i.e. 2D laser arrays) to processing based on multichannel optical interconnects in neural computation. It is quite clear, however, that modeling such complex systems with various inter-element coupling schemes is not an easy task.

In order to abstract some general features of active optoelectronic device arrays we have examined a model based on the dynamics of the light field in the presence of a saturable nonlinearity:

$$\frac{d}{dt}Q_n(t) = \frac{1}{2}[G_n - \Gamma_n - 2i\Omega_n]Q_n(t) + F_n(\kappa, Q_1, \cdots, Q_N), \tag{1}$$

where the coupling function $F_n(\kappa, Q_1, \cdots, Q_N)$ describes various coupling schemes ranging from nearest neighbour to global uniform coupling to the mean field. For simplicity we ignore the population dynamics associated with each device, in which case the model can either be regarded as an array of class A lasers, or as class B lasers (eg semiconductor laser arrays) if it is understood that only the dynamics on timescales $\ll$ upper state lifetime is being probed. This is adequate in determining, for example, necessary (but not sufficient) conditions for phase locking a semiconductor laser array. Equation (1) is actually a discretization of the Ginzburg-Landau equation (used extensively in the modelling of transverse effects in laser dynamics) as in ref.[1]. Here we explicitly allow for complex coupling which corresponds to control over the phase of the interacting fields — a desirable feature in practise — as well as different coupling functions. We also allow for the inevitable technological differences between the coupled elements by imposing various statistical distributions on their natural frequencies.

Our main interest is in enumerating the global dynamics of this system, for which we have found it convenient to introduce the "order parameter" defined as

$$R_o e^{i\Psi_o} = \frac{1}{N}\sum_{j=1}^{N} Q_j. \tag{2}$$

The amplitude, $R_o$, broadly categorizes ordered and disordered states according to whether it is a maximum or a minimum.

The first result is that for most coupling schemes a coupling phase of $\frac{\pi}{2}$ is the most difficult to phase lock (i.e. to achieve a steady state output of the array). This is illustrated in fig.

1 which shows the variation of the order parameter as a function of coupling phase and indicates the transition point at $\frac{\pi}{2}$ beyond which disordered states prevail. For the case of uniform coupling it is possible to prove this result analytically in the thermodynamic limit of an infinite number of oscillators (which we emphasise is distinct from the continuum limit) presented here for the first time. The significance of this result is that the phase of $\frac{\pi}{2}$ corresponds precisely to evanescent waveguide coupling and thus it can be expected that if this is the dominant coupling mechanism, phase locking will be difficult, unless special measures are taken. It is also interesting to observe that the fluctuations of the order parameter defined as

$$\Delta R_o = \overline{(R_o^2 - \bar{R}_o^2)^{\frac{1}{2}}}, \tag{3}$$

and shown by the broken line in fig.1, are maximal at the phase transition point.

Near the phase transition points we have also observed order localization phenomena as illustrated in fig. 2. This feature emerged rapidly from random initial conditions and can be long-lived, depending on the strength of the coupling. It is associated with nearest neighbour coupling and as with phase transition physics in other fields, it appears that the order-disorder transitions in this system can be associated with divergence of correlation lengths. As well as giving examples in which multiple "defects" are formed, we will present the parameter identification of the correlation lengths in this system.
In terms of the possible applications that this system provides, the emergence of spatial structure in the arrays has been shown to related to the coexistence of multiple attractors in the system [1]. Furthermore, it has been suggested [2] that these locatized regions can themselves regarded as information pixels capable of define a flexible optical memory.

# References

[1] Kenju Otsuka, "Self-induced path formation among local attractors and spatiotemporal chaos in a complex Ginzburg-Landau equation", Physics Review A, Vol. 44, No. 2, pp1393-1396 (1991).

[2] R. Chang, G. D'Alessandro,W. J. Firth, J. B. Geddes,R. Indik, J.V. Moloney and E.M. Wright, " Three-dimensional simulations of degenerate counterpropagating beam instabilities in a nonlinear medium", paper NOWe29, Technical Digest, EQEC'91, 27th-30th August, 1991, Edinburgh.

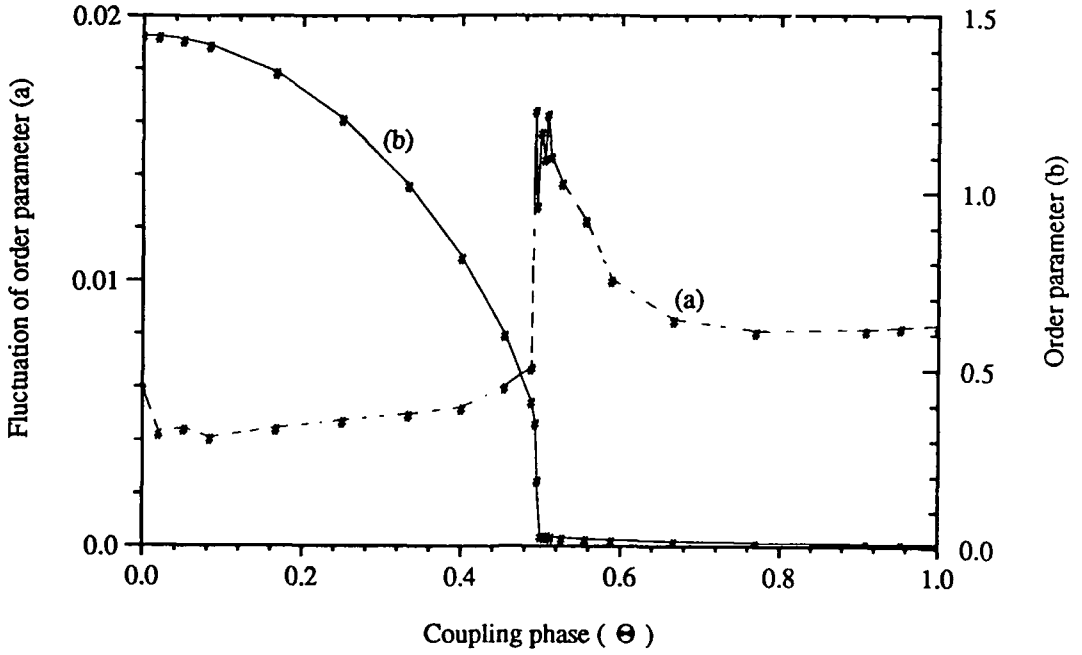


Fig.1: Order parameter $R_o$, and its mean squared deviation, $\Delta R_o = \overline{(R_o^2 - \bar{R}_o^2)}^{\frac{1}{2}}$ (broken line) versus coupling phase $\Theta$ (shown in unit of $\pi$). $\Theta = \frac{\pi}{2}$ is a transition point beyond which the system displays total phase unlocking. Order parameter fluctuations are peaked at the transition point.

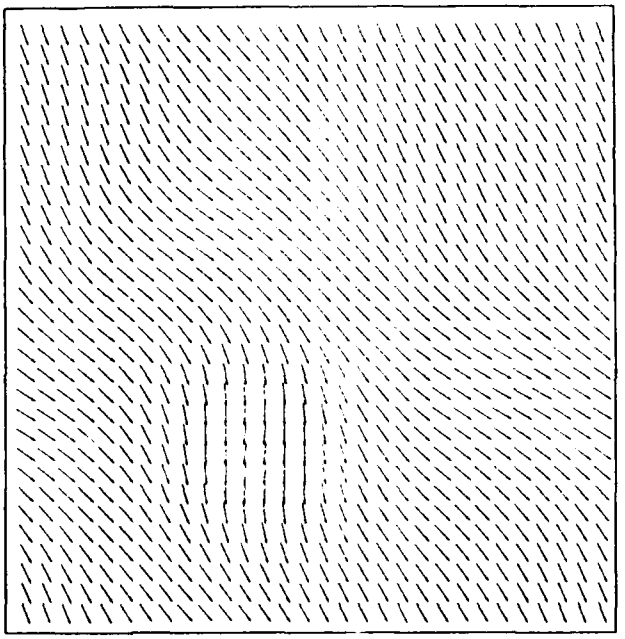

Fig. 2: Near-field flux pattern of $30 \times 30$ array showing region of localized order. Each arrow represents the complex number $Q_n$. The feature emerged rapidly from random initial conditions and can be long lived as desired, according to the coupling strength.

Thursday, June 25, 1992

# Invited Paper Session

**ThC** 4:00pm–5:20pm
Schroedinger Hall

Kenju Otsuka, *Presider*
*NTT Basic Research Laboratories, Japan*

**Network of Chaotic Elements**

Kunihiko Kaneko
Department of Pure and Applied Sciences,
Univ. of Tokyo, Komaba, Meguro, Tokyo 153, Japan

# 1 Introduction

Network of globally coupled chaotic elements is important not only as a model for nonlinear systems with many degrees of freedom, but also from the viewpoint of biological information processing and possible engineering applications.

In nonlinear optics, many modes are interacting through energy source. Each mode can be chaotic for some parameters, and a multi-mode optical system provides an example of globally coupled chaotic elements. Other examples in physics includes the dynamics of vortices in fluid, Josephson junction circuits or charge density wave coupled through electric current.

In neural dynamics, it is known that even a single neuron or a small ensemble of neurons can exhibit chaos. Consequently, the dynamics in the brain consists of an ensemble of elements with complex dynamics and complex coupling. Most of current neural network studies, however, use oversimplified local dynamics (0-1 or a sigmoid function). It is important and of interest to study a model with nontrivial dynamics ( with chaotic response) with simplified global coupling, as another abstraction from neural dynamics. In the dynamics of evolution, constraint from the "environment" leads to a globally coupling. Each species interacts with every species through the environment.

In the talk, we discuss novel aspects in a network of chaotic elements with the use of "globally coupled map" (GCM). A typical example is given by

$$x_{n+1}(i) = (1-\epsilon)f(x_n(i)) + \frac{\epsilon}{N}\sum_{j=1}^{N} f(x_n(j)) \qquad (1)$$

where $n$ is a discrete time step and $i$ is the index of an element ($i = 1, 2, \cdots, N =$ system size). We choose mostly the logistic map $f(x) = 1 - ax^2$, as the simplest model for globally coupled chaotic systems.

The model is a mean-field-theory-type extension of coupled map lattices (CML), extensively investigated as a prototype model for spatiotemporal chaos. Our dynamics (1) consists of a parallel nonlinear transformation and a feedback from the "mean-field". The dynamics (1) is equivalent to $y_{n+1}(i) = f((1-\epsilon)y_n(i) + \frac{\epsilon}{N}\sum_{j=1}^{N} y_n(j))$, as is seen by the transformation $y_n(i) = f(x_n(i))$. In this form, one can see clear correspondence with spin glass or neural nets: If one chooses a sigmoid function (e.g.,$tanh(\beta x)$) as $f(x)$ and random or coded coupling term $\epsilon_{i,j}$, SG or neural nets follow.

# 2 Clustering of Attractors and Phases

The simplest attractor of eq. (1) is a coherent one with $x(i) = x(j)$ for all $i, j$. For the attractor, the motion is governed just by the single logistic map $x_{n+1} = f(x_n)$.

The stability of this attractor is given by $\lambda_0 + \log(1-\epsilon) < 0$.

Besides the above single-clustered coherent attractor, we have attractors with clusterings. Here a cluster is defined as the set of elements in which $x(i) = x(j)$.

Attractors in our GCM are classified by the number of clusters $k$ and the number of elements for each cluster $N_k$. Each attractor is coded by the clustering condition $[k, (N_1, N_2, \cdots, N_k)]$.

The dynamics of a $k$-cluster attractor with $(N_1, N_2, \cdots, N_k)$ is written by the k-dimensional map:

$$X^{\nu}_{n+1} = (1-\epsilon) f(X^{\nu}_n) + \sum_{\mu=1}^{k} \epsilon_\mu f(X^{\mu}_n) \tag{2}$$

where $X^{\nu}_n$ denotes the value of $x_n$ in the $\nu$-th cluster, and the "effective coupling" $\epsilon_\mu$ is given by $\epsilon_\mu = \epsilon \times (N_\mu/N)$.

Our model has the following phases with the change of nonlinearity and coupling.

(i) **Coherent phase**: The coherent attractor ($k = 1$) has occupied (almost) all basin volumes.

(ii) **Ordered phase**: Attractors ($k = o(N)$) with few clusters have occupied (almost) all basin volumes.

(iii) **Partially ordered phase**: Coexistence of attractors with many clusters ($k = O(N)$) and few clusters.

(iv) **Turbulent phase**: All attractors have many ($k = O(N)$; in most cases $k \approx N$) clusters.

# 3 Hierarchical Clustering

In partially ordered phase, we have often encountered with an attractor with a single large cluster and many small clusters (e.g., $N_j = (N/2, 1, 1, \cdots, 1)$). For this type of attractor, the distance between two small clusters $\mid X^{\mu} - X^{\nu} \mid (\mu, \nu > 1)$ is much smaller than the distance between the large cluster and one of the small clusters; $\mid X^1 - X^{\nu} \mid$. To discuss this kind of structure, we have introduced the notion of **precision-dependent clustering**, by defining the "coarse-grained measurement of $x_n(i)$ by $\overline{x}^P_n(i) \equiv [P \times x_n(i)]/P$ where $[\cdots]$ is the integer part of $\cdots$ and $P$ is an integer for the precision. The precision-dependent clustering is defined by the clustering for $\overline{x}^P_n(i)$. The precision-dependent cluster number $k^P_n$ gives the effectived degrees of freedom up to the precision. As the precision is increased, the clusters spilt till their number $k^P$ increases up to $k$. This branching is uniform in the turbulent region, while it is strongly non-uniform in the partialy ordered phase.

In the partially ordered phase, the partition by $[N_1, \cdots, N_k]$ is also strongly non-uniform. To study the non-uniformity of partitions we introduce the probability distribution of partitions, which is given by $\pi(Y)$, where $Y = \sum_j^k (N_j/N)^2$. This probability $\pi(Y)$ gives the variety of partition by clusters.

## 4 Chaotic Itinerancy and Hierarchical Dynamics

Our system leads to a hierarchical dynamics. In a hierarchical dynamical system, there are many units of different levels, organized in a tree structure. A unit interacts strongly with the other units of the same level, and is slaved by the unit of its upper level, with small feedback to the upper level. The upper/lower level is defined according to the precision. The lower-level cluster is influenced by the upper-level cluster, but there is a flow from lower to upper level if chaos is strong enough, leading to the hierarchical dynamics.

When the effective degrees $k_n^P$ are low, a low-dimensional ordered motion emerges from a high-dimensional dynamics. Our system exhibits the intermittent change between the self-organization towards the low-dimensional structure and its collapse to a high-dimensional disordered motion. This type of dynamics has recently been found in optics by Ikeda, Otsuka, and Matsumoto, and in a model of neurodynamics by Tsuda, as have been coined the term **"chaotic itinerancy"** (over attractor ruins). The detaild dynamics will be discussed in the talk.

## 5 Violation of the Law of Large Numbers

Our mean-field $\sum_i f(x(i))$ fluctuates in time. In the turbulent phase, if $x(i)$ takes almost random values almost independently, one might expect that the aggregate $h \equiv (1/N)\sum_j f(x(j))$ obeys the law of large number and the central limit theorem. If this were the case, the variance of the mean-field would decrease as $1/N$ with $N$. We have measured the distribution of mean field $h = (1/N)\sum_i f(x_n(i))$, and have found that the fluctuation of the mean field remains even in the limit of $N \to \infty$. This observation suggests the emergence of hidden coherence in our system. The coherence should be hidden in nature, since the cluster number agrees with $N$.

In the talk, clustering bifurcation, partition information flow, and some extension of globally coupled maps are also given as well as some relevance of network of chaoric elements to the (biological) information processing.

## References

[1] K. Kaneko, Prog. Theor. Phys. 72 (1984) 480; 74 (1985) 1033; Physica 23D (1986) 436; 34D (1989) 1; 37D (1989) 60; *Collapse of Tori and Genesis of Chaos in Dissipative Systems*, (1986 World Sci. Pub.); in *Formation, Dynamics, and Statistics of Patterns* (World Sci. 1990, eds. K. Kawasaki, A. Onuki, and M. Suzuki); J. P. Crutchfield and K. Kaneko, "Phenomenology of Spatiotemporal Chaos", in *Directions in Chaos* (World Scientific, 1987, ed. Hao Bai-lin) pp 272-353 and references cited therein

[2] K. Kaneko, Phys. Rev. Lett. 63 (1989) 219; 65 (1990) 1391; Physica 41D (1990) 38; 54D (1991)5;55D (1992) and references cited therein

# Spatial Correlation Dimension and Critical Phenomena in Complex Ginzburg-Lardan Mode

M. Rabinovich
Nighny Novgorod
Russian Federation

Summary not available at press time.

Friday, June 26, 1992

# Optical Chaos and Noise

**FA** 8:20am–10:20am
Schroedinger Hall

Maxi San Miguel, *Presider*
*University of Balearic Islands, Spain*

# Chaos vs. noise in experimental data

F. Mitschke, M. Dämmig, C. Boden

Institut für Quantenoptik

Universität Hannover

Welfengarten 1

D-3000 Hannover 1

Germany

Tel. Germany-511-762 2502

Fax: Germany-511-762 2211

It is common to quantify chaos through determination of certain invariants. Among experimentalists, the most popular ones are the attractor dimension $D_2$ and entropy $K_2$ with an algorithm by Grassberger and Procaccia /1/ and the largest Lyapunov exponent with an algorithm due to Wolf et al. /2/.

Before it even comes to that, one has to determine whether an observed irregular signal is determistically chaotic, or indeed stochastic. Calculation of above quantities is not helpful for this decision because for random numbers, the first algorithm may and the second certainly will fail to indicate that the data is not chaotic.

Theiler et al. /3/ recently proposed a method that builds on these

algorithms but enhances them by a quantitative criterion about the statistical significance with which deterministic structure can be detected in the signal. This is achieved through comparison of results computed from the original data with those from a number of so-called surrogate data sets, i.e. copies of the original data set which are suitably randomized such as to keep the power spectrum but to destroy the deterministic structure. If results from original and surrogates do not differ (in terms of standard deviations from the mean of the surrogate spread), then most likely there was no deterministic structure in the original either.

We test this proposal with real world data from quantum optical experiments. One is a resonator filled with spin ½ atoms interacting simultaneously with an optical and a weak magnetic field. This system is known to exhibit low-dimensional chaotic behavior /4/. The other experiment is about Brillouin scattering of cw light in optical fibers, which gives rise to an irregular temporal intensity variation. There is a dispute whether this structure is chaotic /5/ or stochastic /6/.

We find that the method works extremely well if applied to dimension or entropy. Data of established chaotic nature is identified as such with high significance (like ten or more standard deviations). The dispute about Brillouin scattering is resolved.

On the other hand, the method fails to give consistent results if applied to the largest Lyapunov exponent. This surprising failure can be explained easily by re-examination of the fine difference between the mathematical concept of Lyapunov exponents and the inner workings of the Wolf algorithm. In particular, it becomes obvious that for random signals, the Wolf algorithm merely gives information on the power spectrum.

/1/ P. Grassberger, I. Procaccia, Physica **9D**, 189 (1983)

/2/ A. Wolf, J. B. Swift, H. L. Swinney, J. A. Vastano, Physica **16D**, 285 (1985)

/3/ J. Theiler, B. Galdrikian, A. Longtin, S. Eubank, J. D. Farmer, in: *Nonlinear Modeling and Forecasting*, SFI Studies in the Sciences of Complexity, Proc. Vol. XII, pp. 163–188, M. Casdagli, S. Eubank (eds.) (Addison-Wesley 1991)

/4/ F. Mitschke, C. Boden, C. Henning, I. Roloff, in: *Coherence and Quantum Optics VI*, p. 759, J. H. Eberly, L. Mandel, E. Wolf (eds.) (Plenum Press 1989); C. Boden, M. Dämmig, F. Mitschke, Phys. Rev. **A** 1992 *(to appear)*

/5/ R. G. Harrison, J. S. Uppal, A. Johnstone, J. V. Moloney, Phys. Rev. Lett. **65**, 167 (1990)

/6/ A. L. Gaeta, R. W. Boyd, Physical Rev. **A44**, 3205 (1991)

# Quantum Noise Reduction in a Spatial Dissipative Structure

L.A. Lugiato and F. Castelli

Dipartimento di Fisica dell' Università, via Celoria 16, 20133 Milano, Italy
phone +39-2-2392264, fax +39-2-2366583

## SUMMARY

We present a novel nonlinear optical effect which arises in a spatial structure of electromagnetic field. Our analysis establishes also, for the first time, a link between the fields of spatial instabilities [1] and of quantum noise reduction [2,3], in nonlinear optical systems.

The phenomena of spontaneous spatial pattern formation in nonlinear dissipative systems has been object of study since many years [4,5]. In particular, the last decade has shown an increasing interest in the spatial and spatio-temporal effects which arise in the structure of the electromagnetic field, in the planes orthogonal to the direction of propagation [1]. For example, it has been shown that passive, nonlinear optical systems can give rise to the spontaneous formation of roll, or hexagonal, or ring patterns [6,7,8].

Both in and out of Optics, the analysis of these phenomena has been limited to a purely classical description. We show, however, that in the case of the model formulated in Ref. 9 one can provide, in a rather straightforward way, a quantum mechanical formulation. The model [9] is presumably the simplest equation that predicts phenomena of spontaneous spatial pattern formation in an optical system. It describes a Kerr medium contained in an optical cavity and driven by a plane-wave coherent field. It has been shown that this model predict the onset of rolls [9] and of hexagonal structures [10] in the transverse planes.

In order to start the analysis of quantum mechanical aspects, we focussed on the simplest case of rolls pattern, which is shown in Fig. 1a in the near field

and in Fig. 1b in the far field, respectively. We calculated the spectrum of the quantum mechanical fluctuations in the intensity difference between the two signal beams $S$ and $S'$ (Fig. 1b), a quantity that can be measured early because the two beams are spatially separated in the far field. We obtained a simple analytical expression which is graphed in Fig. 2. The fact that the value of the spectrum $S(\omega)$ are smaller than 1 indicates that the fluctuation are below the shot-noise level and the fact that $S(\omega = 0) = 0$ shows that there is complete suppression of quantum noise in the intensity difference for zero frequency. The analytical formula for $S(\omega)$ coincide exactly with that for the spectrum of fluctuations in the intensity difference between the signal beams in the optical parametric oscillator [11].

In conclusion, we showed that the two signal beams of the roll pattern are quantum correlated twin beams , exactly as those emitted by an optical parametric oscillator. This results shows that our optical dissipative structure (the roll pattern) is ordered not only from a spatial viewpoint, but also on a quantum mechanical level.

# References


[1] L.A. Lugiato, in "*Proceedings of the Solvay Conference on Quantum Optics*", edited by P. Mandel, Physics Reports, in press.

[2] R. Loudon and P.L. Knight editors, J. Mod. Opt. **34**, (June/July 1987).

[3] H.J. Kimble and D.F. Walls editors, J. Opt. Soc. Am. B **4**, $N^0$ 10 (1987).

[4] G. Nicolis and I. Prigogine, "*Self-Organization in Nonequilibrium Systems*" (Wiley, New York, 1977).

[5] H. Haken, "*Synergetics, an Introduction*" (Springer-Verlag, Berlin, 1977). Opt. Comm. **67** (1988) 363

[6] G. Giusfredi, J.F. Valley, R. Pon, G. Khitrova and H.M. Gibbs, J. Opt. Soc. Am. B **5**, 1181 (1988).

[7] W.J. Firth, J. Mod. Opt. **37**, 151 (1990).

[8] A. Petrossian, M. Pinard, A. Maitze, J.Y. Courtois, and G. Grynberg, submitted for publication.

[9] W.J. Firth, G.S. McDonald, A.J. Scroggie, and L.A. Lugiato, in preparation.

[10] L.A. Lugiato and L. Lefever, Phys. Rev. Lett. **58**, 2209 (1987).

[11] S. Reynaud, C. Fabre, and E. Giacobino, J. Opt. Soc. Am. B **4**, 1520 (1987).

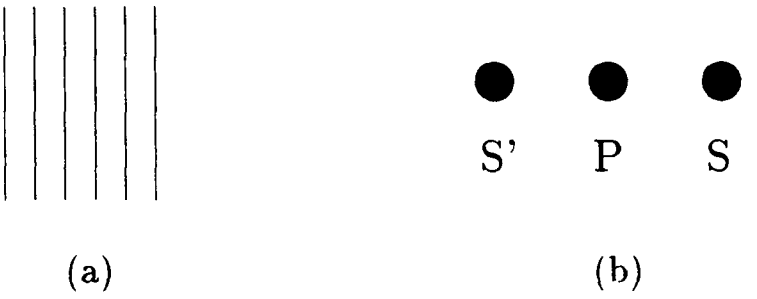


Figure 1: Roll pattern in the transverse plane : (a) near field; (b) far field.

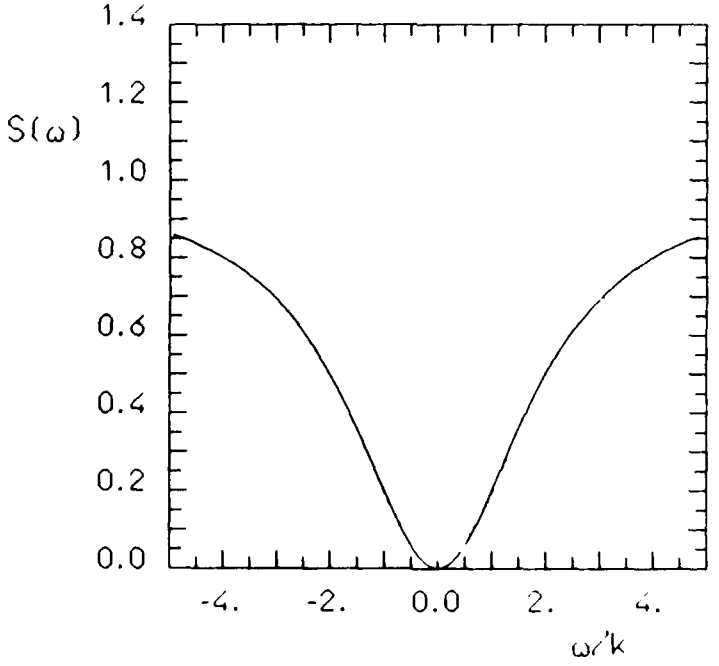


Figure 2: Spectrum of the quantum fluctuation in the intensity difference between the two signal beams of the roll pattern.

# The Influence of Noise and of Spatio–Temporal Nonuniformity on the Evolution of Optically Nonlinear Systems

**H. Ißler, S. Apanasevich[1], J. Grohs, A. Lyakhnovich[1], M. Kuball, J. Steffen, C. Klingshirn**

University of Kaiserslautern, Department of Physics, Erwin–Schrödinger–Straße, D–6750 Kaiserslautern, Germany, Phone –631 / 205 3112, Fax –631 / 205 3300

[1] Division for Optical Problems of Information Technology, Academy of Sciences, Minsk, Republic of Belarus

The investigation of noise induced switching processes in bistable systems is a field of active research [1] due to the omnipresence of noise in real systems. In this paper we extend the research on the influence of noise on the self oscillations of a hybrid ring resonator containing an optically nonlinear or even bistable element. The optically nonlinear element is a ZnSe interference filter showing thermally induced nonlinear refraction [2]. The quasistatic input–output characteristics (IOC) of the filter in reflection and transmission depend on the initial detuning of the Fabry–Perot and by changing this parameter it is possible to obtain bistable as well as monostable but strongly nonlinear behaviour. This element is incorporated in reflection mode into a ring resonator with long round trip time compared to the thermal relaxation time of the nonlinearity. The resonator is a hybrid one consisting of a photodiode transforming the light intensity reflected by the filter into a voltage signal which is delayed electronically and fed back to an electro optical modulator controlling the light falling onto the sample.

Using the photo thermally induced absorption nonlinearity in CdS in conjunction with such a kind of resonator [3] self oscillations of the light intensity in the resonator have been found. The oscillations are mode locked into multiples of the resonator round trip time. There are basic modes with a single maximum per oscillation period and higher modes with more maxima. The transitions between different oscillation modes are given by the Farey–tree structure. Due to the flat lower branch of the IOC used in [3] the basic modes had only one decreasing step in the resonator intensity, and of higher modes only the second Farey–tree generation was observed.

In the present case we can detune the dispersive nonlinear element by changing the angle of light incidence to achieve an IOC with a broad bistable region and higher steepness of the lower branch as it is shown in the inset of Fig. 1. The figure itself shows the oscillation mode obtained with this IOC in the ring resonator with a delay time $\tau_d = 200$ ms much longer than the typical relaxation time of the nonlinearity of about 100 $\mu$s. One can realize that there are three different maxima (two have nearly the same value) during the whole oscillation period of $6\tau_d$. This means that the mode of Fig. 1 belongs to the third generation of the Farey–tree. Additionally, in this mode the lower maximum is due to the part of the lower branch of the IOC with a negative slope.

Using an IOC as it is shown in the inset of Fig. 2 with an almost disappearing bistable region and thus with a very steep middle part we can observe the noise induced destruction of the

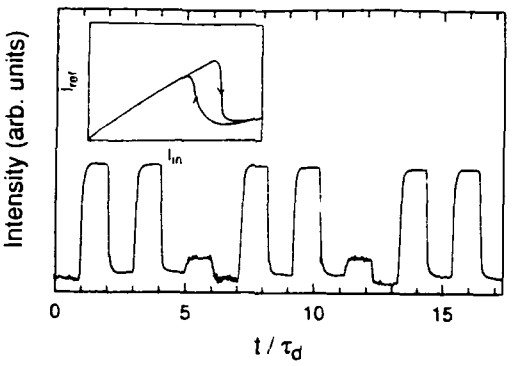


Figure 1: Stable oscillation mode with 3 different maxima per period, i. e. third generation of Farey–tree structure.

mode locked oscillations (Fig. 2, left side). The destruction occurs when the system reaches the critical region of the IOC with a high steepness where the external fluctuations are amplified and, being fed back, lead after some round trips in the resonator to noise induced switching processes. This phenomenon can only occur if the noise spectrum has prominent components at frequencies lower than the inverse response time of the nonlinear element [4]. The simulation is carried out on the basis of an ordinary differential equation for the temperature in the center of the laser spot. Without external noise or in presence of noise containing only too high frequency components the simulation indeed shows a mode locked oscillation, and only with low frequency fluctuations of sufficient amplitude the experimental observation is modeled quite adequately as can be seen from the right side of Fig. 2.

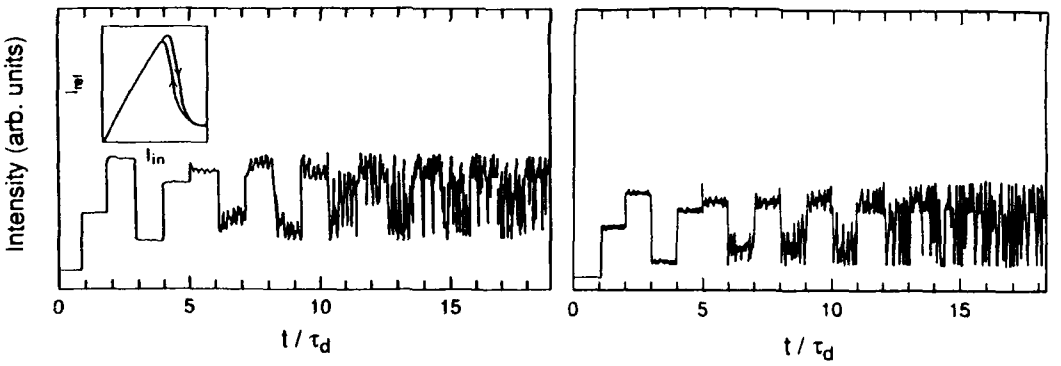


Figure 2: Starting from an empty resonator the mode locked oscillation bound to the delay time is destructed after about $10\tau_d$ by noise (left: experiment, right: simulation).

Apart from temporal changes of the light intensity the nonlinear behaviour may be also influenced drastically by the spatial nonuniformity of the switching process [5]. Further understanding of the latter aspect is gained by taking into account the transverse distribution of light and temperature in the nonlinear element. Because of the longer relaxation time and thus better experimental accessibility we now use the thermally induced absorption nonlinearity in CdS.
In longitudinal direction the problem can be regarded as homogenuous because of the small thickness of the sample of some microns compared with the thermal diffusion length of around

100 microns.

We use a gaussian holding beam with a diameter of about 200 microns and a power level within the bistable region of the hysteresis loop. The crystal is in the low absorbing state. By injecting a temporally ($t_P$ = 2ms) and spatially (d=20 $\mu m$) small pulse we induce a partial switching of the crystal, i. e. minimum transmission in the center of the spot. The resulting spatiotemporal dynamics depends on the energy of the switching pulse deposited into the sample and on the power level of the holding beam. First, the switched area spreads in radial direction but then it may contract again depending on the energy deposited by the switching pulse. The contraction may be up to nearly zero radius, showing again a bell–shaped profile of the transmitted intensity but with lower overall value. The induced temperature profile may be metastable.

After this, the system relaxes to its final state either on the high or low absorbing branch of the bistable loop depending on the energy of the short pulse. The closer the pulse energy is to the value just necessary to induce full switching the longer is the lifetime of the metastable state (typically several ms). This behaviour can be seen in Fig. 3 in the case of a sufficient pulse energy to induce full switching. The radius of the switched area is given as a function of time. The contraction of the switched area and the arise of the metastable intensity profile may be

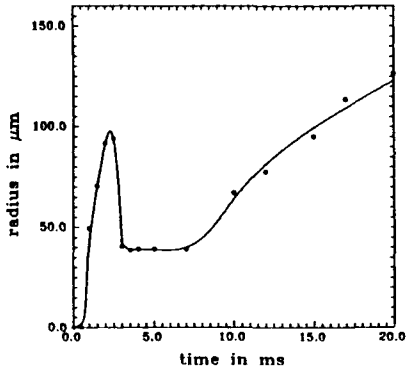


Figure 3: The radius of the high absorbing area of the holding beam as a function of time. The short pulse is switched on at t = 0 ms.

attributed to the presence of the third unstable branch in an optically bistable system. To get a closer correspondence to the three–dimensional relaxation like in the interference filter further investigations will concern the spatio–temporal dynamics of CdS crystals on different substrates.

## References

[1] "Dynamics of First Order Phase Transitions in Equilibrium and Nonequilibrium Systems", S. W. Koch, Lecture Notes in Physics **207**, Springer (1984); W. Lange, F. Mitschke, R. Deserno, J. Mlynek, Phys. Rev. A **32**, 1271, (1985); L. A. Lugiato, G. Broggi and A. Colombo in "Frontiers in Quantum Optics", ed. R. Pike, Hilger, London (1987);

[2] F. V. Karpushko and G. V. Sinitsyn, J. Appl. Spectrosc. **29**, 1323 (1978);

[3] M. Wegener and C. Klingshirn, Phys. Rev. A **35**, 1740 (1987) and Phys. Rev. A **35**, 4247 (1987);

[4] J. Grohs, A. Schmidt, M. Kunz, C. Weber, A. Daunois, A. Rupp, W. Dötter, F. Werner and C. Klingshirn, Proc. SPIE **1127**, 39 (1989);

[5] S. Apanasevich, A. Lyakhnovich, Phys. Stat. Sol. (b), **150**, 507 (1988); H. X. Nguyen, V. D. Egorov, A. Harendt, E. V. Nazvanova, phys. stat. sol. (b) **148**, 407 (1988)

# Transient statistics in the switch-on of class B lasers.

S. Balle, and M. San Miguel, Dep. de Física, Univ. Illes Balears, E-07071 Palma de Mallorca, Spain.

N. B. Abraham, Physics Dept., Bryn Mawr College, Bryn Mawr, PA 19010-2899, USA.

Tel: + 34 71 173234 Fax: + 34 71 438028

The transient evolution of the output of a single-mode class B laser (SML) after it is switched-on has been characterized from an experimental point of view by the evolution of the output intensity,[1, 2] both in the linear and non-linear regimes. However, from a theoretical point of view the characterization of the transient statistics of a SML beyond the linear regime has not been considered in detail.[3-5] Nevertheless, it has been possible to analyze both the linear and non-linear regimes for class A lasers,[6] showing that the transient statistics during the non-linear regime constitute a mapping of the transient statistics in the linear regime. In this case, an approximate solution for a switch-on event can be constructed (QDT approximation, [7]) which allows to examine the correspondence between the transient statatistics in both regimes. The main difficulty for a SML arises from the fact that no analytical solution of the deterministic rate equations is known, though it has been shown numerically[3, 4] that the QDT approximation succesfully explains the transient statistics in both the linear and non-linear regimes. Accordingly, we expect that the transient statistics in the non-linear regime can be understood as a mapping of the Passage Time (PT) statistics. The reason is that the random PT $t^*$ – defined as the time when the intensity reaches a reference value $I_r$ – determines both the beginning of a deterministic stage of evolution and the initial conditions for this period,[3-5] which lasts until the vicinity of the asymptotic steady state is reached.

The PT statistics for a SML can be analytically calculated since they involve only the first stages of evolution, when the intensity is small and a linear approximation holds.[3, 4] Nevertheless, different results are obtained according to whether the SML is gain-switched or Q-switched. In order to clearly distinguish the two cases, the stochastic rate equations equations can be conveniently written in adimensional form,

$$\partial_\tau z = \frac{1+i\theta}{2\epsilon} z \left( \frac{\Delta}{1+\sigma|z|^2} - 1 - L(\tau) \right) + \sqrt{2(\eta_1 + \eta_2 \Delta)} \xi_z(\tau) \ , \tag{1}$$

$$\partial_\tau \Delta = \epsilon \left( 1 + \lambda(\tau) - \Delta - \frac{\Delta}{1+\sigma|z|^2} \right) - \epsilon^2 \sqrt{2(\eta_1 + \eta_2 \Delta)} [z^* \xi_z(\tau) + z \xi_z^*(\tau)] \ , \tag{2}$$

where $z$ is the scaled complex amplitude of the laser field and $\Delta$ is the population inversion scaled to its threshold value. In the case of Q-switching, $\lambda(\tau) = 0$ and $L(\tau) = L_{off}\Theta(-\tau) - L_{on}\Theta(\tau)$, while for gain-switching we have $L(\tau) = 0$ and $\lambda(\tau) = -\lambda_{off}\Theta(-\tau) + \lambda_{on}\Theta(\tau)$. $\xi_z(\tau)$ is a complex white noise of zero mean and correlation

$$< \xi_z(\tau) \xi_z^*(\tau') >= 2\delta(\tau - \tau')$$

modelling spontaneous emission. An approximate solution to the stochastic rate equations can be constructed for both $\tau < \tau^*$ and $\tau > \tau^*$. For $\tau < \tau^*$, the complex electric field is small and its evolution is dominated by spontaneous emission, and the population inversion increases independently of the intensity. For $\tau > \tau^*$ and until the vicinity of the asymptotic steady state is reached, the system evolves unaffected by spontaneous emission noise. Therefore we have that the evolution of the system during the transient non-linear regime is given by

$$\frac{dx}{d\Delta} = f(x, \Delta) \tag{3}$$

where $x = |z|^2$, with initial conditions

$$\tau = \tau^* \Rightarrow \begin{cases} x = x_r \\ \Delta = \Delta(\tau^*) \end{cases} \tag{4}$$

Equations (3) and (4), which are equivalent to (1)-(2) in the domain of validity of the QDT approximation, determine the non-linear mapping of PT statistics into the transient statistics for the non-linear regime. The reason is that (3) defines an autonomous system which is completely determined by the initial condition (4), and provided that the whole influence of spontaneous emission noise is contained in the initial condition (4), the statistical properties at any time are determined by those at the PT, and in particular by the PT statistics. It has to be noted that (4) defines a random initial condition for $\Delta$ at the random time $\tau^*$, but their statistical properties can be calculated in the linear stochastic regime.

The statistical properties of any function $y$ of the dynamical variables $x$ and $\Delta$ are therefore determined as a time-dependent mapping of the PT statistics. However, if we are interested in e. g. the statistical properties of the extreme values of this function, the time dependence can be eliminated, yielding

$$y_{extreme} = F[x_r, \Delta(\tau^*)] \ . \tag{5}$$

Therefore, the statistical properties of $y_{extreme}$ can be determined from those of the PT. In particular, the variance of the PT distribution for SML is rather small and then a linear expansion in $\tau^*$ holds, and so we find that the statistical properties of $y_{extreme}$ are given as a linear transformation of those of the PT.

From such analysis we show that the maximum intensity and the extreme values of the SML frequency during each switch-on event depend linearly on the turn-on time for this particular event. In addition, these quantities scale with the pump rate so that they are given as

$$y_{extreme} = < y^0_{extreme} > + a(\sigma)\lambda_{on}(\tau^* - < \tau^* >) \ , \tag{6}$$

where the parameters $a(\sigma)$ can be calculated from the rate equations. They depend only on the saturation parameter $\sigma$. Numerical evidence of these relations is provided. The main

consequence is that the statistical properties of extreme values of the dynamical variables in the non-linear regime can be obtained by a linear transformation of the PT statistics.

An analytical determination of the coefficients $a(\sigma)$ is not possible since it requires the solution of Eq. (3), which is not known. Nevertheless, assuming that the evolution of $\Delta$ during the peak is governed by its coupling to the laser field, an approximate equation is found that yields approximate values for $a(\sigma)$ which agree with those resulting from the simulation.

Finally, we also show that the main difference between gain-switching and Q-switching is the opposite sign of the slopes $a(\sigma)$ for the same magnitude. The reason is that, during a Q-switching event, the population is almost completely inverted, and the later the PT, the lower its value. However, in gain switching we have that the population inversion is growing due to the action of the high pump until the PT, so that the later the PT occurs, the higher the population inversion.

## References.

[1] F.T. Arecchi, R. Meucci, and J.A. Roversi, Europhys. Lett. **8**, 225 (1989); F.T. Arecchi, W. Gadomski, R. Meucci, and J.A. Roversi, Phys. Rev. A **39**, 4004 (1989); Opt. Commun. **65**, 47 (1988).

[2] P. Spano, A. D'Ottavi, A. Meccozzi, B. Daino, and S. Piazzolla, IEEE J. Quantum Electron. **25**, 1440-1449 (1989).

[3] S. Balle, P. Colet and M. San Miguel, Phys. Rev. A **43**, 498-506 (1991).

[4] A. Mecozzi, P. Spano and A. Sapia, Opt. Lett. **15**, 1067 (1990); P. Spano, A. Mecozzi and A. Sapia, Phys. Rev. Lett. **64**, 3003 (1990).

[5] S. Balle, N. B. Abraham, F. de Pasquale and M. San Miguel, Phys. Rev. A (1992) (to be published).

[6] For reviews, see for instance F. T. Arecchi in *Noise and Chaos in Nonlinear Optical Systems*, edited by F. Moss, L. Lugiato and W. Schleich (Cambridge University Press, 1990) and M. San Miguel, "Statistics of Laser Switch-on", in *Laser Noise*, SPIE Proceedings Vol. 1376, edited by R. Roy, (SPIE, Bellingham, Washington, 1991) 272-283.

[7] F. de Pasquale and P. Tombesi, Phys. Lett. A **72**, 7 (1979); F. de Pasquale, P. Tartaglia and P. Tombesi, Z. Phys. B **43**, 353 (1981); Phys. Rev. A **25**, 466 (1982).

# Two-peaked passage time statistics in a Q-switched $CO_2$ laser near threshold

R. Meucci, M.Ciofini, F.T.Arecchi and Peng-ye Wang*

Istituto Nazionale di Ottica

Largo E. Fermi 6, 50125 Firenze, Italy

Tel.(+)39 55 221179

Fax.(+) 39 55 2337755

In this paper we report experimental evidence of two-peaked transient time statistics in a single mode $CO_2$ laser and we show that this phenomenon is due to the population inversion fluctuations. The same statistical feature has been also observed in dye[1] and semiconductor[2] lasers. However, in the first case two-peaked passage time distributions arise from the coupling between two transverse modes, while in the second case they are induced by the correlation between two successive pulses.

The experimental set up consists of a single mode $CO_2$ laser. The cavity losses are switched by an intracavity electro optic modulator. At t=0 the cavity loss parameter k is changed from an initial high value $k_0$ to a final low value $k_1$. The laser output pulse is detected with a Hg-Cd-Te photodiode having a rise time less than 10 ns. The threshold photon number n, at which the passage time is measured, is set to $n=I_s/2$ [3], where $I_s$ is the saturation value.

Interesting phenomena appear when the initial state is set, adjusting the excitation discharge current, close to the laser threshold. In this case, first passage time distributions with two peaks are observed, as shown in Fig.1 which corresponds to initial laser states ±0.6% from threshold. The two-peaked distributions are observable in a range of current of about 0.08 mA which is larger than the current stability of the power supply (± 0.005 mA).

The class B laser dynamics can be described by two equations for the complex field amplitude $E=|E|\exp(i\phi)$ and population inversion $\Delta$

$$\frac{dE}{dt}=-k(t)E+\frac{G\Delta E}{2}+(GN_2)^{1/2}\xi(t) \qquad (1)$$

$$\frac{d\Delta}{dt}=-\gamma(\Delta-\Delta_0)-2G\Delta|E|^2+(R)^{1/2}\zeta(t) \qquad (2)$$

where k is the decay rate of the field, $\Delta_0$ is the population inversion provided by the pump mechanism, $G=4.6X10^{-8}s^{-1}$ is the field-matter coupling constant[3] and $\gamma=1.0X10^{4}s^{-1}$ is the population decay rate. $\xi(t)$ and $\zeta(t)$ are two uncorrelated stochastic functions with zero mean value and $\delta$-correlated.

In order to compare the experimental results with the model, we have performed numerical simulations of the stochastic rate equations (1) and (2). The following parameter values are used: $k_0=1.12X10^{7}s^{-1}$, $k_1=7.50X10^{6}s^{-1}$, $GN_2=2.0X10^{9}s^{-1}$, $R=6.8X10^{29}s^{-1}$. $\Delta_0$ is estimated via the relation $\Delta_0=Mi$ (where i is the discharge current and $M=7.39X10^{13}mA^{-1}$ is a coupling constant[3]).

Figure 2 shows the simulated passage time distributions in presence of population inversion noise, while in Fig. 3 we report the numerical results with R=0 to confirm the essential role played by the population noise in determining two-peaked distributions.

A theoretical interpretation of this phenomenon can be given making some assumptions about the field during the preparation phase (t<0).

**References**

*Permanent address: Institute of Physics, Academia Sinica, Beijing, China.

[1]A.W.Yu, G.P.Agrawal, and R.Roy, J. of Stat. Phys. **54**, 1223 (1989).

[2]T.M.Shen, IEEE J. of Lightwave Technology, 7 1394 (1989).

[3]F.T.Arecchi, R.Meucci, and J.A.Roversi, Europhys. Lett. **8**, 225 (1989); M.Ciofini, R.Meucci and F.T.Arecchi, Phys. Rev. A **42**, 482 (1990).

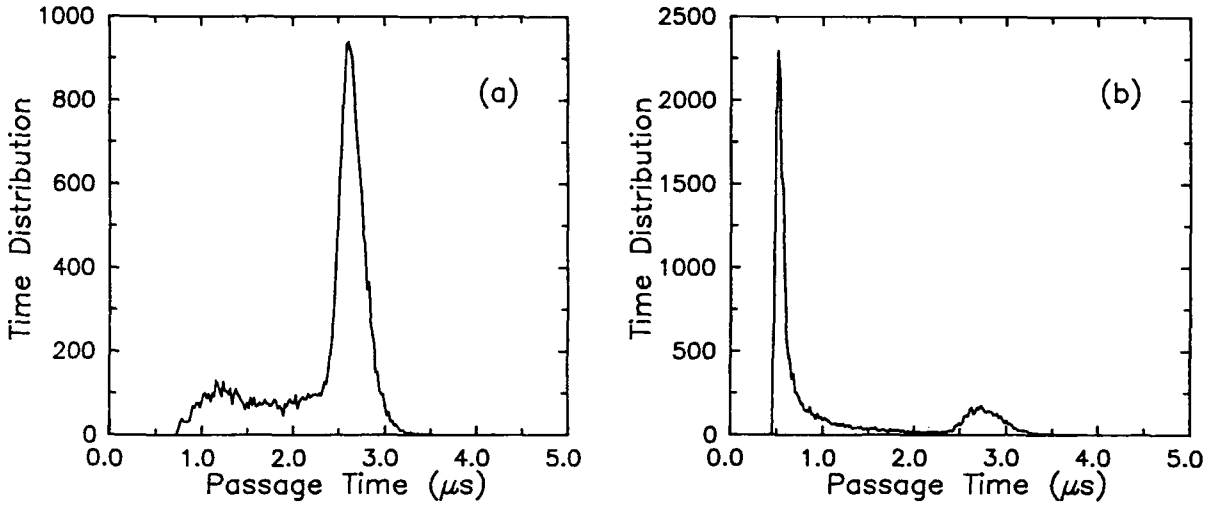


Fig.1. Experimental passage time distributions.

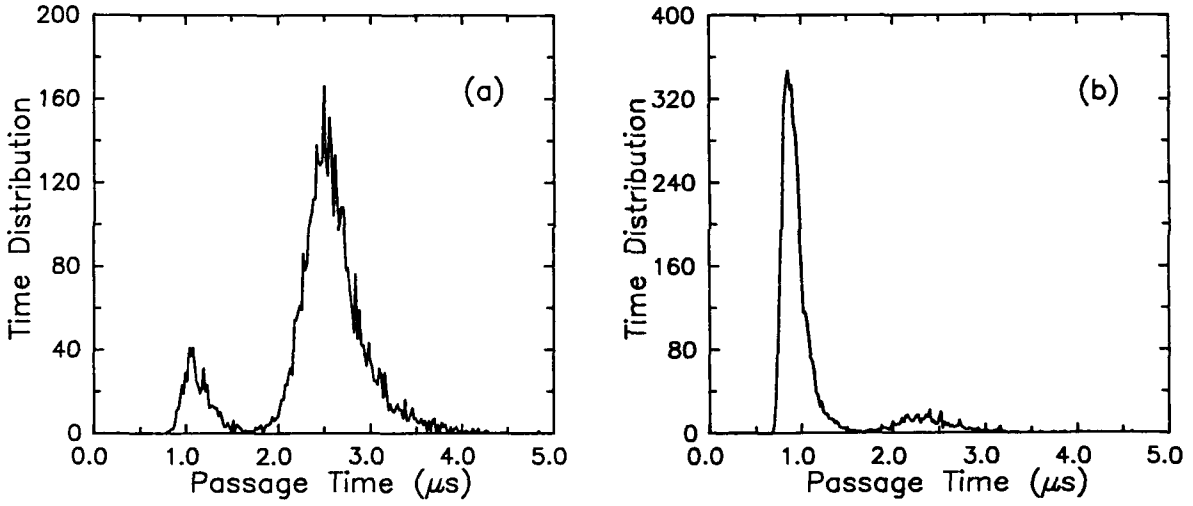


Fig.2. Numerical results close to threshold with 5,000 trajectories.

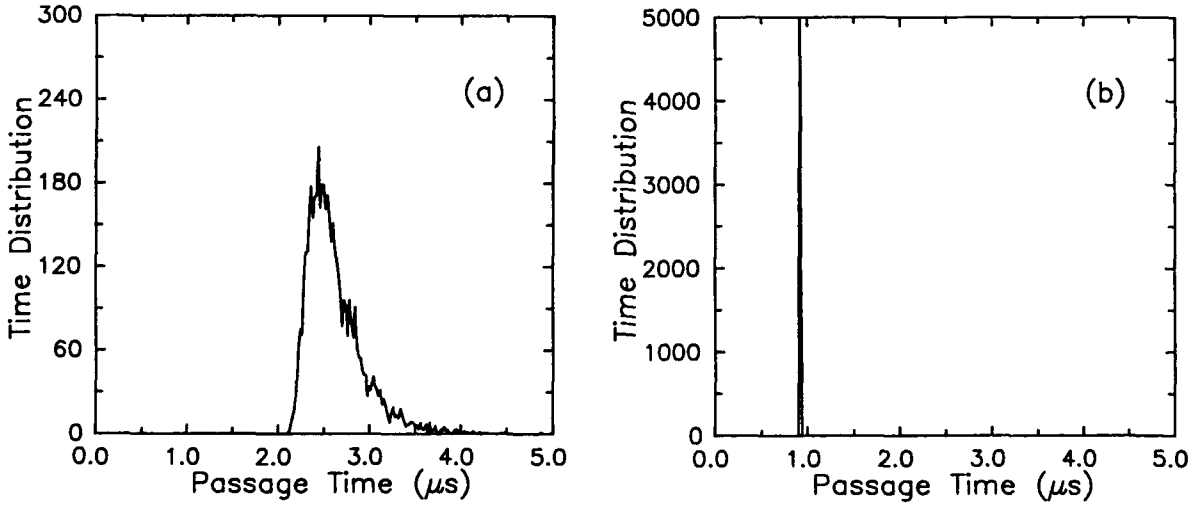


Fig.3. Numerical results as in Fig. 2 with R=0.

# Period-One Oscillation in Chaotic System with Multimodal Mapping

Yun Liu
Graduate School of Electronic Science and Technology
Shizuoka University, 3-5-1 Johoku, Hamamatsu, 432 Japan
Tel +81-53-471-1171 Fax +81-53-475-1764
Junji Ohtsubo
Faculty of Engineering, Shizuoka University
3-5-1 Johoku, Hamamatsu, 432 Japan
Tel +81-53-471-1171 Fax +81-53-475-1764

## 1. Introduction

The behavior of chaotic system described by a differential difference equation (DDE) with a low dimensional mapping has been extensively studied.[1,2] However, the details of the dynamic behaviors especially for a multimodal mapping have not yet been fully understood. It is clear that the usual linear stability analysis can not work for this case, since more than two equilibria exist in the dynamics of the system.

The purpose of this paper is to present some novel results in a chaotic system whose dynamics can be described by a DDE with a multimodal mapping. The physical model is the active interferometer proposed by the authors recently.[3] With an appropriate choice of the control parameters, we can easily realize the multimodal regions in the laser output power. For the case of a small delay time, the output power in such region shows a relaxation-like oscillation. With the increase of the delay time $t_r$, the waveform evolves into a steady state oscillation which has the period near the delay time. We call this new type of oscillation period-one oscillation to distinguish such as period-$2t_r$, $2t_r/3$, $2t_r/5$,... oscillations in usual period-doubling bifurcation scenarios. The experimental results are coincide with the numerical simulations calculated from the corresponding DDE.

## 2. Theoretical Model and Simulation

The experimental model for our system is shown in Fig.1. The light output from a laser diode is directed into a Twyman-Green interferometer. The interference signal is detected by a photodiode and fed back into the injection current to the laser diode. The feedback loop consists of an amplifier and a digital delay circuit. The important point is that the laser output power is nonlinearly converted to the injection current through the interference signal and, accordingly, the relation forms the nonlinearity of the whole system. The dynamics of such system can be described by a DDE as

$$\tau \frac{dX(t)}{dt} + X(t) = P_b - \mu X(t - t_r)\{1 + b\cos[\kappa X(t - t_r) - \phi_0]\}, \qquad (1)$$

where $X(t)$ is the time-dependent laser output power at time $t$ and $\tau$ is the response time of the system. $P_b$ represents the bias output power of the laser diode and is linearly proportional to the bias injection current. $\mu$ is a measure of the damping factor for the light output power in one open feedback loop and can be controlled by the feedback gain. $\kappa$ is a parameter proportional to the optical path difference of the interferometer arms. $b$ and $\phi_0$ are the constants of the system.

Generally, the periodic term in the right hand-side of above equation yields the multimodal mapping when the differential term can be disregarded. In this paper, we discuss the behavior of the system in which more than two humps are involved in the output power regions. Fig.2 schematically shows a multimodal mapping having two equilibria $p_1$ and $p_2$

within the range of the output variations. We numerically calculated the output power from Eq.(1) and investigate how the output power varies when the differential term in Eq.(1) is taken into consideration.

Fig.3 shows the main results of the numerical simulations. In Fig.3, $P_b$ is fixed at 1.29mW and the delay times are set to be 2.7 and 5.0 (in unit of the system's response time $\tau$) for (a) and (b), respectively. The other parameters are fixed as $\mu$=0.4, $b$=0.8, $\kappa$=4.8$\pi$, and $\phi_0$=0. The waveform in Fig.3(a) is a relaxation-like oscillation with the period of the envelope being 48.76$t_r$. The fine oscillation having the period near the delay time can be also seen in this figure. When the delay time is increased, the relaxation oscillation disappears and the output power is dominated by the period-one oscillation as is shown in Fig.3(b). The calculated period of the oscillation in this state is 1.11$t_r$.

## 3. Experimental Results

The light source used in the experiment is a single mode laser diode of a 5mW maximum power with a 780nm oscillation frequency. In the experiment, we fixed $\mu$ at about 0.4 and the optical path difference of the interferometer arms to be 0.9cm which results $\kappa$ being 4.8$\pi$[mW$^{-1}$]. The bias injection current to the laser diode and the delay time are varied to search the regions for the relaxation-like and period-one oscillations. It is found that for a fixed delay time, such region and the normal region appear alternately. Here, the normal region means the region in which the usual period-doubling bifurcation schemes are observed. The same results are also obtained in the numerical simulations.

Fig.4 shows two instances for the experimental results at two different delay times. Fig.4(a) and (b) are the results for $t_r$=0.5 and 1.0ms, respectively. The periods for the relaxation and fine oscillations in Fig.4(a) are measured to be 11.70 and 0.56ms, respectively. The period of the period-one oscillation in Fig.4(b) is 1.08ms. As expected from the simulation, the output power evolves into the period-one oscillation when the delay time increases. It is noted that, in comparison with the simulation results, the phenomenon of frequency locking can be seen in the waveform in Fig.4(b). With the further increase of the delay time, even the second harmonic solution of the period-one oscillation can be observed not only in the simulation but also in the experiment. We also investigate the dependence of the duty ratio of the period-one oscillation on the control parameters.

## 4. Summary

We have observed the relaxation-like and period-one oscillations in the light output power in a chaotic system which consists of a laser diode active interferometer. The dynamics of such a system is described by a DDE with a multimodal mapping. The simulations agrees well with the experimental results. Obviously, such relaxation and period-one oscillations can not be explained by the counterparts in the discrete mapping. This phenomenon implies the fact that the coupling between the discrete and continuous properties of actual physical system leads to very complicated dynamical behaviors of the system output.

## References

[1] K. Ikeda, Opt. Comm. **30** (1979) 257.
[2] J.Y. Gao, L.M. Narducci, H. Sadiky, M. Squicciarini, and J.M. Yuan, Phys. Rev. A **30** (1984) 901.
[3] Y. Liu and J. Ohtsubo, to be published in J. Opt. Soc. Am. B.

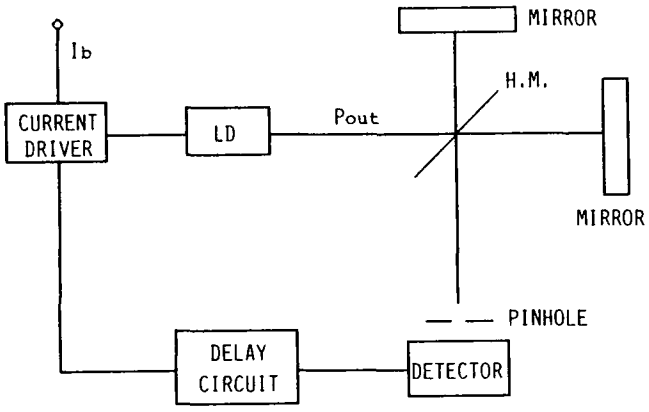


Fig.1 Experimental setup. LD: laser diode. H.M.: half mirror.

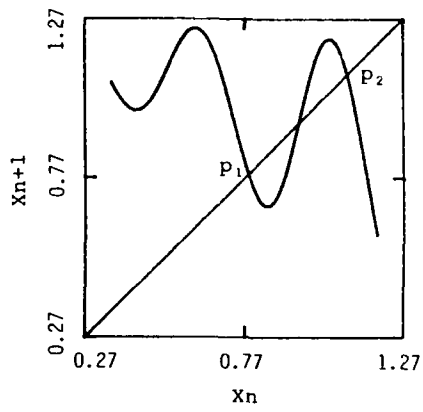


Fig.2 Multimodal mapping between $X_{n+1}$ and $X_n$. Two equilibria case.

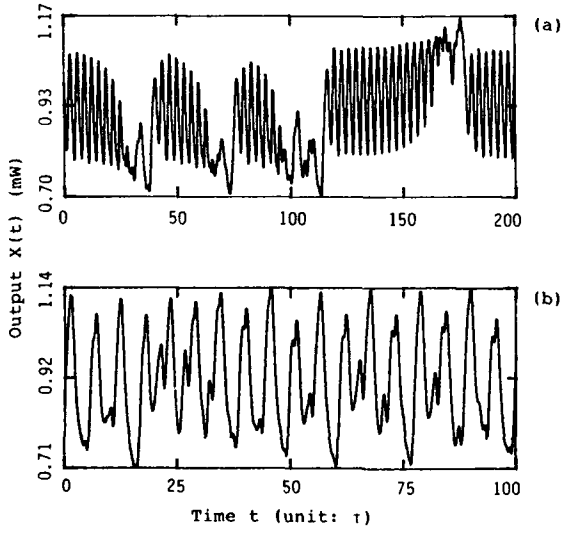


Fig.3 Numerical results at $P_b$=1.29mW. (a) the relaxation oscillation at $t_r$=2.7, and (b) the period-one oscillation at $t_r$=5.0.

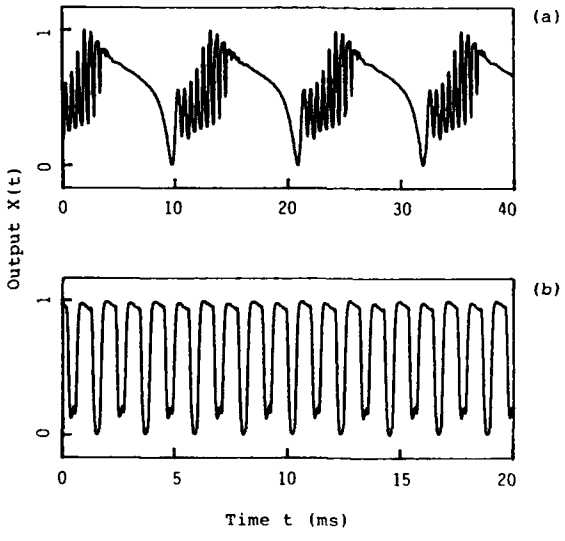


Fig.4 Experimental observations at $P_b$=1.2mW. (a) the relaxation oscillation at $t_r$=0.5ms, and (b) the period-one oscillation at $t_r$=1.0ms.

Friday, June 26, 1992

# Special Topics in Chaos

**FB** 10:40am–12:00m
Schroedinger Hall

Govind R. Agrawal, *Presider*
*University of Rochester, U.S.A.*

# Radiation-trapping: a new mechanism for chaos in optical systems

M. Möller, W. Lange

*Institut für Angewandte Physik, Westfälische Wilhelms-Universität,*
*Corrensstr. 2/4, D-W-4400 Münster, Germany*
*Tel. +49-251-833535, Fax +49-251-833513*

Chaos in simple optical systems can be caused by a number of known mechanisms such as time delays or modulated parameters, or by more intrinsic effects like Rabi oscillations – described by the "Laser-Lorenz equations" – or by the light shift in conjunction with an external magnetic field. We show that the effect of radiation trapping, i.e. the reabsorption of fluorescence light, can produce chaos as well.

The system we study is a sodium-filled Fabry-Perot resonator that is known to show self-oscillations due to spin precession in the ground state under the influence of a transverse static magnetic field [1]. These oscillations can become chaotic if the magnetic field is not perpendicular to the optical axis [3]. In the experiment we observe wide parameter ranges of irregular behaviour, chiefly a range of quasiperiodic oscillation followed by period-doubling into chaos [4]. After running through the sequence described, the system will switch into a state of high transmission, in which further oscillatory behaviour including chaos is possible. The experiment shows that upon this switching, the former nearly Gaussian transmitted beam changes to a transverse structure that can be described as a superposition of low-order Gauss-Laguerre or Gauss-Hermite modes. Its exact shape was not reproducible, since it depends on very small alignment inaccuracies. For that reason, we inserted an aperture into the resonator to prevent premature mode switching and restricted our measurements to the region before the switching. As this proved to have no influence on the dynamical behaviour in this range, there is no transverse dynamics dominating these nonlinear oscillations.

The two regions of chaotic behavior correspond to two different ranges of the resonator phase. In Fig. 1

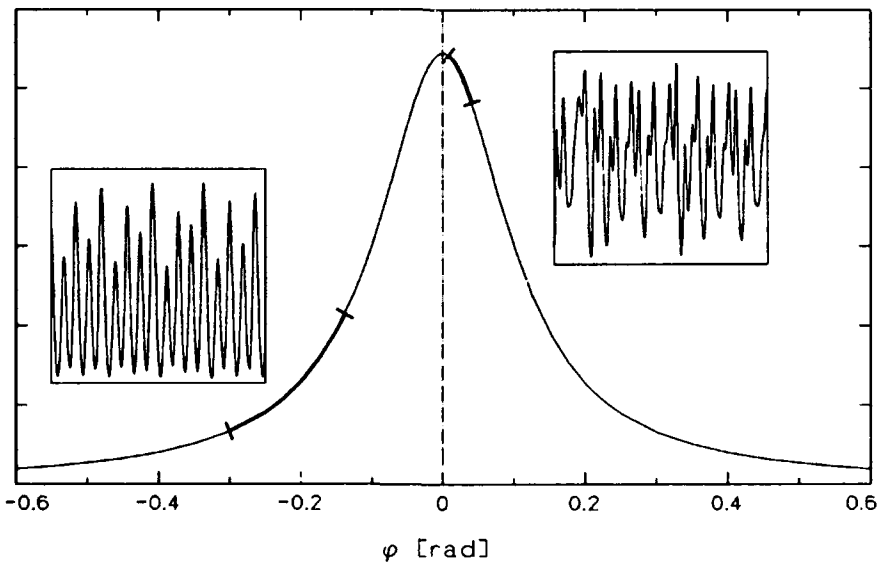


Figure 1: Resonance curve of the Fabry-Perot resonator as a function of the total resonator phase shift (see text). Shown are typical phase ranges covered during oscillation for radiation-trapping induced chaos (left hand slope) and light-shift induced chaos (right hand slope).

the resonance curve (Airy function) of the resonator is shown, its argument being the total resonator phase shift $\varphi$. This quantity consists of a linear component $\varphi_0$, determined by the optical round-trip length in the absence of nonlinear effects, and a nonlinear component $\varphi_{nl}$, depending on the dynamical variables. The high transmission state corresponds to a phase range near the top of the maximum, for positive values of $\varphi$, while the oscillations before the switching take place in a range of negative $\varphi$. In the experiment, a distinction between both types is possible via phase scans and by differences in the signal shapes, especially in the modulation contrast.

Dimension estimations performed on about a hundred measured time series show that attractor dimensions do not exceed a value of about 2.3 for both types, suggesting that the fundamental dynamics of each might be contained in 3-dimensional models. The microscopic model presented in [1] and [2], however, involves the three cartesian components of the spin expectation value in the ground state plus the population of the excited state – unless its decay constant is large enough to permit adiabatic elimination. It has recently been shown by Boden et al.[5] that a reduced model comprising only the ground state polarization shows chaos on the right slope of the Airy function, and that in that model light-shift is the predominant physical mechanism.

Introducing phenomenologically the effect of radiation trapping [6], i.e. the reabsorption of fluorescence light, adds an incoherent pump mechanism that acts destructively on the ground state orientation and simultaneously leads to a seemingly longer lifetime of the excited state population. Thus it provides a strong nonlinear coupling between the excitation and the spin component parallel to the optical axis. There is a striking quantitative agreement between simulations using this model and the experimental measurements on the left side of the Airy function (Fig. 2), in particular in attractor dimension and entropy values.

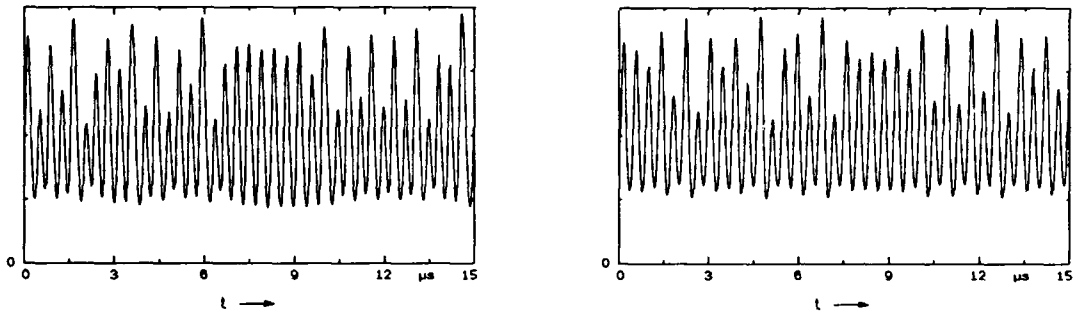


Figure 2: Measured (left) and simulated (right) time series of chaos of the radiation-trapping type.

It is also possible to reduce the model to three dimensions by considering instead a purely transverse magnetic field and completely neglecting the light-shift contribution. The remaining variables are the two spin components perpendicular to the magnetic field and the excited state population. Performing the simulation using this second reduced model yields – without changing the values of any parameters - qualitatively the same behavior as the full four-dimensional model. Thus the effect of radiation trapping, although introduced here in a most simplified way, turns out to be responsible for the generation of the new type of chaotic behavior in sodium-filled Fabry-Periot resonators studied here.

**References**

[1] F. Mitschke, R. Deserno, W. Lange, J. Mlynek: Phys. Rev. A33, 3219 (1986)

[2] J. Nalik, W. Lange, F. Mitschke: Appl. Phys. B49, 191 (1989)

[3] F. Mitschke, C. Boden, C. Henning, I. Roloff: in "Coherence and Quantum Optics VI", J.H. Eberly, L. Mandel and E. Wolf, Eds., (Plenum 1989), p.759

[4] W. Lange, M. Möller, K. Iwankiw, M. Oestreich, J. Nalik: in "Nonlinear Dynamics in Optical Systems", (Opt. Soc. of. Am, Wash. DC 1990), pp.FB4-1/439,

[5] C. Boden, M. Dämmig, F. Mitschke: preprint

[6] M. Möller, W. Lange: to be published

# Space-time representation of a delayed dynamical system

F.T. Arecchi (+), G. Giacomelli, A. Lapucci and R. Meucci

Istituto Nazionale di Ottica
Largo E. Fermi 6, 50125 Firenze - Italy
Phone 39 -55 - 221179, Fax 39 - 55 -2337755

Summary

In nonlinear optics the transition to high dimensional chaos is realized either by letting many modes to compete in an optical resonator [1] or by introducing a delayed feedback [2]. Whenever data can be organized on a two dimensional domain, some hidden features of the complex dynamics appear explicitely as suitable patterns.

We make use of an equivalent two dimensional representation to organize the data provided by an experimental system with DD dynamics (delay-differential). This data reorganization sheds light on two non trivial types of correlations.

The experimental system consists of a single mode $CO_2$ laser with an intracavity loss modulation driven by a signal proportional to the output laser intensity. In the feedback loop from the detector to the modulator we insert a delay line and an amplifier. The chaotic laser intensity had a correlation time $T_c$ of a few tens of microseconds.

Here we investigate what happens when we insert a delay $\tau = 1,400\mu s$, that is, ten times longer than $T_c$.

By measuring the time correlation over long times a new feature appears. While the correlation function decays over a $T_c$ varying over tens of microseconds it has a revival after a time $\tau$. In such a case, the interplay of nonlinearity and delay implies two different relevant time scales.

A two dimensional re-organization of the data follows closely the numerical technique which solves DD equations [3]. The state of a DD equation such as

$$\dot{x}(t) = F(x(t), x(t-\tau)) \qquad (1)$$

is determined by all the values of the function $x$ in the interval $(t,\ t-\tau)$. This

function can be approximated by $N$ samples taken at intervals $\Delta t = \tau/(N-1)$. The evolution consists in a $N$-dimensional discrete mapping. Choosing the Euler integration scheme for Eq. (1), that is,

$$x(t+\Delta t) = x(t) + F\left(x(t), x(t-\tau)\right)\Delta t \quad , \tag{2}$$

the $N$-dimensional mapping is defined by the generic term [3]

$$x_s(k+1) = x_{s-1}(k) + F\left[x_{s-1}(k+1), x_s(k)\right] \tag{3}$$

where we have denoted by $s$ an index ranging from 1 to $N$ and corresponding to a single delay interval, and by $k$ a discrete index counting the delay units. Eq. (3) is completed by two slightly different equations at the boundaries $s = 1$ and $s = N$, as shown in Ref. 3.

The above procedure suggests an organization of the data in a two dimensional "space-time" domain $s - k$, where the space cell corresponds to a single delay and the unbounded time is spanned in terms of delay units.

As long as $\tau < T_c$, all points along the $s$ axis are strongly correlated and hence the two dimensional representation is a pure visualization of the technique leading to Eq. (2) but it does not bring any physical insight. In contrast, when $\tau >> T_c$ the points along the $s$ axis decorrelate, and then the correlation revives after $\tau$, as indicated by Eq. (3), yielding a nontrivial two dimensional representation. An organization of data along these lines (Fig. 1) shows indeed a cellular structure as in space-time turbulence [4].

Putting a threshold at 0.3 of the maximum pulse height, we obtain (Fig. 2) a digitized space-time picture in black (above threshold) and white (below threshold). The two dimensional representation provides a visual discrimination among the different types of chaotic behavior.

## References


1. F.T. Arecchi, G. Giacomelli, P.L. Ramazza and S. Residori, Phys. Rev. Lett. **65**, 2531 (1990).
2. K. Ikeda and K. Matsumoto, Physica **29D**, 223 (1989).
3. J.D. Farmer, Physica **4D**, 366 (1982).
4. B.I. Shraiman, Phys. Rev. Lett. **57**, 325 (1987).

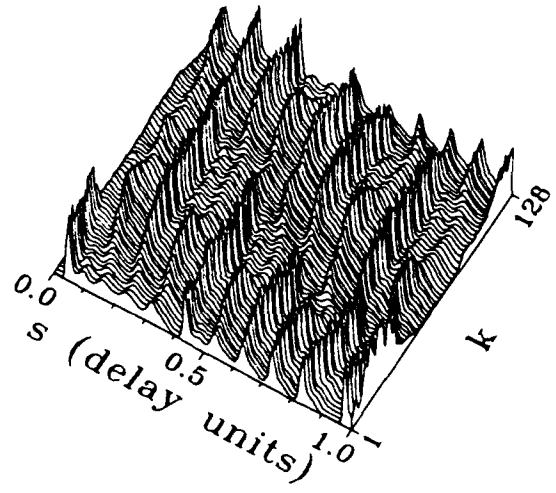


Fig. 1 Cellular pattern obtained by plotting the signal $x(s,k)$ versus $s$ $(0 < s < \tau)$ for successive $k$. The decay of the correlations along $s$ occurs over a time $T_c$ (around 0.1 delay units) while along $k$ correlations last for tens of delay units.

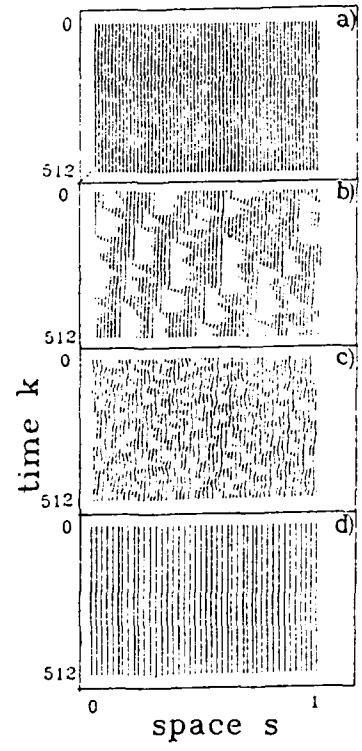


Fig. 2 Two dimensional representations of the laser signals for different value of the control parameter. The horizontal axis ranges over one delay unit while the vertical axis covers 512 delay units. The black regions correspond to data above the threshold and white regions to data below the threshold. Panels b) and c) show chaotic behaviors with different two dimensional patterns.Panel d) corresponds to a locked regime.

# Generalised Approach to the Theory of Radiation-Atom Interaction

Weihan Tan*, Weiping Lu and Robert G. Harrison

Department of Physics, Heriot-Watt University, Edinburgh EH14 4AS, U.K.

*On leave from Shanghai Institute of Optics and Fine Mechanics, P.R.C.

In describing the nonlinear interaction of radiation with matter it is well known that the perturbation expansion technique is used to calculate the atomic wave functions and the transitions between the states of a system. However the technique, though involving all states of the system, is valid only in the limit of weak interaction fields and non-resonant interactions. For strong fields and resonant interactions, density matrix or dressed atom formulisms are commonly used though these exact treatments are restricted to simple two level schemes or approximations of these; their application to general resonant-near resonant multilevel interactions being prohibitively complex.

In this letter we report on a generalised treatment for the interaction of optical fields of arbitrary field strengths with a multilevel system. This work is currently motivated by our susceptibility calculations of multilevel atomic systems, though we foresee the value of this treatment in wide range of radiation-atom interactions.

In this treatment the Hamiltonian is partitioned into two parts, one forming a dressed atomic state, the other for excitation between the states. This new formulism (TLH for short) allows for a natural change in the energy distribution of the two parts of the Hamiltonian according to the strength of the interaction. On reducing the field interaction strength, the level characterisation of the dressed states are changed until in the limit of weak field interaction the level features reduce to those of the unperturbed system. In general both parts of the Hamiltonian (dressed and excitation parts) exist simultaneously, their relative magnitudes depending on the field strength, the frequency detuning of the field from the atomic transitions and the degree of

coherence of the interaction according to the relative dephasing and de-energisation rates. Significantly for strong fields we find that most of the field energy is taken up in modifying the states, as for standard dressed states, only in the limit of incoherent interaction, while for coherent interaction this is limited to at most equal partitioning of the field energy to dressing and exciting the states.

The formulation is best understood by considering first a simple two level (m,g) system in which we define the partition parameter $\beta$ such that $(1-\beta)V$ is the dressing energy and $\beta V$ the energy for excitation. The parameter $\beta$ is determined by the field strength $x=\frac{\Omega_{mg}}{\sqrt{\bar{\Delta}^2+v^2}}$, $v=\frac{1}{T_2}$ and the degree of interaction coherence $\lambda=\frac{T_2}{T_1}\leq 2$ through the equation

$$(1-\beta)x=-\left(\frac{1}{2\lambda}+\frac{x}{2\lambda}\right)+\sqrt{\left(\frac{1}{2x}+\frac{x}{2\lambda}\right)^2+\frac{x^2}{\lambda}} \qquad (1)$$

Figs. 1,2 show the curves of $(1-\beta)x$ vs. x and $\beta$ vs. x for $\lambda = 2, 0.1$, respectively. From these figures, in the limit of coherent interaction $\lambda=\frac{T_2}{T_1}=2$, we have $1-\beta=\beta=0.5$; one half of the interaction energy is used for dressing and the other half for excitation. In the limit of incoherence interaction $\lambda << 1$, it is easily proved that $\beta \approx \lambda$ and a large part $(1-\beta)V$ is used for dressing, with a remaining small part, $\beta V$, for excitation.

In addition to eqn. (1), the following corresponding relation between weak field and strong resonant field interaction is established as:

$$\frac{\Omega_{mg}}{\omega-\omega_{mg}} \quad \Rightarrow \quad \frac{\beta\Omega_{mg}(\bar{\Delta}-iv)}{(1-\beta)^2\Omega_{mg}^2+\bar{\Delta}^2+v^2} \qquad (2)$$

Eqns. (1,2) constitute the main relations used to modify conventional theory such that it can be applied to strong and resonant interactions. For a particular system $\beta$ is determined from spectroscopic data.

In generalising this treatment to a multilevel system, we first note that conventional perturbation expansion theory usually consists of a multiple of factors of the form $\frac{\Omega_{mg}}{\omega-\omega_{mg}}$. By the relation (1), (2) each of these factors can be replaced by a corresponding factor subject to the conditions that not more than one of the level transitions is resonantly excited, the others being

off resonant ($\overline{\Delta} \gg \nu$). In practice this is descriptive of most real multilevel atomic and molecular interactions, the treatment thus providing an analytic basis for describing multilevel atomic-radiation interaction for arbitrary field strengths.

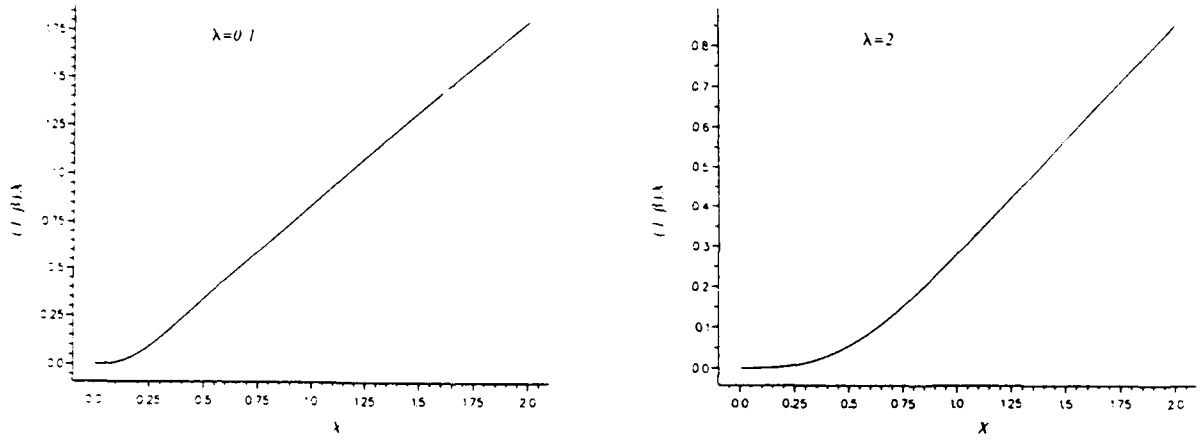


Fig. 1.

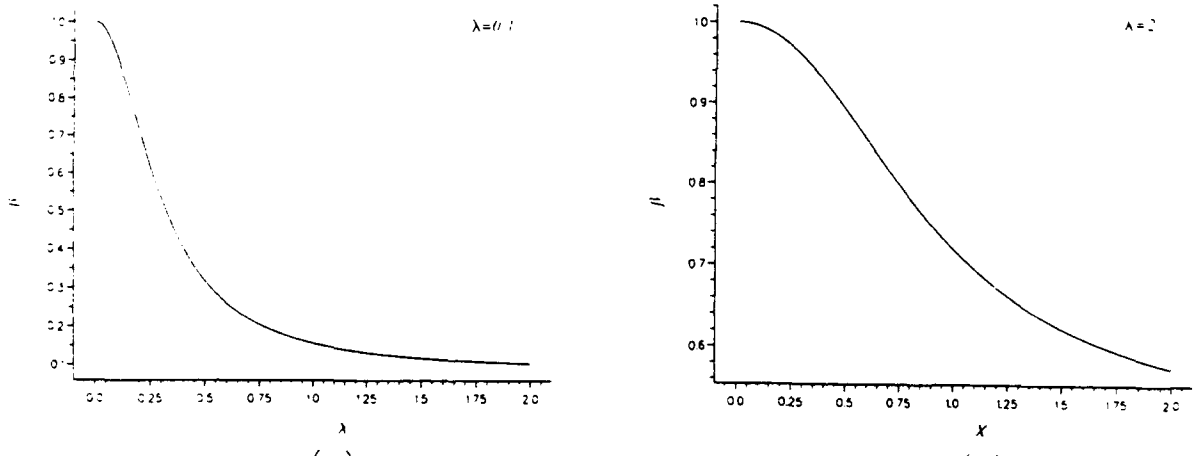


Fig. 2.

Fig. 1. Dressing splitting $(1-\beta)x$ vs. x. (a) $\lambda = 0.1$, (b) $\lambda = 2$.

Fig. 2 Partition parameter $\beta$ versus x. (a) $\lambda = 0.1$, (b) $\lambda = 2$.

# Neural Network Applications to Optical Chaos

S. D. Pethel, C. M. Bowden, and C. C. Sung
Weapons Sciences Directorate, AMSMI–RD–WS–ST
Research, Development, and Engineering Center
Redstone Arsenal, AL 35898–5248
Phone: 205-876-2650

## Summary

Modeling, characterization and prediction with regard to chaotic systems has been an area of vigorous pursuit for many years. Linear methods, such as Fourier decomposition, do not distinguish chaotic dynamical behavior from noise. Of fundamental importance is the characterization of the physical system or the underlying equations from a given time series or phase space attractor, as well as the influence of noise in coupling across basin boundaries and modifications of the otherwise purely deterministic dynamics. Local approximation methods in relation to arbitrary chaotic attractors, in general, are insufficient to deduce the generating equations and conditions.[1] A forward–feed, hidden–layer, neural network (FFNN), on the other hand, is manifestly a function generator, and when trained adequately on a chaotic time series, is shown to constitute a global approximation to the attractor.[2] That is, a FFNN, trained upon a chaotic time series, becomes a functional realization of that time series, in the global sense. Furthermore, a FFNN is shown to course grain the noise, in a time series during training, in the least–squares sense.[3] The functional realization property of the FFNN allows the possibility for data window extension, once it is trained on a stationary time series, which can be, in fact, a rather narrow window. This is accomplished in the FFNN by choosing the input, in the form of delay coordinates, from a portion of the original time series which was not part of the training set, and then feeding the output into the input; thus, the trained FFNN becomes self–generating, and facilitates data window extension.

Lapedes and Farber[4] showed earlier that FFNN's with nonlinear transfer function are quite capable of learning underlying rules from chaos, given even a short segment of the time series. Their training algorithm, however, uses a well-known, conventional version of the backpropagation, steepest descents approach and requires the computational capability of a CRAY. We have derived a new, unique, fast, and efficient training algorithm that accomplishes training on a 386-level PC in minutes, or seconds, what requires a half-hour CPU time on a CRAY using the conventional backpropagation procedure. Thus, our training method renders the use of FFNN's for chaotic time series analysis and characterization as practical.

We further extend the work of Lapedes and Farber[4] to applications in nonlinear optical systems, using as models the Lorenz system, Ikeda and Duffing oscillator,[5] and demonstrate characterization with respect to the phase space attractors, self–generation (stationary data window extension), and multistep prediction commensurate with the associated Lyapunov critical exponent. We also apply our new method of analysis to the study of stimulated Brillouin

scattered light from a CW pumped optical fiber.[6,7] Since controversy lingers over the interpretation of the results of several independent experiments,[7] we use our FFNN method to clearly demonstrate purely deterministic from purely stochastic contributions in the SBS temporal evolution using signal generation from the standard stochastic SBS equations. Results are analyzed for regions of the parameter space and conditions which include those corresponding to the experiments.[6,7]

As a generic example, the method was applied to the chaotic time series generated from the Lorenz equations. The training data to the FFNN is generated from integration of the Lorenz equations and in the form of delay coordinates[8]. The attractor associated with the embedding[8] from the time series generated from integration of the equations is shown in Fig. 1. Shown in Fig. 2 is the corresponding attractor, self–generated from the FFNN after training, and is qualitatively the same as in Fig. 1. To this degree, the FFNN has become, through its training, a functional realization of the integration of the Lorenz system. If the time series were experimental data, the FFNN trained on the data would be interpreted as a functional realization of the time series, and thus a characterization of the system, whereas, the self–generated data subsequent to training represented in Fig. 2, could be useful as data window extension, which may be necessary, under experimental conditions, to accommodate the calculation of such parameters as a Lyapunov critical exponent.

## References


1. M. Casdagli, Physica **D35**, 335 (1989).

2. S. D. Pethel, C. M. Bowden, and C. C. Sung, "Fast–training Algorithm for Hidden–layer, Forward–feed Neural Networks," Submitted to Journal of Neural Networks.

3. C. M. Bowden, C. E. Hall, Jr., S. D. Pethel, and C. C. Sung, in *OSA Proceedings on Nonlinear Dynamics in Optical Systems*, Vol. **7**, edited by N. B. Abraham, E. M. Garmire, and P. Mandel, (1991), p. 278. Also, S. D. Pethel, C. M. Bowden, and C. C. Sung, in preparation.

4. A. Lapedes and R. Farber, Technical Report LA–UR–87–2662, Los Alamos National Laboratory (1987).

5. P. W. Milonni, M.–L. Shih and J. R. Ackherhalt, *Chaos in Laser–Matter Interactions*, (World Scientific, Singapore, 1987).

6. R. G. Harrison, J. S. Uppal, A. Johnstone, and J. V. Moloney, Phys. Rev. Lett. **65**, 167 (1990).

7. A. L. Gaeta and R. W. Boyd, Phys. Rev. Lett. **44**, 3205 (1991).

8. P. Grassberger and I. Procaccia, Phys. Rev. Lett. **50**, 346 (1983).

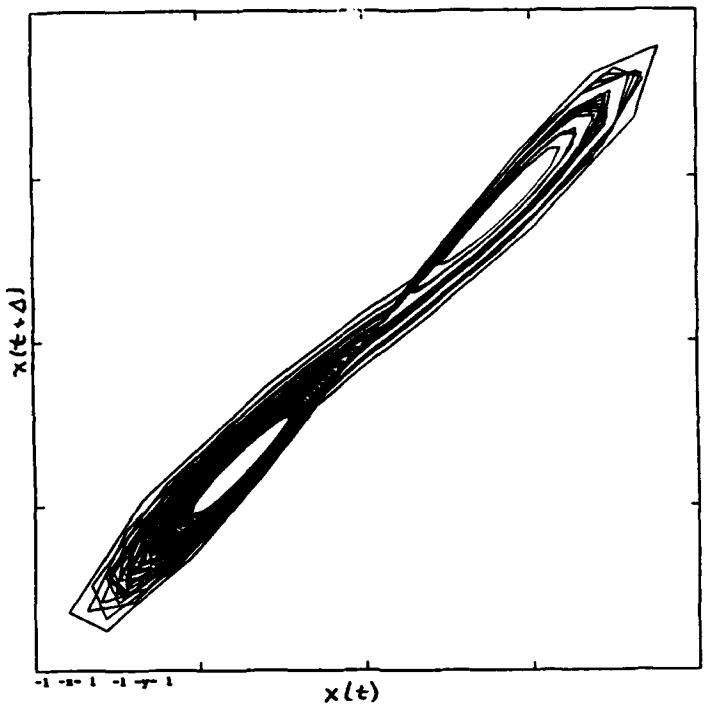


Figure 1. Lorenz attractor, generated from embedding using the x-variable, from time series obtained by integration of the Lorenz equations (Ref. 5, page 125) for values of the parameters[5] s = 16, b = 14, r = 40. The embedding dimension is d = 4, and the embedding time is D = 0.01. The plot corresponds to 2500 pts.

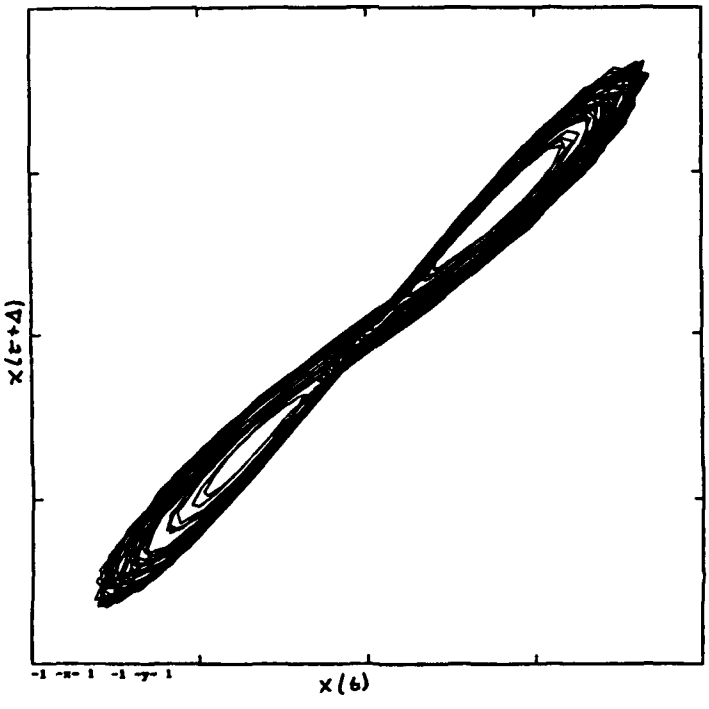


Figure 2. Attractor generated from embedding using time series self-generated from trained neural network. The training data is identical to that used to calculate results shown in Fig. 1. The FFNN consists of 4 inputs and one output, with a 44 element hidden layer and fully connected. A hyperbolic tangent thresholding function was applied to each hidden–layer neuron. The plot consists of 2500 pts.

# Mechanisms of Amplification with Inversion

Olga Kocharovskaya
Russian Academy of Sciences
Russian Federation

We analyze the physical origin of the gain in all schemes of inversionless amplification proposed to date and define two different mechanisms responsible for this process.

# POLARIZATION-SENSITIVE POPULATION TRAPPING IN AN OPTICALLY PUMPED LASER.

E. Roldán, R. Vilaseca,

Departament d'Optica, Universitat de València, 46100 Burjassot, Spain, T/. 34-6-3864343.

G. J. de Valcárcel,

Departament de Física Aplicada, Universitat Politècnica de València, 46020 València, Spain.

M. Arjona, J. Pujol,

Departament d'Optica i Optometria, Universitat Politècnica de Catalunya, 08222 Terrassa, Spain.

and R. Corbalán

Departament de Física, Universitat Autònoma de Barcelona, 08193 Bellaterra, Spain, T./. 34-3-5811653.

As we have shown recently /1/, the efficiency of an optically pumped laser is strongly sensitive to the structure of the atomic (or molecular) levels involved in the amplifying process, in particular to M-degeneracy. Specifically, when the common level b shared by the pump and laser transitions in a typical three-level configuration (Fig.1) has two sublevels m=±1 and the pump and laser fields are both linearly polarized (such as in the case, for instance, of the ammonia far-infrared laser /2/), there is a large difference in the dynamics of the laser when the pump and laser field polarizations are parallel or orthogonal /1,2/.

To explain the origin of the observed behavior we present in this contribution an analytical study of this class of laser. For the sake of simplicity only the case in which the sublevels m=±1 of level b (Fig.1) are degenerate will be considered.

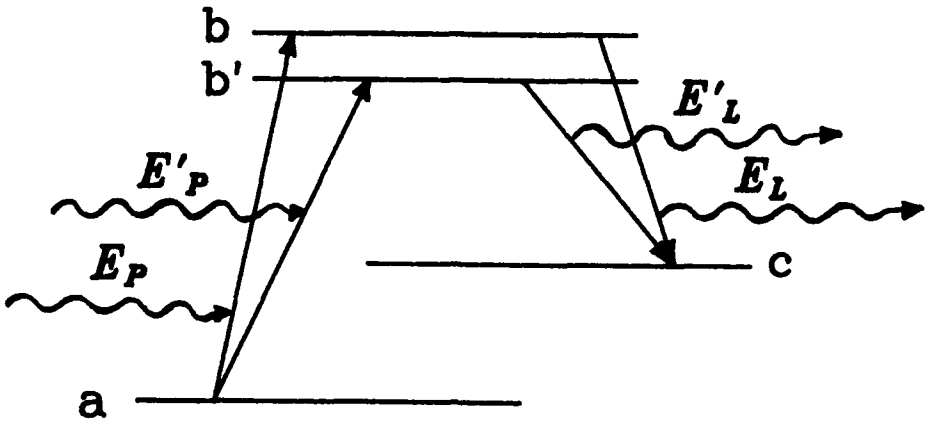


**Fig.1**.- Level diagram and fields in an optically pumped laser. a and c are J = 0 levels and b,b' are m = ±1 degenerate sublevels of a J = 1 level. The circularly polarized $E_p$ ($\sigma^+$) and $E'_p$ ($\sigma^-$) pump fields define a linearly polarized field, and the $E_L$ ($\sigma^+$) and $E'_L$ ($\sigma^-$) laser fields also define a linearly polarized field (either parallel or orthogonal to the pump field).

The analysis is performed first in the basis of the bare-atom states:

$$|a>,\ |b>,\ |b'>,\ |c>$$

in which we obtain the stationary solutions in both cases of parallel and orthogonal polarizations.

The most clear interpretation of the origin of the observed behavior, however, is obtained when the analysis is performed in the basis of the dressed states:

$$|\tilde{b}>,\ |r_+>,\ |r_->,\ |c>$$

where the first three states represent the eigenstates of the interaction Hamiltonian in the interaction picture when only the pump field is present. The state $|\tilde{b}>$ is a linear superposition of the bare-atom states $|b>$ and $|b'>$, whereas the states $|r_+>$ and $|r_->$ are a linear superposition of the states $|b>$, $|b'>$, and $|a>$. When the (weak) laser field has parallel linear polarization, it connects the state $|c>$ with the states $|r_+>$ and $|r_->$ (but not with the state $|\tilde{b}>$), and therefore Raman pumping is possible. When the laser field is orthogonally polarized, however, it connects the state $|c>$ with the dressed state $|\tilde{b}>$ only, so that in this case Raman pumping is forbidden. Furthermore, the population of the dressed state $|\tilde{b}>$ remains smaller than the (small) population of $|c>$ whenever $\Gamma < \Gamma_{th}$

($\Gamma$ represents the relaxation rate for the two-photon coherence $\rho_{bb'}$ induced by the pump field, and the threshold $\Gamma_{th}$ is given by an analytical expression), so that the population excited by the pump field from level a to level b remains essentially "trapped" in the states $|r_+>$ and $|r_->$. Only for $\Gamma > \Gamma_{th}$ laser emission can be achieved.

For $\Gamma = \gamma_{II}$ (i.e. the smallest possible value of $\Gamma$, equal to the longitudinal relaxation rate $\gamma_{II}$) the orthogonally polarized optically pumped laser is exactly equivalent to an incoherently pumped two-level laser (i.e. to a Lorenz-Haken laser), in the sense that optical pumping is unable to generate laser emission and only additional incoherent pumping of the upper level could give rise to laser emission.

It is worth noting that the double-V system here considered (Fig.1) is exactly the inverted case of the double-$\Lambda$ configuration which is being intensively studied presently /3/ in the context of "lasing without inversion". Hence it can be said that our system represents an example of polarization-sensitive "inversion without lasing". Our analysis is more general than those of refs. /3/ in the sense that the relative orientation of the electric field vectors of the pump and laser waves has been clearly taken into account. The typical condition of very small $\Gamma$ for the appearance of trapping in the cases of refs. /3/ is not required here.

[Permanent address of one of the authors (R.Vilaseca): Departament de Física (E.T.S.E.I.), Universitat Politècnica de Catalunya, 08222-Terrassa, Spain].

/1/ M. Arjona, R. Corbalán, F. Laguarta, J. Pujol, and R. Vilaseca: Phys. Rev. A (Rapid Commun.) 41, 6559 (1990).

/2/ E. Hogenboom, W. Klische, C.O. Weiss, and A. Godone: Phys. Rev. Lett. 55, 2571 (1985).

C. O. Weiss, N. B. Abraham, and U. Hübner: Phy. Rev. Lett. 61, 1587 (1988).

/3/ M. O. Scully, S.- Y. Zhu, and A. Gavrielides: Phys. Rev. Lett. 62, 2813 (1989).

O. Kocharovskaya and P. Mandel: Phys. Rev. A 42, 523 (1990)

O. Kocharov skaya, F. Mauri, and E. Arimondo: Optics. Comm. 84, 393 (1991).

L. M. Narducci, M. O. Scully, C. H. Keitel, S.- Y. Zhu, and H. M. Doss: Optics Comm. 86, 324 (1991) (and refs. therein).

A. Karawajczyk, J. Zakrzewski, and W. Gawlik: Phys. Rev. A 45 (January 1992).

Abraham, Neal B. — WA, WB3, FA4
Afanasev, A. A. — TuC2
Agrawal, Govind P. — FB
Anishchenko, V. S. — TuC14, TuC26
Apanasevich, S. — FA3
Arecchi, E. T. — WA2, FB2
Arjona, M. — FB6

Balle, S. — TuC10, WB3, FA4
Bandy, D. K. — MB6
Bärwolff, A. — ThA2
Bava, G. P. — TuC15
Belenov, E. M. — MC4
Belinsky, A. V. — TuC21
Berger, G. — ThA2
Berry, Michael — WC1
Besnard, P. — TuC8
Bielawski, S. — TuA4, TuA5
Blouin, A. — WA5
Boden, C. — FA1
Boggavarapu, D. — ThA7
Boixader, Francesc — TuC17, TuC27
Bossert, David J. — ThA4
Bouazaoui, M. — TuA4, TuA5
Bowden, C. M. — FB4
Boyd, R. W. — WA5
Brambilla, M. — WA3, WB1
Brivio, F. — TuC9
Bucholtz, F. — TuB6

Carr, Thomas — MC10
Castelli, F. — TuC15, WA3, FA2
Cattaneo, M. — WB1
Chen, Z. — WB3
Chern, Jyh-Long — MC5, ThB1
Chow, Weng W. — ThA7
Christiansen, P. L. — MA6
Chunfei, Li — TuC19
Ciofini, M. — FA5
Coates, A. B. — WB1
Colet, Pere — MC30, TuA2, ThB2
Corbalán, R. — FB6
Cormier, Jean-François — MC1
Coullet, Pierre — WA1

Dambly, L. — TuC22
Dämmig, M. — FA1
Danckaert, J. — TuC16
D'Angelo, E. J. — WB1, WB3
Dangoisse, D. — WB2
Davis, Peter — ThB
Dayawansa, W. P. — TuA1
Debernardi, P. — TuC15
DeFreez, Richard K. — ThA4
De Jagher, P. C. — ThA5
Dente, Gregory C. — ThA4
Derozier, D. — TuA4, TuA5
de Valcárcel, G. J. — FB6
Dienes, A. — MA5
Dunlop, A. M. — MA3

Elsässer, W. — MC29, ThA3
Erneux, Thomas — MC10, MC25, ThB5
Etrich, C. — TuC7

Fabiny, Larry — ThB2
Farjas, Jordi — TuC17
Fedorov, S. V. — TuC20
Firth, William J. — MA, MA3, TuC1, WA6, WB6
Fischer, I. — MC29
Fork, Richard L. — MA4
Forysiak, W. — MC2

Gao, Jinyue — TuC18
Garus, Dieter — MC26, TuB2
Gatti, A. — WA3
Geddes, J. B. — WB6
Geisler, T. — MA6
Georgiou, M. — MB3
Giacomelli, G. — WA2, FB2
Gibbs, H. M. — ThA7
Gills, Zelda — TuA3
Glorieux, P. — TuA4, TuA5, TuC22, WB2, ThD
Gobel, E. O. — MC29, ThA3
Goosev, I. V. — TuB5
Grantham, J. W. — ThA7
Grebogi, Celso — TuA1
Green, C. — WB1
Grohs, J. — FA3
Grynberg, G. — WA5

Haeltermann, M — MC8
Haken, H. — MB5, WC2
Harkness, G. K. — TuC1
Harrison, Robert G. — TuB1, WC, FB3
Hart, D. E. — TuC5
Heatley, D. R. — MA3
Hennequin, D. — WB2
Hereth, Ralf — MC26, TuB2
Heritage, J. P. — MA5
Herrero, Ramon — TuC27
Hoffer, L. M. — WA4
Hong, Feng-Lei — MB2, MC7
Hong, M. Y. — MA5
Hu, Y. Z. — ThA7
Hunt, E. R. — TuA3

Indik, R. — WB6, ThB4
Irie, Tomoyoshi — ThA1
Issler, H. — FA3
Ivanov, V. V. — MC24

Jakobsen, P. K. — MC6, WB5
Jiang, Ziping — ThB6
Jinyue, Gao — TuC18
Johnstone, A. — TuB1
Jones, D. J. — MB6

Kachanov, A. A. — MC24
Kaiser, F. — TuC3
Kaneko, Kunihiko — ThC1
Kawaguchi, Hitoshi — ThA1
Kent, A. J. — WB1
Khandokhin, P. A. — MB7

Khanin, Yakov I. — MB, MB7, MC19
Khitrova, G. — ThA7
Khodova, G. V. — TuC20
Kilin, S. Ya — TuC24
Klehr, A. — ThA2
Klingshirn, C. — FA3
Koch, S. W. — ThA7, ThB4
Kocharovskaya, Olga — FB5
Koryukin, I. V. — MC19
Kostritskaya, K. S. — TuC20
Kotomtseva, L. A. — MC15
Kovalenko, S. A. — MC24
Kreuzer, M. — TuC6
Krivoschekov, V. A. — TuB5
Kuball, M. — FA3
Kuznetsov, A. P. — TuC25
Kuznetsov, S. P. — TuC25

Ladjouze, H. — MC23
Lange, W. — WA4, FB1
Lapucci, A. — FB2
Lee, Zhang — TuC19
Lefever, R. — WA6
Leite, Jose R. R. — WA5
Lenstra, Daan — ThA, ThA5
Lepers, C. — WB2
Li, Chunfei — TuC19
Li, Hua — ThA6
Li, Ruo-Ding — ThB5
Lim, D. S. — TuB1
Lippi, G. L. — WA4
Liu, Yun — FA6
Logvin, Yu. A. — TuC12
Loiko, N. A. — MC13
Louvergneaux, E. — WB2
Lu, Weiping — TuB1, FB3
Lugiato, L. A. — TuC15, WA3, WA6, WB1, FA2
Luther, G. G. — TuC5
Lyakhnovich, A. — FA3

Maier, T. D. — TuA3
Maitre, A. — WA5
Mak, A.A. — MB4, MC21
Malev, A. V. — TuC23
Mandel, Paul — MB3, TuC7, WB, WE
Mark, J. — MA6
Massaneda, Josep — TuC17
Mazzoleni, S. — TuC9
McCall, Martin — ThB6
McDonald, G. S. — WA6, WB6
McInerney, John G. — ThA6
Melnikov, L. A. — MC14, MC16, MC18, TuC4
Meucci, R — FA5, FB2
Meziane, B. — MC23, TuC8
Milani, M. — TuC9
Mitschke, Fedor M. — TuA, FA1
Möller, M. — FB1
Moloney, Jerome V. — MC2, MC6, TuC5, WB5, WB6, WD, ThB4
Mork, J. — MA6
Müller, R. — ThA2
Murphy, T. W., Jr. — TuA3

Nalik, J. — WA4
Nazarkin, A. V. — MC4
Neiman, A. B. — TuC14, TuC26
Neubecker, R. — TuC6
Newell, A. C. — WB5
Nichols, D. T. — TuC13
Ning, C. Z. — MB5

Ohtsubo, Junji — FA6
Oppo, G. L. — WB1
Oraevsky, A. N. — MB6, MC22
Orlov, O. A. — MB4, MC21
Orriols, Gaspar — TuC17, TuC27
Otsuka, Kenju — MB3, MC5, TuC7, ThB1, ThC
Ott, Edward — TuA1

Peng-ye, Wang, — FA5
Pesquera, L. — MC30, TuC28
Pethel, S. D. — FB4
Pettiaux, Nicolas P. F. — MC25
Pi, Francesc — TuC17, TuC27
Piché, Michel — MA2, MC1
Pinard, M. — WA5
Pirovano, R. — WB1
Prati, F. — WA3, WB1
Protsenko, I. E. — MC27
Pujol, J. — FB6

Rabinovich, M. — ThC2
Rahman, Lutfur — ThB3
Ramazza, P. L. — WA2
Residori, S. — WA2
*Rios Leite, J. R.* — WA5
Rivlin, L. A. — MC11
Rodriguez, M. A. — TuC28
Roldán, E. — FB6
Romeiras, Filipe J. — TuA1
Rosanov, N. N. — TuC20, TuC21
Rosell, Joan I. — TuC27
Roy, Rajarshi — TuA2, TuA3, TuB, ThB2
Ru, P. — MC6, ThB4

Sacher, J. — MC29, ThA3
Salin, François — MA2
Samson, A. M. — MC13, MC15, TuC12
Samson, B. A. — TuC2
San Miguel, Maxi — MC30, TuC10, FA, FA4
Sancho, J. M. — TuC10
Sargent, Murray, III — ThA7
Sarkissian, T. V. — MB6
Sataev, I. R. — TuC25
Sauer, M. — TuC3
Schliep, F. — MC26
Scroggie, A. J. — WA6
Shaw, Kenneth D. — TuB4
Shelaev, A. N. — MC3
Shimizu, Todao — MB2, MC7
Shore, K. A. — MA6, TuC11
Smith, Sandra L. — MA4
Sokolov, A. A. — TuC4
Song, Yinglin — TuC19
Sorenson, M. P. — MA6
Staliunas, K. — WB4

Steffen, J. — FA3
Stephan, G. — TuC8
Sugawara, Toshiki — MB2, MC7
Sung, Chi C. — FB4
Sviridenkov, E. A. — MC24

Tachikawa, Maki — MB2, MC7
Tan, Weihan — FB3
Tan-no, Naohiro — ThA1
Tang, D. Y. — MB1
Tanii, K. — MC7
Tatarkov, G. N. — MC16, TuC4
Tatarkova, S. A. — MC17
Thienpont, H. — TuC16
Tohei, Takehisa — MB2, MC7
Toronov, V. Yu. — MC14, MC18
Torrent, M. C. — TuC10
Tredicce, J. R. — WB1, WB3
Trillo, S. — MC8, TuB3
Tschudi, T. — TuC6
Tuchin, V. V. — MC17

Uppal, J. S. — TuB1
Ustyugov, V. — MB4, MC21

Valle, A. — MC30, TuC28
Veretennicc Irina P. — TuC16
Veshneva, I — TuC4
Viktorov, E. A. — MB4, MC21
Vilaseca, R — FB6
Vinogradov, S. E. — MC24
Vitrischak, I B. — MB4
Vladimirov, A. G. — MC20
Vohra, S. T. — TuB6
Volkov, V. M. — TuC2
Vorgerd, C. — WA4
Vorontsov, M A. — WA7
Voss, M — hA2

Wabnitz, S — MC8, TuB3
Wang, Peng ye — FA5
Weihan, Ta — FB3
Weiss, C. O — MB1, WB1, WB4
Wenden, S. G. — WB5
Winful, Herbert G. — TuC13, ThA4, ThB3
Wright, E. M. — TuC5, ThB4
Wu, Song — MA4

Ye, Jun — ThA6
Yee, W. M. — TuC11
Yinglin, Song — TuC19

Zadernovsky, A. A. — MC11
Zeghlache, H. — TuC22
Zeldovich, B. Ya. — TuB5
Zha, Zizhong — TuC19
Zhang, Lei — TuC19
Zheng, Zhiren — TuC18
Zhiren, Zheng — TuC18
Zizhong, Zha — TuC19